ESTIMATION OF REMAINING SERVICE LIFE OF FLEXIBLE PAVEMENTS FROM SURFACE DEFLECTIONS

by

DABA SHABARA GEDAFA

B.S., Addis Ababa University, Ethiopia, 2001
M.Tech., Indian Institute of Technology Bombay, India, 2005

AN ABSTRACT OF A DISSERTATION

submitted in partial fulfillment of the requirements for the degree

DOCTOR OF PHILOSOPHY

Department of Civil Engineering
College of Engineering

KANSAS STATE UNIVERSITY
Manhattan, Kansas

2008

Abstract

Remaining service life (RSL) has been defined as the anticipated number of years that a pavement will be functionally and structurally acceptable with only routine maintenance. The Kansas Department of Transportation (KDOT) has a comprehensive pavement management system, network optimization system (NOS), which uses the RSL concept. In support of NOS, annual condition surveys are conducted on the state highway system. Currently KDOT uses an empirical equation to compute RSL of flexible pavements based on surface condition and deflection from the last sensor of a falling-weight deflectometer (FWD). Due to limited resources and large size, annual network-level structural data collection at the same rate as the project level is impractical. A rolling-wheel deflectometer (RWD), which measures surface deflections at highway speed, is an alternate and fast method of pavement-deflection testing for network-level data collection. Thus, a model that can calculate RSL in terms of FWD first sensor/center deflection (the only deflection measured by RWD) is desired for NOS.

In this study, RWD deflection data was collected under an 18-kip axle load at highway speed on non-Interstate highways in northeast Kansas in July 2006. FWD deflection data, collected with a Dynatest 8000 FWD on the KDOT network from 1998 to 2006, were reduced to mile-long data to match the condition survey data collected annually for NOS. Normalized and temperature-corrected FWD and RWD center deflections and corresponding effective structural numbers (SNeff) were compared. A nonlinear regression procedure in Statistical Analysis Software (SAS) and Solver in Microsoft Excel were used to develop the models in this study.

Results showed that FWD and RWD center deflections and corresponding SNeff are statistically similar. Temperature-correction factors have significant influence on these variables. FWD data analysis on the study sections showed that average structural condition of pavements of the KDOT non-Interstate network did not change significantly over the last four years. Thus, network-level deflection data can be collected at four-year intervals when there is no major structural improvement.

Results also showed that sigmoimal relationship exists between RSL and center deflection. Sigmoidal RSL models have very good fits and can be used to predict RSL based on center deflection from FWD or RWD. Sigmoidal equivalent fatigue crack-models have also

shown good fits, but with some scatter that can be attributed to the nature and quality of the data used to develop these models. Predicted and observed equivalent transverse-crack values do not match very well, though the difference in magnitude is insignificant for all practical purposes.

ESTIMATION OF REMAINING SERVICE LIFE OF FLEXIBLE PAVEMENTS FROM SURFACE DEFLECTIONS

by

DABA SHABARA GEDAFA

B.S., Addis Ababa University, Ethiopia, 2001
M.Tech., Indian Institute of Technology Bombay, India, 2005

A DISSERTATION

submitted in partial fulfillment of the requirements for the degree

DOCTOR OF PHILOSOPHY

Department of Civil Engineering
College of Engineering

KANSAS STATE UNIVERSITY
Manhattan, Kansas

2008

Approved by:

Major Professor
Dr. Mustaque Hossain

Copyright

Abstract

Remaining service life (RSL) has been defined as the anticipated number of years that a pavement will be functionally and structurally acceptable with only routine maintenance. The Kansas Department of Transportation (KDOT) has a comprehensive pavement management system, network optimization system (NOS), which uses the RSL concept. In support of NOS, annual condition surveys are conducted on the state highway system. Currently KDOT uses an empirical equation to compute RSL of flexible pavements based on surface condition and deflection from the last sensor of a falling-weight deflectometer (FWD). Due to limited resources and large size, annual network-level structural data collection at the same rate as the project level is impractical. A rolling-wheel deflectometer (RWD), which measures surface deflections at highway speed, is an alternate and fast method of pavement-deflection testing for network-level data collection. Thus, a model that can calculate RSL in terms of FWD first sensor/center deflection (the only deflection measured by RWD) is desired for NOS.

In this study, RWD deflection data was collected under an 18-kip axle load at highway speed on non-Interstate highways in northeast Kansas in July 2006. FWD deflection data, collected with a Dynatest 8000 FWD on the KDOT network from 1998 to 2006, were reduced to mile-long data to match the condition survey data collected annually for NOS. Normalized and temperature-corrected FWD and RWD center deflections and corresponding effective structural numbers (SNeff) were compared. A nonlinear regression procedure in Statistical Analysis Software (SAS) and Solver in Microsoft Excel were used to develop the models in this study.

Results showed that FWD and RWD center deflections and corresponding SNeff are statistically similar. Temperature-correction factors have significant influence on these variables. FWD data analysis on the study sections showed that average structural condition of pavements of the KDOT non-Interstate network did not change significantly over the last four years. Thus, network-level deflection data can be collected at four-year intervals when there is no major structural improvement.

Results also showed that sigmoimal relationship exists between RSL and center deflection. Sigmoidal RSL models have very good fits and can be used to predict RSL based on center deflection from FWD or RWD. Sigmoidal equivalent fatigue crack-models have also

shown good fits, but with some scatter that can be attributed to the nature and quality of the data used to develop these models. Predicted and observed equivalent transverse-crack values do not match very well, though the difference in magnitude is insignificant for all practical purposes.

Table of Contents

List of Figures

List of Tables

Acknowledgements

I would like to take this opportunity to express my deepest sense of gratitude to my major professor **Dr. Mustaque Hossain** for his invaluable guidance, motivation, and constant encouragement without which this dissertation could not have this shape. In addition to my dissertation work, his encouragement in publishing technical papers and developing my profession has been incredible.

I would also like to thank **Dr. Paul Nelson** for agreeing to be my committee member and for his frequent advice during this dissertation work. I also thank **Dr. Stefan Romanoschi** for being my committee member and providing data on perpetual pavement sections on US-75. I am also grateful to **Dr. Sunanda Dissayanake** for being my committee member and such a friendly person.

I also appreciate **Mr. Rick Miller** of the Kansas Department of Transportation (KDOT) for providing network-level FWD deflection and distress data. I am also grateful to **Mr. Douglas Steele** of Applied Research Associates (ARA) for providing RWD deflection data. I would also like to acknowledge the Federal Highway Administration (FHWA) for funding this study.

I would also thank my relatives and friends who have been involved directly or indirectly for the completion of my dissertation.

Finally, I want to thank God Almighty for giving me strength to overcome all the challenges I have faced throughout my life, particularly for comforting me after the loss of my beloved father.

Dedication

This dissertation is dedicated to my late father, **Mr. Shabara Gedafa Hatew**, who understood the importance of education without being educated and supported me throughout my undergraduate and graduate education until he passed away.

CHAPTER 1 INTRODUCTION

1.1 General

A major goal of most transportation systems is the safe, rapid, and convenient movement of people and goods from one place to another in order to enhance economic activity and development. Development of transportation facilities raises living standards, and improves the aggregate of community values. In the United States, transportation over the course of its historical development has been fundamentally influenced and shaped by legislation. Whereas technological advances have made it possible to transport people and goods in a more *efficient* manner, major improvements in the transportation industry have been shaped by the larger institutional systemic framework that determines present and future needs and seeks to give them *cost-effective* yet far-reaching solutions. Roads are the dominant means of transportation in many countries today *(Mitchell and Maree, 1994).* As roads play an essential role in achievement of a government's overall social, economic, security, and developmental goals, much capital has been expended in developing extensive road networks worldwide. The United States' network of major highways incorporates almost four million miles of pavements (*FHWA, 1993*). This pavement network forms a significant portion of the national transportation infrastructure and represents a cumulative investment of hundreds of billions of dollars over several decades. Therefore, despite increasingly limited national funds for infrastructure maintenance in the 1980s and 1990s, there has been a growing need for strategic management of the national pavement network to preserve this large capital investment. To address this problem, the Intermodal Surface Transportation Efficiency Act (ISTEA) was passed in 1991. ISTEA's mandates include development and implementation of various infrastructure management and monitoring systems: pavement, bridge, highway safety, traffic congestion, public transportation facilities and equipment, and intermodal facilities and systems management systems. The goal was to optimize available funds in preserving the national transportation infrastructure. Consequently, to continue to qualify for federal funds, states, and their local jurisdictions were to implement working infrastructure management systems, consisting of all seven mandated categories *(Amekudzi and Attoh-Okine, 1996).*

The pavement management system (PMS) was initiated in the mid 1970s based on integration of systems principles, engineering technologies, and economic evaluation as a result of the shift from the design-and-build mode to the repair-and-maintain mode *(Kulkarni and Miller, 2003; Haas, 2001).* Systems developed in the 1990s use integrated techniques of performance prediction, network and project-level optimization, multi-component prioritization, and the geographical information system (GIS). Key elements to be addressed by PMS are data collection and management, pavement performance prediction, economic analysis, priority evaluation, optimization, institutional issues, and information technology. Successful implementation of a PMS depends mainly on three factors: reliable data, realistic models for analyzing the data, and user-friendly software for organizing the inputs and presenting the outputs *(Chen et al., 1993).*

The Kansas Department of Transportation (KDOT) uses a comprehensive, successful PMS. The network-level PMS of KDOT is popularly known as the network optimization system (NOS). In support of NOS, annual condition surveys are conducted based on methodologies proposed by Woodward Clyde Consultants (now URS Corp.) and subsequently, refined by the KDOT pavement management section. Current annual condition surveys include roughness, rutting, fatigue cracking, transverse cracking, and block cracking for flexible and composite pavements; and roughness, faulting, and joint distresses for rigid pavements. Different severity levels and extents are measured in the survey. While roughness, rutting, and faulting data are collected using automated methods, cracking and joint-distress surveys are done manually. These survey results constitute the basic condition inputs into the NOS system. The performance prediction methodology in the NOS system is based on the Markov process. The technique uses transition matrices to predict future conditions based on current conditions for multi-year programming *(Kulkarni et al., 1983).* Based on functional class, pavement type, traffic loading, and roadway width, the statewide network is divided into 23 road categories and six administrative districts.

Remaining service life (RSL) is the anticipated number of years that a pavement is in acceptable condition to accumulate enough functional or structural distress under normal conditions, given that only routine maintenance is performed *(Baladi, 1991).* KDOT adopted a similar definition for RSL. RSL is calculated from the condition of the pavement during that year and the projected number of years until rehabilitation is required. Once RSL is estimated for each

pavement section in the network, the sections are grouped into different categories *(Dicdican et al., 2004)*. This combines severity and extent of different distresses and rate of deterioration. RSL also requires development of a performance model and establishment of a threshold value for each distress type. Based on these threshold values, current distress level, and deterioration model for each particular distress, time for each distress to reach the threshold value can be computed *(Baladi,1991)*. Calculating RSL has been a complex task due to lack of adequate performance prediction models required for determining timing of the rehabilitation project. In general, there are three RSL estimation procedures: (i) functional failure-based approach; (ii) structural failure-based approach; and (iii) functional and structural failure-based approaches *(Witczak, 1978)*.

Deflection testing is now widely recognized as an important tool for pavement structural evaluation. Current deflection testing devices measure deflection response to a known load applied at the pavement surface. Although deflection data analysis is a matter of continuing research, surface-deflection testing is accepted by most highway agencies as a standard practice for the advantages of being fast and reliable in most cases *(Hossain et al., 2000)*.

At the network level, deflection testing can identify the beginning and end of management sections and group pavement sections with similar structural capacities for condition prediction, and can also identify projects for project-level testing and evaluation. The structural evaluation provides a wealth of information concerning the expected behavior of pavements. However, due to expenses involved in data collection and analysis, structural capacity is not currently evaluated at the network level of pavement management by many agencies, though it is routinely done at the project level. *Haas et al. (1994)* argue that structural-capacity information, even derived from less intensive sampling than for project-level purposes, can be very useful at the network work level for project prioritization purposes. The practice exists in a few states and Canadian provinces such as Idaho, Minnesota, Utah, Alberta, and Prince Edward Island *(Haas et al., 1994)*.

1.2 Problem Statement

Currently a falling-weight deflectometer (FWD) is the most popular device for project-level deflection testing. However, during the last decade, many highway agencies have adopted FWD as a tool for assessing structural adequacy of the pavements at the network-level

(Damnjanovic and Zhang, 2006). KDOT uses recently developed remaining-life equations primarily driven surface distresses, but use one input from pavement surface-deflection testing for NOS. KDOT owns and operates two Dynatest 8000 FWD. Currently, each unit is capable of testing up to 20 lane-miles in a 10-hour day during a deflection survey period that runs from April through October. At this production level, to test the entire network (11,186 lane-miles) annually, 200 days of testing would be necessary. This does not include time spent in travel from one project to the other. An alternate, faster method of deflection testing that can be used on the whole network or on a representative sample of the network, is needed. A rolling- wheel deflectometer (RWD), which measures surface deflections at highway speed, appears to be very promising for this purpose. Thus, this study was initiated to assess the feasibility of using RWD for deflection measurements at the network level and using the measured deflections for predicting RSL as well as some distresses that are measured during condition survey for NOS.

Structural capacities of flexible pavements are determined using deflection measurements. The most important environmental factor affecting surface deflections of flexible pavements is the temperature of the asphaltic layers *(Kim et al., 1995; Park et al., 2002; Shao et al., 1997)*. All such deflection data should be adjusted to a reference temperature *(Chen et al., 2000)*. The temperature can be measured directly by drilling holes into the pavement, but the procedure is time consuming and multiple holes are needed to capture the temperature gradient. Temperature estimates based on correlations with externally measurable variables are preferable. Some of the methods are based on graphs and charts and are time consuming to use at the network level. A method which is accurate enough and easy to use at the network level also needs to be identified if the center deflection is used routinely.

Currently, KDOT uses an equation which computes the design life of flexible pavements based on the equivalent thickness of the action (rehabilitation strategy), equivalent transverse cracking before the action, design-lane average daily load (ADL- average daily 18-kip equivalent single-axle loads) during the year of the action, and average deflection from the sixth sensor of an FWD. However, it is not feasible from time, cost, and safety points of view to use FWD at the network level. RWD, which is state-of-the-art equipment to measure pavement surface deflections at highway speed, can be used to collect data at the network level. However, only center deflection is measured with RWD. Thus, a model that can estimate the remaining service life of pavements in terms of center deflection is required.

KDOT collects fatigue and transverse cracking data on a yearly basis as part of a NOS survey. Three, 100-ft randomly selected test sections are used to determine the expected condition for any mile-long PMS segment. The three, 100-ft sections may not represent the condition of the pavement in a mile since the method is subjective. Also, quality of the data depends on the experience and personal judgment of the personnel involved. The manual survey method is slow, distracts the flow of traffic, and is unsafe, especially in urban areas. This method is also neither time nor cost effective. Prediction models for fatigue and transverse cracking, in terms of objectively measured data such as deflection, will help KDOT avoid the drawbacks of the existing practice requiring manual surveys.

1.3 Objectives of the Study

The main objectives of this study are:

- To compare FWD and RWD center deflections and corresponding effective structural numbers computed from the FWD and RWD deflection measurements;
- To develop and validate remaining service life (RSL) models using layer thickness, traffic, distress, deflection, and structural data; and
- To develop and validate prediction models for fatigue and transverse cracking in terms of pavment surface deflections and other objective variables.

The study will also determine effects of temperature-correction methods on center deflections and corresponding computed effective structural numbers and the frequency of deflection measurements at the network level. A comparison of structural numbers (SN) based on the AASHTO method and KDOT procedures will also be done.

1.4 Organization of Dissertation

This dissertation is divided into six chapters. The first chapter covers a brief introduction, problem statement, study objectives, and outline of the dissertation. Chapter 2 is a review of the literature. Chapter 3 describes the test sections and data collection procedure. Chapter 4 presents analysis and discussion of test results. Chapter 5 presents prediction models for RSL, fatigue, and transverse cracking. Finally, Chapter 6 presents conclusions and recommendations based on this study.

CHAPTER 2 LITERATURE REVIEW

2.1 Introduction

The basic components and management levels of the pavement management system (PMS), from inception to current status, have been reviewed. Three components of the Kansas Department of Transportation (KDOT) PMS–network optimization system (NOS), project optimization system (POS), and pavement management information system (PMIS)–have been discussed. Remaining service life (RSL) and its estimation procedures have been reviewed. Pavement performance prediction and model development have been described. Four types of pavement deflection devices and integration of deflection data into the PMS have also been reviewed. Pavement temperature prediction and deflection correction procedures have been outlined. Structural capacity of pavement has also been described.

2.2 Pavement Management System

The pavement management system (PMS) was first conceived in the late 1960s to 1970s as a result of pioneering work by *Hudson et al. (1968)* and *Finn et al. (1977)* in the United States, and by *Haas (1977)* in Canada. *AASHTO (1990)* defines PMS as follows: "A PMS is a set of tools or methods that assist decision makers in finding optimum strategies for providing, evaluating, and maintaining pavements in a serviceable condition over a period of time." The products and information that can be obtained and used from a PMS include planning, design, construction, maintenance, budgeting, scheduling, performance evaluation, and research *(Hugo et al., 1989; AASHTO, 1990)*. The goal of a PMS is to yield the best possible value for available funds in providing and operating smooth, safe, and economical pavements *(Lee and Hudson, 1985)*. The functions of a PMS is to improve the efficiency of decision making, to expand the scope and provide feedback on the consequences of the decisions, to facilitate coordination of activities within the agency, and to ensure consistency of decisions made at different levels within the same organization *(Haas et al., 1994)*. A PMS provides a systematic, consistent method for selecting maintenance and rehabilitation (M&R) needs and determing priorities and the optimal time of repair by predicting future pavement conditions *(Shahin, 2005)*.

2.2.1 Basic Components

Most formal definitions of PMS agree on five key components. These are pavement condition surveys, database containing all related pavement information, analysis scheme, decision criteria, and reporting procedures. Figure 2-1 shows the basic components of a PMS.

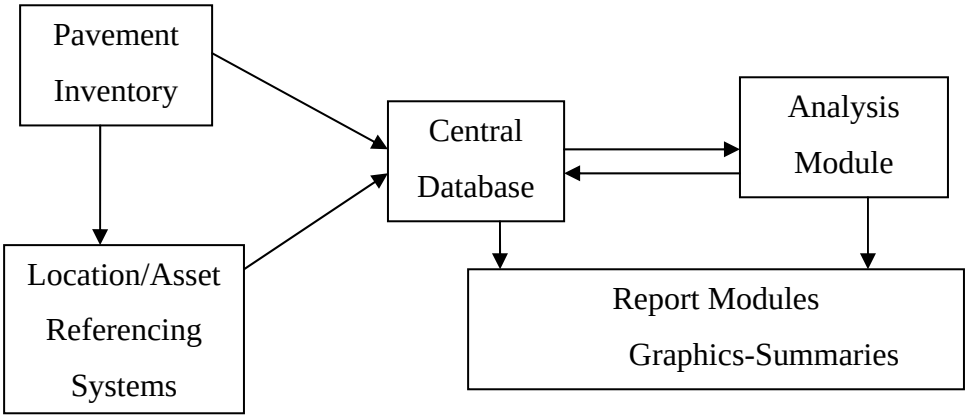

Figure 2-1 Basic Components of PMS *(USDOT, 1991)*

2.2.2 Pavement Management Levels

To determine the direction and specificity of project development and planning, decisions can be carried out at two management levels depending on the choice of the decision maker to get into the details: network level and project level *(Panigraphi, 2004)*.

Network level uses a systems methodology to combine methods, procedures, aggregate data, software, policies, and decisions to produce solutions that are optimized for the entire pavement network, and decisions are concerned with programmatic and policy issues for an entire network. These decisions include establishing pavement preservation policies; identifying priorities; estimating funding needs; and allocating budgets for maintenance, rehabilitation, and reconstruction (MR&R).

At the project level, only selected segments of the whole network are analyzed at a higher level of technical detail to determine the specific nature and type of treatment for the segment. Such detailed analysis at the project level requires a more detailed data collection, data storage, and data analysis *(Panigraphi, 2004)*. Detailed consideration is also given to alternative conditions, MR&R assignments, and unit costs for a particular section of project within the overall program. The objective is to provide the desired benefits or levels of service at the least total cost over the analysis period. This level of management involves assessing causes of

pavement deterioration, determining potential solutions, assessing effectiveness of alternative repair techniques, and selecting solution and design parameters. The purpose is to provide the most cost-effective feasible original design, maintenance, and rehabilitation or reconstruction strategy possible for a selected section of pavement for the available funds *(AASHTO, 2001)*.

Some PMS literature introduces an innovative PMS model with three decision levels, differentiating the network level into the program and project selection levels *(Lee and Hudson, 1985; Haas et al., 1994).* Program level involves planning and allocating budgets for network optimization. Project selection level ranks candidate projects within the constraints of the available budget. Project level is concerned with detailed design decisions for implementing individual projects chosen at the project selection level. Figure 2-2 illustrates PMS information flows.

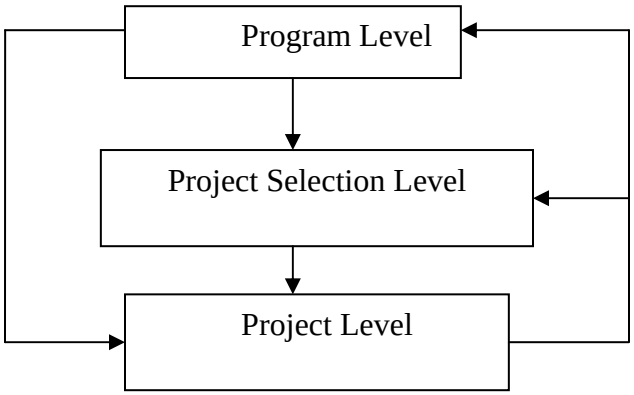

Figure 2-2 PMS Structure and Information Flows *(Amekudzi and Attoh-Okine, 1996)*

2.3 Kansas Department of Transportation (KDOT) PMS

The concept for a PMS for KDOT was first discussed in an issue paper in 1979. Woodward Clyde Consultants (now URS Corp.) was contracted in 1980 to develop the system in three phases. Phase I of the study examined the feasibility of developing a PMS and concluded that an appropriate PMS could be developed to meet the goals of KDOT within its available resources. The feasibility report included a five-year schedule with the major developmental effort in the first three years. The conceptual framework of a PMS identified in the feasibility study consisted of three major components: (a) network optimization system (NOS), (b) project optimization system (POS), and (c) pavement management information system (PMIS). Phase II completed a major portion of the NOS and a significant portion of the PMIS *(Kulkarni et al.,*

1983). In phase III, a POS was developed and NOS predictions models were finalized *(Kulkarni et al., 1988)*. The KDOT PMS process is shown in Figure 2-3.

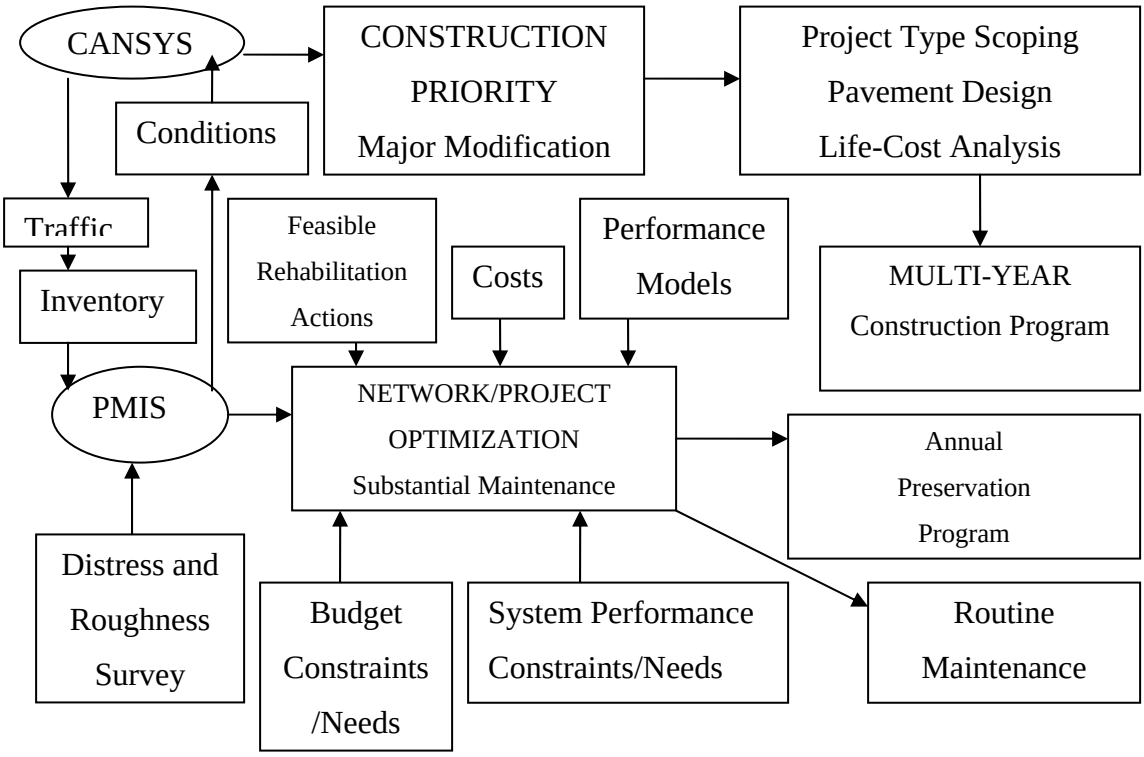

Figure 2-3 KDOT PMS System *(Kulkarni et al., 1988)*

2.3.1 Methodology for KDOT Network Optimization System (NOS)

The NOS methodology is based on formulating the problem as a Markov Decision Process (MDP) and converting it into a linear program. MDP is the most popular network optimization method for managing pavements and bridges. It has been implemented in PMS by agencies all over the world *(Golabi et al., 1982; Thompson et al., 1987; Harper and Majidzadeh, 1993; Wang et al., 1994)* since the first pavement network optimization system based on MDP was developed by *Golabi et al. (1982)*.

Road segment is defined in KDOT NOS as the pavement structural section on a one-mile (± 0.5-mile) interval of the state highway network. A transition probability, $p_{ij}(a_k)$, specifies the likelihood that the road segment will move from state i to state j in unit time if the rehabilitation action a_k is applied to the segment at the present time. Under the assumptions of a Markov process, the specification of condition state and transition probability permits one to

calculate the probabilities that a road segment would be in a different condition state at any given time period for an assumed rehabilitation policy.

The objective of the NOS is to find the rehabilitation policy that would achieve desired performance at a minimum cost or would maximize user benefits for a fixed budget. This applies to 11,186 miles of the state highway system. Major outputs from a NOS include annual rehabilitation budgets over a selected planning horizon (such as five years), location of candidate rehabilitation projects, minimum performance requirements for a fixed budget, optimal rehabilitation actions, etc.

2.3.2 Implementation of the NOS

2.3.2.1 Identification of Road Categories

Based on functional class, pavement type, traffic loading, and roadway width, the statewide network is divided into 23 categories as shown in Table 2-1 . The NOS operates independently on each road category. Thus, basic inputs (condition state, costs, transition probability, feasible actions, and performance standards) can be varied for each category.

2.3.2.2 Determination of Distress Types, Influence Variables, and Distress States

Distress types define specific pavement deficiencies which trigger rehabilitation actions. Influence variables allow for prediction of future levels of distress types. The influence variable "index to the first distress, IFD" is used to differentiate between expected life cycles for alternative rehabilitation treatments. The differences in future performance of different rehabilitation treatments can be handled properly through use of the index to the first distress. Table 2-2 shows distress types and influence variables.

2.3.2.3 Condition States (CS)

The condition state defines one particular combination of given levels of selected distress types and influence variables for a particular road category. In defining a condition state, the following sequence of variables is used: IFD, roughness, combination of primary distress type and rate of change for the first distress type, and combination of secondary distress type and rate of change for the secondary distress type. Total condition states will then be: 4x3x6x6=432 or 4x3x6x3=216. Since efficiency of the linear program and ease of developing performance

prediction models would increase with a reduced number of rates of change of distress, 216 condition states are normally used by KDOT.

Table 2-1 KDOT Road Categories *(Kulkarni et al., 1983)*

Functional Class	Pavement Type	Roadway Width (m)	Traffic Loading	Road Category
Interstate	PCCP	All	0-749	1
			750-up	2
	Composite		0-749	3
			750-up	4
	FDBIT*		All	5
Other	PCCP		0-87	6
			88-162	7
			163-up	8
	Composite		0-87	9
			88-162	10
			163-up	11
	FDBIT*	<9.80	0-22	12
			23-50	13
			51-up	14
		≥9.80	0-22	15
			23-50	16
			51-up	17
	PDBIT**	<9.80	0-22	18
			23-50	19
			51-up	20
		≥9.80	0-22	21
			23-50	22
			51-up	23

* Full-Design Bituminous Pavement; ** Partial-Design Bituminous Pavement

Table 2-2 Distress Types and Influence Variables for Given Pavement Types

Pavement Type	Distress Types	Influence Variables
Full-Design Bituminous/Composite	Roughness	Change in transverse cracks
	Transverse cracks	Index to first transverse crack
	Rutting	Change in rutting
Partial-Design Bituminous	Roughness	Change in fatigue cracks
	Fatigue cracks	Index to first fatigue crack
	Transverse cracks	Change in transverse cracks
PCC	Roughness	Change in joint distress
	Joint distress	Index to first joint distress
	Faulting	Change in faulting

2.3.2.4 Feasible Maintenance and Rehabilitation Actions

After the list of actions or rehabilitation alternatives applicable to a given road category is prepared, feasible actions from this list for each condition state need to be specified. This would include actions that would adequately correct given distress levels. However, some actions may be permitted because of budget limitations, even if they do not correct the distresses. A list of maintenance and rehabilitation actions is shown in Table 2-3.

2.3.2.5 Costs of Different Actions

The total cost, $C(i,k)$ of action k for pavements in condition state i is given by the following:

$$C(i,k) = RMC_k(R(i), D_1(i), D_2(i) + CS_k(R(i), D_1(i), D_2(i)) \quad (2.1)$$

where

$R(i)$ = level of roughness corresponding to CS i;

$D_1(i)$ = level of primary distress type corresponding to CS i;

$D_2(i)$ = level of secondary distress type corresponding to CS i;

$RMC_k(R(i), D_1(i), D_2(i)$ = routine maintenance cost during the year following the action a_k for a distress state specified by $R(i), D_1(i)$ and $D_2(i)$; and

$CS_k(R(i), D_1(i), D_2(i))$ = construction cost of action a_k on a pavement with the distress state specified by $R(i), D_1(i)$, and $D_2(i)$.

Table 2-3 List of Maintenance and Rehabilitation Actions *(Kulkarni et al., 1983)*

Feasible Action	Pavement Type			
	FDBIT	**PDBIT**	**Composite**	**PCC**
Do Nothing	X	X	X	X
Routine Maintenance	X	X	X	X
Seals	X	X	X	
Overlays	X	X	X	X
Surface Recycle with Overlay	X	X	X	
Cold Milling	X		X	
Cold Mill with Hot Recycle	X	X	X	
Stress-Absorbing Membrane	X	X	X	
Type F Crack Repair	X			
Type P Crack Repair		X		
Cold Recyle with Overlay		X		
Joint Repair with PCC			X	X
Joint Repair with AC			X	X
PCC Pavement Patching				X
PCC Concrete Overlay				X
PCC Patching with Overlay				X
Grinding PCC				X

2.3.2.6 Optimal Rehabilitation Policies

An integrated set of computer programs, which accepts inputs and determines the optimal rehabilitation policies, is used in a NOS. The main steps are as follows:

1. An optimal steady state policy is determined for selected long-term performance standards for the given road category;
2. An optimal transition policy is determined in which optimal steady state distribution of road segments in different condition states is achieved; and

3. The optimal transition policy determined in Step (2) provides a recommended action for road segments in each condition state.

2.3.3 Project Optimization System (POS)

The objective of a POS is to determine the optimal assignment of one out of several feasible actions to each project scheduled for rehabilitation during the planning year. The assignment should maximize total benefits over the portfolio of rehabilitation projects, subject to meeting constraints on the total available rehabilitation budget for the planning year and subject to matching the NOS performance requirements for each project. An integer program is used for this purpose.

The POS is specifically oriented toward engineering and technical needs of pavement management. The POS develops the potential for better performance for the total target cost of all the projects. This is accomplished by using site-specific cost and engineering data, and actions not available to the NOS because of its broad network prospective. Components of a POS include a set of prediction models to estimate the probabilities of reaching different distress levels as a function of age, traffic, overlay thickness, and environmental factors; and an integer programming algorithm which determines the optimal assignment of one out of several feasible actions to each project scheduled for rehabilitation during the planning year *(Kulkarni et al., 1988).*

2.3.4 Pavement Management Information System (PMIS)

PMIS is a user-friendly operation to sort, query, and process data. It provides necessary information for the NOS and POS models. Relational database management (RDBM) software running in an OS/2 operating environment is used. The system is designed for the computer platform, Intergraph Interserve 3005.

2.4 Remaining Service Life (RSL)

The remaining service life (RSL) is the anticipated number of years that a pavement is in acceptable condition to accumulate enough functional or structural distress under normal conditions, given that no further maintenance is performed or distress points equal to an as-defined threshold value *(Baladi, 1991).* RSL is calculated from the condition of the asset during that year and the projected number of years until rehabilitation is required. Once RSL is

estimated for each pavement section in the network, the sections are grouped into different categories *(Dicdican et al., 2004)*. It combines the severity and extent of different distresses and the rate of deterioration. It requires development of a performance model and establishment of a threshold value for each distress type. Based on these threshold values, the current distress level and deterioration model for each particular distress, and time for each distress to reach the threshold value, can be computed. The shortest of these time periods is the RSL of the pavement section *(Baladi, 1991)*. The definition of the threshold values depends on the criteria used to control long-term network conditions *(Kuo et al., 1992)*. Existing methods rely on various concepts from purely empirical to truly mechanistic. Lack of adequate performance prediction models has been the major impediment in predicting remaining life *(Vepa et al., 1996)*.

RSL is used for future planning and budgeting purposes. This is not only useful for timing a major rehabilitation but also assists managers in forecasting long-term needs of the network. The evaluation of RSL is necessary to make optimal use of the structural capacity of in-service pavements. Knowledge of RSL facilitates decision making in regard to strategies for reconstruction-rehabilitation of roads, thereby leading to efficient use of existing resources *(Vepa et al., 1996)*. Accurate RSL models improve the process of allocating funds and resources for maintenance and rehabilitation of asphalt pavements *(Romanoschi and Metcalf, 2000)*.

To calculate RSL for a pavement section, the agency needs its current condition, a definition of unserviceable condition, and a mechanism to predict deterioration of the pavement condition. Figure 2-4 shows the information required to calculate RSL.

2.4.1 RSL Estimation Procedures

Failure of a pavement can be categorized as structural or functional failure. In the functional failure-based approach, RSL is computed on the basis of performance of the pavement. On the other hand, reduction of structural capacity is the primary concern in the structural failure-based approach. RSL estimates based on functional failure are greater than those based on structural failure (*Witczak, 1978)*.

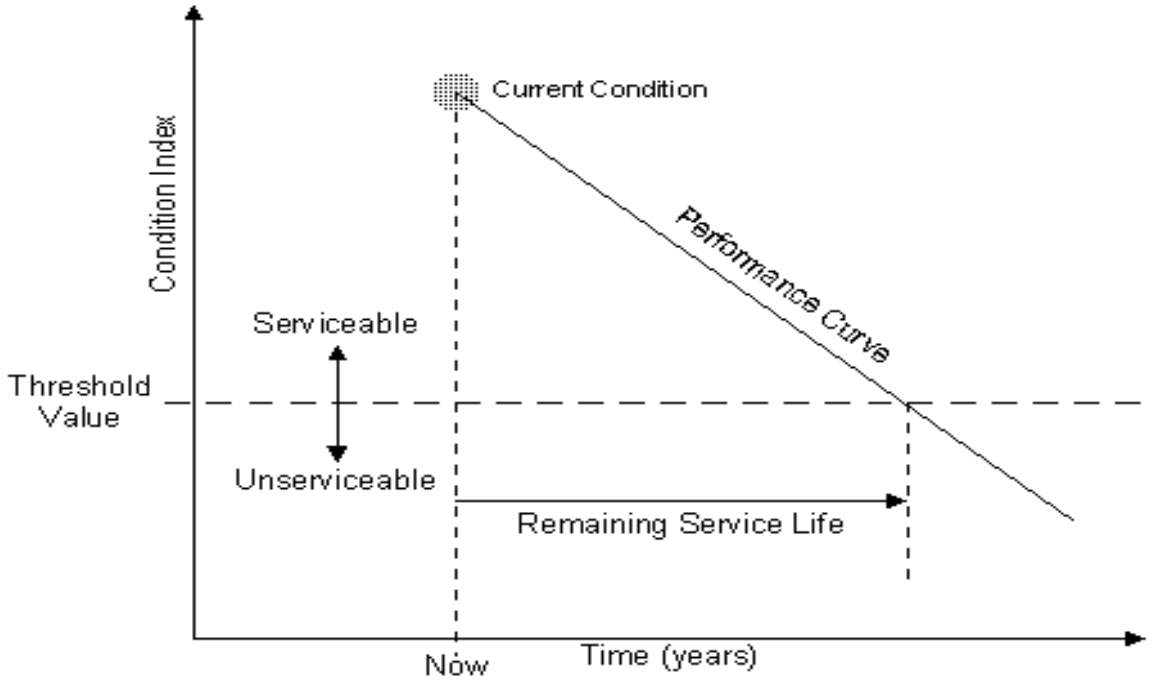

Figure 2-4 Calculating RSL for an Individual Condition Index *(FHWA, 1998)*

2.4.1.1 Functional Failure-Based Approaches

In this approach, decrease in the performance index with age or traffic is charted in conjunction with a functional failure criterion. *AASHTO (1986)* describes three approaches for estimating RSL. Traffic approach is used if reasonably accurate historical traffic data is available. RSL can be determined from Equation (2.2):

$$RSL_x = \frac{N_f - X}{N_f} \times 100 \tag{2.2}$$

where

RSL_x = remaining service life of pavement (percent);

N_f = total number of traffic applications to failure; and

X = cumulative number of 18-kip ESALs.

Time approach is used if specific traffic information is not available. RSL can be determined using Equation (2.3). Serviceability approach is used if the present serviceability

index of a pavement is known along with the initial structural number. RSL can be estimated by a graphical procedure.

$$RSL_x = \frac{T_f - t}{T_f} = \frac{(1+r)^{T_f} - (1+r)^t}{(1+r)^{T_f} - 1} \tag{2.3}$$

where

RSL_x = remaining service life of pavement (percent);

t = time existing pavement has been in service;

T_f = best estimate of the probable time that the pavement can last before any overlay is required; and

r = annual traffic growth rate.

Ullidtz (1993) calculated RSL using an empirical expression developed in terms of the present serviceability rating (PSR) affected by traffic (to terminal PSR of 2.0) and non-load-associated degradation. An annual PSR decrease of 0.1 was assumed for non-load-associated degradation.

$$RSL = \frac{PSR-2}{2 \times min\ [\{AASHTO\ Cumulative\ Design\ W18/Yearly\ W18\},\ 20]} \tag{2.4}$$

where

RSL = remaining service life of the pavement (years); and

$W18$ = number of 18-kip ESALs.

When historical pavement performance data are available, this information can be used to compile survivor curves, which can then be used to estimate RSL. Survival of a pavement is determined by the amount of time it lasts before major maintenance or rehabilitation must be performed. Attempts have been made to estimate average RSL of a particular type of pavement by computing total area under the survivor curves *(Winfrey and Ferrel, 1940; Ferrel and Paterick, 1948; Winfrey and Howell, 1968; Millard et al., 1971; Garcia-Diaz et al., 1983). Vepa et al. (1996)* have used performance histories of flexible pavements from the Mississipi DOT

PMS database, following the work of *Garcia- Diaz et al. (1983)*. Survivor functions developed assumed the following form:

$$\nu = 1 - \exp\left(\frac{-q}{W^r}\right) \tag{2.5}$$

where

ν = percentage of surviving pavement length (mi);

q = location parameter (i.e., parameter affecting location of the survivor curve);

r = shape parameter (i.e., parameter affecting shape of the curve); and

W = cumulative ESALs from date of construction.

Traffic was used as a surrogate for pavement life to estimate RSL as shown in Figure 2-5. The percentage of RSL was calculated for pavements that sustained traffic volume (*W),* estimated in terms of 18-kip ESAL.

$$RSL_x = \left(\frac{A_1}{A_0}\right) \times 100 \tag{2.6}$$

where

RSL_x = remaining service life of pavement (percent);

A_0 = total area under the curve or mean value of service life of pavement; and

A_1 = remaining area under the curve after traffic W passes.

By using a percentage of remaining service life (RSL_x) from Equation (2.6), RSL in years can be calculated using Equation (2.7).

$$RSL = \frac{RSL_x}{100 - RSL_x} \times \text{Age of pavement} \tag{2.7}$$

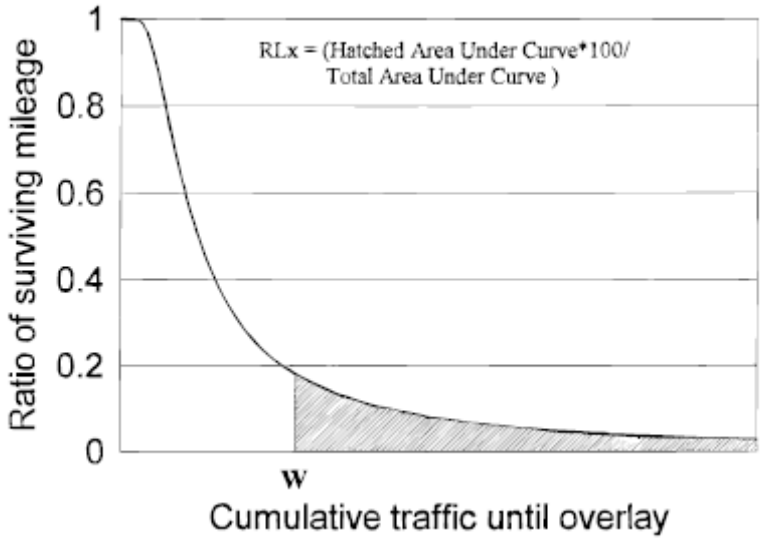

Figure 2-5 RSL Using Survivor Curve *(Vepa et al., 1996)*

2.4.1.2 Structural Failure-Based Approaches

These approaches make use of fatigue principles that require effective thickness or modulus derived from in situ measurements. Many researchers have used back-calculated layer moduli in an appropriate equation to estimate RSL *(Fernando et al., 1984; Richter and Irwin, 1988; Kilareski, 1989).* RSL can be calculated by a unique curve (Figure 2-6) relating the condition factor (CF) and the RSL *(AASHTO, 1986; AASHTO, 1993).* The condition factor (CF) is defined as the ratio of the effective structural number to the original structural number for flexible pavements. AASHTO suggested two different approaches for estimating CF. The first is to evaluate pavements in service using FWD sensor deflections. The second is to estimate overall CF based on its visual condition by modifying the layer coefficient of each layer commensurate with surface damage.

Marchionna et al. (1987) used mechanistic principles to develop a graphical procedure relating the percentage of RSL. Equivalent-layer thickness and critical strains in the pavement layers have been used by *Horak (1988)* to compute RSL through a series of graphical procedures. *George (1989)* developed a graphical procedure to determine RSL based on the effective thickness ratio (ETR) derived from nondestructive test (NDT) deflections. On the basis of experimental data from the field sections, *Croney (1990)* developed deflection and life contours to estimate RSL. *Mamlouk et al. (1990)* computed RSL based on a fatigue model

(considering the rate of crack development in Arizona) and in conjunction with the back-calculated moduli.

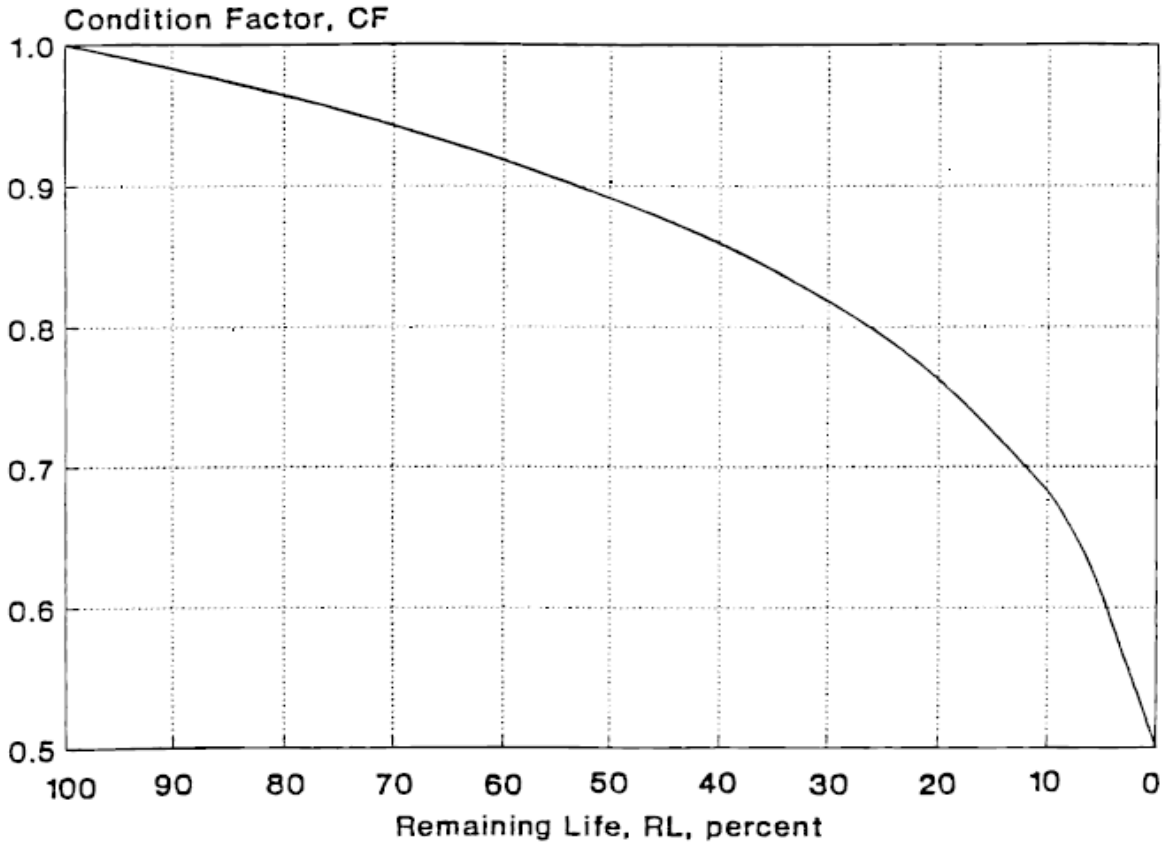

Figure 2-6 Relationship between Condition Factor and RSL *(AASHTO, 1993)*

Park and Kim (2003) developed RSL prediction methods for flexible pavements using FWD multiload-level deflections and based on pavement response and performance models. The pavement response models were designed to predict critical pavement responses from surface deflections and deflection basin parameters. Theoretical pavement responses were computed using the ABAQUS finite-element program for dynamic analysis based on three load levels. The pavement performance models were used to develop the relationships between critical pavement responses obtained from pavement response models and actual pavement performance.

Werkmeister and Alabaster (2007) have used accelerated pavement test results from the Canterbury Accelerated Pavement Testing Indoor Facility in New Zealand to develop a new pavement performance criterion that predicts rutting of a low-volume road. The RSL prediction procedure has been based on center deflections from FWD measurements and used the change in

FWD test results between the start and end of the post-compaction period. They have developed Equation (2.8) to predict RSL in terms of ESAL.

$$N \geq 5{,}000{,}000e^{(-0.0206 \times \Delta d_0)} \tag{2.8}$$

where

N = average RSL (ESALs)-load cycles to failure (15-mm rut depth); and

Δd_0 = percentage of change in central deflections during post-compaction period.

2.4.1.3 Functional and Structural Failure-Based Approaches

Allison (1983) developed a procedure to estimate RSL for the Texas flexible pavement network based on predicted ride and distress conditions. These conditions were forecasted using equations that involved measurable values of material properties, climatic conditions, and design factors. *George (1989)* has developed equations that can be used to forecast the pavement condition rating (PCR) of five types of pavements using the Mississippi DOT PMS database. With projected PCR and a trigger value of 65, RSL of pavement segments can be calculated. *Santha et al (1990)* developed a simple, mechanistic rut-depth prediction model that, when used with estimated current traffic, yields the RSL. *Scullion and Chester (1995)* calculated the remaining service life based on the fatigue life from the deflection data, as well as existing cracking and rutting information. *Zaghloul and Elfino (2000)* have used back-calculated layer moduli and expected traffic volumes to estimate the RSL of homogeneous sections.

2.5 Pavement Performance Prediction

Three generally accepted measures of pavement performance are safety, structural, and functional. Safety is most commonly measured in terms of frictional characteristics of a pavement. Structural performance is a measure of the pavement's ability to resist deformation under traffic loads. It is most commonly measured in terms of various distresses such as cracking or rutting. Functional performance is a measure of the pavement's ability to serve the user over time. It is usually measured in terms of roughness or ride quality of the pavement surface *(Hand et al., 1999).*

Modeling pavement deterioration in terms of surface distress is a critical engineering process in PMS. Pavement performance models vary depending on the type of performance that

is being modeled. Performance models could be developed for each individual distress mechanism or for the condition index, depending on the decision process within the agency. A number of different modeling techniques can also be used, depending on use of models within the agency *(FHWA, 1998)*.

A pavement performance prediction model is a mathematical description of the expected values that a pavement attribute will take during a specified analysis period. An attribute is a property of a pavement section or class of pavements that provides a significant measure of the behavior, performance, adequacy, cost, or value of the pavement *(Hudson et al., 1979)*. Pavement deterioration models express the future state of a pavement as a function of explanatory variables or causal factors. A partial list of causal factors includes pavement structure, age, traffic loads, environmental variables, etc. Time

Figure 2-7 shows a typical pavement deterioration curve.

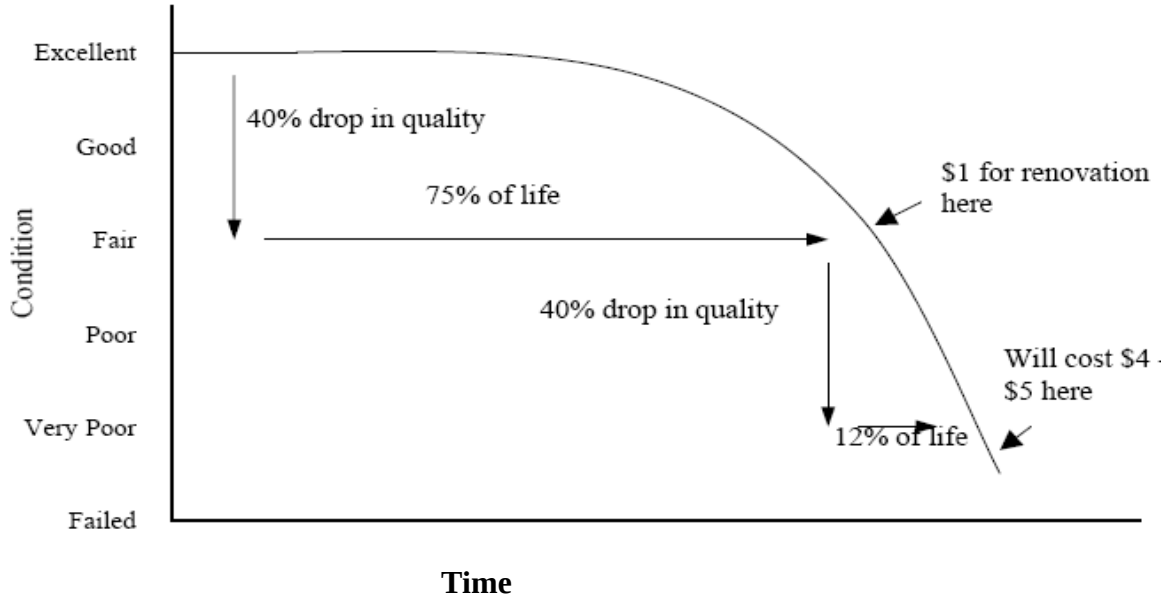

Figure 2-7 Pavement Deterioration Curve *(FHWA, 1985)*

The normal method of depicting pavement performance is by a pavement performance curve. Functional conditions usually employed are the RSL of the pavement. It is also one of the most challenging steps because of various factors that have to be taken into consideration and the difficulty involved in pinpointing the factor that causes deterioration in the pavement. Condition prediction models are used at both network and project levels to analyze the condition and determine maintenance and rehabilitation requirements.

At the network level, pavement performance prediction is important for adequate activity planning, project prioritization, and budget allocation *(Chen et al., 1993)*. Pavement performance models are an important component of a network-level, multi-year analysis for the following types of activities *(FHWA, 1998)*:

- Estimating type and timing of maintenance and/or rehabilitation as part of a multi-year improving program;
- Predicting length of time until a lower limit of acceptable pavement condition is reached;
- Optimizing the combination of projects, treatments, and timing to achieve agency goals;
- Evaluating long-term impacts of various program scenarios;
- Providing a feedback loop to the pavement design process;
- Estimating pavement life-cycle costs; and
- Summarizing impacts of different maintenance and rehabilitation strategies in terms of overall network conditions.

At the project level, prediction models are used to design pavements, perform life-cycle cost analyses, select optimal designs with the least total cost, and in trade-off analyses in which annualized costs of new construction, maintenance, rehabilitation, and user costs are considered for a specific pavement design. Better prediction models make a better PMS, which leads to considerable cost savings *(Way, 1985; Paterson, 1987; Markov, 1990; Mohseni et al., 1990; FHWA, 1998)*.

2.5.1 Classification of Performance Prediction Models

Prediction models are classified into various categories depending on predicted variables, method of development, and whether individual or composite attributes are predicted. A commonly used classification recognizes two types: deterministic and probabilistic. A deterministic model predicts a single value of the dependent variable *(Lytton, 1987)*. The probabilistic models, on the other hand, predict a distribution of the attribute. Another classification groups the prediction models into four categories: (1) mechanistic models, (2) empirical models, (3) mechanistic-empirical models, and (4) subjective models. Depending on whether a single measure or a compound measure is predicted, other classifications in use are disaggregate and aggregate models. Aggregate models predict composite measures such as

damage index, condition rating, or serviceability that determine overall health of the network. Disaggregate models predict the evolution of an individual measure or distress. Table 2-4 shows the classification of prediction models.

Table 2-4 Classification of Prediction Models *(Haas et al., 1994)*

	Types of Models						
	Deterministic				**Probabilistic**		
Levels of Pavement Management	**Primary Response**	**Struc-tural**	**Func-tional**	**Dam-age**	**Survivor Curves**	**Transition Process Models**	
	Deflection	Distress	PSI	Load Equi.		Markov	Semi-Markov
	Stress	Pavement	Safety				
	Strain	Condition					
National Network				X	X	X	X
State Network		X	X	X	X	X	X
District Network		X	X	X	X	X	X
Project	X	X	X	X			

Regression is one of the most powerful and widely used analysis techniques available for constructing performance models. This approach is primarily used in agencies with a historical database available. To judge how well an equation fits the actual data, a number of parameters can be used. These include the coefficient of determination (R^2) that explains how much of the total variation in the data is explained by the regression equation and the root mean square error (RMSE), which is the standard deviation of the predicted values for a specific value of independent variable. Hypothesis tests on regression constants, which are generally based on the t-statistic, are also used *(FHWA, 1998)*.

Washington State DOT (WSDOT) uses a pavement management program referred to as the Washington State Pavement Management System (WSPMS). The WSDOT developed performance models to achieve a predictive capability based on a combined rating. The combined rating provided the department with the ability to rank projects and provide a pavement management condition rating versus age relationship so that time to failure might be

predicted. The general form of the performance equation used by WSPMS to relate pavement condition to age is shown in Equation (2.9) *(FHWA, 1998)*:

$$PCR = C - mA^p \tag{2.9}$$

where

PCR = pavement condition rating;

A = age;

C = model constant for a maximum rating (approximately 100);

m = slope coefficient; and

p = selected constant that controls the degree of curvature of the performance curve.

The S-shaped curve-fitting technique is useful when predicting change in the dependent variable as a function of one independent variable. *Smith (1986)* used an S-shaped model for relating PCI to pavement age. The model had the following form:

$$PCI = 100 - \frac{\rho}{(\ln(\alpha) - \ln(AGE))} \times \left(\frac{1}{\beta}\right) \tag{2.10}$$

where

$\rho, \alpha,$ and β = constants.

The α constant controls the age at which the PCI is projected to reach zero. The β constant controls how sharp the curve bends. The ρ constant controls the location of the inflection point in the curve. These three constants are determined using regressions analysis.

2.6 Model Development

Darter (1980) outlined four basic criteria that should be followed to develop reliable performance models at any level within the transportation agency: an adequate database, inclusion of all significant variables that affect performance, adequate functional form of the model, and satisfaction of statistical criteria concerning precision of the model. There are other factors that must be accounted for in development of pavement performance models *(Lytton, 1987)*. These include an understanding of the principles underlying each type of model, selection of the appropriate model form, role of statistics and mechanics in developing an appropriate

model, identification of the data needed for a specific model, modification of the models to represent the effects of maintenance, and limitations and uses of different types of models.

Data requirements for performance models vary depending on the type of model being developed. Inventory and monitoring information are the most basic levels used to develop the models. Inventory data include any network information that does not change with time or traffic. Monitoring data are influenced by time and traffic and are most commonly used as dependent variables in developing performance models. Types of data used for each of the predominant modeling approaches are as shown in Table 2-5 *(Lytton, 1987).*

Table 2-5 Data Used to Develop Different Types of Performance Models *(Lytton, 1987)*

Data Requirements	Deterministic	Probabilistic (Markovian)
(a) Inventory Data		
Pavement Structure	Required	Required
Joint Features	Useful	Useful
Drainage Characteristics	Useful	Useful
Age	Required	Required
Prior Condition/Traffic	Required	Required
Environmental/Climatic	Useful	Useful
Material Properties	Useful	Useful
(b) Monitoring Data		
Distress Data	Required	Required
Traffic	Required	Required
Deflection	Useful	Useful
Profile	Useful	Useful
Maintenance History	Useful	Not required
Condition Index	Required	Required

2.6.1 Nonlinear Regression Procedure in Statistical Analysis Software (SAS)

The NLIN procedure in SAS implements iterative methods that attempt to find least-squares estimates for nonlinear models. The NLIN procedure first examines starting- value specifications of the parameters. Parameter names, starting values, and expressions for the model

must be specified. If a grid of values is specified, PROC NLIN evaluates the residual sum of squares at each combination of parameter values to determine the set of parameter values producing the lowest residual sum of squares (SSE). These parameter values are used for the initial step of the iteration. PROC NLIN does not necessarily produce a good solution the first time. Much depends on specifying good initial values for the parameters. PROC NLIN uses one of these four iterative methods: Gauss-Newton method (default), Newton method, Marquardt method, or Gradient method. These methods use derivatives or approximations to derivatives of the SSE, with respect to the parameters, to guide the search for the parameters producing the smallest SSE. The Gauss, Newton, and Marquardt methods are more robust than the Gradient method.

2.6.1.1 Computational Methods

For the system of equations represented by the nonlinear model in Equation (2.11), there are two approaches to solving for the minimum.

$$Y = F(\beta_0, \beta_1, ..., \beta_\tau, Z_1, Z_2, ..., Z_n) + \varepsilon = F(\beta^*) + \varepsilon \tag{2.11}$$

where

Z = a matrix of the independent variables;

β = a vector of the parameters;

ε = the error vector; and

F =a function of the independent variables and parameters.

The first method is to minimize Equation (2.12).

$$L(\beta) = 0.5(e'e) \tag{2.12}$$

where

$e = Y - F(\beta)$ and β is an estimate of β^*.

The second method is to solve the nonlinear "normal" equations:

$$X'F(\beta) = X'Y \tag{2.13}$$

where

$$X = \frac{\partial F}{\partial \beta}.$$

In the nonlinear situation, both X and $F(\beta)$ are functions of β, and a closed-form solution generally does not exist. Thus, PROC NLIN uses an iterative process: a starting value for β is chosen and continually improved until the error sum of squares $\varepsilon'\varepsilon$ is minimized.

The iterative techniques that PROC NLIN uses are similar to a series of linear regressions involving the matrix X evaluated for the current values of β and $e = Y - F(\beta)$, the residuals evaluated for the current values of β. The iterative process begins at some point β_0. Then X and Y are used to compute Δ such that $SSE(\beta_0 + k\Delta) < SSE(\beta_0)$. The four methods differ in how Δ is computed to change the vector of parameters.

2.6.1.1.1 Gauss-Newton

The Gauss-Newton method uses the Taylor series. The Gauss-Newton iterative method regresses the residuals onto the partial derivatives of the model with respect to the parameters until the estimates converge.

$$F(\beta) = F(\beta_0) + X(\beta - \beta_0) + \ldots$$

where

$X = \partial F / \partial \beta$ is evaluated at $\beta = \beta_0$.

Substituting the first two terms of this series into the normal equations

$$X'F(\beta) = X'Y$$

$$X'(F(\beta_0) + X(\beta - \beta_0)) = X'Y$$

$$(X'X)(\beta - \beta_0) = X'Y - X'F(\beta_{0)}$$

$$(X'X)\Delta = X'e$$

$$\Delta = (X'X)^{-}X'e \qquad (2.14)$$

2.6.1.1.2 Newton

The Newton method uses the second derivatives and solves the equation. The Newton iterative method regresses the residuals onto a function of the first and second derivatives of the

model with respect to the parameters until the estimates converge. Analytical first- and second-order derivatives are automatically computed.

$$\Delta = (G^{-})X'e \tag{2.15}$$

where

$$G = (X'X) + \sum_{i=1}^{n} H_i(\beta)e_i$$

$H_i(\beta)$ = the Hessian of e

2.6.1.1.3 Marquardt

The Marquardt iterative method regresses the residuals onto the partial derivatives of the model with respect to the parameters until the estimates converge. It is a compromise between the Gauss-Newton and Gradient. It is equivalent to performing a series of ridge regressions and is useful when the parameter estimates are highly correlated or the objective function is not well approximated by a quadratic.

$$\Delta = (X'X + \lambda diag(X'X))^{-}X'e \tag{2.16}$$

2.6.1.1.4 Gradient

The Gradient (steepest descent) method is based on the gradient of $\varepsilon'\varepsilon$. The quantity $-X'e$ is the gradient along which $\varepsilon'\varepsilon$ increases. Thus, Equation (2.17) is the direction of steepest descent.

$$\Delta = X'e \tag{2.17}$$

2.7 Pavement Deflection Devices

Structural conditions of pavements can be determined using destructive and nondestructive means. Since most nondestructive testing (NDT) means have very low operational cost, short-test duration, no disturbance effects, automated data collection, full-scale model tests, and geometric and stress conditions similar to those of real traffic loads, they are most widely used *(Elton and Harr, 1988; Parvini, 1997)*.

Two main techniques of NDT are seismic techniques (time measurements) and surface loading (surface deflection measurements). The main drawback of the seismic technique is the difference between the test and real pavement loading conditions *(Lytton, 1989)*, although it is a sophisticated method of pavement evaluation. Some of the drawbacks are the time required to run the test and complexities in data analysis; provides horizontal properties of the pavement components instead of vertical properties; ignores the anistropic nature of the materials; and applies to only low-strain levels. Deflection-based techniques are being widely used in structural evaluation of pavements due to their speed, ease of operation (simplicity), and ability to model real traffic load intensities and durations (*Hoffman and Thompson, 1982; Sebaaly and Mamlouk, 1986).*

Deflections of pavements can be induced and measured non-destructively using various commercially available devices. These devices are designed based on a variety of loading modes and measuring sensors. Pavement deflections are highly dependent on loading mode *(Hoffman and Thompson, 1982).* The loading modes can be static, steady state vibratory, and impulse loading, while the resulting responses are measured with sensors that include geophones, accelerometers, and linear-variable differential transformers (LVDT) *(Choubane et al., 2006).* Recently, automated mobile dynamic-load method devices have emerged as the fourth loading mode.

2.7.1 Static or Slow-Moving Devices

Devices that measure the deflection response of a pavement to slowly applied loads are generally classified as static deflection equipment *(Smith and Lytton, 1985).* Some of the devices in this category are summarized in Table 2-6.

2.7.2 Steady State Devices

These devices place a static load on a plate on the pavement surface. A steady state sinusoidal vibration is then induced in the pavement with a dynamic-force generator. These devices are stationary when measurements are taken, with the force generator started and deflection sensors lowered to the pavement surface. The most commonly used steady state dynamic deflection devices are summarized in Table 2-7 *(FHWA, 1989).*

Table 2-6 Summary of Static or Slow-Moving Devices

Name of Device	Loading Range (lb)	Principle of Operation	Speed (kph)	Load Actuator System	Deflection measuring device	Number of sensors
Benkelman Beam	18,000	Deflection Beam	0.00	Loaded Truck Axle	Dial Indicator	1
La Croix Deflectograph	12,000-26,000	Mechanized Deflection Beam	2-5	Moving Weighted Truck	Inductive Displacement Transducers	2
California Travelling Deflectometer	18,000	Mechanized Deflection Beam	2-5	Moving weighted truck	Dial Indicator	1
South African Curvature Meter		Beam Type				
Road Surface Deflectometer		Mechanized Deflection Beam			LVDT	
French Flexigraph					Laser-Photocell Combination	

Table 2-7 Summary of Steady State Vibratory Devices

Deflection Device	Load Actuator System	Peak-to-Peak Load (lb)	Type of Load Transmission	Fre-quency (Hz)	Deflection Measuring Device	Number of Sensors
Dynaflect	Counter-Rotating Masses	1000	Two 16'' Diameter Steel Wheels	8	Velocity Transducers	5
Road Rater Model 400B	Hydraulic-Actuated Masses	500-3000	Two 4x7 Steel Pads	25	Velocity Transducers	4
Road Rater Model 2000	Hydraulic-Actuated Masses	1000-5,500	18'' Diameter Circular Plate	6-60	Velocity Transducers	4
Road Rater Model 2008	Hydraulic-Actuated Masses	1000-8,000	18'' Diameter Circular Plate	6-60	Velocity Transducers	4
WES 16kip Vibrator	Hydraulic-Actuated Masses	30,000	18'' Diameter Circular Plate	5-100	Velocity Transducers	3

2.7.3 Impact (Impulse)-Load Response Devices

All impact-load devices deliver a transient impulse load, recorded by a load cell, to the pavement surface through a buffered circular load plate that helps distribute the load uniformly over the loading area. These classes of devices are currently the most common structural evaluation tool *(Roesset and Shao, 1985; Abdallah et al., 2001).* A single analog integration of a signal generates the deflection-time trace. The deflection measurements are recorded by the data acquisition sensors commonly known as geophones (velocity transducers) or seismic deflection transducers *(Choubane et al., 2006).* These sensors are located radially in the tow vehicle. A falling-wheel deflectometer (FWD) is a typical impulse-load response device. Table 2-8 shows a summary of devices in this class.

2.7.3.1 Falling-Wheel Deflectometer (FWD)

FWD testing has been established worldwide as one of the most effective tools for measuring deflections for pavement evaluation purposes. The FWD is a trailer-mounted device which applies a load to the pavement surface through a circular plate with a diameter of 11.8-in. A mass is dropped onto the plate with a rubber pad generating an impulse load on the pavement, which is similar to the stress pulse generated by moving trucks. The magnitude of the FWD force on the pavement can be varied by altering either the mass of the drop weight or the drop height. Varying the drop mass and/or height of the FWD provides a direct opportunity to evaluate the stress sensitivity of the materials in the pavement structure. Peak force and maximum deflections at various points along the surface are measured by load cells and velocity transducers, commonly known as geophones. A single analog integration of a signal generates the deflection-time trace. Deflection measurements are recorded by the data acquisition system typically located in the tow vehicle.

Table 2-8 Summary of Impulse-Load Response Devices

Deflection Device	Load-Actuator System	Loading Range (lb)	Type of Load Transmission	Duration (msec)	Deflection Measuring Mevice	Number of Sensors
Dynatest FWD 8002	Dropping Mass	1,500-27,000	Circular Plate 11.8'' Diameter	25-30	Velocity Transducers	7
KUAB FWD	Two dropping Masses	2,700-33,700	Segmented Circular Plate 18'' Diameter	28	Seismic Deflection Transducers	5
Phonix FWD	Dropping Mass	2,300-23,000	Circular Plate 11.8'' Diameter		Velocity Transducers	3
WES FWD	Dropping Mass	15,000	Circular Plate 11.8'' Diameter		Velocity Transducers	2
Shell FWD			Circular Plate 11.8'' Diameter		Velocity Transducers	4

2.7.4 Automated Mobile Dynamic-Load-Method Devices

Recently, efforts have been made around the world to produce a high-speed monitoring device for measuring pavement-bearing capacity. The major reason for the need for such a device is the increasing amount of traffic on major roads. Stationary tests are difficult in such cases for safety reasons, and they also provide information at discrete points that could often be separated several hundred meters apart. It is expected this type of equipment will play a major role in monitoring network-level structural condition in the near future. Table 2-9 shows a summary of automated mobile dynamic-load-method devices. A rolling-wheel Deflectometer (RWD) is typical of this class. It has been discussed in detail.

2.7.4.1 Rolling-Wheel Deflectometer (RWD)

An RWD is an innovative device for the efficient, fast determination of pavement structural response. The current prototype was developed jointly by the Federal Highway Administration (FHWA) Office of Asset Management and Applied Research Associates, ARA *(ARA, 2007)*. An RWD consists of a set of four triangulation lasers attached to an aluminum beam mounted beneath a custom-designed 53-ft trailer. The trailer is sufficiently long to isolate the deflection basin produced by the RWD trailer's 18-kip, dual-tire, single-axle from deflections produced by the RWD tractor. Figure 2-8 shows an overview of the RWD truck, trailer, and laser-mounting beam. In addition, the natural frequency of the trailer's suspension of 1.45 to 1.8-Hz is low enough that it does not couple with the high-frequency vibration of the 25.5-ft aluminum beam used to support the lasers. The beam uses a curved extension to pass under and between the dual tires, placing the rearmost laser approximately six inches behind the axle centerline and seven inches above the roadway surface, as shown in Figure 2-8. The wheels have been spaced a safe distance from the laser and beam using custom lugs and a spacer.

Table 2-9 Summary of Automated Mobile-Dynamic Devices

Name of Device	Manufacturer	Loading Range (lb)	Speed Range (mph)	Deflection Measuring
Rolling Dynamic Deflectometer	University of Texas, Austin	1000 static and 5000 dynamic	1	Geophones
Highway Rolling-Weight Deflectometer	Dynatest Consulting and Quest Integrated	9000	20	
Rolling-Wheel Deflectometer	Applied Research Associates	18,000-24,000	45-65	Lasers
Rolling Deflection Tester	Swedish National Road Administration and VTI	8,000-14,000	60	
High-Speed Defletograph	Greenwood Engineering, Denmark	11,000	50	Laser Doppler Sensors

Figure 2-8 Overview of RWD and Laser D between Dual-Tires *(ARA, 2007)*

The RWD truck is 8.5-ft wide, 12-ft high, and 75-ft long. Center-to-center distance for the single-axle dual tire is 17 inches wide to accommodate laser D, as shown in Figure 2-9(a). The RWD truck has an 8,900-lb single-axle, single-tire steering axle; a 19,200-lb dual-tire tandem axle at the back of the tractor; and an 18,000-lb dual-tire single axle in the rear of the trailer as can be seen from Figure 2-9(b). Total truck weight is 46,100 lbs.

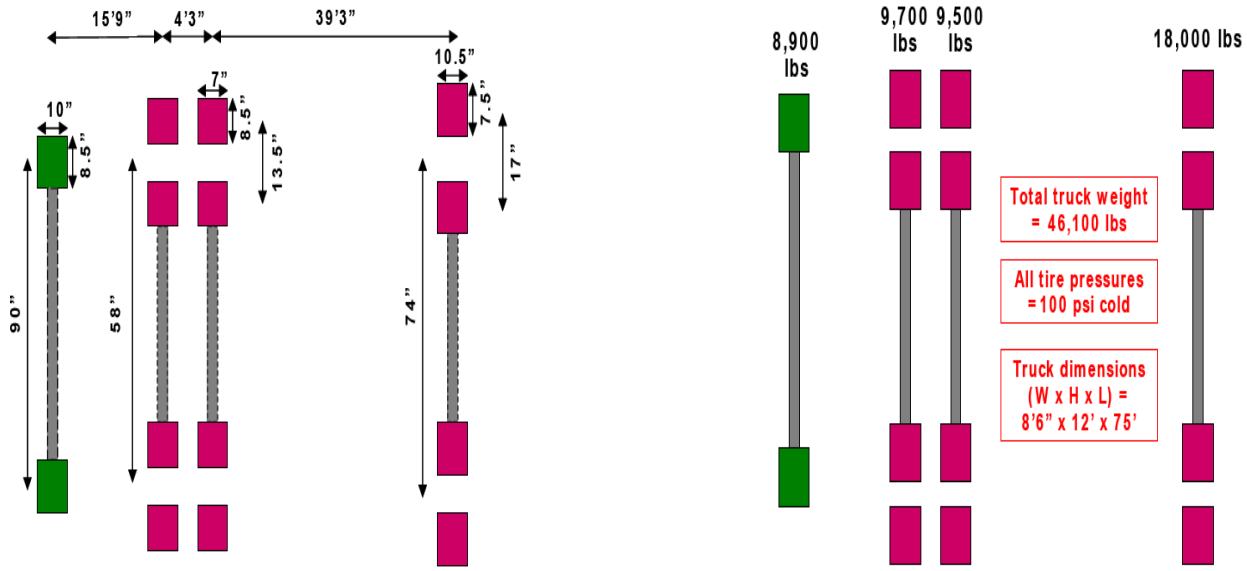

(a) Wheel Configurations (b) Wheel Loads

Figure 2-9 RWD Wheel Configurations and Loads *(ARA, 2007)*

2.7.4.1.1 Deflection Measurement Principle

The RWD uses a "spatially coincident" methodology for measuring pavement deflection. Three lasers placed forward of the loaded axle are used to define the unloaded pavement surface profile, and a fourth laser (D) placed between the dual tires measures the deflected pavement surface. Deflection is calculated by comparing the undeflected pavement surface with the deflected pavement profile at the same location. This method was originally developed by the Transportation and Road Research Laboratory (TRRL) and further developed by Dr. Milton Harr at Purdue University (*Harr and Ng-A-Qui, 1977*). Figure 2-10 shows an illustration of the concept.

The spatially coincident method utilizes three lead sensors, A, B, and C, to define the undeflected pavement profile at time, t=0. When the RWD advances eight ft, sensors B, C, and D measure the profile previously defined by lasers A, B, and C. Due to dynamic truck effects, readings B2 and C2 will be different from the previous corresponding readings, A1 and B1. Assuming the beam is rigid with negligible bending, the profile defined by readings B2 and C2 is shifted in slope and magnitude to fit the previous readings at the same locations, A1 and B1. This allows for a comparison of the pavement surface at the same location between its undeflected and deflected states (i.e., D2 and C1). Deflection is then calculated using Equation (2.18) (*Steele et al., undated*):

$$Deflection = [(B_2 - 2C_2 + D_2) - (A_1 - 2B_1 + C_1)] \quad (2.18)$$

where

A_1, B_1 and C_1 = laser readings at A, B, and C at time=0; and

B_2, C_2 and D_2 = laser readings at B, C, and D after 8 ft of travel.

2.7.4.1.2 Data Acquisition System, Operating and Data Analysis Software

Laser signals are acquired by a data acquisition board installed in a desktop computer located in the RWD trailer. ARA has developed software that powers the lasers, generates output files, and stores the files on the computer harddrive. The laser readings are referenced longitudinally by monitoring the anti-lock braking system (ABS) tone counter that is part of the rear-axle braking system. The data acquisition system is also capable of handling outputs from the accelerometers mounted on the aluminum beam. The accelerometers are used for monitoring

beam movements and diagnostic purposes during prototype development. Currently, the data are post-processed within minutes of collection on the computer used for data collection.

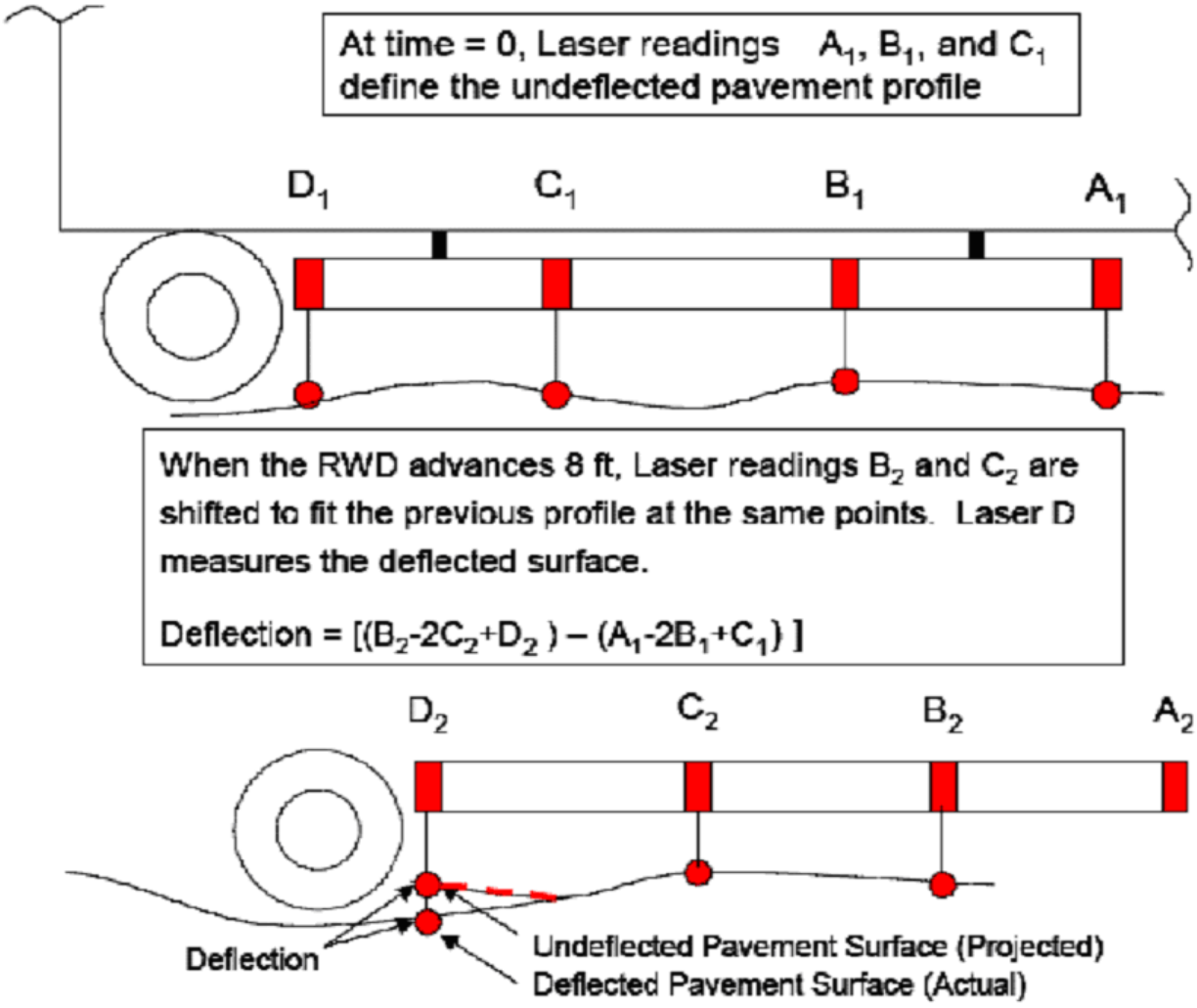

Figure 2-10 Spatially Coincident Profiles of Pavement *(Steele et al., undated)*

2.8 Correcting Deflections for Pavement Temperature

2.8.1 Pavement Temperature Prediction

Structural capacities of flexible pavements can be determined from surface-deflection measurements. The most important environmental factor affecting surface deflections of flexible pavements is the temperature of the asphaltic layers *(Kim et al., 1995; Shao et al., 1997; Park et*

al., 2002). All deflection data need to be adjusted to a constant temperature *(Chen et al., 2000)*. The temperature can be measured directly by drilling holes into the pavement, but the procedure is time consuming and multiple holes are needed to capture the temperature gradient. Temperature estimates based on correlations with externally measurable variables are preferable.

Leland et al. (1992) developed Equation (2.19) by the quasi-Newton method of numerical optimization SYSTAT, a statistical computer program, based on pavement depth, time of FWD testing, and pavement surface temperature data from the Michigan Department of Transportation (MDOT) database.

$$T_z = T_{surf} + (-0.345 - 0.0432z^2 + 0.00196z^3)\sin(-6.3252t + 5.0967) \quad (2.19)$$

where

T_z = AC pavement temperature at depth z (^{o}C);

T_{surf} = AC pavement temperature at the surface (^{o}C);

z = depth at which temperature is to be determined (cm); and

t = time when AC surface temperature was measured [days; $0<T<1$(e.g., 1:30pm=13.5/24=0.5625 days)]

Jameson (1993) has recommended Equation (2.20) to calculate asphalt-concrete layer, mid-depth temperature at testing time.

$$T_{mac} = -2.6 + 0.842 \times (T_s + T_{ma}) + 1.31 \times \log(AC_t) - 0.165 \times (T_s + T_{ma}) \times \log(AC_t) \quad (2.20)$$

where

T_{mac} = asphalt-concrete layer mid-depth temperature (^{o}F) at testing time;

AC_t = asphalt layer thickness (mm);

T_s = temperature at pavement surface; and

T_{ma} = mean air temperature of the month of deflection testing.

Solaimanian and Kennedy (1993) have developed a simple regression equation for air and pavement temperature based on analysis using the energy balance at the pavement surface and the resulting temperature equilibrium:

$$T_d = T_s(1 - 2.48\times10^{-3}d + 1.1\times10^{-5}d^2 - 2.44\times10^{-8}d^3) \quad (2.21)$$

where

T_d = pavement temperature at a given depth, d (^{o}C);

T_s = pavement surface temperature (^{o}C); and

d = depth below surface (mm).

Watson et al. (2004) have developed an equation that allows prediction of pavement temperature at any depth based on surface temperature data from the Strategic Highway Research Program (SHRP) temperature database.

$$T_d = T_{surf}(1 - 0.063d + 0.007d^2 - 0.0004d^3) \quad (2.22)$$

where

T_d = pavement temperature (^{o}F);

T_{surf} = surface temperature (^{o}F); and

d = pavement depth (in).

By using measured pavement-depth temperatures from SHRP's long term pavement performance (LTPP) database, BELLS equation was developed as a means of predicting the one-third-depth temperature (*Inge and Kim, 1995*). A third model, BELLS3, was subsequently developed for use during routine FWD testing when pavement surface is typically shaded for less than a minute. BELLS3 model has been used in this study to calculate mid-depth pavement temperature *(FHWA, 2000)*.

$$T_d = 0.95 + 0.892T_s + (\log d - 1.25)\times\left[1.83\sin\left(2\pi\frac{A}{18}\right) - 0.448T_s + 0.621T_{avg}\right] + 0.042T_s\sin\left(2\pi\frac{B}{18}\right) \quad (2.23)$$

where

T_d = pavement temperature at layer mid-depth (^oC);

T_s = infrared surface temperature (^oC);

T_{avg} = average of high and low air temperatures on the day before testing (^oC); and

d = layer mid-depth (mm) where A and B are computed as follows:

$$A = \begin{cases} t_d + 9.5 & if \quad 0 \le t_d < 5 \\ -4.5 & if \quad 5 \le t_d < 11 \\ t_d - 15.5 & if \quad 11 \le t_d < 24 \end{cases} \quad \text{and} \quad B = \begin{cases} t_d + 9.5 & if \quad 0 \le t_d < 3 \\ -4.5 & if \quad 3 \le t_d < 9 \\ t_d - 13.5 & if \quad 9 \le t_d < 24 \end{cases}$$

where

t_d = the time of day (in decimal hours).

The last two variables are used as arguments to a pair of sine functions with 18-hour periods, and 15.5- and 13.5-hour phase lags, respectively. One cycle per day is allowed. During the other six hours of the day, A and B are set equal to -4.5 so that the sine functions return a value of -1.

2.8.2 Deflection Correction

Deflection measurements in flexible pavements must be corrected to a particular type of loading system and to a predefined environmental condition. The loading system factor is dependent on the type of nondestructive testing device, frequency of loading, and load level. It is also well known that the most critical environmental factor affecting deflections in flexible pavements is the temperature of the asphalt concrete (AC) layer (*Park et al., 2002*). Because of the urgent need to develop a realistic temperature-correction procedure, many researchers have developed models for temperature-deflection correction based on a statistical analysis of data obtained from a limited range of mixture types or pavement profiles *(AASHTO, 1993; Kim et al., 1995).*

AASHTO (1993) recommends a linear relationship between the temperature and the temperature-correction factor. The relationship is presented on a nomogram form; the slopes of the lines depend on the thickness of the asphalt layer. It is important to note that the guide

recommends two different nomograms: one for pavements with granular and asphalt-treated bases and another for pavements with cement and pozzolanic-treated bases. *Kim et al. (1995)* proposed Equation (2.24) to correct the maximum surface deflection to a reference temperature.

$$D_{68} = D_T \times \left[10^{\alpha(68-T)}\right] \tag{2.24}$$

where

D_{68} = adjusted deflection to the reference temperature of 68°F (in);

D_T = deflection measured at temperature T (°F) (in.);

$\alpha = 3.67\times10^{-4}\times t^{1.4635}$ for wheelpaths, and $3.65\times10^{-4}\times t^{1.4241}$ for lane centers;

t = thickness of the AC layer (in.); and

T = AC layer mid-depth temperature (°F) at time of FWD testing.

Park and Kim (1997) have developed deflection-correction procedures based on the linear viscoelasticity theory and time-temperature superposition principle. These procedures explicitly account for the thermorheological properties of the mixture. A series of field and laboratory tests were performed and the data were used to verify the proposed procedures.

Chen et al. (2000) have developed the universal temperature-correction equation for deflection for flexible pavements in Texas using an optimization technique based on the concept of the minimum least-square difference between the target values and the predicted results.

$$W^1_{T_w} = W^1_{T_c}\left(\frac{1.0823^{-0.0098\times t}}{0.8631}\right)\times T_w^{0.8316}\times T_d^{-0.8419} \tag{2.25}$$

where

$W^1_{T_w}$ = deflection adjusted to temperature T_w (mm);

$W^1_{T_c}$ = deflection measured in the field (mm);

t = thickness of the pavement (mm);

T_d = mid-depth pavement temperature at time of FWD data collection (°C); and

T_w = temperature to which deflection is adjusted (°C).

2.9 Pavement Structural Capacity

Structural number (SN) is the most powerful concept because of its applicability and adaptability to various material types and environmental conditions (*Romanoschi and Metcalf, 1999).* SN expresses the capacity of pavements to carry loads for a given combination of soil support, estimated traffic, terminal serviceability, and environment.

Many researchers have developed different approaches to estimate the SN of an existing pavement directly from FWD deflections. *Jameson (1992)* has developed a mechanistic procedure to estimate the SN from FWD deflections:

$$SN = 13.47 - 6.47 \times \log(DEF_0) + 3.697 \times \log(V_{900}) \quad (2.26)$$

where

SN = structural number of the pavement;

DEF_0 = temperature-corrected central deflection (microns); and

V_{900} = normalized deflection at 900-mm offset (microns).

AASHTO (1993) describes a method for calculating effective SN (SNeff) of existing flexible pavements based on the condition survey data. Structural layer coefficients for the surface and base layers are assigned according to severity of distresses at the pavement surface. Equation (2.27) has been recommended by *AASHTO (1993)* to calculate SN.

$$SN = \sum m_i \times a_i \times h_i \quad (2.27)$$

where

a_i = structural coefficient of layer i;

h_i = layer thickness of layer i (in); and

m_i = drainage coefficient, applied only to granular materials.

The layer coefficients describe the contribution of each material to the performance of the pavement structure. They were derived from stress-and-strain calculations in a multilayered pavement system and correlated with performance on the basis of the AASHTO Road Test (*Til*

et al., 1972). Typical values for the structural-layer coefficients for different pavement materials have been given by *Witczak and Yoder (1975*) and *Paterson (1987)*.

AASHTO (1993) has also recommended calculating SN from the NDT deflection test results. The AASHTO algorithm suggests that at a sufficiently large distance from the load center, deflections measured at the pavement surface are due to subgrade deformation only, and are also independent of the size of the load plate. This allows the back-calculation of the subgrade-resilient modulus from a single-deflection measurement and load magnitude Equation (2.28).

$$M_R = \frac{0.24 \times P}{d_r \times r} \tag{2.28}$$

where

M_R = back-calculated subgrade-resilient modulus (psi);

P = applied load (psi); and

d_r = deflection at a distance r (in) from the center of the load (in).

To use a particular sensor deflection to estimate the subgrade-resilient modulus, the deflection must be measured far enough away from the load so that it provides a good estimate of the subgrade modulus, independent of the effects of any layer above, but also close enough so that it is not too small to be measured accurately. The AASHTO Guide further suggests that the minimum distance be determined based on the radius of the stress bulb at the subgrade-pavement interface *(AASHTO, 1993)*.

$$r = 0.7\sqrt{a^2 + \left\{ D\sqrt[3]{\frac{E_P}{M_R}} \right\}^2} \tag{2.29}$$

where

a = radius of load plate (in);

D = total thickness of pavement layers above the subgrade (in); and

E_p = effective modulus of all pavement layers above the subgrade (psi).

When the subgrade resilient modulus and total thickness of all layers above the subgrade are known, the effective modulus (E_p) of the entire pavement structure (all pavement layers above the subgrade) may be determined from the deflection measured at the center of the load plate *(AASHTO, 1993)*.

$$\frac{M_R d_0}{qa} = 1.5\left\{\frac{1}{\sqrt{1+\left(\frac{D}{a}*\sqrt[3]{\frac{E_P}{M_R}}\right)^2}}+\frac{\left[1-\frac{1}{\sqrt{1+\left(\frac{D}{a}\right)^2}}\right]}{\left(\frac{E_P}{M_R}\right)}\right\} \tag{2.30}$$

where

E_p = effective modulus of all pavement layers above the subgrade (psi);

d_0 = deflection measured at the center of the load plate (and adjusted to a standard temperature of 68^{o}F) (in);

q = NDT load plate pressure (psi);

a = NDT load plate radius (in);

D = total thickness of pavement layers above the subgrade (in); and

M_R = subgrade-resilient modulus (psi).

Equation (2.31) shows an AASHTO procedure to compute the effective structural number (SNeff).

$$SN_{eff} = 0.0045 \times D \times \left(E_P\right)^{1/3} \tag{2.31}$$

where

D = total thickness of pavement layers (in); and

E_p = effective pavement modulus of all layers above the subgrade (psi).

Rohde (1994) has used the layered-elastic theory and the back-calculation procedure, a theoretical procedure without any laboratory tests to determine layer coefficients for different materials, to develop an SN equation suitable for climatic conditions and pavements in South Africa. Using this theoretical approach, he has developed Equation (2.32).

$$SN = k_1 \times (DEF_0 - D_{1.5\times Hp})^{k_2} \times H_p^{k_3} \tag{2.32}$$

where

H_p = total pavement thickness (mm); and

k_1, k_2 and k_3 = regression coefficients.

Romanoschi and Metcalf (1999) in Louisiana have developed relationship between the SN and the FWD deflections separately for pavement structures with granular foundation layers and for pavement structures with stabilized foundation materials from a relatively small data set. Equation (2.33) has been selected based on the coefficient of determination, standard error, and conditions to satisfy sign for the coefficients for the pavement structures with cement treated layers.

$$SN = 6.45 - 3.676 \times \log(DEF_0) + 3.727 \times \log(D_{1500}) \tag{2.33}$$

where

V_{1500} = normalized deflection at a 1500 mm offset (microns).

Similarly, *Romanoschi and Metcalf (1999*) have selected Equation (2.34) for pavement structures with cement-treated layers.

$$SN = 6.96 - 0.196 \times \left[(AREA) - 450 \times \left(D_{1200}\right)\right]^{0.5} \tag{2.34}$$

where

$$AREA = 25.4 \times \left[4 \times DEF_0 + 6 \times D_{200} + 5 \times D_{300} + 3 \times D_{450}\right]$$

where

$D_{200}, D_{300}, D_{450}$ *and* D_{1200} = normalized deflection at 200-, 300-, 450- and 1200-mm offsets (microns).

Hoffman (2003) has developed YONAPAVE, a direct and simple method for evaluating structural needs of flexible pavements based on interpretation of measured FWD deflection basins using mechanistic and practical approaches. It estimates the SNeff and equivalent subgrade modulus independently of pavement-layer thicknesses. The method relies on the Hogg model of an infinite plate on an elastic subgrade of finite or infinite thickness.

2.10 Integration of Pavement Deflection Data into PMS

Deflection data has become an essential tool for evaluation of the structural capacity and integrity of existing, rehabilitated, and newly constructed pavements. FWD center-deflection data reflects the overall structural capacity of the pavement. Normalized center-deflection data can be directly used for pavement evaluation and overlay design *(Noureldin et al., 2003).*

The FWD test is the widely used nondestructive dynamic test for evaluation of the quality of pavement structures. Maintenance strategies in many countries all over the world are based on results of this test *(Al-Khoury et al., 2000).* The FWD analysis provides additional information which helps in making a more cost-effective rehabilitation treatment decision. Implementing the FWD program as part of the PMS will also help in establishing a pavement structural-adequacy database. The data available in this database can be used in developing accurate structural prediction models. Also, it will help in developing more cost-effective maintenance and rehabilitation programs and improving design, maintenance, and rehabilitation techniques currently used.

NDT methods are typically used to measure variations in the modulus of different pavement layers. The critical strains necessary for the estimation of remaining life of a pavement structure are then determined from the estimated moduli *(Meshkani et al., 2003).* Numerous field and laboratory investigations have been performed to develop relationships between pavement performance and deflection *(Hveem, 1955; Bergen and Monismith, 1972; Lister and Kennedy, 1977; Majidzadeh and Ilves, 1981).*

2.11 Summary of Literature Review

A pavement management system (PMS) has been used to assist decision makers in finding optimum strategies for providing, evaluating and maintaining pavements in a serviceable condition over a period of time since the late 1960s. KDOT uses a comprehensive PMS and conducts annual condition surveys for NOS. RSL is the anticipated number of years that a pavement is in acceptable condition to accumulate enough functional or structural distress under normal conditions, given that no further maintenance is performed. Many researchers and agencies have used functional, structural, and/or both approaches to compute RSL. Modeling pavement deterioration is a critical engineering process in PMS. Prediction models are classified into various categories depending on the predicted variables, method of development, and whether individual or composite attributes are predicted. Many researchers and/agencies have used different techniques to develop prediction models depending on the needs and availability of data. Structural conditions of pavements based on nondestructive testing (NDT) deflection techniques are widely used due to their speed, ease of operation, and their ability to model real traffic load intensities and durations. There are four different types of pavement-deflection loading modes. The most important environmental factor affecting surface deflections of flexible pavements is the temperature of the asphaltic layers. Many researchers and institutions have developed equations to calculate pavement temperature and then correct pavement deflection to the standard temperature. Structural number (SN) is the most powerful concept because of its applicability and adaptability to various material types and environmental conditions. Many researchers have developed different approaches to estimate the SN of an existing pavement directly from normalized and temperature-corrected deflections. Deflection data has become an essential tool for evaluation of the structural capacity and integrity of existing, rehabilitated, and newly constructed pavements.

CHAPTER 3 TEST SECTIONS AND DATA COLLECTION

3.1 Test Sections

Experimental sections (perpetual pavement sections) and the highway network (asphalt pavements only) have been used as test sections for rolling-wheel Deflectometer (RWD) and falling-wheel Deflectometer (RWD) deflection data collection.

3.1.1 Experimental Sections

Figure 3-1 shows the spatial distribution of all test sections as recorded by an RWD global positioning system (GPS). Experimental sections on US-75 are perpetual pavement sections, which KDOT built as a field trial to investigate suitability of the perpetual pavements concept for Kansas highway pavements. The experiment involved construction of four, thick-pavement structures on a new alignment of US-75 near Sabetha, Kansas in Brown County. They were built to have a perpetual life and layer thicknesses close to those recommended by KDOT's structural design method for flexible pavements based on the 1993 AASHTO Design Guide. To verify the approach of designing perpetual pavements based on an endurance strain limit, four pavements were instrumented with gages for measuring strain at the bottom of the asphalt base layers. A research team from Kansas State University placed instrumentation systems in the four pavement structures during their construction in June 2005. Table 3-1 shows the pavement structures. The estimated design cumulative traffic for these pavements is 2.6 million ESALS/lane for 10 years and 5.7 million ESALS/lane for 20 years *(Romanoschi et al., 2007)*.

The Kansas Asphalt Pavement Association (KAPA) provided the design of Sections 1, 2, and 3. The tensile strain at the bottom of the asphalt layer of these sections is smaller than 70 microstrains, the endurance limit proposed in the literature based on laboratory fatigue tests on asphalt mixes. Section 4 was designed by KDOT. Sections 1 and 3 have the same thickness, but a softer binder was used in the construction of the base asphalt mix (PG 64-22 instead of PG70-22), and a richer and more ductile asphalt mix was used in the bottom lift of the base layer for Section 3. This mix had a binder content of 6.0%, and different volumetric properties (design air voids = 3%±2%; VFA=77%) than the mix used in the same lift in Section 1 (binder content=

5.7%, design air voids = 4%±2%; VFA=72%). It is expected this mix will have a longer fatigue life. Section 2 was designed by *Thompson (2003)*, which is a thin section (11 in) with a predicted fatigue life of 30 million ESALs/lane. This corresponds to a reliability level of 85% and has been named as the high-reliability section.

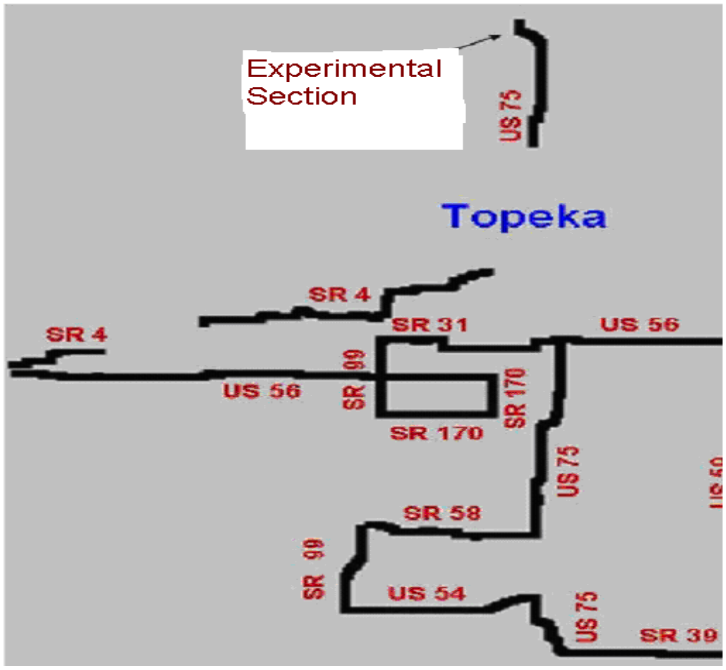

Figure 3-1 Kansas RWD Test Roads *(ARA, 2007)*

Table 3-1 Configuration of Experimental Sections *(Romanoschi et al., 2007)*

Section	**1**	**2**	**3**	**4**
Acronym	**KAPA (Standard)**	**High Reliability**	**KAPA 2 (Modified)**	**KDOT**
Surface Course	1.5 in., SM 9.5 A (PG70-28)			
Binder Course	2.5 in., SM 19 A (PG70-28)			
Base Course	9 in., SM 19A (PG70-22)	7 in., SM 19 A (PG64-22)	9 in., SM 19 A (PG64-22)*	12 in., SM 19A (PG64-22)
Stabilized Subgrade	6 in., 6% hydrated lime mixed with the natural soil			
Natural Subgrade	High plasticity clay (A-7-6)			

(*) the bottom 3" was designed at 3% air voids for a binder-rich layer.

(*P_b= 6.0%, Design Air Voids = 3%±2%; VFA=77%*)

3.1.2 Highway Network

Deflection data was collected on the highway network (asphalt pavements only) in Districts I and IV of KDOT in July 2006 using a rolling-wheel deflectometer (RWD). KDOT maintains two types of asphalt pavements: full-design and partial-design bituminous pavements. Full-design bituminous (FDBIT) pavements were designed for current and projected traffic. They usually carry heavier traffic than the partial-design bituminous (PDBIT) pavements, which resulted from paving and maintenance of farm-to-market roads in 1940s and 1950s. Districts I and IV were chosen in the test network since their pavements mileage most closely approximates the pavement types on the entire KDOT network, and their closeness to Topeka. Deflection data collected on these districts would be representative of the entire KDOT network.

Total mileage and study mileage of the FDBIT and PDBIT sections in Districts I and IV is shown in Table 3-2. Study sections varied from 5 to 11% in total mileage of FDBIT and PDBIT in these districts. Table 3-3 shows general characteristics of the sections on which FWD deflection data was taken from 1998 to 2006 for comparison purposes. It is to be noted that RWD deflection data was taken on 506 lane-miles, but some of the sections do not have FWD deflection data and thus were not included in Table 3-3. Daily 18-kip, equivalent single-axle loads (ESALs) varied from six to 437 and are fairly representative of the traffic loads on KDOT's non-Interstate network. On average, loading on the FDBIT pavements was three to four times the loading on PDBIT pavements. Some of the sections had thin overlays at different time.

Table 3-2 FBIT and PDBIT in Districts I and IV

District	Full-Depth Bituminous			Partial-Depth Bituminous		
	Total (mi)	Study (mi)	Study (%)	Total (mi)	Study (mi)	Study (%)
I	475	54	11.4	731	65	8.9
IV	624	60	9.6	559	28	5.0

Table 3-3 General Characteristics of Study Sections

Sec	Route	County	Pavement Type	AADT[1]	EAL[2]	Last Rehabilitation	
						Type	Year
1	K-4	Wabaunsee	Partial Design	2218	105	-	-
2	K-31	Osage	Partial Design	523	60	0.9'' SM-9.5A[3]	2004
3		Wabaunsee	Partial Design	278	13	0.9'' SM-9.5A[3]	2001
4	K-39	Neosho	Full Design	1110	66	-	-
5	US-54	Greenwood	Full Design	1165	156	-	-
6		Woodson	Full Design	1840	100	-	-
7	US-56	Douglas	Full Design	1076	127	0.9'' SM-9.5A[3]	2004
8		Morris	Full Design	2818	178	1'' BM-2	2003
9		Osage	Partial Design	498	80	1'' SM-12.5A[4]	2003
10	US-59	Allen	Full Design	630	63	-	-
11		Anderson	Full Design	1004	79	-	-
12		Neosho	Partial Design	275	6	-	-
13	US-75	Brown	Full Design	1807	320	-	-
14		Coffey	Full Design	2098	437	0.9'' SM-9.5A[3]	2003
15		Jackson	Full Design	1411	321	0.9'' SM-9.5T[5]	2004
16		Osage	Full Design	310	35	-	-
17		Woodson	Full Design	482	19	1'' SM-12.5A[4]	2002
18	K-99	Greenwood	Partial Design	458	97	-	-
19		Lyon	Partial Design	612	98	0.9'' BM-1[6]	1999
20		Wabaunsee	Partial Design	463	20	-	-
21	K-170	Lyon	Partial Design	693	210	0.9'' SM-9.5A	2000
22		Osage	Partial Design	698	114	0.9'' SM-9.5A	2000

[1]AADT = annual average daily traffic; [2]EAL=equivalent axle load (daily) on design lane; [3, 4]Superpave mix, nominal aggregate size 9.5 and 12.5 mm, respectively, above maximum density; [5]Superpave recycled mix, nominal aggregate size 9.5 mm, friction course mix; and [6]Bituminous mix with combined aggregates, 30% crushed material, 15% natural sand.

3.2 Deflection Data

3.2.1 RWD Deflection Data

Applied Research Associates (ARA) collected deflection data using RWD on 17 US and state routes (SR) as shown in Figure 3-1 from July 28 to August 1, 2006. Testing was performed in one direction and referenced using the reference marker system posted in the field. A total of 506 lane-miles were tested over three days. In addition, ARA tested the four perpetual pavement sections located on US-75 near Sabetha. On US-75, the RWD made 16 passes (15 northbound and one southbound) over an approximately 1.5-mi-long test section. In general, the RWD tested at normal highway speeds (i.e., 50- to 65-mph) whenever conditions permitted. On that day, KDOT also performed FWD testing on perpetual pavement sections at 50-ft intervals.

3.2.2 FWD Deflection Data

FWD deflection data was collected with a Dynatest 8000 FWD shown in Figure 3-2. FWD data were typically collected on the outer wheel path of the travel lane. The study used data collected from 1998 to 2006. More than 400,000 deflection data points have been averaged and reduced to data for about 13,000 lane-miles in order to match this data with the distress and traffic data collected annually by KDOT on the mile-long PMS segments.

3.3 Stress-and-Strain Data

Stress-and-strain data have been collected on only four perpetual pavement sections. Each test section has multiple gauges, with half of the sensors located in the right-vehicle wheel path, and the other half located six inches to the right. Seven sets of pavement response measurements under known wheel load were performed between July 2005 and October 2007, before and after the pavement sections were opened to traffic. In each session, a single axle dump truck, an FHWA Class 5 vehicle, was used as the loading vehicle. The same loading vehicle was used for all measurements. Before the runs were done, the static weight of each wheel was measured by the Kansas Highway Patrol using calibrated scales. On each pavement, three sets of five passes of the loading vehicle were performed. Five passes were performed with the truck passing at 20- to 25-mph, 40- to 45-mph, and 55- to 60-mph, in order to determine the

effect of vehicle speed on pavement response. In addition to the KDOT truck, RWD was also used to collect stress-and-strain data in August 2006 on the same sections.

Figure 3-2 KDOT FWD Dynatest 8000

Horizontal strains and the vertical stress at the bottom of the asphalt concrete layer, as well as the position of the loading vehicle, were recorded with a National Instruments data acquisition system at a rate of 300 records per second. A sampling rate of 3,000-Hz was used and the average value for ten samples was recorded. The data was recorded in text format in separate files for each passes of the vehicle and was then processed using Microsoft Excel *(Romanoschi et al., 2007).*

3.4 Temperature Data

3.4.1 Pavement Surface Temperature

Pavement surface temperatures, in conjunction with air temperature and AC layer thickness, are needed to adjust field deflections to a standard temperature of 68 ºF. RWD

continuously measures pavement surface temperature with an infrared thermometer. Pavement surface temperature is also measured with an FWD infrared sensor.

3.4.2 Pavement Mid-Depth Temperature

Pavement mid-depth temperature was measured only on perpetual pavement sections during each data collection session. The thermocouple of a temperature gage was lowered into the holes drilled in the AC layers and filled with oil to measure the temperature at the mid-depth of each AC layer at the time of response measurement *(Romanoschi et al., 2007).*

3.5 KDOT PMS Data

3.5.1 Cracking Data

KDOT uses segments approximately one-mile long as PMS sections. Each of these segments is randomly assigned three, 100-ft sample survey locations for a visual rating of fatigue and transverse cracking on bituminous and composite pavements. For each cracking type on bituminous pavements, codes are used to define severity and extent.

Raters, traveling on the shoulder in a van at a slow speed, use an electronic data entry panel and software developed by International Cybernetics Corporation (ICC) to enter distress data in the field. Pressing the appropriate button on the data entry panel whenever a crack of a particular code is encountered enters the number or length of the cracks. The extent can also be coded by entering the total number of occurrences of a particular code of crack and then pressing the appropriate key. This data is summarized in the office as the cracks of each type in each severity category expected on any 100-ft sample of the mile-long PMS segments.

3.5.1.1 Fatigue Cracking Data

Fatigue cracking, commonly called alligator cracking, is caused by traffic and will normally occur in wheel path areas. The first sign of fatigue cracking is usually one or more longitudinal parallel cracks in the wheel path. After repeated traffic loading, the cracks connect, forming many-sided, sharp-angled pieces that develop a pattern resembling the skin of an alligator. Advanced stages of fatigue cracking include spalling of the cracks, pumping, and shoving. Shoving may occur without evidence of fatigue cracking.

Fatigue cracking ratings are summarized by severity and extent of interconnected longitudinal cracks in the wheel paths. Severity levels are based on density of the crack pattern and spalling of the pieces between cracks. The extent of fatigue cracking is measured and recorded by KDOT as the lineal feet of wheel path which are cracked and/or shoved.

Fatigue cracking severity is assigned Code 1, 2, 3, or 4. According to the KDOT field operations manual (*KDOT, 2006*), Code 1 fatigue cracking represents hairline alligator cracking with pieces which are non-removable. Code 2 refers to cracking with pieces which are non-removable, but which are spalled. Code 3 refers to pieces that are spalled, loose, and removable. Pavement will probably pump with loading. Code 4 refers to pavement that has shoved to the extent that a ridge of asphalt material has risen adjacent to the wheelpath. Sometimes the pavement moves laterally rather than forming a ridge.

URS Corp. (2000) developed coefficients based on the time from when the severity level was first detected until the highest severity level was reached. These coefficients can then be used to combine the number and severity of cracks into a continuous variable called equivalent Code 4 cracks. Different combinations of the coded cracks will result in an equivalent number of Code 4 cracks for the PMS segment, and this is used as an input for the cracks into NOS. Equivalent fatigue cracking (EFCR) is calculated using Equation (3.1):

$$EFCR = 0.078FC1 + 0.127FC2 + 0.299FC3 + FC4 \quad (3.1)$$

where

$EFCR$ = equivalent fatigue cracking in Code 4; and

$FC1, FC2, FC3\ and\ FC4$ = Code 1, Code 2, Code 3, and Code 4 fatigue cracking, respectively.

3.5.1.2 Transverse Cracking Data

Transverse cracks extend across the pavement approximately perpendicular to the centerline. They are not usually load associated and are caused by shrinkage of the AC pavement and reflection cracks in a PCC pavement through an overlay. KDOT is concerned with the extent and severity of transverse cracks. The extent of transverse cracking is measured and recorded as the number of full roadway-width cracks in the survey section. Severity is coded as 0, 1, 2, or 3, based on crack width, roughness, secondary cracks, and sealed cracks.

The four severity codes associated with transverse cracking are defined in the KDOT field operations manual (*KDOT, 2006*). TRzero refers to sealed cracks with no roughness and sealant breaks less than one-ft/lane. TR1 represents no roughness, 0.25-in or wider, with no secondary cracking; or any width with secondary cracking less than a four-ft/lane; or any width with a failed seal ($\geq$ one-ft/alne). TR2 refers to any width with noticeable roughness due to depression or bump or wide crack (one-in plus); also, cracks that have more than four-ft of secondary cracking per lane but no roughness; also, sealed cracks with noticeable roughness. TR3 describes any width with noticeable significant roughness due to depression or bump. Secondary cracking will be more severe than Code 2.

URS Corp. (2000) developed the coefficients to relate Code 1 and Code 2 transverse cracks to Code 3 using the transition time between appearance of a Code 1 or 2 cracks and a Code 3 crack. These coefficients can then be used to combine the number and severity of cracks into a continuous variable called equivalent Code 3 cracks. Different combinations of the coded cracks will result in an equivalent number of Code 3 cracks for the PMS segment, and this is used as an input for the cracks into NOS. Equivalent transverse cracking (ETCR) is calculated using Equation (3.2):

$$ETCR = 0.2079TR1 + 0.4099TR2 + TR3 \quad (3.2)$$

where

$ETCR$ = equivalent transverse cracking corresponding to Code 4; and

$TR1, TR2$ *and* $TR3$ = Code 1, Code 2, and Code 3 transverse cracking, respectively.

It is to be noted that TRzero is not included in the equation since it does not have any coefficient. The coefficients were determined based on the time from when that severity level was first detected until the highest severity level was reached. TRzero clearly does not fit in the progression since some were already TR1 cracks that had been sealed.

3.5.2 Rutting Data

Rutting is the longitudinal depression on the wheel path in asphalt concrete pavements, which stems from the permanent deformation in any or all of the pavement layers or the subgrade. It usually results from the relative movement of materials due to traffic loading (*Huang, 2004*). While deep ruts may be interpreted as a structural failure, they are also a serious

safety issue for road users because there is a potential for hydroplaning if water accumulates in the ruts.

Measurement of rut depth has become an integral component of the condition survey of bituminous and composite pavements for KDOT. Automated transverse profile data allow for numerous methods to calculate rut depths. KDOT makes automated rut-depth measurements using a rut bar mounted on a vehicle with three sensors that also do profile measurements. In a three-point system, data are collected in each wheel path and in mid lane. With the three-point system, rut depth is calculated as the difference in elevation between the mid-lane measurement and the wheel path measurement *(Miller et al., 2004).*

KDOT measures rutting using a South Dakota-type profilometer. KDOT assigns a rut code for input into the NOS based on the rut depths: Code 0 (0.0 to 0.25-in.), Code 1 (0.25 to 0.50-in.), Code 2 (0.5 to 1.0-in.), or Code 3 (>1.0-in.). The rut-depth values are computed from the profile data with RP090L software for the three-point rut-depth algorithm. If h_1, h_2, and h_3 are the elevation measurements at the three sensors (on the wheel paths and between the wheel paths), the total rut depth for both wheel-paths is calculated as (*KDOT, 1996*).

$$RD_{total} = h_1 + h_3 - 2h_2 \tag{3.3}$$

Then the average rut depth is

$$RD_{avg} = \frac{(h_1 + h_3 - 2h_2)}{2} \tag{3.4}$$

3.5.3 Layer Thickness

Layer information data for all KDOT pavement cross sections is stored in CANSYS, a master database of the KDOT highway network. In this study, bound layer-thickness information since 1920 has been extracted from CANSYS.

3.5.4 Traffic Data

Traffic monitoring activities at KDOT are primarily carried out by the Traffic and Field Operations (TFO) Unit of the Bureau of Transportation Planning. This unit is responsible for all

aspects of traffic data collection: procurement, repair, and service of the data collection equipment; and tabulation, analysis, evaluation, and retention of collected data *(KDOT, 2003)*.

The average daily traffic (ADT) data for all roads with Interstate, US, and Kansas route numbers are maintained in the CANSYS/CANSYS II database for each highway section. Traffic counts are collected every year on Interstate and divided four-lane facilities. Traffic counts are collected every other year on the rest of the state system (north half of State in odd-numbered fiscal years and south half of the state in even-numbered fiscal years). If a new traffic count is not collected, then an expansion factor is used to adjust the count from the previous year. Annual average daily traffic (AADT) and equivalent standard daily traffic (EAL) data on the PMS segments were provided by KDOT for this study.

3.5.5 RSL Data

KDOT uses Equation (3.5), developed by *URS Corp (2000),* to calculate the design life of a non-routine maintenance action for flexible pavements. RSL was taken as the difference between the design life and the FWD test date in this study.

$$DL\_Flex = 15.4 + 0.873 \times FDBit + 1.05 \times EqThick - 3.27 \times \ln(TCR_{prior} + 1) - 1.78 \times \ln\left(\frac{D - ADL}{EqThick}\right) - 0.0662 \times d_6 \quad (3.5)$$

where

DL_Flex = design life of a non-routine maintenance action (years);

$FDBit$ = full-design bituminous (FDBit) index (FDBit pavement =1; otherwise = 0);

$EqThick$ = equivalent thickness (in) of the action;

TCR_{prior} = equivalent transverse cracking before the action;

$D - ADL$ = design lane ADL (80kN/day) in the year of the action; and

d_6 = average deflection (microns) from the most distant sensor.

FWD and RWD deflection data have been analyzed and detailed results are given in Chapter 4. Condition survey and deflection data have been used to develop RSL, EFCR, and ETCR models. Methodologies to develop the models and the results have been discussed in Chapter 5.

CHAPTER 4 DATA ANALYSIS AND DISCUSSIONS

4.1 Introduction

Structural-capacity analysis has been done using FWD deflection data collected from 1998 to 2006 and RWD deflection data collected in summer of 2006. Comparison of normalized and temperature-corrected FWD and RWD center deflections and corresponding SNeff has also been done. The effect of the temperature-correction method on center deflections and corresponding SNeff has been performed using FWD deflection data. Analysis has also been carried out to determine the frequency of deflection measurements at the network level using FWD deflection data over the test years and corresponding SNeff. Comparison has been done for measured and calculated mid-depth pavement temperature using temperature data collected for the experimental (perpetual pavement) sections on US-75 in Kansas. SNeff has also been computed using KDOT procedures and comparison has been made with SNeff from the AASHTO method. Finally, significant-difference tests based on paired t-test and linear regression have been done using the Statistical Analysis Software (SAS).

4.2 Deflection Data

Loads measured by the FWD load cell for two consecutive drops are not the same during testing, even for the same equipment configuration and fall height. The variations are small but must be taken into consideration in the analysis. Deflection normalization is the process of correcting the deflection measured at any load to a standard load of 9,000 lbs. It is assumed that surface deflections vary linearly with the load for a relatively narrow interval of the loads (less than 1,000 lbs) and for the load duration period of 20 to 35 milli seconds. All deflections measured using FWD were normalized to the standard load of 9,000 lb using Equation (4.1).

$$d_i = \frac{d_{mi} \times P}{9{,}000} \tag{4.1}$$

where

d_{mi} = deflection measured by geophone i under any load P; and

d_i = normalized deflection.

At 55 mph, the RWD's two-kHz lasers take readings at approximately every 0.5-inch intervals, resulting in extremely large data sets. To make the data set manageable and to reduce the random error of individual readings, data are averaged over an interval suitable for pavement management purposes, typically 0.1 mile. At normal highway speeds, a 0.1-mile contains approximately 60,000 individual laser readings. RWD deflection was not normalized since a standard load of 9,000 lbs was used.

Structural capacities of flexible pavements can be determined from surface deflection measurements. The most important environmental factor affecting surface deflections of flexible pavements is the temperature of the asphaltic layers *(Kim and Lee, 1995; Shao et al., 1997; Park et al., 2002).* All deflection data need to be adjusted to a constant temperature *(Chen et al., 2000). BELLS3 and Watson et al. (2004)* methods have been used to calculate mid-depth pavement temperature. *AASHTO and Chen et al. (2000)* approaches have been used to correct pavement deflection to a standard temperature of 68^{o}F.

4.2.1 Repeatability

Repeatability of RWD and FWD has been discussed. RWD deflection data on experimental (perpetual pavement) sections has been used to evaluate repeatability of RWD. Literatures on the repeatability of FWD have been reviewed.

4.2.1.1 Repeatability of RWD

Sixteen runs were made on the experimental (perpetual pavement) sections on Aug. 1, 2006, with 15 of them in the same direction. Run number three has not been included in this analysis since it was in a different direction. The mean of 15 runs has been computed and included in Figure 4-1. Run 14 shows the highest deflection for all sections except Section 1. All sections have lowest deflection at different runs. Mean RWD deflection is higher than the FWD center deflection for all sections except Section 3. This difference, however, is insignificant from a practical point of view. This shows that RWD has a reasonably good repeatability.

4.2.1.2 Repeatability of FWD

Bentsen et al. (1989) have collected FWD deflection data in five series of five drops each on flexible pavements. The study found that FWD showed good repeatability, within the limit of the manufacturers. *Rocha et al. (2003)* found that FWD showed a good repeatability for the

Texas Department of Transportation. *Choubane et al. (2006)* have done research for the Florida Department of Transportation to assess the level of precision of FWD measurements on flexible pavements. The study demonstrated a generally high level of FWD repeatability.

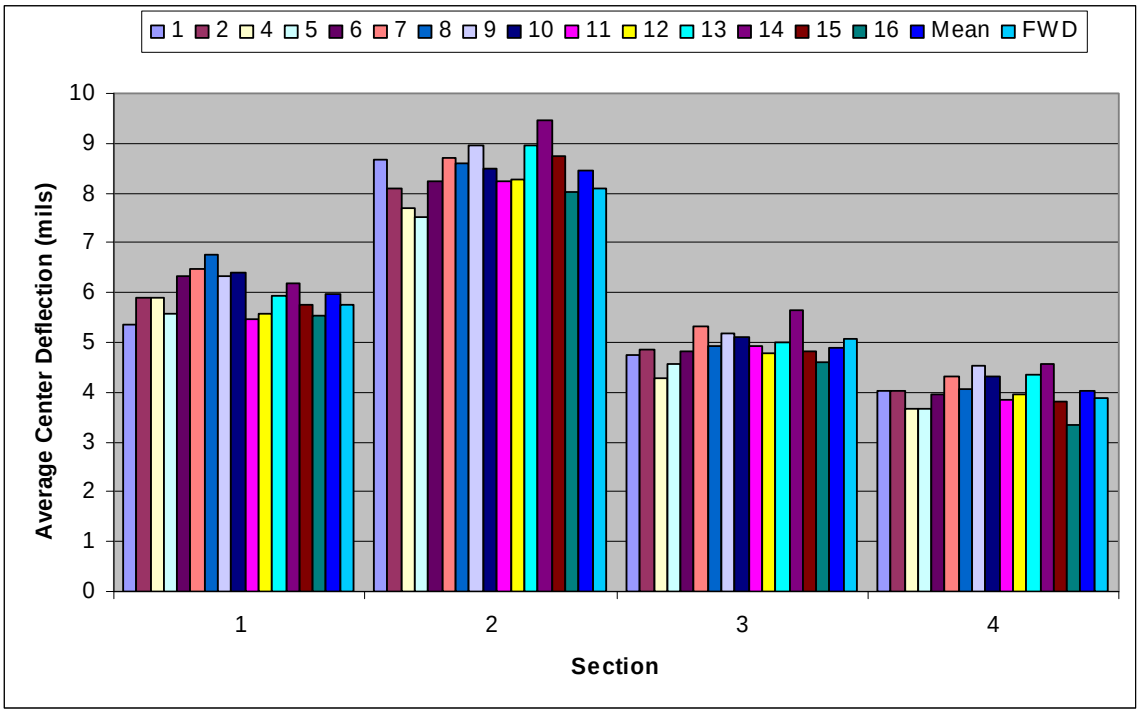

Figure 4-1 Mean FWD and RWD Center Deflections for Experimental Sections

4.2.1.3 Significant-Difference Test

Paired t-tests have been done to determine statistical differences between RWD center deflections of different runs. Paired data arise when two dependent samples are observed using two measurement methods on a subject. The hypothesis test will be performed on the difference of the means of the two samples. The default value is zero, which results in a test where the two population means are equal..

Confidence interval produces a symmetrical two-sided interval around the mean. Lower bound produces a one-sided interval with a lower endpoint. Upper bound produces a one-sided interval with an upper endpoint. The confidence level represents the percentage of time the interval covers the true (unknown) parameter value..

The Statistical Analysis Software (SAS) was used to do paired t-tests and confidence intervals for mean differences at the 5% level of significance. For brevity, only runs 1, 5, 10, and

15 have been included as shown in Table 4-1. Run 1 is significantly different from run 10 for Section 1; and run 5 for Sections 2 and 4. Run 5 is significantly different from run 10 for all sections and from run 15 for Section 2. Run 10 is significantly different from run 15 only for Section 4. The results show that RWD is fairly repeatable device.

Table 4-1 Significant-Difference Test for Repeatability of RWD

Compare		Section 1		Section 2		Section 3		Section 4	
Run	**Run**	**Pr>|t|**	**Similar**	**Pr>|t|**	**Similar**	**Pr>|t|**	**Similar**	**Pr>|t|**	**Similar**
1	5	0.51	Yes	<.0001	No	0.57	Yes	0.04	No
	10	0.01	No	0.47	Yes	0.23	Yes	0.09	Yes
	15	0.42	Yes	0.80	Yes	0.79	Yes	0.15	Yes
5	10	0.01	No	<.0001	No	0.00	No	<.0001	No
	15	0.70	Yes	<.0001	No	0.28	Yes	0.33	Yes
10	15	0.17	Yes	0.22	Yes	0.10	Yes	0.01	No

4.2.2 FWD and RWD Center Deflection

BELLS3 Equation (2.23) has been used to calculate the pavement mid-depth temperature, and the AASHTO method has been used to correct FWD and RWD center deflections to a standard temperature. Comparison of FWD and RWD center deflections has been done on a mile-by-mile basis for all projects except for the experimental sections. It is to be noted that FWD and RWD deflection data were not collected at the same time for all projects, except for the experimental sections. Some of the projects had rehabilitation actions between the time FWD and RWD deflection data were collected, and those sections have been discussed separately.

AASHTO Guide (1993) recommends a linear relationship between the temperature and the temperature-correction factor. The relationship is presented on a nomogram form–the slopes of the lines depend on the thickness of the asphalt layer. It is important to note that the guide recommends two different nomograms: one for pavements with granular and asphalt-treated bases and another for pavements with cement and pozzolanic-treated bases. The AASHTO method has been used to correct FWD and RWD center deflections to a standard temperature of 68^{o}F. Comparison of FWD and RWD center deflections for experimental sections, projects without and with rehabilitation actions, significant-difference tests, and linear regression have

also been done. Results for some of the projects without and with rehabilitation actions have been included in Appendix A.

4.2.2.1 Experimental Sections

FWD and RWD deflection data have been taken on the same date and it is more reasonable to compare these results. Section 1 has a slope and an R^2 value of 0.42 and 0.78, respectively, as indicated in Figure 4-2(a), and there is no significant variation. Figure 4-2(b) shows the FWD and RWD deflections for Section 2, which shows some variation. Figure 4-2(c) and (d) show some scatter and outliers for Sections 3 and 4, respectively. The increase in variation may be due to a high test temperature.

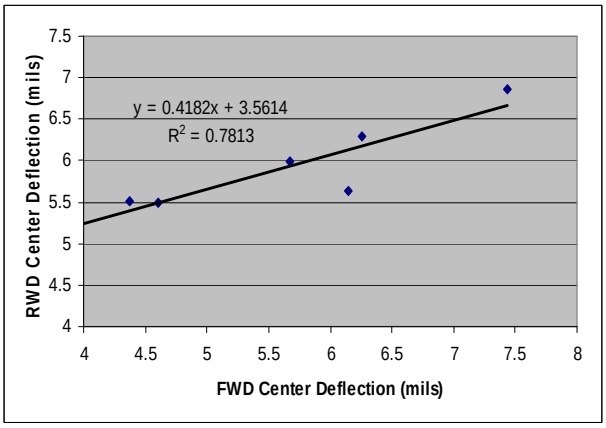

(a) Section 1

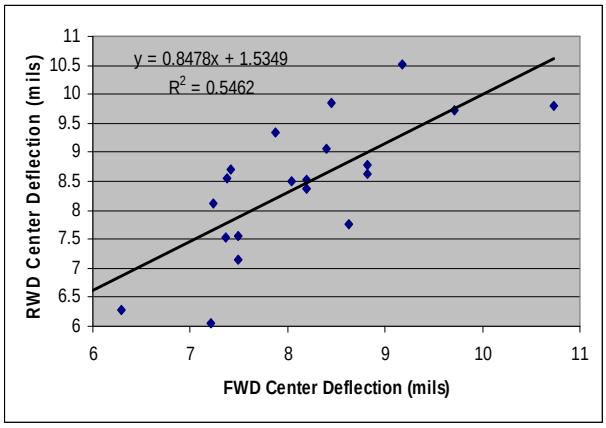

(b) Section 2

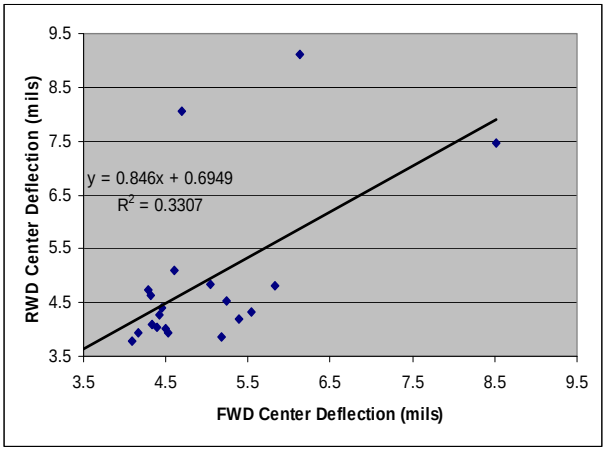

(c) Section 3

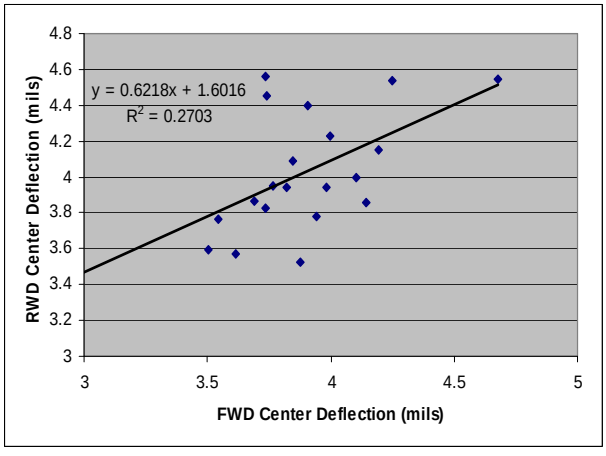

(d) Section 4

Figure 4-2 FWD and RWD Center Deflections for Experimental Sections

4.2.2.2 Without Rehabilitation Actions

US-59 in Anderson County shows some scatter, relatively low slope, and R^2 as indicated in Figure 4-3(a). Figure 4-3(b) indicates a relatively low scatter and high slope for US-75 in Brown County. US-75 in Coffey County has a slope and an R^2 value of 0.85 and 0.65, respectively, as indicated in Figure 4-3(c). US-75 in Jackson County has a low slope and a low R^2 value as indicated in Figure 4-3(d). This may be due to four years difference in test time for these two pieces of equipment.

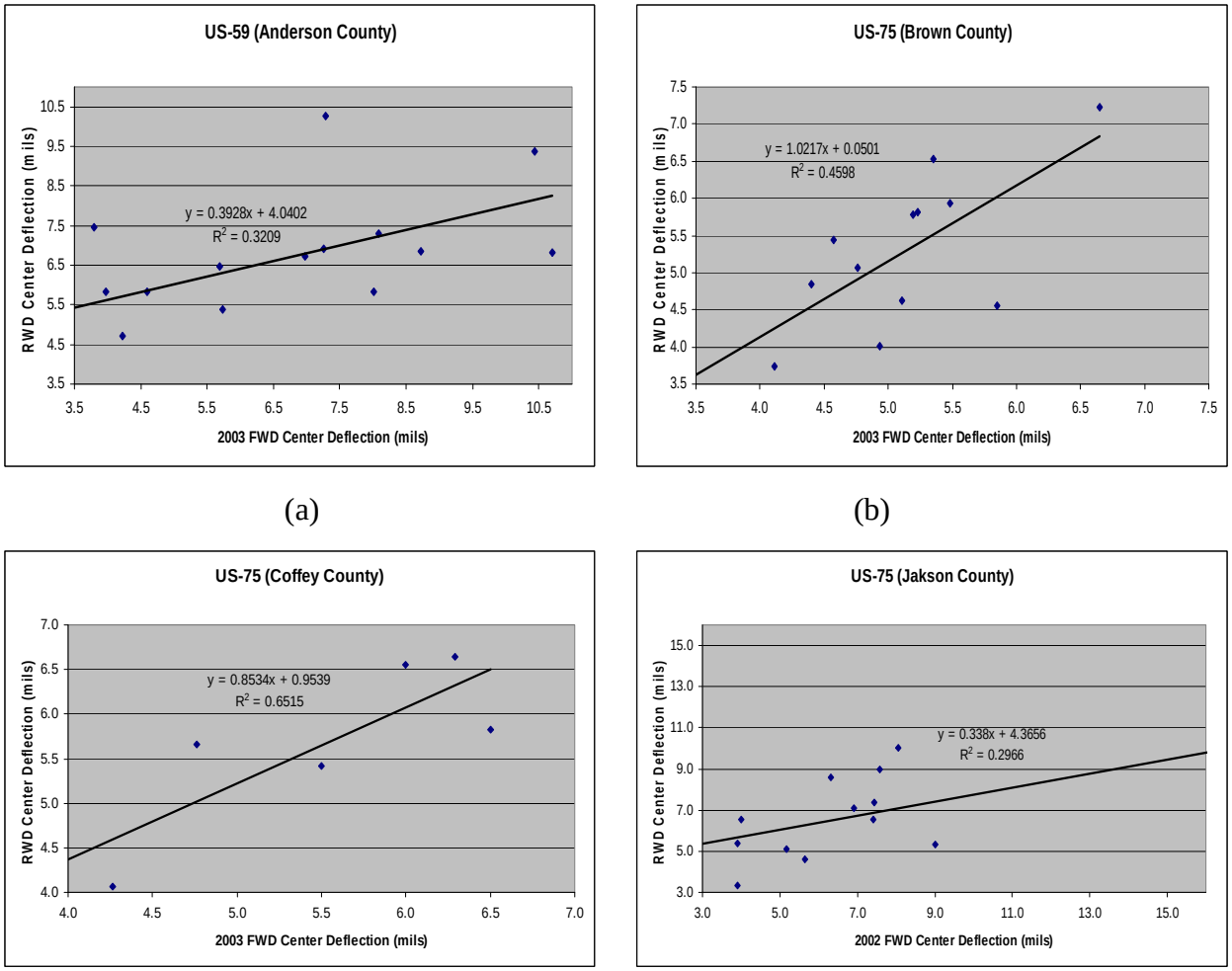

Figure 4-3 FWD and RWD Center Deflections for US-59 and US-75

4.2.2.3 With Rehabilitation Actions

K-31 in Osage County has a slope and an R^2 value of 0.62 and 0.84, respectively, as indicated in Figure 4-4(a). K-31 in Wabaunsee County has a low slope and a small R^2 value as indicated in Figure 4-4(b), probably due to the effect of rehabilitation action between FWD and RWD deflection test dates. The effects of the rehabilitation action taken is not evident from Figure 4-4(c) for K-99 in Lyon County, since RWD shows higher deflection at some points and lower at others. FWD deflection is higher than the RWD deflection at all points for K-99 in Wabaunsee County, as indicated in Figure 4-4(d), due to rehabilitation action.

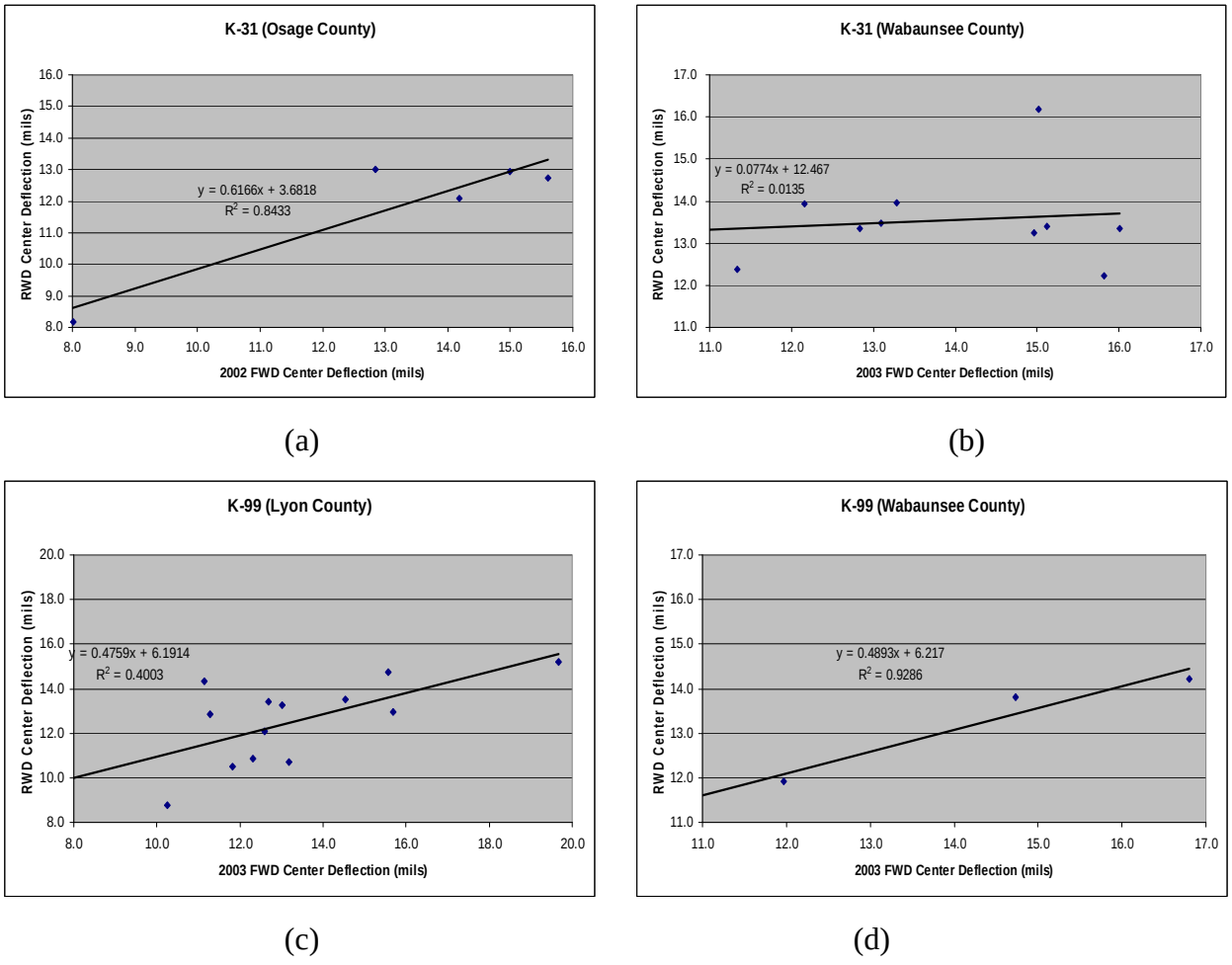

Figure 4-4 FWD and RWD Center Deflections for K-31 and K-99

RWD shows higher deflections at relatively lower deflection values for US-54 in Greenwood County as in indicated in Figure 4-5(a). RWD center deflection is lower than the FWD center deflections at all points for US-56 in Douglas County, mainly due to the rehabilitation action as indicated in Figure 4-5(b). FWD shows higher deflection in some cases and vice versa for US-56 in Norris County as indicated in Figure 4-5 (c). Figure 4-5(d) shows quite scattered center deflections for US-56 in Osage County. The effect of rehabilitation action is not clear.

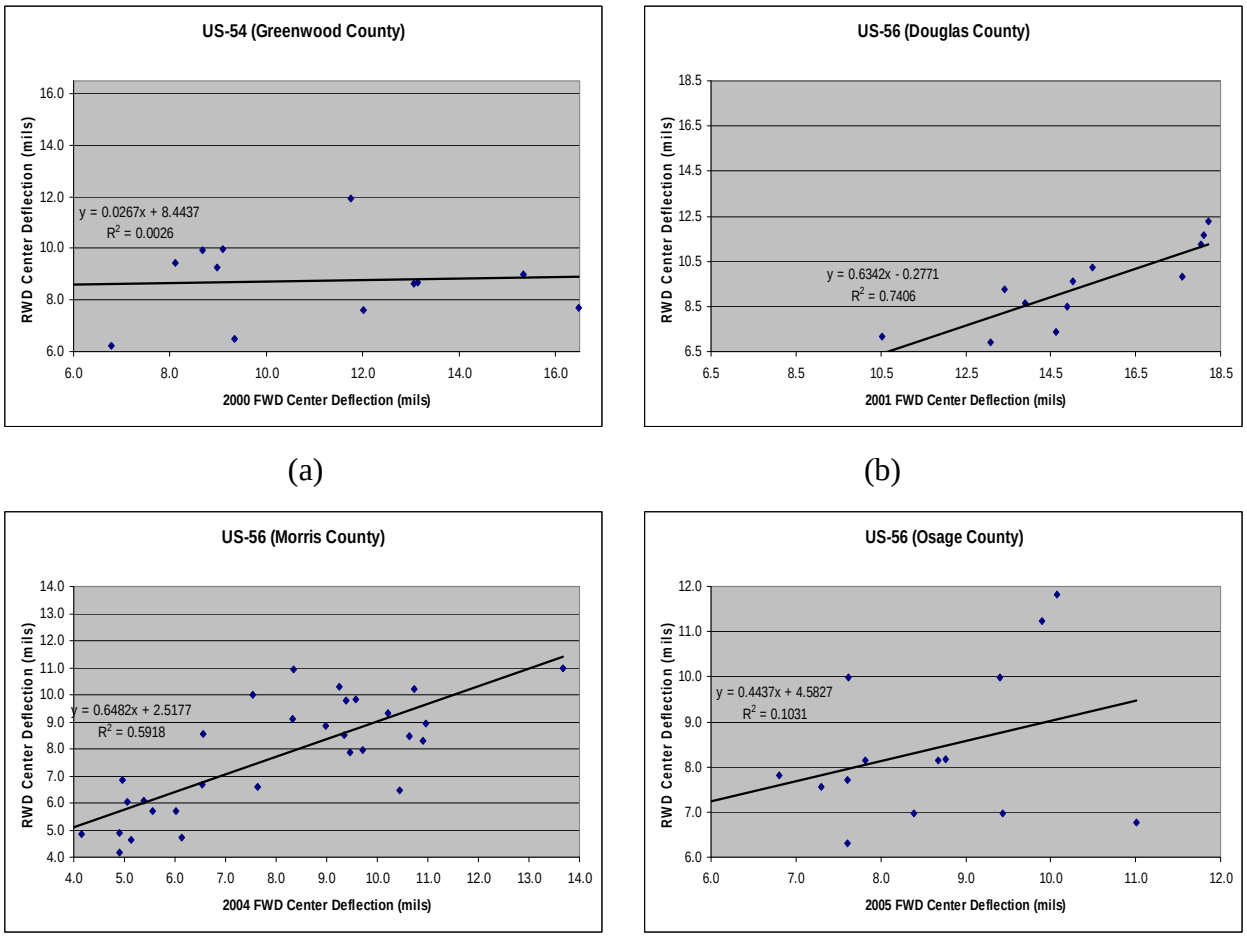

(a) (b)

(c) (d)

Figure 4-5 FWD and RWD Center Deflections for US-54 and US-56

4.2.2.4 Significant-Difference Test

Average RWD center deflection is slightly higher than that of FWD in all experimental sections except on Section 3, though the difference is not significant from a practical point of view as shown in Figure 4-6. The numerical values are shown in Table 4-2.

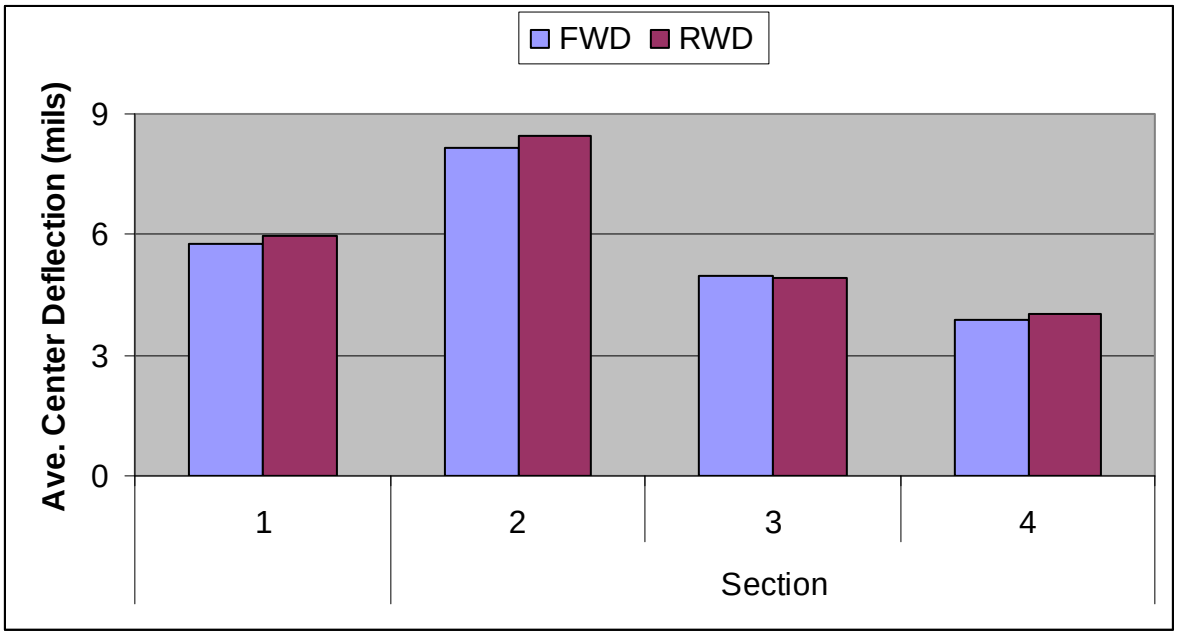

Figure 4-6 Average FWD and RWD Center Deflections for Experimental Sections

Table 4-2 shows significant-difference test results for experimental sections. There is no significant difference in FWD and RWD center deflections. The mean difference between FWD and RWD center deflections is positive only for Section 3, which shows that RWD center deflection is slightly higher than FWD center deflection for other sections. This is a reasonable comparison since deflection data has been taken on the same date, and it supports that RWD can be used to take deflection data instead of FWD. It is to be noted that the number of data points are not mile-based, unlike other projects.

Table 4-2 Significant-Difference Test of Center Deflection for Experimental Sections

Section	Avg. d_0		Paired T-Test for Difference (FWD-RWD)					No. of Data Points
	FWD	RWD	Lower	Mean	Upper	Pr>|t|	Similar	
1	5.75	5.96	-0.96	-0.22	0.53	0.49	Yes	6
2	8.15	8.44	-0.67	-0.30	0.08	0.11	Yes	20
3	4.98	4.91	-0.50	0.07	0.65	0.80	Yes	20
4	3.90	4.03	-0.27	-0.13	0.02	0.08	Yes	20

Average RWD center deflection is slightly higher than that of FWD in four out of seven projects without rehabilitation actions as shown in Figure 4-7. Average FWD center deflection is higher than RWD for all projects with rehabilitation actions except K-170 in Lyon County and US-75 in Osage County. Numerical values of average FWD and RWD center deflections are given in Table 4-3.

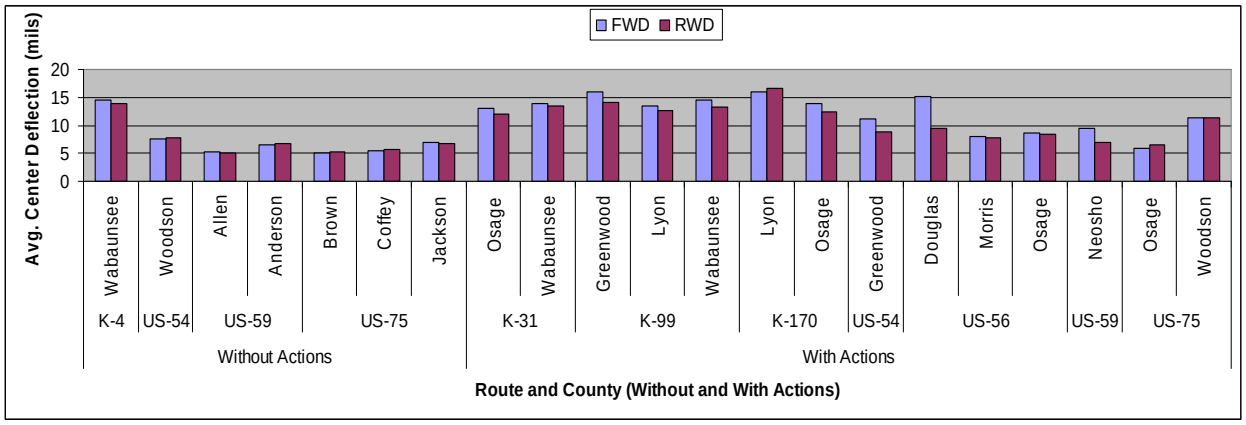

Figure 4-7 Average FWD and RWD Center Deflection

The Statistical Analysis Software (SAS) was used to do paired t-tests and confidence intervals for mean differences at the 5% level of significance. Table 4-3(a) shows that the mean center deflections from RWD and FWD are statistically similar on all routes without rehabilitation actions between the dates FWD and RWD data had been taken. Table 4-3(b) shows the results for routes which had rehabilitation actions between the dates FWD and RWD deflection data had been taken. FWD center deflection is significantly different from the RWD center deflection on only five out of 14 routes with rehabilitation actions. These results tend to indicate that RWD can be a valuable tool to collect deflection data at the network level.

Table 4-3 Significant-Difference Test for FWD and RWD Center Deflection

Route	County	Average d_0		Paired T-Test for Difference (FWD-RWD)					Length (mi)
		FWD	RWD	Lower	Mean	Upper	Pr>|t|	Similar	
(a) Without Rehabilitation Actions									
K-4	Wabaunsee	14.45	13.88	-1.34	0.57	2.48	0.53	Yes	12
US-54	Woodson	7.50	7.77	-1.10	-0.27	0.56	0.44	Yes	6
US-59	Allen	5.33	4.98	-0.36	0.35	1.06	0.28	Yes	8
	Anderson	6.59	6.64	-1.13	-0.05	1.04	0.93	Yes	15
US-75	Brown	5.13	5.28	-0.61	-0.15	0.31	0.49	Yes	12
	Coffey	5.57	5.70	-0.74	-0.13	0.48	0.60	Yes	6
	Jackson	7.02	6.74	-1.33	0.28	1.90	0.71	Yes	15
(a) With Rehabilitation Actions									
K-31	Osage	13.12	11.98	-0.45	1.34	3.13	0.11	Yes	5
	Wabaunsee	13.96	13.56	-0.92	0.40	1.72	0.51	Yes	10
K-99	Greenwood	16.08	14.21	0.45	1.87	3.28	0.01	No	20
	Lyon	13.38	12.56	-0.37	0.82	2.00	0.16	Yes	13
	Wabaunsee	14.50	13.30	-1.97	1.20	4.37	0.25	Yes	3
K-170	Lyon	16.06	16.59	-2.34	-0.53	1.28	0.50	Yes	7
	Osage	13.93	12.43	0.48	1.50	2.52	0.00	No	13
US-54	Greenwood	11.07	8.74	0.20	2.33	4.45	0.03	No	12
US-56	Douglas	15.23	9.40	5.03	5.83	6.64	0.00	No	12
	Morris	8.01	7.72	-0.30	0.30	0.88	0.32	Yes	30
	Osage	8.60	8.40	-0.80	0.20	1.20	0.67	Yes	14
US-59	Neosho	9.54	6.85	1.82	2.69	3.56	0.00	No	8
US-75	Osage	5.90	6.58	-3.70	2.34	1.46	0.57	Yes	5
	Woodson	11.44	11.43	-1.04	0.01	1.05	0.98	Yes	11

4.2.2.5 Linear Regression

Linear regression analysis was conducted for all experimental sections, projects without and with rehabilitation actions to determine whether FWD center deflection can be predicted from RWD center deflection and vice versa. RWD deflection was taken as the dependent variable in this analysis. There is a linear relationship between FWD and RWD center deflections for all experimental sections as shown in Table 4-4. Slope and R^2 value varies from 0.42 to 0.85 and 0.27 to 0.78, respectively. Section 1 has the lowest slope, but it is compensated by high intercept. In general, RWD deflection can be predicted from FWD deflection data.

Table 4-4 Linear Regression of Center Deflection for Perpetual Pavement Sections

Section	Intercept	Slope	C.I.* for Slope		Pr>|t|	Linear Relation	R^2	No. of Data Points
			Lower	Upper				
1	3.56	0.42	0.11	0.73	0.02	Yes	0.78	6
2	1.53	0.85	0.47	1.23	0.00	Yes	0.55	20
3	0.69	0.85	0.25	1.44	0.01	Yes	0.33	20
4	1.60	0.62	0.12	1.13	0.02	Yes	0.27	20

* confidence interval for slope at 95% confidence level

The slope and R^2 value varies from 0.47 to 1.08 and 0.40 to 0.91, respectively. There is a linear relationship between FWD and RWD center deflections for all projects without rehabilitation action except on K-4 in Wabaunsee County and US-54 in Woodson County as shown in Table 4-5(a). Table 4-5(b) shows there is no linear relationship between FWD and RWD center deflection for half of the projects with rehabilitation action.. Slope varies from 0.33 to 1.09 and R^2 value varies from 0.30 to 0.63 for those projects in which there is a linear relationship between FWD and RWD center deflections. This shows that RWD center deflection can be predicted from the FWD center deflection with reasonable accuracy at the network level. This implies that RWD can be used to collect deflection data at the network level instead of FWD.

Table 4-5 Linear Regression of FWD and RWD Center Deflection

Route	County	Inter-cept	Slope	C.I.* for Slope		Pr>|t|	Linear Relation	R^2	Length (mi)
				Lower	Upper				
(a) Without Rehabilitation Actions									
K-4	Wabaunsee	14.17	-0.02	-0.47	0.43	0.92	No	0.00	12
US-54	Woodson	0.91	0.91	-0.61	2.44	0.17	No	0.41	6
US-59	Allen	0.65	0.81	-0.14	1.76	0.08	Yes	0.42	8
	Anderson	4.02	0.40	0.05	0.74	0.03	Yes	0.32	15
US-75	Brown	-0.29	1.09	0.32	1.84	0.01	Yes	0.50	12
	Coffey	1.02	0.84	-0.06	1.74	0.06	Yes	0.63	6
	Jackson	4.50	0.33	-0.01	0.69	0.05	Yes	0.30	15
(b) With Rehabilitation Actions									
K-31	Osage	3.78	0.61	0.12	1.10	0.03	Yes	0.84	5
	Wabaunsee	12.5	0.08	-0.47	0.62	0.76	No	0.01	10
K-99	Greenwood	9.45	0.30	-0.17	0.76	0.20	No	0.09	20
	Lyon	6.26	0.47	0.09	0.86	0.02	Yes	0.40	13
	Wabaunsee	6.20	0.49	-1.35	2.33	0.18	No	0.92	3
K-170	Lyon	15.78	0.05	-1.05	1.16	0.89	No	0.01	7
	Osage	2.95	0.68	0.50	0.86	0.00	Yes	0.86	13
US-54	Greenwood	8.38	0.03	-0.34	0.40	0.85	No	0.00	12
US-56	Douglas	-0.20	0.63	0.36	0.90	0.00	Yes	0.73	12
	Morris	2.53	0.65	0.44	0.86	0.00	Yes	0.59	30
	Osage	4.47	0.46	-0.36	1.27	0.25	No	0.11	14
US-59	Neosho	0.48	0.67	0.46	0.87	0.00	Yes	0.91	8
US-75	Osage	9.98	-0.58	-3.13	1.98	0.53	No	0.15	3
	Woodson	-0.93	1.08	0.53	1.63	0.00	Yes	0.69	11

* confidence interval for slope at 95% confidence level

4.2.3 Effect of Temperature-Correction Method

Since RWD measures only center deflection, the effect of the temperature-correction factor can be very pronounced. Thus temperature-correction factors used in this study were investigated in greater detail using recent FWD center-deflection data. The BELLS3 equation was used to calculate pavement mid-depth temperature and the AASHTO method to correct pavement deflection to a standard temperature. This is referred to as Method II in this study. *Watson et al. (2004)* and *Chen et al. (2000)* equations have been used to calculate pavement mid-depth temperature and adjust center deflection to standard temperature, respectively. This correction method is referred to as method I in this study.

Results have been presented for the Kansas and US routes separately. Significant-difference tests have been done using the paired t-test. Finally, linear regression has been done using SAS, in which the FWD center deflection, using Method II (BELLS3 and AASHTO method), was taken as the dependent variable and Method I (Watson and Chen method) deflection as the independent variable. Effect of the pavement temperature-correction method on the FWD center deflection for Kansas and US routes (the same route in different Counties combined), different routes in the same county, and in the district have been completed and the results are in Appendix A.

4.2.3.1 Kansas Routes

Three of the center-deflection points are quite different from the rest of the data points and as a result, R^2 value is low for K-4 in Wabaunsee County as shown in Figure 4-8(a). K-31 in Osage and Wabaunsee Counties has higher slope and R^2 values that show the two temperature-correction methods give similar results for this project as shown in Figure 4-8(b) and (c), respectively. The slope is relatively low, which shows that Method II gives lower FWD center deflection ($FWDd_0$) as the center deflection increases in magnitude as shown in Figure 4-8(d).

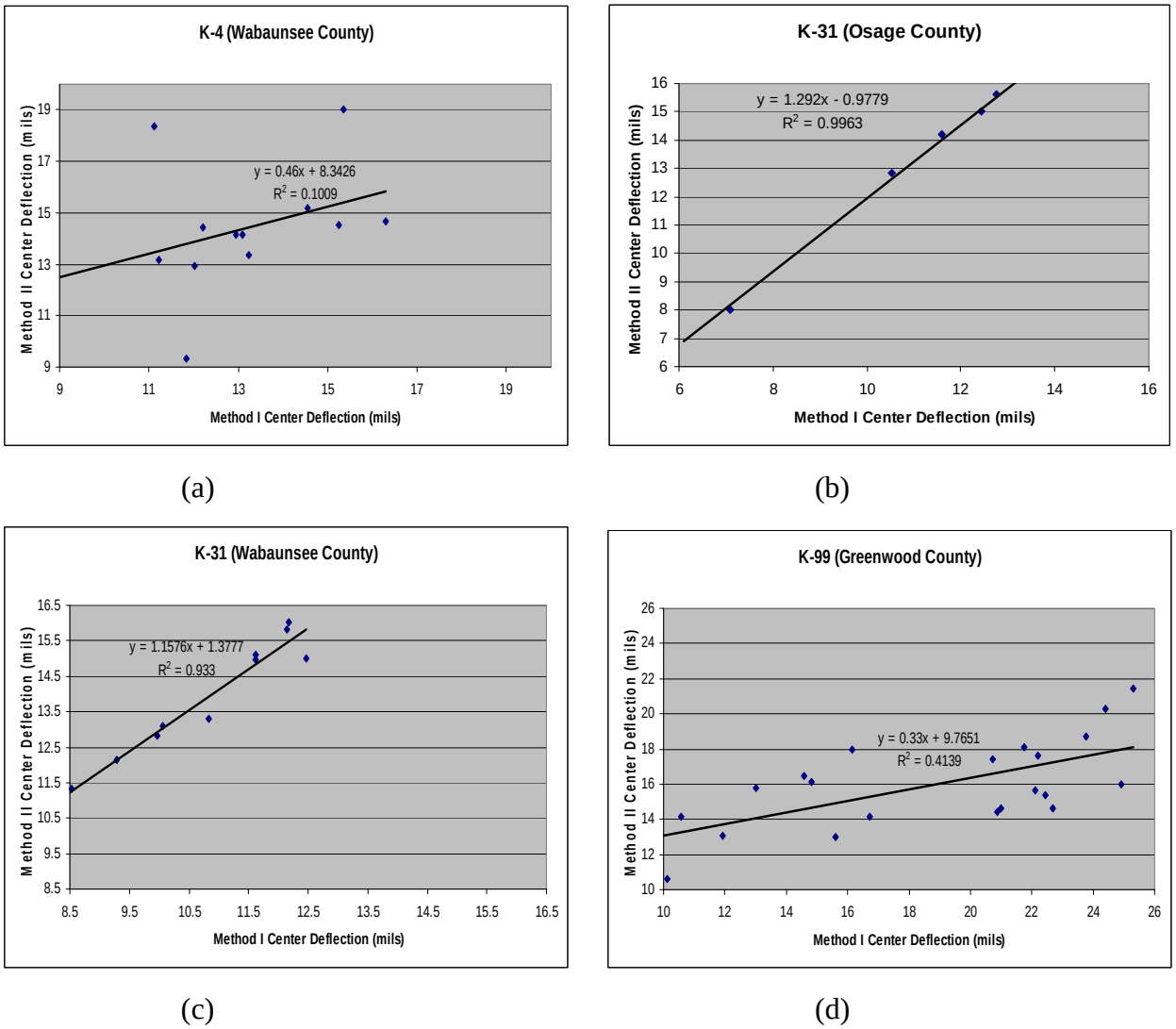

Figure 4-8 Effect of Temperature-Correction Method on $FWDd_0$ for K-4, K-31, and K-99

Temperature-correction Methods I and II show similar results with slope close to one and high R^2 value for K-99 in Lyon and Wabaunsee Counties, as shown in Figure 4-9(a) and (b). Temperature-correction Method II consistently shows higher center deflection than Method I with some scatter for K-170 in Lyon County as shown in Figure 4-9 (c). The two temperature-correction methods consistently show similar results for K-170 in Osage County as shown in Figure 4-9(d).

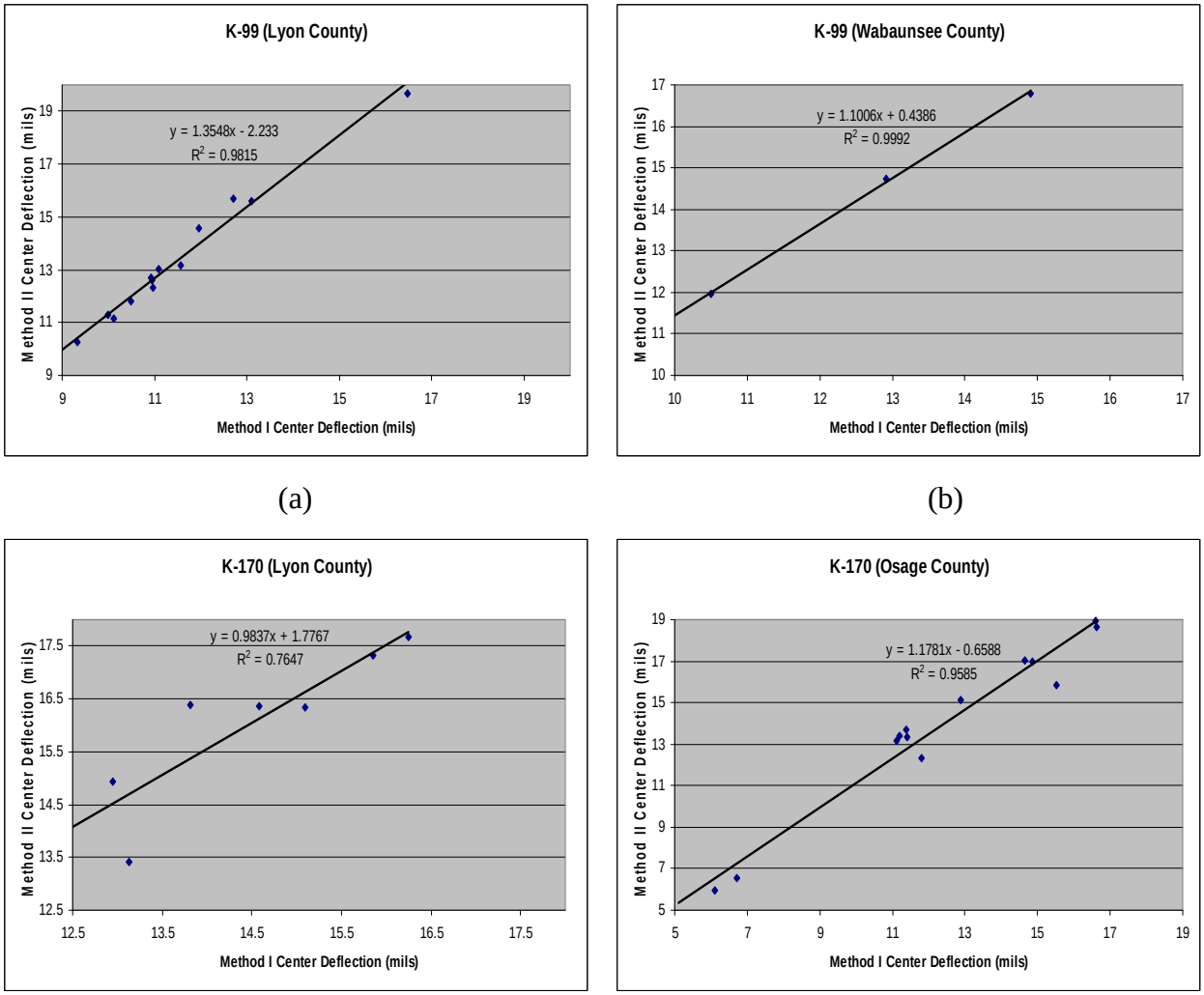

Figure 4-9 Effect of Temperature-Correction Method on $FWDd_0$ for K-99 and K-170

4.2.3.2 US Routes

Figure 4-10(a) shows nearly no linear relationship between the center deflections based on the two temperature-correction methods for US-54 in Greenwood County. Figure 4-10(b) shows good linear relationship, though temperature-correction Method II consistently gives slightly higher center deflections for US-54 in Woodson County. Center deflections using the two temperature-correction methods have linear relationships for US-56 in Morris County as shown in Figure 4-10(c). There is significant scatter in center deflection using the two correction methods for US-56 in Osage County as shown in Figure 4-10(d).

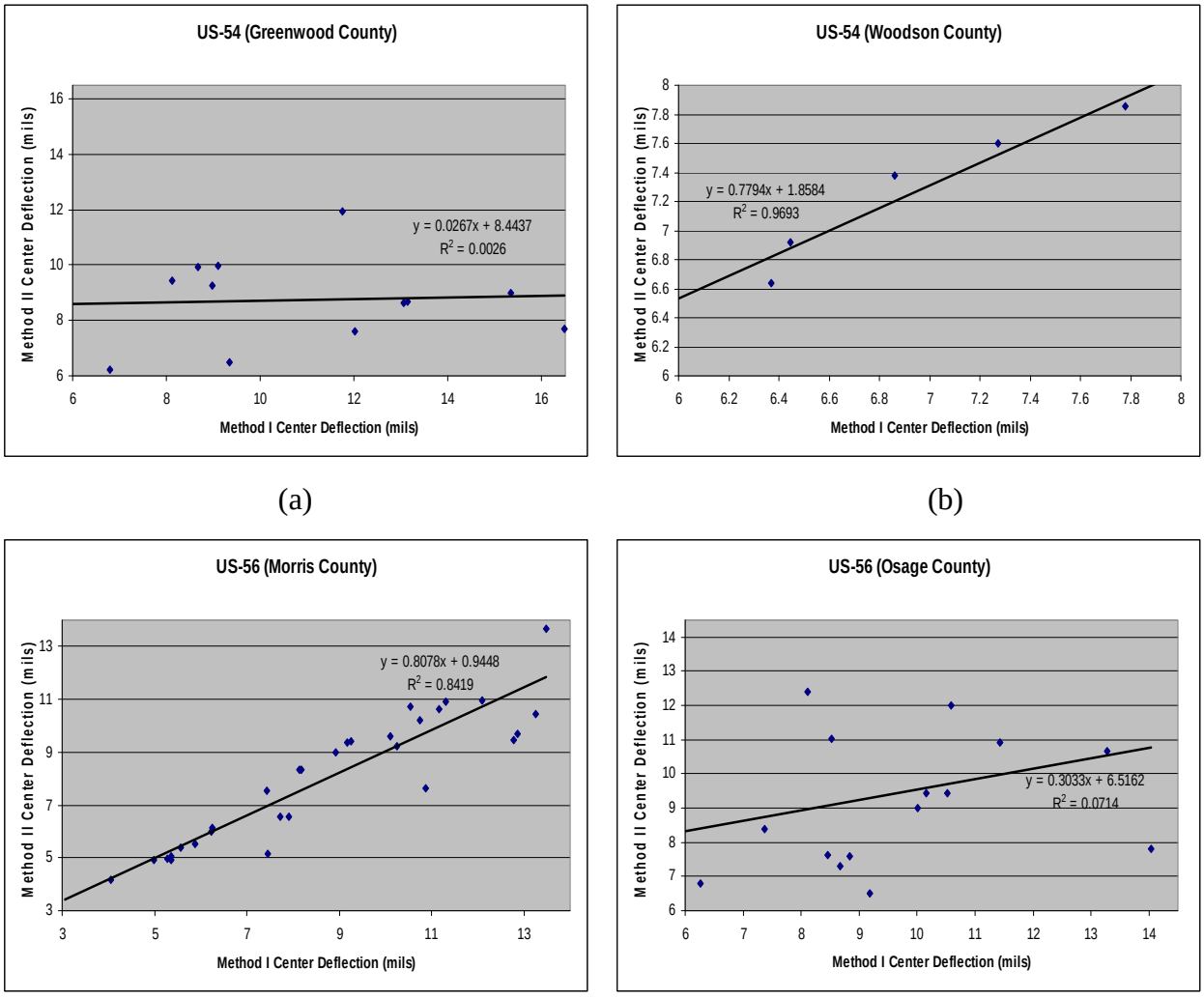

(a) (b)

(c) (d)

Figure 4-10 Effect of Temperature-Correction Method on $FWDd_0$ for US-54 and US-56

FWD center deflections using the two temperature-correction methods have a linear relationship for US-59 in Neosho County as shown in Figure 4-11(a). Very low slope shows that temperature-correction Method II gives significantly smaller center deflection than Method I for US-75 in Brown County as shown in Figure 4-11(b). Center deflections based on the two methods show a linear relationship for US-75 in Coffey and Jackson counties, though Method II shows smaller center deflection for US-75 in Coffey as shown in Figure 4-11(c) and (d).

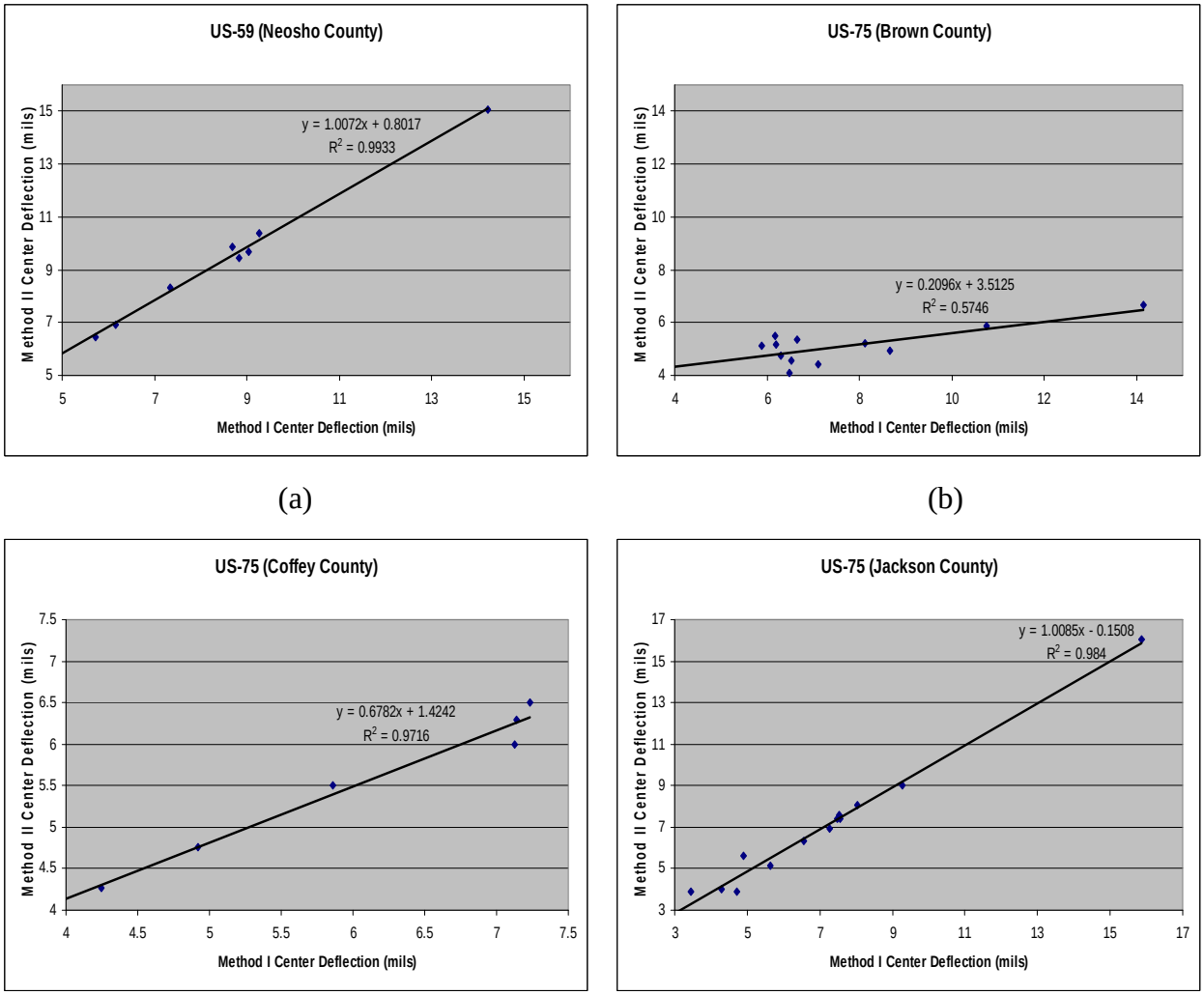

Figure 4-11 Effect of Temperature-Correction Method on FWDd_0 for US-59 and US-75

4.2.3.3 Significant-Difference Test

Figure 4-12 shows the effect of the two pavement temperature-correction methods on the FWD center deflection. Method II (BELLS3 and AASHTO) shows higher average FWD center deflections for all Kansas routes except K-99 in Greenwood County. Method I (Watson and Chen method) shows slightly higher average FWD center deflection for all US routes except for US-54 and US-75 in Woodson County and US-59 in Neosho County. Numerical values of average FWD center deflections are tabulated in Table 4-6.

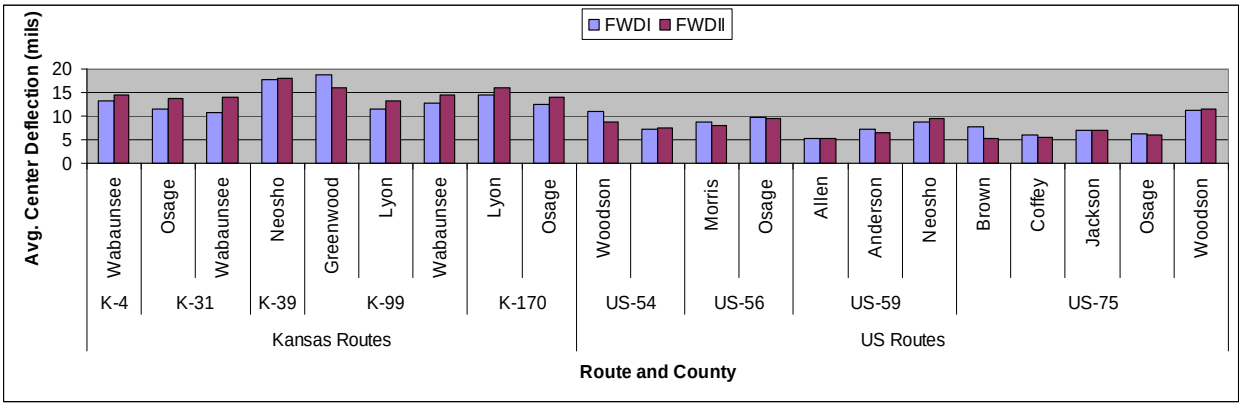

Figure 4-12 Effect of Temperature-Correction Method on Average $FWDd_0$

There is significant difference between the center deflections using the two temperature-correction methods for all Kansas routes except K-4 in Wabaunsee and K-39 in Neosho counties as shown Table 4-6(a). There is also significant difference for all US routes except US-56 in Osage County, US-59 in Allen County, and US-75 in Jackson and Osage counties as shown in Table 4-6(b). The reason why most sections show significant difference is that one temperature-correction method consistently shows higher center deflection than the other method. Temperature-correction Method II (BELLS3 and AASHTO) shows higher center deflection for nine out of 15 sections. It appears that Method I (Watson and Chen) results in higher center deflection for thicker sections whereas Method II (BELLS3 and AASHTO) results in higher center deflection for thinner sections. Method I (Watson and Chen) is easier to use and should be accurate enough for temperature correction at the network level.

Table 4-6 Significant-Difference Test for Effect of Temp.-Correction Method on $FWDd_0$

Route	County	Avg. d_0		Paired T-Test for Difference (I-II)					Length (mi)
		I	II	Lower	Mean	Upper	Pr>|t|	Similar	
(a) Kansas Routes									
K-4	Wabaunsee	13.26	14.44	-2.80	-1.18	0.44	0.14	Yes	12
K-31	Osage	11.45	13.82	-3.15	-2.37	-1.58	0.00	No	6
	Wabaunsee	10.87	13.96	-3.43	-3.09	-2.75	0.00	No	10
K-39	Neosho	17.73	18.11	-3.94	-0.38	3.19	0.41	Yes	2
K-99	Greenwood	18.84	15.98	1.12	2.86	4.61	0.00	No	21
	Lyon	11.51	13.37	-2.30	-1.85	-1.41	0.00	No	13
	Wabaunsee	12.78	14.50	-2.30	-1.72	-1.15	0.01	No	3
K-170	Lyon	14.52	16.06	-2.19	-1.54	-0.89	0.00	No	7
	Osage	12.38	13.92	-2.16	-1.55	-0.93	0.00	No	13
(b) US Routes									
US-54	Greenwood	11.07	8.74	0.20	2.33	4.45	0.03	No	12
	Woodson	7.24	7.50	-0.51	-0.26	-0.02	0.04	No	6
US-56	Morris	8.75	8.02	0.32	0.74	1.15	0.00	No	30
	Osage	9.75	9.47	-1.13	0.27	1.68	0.68	Yes	16
US-59	Allen	5.35	5.33	-0.24	0.02	0.29	0.84	Yes	8
	Anderson	7.35	6.59	0.49	0.75	1.02	0.00	No	15
	Neosho	8.66	9.52	-1.05	-0.86	-0.68	0.00	No	8
US-75	Brown	7.75	5.14	1.35	2.61	3.88	0.00	No	12
	Coffey	6.09	5.55	0.07	0.54	1.00	0.03	No	6
	Jackson	7.12	7.03	-0.15	0.09	0.33	0.44	Yes	13
	Osage	6.29	5.90	-1.36	0.39	2.15	0.57	Yes	5
	Woodson	11.18	11.43	-0.48	-0.25	-0.02	0.04	No	11

4.2.3.4 Linear Regression

There is a linear relationship between FWD center deflections using the two temperature-correction methods for all Kansas routes except K-4 in Wabaunsee County. Slope and R^2 value vary from 0.33 to 1.35 and 0.41 to 1.0, respectively, for Kansas routes as shown in Table 4-7(a).

There is a linear relationship for all US routes except three: US-54 in Greenwood County, and US-56 and US-75 in Osage County, as shown in Table 4-7(b). The slope and R^2 value vary from 0.21 to 1.01 and 0.57 to 0.98, respectively. Most of the projects show slope close to 1.0 and R^2 value greater than 0.90, which shows that FWD center deflection using one temperature-correction method can be calculated from another method with good accuracy.

Table 4-7 Linear Regression for Effect of Temperature-Correction Method on $FWDd_0$

Routes	County	Intercept	Slope	C.I.* for Slope			Linear Relation	R^2	Length (mi)
				Lower	Upper	Pr>|t|			
(a) Kansas Routes									
K-4	Wabaunsee	8.34	0.46	-0.51	1.43	0.31	No	0.10	12
K-31	Osage	-0.98	1.29	1.18	1.40	0.00	Yes	1.00	6
	Wabaunsee	1.38	1.16	0.90	1.41	0.00	Yes	0.93	10
K-99	Greenwood	9.77	0.33	0.14	0.52	0.00	Yes	0.41	21
	Lyon	-2.23	1.35	1.23	1.48	0.00	Yes	0.98	13
	Wabaunsee	0.44	1.10	0.70	1.51	0.02	Yes	1.00	3
K-170	Lyon	1.78	0.98	0.36	1.01	0.01	Yes	0.76	7
	Osage	-0.66	1.18	1.02	1.34	0.00	Yes	0.96	13
(b) US Routes									
US-54	Greenwood	8.44	0.03	-0.34	0.40	0.88	No	0.00	12
	Woodson	1.85	0.78	0.59	0.97	0.00	Yes	0.97	6
US-56	Morris	0.94	0.81	0.67	0.94	0.00	Yes	0.84	30
	Osage	6.52	0.30	-0.32	0.93	0.32	No	0.07	16
US-59	Allen	0.07	0.98	0.61	1.35	0.00	Yes	0.88	8
	Anderson	-0.79	1.01	0.88	1.13	0.00	Yes	0.96	15
	Neosho	0.80	1.01	0.92	1.09	0.00	Yes	0.99	8
US-75	Brown	3.51	0.21	0.08	0.34	0.00	Yes	0.57	12
	Coffey	1.42	0.68	0.52	0.84	0.00	Yes	0.97	6
	Jackson	-0.15	1.01	0.92	1.09	0.00	Yes	0.98	13
	Osage	3.20	0.43	-0.12	0.98	0.10	No	0.67	5
	Woodson	-0.50	1.07	0.95	1.19	0.00	Yes	0.98	11

4.2.4 Frequency of Deflection Measurement Using FWD Center Deflection

FWD data collected on the study sections from 1998 to 2006 were used to find the frequency of deflection measurements at the network level. For each section under study, FWD data was analyzed and compared for two test years. Test intervals varied from four to five years. Normalized FWD center deflection over the years was used to determine frequency of deflection measurements at the network level. Temperature-correction Method I (Watson and Chen) has been used. There were rehabilitation actions between the two test years for some of the projects, and analysis was done separately. Paired t-tests have been used for significant-difference test at the 5% level of significance. Linear regression has also been done using recent FWD center deflection as the dependent variable and the earliest FWD center deflection as the independent variable. Results for some of the projects are detailed in Appendix A.

4.2.4.1 Without Rehabilitation Actions

FWD center deflections in 1999 and 2003 are linearly related for US-54 in Woodson County as shown in Figure 4-13(a). Figure 4-13(b) shows some scatter, and R^2 value of 0.34 is also relatively low for US-59 in Allen County. There is no change in FWD center deflection for both projects.

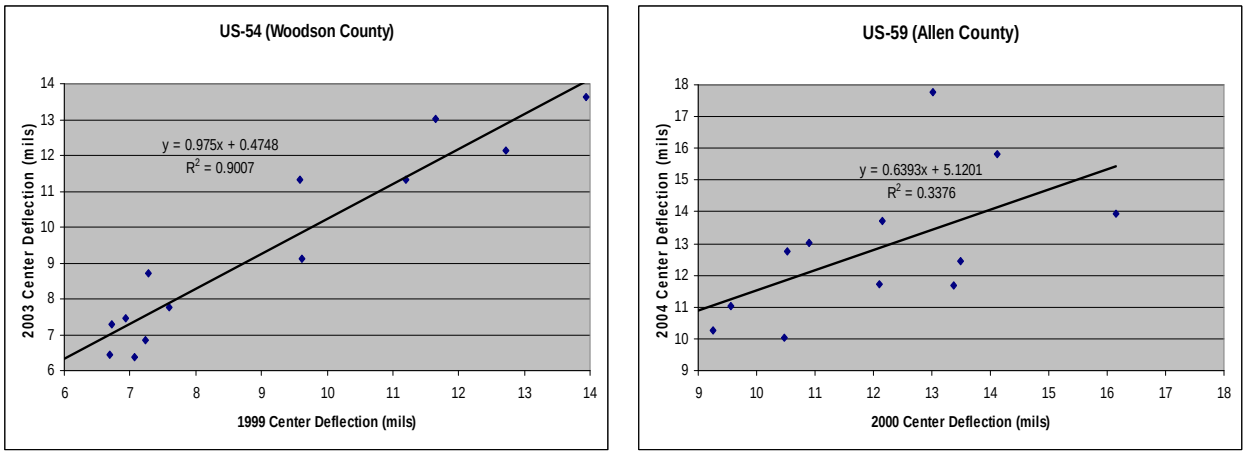

(a) (b)

Figure 4-13 FWD Center Deflections over Years for US-54 and US-59

FWD center deflection in 2003 is higher than the data in 1999 in some cases and vice versa, as shown in Figure 4-14(a). FWD center deflection in 2003 is lower than the data in 1999, and the slope is negative contrary to engineering expectations as shown in Figure 4-14(b). It might be due to localized rehabilitation action that was not included in the database. FWD center deflection in 1999 is nearly the same as in 2003 as shown in Figure 4-14(c) and as a result, R^2 value is close to zero. US-75 in Jackson County shows some scatter as shown in Figure 4-14(d).

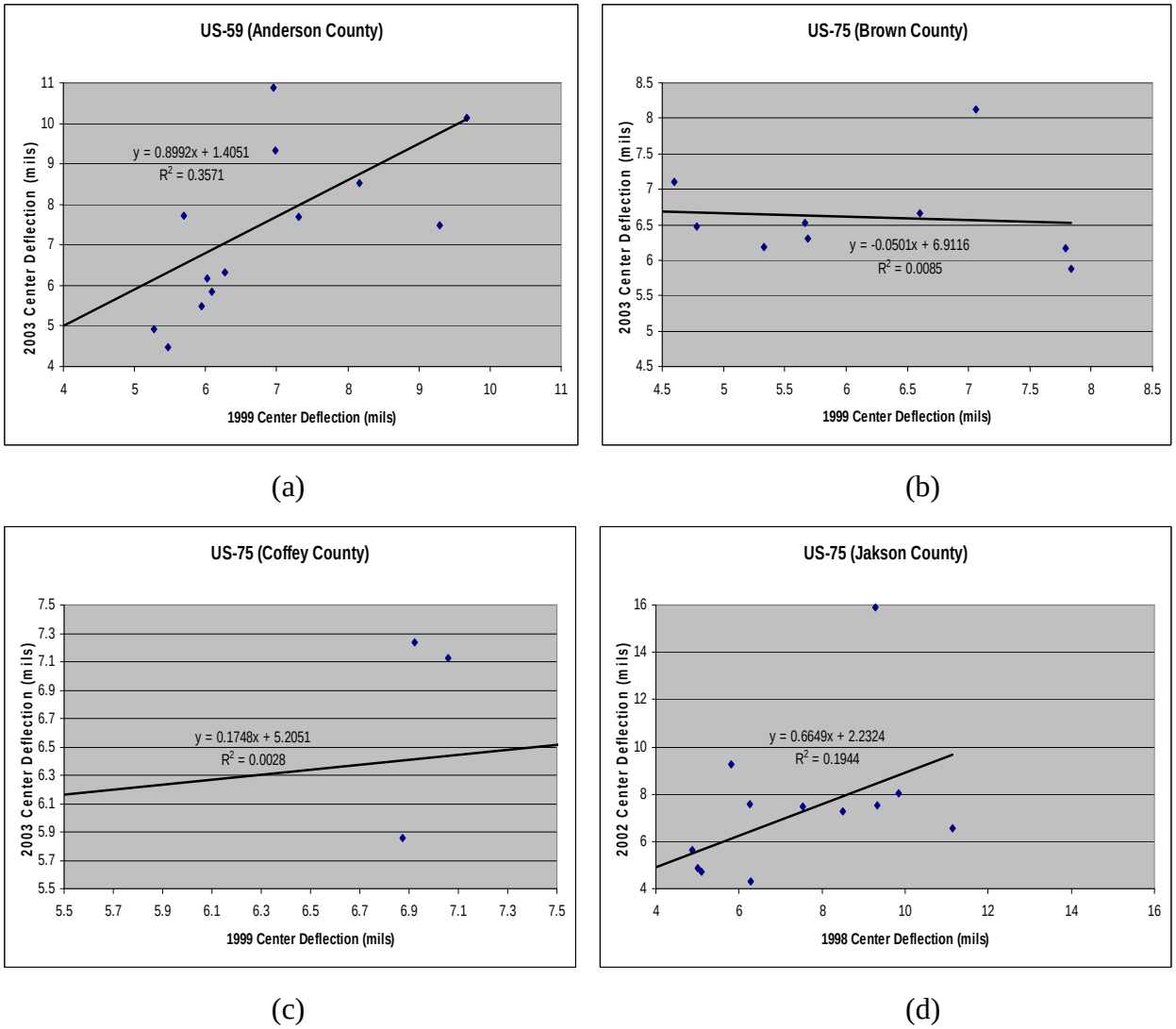

Figure 4-14 FWD Center Deflections over Years for US-59 and US-75

4.2.4.2 With Rehabilitation Actions

FWD center deflection in 2003 is clearly less than the data in 1999 for K-31 in Wabaunsee County and the data in 1998 for K-99 in Lyon County, as shown in Figure 4-15(a) and (b) due to rehabilitation action. FWD center deflections in 1999 and 2004 are related negatively for K-170 in Lyon County, as shown in Figure 4-15(c). There is no significant reduction in center deflection due to rehabilitation action for K-170 in Osage County as shown in Figure 4-15(d).

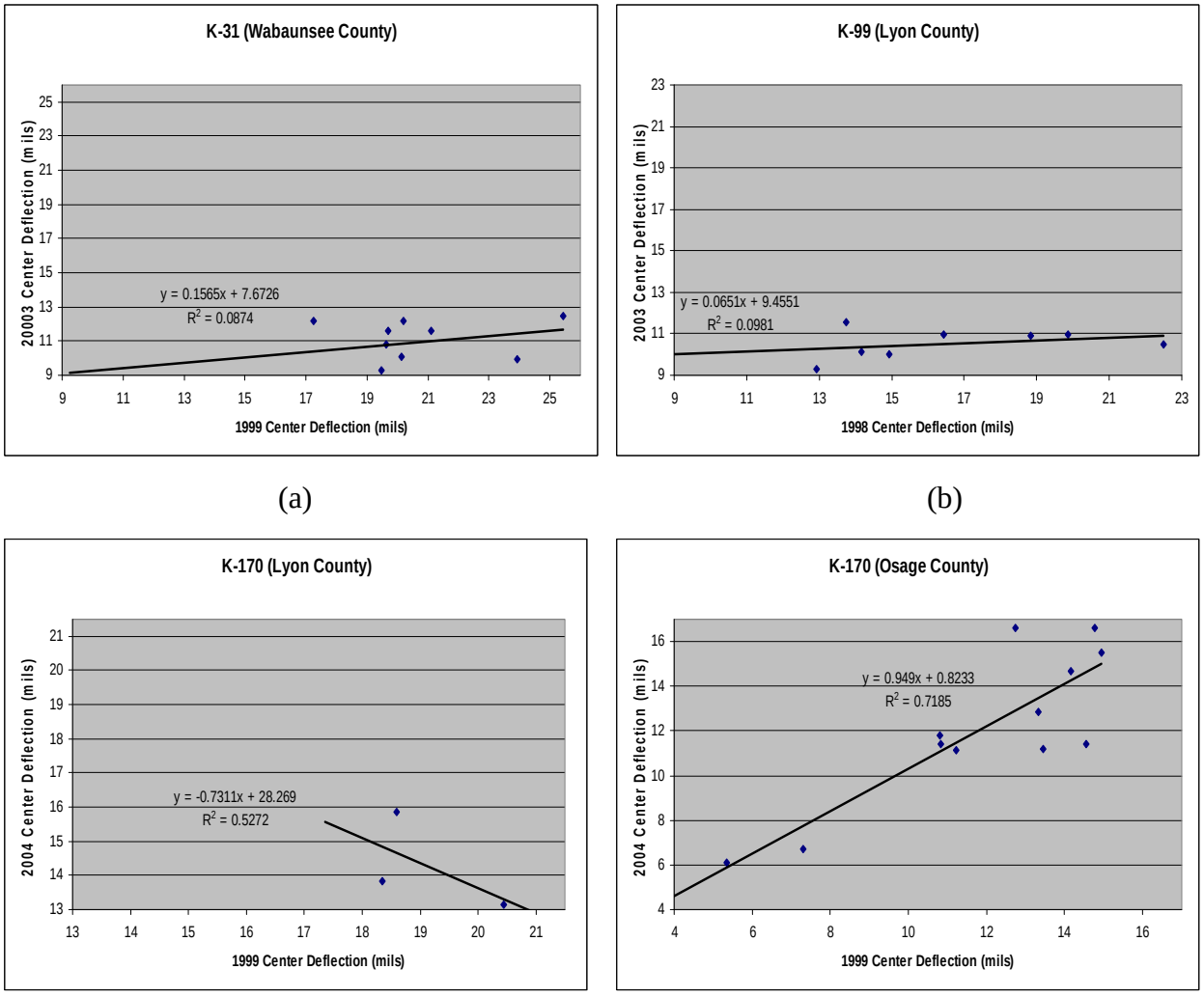

Figure 4-15 FWD Center Deflection over Years for K-31, K-99, and K-170

FWD center deflection in 2004 is slightly lower than the data in 1999 for US-56 in Morris County due to rehabilitation action as shown in Figure 4-16(a). FWD center deflection in 2005 remains more or less constant as the FWD center deflection in 2001 increases for US-56 in Osage County as shown in Figure 4-16(b).

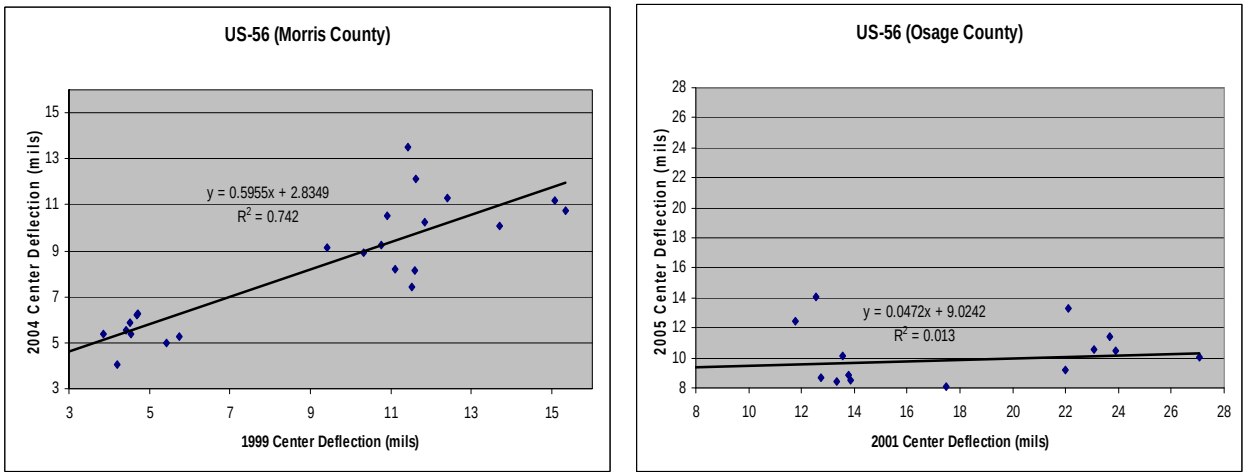

(a) (b)

Figure 4-16 FWD Center Deflection over Years for US-56

4.2.4.3 Significant-Difference Test

Figure 4-17 shows average FWD center deflection remains more or less constant over the two test years for routes without rehabilitation action. Figure 4-17 shows a significant reduction in FWD center deflection for most of the routes which had rehabilitation actions between the two test years. Table 4-8 shows the numerical values of average FWD center deflections over the two years.

Table 4-8(a) shows no significant difference in FWD center deflection over the two test years for the projects without rehabilitation action. Table 4-8(b) shows a significant difference in FWD center deflection for all projects with rehabilitation action except, for K-170 in Osage County and US-56 in Morris County. No rehabilitation was done on K-4 in Wabaunsee County, and the mean center deflections on this project after five years were not significantly different. No significant difference in mean center deflections was observed for four years for six other projects. It appears that network-level deflection data may be collected at five-year intervals when there is no structural rehabilitation.

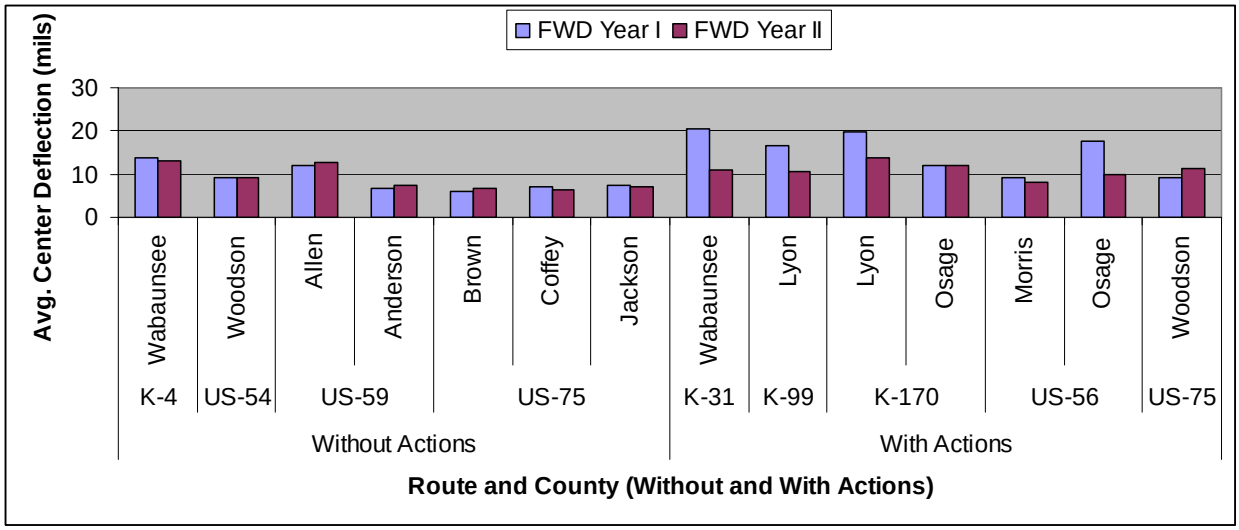

Figure 4-17 Average FWD Center Deflection over Years

Table 4-8 Significant-Difference Test for FWD Center Deflection over Years

Routes	County	Avg. d_0		Paired T-Test for Difference(FWD-RWD)					Length (mi)
		FWD	RWD	Lower	Mean	Upper	Pr>|t|	Similar	
(a) Without Rehabilitation Actions									
K-4	Wabaunsee	13.93	12.90	-1.27	1.03	3.34	0.31	Yes	7
US-54	Woodson	9.10	9.34	-0.75	-0.25	0.25	0.30	Yes	13
US-59	Allen	12.09	12.85	-2.01	-0.76	0.50	0.21	Yes	12
	Anderson	6.61	7.35	-1.76	-0.74	0.28	0.14	Yes	15
US-75	Brown	6.15	6.60	-1.57	-0.45	0.66	0.37	Yes	9
	Coffey	7.15	6.46	-0.62	0.70	2.01	0.22	Yes	5
	Jackson	7.35	7.12	-1.52	0.23	1.98	0.78	Yes	13
(b) With Rehabilitation Actions									
K-31	Wabaunsee	20.44	10.87	7.77	9.56	11.37	<.0001	No	10
K-99	Lyon	16.68	10.54	3.42	6.14	8.85	0.00	No	8
K-170	Lyon	19.60	13.94	1.73	5.67	9.60	0.02	No	4
	Osage	11.96	12.17	-1.36	-0.21	0.94	0.69	Yes	12
US-56	Morris	9.09	8.25	-0.05	0.84	1.74	0.06	Yes	23
	Osage	17.74	9.86	5.04	7.88	10.72	<.0001	No	16
US-75	Woodson	9.10	11.18	-3.53	-2.08	-0.62	0.01	No	11

4.2.4.4 Linear Regression

Table 4-9(a) shows a linear relationship between FWD center deflections over the two test years for only three projects without rehabilitation action: US-54 in Woodson County, and US-59 in Allen and Anderson counties. Table 4-9(b) shows that FWD center deflections over the two test years have linear relationships for K-170 in Osage County and US-56 in Morris County. These projects also have relatively high slope and R^2 values, though they were rehabilitated in between the two test years. Slope and R^2 value vary from 0.64 to 0.90 and 0.34 to 0.90, respectively, for those projects which show linear relations.

Table 4-9 Linear Regression for Frequency of Deflection Measurement Using Deflection

Route	County	Inter-cept	Slope	C.I.* for Slope		Pr>|t|	Linear Relation	R^2	Length (mi)
				lower	upper				
(a) Without Rehabilitation Actions									
K-4	Wabaunse	8.29	0.33	-0.39	1.05	0.29	No	0.22	7
US-54	Woodson	0.47	0.98	0.76	1.19	0.00	Yes	0.90	13
US-59	Allen	5.12	0.64	0.01	1.27	0.04	Yes	0.34	12
	Anderson	1.41	0.90	0.18	1.62	0.02	Yes	0.36	15
US-75	Brown	6.91	-0.05	-0.53	0.43	0.81	No	0.01	9
	Coffey	5.21	0.17	-5.85	6.20	0.93	No	0.00	5
	Jackson	2.23	0.66	-0.23	1.56	0.13	No	0.19	13
(b) With Rehabilitation Actions									
K-31	Wabaunse	7.67	0.16	-0.26	0.57	0.41	No	0.09	10
K-99	Lyon	9.46	0.07	-0.13	0.26	0.45	No	0.10	8
K-170	Lyon	28.27	-0.73	-2.84	1.38	0.27	No	0.53	4
	Osage	0.82	0.95	0.53	1.37	0.00	Yes	0.72	12
US-56	Morris	2.83	0.60	0.44	0.75	0.00	Yes	0.74	23
	Osage	9.02	0.05	-0.19	0.28	0.67	No	0.01	16
US-75	Woodson	7.40	0.41	-0.19	1.02	0.16	No	0.21	11

* confidence interval for slope at 95% confidence level

4.2.5 Measured and Calculated Pavement Temperature

Pavement temperature at mid-depth of surface, binder, and base layers was measured seven times from June 2005 to April 2007 for the four experimental sections on US-75. Three equations were used to calculate mid-depth pavement temperature: *Leland et al. (1992)* and *BELLS3*, and *Watson et al. (2004)*. The three equations are (2.19), (2.23), and (2.22). Three of the seven pavement temperature-measurement sessions are discussed in this section: one in spring, one in summer, and one in fall. Results for the rest have been included in Appendix A.

4.2.5.1 Spring 2006

Mid-depth pavement temperatures for the surface layer in ascending order: BELLS3, Watson, Leland and measured method for all sections except Section 1. In Section 1, the Watson method shows the lowest value as shown in Figure 4-18. Watson, Leland, BELLS3 and measured method show the lowest to highest mid-depth pavement temperatures for the binder and base layers for Sections 1 and 2, as shown in Figure 4-18(a) and (b). Leland and BELLS3 switch positions in the binder layer for Section 2. BELLS3, Watson, Leland, and measured method show the lowest to the highest mid-depth temperature for Section 3 whereas BELLS3 and Leland switch positions for Section 3 for the binder layer as shown in Figure 4-18(c) and (d). For the base layer, the lowest to the highest mid-depth temperature is shown by Watson, BELLS3, Leland, and measured method as shown in Figure 4-18(c) and (d).

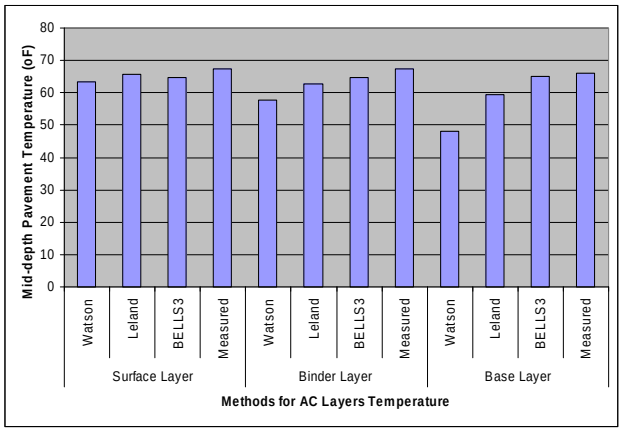

(a) Section 1

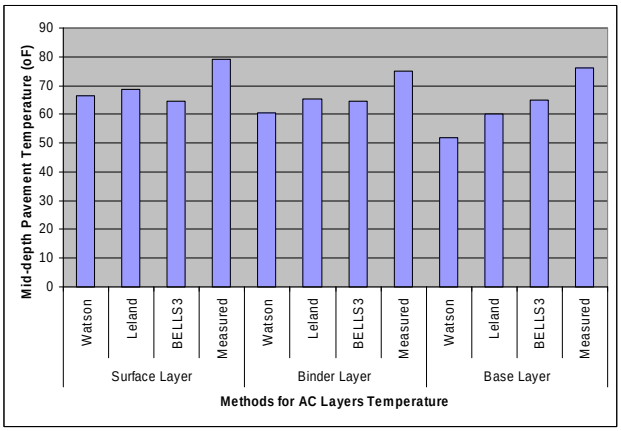

(b) Section 2

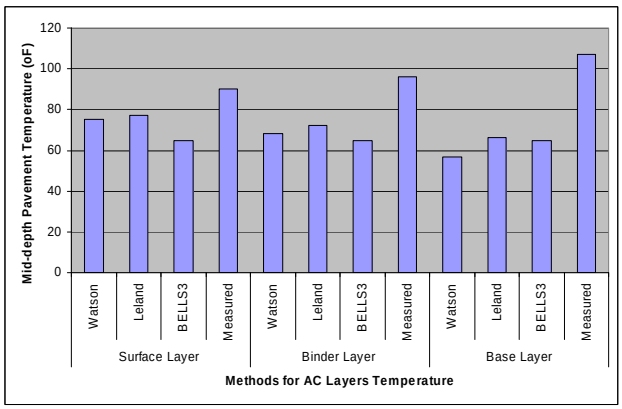

(c) Section 3

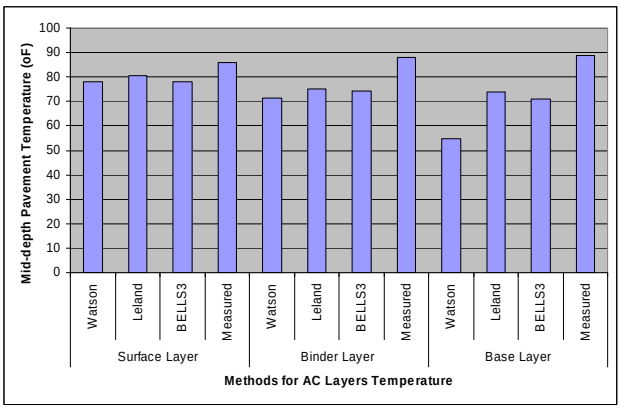

(d) Section 4

Figure 4-18 Pavement Temperature for Experimental Sections (Test Date: 04/13/2006)

4.2.5.2 Summer 2006

Pavement temperature was not measured on Section 3 and comparison was made only for calculated pavement temperatures. The lowest to the highest mid-depth pavement temperatures were obtained from BELLS3, Watson, Leland, and measured method for all sections for the surface layer as shown in Figure 4-19. The order changes to Watson, Leland, BELLS3, and measured method for all sections for the binder and base layers as shown in Figure 4-19. When the pavement surface temperature is high, BELLS3 and measured mid-depth pavement temperatures are close for the binder and base layers. Pavement temperature decreases with depth when the pavement surface temperature is high.

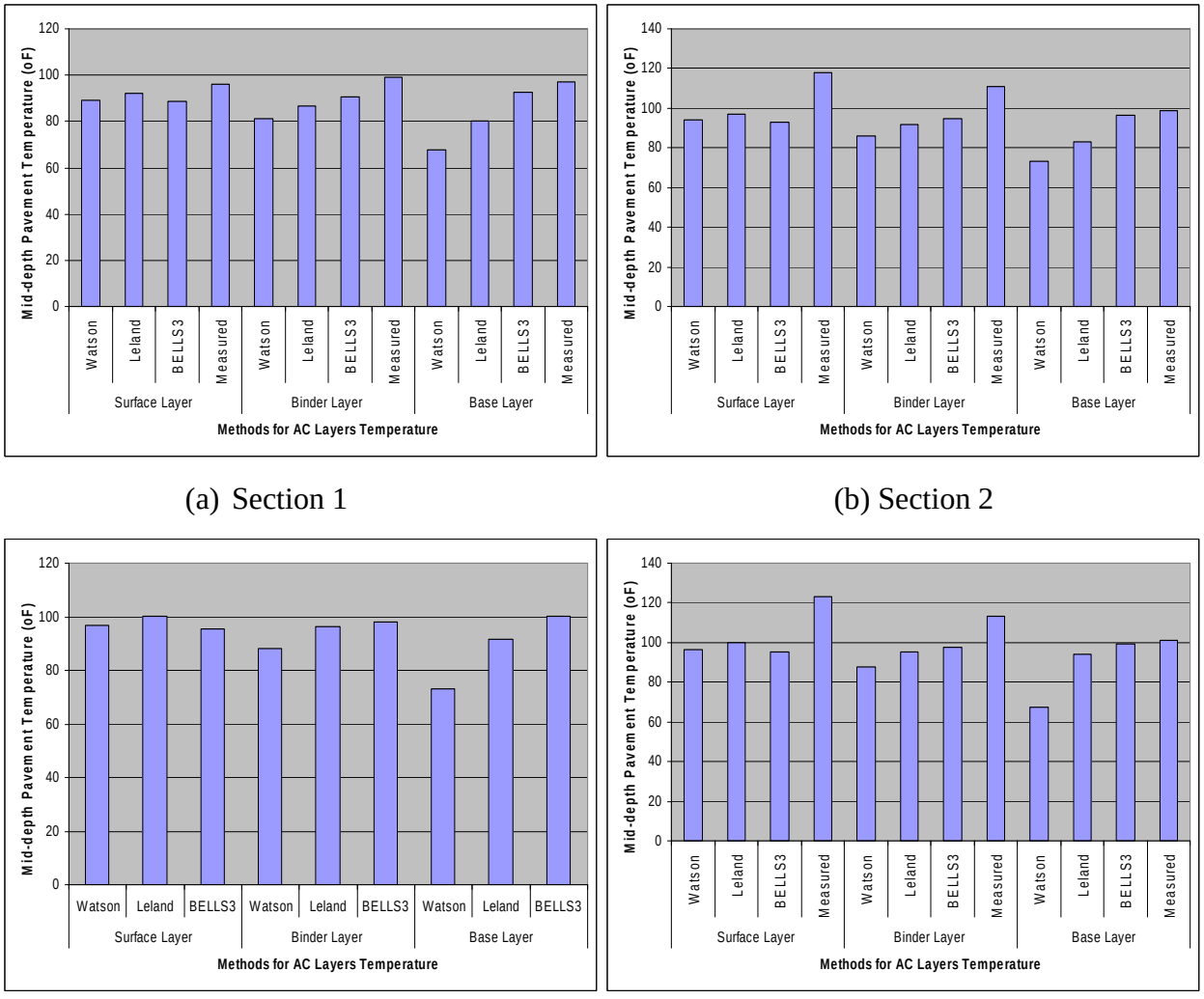

(a) Section 1 (b) Section 2

(c) Section 3 (d) Section 4

Figure 4-19 Pavement Temperature for Experimental Sections (Test Date: 8/1/2006)

4.2.5.3 Fall 2006

Surface and mid-depth temperature data were collected in October 2006. Watson, Leland, BELLS3, and measured method show the lowest to the highest mid-depth temperatures for Sections 1, 3, and 4 in all layers as shown in Figure 4-20(a), (c), and (d). BELLS3, Watson, Leland, and measured method show the lowest to the highest mid-depth pavement temperatures for Section 2 for the surface layer as shown in Figure 4-20(b). The order changes to Watson, Leland, measured, and BELLS3 method for the binder and base layers. The variation of calculated mid-depth temperature is highest for the base layers for all sections as shown in Figure 4-20.

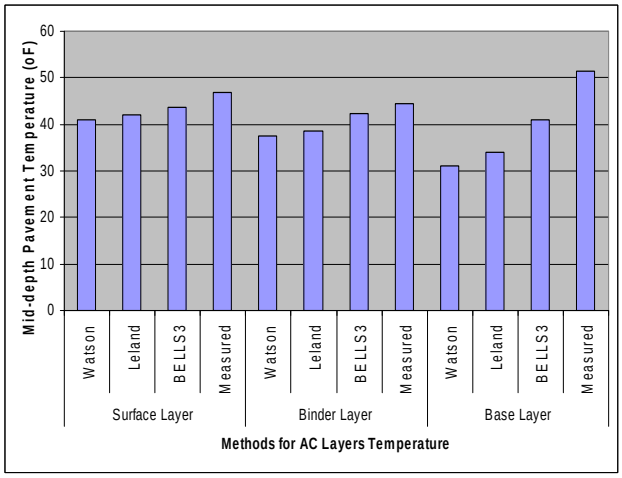

(a) Section 1

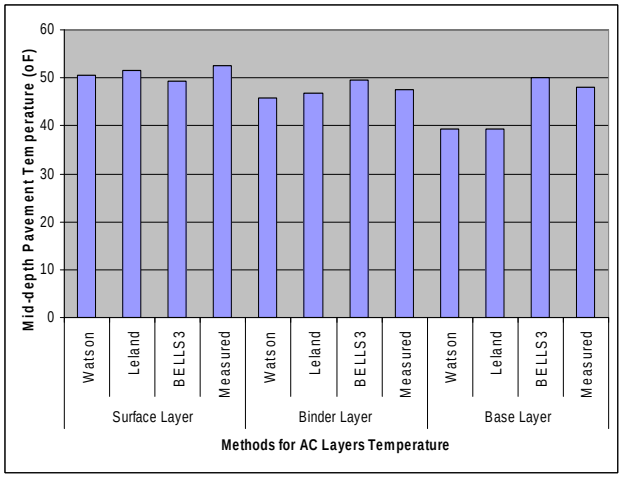

(b) Section 2

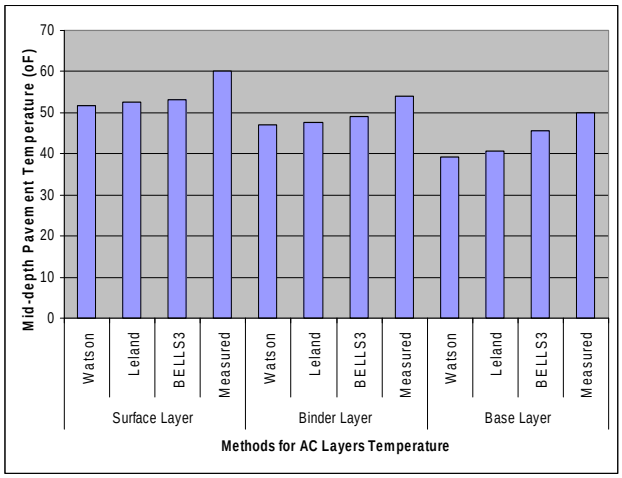

(c) Section 3

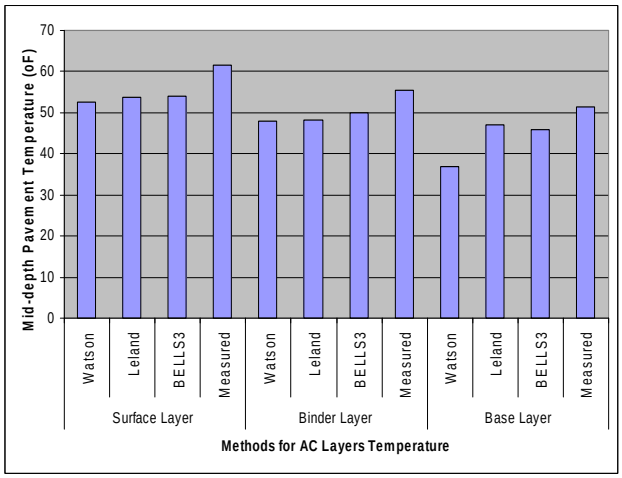

(d) Section 4

Figure 4-20 Pavement Temperature for Experimental Sections (Test Date: 10/13/2006)

4.2.5.4 Significant-Difference Test

Average mid-depth pavement temperature was calculated based on mid-depth thickness and mid-depth temperature for surface, binder, and base layers using Odemark's equation. Figure 4-21 is based on pavement surface and mid-depth data collected in April 2006, August 2006, and October 2006. Data was not collected on Section 3 in August 2006. Watson, Leland, BELLS3, and measured method show the lowest to highest average mid-depth pavement temperatures for Sections 1 and 2 as shown in Figure 4-21(a); for all sections as shown in Figure 4-21(b); and for Sections 1 and 3 as shown in Figure 4-21(c). Watson, BELLS3, Leland, and measured mid-depth pavement temperatures are lowest to the highest for Sections 3 and 4 as shown in Figure 4-21(a), and Section 4 as shown in Figure 4-21(c). In general, BELLS3 gives the mid-depth pavement temperature that is closest to the measured one, and it is recommended this method be used when there is no measured mid-depth pavement temperature.

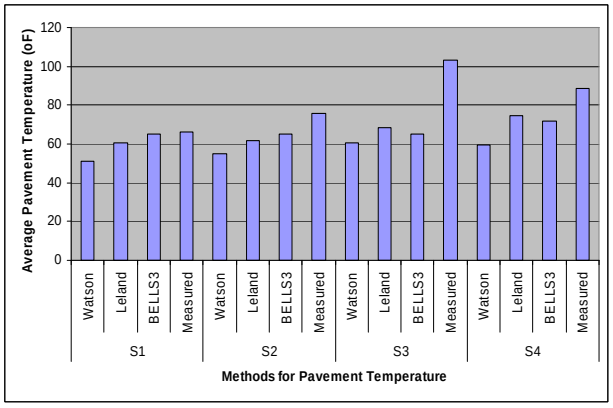

(a) Test Date:04/13/2006

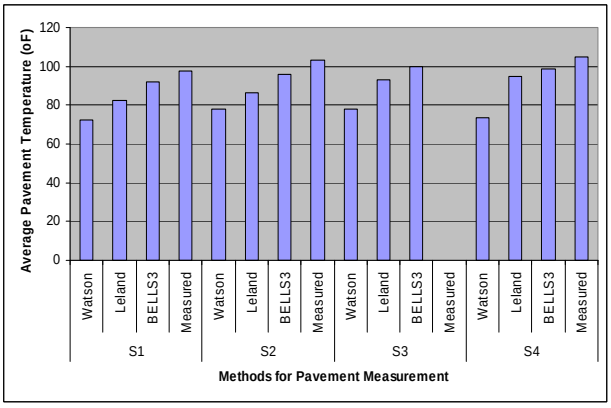

(b) Test Date:08/01/2006

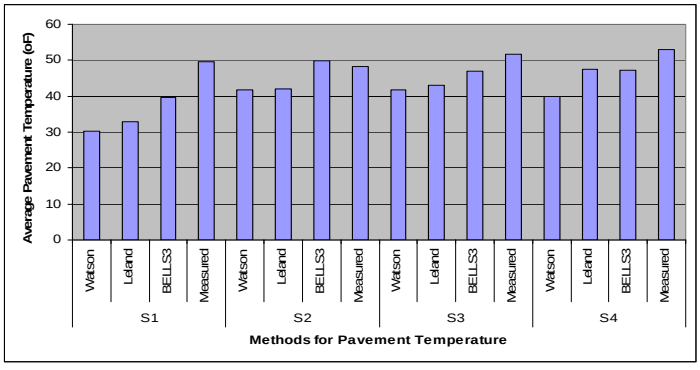

(c) Test Date: 10/13/2006

Figure 4-21 Average Calculated and Measured Mid-Depth Pavement Temperatures

Significant-difference tests were done using the paired t-test. There is a significant difference between the calculated and measured mid-depth pavement temperatures for all sections as shown in Table 4-10. BELLS3 equation gives results closest to the measured mid-depth pavement temperatures from a practical point of view.

Table 4-10 Significant-Difference Tests for Mid-Depth Pavement Temperatures

Test Date	Compare		Section 1		Section 2		Section 3		Section 4	
	Method	Method	Pr>|t|	Simi-lar	Pr>|t|	Simi-lar	Pr>|t|	Simi-lar	Pr>|t|	Simi-lar
4/13/06	Watson	Leland	0.00	No	0.00	No	0.00	No	0.00	No
		BELLS3	0.00	No	0.00	No	0.00	No	0.00	No
		Measured	0.00	No	0.00	Yes	0.00	No	0.00	No
	Leland	BELLS3	0.00	No	0.00	No	0.00	No	0.00	No
		Measured	0.00	No	0.00	No	0.00	No	0.00	No
	BELLS3	Measured	0.00	No	0.00	No	0.00	No	0.00	No
8/1/06	Watson	Leland	0.00	No	0.00	No	0.00	No	0.00	No
		BELLS3	0.00	No	0.00	No	0.00	No	0.00	No
		Measured	0.00	No	0.00	No	-	-	0.00	No
	Leland	BELLS3	0.00	No	0.00	No	0.00	No	0.00	No
		Measured	0.00	No	0.00	No	-	-	0.00	No
	BELLS3	Measured	0.00	No	0.00	No	-	-	0.00	No
10/13/06	Watson	Leland	0.00	No	0.01	No	0.00	No	0.00	No
		BELLS3	0.00	No	0.00	No	0.00	No	0.00	No
		Measured	0.00	No	0.00	No	0.00	No	0.00	No
	Leland	BELLS3	0.00	No	0.00	No	0.00	No	0.01	No
		Measured	0.00	No	0.00	No	0.00	No	0.00	No
	BELLS3	Measured	0.00	No	0.00	No	0.00	No	0.00	No

4.3 Pavement Structural Capacity

Normalized and temperature-corrected pavement deflection has been used to compute effective structural number (SNeff) using the AASHTO method (*AASHTO, 1993)*. Comparison of effective structural number (SNeff) from FWD and RWD deflections, effect of temperature-correction method on SNeff, and frequency of deflection measurements at network level using SNeff have been discussed in this section. Later SNeff obtained from the AASHTO method has also been compared to SNeff computed using a current KDOT algorithm.

It is to be noted that RWD measures deflection only under the load. This means only center deflection data is available. However, during existing pavement modulus computation from Equation (2.30), knowledge of the subgrade modulus is necessary. Since subgrade modulus of an existing pavement remains relatively unchanged *(Croney and Croney, 1991; Khogali and Anderson, 1996; Hossain et al., 2000)*, subgrade modulus can be obtained from previous FWD data or alternative means such as the California bearing ratio (CBR) tests, dynamic cone penetration (DCP) or based upon the plasticity index (PI) and gradation.

4.3.1 FWD and RWD SNeff

Temperature-corrected RWD deflection in 2006 and FWD deflection (normalized and temperature corrected) from 1998 to 2006 have been used to compute SNeff. Comparison has been made for experimental sections, the routes without and with rehabilitation actions.

4.3.1.1 Experimental Sections

FWD and RWD SNeff are negatively related for the perpetual pavement Section 1 as shown in Figure 4-22(a). Figure 4-22(b) shows some scatter, and low slope and R^2 value for Section 2. The relationship between FWD and RWD SNeff for Section 3 is insignificant as shown in Figure 4-22(c). There is a weak linear relationship between FWD and RWD SNeff for Section 4 as shown in Figure 4-22(d). In general, there is a weak or negative linear relationship between FWD and RWD SNeff for all sections in contrast to the FWD and RWD center deflections. This may be due to the effect of variables used to calculate SNeff other than center deflection.

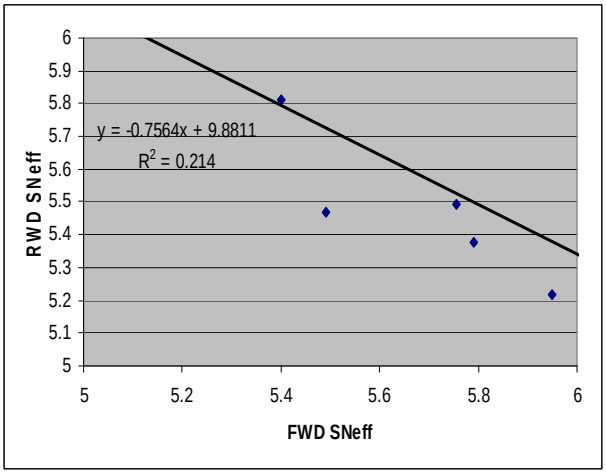

(a) Section 1

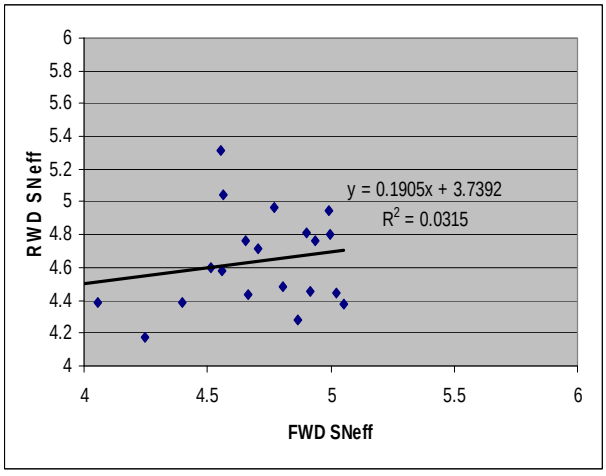

(b) Section 2

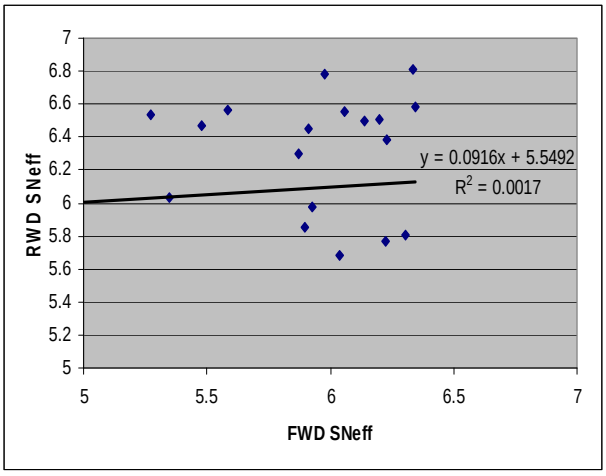

(c) Section 3

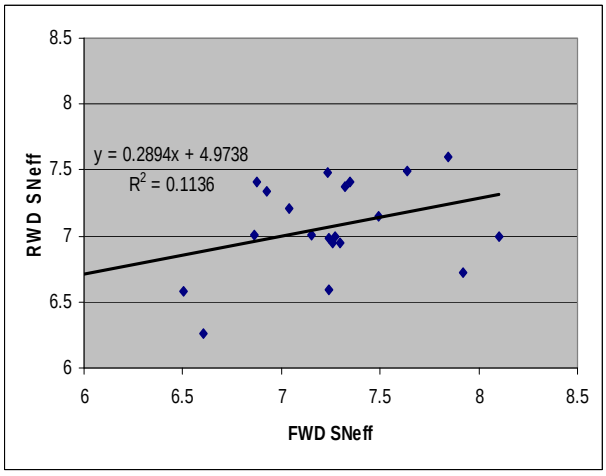

(d) Section 4

Figure 4-22 FWD and RWD SNeff for Experimental Sections

4.3.1.2 Without Rehabilitation Actions

FWD and RWD SNeff have a poor linear relationship with scattered results, low slope, and R^2 value for US-59 in Anderson County, and US-75 in Brown, Coffey, and Jackson counties as shown in Figure 4-23. Low slope is evident for low RWD SNeff as FWD SNeff increases. The R^2 value is very low as well.

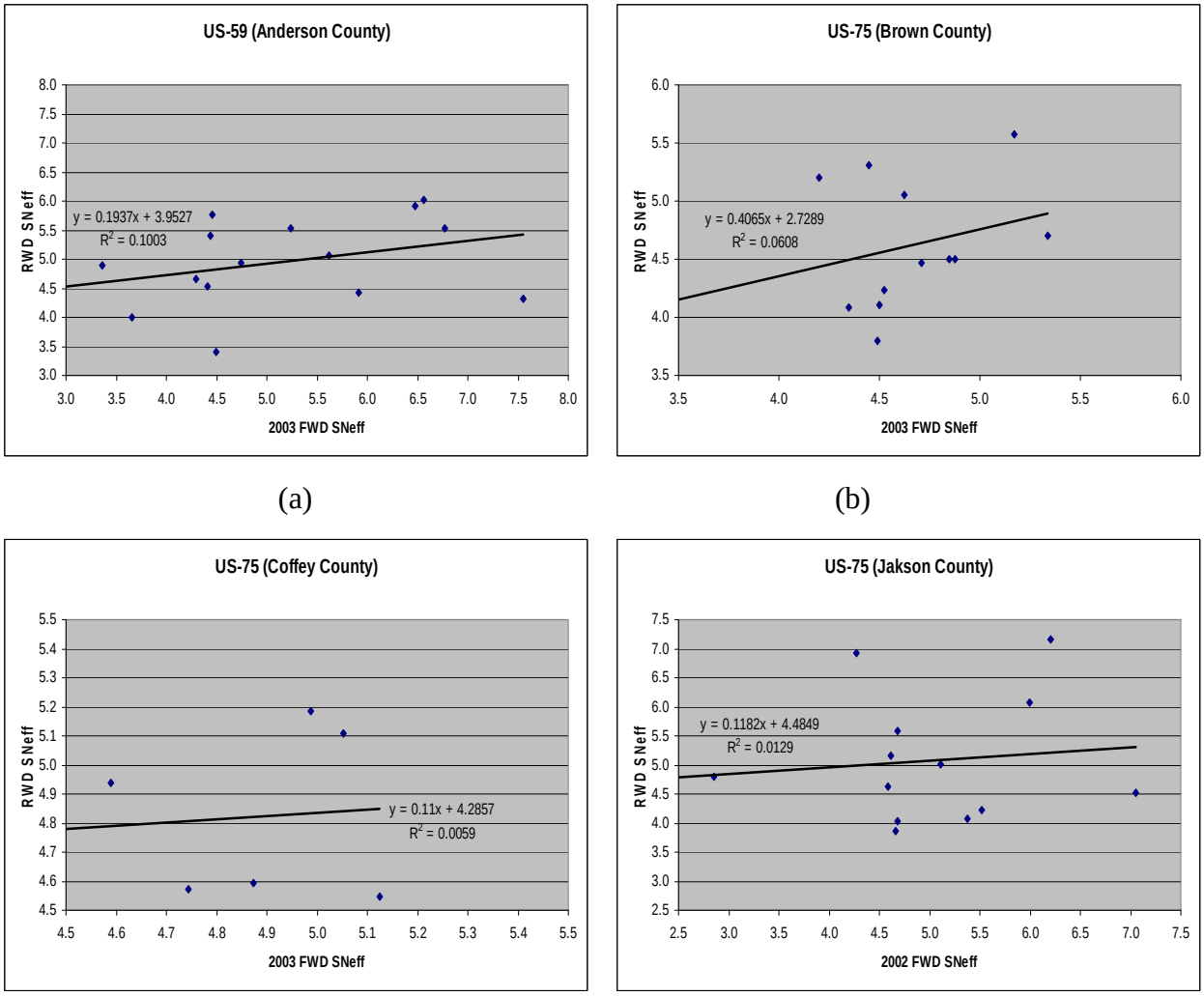

Figure 4-23 FWD and RWD SNeff for US-59 and US-75

4.3.1.3 With Rehabilitation Actions

FWD and RWD SNeff have a very good linear relationship and one can be predicted from the other with reasonably high accuracy for K-31 in Osage County as shown in Figure 4-24(a). FWD and RWD SNeff for K-31 in Wabaunsee have a low negative slope and R^2 value in contrast to the FWD and RWD center-deflection relationship as shown in Figure 4-24(b). The slope for K-99 in Lyon County is fairly high, but the R^2 value is low due to the scatter in data points as shown in Figure 4-24(c). FWD and RWD SNeff are also poorly related for K-99 in Wabaunsee County as shown in Figure 4-24(d).

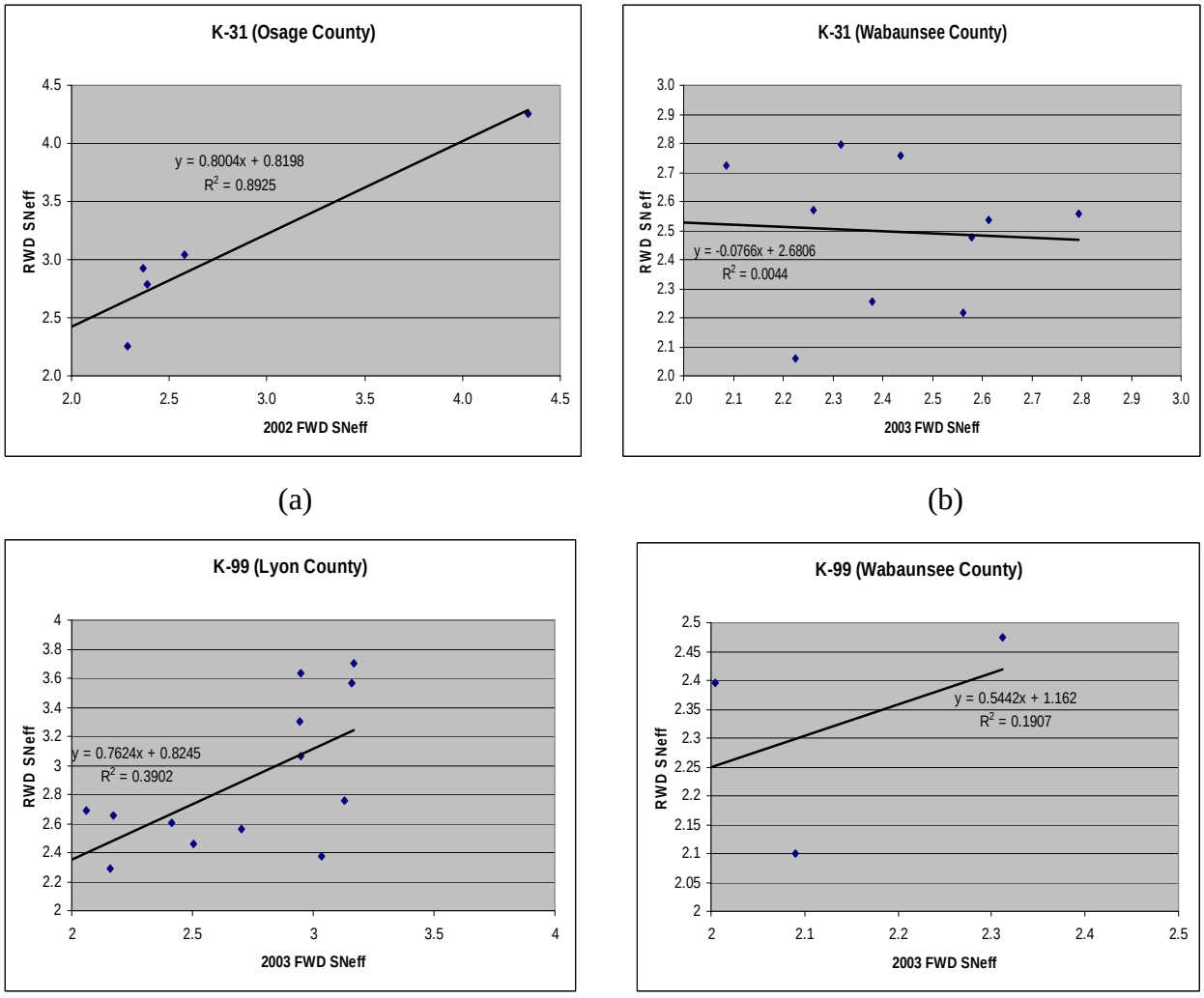

Figure 4-24 FWD and RWD SNeff for K-31 and K-99

Figure 4-25(a) shows that RWD SNeff remains more or less constant as FWD SNeff increases with slope and R^2 value close to zero for US-54 in Greenwood County. The relationship does not reflect the effect of rehabilitation action. RWD SNeff is greater than FWD SNeff at all points due to rehabilitation action for US-56 in Douglas County as shown in Figure 4-25(b). FWD and RWD SNeff show linear relationship with some scatter, and relatively low slope and R^2 value for US-56 in Norris County as shown in Figure 4-25(c), and the effect of rehabilitation action is not clear. Widely scattered SNeff results in very low R^2 for US-56 in Osage County as shown in Figure 4-25(d), and RWD SNeff is lower than FWD SNeff due to rehabilitation action.

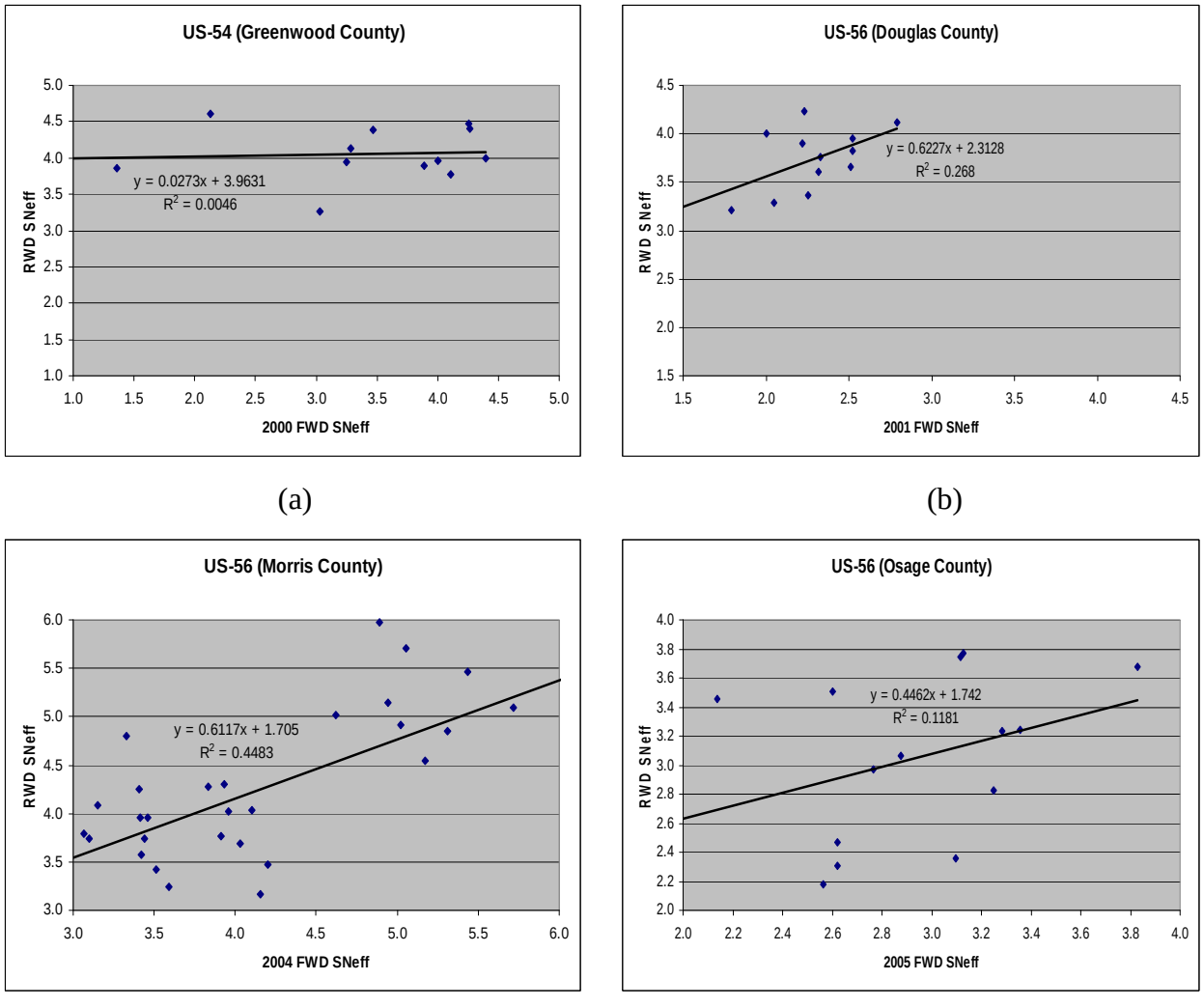

Figure 4-25 FWD and RWD SNeff for US-54 and US-56

4.3.1.4 Significant-Difference Test

Figure 4-26 shows the average FWD and RWD SNeff for all perpetual pavement sections; the numerical values are given in Table 4-11. FWD SNeff is slightly higher than RWD SNeff for all sections except Section 3. Table 4-11 shows no significant difference between FWD and RWD SNeff for experimental sections.

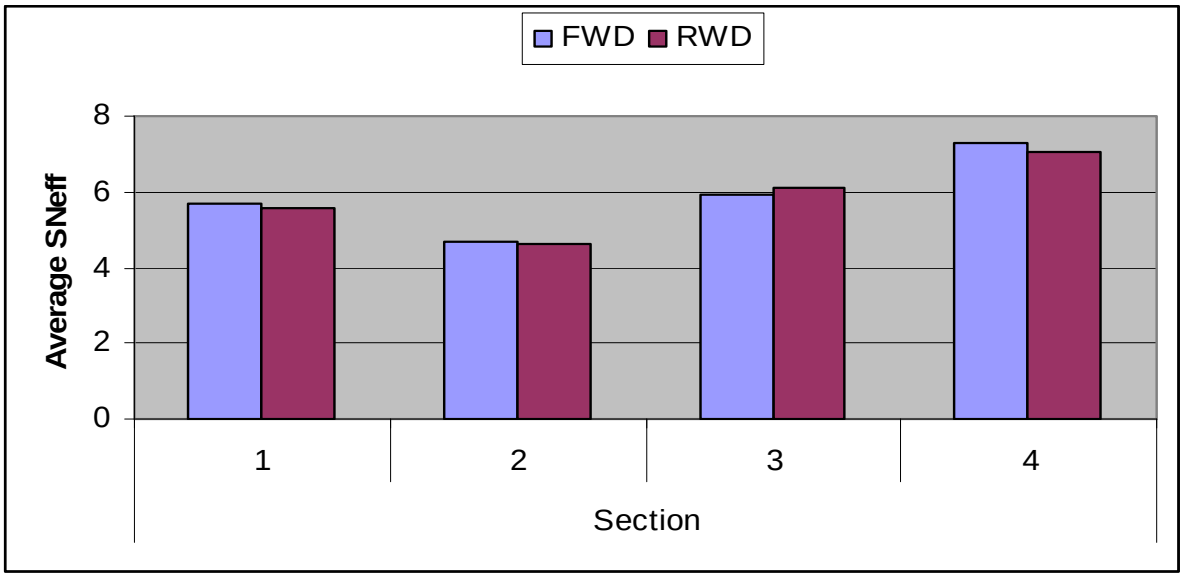

Figure 4-26 FWD and RWD SNeff for Experimental Sections

Table 4-11 Significant-Difference Test of SNeff for Experimental Sections

Section	Avg.SNeff		Paired T-Test for SNeff Difference(FWD-RWD)					No. of Data Points
	FWD	RWD	Lower	Mean	Upper	Pr>|t|	Similar	
1	5.68	5.58	-0.38	0.10	0.58	0.62	Yes	6
2	4.71	4.64	-0.10	0.07	0.27	0.37	Yes	20
3	5.94	6.09	-0.53	-0.15	0.23	0.41	Yes	20
4	7.26	7.07	-0.02	0.18	0.39	0.08	Yes	20

There is no significant difference in FWD and RWD SNeff for those projects without rehabilitation action. There are significant differences in mean SNeff for US-54 in Greenwood County, US-56 in Douglas County, and US-59 in Neosho County as shown in Figure 4-27.

Average RWD SNeff is consistently higher than average FWD SNeff due to rehabilitation action. Numerical values of FWD and RWD SNeff are shown in Table 4-12.

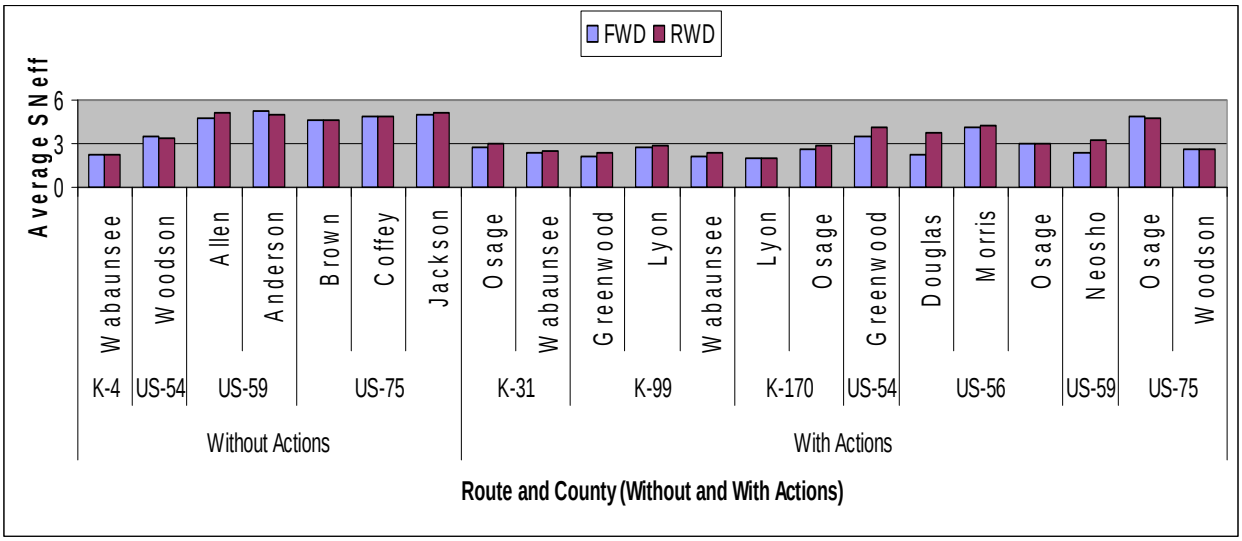

Figure 4-27 Average FWD and RWD SNeff

FWD and RWD SNeff are not significantly different from each other for all projects without rehabilitation actions as shown in Table 4-12(a). There is no significant difference between FWD and RWD SNeff for all projects with rehabilitation action except K-99 in Greenwood County, US-56 in Douglas County, and US-59 in Neosho County as shown in Table 4-12(a). RWD SNeff is greater than FWD SNeff for the three projects, which shows the effect of rehabilitation action.

Table 4-12 Significant-Difference Test for FWD and RWD SNeff

Routes	County	Avg. SNeff		Paired T-Test for Difference (FWD-RWD)					Length (mi)
		FWD	RWD	Lower	Mean	Upper	Pr>|t|	Similar	
(a)Without Rehabilitation Actions									
	Wabaunsee	2.23	2.28	-0.41	-0.04	0.33	0.81	Yes	12
	Woodson	3.52	3.43	-0.28	0.08	0.44	0.58	Yes	6
	Allen	4.69	5.08	-1.02	-0.39	0.24	0.19	Yes	8
	Anderson	5.21	4.95	-0.43	0.25	0.94	0.44	Yes	15
	Brown	4.66	4.63	-0.34	0.03	0.39	0.88	Yes	12
	Coffey	4.90	4.82	-0.26	0.08	0.43	0.56	Yes	6
	Jackson	5.05	5.08	-0.89	-0.03	0.83	0.94	Yes	13
(b)With Rehabilitation Actions									
K-31	Osage	2.80	3.06	-0.56	-0.26	0.04	0.07	Yes	5
	Wabaunsee	2.43	2.51	-0.32	-0.08	0.16	0.47	Yes	10
K-99	Greenwood	2.10	2.40	-0.52	-0.30	-0.09	0.01	No	20
	Lyon	2.72	2.92	-0.43	-0.20	0.03	0.08	Yes	13
	Wabaunsee	2.13	2.33	-0.70	-0.20	0.30	0.23	Yes	3
K-170	Lyon	2.03	1.97	-0.17	0.06	0.28	0.56	Yes	7
	Osage	2.68	2.90	-0.45	-0.22	0.00	0.05	Yes	13
US-54	Greenwood	3.46	4.07	-1.23	-0.61	0.01	0.05	Yes	12
US-56	Douglas	2.28	3.75	-1.65	-1.47	-1.28	0.00	No	12
	Morris	4.16	4.26	-0.34	-0.09	0.15	0.44	Yes	30
	Osage	2.95	3.06	-0.46	-0.11	0.23	0.48	Yes	14
US-59	Neosho	2.43	3.31	-1.10	-0.89	-0.67	0.00	No	8
US-75	Osage	4.86	4.76	-2.43	0.10	2.63	0.92	Yes	5
	Woodson	2.58	2.61	-0.26	-0.03	0.21	0.80	Yes	11

4.3.1.5 Linear Regression

There is no linear relationship between FWD and RWD SNeff for all experimental sections as shown in Table 4-13. The slope for Section 1 is negative.

Table 4-13 Linear Regression of FWD and RWD SNeff for Perpetual Pavement Sections

Section	Intercept	Slope	C.I.* for Slope		Pr>|t|	Linear Relation	R^2	No. of Data Points
			lower	upper				
1	9.88	-0.76	-2.77	1.26	0.36	No	0.21	6
2	3.74	0.19	-0.33	0.71	0.45	No	0.03	20
3	5.54	0.09	-1.00	1.18	0.86	No	0.00	20
4	4.97	0.29	-0.11	0.69	0.15	No	0.11	20

* confidence interval for slope at 95% confidence level

There is no linear relationship between the FWD and RWD SNeff for all projects without rehabilitation action as shown in Table 4-14(a). FWD and RWD SNeff have linear relationships in only five of 14 projects with rehabilitation action as shown in Table 4-14(b). Slope and R^2 value vary from 0.61 to 0.93 and 0.43 to 0.91, respectively, for projects that show linear relations.

4.3.2 Effect of Temperature-Correction Method on SNeff

The effect of the two temperature correction methods on FWD center deflection has been discussed. Effect on center deflections is translated into effect on corresponding SNeff. It has been investigated separately for Kansas and US routes. Significant-difference tests using paired t-test and linear regression have been done. Effect of the pavement temperature-correction method on FWD SNeff for Kansas and US routes (the same route in different counties combined), and different routes in the same county and district, have been done and results are shown in Appendix A.

Table 4-14 Linear Regression for FWD and RWD SNeff

Routes	County	Intercept	Slope	C.I.* for Slope		Pr>t	Linear Relation	R^2	Length (mi)
				Lower	Upper				
(a)Without Rehabilitation Actions									
K-4	Wabaunsee	2.42	-0.06	-0.42	0.29	0.70	No	0.02	12
US-54	Woodson	7.72	-1.22	-3.88	1.44	0.27	No	0.29	6
US-59	Allen	3.05	0.43	-3.53	4.39	0.80	No	0.01	8
	Anderson	4.00	0.18	-0.16	0.53	0.27	No	0.09	15
US-75	Brown	2.70	0.41	-0.71	1.53	0.43	No	0.06	12
	Coffey	3.70	0.23	-1.68	2.14	0.76	No	0.03	6
	Jackson	4.50	0.11	-0.57	0.80	0.72	No	0.01	13
(b)Without Rehabilitation Actions									
K-31	Osage	0.69	0.85	0.41	1.29	0.01	Yes	0.93	5
	Wabaunsee	2.76	-0.10	-1.01	0.81	0.80	No	0.01	10
K-99	Greenwood	2.44	-0.02	-0.57	0.53	0.95	No	0.00	20
	Lyon	0.71	0.81	0.19	1.43	0.02	Yes	0.43	13
	Wabaunsee	1.11	0.57	-15.15	16.29	0.72	No	0.18	3
K-170	Lyon	2.18	-0.10	-0.74	0.53	0.69	No	0.03	7
	Osage	0.72	0.82	0.64	1.00	0.00	Yes	0.91	13
US-54	Greenwood	3.95	0.03	-0.24	0.31	0.79	No	0.01	12
US-56	Douglas	2.35	0.61	-0.10	1.32	0.08	No	0.27	12
	Morris	1.73	0.61	0.35	0.87	0.00	Yes	0.44	29
	Osage	1.97	0.37	-0.39	1.13	0.31	No	0.09	14
US-59	Neosho	1.62	0.70	-0.41	1.80	0.17	No	0.28	8
US-75	Osage	-0.91	1.17	-4.62	6.96	0.57	No	0.12	5
	Woodson	0.21	0.93	0.37	1.48	0.00	Yes	0.61	11

* confidence interval for slope at 95% confidence level

4.3.2.1 Kansas Routes

Method I shows higher SNeff than Method II with some scatter for K-4 in Wabaunsee County as shown in Figure 4-28(a). There is a very good linear relationship between SNeff based on the two methods, though Method II shows higher SNeff consistently for K-31 in Osage County as shown in Figure 4-28(b). Relatively low slope shows that SNeff based on Method I is higher than the one using Method II for K-31 in Wabaunsee County as shown in Figure 4-28(c). Method II gives higher SNeff for low SNeff and vice versa for high SNeff for K-99 in Greenwood County as shown in Figure 4-28(d).

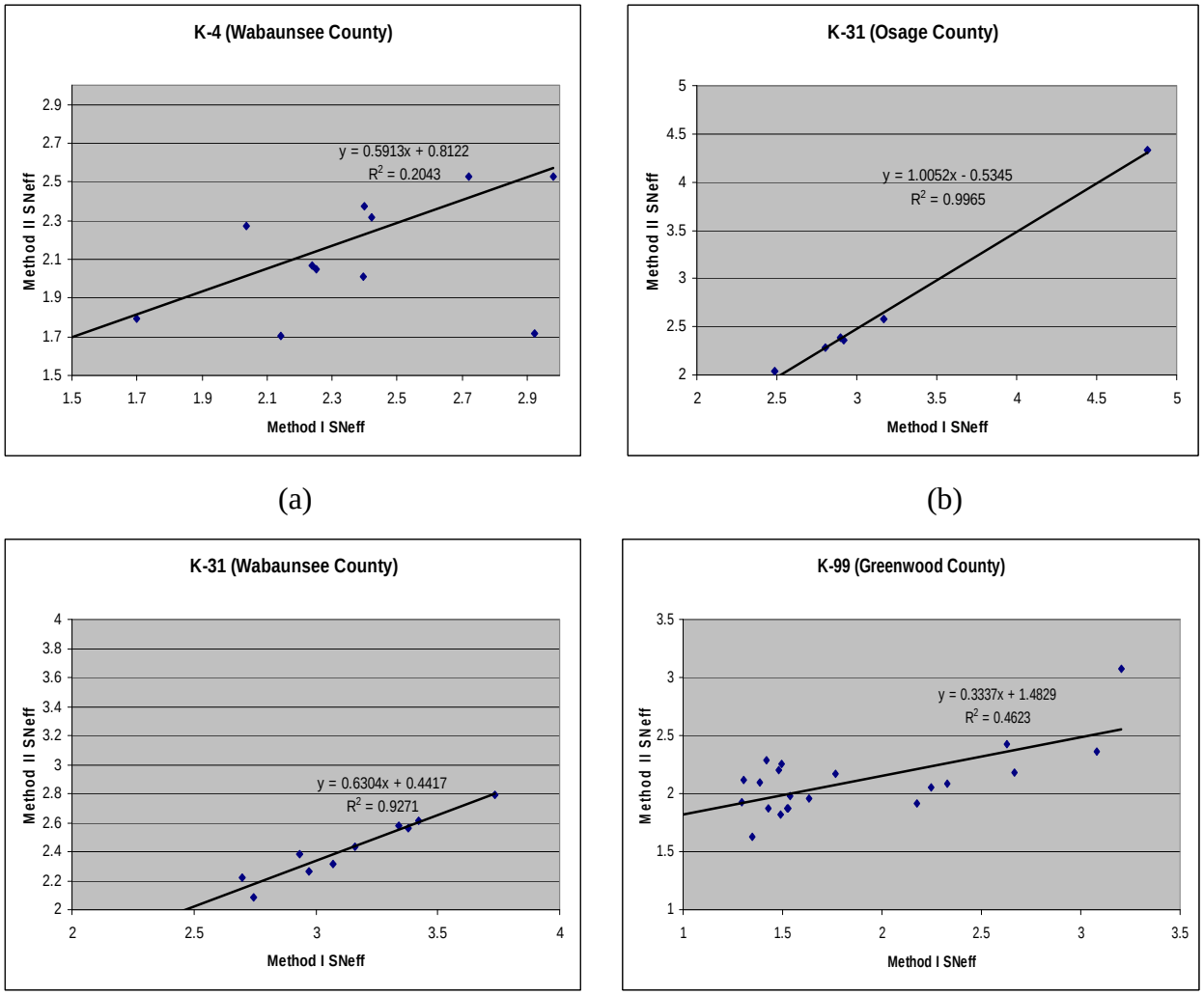

Figure 4-28 Effect of Temperature-Correction Methods on SNeff for K-4, K-31, and K-99

Figure 4-29 shows a very good linear relationship between SNeff based on both methods. Method I consistently gives higher SNeff than Method II for all projects as shown in Figure 4-29. This results in significant difference in SNeff based on the two methods.

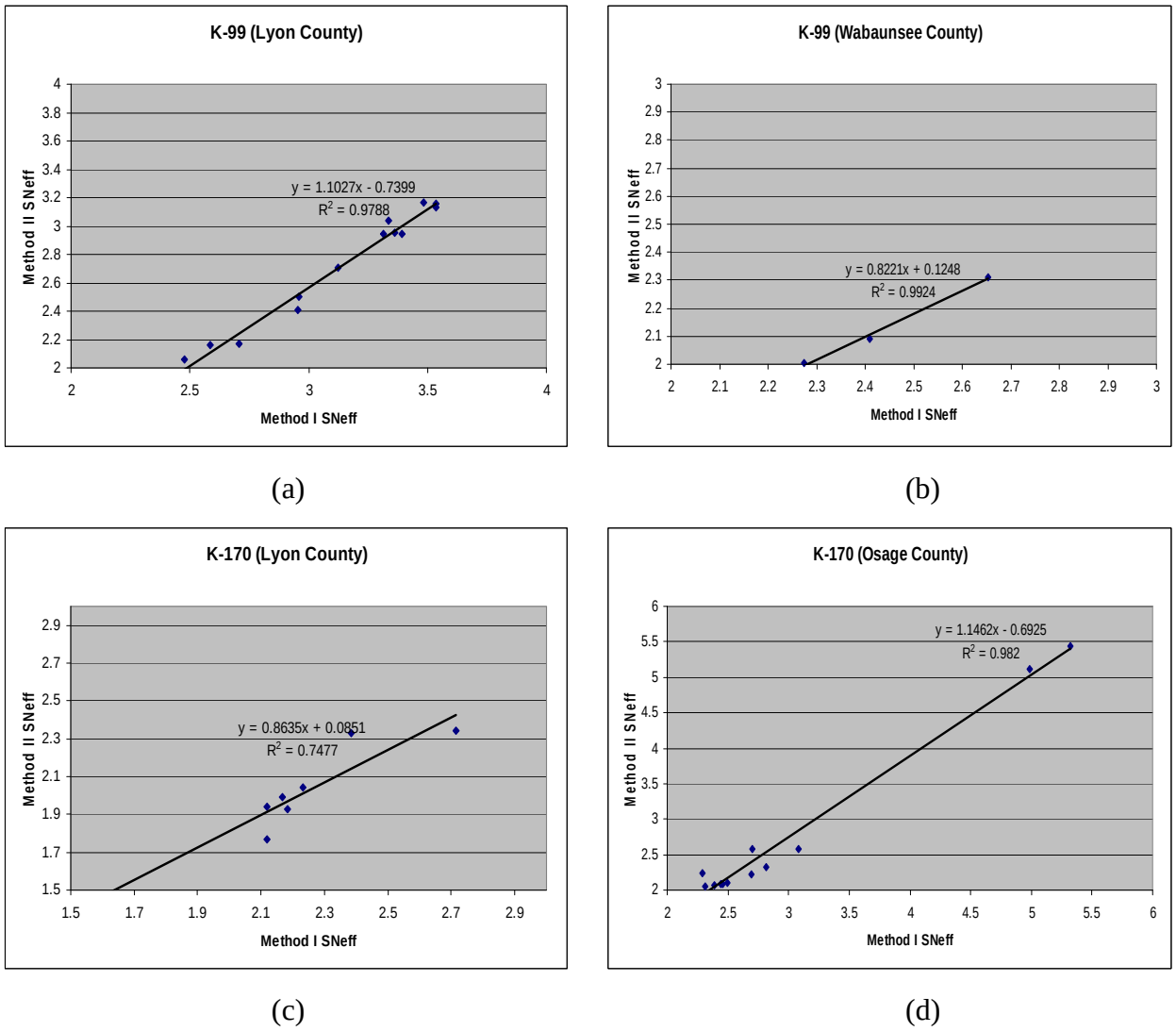

Figure 4-29 Effect of Temperature-Correction Method on SNeff for K-99 and K-170

4.3.2.2 US Routes

There is no linear relationship between SNeff based on the two methods for US-54 in Greenwood County as shown in Figure 4-30(a). Method I gives higher SNeff than Method II at all points for US-54 in Woodson County as shown in Figure 4-30(b). The two methods give very close SNeff for US-56 in Morris County as shown in Figure 4-30(c). Figure 4-30(d) shows highly scattered SNeff in which SNeff based on the two methods are negatively related.

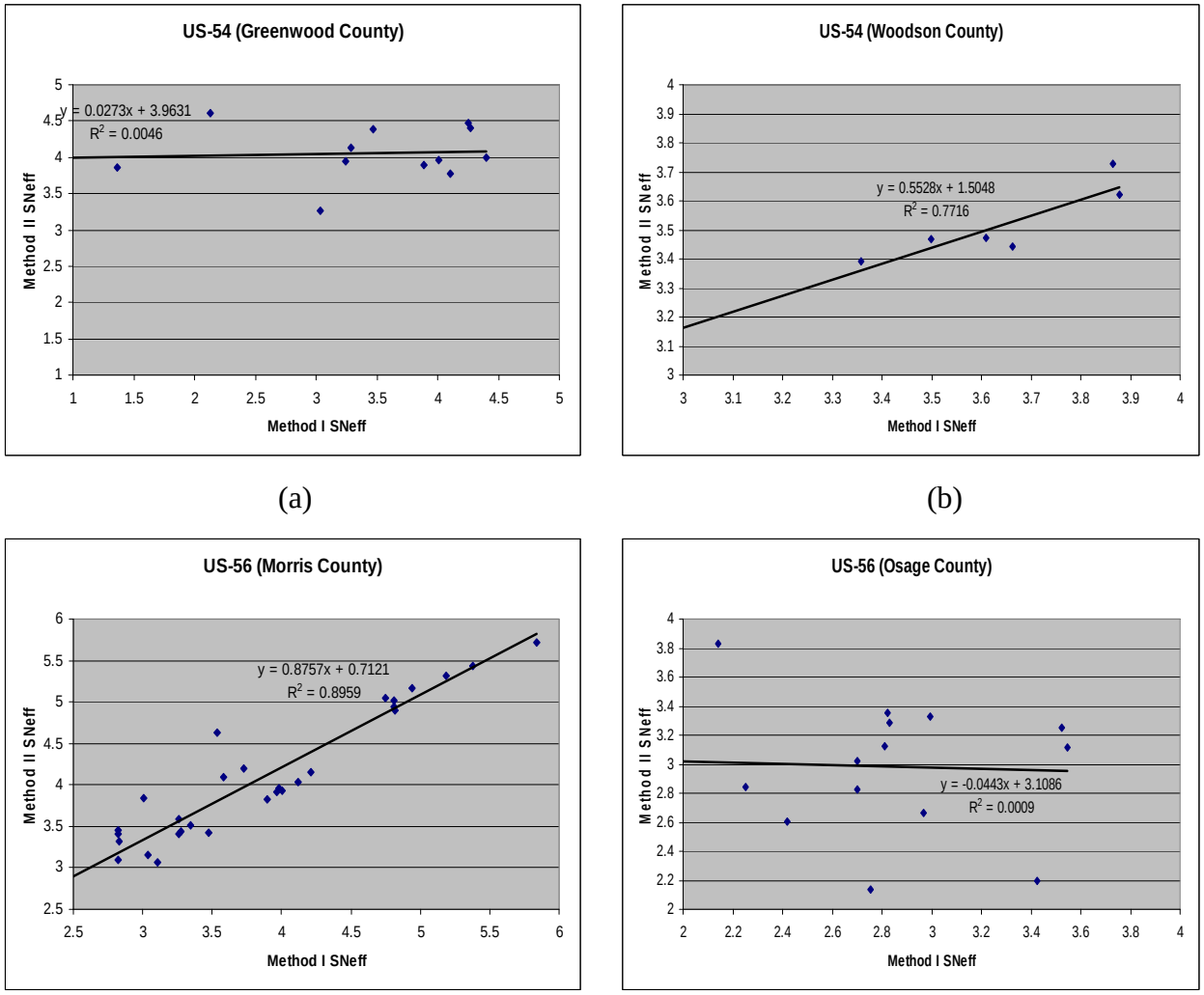

Figure 4-30 Effect of Temperature-Correction Method on SNeff for US-54 and US-56

Figure 4-31(a) shows a very good linear relationship between SNeff based on the two temperature-correction methods, though Method I consistently gives higher SNeff. Slope is low, though Method II consistently gives higher SNeff and R^2 values are low due to the scatter for US-75 in Brown County as shown in Figure 4-31(b). Figure 4-31(c) and (d) show good linear relationships for SNeff based on the two temperature-correction methods, though Method II consistently gives higher SNeff for US-75 in Coffey County and vice versa for US-75 in Jackson County.

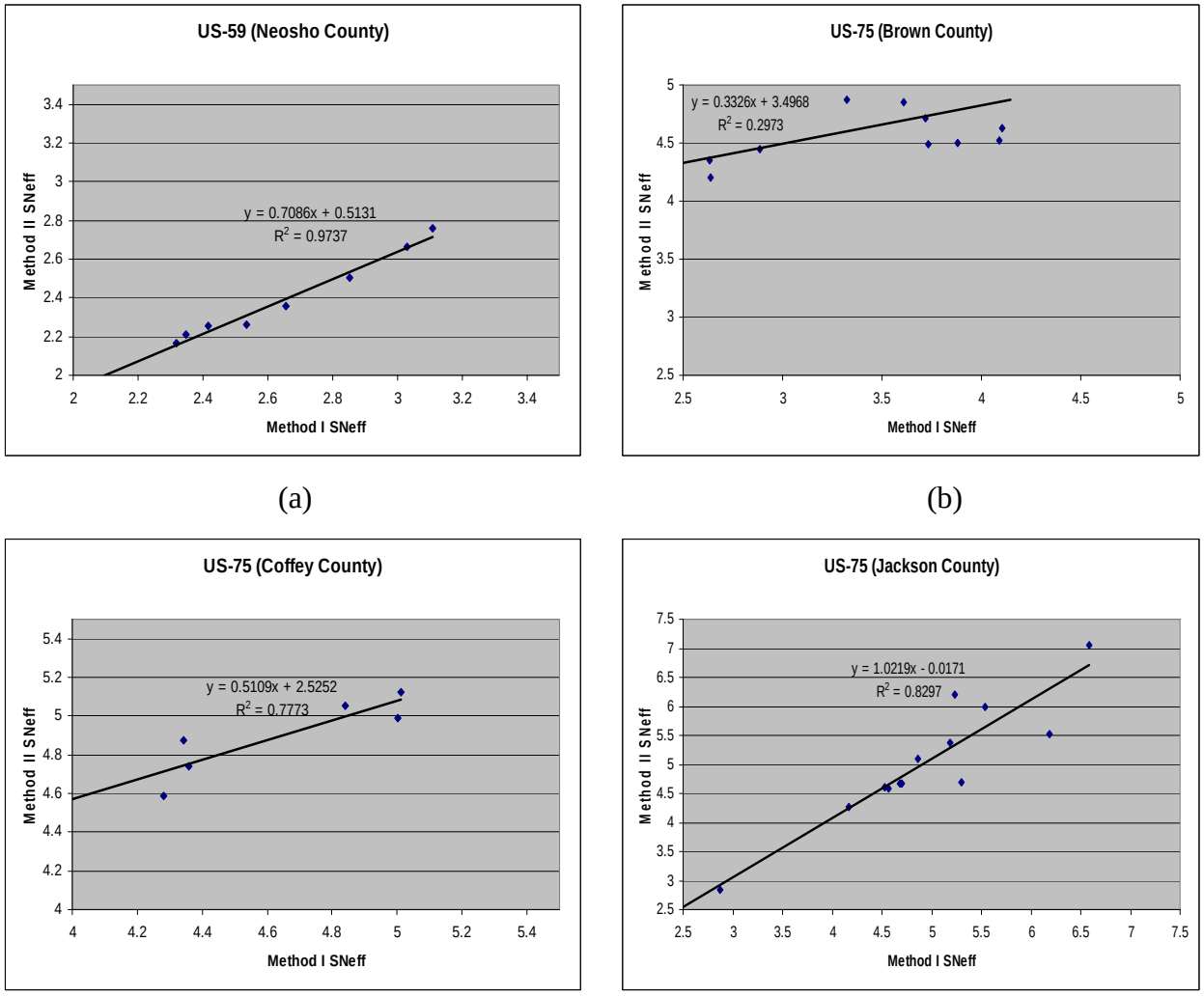

Figure 4-31 Effect of Temperature-Correction Method on SNeff for US-59 and US-75

4.3.2.3 Significant-Difference Test

The effect of a temperature-correction factor on the computed effective structural number was also investigated. Method I shows higher average SNeff for eight out of the nine Kansas routes, whereas Method II shows higher/equal average SNeff for ten of the 12 US routes as shown in Figure 4-32. However, the difference is not significant from a practical point of view. In general, US routes are thicker than the Kansas routes, and this leads to a conclusion that Method I tends to predict higher values for thinner sections and Method II tends to predict higher values for thicker sections. Numerical values of average SNeff are tabulated in Table 4-15.

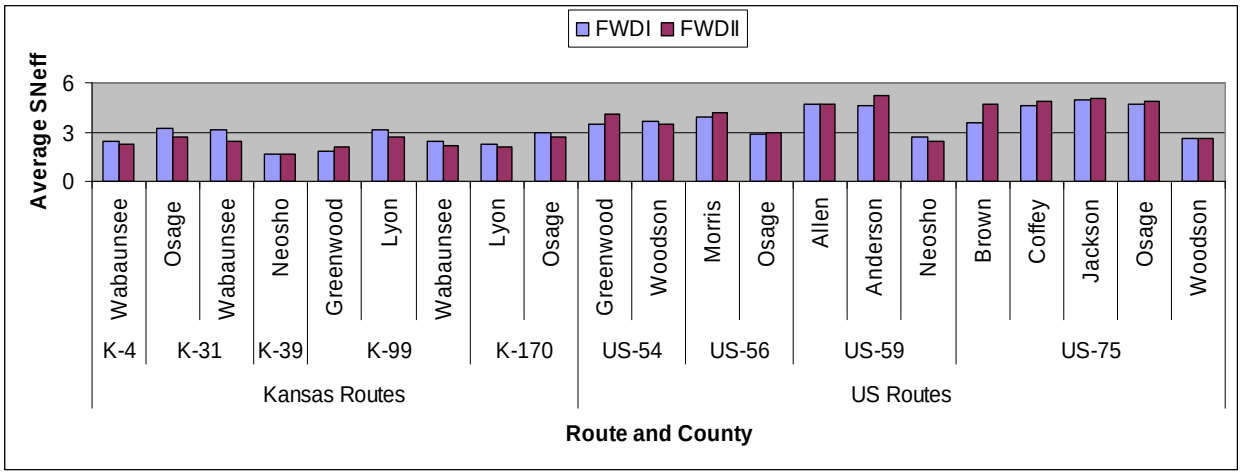

Figure 4-32 Effect of Temperature-Correction Method on Average SNeff

There is no significant difference between SNeff based on the two temperature-correction methods for two of eight Kansas routes, K-4 in Wabaunsee and K-39 in Neosho County, as shown in Table 4-15(a). Method II gives higher average SNeff for all Kansas routes. It shows significant difference for all except K-99 in Greenwood County. There are significant differences in SNeff based on the two temperature-correction methods for six of 12 US routes as shown in Table 4-15(b). Method II gives higher average SNeff for four out of the six US routes. In general, most routes show significant difference since one or the other method consistently gives higher SNeff. The results signify that effect of the method of temperature-correction factor can be very pronounced at times.

Table 4-15 Significant-Difference Test for Effect of Temp.-Correction Method on SNeff

Route	County	Avg.SNeff		Paired T-Test for Difference (I-II)					Length (mi)
		I	II	Lower	Mean	Upper	Pr>|t|	Similar	
(a) Kansas Routes									
K-4	Wabaunsee	2.41	2.24	-0.12	0.17	0.47	0.22	Yes	12
K-31	Osage	3.18	2.66	0.47	0.52	0.57	0.00	No	6
	Wabaunsee	3.15	2.42	0.63	0.72	0.82	0.00	No	10
K-39	Neosho	1.68	1.64	-0.39	0.04	0.47	0.43	Yes	2
K-99	Greenwood	1.86	2.10	-0.46	-0.25	-0.04	0.02	No	21
	Lyon	3.14	2.72	0.38	0.42	0.46	0.00	No	13
	Wabaunsee	2.45	2.14	0.22	0.31	0.40	0.00	No	3
K-170	Lyon	2.27	2.05	0.12	0.23	0.33	0.00	No	7
	Osage	2.94	2.68	0.13	0.26	0.39	0.00	No	13
(b) US Routes									
US-54	Greenwood	3.45	4.06	-1.23	-0.60	0.02	0.06	Yes	12
	Woodson	3.65	3.52	0.01	0.13	0.24	0.04	No	6
US-56	Morris	3.95	4.17	-0.33	-0.22	-0.11	0.00	No	30
	Osage	2.85	2.98	-0.53	-0.13	0.26	0.48	Yes	16
US-59	Allen	4.69	4.70	-0.19	-0.01	0.16	0.86	Yes	8
	Anderson	4.65	5.20	-0.86	-0.55	-0.24	0.00	No	15
	Neosho	2.66	2.40	0.18	0.26	0.34	0.00	No	8
US-75	Brown	3.54	4.67	-1.43	-1.14	-0.84	0.00	No	12
	Coffey	4.64	4.90	-0.46	-0.26	-0.05	0.02	No	6
	Jackson	4.95	5.05	-0.35	-0.09	0.17	0.45	Yes	13
	Osage	4.70	4.88	-1.03	-0.18	0.68	0.60	Yes	5
	Woodson	2.62	2.58	-0.01	0.04	0.10	0.09	Yes	11

4.3.2.4 Linear Regression

Table 4-16(a) shows a linear relationship between SNeff based on the two temperature-correction methods for all Kansas routes except K-4 and K-99 in Wabaunsee County. Slope

varies from 0.33 to 1.15, though most of the sections have slopes close to 1.0. Some sections have R^2 value greater than 0.90.

Table 4-16 Linear Regression of Effect of Temperature-Correction Method on SNeff

Route	County	Inter-cept	Slope	C.I.* for Slope		Pr>|t|	Linear Relation	R^2	Length (mi)
				lower	upper				
(a) Kansas Routes									
K-4	Wabaunsee	0.81	0.59	-0.23	1.41	0.14	No	0.20	12
K-31	Osage	-0.53	1.01	0.92	1.09	0.00	Yes	0.93	10
	Wabaunsee	0.44	0.63	0.47	0.77	0.00	Yes	0.93	10
K-99	Greenwood	1.48	0.33	0.16	0.51	0.00	Yes	0.46	21
	Lyon	0.09	0.86	0.29	1.44	0.01	Yes	0.75	7
	Wabaunsee	0.12	0.82	-0.09	1.74	0.06	No	0.99	3
K-170	Lyon	0.09	0.86	0.29	1.44	0.01	Yes	0.75	7
	Osage	-0.69	1.15	1.04	1.25	0.00	Yes	0.98	13
(b) US Routes									
US-54	Greenwood	3.96	0.03	-0.25	0.31	0.83	No	0.01	12
	Woodson	1.50	0.55	0.14	0.97	0.02	Yes	0.77	6
US-56	Morris	0.71	0.88	0.76	0.99	0.00	Yes	0.90	30
	Osage	3.11	-0.04	-0.91	0.82	0.91	No	0.001	16
US-59	Allen	2.65	0.44	-0.18	1.05	0.13	No	0.33	8
	Anderson	-1.18	1.37	1.04	1.71	0.00	Yes	0.86	15
	Neosho	0.51	0.71	0.59	0.82	0.00	Yes	0.97	8
US-75	Brown	3.50	0.33	-0.03	0.69	0.07	No	0.30	12
	Coffey	2.52	0.51	0.13	0.89	0.02	Yes	0.78	6
	Jackson	-0.02	1.02	0.71	1.33	0.00	Yes	0.83	13
	Osage	3.20	0.36	-1.91	2.62	0.65	No	0.08	5
	Woodson	-0.16	1.04	0.91	1.18	0.00	Yes	0.97	11

* confidence interval for slope at 95% confidence level

Table 4-16(b) shows a linear relationship between SNeff based on the two temperature-correction methods for seven of 12 US routes. Slope and R^2 value varies from 0.51 to 1.37 and 0.77 to 0.97, respectively. In general, most Kansas and US routes that show a linear relationship have slopes close to 1.00 and R^2 values greater than 0.90. This shows that the two methods give comparable SNeff.

4.3.3 Frequency of Deflection Measurements Using SNeff

Frequency of deflection measurements using SNeff has been analyzed using normalized and temperature-corrected (Method I) FWD deflection data over two test years. Analysis and discussions have been done for the projects without and with rehabilitation actions. Results for some of the projects are shown in Appendix A.

4.3.3.1 Without Rehabilitation Actions

There is a good linear relationship between FWD SNeff in 1999 and 2003, with minor scatter for US-54 in Woodson County as shown in Figure 4-33(a). Figure 4-33(b) shows scatter with higher FWD SNeff in 2000 than those in 2004 for US-59 in Allen County.

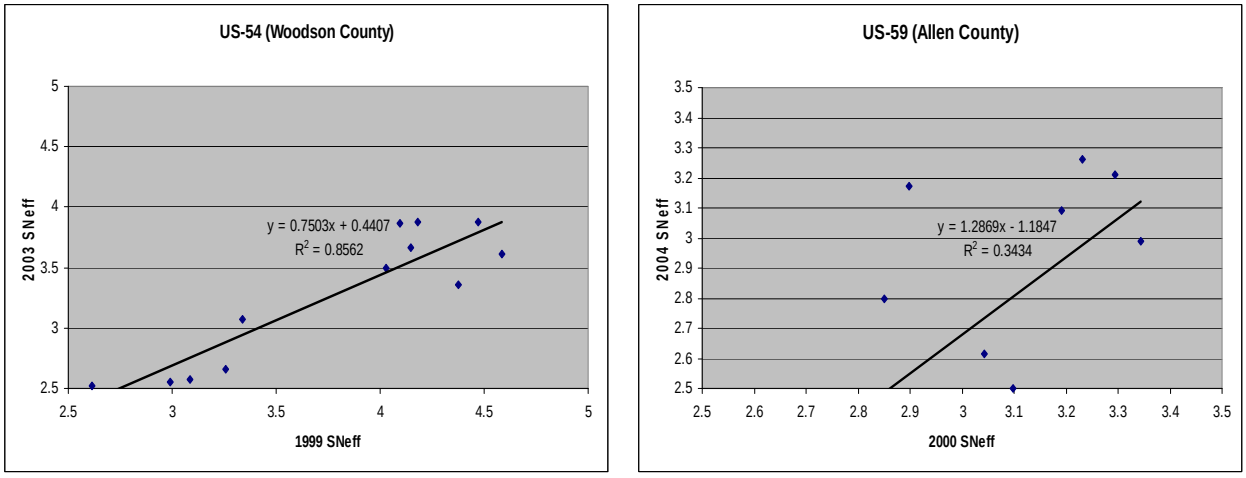

(a) (b)

Figure 4-33 FWD SNeff over Years for US-54 and US-59

Figure 4-34(a) shows that FWD SNeff in 1999 is higher than the one in 2003, though some of the points are scattered for US-59 in Anderson County. Very low slope in Figure 4-34(b) shows the deterioration of US-75 in Brown County from 1999 to 2003. FWD SNeff in 1999 and 2003 are negatively related for US-75 in Coffey County as shown in Figure 4-34(c). FWD SNeff in 2002 is higher than FWD SNeff in 1998, though there was no rehabilitation action for US-75 in Brown Jackson County as shown in Figure 4-34(d). This may be due to some maintenance actions which were done by KDOT and not reported as rehabilitation action.

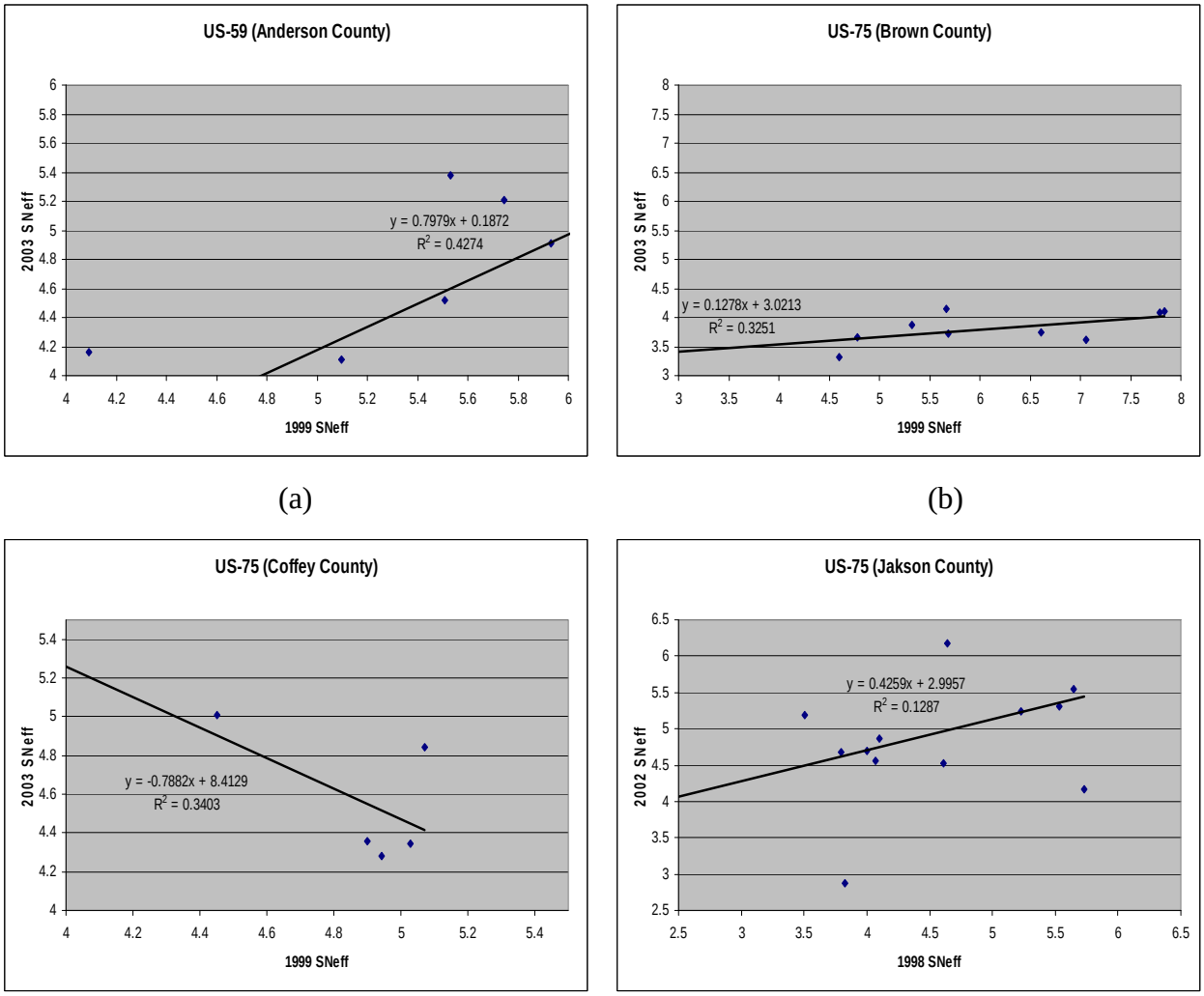

(a) (b)

(c) (d)

Figure 4-34 FWD SNeff Over Years for US-59 and US-75

4.3.3.2 With Rehabilitation Actions

FWD SNeff in 2003 is higher than the data in 1999 at all points due to rehabilitation action, though they are negatively related for K-31 in Wabaunsee as shown in Figure 4-35(a). Figure 4-35(b) shows low slope and R^2 values for K-99 in Lyon County and an increase in SNeff due to rehabilitation action. The slope is high, though R^2 is very low due to scatter of SNeff data for K-170 in Lyon County as shown in Figure 4-35(c). There is a good linear relationship between SNeff in 1999 and 2004, but the effect of rehabilitation action on SNeff is not clear from Figure 4-35(d) for K-170 in Osage County.

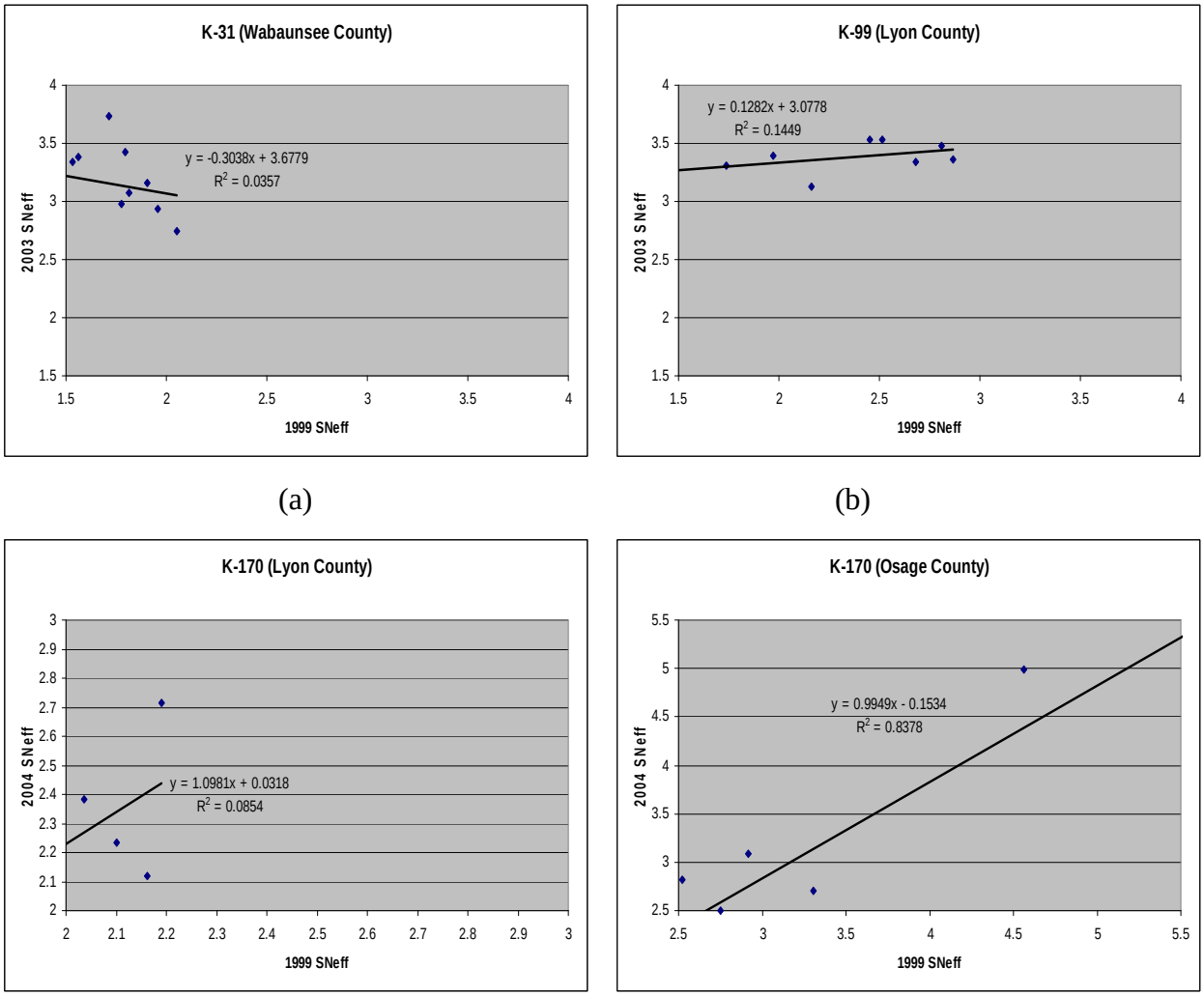

Figure 4-35 FWD SNeff over Years for K-31, K-99, and K-170

The slopes of the relationship between SNeff in 1999 and 2004 are relatively low. It shows that SNeff in 2004 is lower than the data in 2004 (though there had been rehabilitation action between 1999 and 2004) for US-56 in Morris County as shown in Figure 4-36(a). Figure 4-36(b) shows some scatter and negative relationship between SNeff in 2001 and 2005, though SNeff in 2005 is higher due to rehabilitation action.

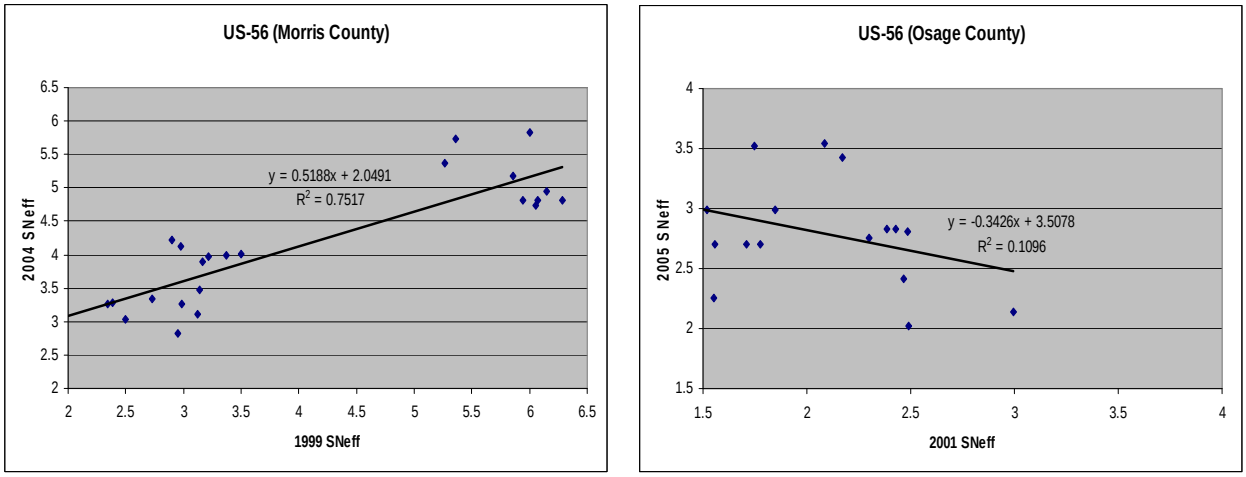

(a) (b)

Figure 4-36 FWD SNeff over Years for US-56

4.3.3.3 Significant-Difference Test

The effective structural numbers computed from the FWD test data were also investigated to assess the suitable test frequency for network-level deflection data collection. Results are shown in Figure 4-37. All projects without rehabilitation action show reduction in SNeff except K-4 in Wabaunsee County and US-75 in Jackson County. This may be due to pavement test temperature, heavy maintenance actions by KDOT, and increase in pavement stiffness due to aging. All projects with rehabilitation action show an increase in SNeff except K-170 in Osage County and US-75 in Woodson County. Numerical values of average FWD SNeff over two test years are shown in Table 4-17.

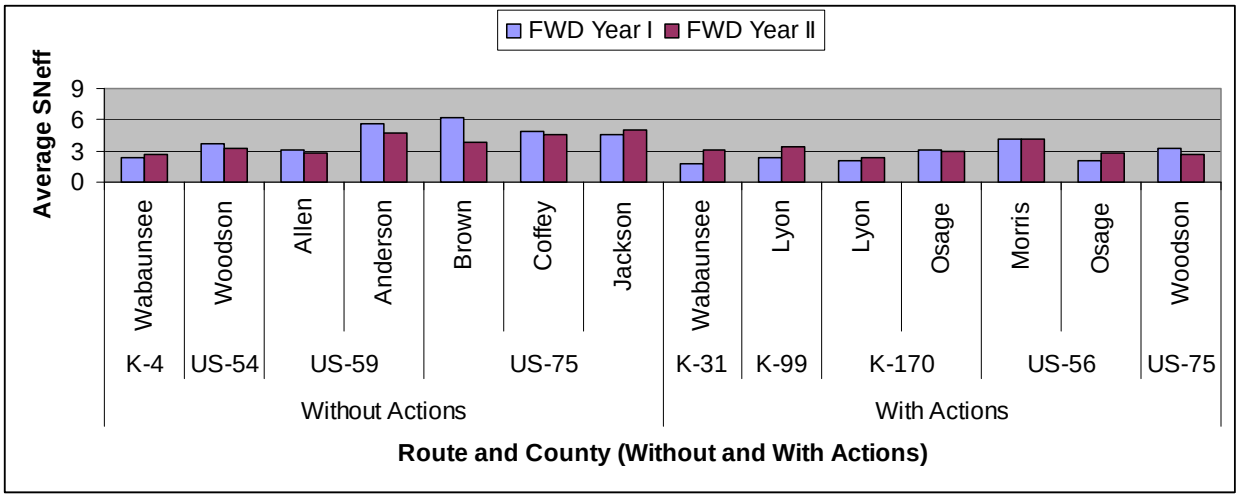

Figure 4-37 Average FWD SNeff over Years

There is no significant difference in SNeff over the two test years, only for three of the seven projects without rehabilitation actions: K-4 in Wabaunsee County, and US-75 in Coffey and Jackson counties as shown in Table 4-17(a). There is no significant difference in SNeff over the test interval for K-170 in Lyon and Osage counties and US-56 in Morris County, as shown in Table 4-17(b). This shows that rehabilitation action may not necessarily result in an increase in structural capacity or fast deterioration in some cases. It was observed that a small difference in mean center deflection results in a significant difference in SNeff when the pavement is thick. This result shows the frequency of deflection data collection should be four years. In other words, 25% of the network can be tested each year for a four-year test cycle.

4.3.4 AASHTO and KDOT SN_{eff}

The effective structural number (SN_{eff}) based on deflection data was computed using Equation (2.31) given by the AASHTO method. SN_{eff} based on the KDOT procedure was computed using different coefficients for the pavement materials in different layers. These coefficients were obtained from the Kansas Highway Pavement Design manual *(KDOT, undated)* as well as from a 1972 NCHRP report number 128 *(Til et al., 1972)*. The coefficients depend on the age of the pavement as shown in Table 4-18. One-third of total AC thickness was considered as the surface course, and the lower two-third was considered as the base course in this study. Comparison was made between the two SNeff for experimental sections, road

category-wise, district-wise, and state-wide. Some district-wise and statewide results are shown in Appendix A. Finally, significant- difference tests using paired t-tests were also done.

Table 4-17 Significant-Difference Test of FWD SNeff over Years

Route	County	Avg. SNeff		Paired T-Test for Difference (I-II)					Length (mi)
		Year I	Year II	Lower	Mean	Upper	Pr>|t|	Similar	
(a)Without Rehabilitation Actions									
K-4	Wabaunsee	2.43	2.60	-0.66	-0.17	0.32	0.43	Yes	7
US-54	Woodson	3.68	3.20	0.31	0.48	0.65	0.00	No	13
US-59	Allen	3.06	2.76	0.11	0.31	0.50	0.01	No	12
	Anderson	5.59	4.65	0.59	0.94	1.30	0.00	No	15
US-75	Brown	6.14	3.81	1.50	2.34	3.18	0.00	No	9
	Coffey	4.88	4.57	-0.33	0.31	0.96	0.25	Yes	5
	Jackson	4.60	4.95	-0.94	-0.36	0.23	0.21	Yes	13
(b)With Rehabilitation Actions									
K-31	Wabaunsee	1.75	3.15	-1.69	-1.40	-1.10	0.00	No	10
K-99	Lyon	2.40	3.39	-1.30	-0.99	-0.67	0.00	No	8
K-170	Lyon	2.12	2.36	-0.63	-0.24	0.15	0.15	Yes	4
	Osage	3.17	3.00	-0.10	0.17	0.43	0.19	Yes	12
US-56	Morris	4.10	4.18	-0.45	-0.08	0.29	0.67	Yes	23
	Osage	2.10	2.79	-1.08	-0.70	-0.31	0.00	No	16
US-75	Woodson	3.28	2.62	0.38	0.66	0.95	0.00	No	11

Table 4-18 Layer Coefficients for Pavement Materials *(KDOT, undated; Til et al., 1972)*

Mix Designation	Initial Year	Year 10	Year 20
Bituminous Surface	0.42	0.34	0.28
Bituminous Base	0.34	0.28	0.20
Aggregate Base	0.14	0.11	0.08
Cold-in-Place Recycle	0.25	0.18	0.11
Lime-Treated Subgrade	0.11	0.08	0.00
Rubblized PCCP	0.20	0.16	0.12

4.3.4.1 Experimental Sections

Figure 4-38 shows that SNeff AASHTO is greater than SNeff KDOT for all experimental sections.

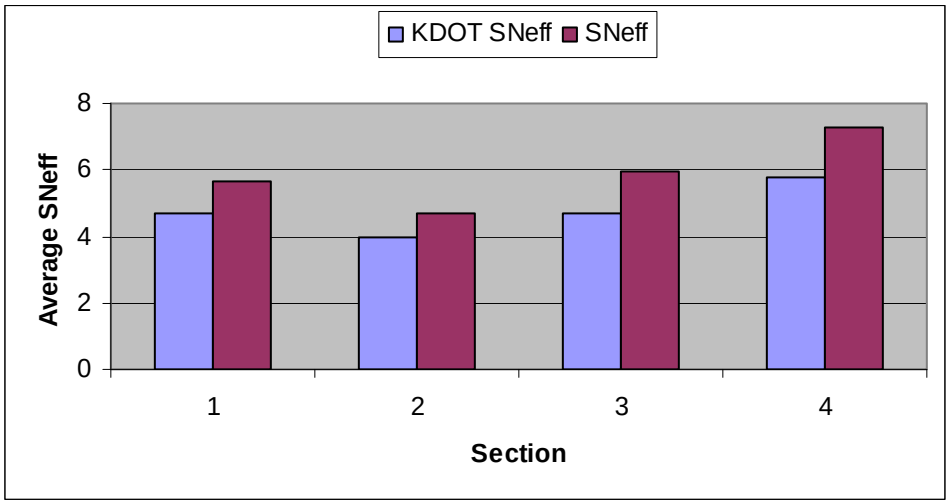

Figure 4-38 SNeff AASHTO and KDOT for Experimental Sections

4.3.4.2 Road Category-Wise

SNeff, using the AASHTO method and KDOT procedure, show some linear relationships with low slope and R^2 value for road category 12 as shown in Figure 4-39(a). There is almost no linear relationship between SNeff using the AASHTO method and KDOT procedure for road categories 13, 14, and 15 as shown in Figure 4-39(b), (c), and (d).

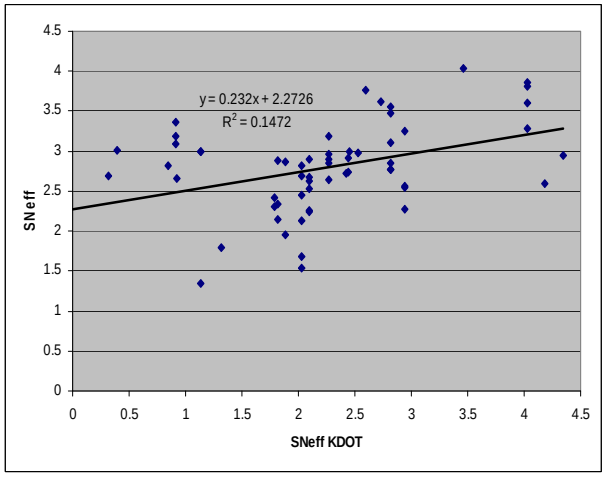

(a) Road Category 12

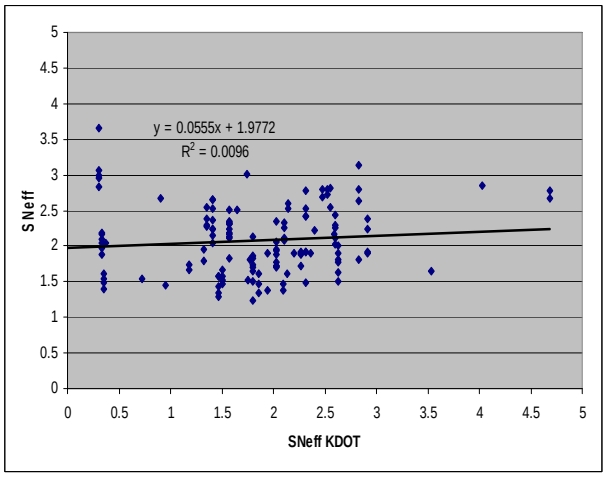

(b) Road Category 13

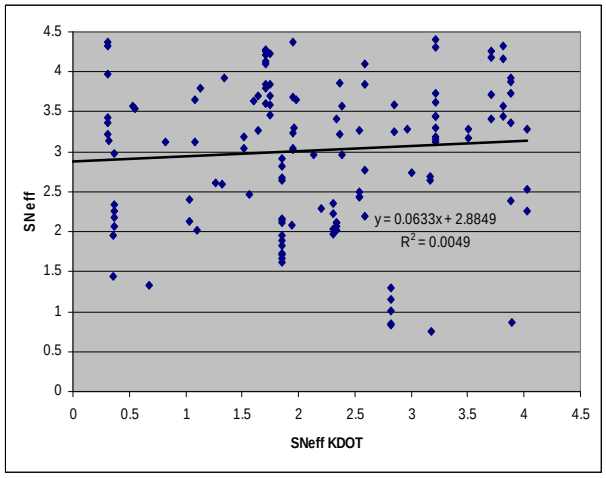

(c) Road Category 14

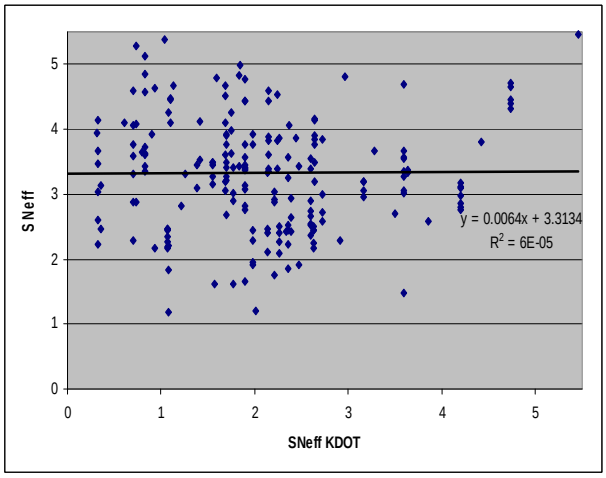

Road Category 15

Figure 4-39 SNeff AASHTO and KDOT for Road Categories 12 to 15

Figure 4-40 shows insignificant linear relationship between SNeff using the AASHTO method and KDOT procedure for road categories 16, 17, 18, and 19. It shows that SNeff using the AASHTO method remains more or less constant as SNeff using the KDOT procedure increases.

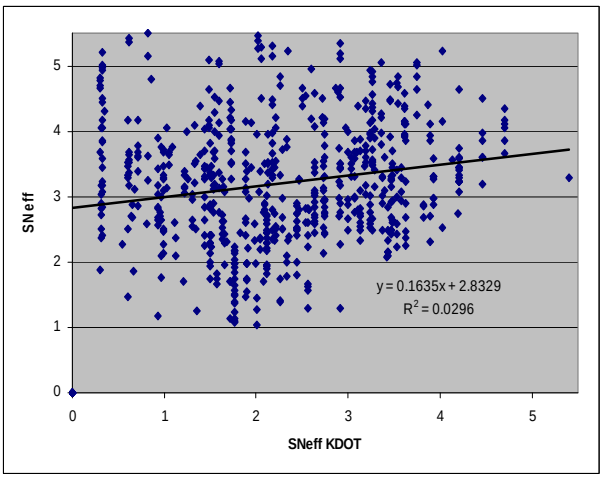

(a) Road Category 16

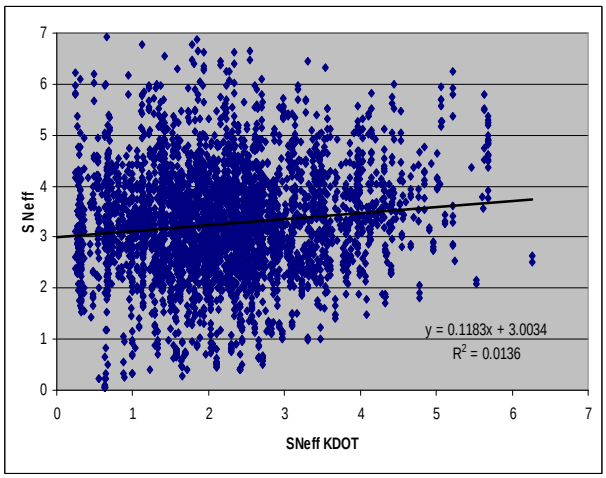

(b) Road Category 17

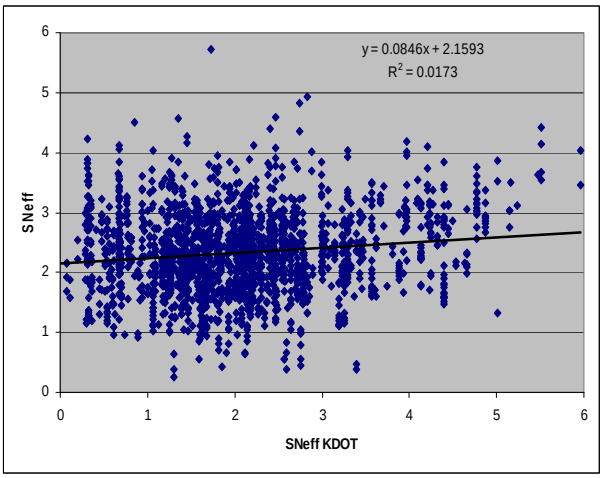

(c) Road Category 18

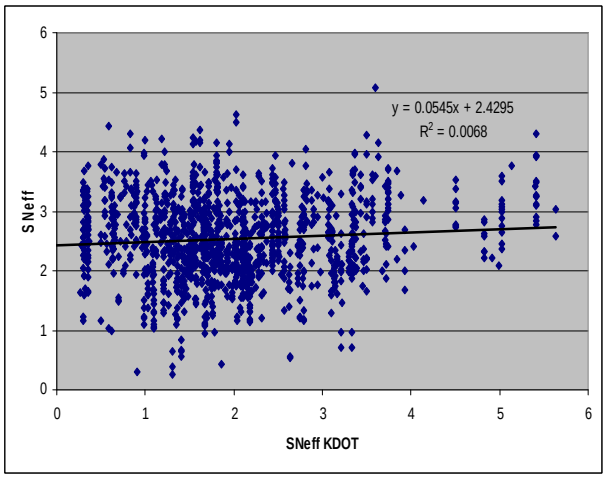

(d) Road Category 19

Figure 4-40 SNeff AASHTO and KDOT for Road Categories 16 to 19

Figure 4-41 shows large data scatter with low slope and R^2 value, and there is almost no linear relationship between SNeff based on the AASHTO method and KDOT procedure for road categories 20, 21, 22, and 23.

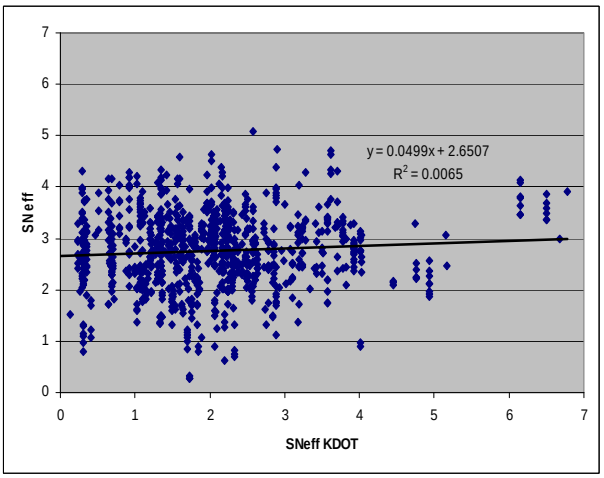

(a) Road Category 20

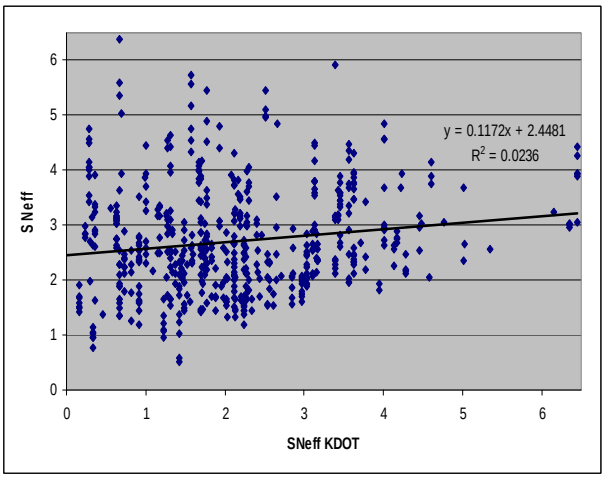

(b) Road Category 21

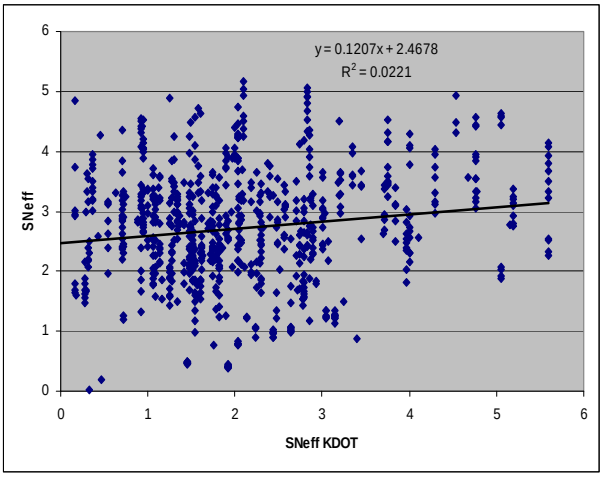

(c) Road Category 22

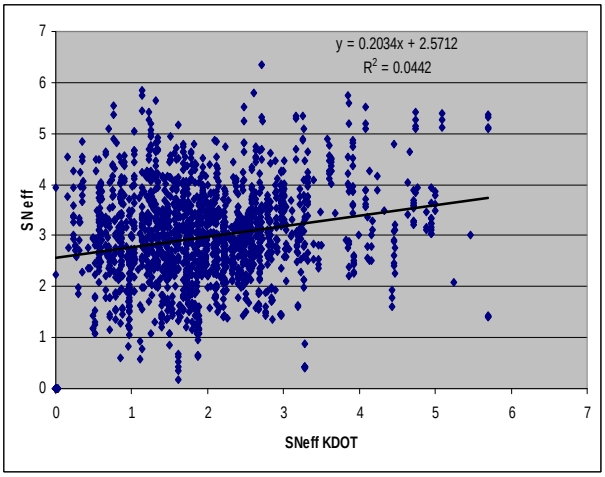

(d) Road Category 23

Figure 4-41 SNeff AASHTO and KDOT for Road Categories from 20 to 23

4.3.4.3 District-Wise

Figure 4-42(a) shows that SNeff AASHTO and KDOT are negatively related, though the slope is very close to zero. There is a weak linear relationship between SNeff AASHTO and KDOT for Districts 2, 3, and 4 as shown in Figure 4-42(b), (c), and (d). Results for Districts 4, 5, and statewide have been shown in Appendix A.

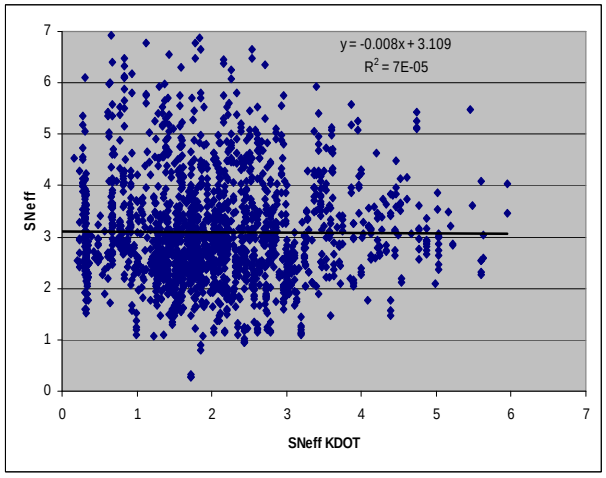

(a) District 1

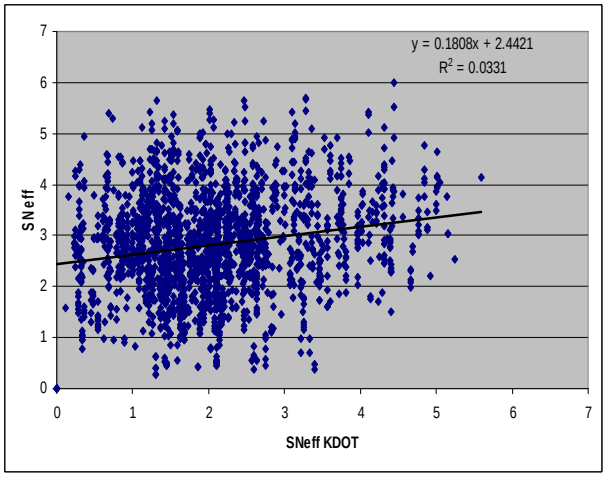

(b) District 2

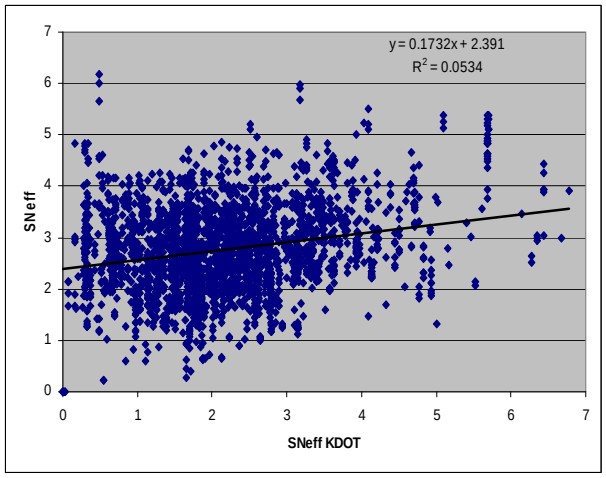

(c) District 3

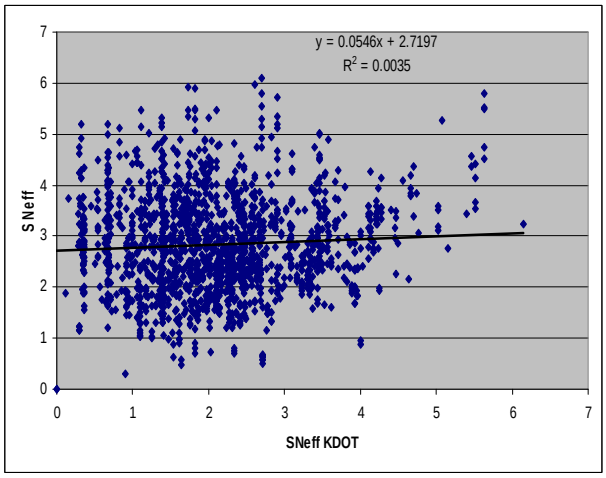

(d) District 4

Figure 4-42 SNeff AASHTO and KDOT for Districts 1 to 4

4.3.4.4 Significant-Difference Test

Figure 4-43 shows that average SNeff using the AASHTO method is greater than SNeff using the KDOT procedure for all road categories, districts, and overall. In general, SNeff KDOT is greater than SNeff AASHTO for new pavements and less than SNeff AASHTO for aged pavements. This may be due to the coefficients assigned to different materials in different pavement layers. Some pavements may not lose SNeff significantly with time. Numerical values of average SNeff AASHTO and KDOT are shown in Table 4-19.

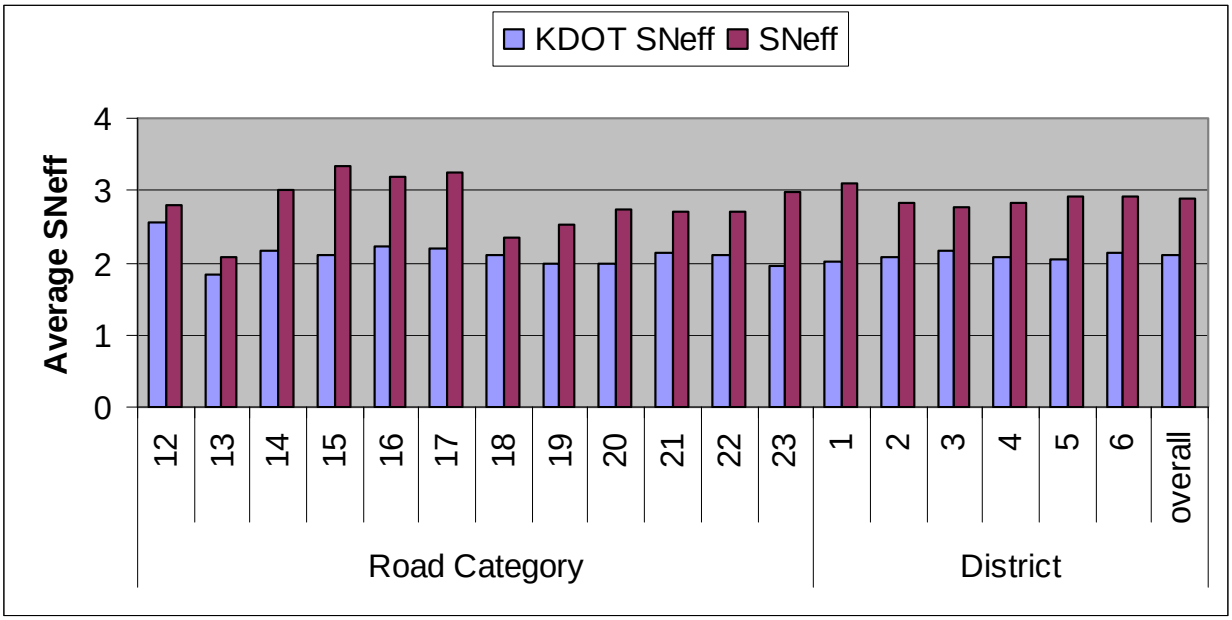

Figure 4-43 Average SNeff AASHTO and KDOT

There is significant difference between SNeff KDOT and SNeff AASHTO for all road categories, districts, and overall (the state) as shown in Table 4-19.

Table 4-19 Significant-Difference Test of SNeff AASHTO and KDOT

Road Category	Avg.SNeff		Paired T-Test for Difference (I-II)					Length (mi)
	I	II	Lower	Mean	Upper	P(t)>|t|	Similar	
(a)Road Category-Wise								
12	2.56	2.80	-0.77	-0.54	-0.31	<.0001	No	59
13	1.84	2.08	-0.39	-0.24	-0.08	0.00	No	134
14	2.18	3.02	-1.08	-0.85	-0.61	<.0001	No	136
15	2.10	3.33	-1.42	-1.23	-1.04	<.0001	No	204
16	2.23	3.20	-1.07	-0.97	-0.86	<.0001	No	657
17	2.19	3.26	-1.12	-1.07	-1.03	<.0001	No	3992
18	2.10	2.34	-0.30	-0.25	-0.19	<.0001	No	1871
19	1.98	2.54	-0.63	-0.56	-0.50	<.0001	No	1348
20	1.99	2.75	-0.84	-0.76	-0.67	<.0001	No	952
21	2.14	2.70	-0.68	-0.56	-0.44	<.0001	No	563
22	2.11	2.72	-0.71	-0.61	-0.51	<.0001	No	761
23	1.96	2.97	-1.06	-1.00	-0.95	<.0001	No	1790
(b)District-Wise								
1	2.03	3.09	-1.13	-1.06	-1.00	<.0001	No	1843
2	2.08	2.82	-0.80	-0.74	-0.68	<.0001	No	2020
3	2.17	2.77	-0.65	-0.60	-0.55	<.0001	No	2527
4	2.08	2.83	-0.82	-0.76	-0.69	<.0001	No	1657
5	2.05	2.92	-0.93	-0.88	-0.82	<.0001	No	2145
6	2.15	2.93	-0.84	-0.78	-0.72	<.0001	No	2262
State	2.10	2.89	-0.82	-0.79	-0.77	<.0001	No	12454

CHAPTER 5 PREDICTION MODELS

5.1 Introduction

Remaining service life (RSL), fatigue, and transverse cracking prediction models have been developed using KDOT statewide mile-long PMS data from 1998 to 2006. The model forms are linear, quadratic, and sigmoidal. Linear RSL models have been developed for road categories 12 to 23, districts, state, and for perpetual pavement sections on US-75. Stress, strain, deflection, and temperature data collected from June 2005 to April 2007 have been used to develop linear RSL models for perpetual pavement sections on US-75. Quadratic RSL models have been developed for the districts only. Sigmoidal RSL models with linear sub-models (with and without cracking data) have been developed for road categories 12 to 23, districts, and the state. Sigmoidal models with quadratic sub-models have been developed for districts and the state. Finally, sigmoidal models have been developed using statewide data using the logarithm of equivalent axle load (logEAL).

Linear equivalent fatigue cracking (EFCR) and equivalent transverse cracking (ETCR) models have been developed for road categories 12 to 23, districts, and the state. Quadratic EFCR and ETCR models have been developed for districts only. Road category-wise, district-wise, and statewide sigmoidal EFCR models with linear sub-models and sigmoidal ETCR models with linear sub-models (with and without SNeff) have also been developed. Sigmoidal EFCR and ETCR models with quadratic sub-models have been developed for districts and the state. Sigmoidal EFCR and ETCR models have been developed using statewide data based on logEAL.

5.2 Model Development

In Kansas, road categories 12 to 17 are full-design bituminous (FDBIT) pavements, and road categories 18 to 23 are partial-design bituminous (PDBIT) pavements. Ninety percent of the data was used to develop the models and the rest was used to validate them. There was not been enough data to develop and validate models for road categories 1 to 12. These road categories are concrete and composite pavements where FWD data is not routinely collected. A nonlinear regression (NLIN) procedure in the Statistical Analysis Software (SAS) and Solver in Microsoft Excel have been used to develop the models.

The sigmoidal RSL model chosen is shown in Equation (5.1) followed by four linear sub-models. The four sub-models are sigma (δ), alpha (α), beta (β), and gamma (γ). All linear sub-models include the same variables. RSL has been used as a dependent variable whereas center deflection (d_0) has been taken as an independent variable. Pavement thickness, traffic, cracking, rutting, and structural data have also been included in the model. Similar sigmoidal models have been developed for EFCR and ETCR with different variables in the sub-models, in which EFCR and ETCR have been used as the dependent variables and center deflection *(d_0)* as an independent variable. Sigmoidal models with quadratic sub-models have also been developed in which the same variable has the coefficients for linear and quadratic parts. For example, the coefficient for total pavement thickness above subgrade in δ sub-model is δ_1 and δ_{22} for the linear and quadratic parts, respectively.

$$RSL = \delta + \frac{\alpha}{1 + e^{\beta - \gamma d_0}} \tag{5.1}$$

$$\delta = \delta_0 + \delta_1 D + \delta_2 EAL + \delta_3 ETCR + \delta_4 EFCR + \delta_5 Rut + \delta_6 SN_{eff} \tag{5.1a}$$

$$\alpha = \alpha_0 + \alpha_1 D + \alpha_2 EAL + \alpha_3 ETCR + \alpha_4 EFCR + \alpha_5 Rut + \alpha_6 SN_{eff} \tag{5.2b}$$

$$\beta = \beta_0 + \beta_1 D + \beta_2 EAL + \beta_3 ETCR + \beta_4 EFCR + \beta_5 Rut + \beta_6 SN_{eff} \tag{5.3c}$$

$$\gamma = \gamma_0 + \gamma_1 D + \gamma_2 EAL + \gamma_3 ETCR + \gamma_4 EFCR + \gamma_5 Rut + \gamma_6 SN_{eff} \tag{8d}$$

where

RSL = remaining service life (year);

D = total pavement thickness above subgrade (in);

EAL = equivalent axle load (ESAL/day);

ETCR = equivalent transverse cracking*;*

EFCR = equivalent fatigue cracking;

Rut = rut depth (in); and

SN_{eff} = effective structural number.

5.2.1 NLIN Procedure

The NLIN procedure implements iterative methods that attempt to find least-square estimates for nonlinear models. To begin this process, the NLIN procedure first examines the starting value specifications of the parameters. If a grid of values is specified, PROC NLIN evaluates the residual sum of squares at each combination of parameter values to determine the set of parameter values producing the lowest residual sum of squares. These parameter values are used for the initial step of the iteration. Then, PROC NLIN uses one of these four iterative methods: GAUSS-NEWTON method (default method), NEWTON method, MARQUARDT method, and GRADIENT method. These methods use derivatives or approximations to derivatives of the sum of squares for error (SSE) with respect to the parameters to guide the search for the parameters producing the smallest SSE. The GAUSS-NEWTON, MARQUARDT, and NEWTON methods are more robust than the GRADIENT method.

The GAUSS-NEWTON method uses the Taylor series. The NEWTON method uses the second derivatives and solves the equation. The MARQUARDT method is a compromise between the GAUSS-NEWTON and the GRADIENT methods. It is equivalent to performing a series of ridge regressions and is useful when parameter estimates are highly correlated or the objective function is not well approximated by a quadratic. Details of these methods have been discussed in Chapter 2.

Initial (seed) values have been used to run PROC NLIN in SAS based on the four iterative methods. Final values after convergence have been used in Solver to optimize the models.

5.2.2 Solver Procedure

Solver in Microsoft Excel has been used to optimize RSL, EFCR, and ETCR models. The objective is to minimize the sum of squared differences between each observation and the corresponding predicted value. It uses the generalized reduced-gradient (GRG2) nonlinear optimization code. The GRG2 code has been proven over many years use as one of the most robust and reliable approaches to solving difficult nonlinear programming (NLP) problems. The model with the least sum of squared differences has been taken as the best. It should be noted that solver procedure and NLIN procedure give the same SSE, but the former is fast and has been used to optimize using many seed values.

5.2.3 Goodness of Fit

The quality of fit of a linear model is expressed in terms of the coefficient of determination (R^2). In nonlinear regression, such a measure is not readily defined. One of the problems with the R^2 definition is that it requires the presence of an intercept, which most nonlinear models do not have. Adjusted R^2 values were computed taking into account the degrees of freedom using Equation (5.2) as an approximate goodness of fit measurement:

$$R^2 = 1 - \left(\frac{n-p}{n-1}\right) \times \left(\frac{SSE}{SST}\right) \tag{5.2}$$

where

n =number of data points;

P =number of regression constants;

$n - P$ =degrees of freedom;

SSE =sum of squares for errors; and

SST =sum of squares of total.

5.2.4 Mean Absolute Deviation

Mean absolute deviation for observed and predicted RSL, EFCR, and ETCR has been calculated using Equation (5.3).

$$MAD = \frac{\sum_{i=1}^{n} \left| x_i - \bar{x} \right|}{n} \tag{5.3}$$

where

x_i = individual observed or predicted values;

$\bar{x}$ = mean observed or predicted values; and

n = number of data points.

5.3 Remaining Service Life (RSL) Models

Linear, quadratic, and sigmoidal RSL models have been developed for road categories 12 to 23, districts, and the state. Only linear RSL models have been developed for perpetual pavement sections on US-75 since there is no enough data to develop sigmoidal models.

5.3.1 Linear Regression

RSL models have been developed for road categories 12 to 23, districts, and the state. In addition, linear RSL models have been developed for perpetual pavement sections on US-75 using SAS. Some of the variables were dropped based on the 5% significance level.

5.3.1.1 Experimental Sections

Linear models have been developed for experimental sections using seven sets of data collected from June 2005 to April 2007: longitudinal strain at the bottom of HMA at 20-, 40-, and 60-mph truck speeds (*L20, L40, and L60)*; transverse strain at the bottom of HMA at 20-, 40-, and 60-mph truck speeds (*T20, T40, and T60);* stress on top of subgrade at 20-, 40-, and 60-mph truck speeds (*P20, P40, and P60);* mid-depth pavement temperature *(T_{pav})* and normalized and temperature-corrected FWD center deflection *(d_0)*. Total HMA design thickness *(D)* was also used. Linear models have been developed for all sections and overall conditions using average, maximum, minimum, and overall strain-and-stress data. Relationships between the center deflection and the average, maximum, minimum, and overall stress and strain at various speeds have also been investigated and results are shown in detail in Appendix B. Significant-difference tests between the strains and stresses at 20-, 40-, and 60-mph truck speeds have been carried out and are detailed in Appendix B.

Table 5-1 shows there is a positive linear relationship between RSL and d_0 when average, maximum, and minimum data is used to develop the models. There is no linear relationship between RSL and d_0 for Section 3 and overall. Intercept is not significant for Section 2 when average and maximum data are used; for Section 3; and overall when minimum data is used to develop RSL linear models for perpetual pavement sections. Coefficients of determination are high.

Table 5-1 Linear RSL Models for Experimental Sections

Data	Section	Model	R^2	N
Average	**1**	$RSL = 3.71739 + 0.12313 d_0 + 0.09935 L_{60}$	0.96	6
	2	$RSL = -0.17817 d_0 + 0.04646 T_{pav} + 0.00457 L_{20}$	1.00	5
	3	$RSL = 12.54029 - 0.11158 T_{pav}$	0.94	4
	4	$RSL = 7.99151 - 0.26721 d_0 + 0.04432 T_{pav}$	0.99	5
	Overall	$RSL = -14.11332 + 1.48251 D$	0.97	19
Maximum	**1**	$RSL = 3.80765 + 0.08607 d_0 + 0.03835 L_{20}$	0.90	6
	2	$RSL = -0.060830 d_0 + 0.03821 T_{pav}$	0.99	5
	3	$RSL = 6.13445 - 0.10725 d_0 + 0.01576 L_{20}$	1.00	4
	4	$RSL = 7.96633 - 0.17271 d_0 + 0.03807 T_{pav}$	0.98	5
	Overall	$RSL = 7.42154 - 0.24977 d_0$	0.17	20
Minimum	**1**	$RSL = 4.48309 + 0.08773 d_0 + 0.42892 P_{20}$	0.96	6
	2	$RSL = 1.01542 - 0.11568 d_0 + 0.02885 T_{pav}$	0.92	5
	3	$RSL = 0.42086 d_0 + 2.97902 P_{20}$	1.00	4
	4	$RSL = 7.87601 - 0.42424 d_0 + 0.05657 T_{pav}$	0.96	5
	Overall	$RSL = 0.43850 D$	0.88	20
Overall	**1**	$RSL = NA$		
	2	$RSL = 1.80333 - 0.01756 L_{20} + 0.04320 L_{60}$	0.46	15
	3	$RSL = NA$	0.98	12
	4	$RSL = NA$		
	Overall	$RSL = 5.44456 - 0.37099 d_0 + 0.03417 T_{pav}$	0.26	57

5.3.1.2 Road Category (RC)-Wise

There is a linear relationship between the center deflection (d_0) and RSL for all road categories except 16, 22, and 23 as shown in Table 5-2. RSL decreases as d_0 increases for all road categories except for 15. Intercept is not significant for only road category 14.

The coefficient of determination (R^2) varies from 0.02 to 0.59. It decreases with an increase in the number of data prints. Low R^2 shows that much of the variation is not explained and as a result, the models are not good enough to predict RSL accurately.

5.3.1.3 District-Wise and Statewide

There is a negative linear relationship between RSL and center deflection (d0) for districts and the state, except for Districts 2 and 6 as shown in Table 5-3. A negative relationship shows that RSL decreases as d0 increases, which meets engineering expectation. The coefficient of determination varies from 0.01 to 0.20, which is very low and the models may not be good enough to predict RSL. Since R2 values are very low, quadratic regression has been done for all districts and results are included in Appendix B.

Table 5-2 Road Category (RC)-Wise Linear RSL Models

RC	Model	R^2	N
12	$RSL = 7.622 - 0.136d_0 + 0.164D + 0.002AADT - 4.723ETCR - 0.451EFCR$	0.59	55
13	$RSL = 10.158 - 0.172d_0 - 0.736EFCR - 17.578Rut$	0.47	111
14	$RSL = -0.0605d_0 + 2.565AADT - 0.231EFCR$	0.16	221
15	$RSL = 4.443 + 0.127d_0 - 0.0026AADT + 0.0727EAL - 0.490EFCR - 10.685Rut$	0.48	66
16	$RSL = 5.990 - 0.924ETCR$	0.04	600
17	$RSL = 6.668 - 0.009d_0 - 0.037D - 6.384Rut$	0.04	3,702
18	$RSL = 5.277 - 0.025d_0 - 0.180EFCR$	0.05	1,873
19	$RSL = 30.802 - 0.0124d_0 - 24.426PL1 - 25.837PL2 - 25.666PL3 + 0.0216EAL - 0.464RTCR - 0.0713EFCR - 10.631Rut$	0.16	1,312
20	$RSL = 8.547 - 0.056d_0 - 0.007EAL - 1.182ETCR - 0.142EFCR - 7.955Rut$	0.19	779
21	$RSL = 7.178 - 0.081d_0 - 0.193D + 0.0015AADT$	0.09	197
22	$RSL = 5.281 + 0.120D$	0.02	662
23	$RSL = 5.474 + 0.069D - 1.365ETCR$	0.05	1,552

Table 5-3 District-Wise and Statewide Linear RSL Models

Dist.	Model	R^2	N
1	$RSL = 6.433 - 0.0103d_0 - 1.089ETCR - 6.023Rut$	0.07	1,321
2	$RSL = 6.881 - 1.837ETCR + 0.033EFCR - 2.811Rut$	0.16	1,355
3	$RSL = 13.827 - 0.0376d_0 - 7.042PL1 - 9.664PL2 - 8.86PL3 - 0.0876EFCR - 4.406Rut$	0.20	1,625
4	$RSL = 6.293 - 0.126d_0 - 0.046EFCR$	0.08	1,164
5	$RSL = 6.931 - 0.071d_0 - 606ETCR - 5.310Rut$	0.07	1,509
6	$RSL = 5.902 - 0.0465D - 0.440ETCR - 0.090EFCR$	0.04	1,455
State	$RSL = 5.776 - 0.0219d_0$	0.01	11,401

AADT-average annual daily traffic; PL1, PL2 and PL3-performance level 1, 2 and 3

5.3.1.4 Summary of RSL Linear Regression

Linear RSL models have been developed for experimental sections, road categories 12 to 23, districts, and the state. There is a positive linear relationship between RSL and center deflections in general. Coefficient of determination is high for experimental sections, though the number of data points used was low. Coefficients of determination for road categories, districts, and the state are low, which shows most of the variations have not been explained and the models are not recommended. As a result, it was decided to develop sigmoidal RSL models.

5.3.2 RSL Sigmoidal Model with Linear Sub-Models

Sigmoidal RSL models with no cracking data in the linear sub-models have been developed and results have been included in Appendix B. Sigmoidal RSL models with linear sub-models are shown in Equation (5.1). Six variables have been included in all sub-models and results have been discussed in this section.

5.3.2.1 Road Category (RC)-Wise

In each sub-model for all FDBIT, β_0 has the largest absolute value whereas γ_0 tends to be the smallest. Absolute magnitude of the coefficients is high for the variables which are small in magnitude. Table 5-4 shows coefficient of determination value varies from 0.17 to 0.95.

Table 5-4 FDBIT Sigmoidal RSL Model with Linear Sub-Models

RC		0	1(D)	2(EAL)	3(ETCR)	4(EFCR)	5(Rut)	6(SNeff)	R^2	N
12	δ	18.445	0.106	-0.121	-7.892	0.403	-42.618	-2.504	1.00	46
	α	-12.676	2.292	-0.330	64.041	-697.100	116.100	-4.642		
	β	31.688	-2.326	2.386	-51.290	12.493	-57.159	-11.731		
	γ	-0.478	-0.143	0.243	-4.119	0.848	-1.017	-0.515		
13	δ	9.527	0.087	-0.099	16.748	-0.900	8.500	-0.965	0.99	79
	α	-12.817	0.120	0.242	-15.400	0.559	-23.156	2.013		
	β	-499.21	-75.48	7.175	38.674	-228.315	-482.423	176.698		
	γ	1.625	-4.778	0.490	15.027	-28.877	-220.871	4.003		
14	δ	-0.437	0.151	0.157	7.657	2.726	6.230	-0.832	0.96	115
	α	2.019	-0.149	-0.191	-4.036	-2.929	0.429	1.894		
	β	184.381	-33.23	0.699	70.106	-44.682	-27.146	96.317		
	γ	-3.674	-5.505	0.291	0.503	-2.486	3.202	19.395		
15	δ	2.679	0.360	-0.024	-0.339	0.047	-7.715	0.062	0.95	109
	α	8.404	-2.040	0.547	-18.261	2.908	95.178	-0.055		
	β	-19.025	-2.317	-0.372	2.766	15.342	90.030	5.520		
	γ	-0.168	-0.103	-0.043	0.216	0.553	0.586	0.031		
16	δ	12.426	-0.455	-0.101	0.202	-0.110	-16.082	-0.170	0.58	447
	α	-4.251	0.370	0.102	-1.545	-0.001	5.361	0.348		
	β	-692.71	-43.24	14.267	45.428	117.441	-1317.67	-54.475		
	γ	-34.448	-1.110	1.878	3.230	12.175	-34.542	-30.428		
17	δ	13.598	-0.426	-0.010	-1.205	0.034	-7.221	-0.684	0.17	2,425
	α	-8.451	0.489	0.012	-0.104	-0.103	9.603	0.497		
	β	32.220	-1.360	-0.193	20.051	-1.575	40.804	-1.634		
	γ	2.582	-0.212	-0.011	0.782	-0.074	2.033	0.168		

Table 5-5 shows that β_0 has the largest absolute magnitude for most PDBIT road categories. It also shows that R^2 value varies from 0.34 to 0.79 and decreases with an increase in number of data points.

Table 5-5 PDBIT Sigmoidal RSL Model with Linear Sub-Models

RC		0	1(D)	2(EAL)	3(ETCR)	4(EFCR)	5(Rut)	6(SNeff)	R^2	N
18	δ	7.341	0.339	-0.183	0.866	0.039	10.645	-2.342	0.37	1,200
	α	-4.271	-0.123	0.229	-2.843	0.015	-18.833	2.508		
	β	164.560	-17.42	1.630	38.125	10.022	-220.302	-124.37		
	γ	11.515	-1.419	0.121	0.872	0.474	-9.601	-6.549		
19	δ	7.143	-0.244	-0.129	1.487	0.073	-9.710	2.393	0.40	931
	α	-1.607	0.500	0.163	-1.402	-1.207	-19.582	-3.651		
	β	55.934	1.124	-0.570	-1.913	1.438	-73.135	-9.803		
	γ	4.109	0.155	-0.057	0.144	0.033	-10.631	-0.472		
20	δ	-2.842	0.219	0.200	-0.303	0.006	-12.168	-2.027	0.64	542
	α	8.530	0.245	-0.235	0.243	-0.141	0.487	1.943		
	β	-7.675	1.429	0.120	-2.822	6.664	-80.477	-5.446		
	γ	0.480	0.128	0.011	-0.394	0.508	-4.890	-0.842		
21	δ	18.448	-1.702	-0.265	-1.139	-0.219	8.013	-0.334	0.79	281
	α	-16.114	1.871	0.198	0.024	0.506	-13.965	1.236		
	β	17.342	-18.69	-2.530	83.471	167.507	-524.689	39.941		
	γ	0.728	-1.531	-0.002	3.096	12.753	-30.728	2.926		
22	δ	14.892	0.009	-0.142	1.073	-0.234	-4.896	-1.632	0.56	455
	α	-16.515	0.051	0.180	-2.346	0.505	0.275	3.574		
	β	225.977	-1.841	-3.628	124.60	42.482	-272.828	-32.269		
	γ	21.844	-0.155	-0.134	7.330	2.115	-4.242	-6.244		
23	δ	3.749	-0.394	0.016	0.760	-0.238	-1.789	0.048	0.34	951
	α	0.938	0.726	-0.007	-2.941	0.164	4.719	-0.856		
	β	-7.664	-0.224	0.161	-1.448	-0.003	-7.364	0.287		
	γ	-0.877	-0.046	0.009	-0.260	0.024	-1.419	0.394		

5.3.2.1.1 Model Plots

Some of the points have higher deviation from the 45^{o} slope line when the predicted RSL is higher than the observed RSL in general for road category 12 as shown in Figure 5-1(a). For road category 13, observed and predicted RSL are somewhat balanced, though a majority of the points show higher predicted RSL as shown in Figure 5-1(b). Unlike many other road categories, few points show higher observed RSL when RSL is low for road category 14 as shown in Figure 5-1 (c). Figure 5-1(d) shows a well fit model, though a majority of the points show predicted RSL is higher than observed RSL.

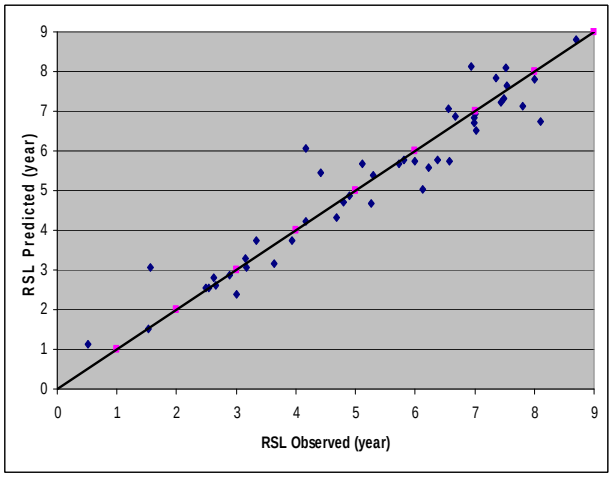

(a) Road Category 12

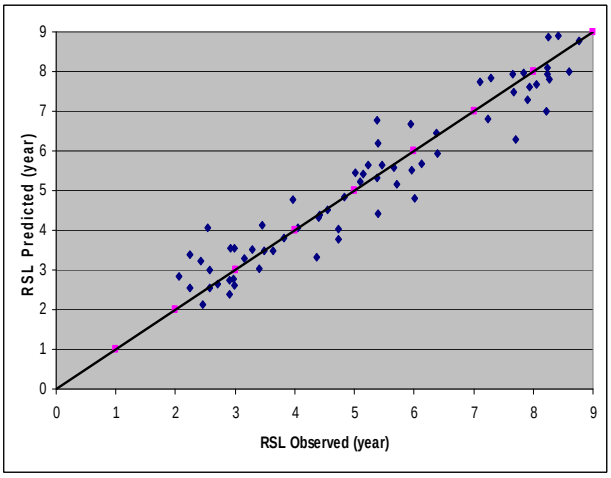

(b) Road Category 13

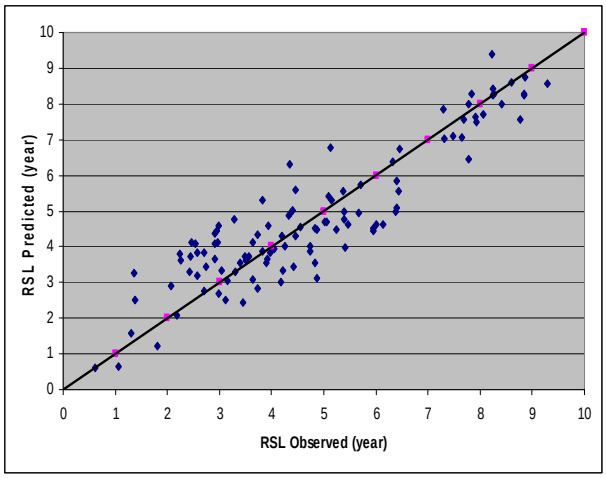

(c) Road Category 14

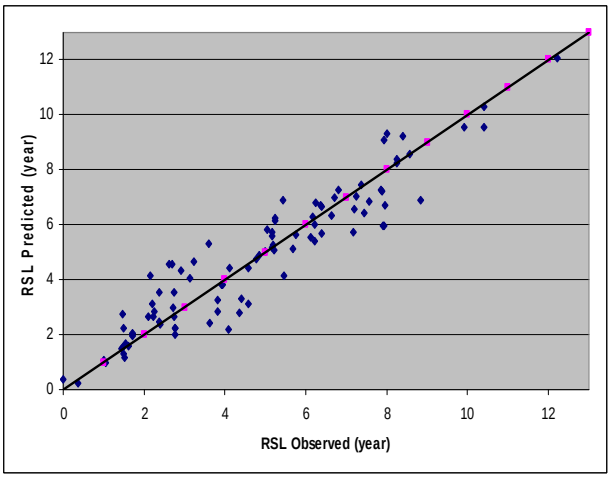

(d) Road Category 15

Figure 5-1 Sigmoidal RSL Model with Linear Sub-Models for RC 12 to 15

Sigmoidal RSL models with linear sub-models are a good fit for road category 16 since observed and predicted RSL are more or less uniform around the 45^{o} slope line as shown in Figure 5-2(a). Sigmoidal models with linear sub-models with cracking data are better than the ones with no cracking data for road categories 17 and 18. Inclusion of more points shows higher predicted RSL when RSL is low and vice versa, as shown in Figure 5-2(b) and (c). Observed and predicted RSL are well balanced except when RSL is low for road category 19 as shown in Figure 5-2(d). In general, sigmoidal models with linear sub-models that include cracking data are a better fit than the ones without cracking data for road categories 16 to 19.

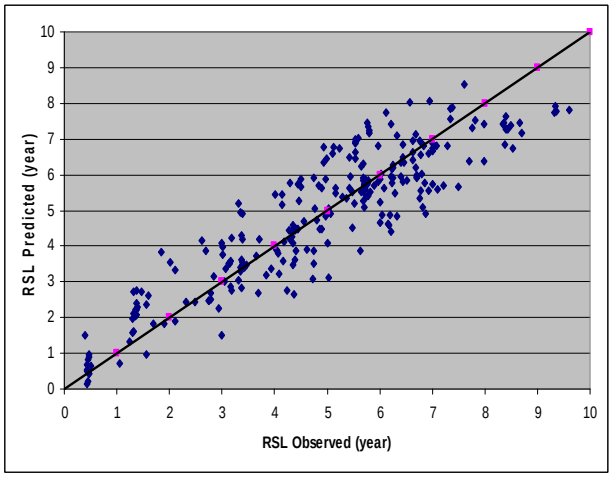

(a) Road Category 16

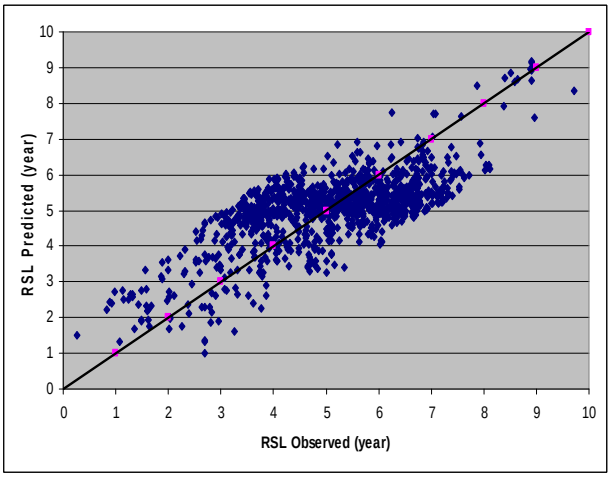

(b) Road Category 17

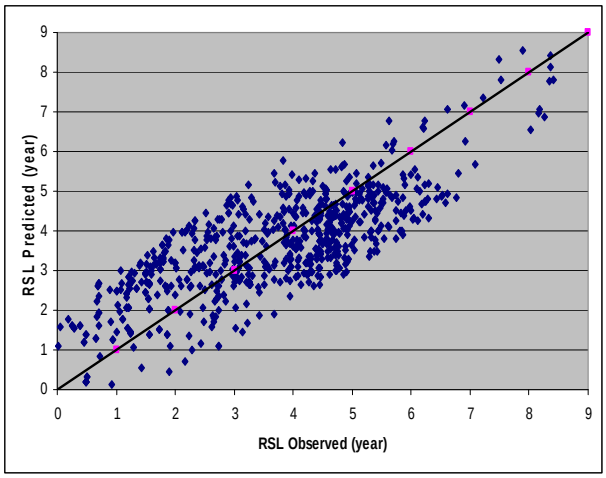

(c) Road Category 18

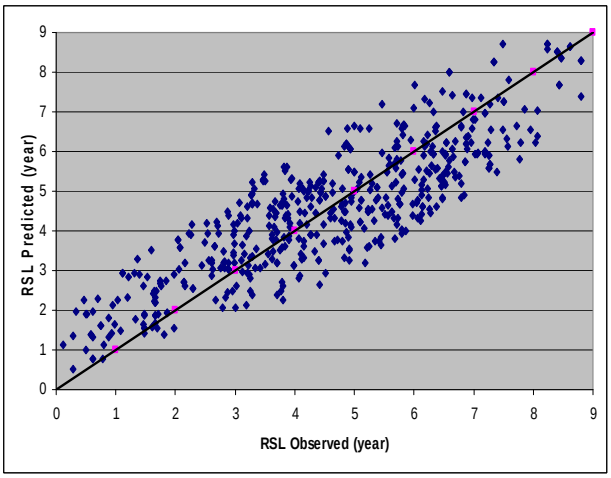

(d) Road Category 19

Figure 5-2 Sigmoidal RSL Model with Linear Sub-Models for RC 16 to 19

Observed and predicted RSL are well balanced around the 45^{o} slope line for road category 20 as shown in Figure 5-3(a). Road categories 21, 22, and 23 are also well fit as shown in Figure 5-3(b), (c), and (d). In general, sigmoidal models with linear sub-models which include cracking data are better than the ones with no cracking data for road categories 20 to 23.

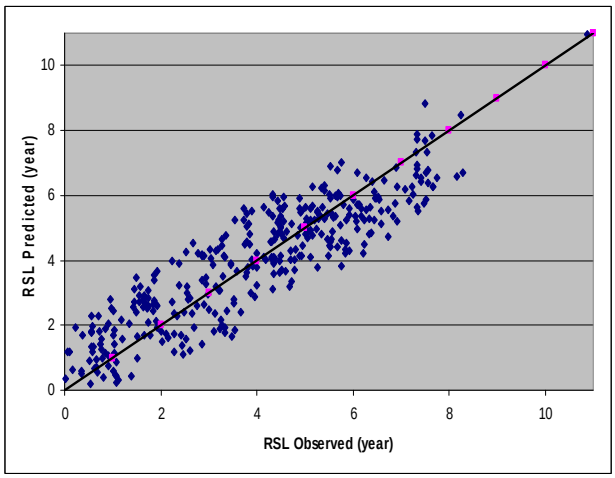

(a) Road Category 20

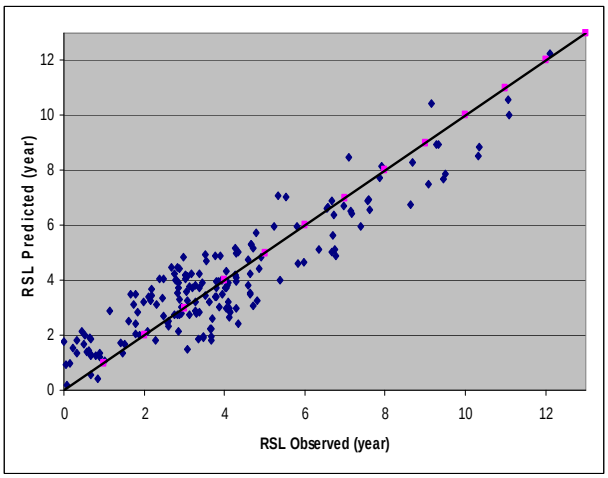

(b) Road Category 21

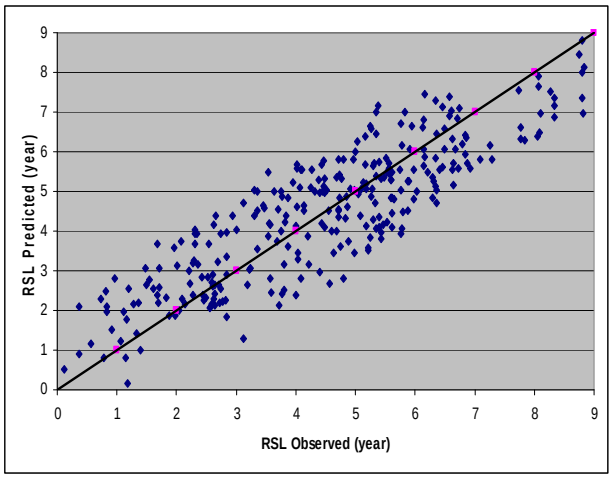

(c) Road Category 22

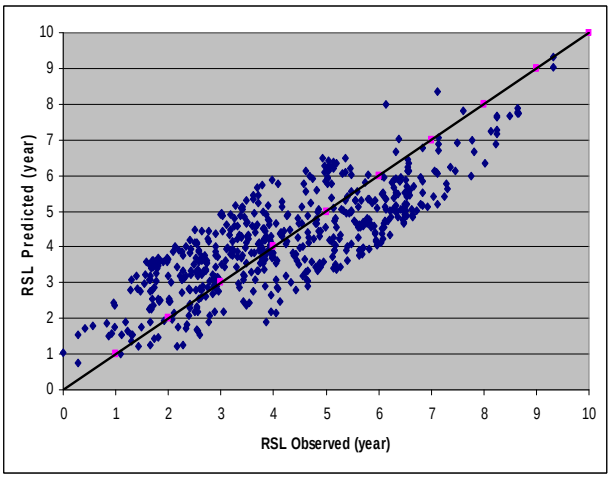

(d) Road Category 23

Figure 5-3 Sigmoidal RSL Model with Linear Sub-Models for RC 20 to 23

5.3.2.1.2 Validation Plots

Observed and predicted RSL match exactly for road categories 12, 13, and 15 as shown in Figure 5-4(a), (b), and (d). Most of the points show that observed RSL is greater than predicted RSL for road category 14 as shown in Figure 5-4(c).

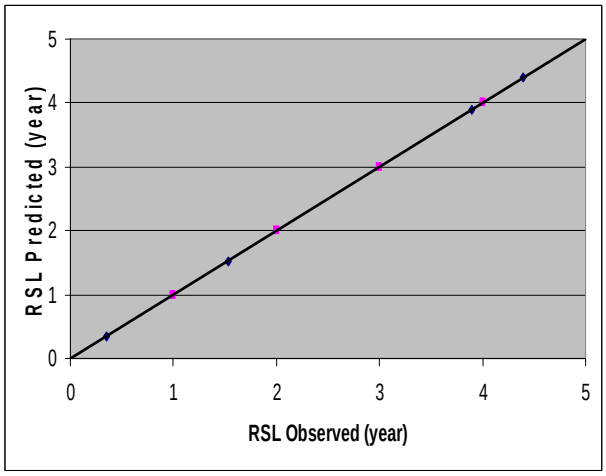

(a) Road Category 12

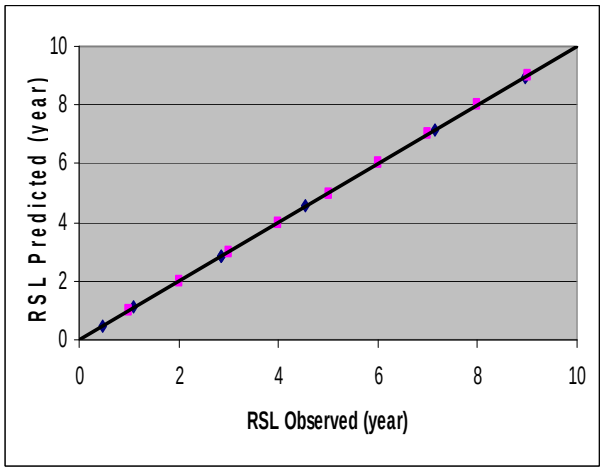

(b) Road Category 13

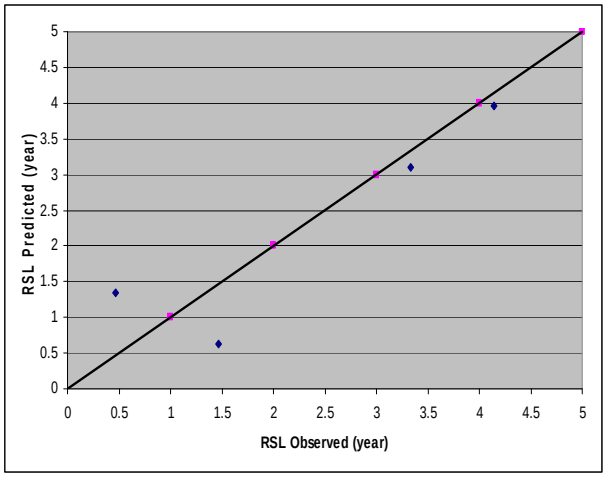

(c) Road Category 14

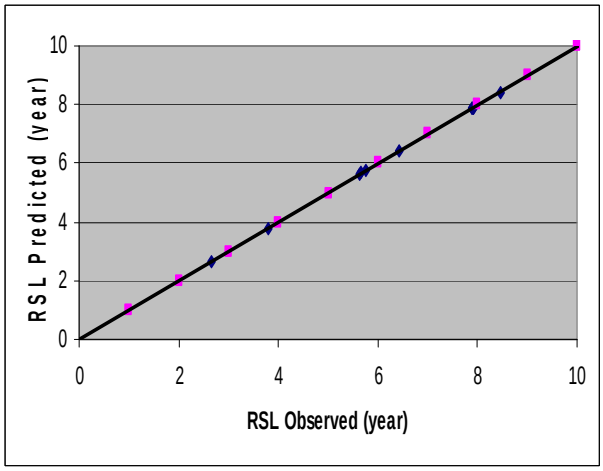

(d) Road Category 15

Figure 5-4 Sigmoidal RSL Model with Linear Sub-Models Validation for RC 12 to 15

Predicted RSL is higher than observed RSL when RSL is low, and high whereas it is lower when RSL is in between for road category 16 as shown in Figure 5-5(a). Most of the points show that predicted RSL is higher than observed RSL when RSL is low and vice versa for road category 17 as shown in Figure 5-5(b). Validation plots for road categories 18 and 19 show that observed and predicted RSL are somewhat balanced, though a majority of the points show higher predicted RSL as shown in Figure 5-5(c) and (d).

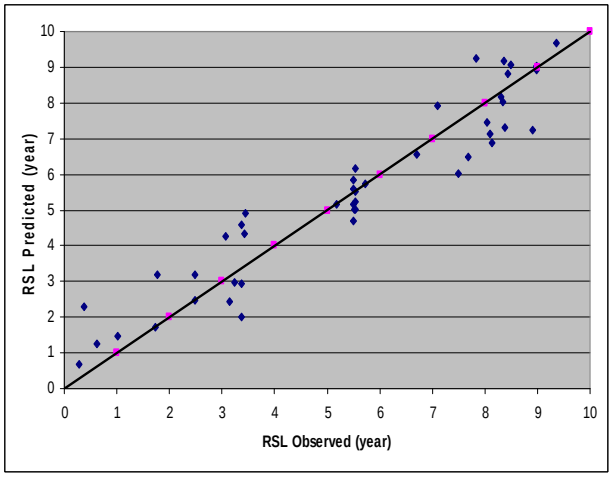

(a) Road Category 16

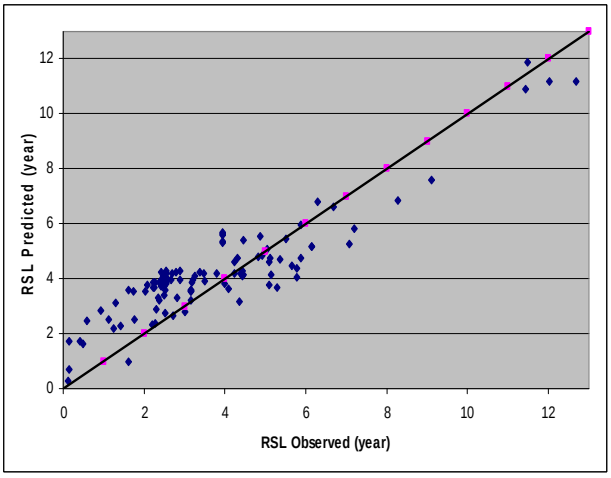

(b) Road Category 17

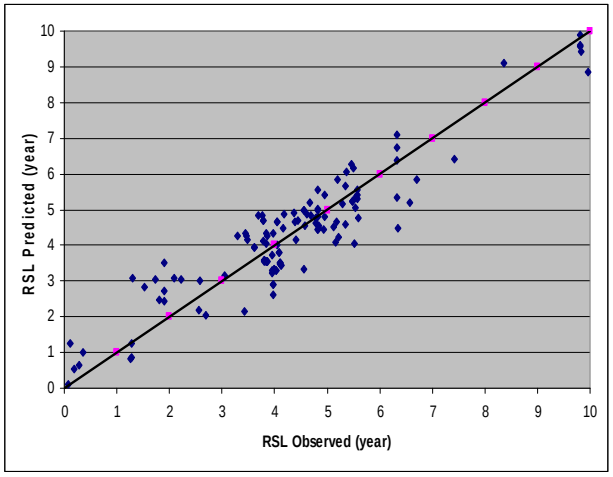

(c) Road Category 18

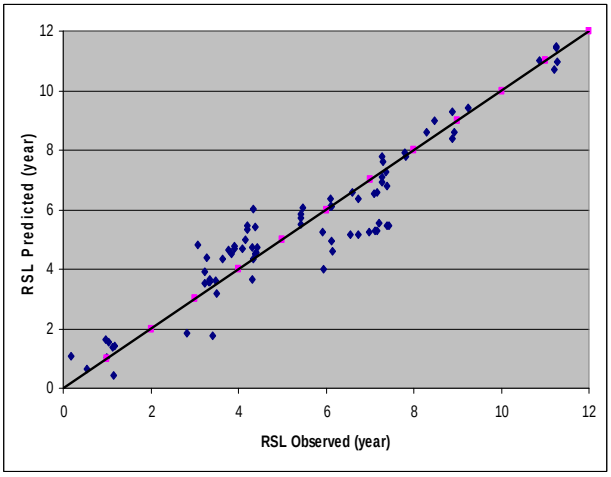

(d) Road Category 19

Figure 5-5 Sigmoidal RSL Model with Linear Sub-Models Validation for RC 16 to 19

A majority of the points show that predicted RSL is greater than observed RSL when RSL value is low and vice versa. There is almost no observed or predicted RSL when RSL is

between four and six years as shown in Figure 5-6(a). Observed and predicted RSL match almost around the 45^{o} slope line for road category 21 as shown in Figure 5-6(b). Observed and predicted RSL are more or less balanced for road categories 22 and 23, shown in Figure 5-6(c) and (d).

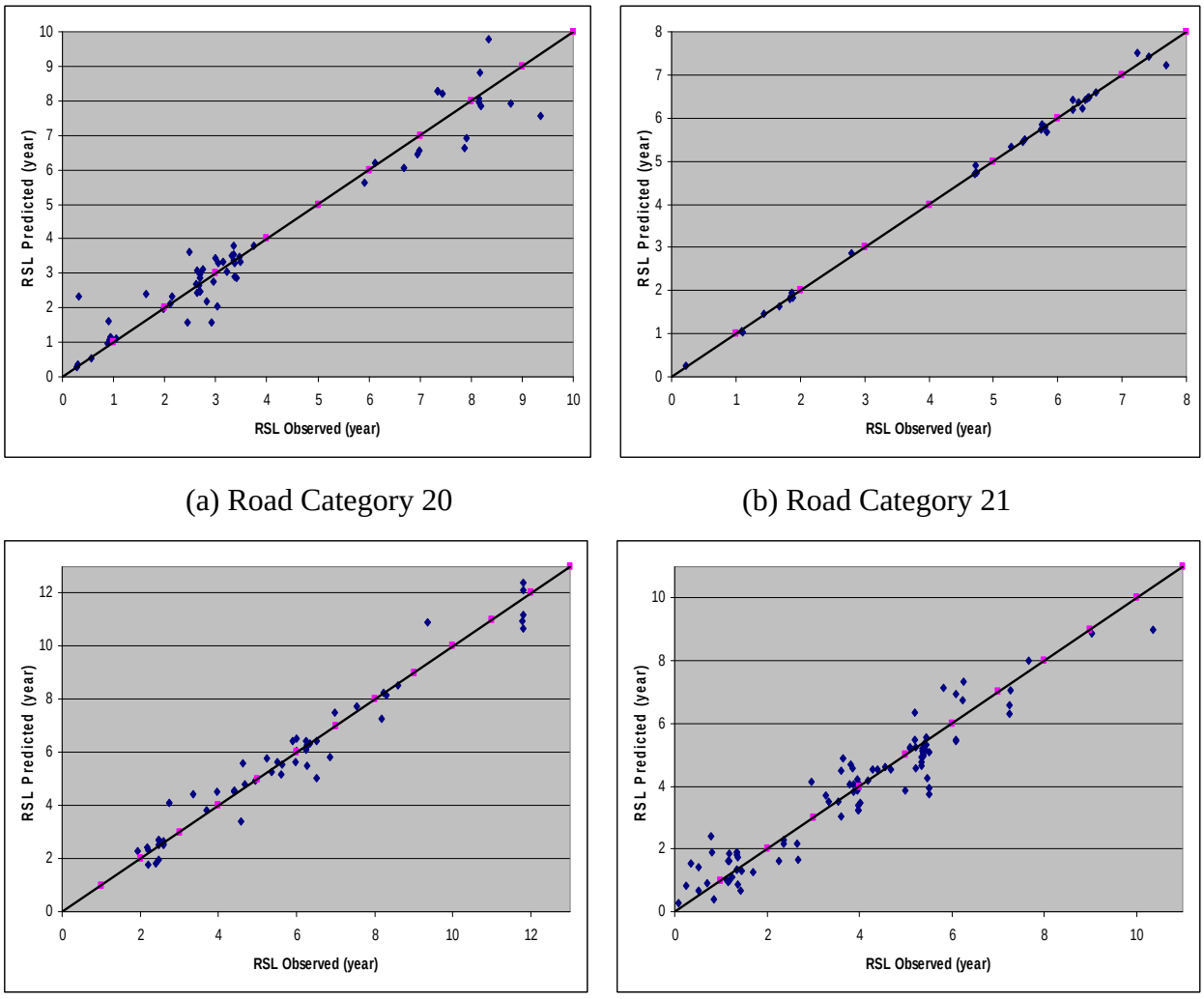

(a) Road Category 20 (b) Road Category 21

(c) Road Category 22 (d) Road Category 23

Figure 5-6 Sigmoidal RSL Mode with Linear Sub-Models Validation for RC 20 to 23

5.3.2.2 District-Wise and Statewide

The coefficient for rutting and EAL is the largest and smallest in magnitude, respectively. Table 5-6 shows the coefficient of determination varies from 0.10 to 0.45.

Table 5-6 District-Wise and Statewide Sigmoidal RSL Model with Linear Sub-Models

Dist.		0	1(D)	2(EAL)	3(ETCR)	4(EFCR)	5(Rut)	6(SNeff)	R^2	N
1	δ	4.345	0.712	0.039	-47.981	-2.467	161.230	-3.337	0.10	1,235
	α	0.927	-0.672	-0.039	47.891	2.435	-164.374	3.215		
	β	146.90	22.206	-1.910	-546.89	-5.095	-3847.89	0.718		
	γ	7.172	0.009	-0.140	-20.111	-0.887	-126.711	6.374		
2	δ	7.326	-0.423	-0.049	-8.734	0.355	-19.253	0.612	0.45	1,220
	α	3.845	0.016	0.042	5.982	-0.234	12.729	-0.410		
	β	3.052	-0.734	-0.014	-1.423	0.408	1.994	0.222		
	γ	0.013	-0.026	0.001	0.062	0.008	0.373	-0.035		
3	δ	8.685	0.278	0.155	1.087	-0.374	-19.445	-2.048	0.41	1,404
	α	-4.903	-0.072	-0.122	-1.025	0.116	8.637	1.479		
	β	46.102	2.927	-0.863	-28.713	1.460	26.830	2.496		
	γ	2.286	0.394	-0.032	-1.542	0.003	-3.963	0.180		
4	δ	2.883	0.184	0.000	-1.029	-0.034	-3.881	0.365	0.39	1,007
	α	-19.198	0.156	0.123	984.418	1.753	-30.869	4.121		
	β	-26.322	-0.267	0.038	63.183	11.934	-3.048	4.878		
	γ	-3.719	-0.053	0.004	3.120	0.639	1.630	0.630		
5	δ	4.611	-0.057	0.007	-1.201	-0.297	-0.320	-0.279	0.32	1,385
	α	5.236	-0.042	-0.018	-0.621	0.273	-0.782	-0.310		
	β	2.905	0.609	0.119	1.357	-0.868	-19.104	-3.756		
	γ	-0.355	0.100	0.006	0.212	-0.020	-2.498	-0.147		
6	δ	6.184	0.779	0.424	-2.390	-2.205	-7.614	-6.043	0.29	1,289
	α	-4.353	-0.606	-0.425	0.979	2.153	11.950	6.495		
	β	5.928	0.219	0.019	8.200	-3.574	-12.439	-1.591		
	γ	-0.208	0.021	0.006	0.461	10.831	-0.508	0.142		
State	δ	3.074	0.089	0.001	-0.824	-0.023	-2.066	0.290	0.14	7,587
	α	4.509	-0.703	0.004	-0.533	0.147	-5.069	1.386		
	β	-11.569	0.695	0.013	0.506	0.797	-17.166	2.535		
	γ	-0.810	0.080	0.001	0.079	0.035	-1.680	0.075		

5.3.2.2.1 Model Plots

Predicted RSL remains more or less constant as observed RSL increases with the exception of a few points which show better match between observed and predicted RSL for District 1 as shown in Figure 5-7(a). Observed and predicted RSL are well balanced around the 45^{o} slope line, though predicted RSL is somehow greater than observed RSL when RSL is low for Districts 2, 3, and 4 as shown in Figure 5-7(b), (c), and (d). Sigmoidal RSL models with linear sub-models that include cracking data are a better fit than the ones without cracking data.

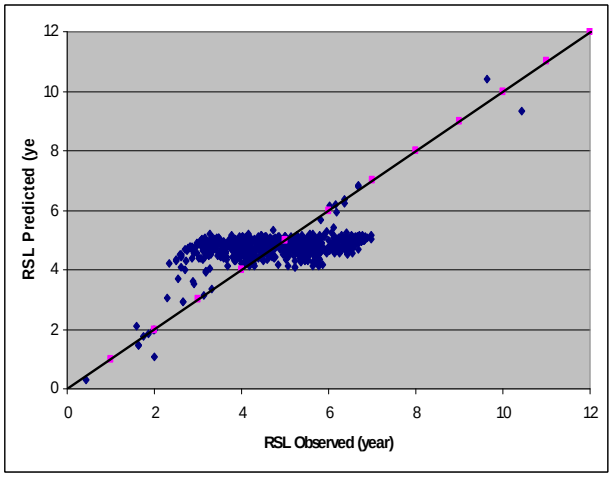

(a) District 1

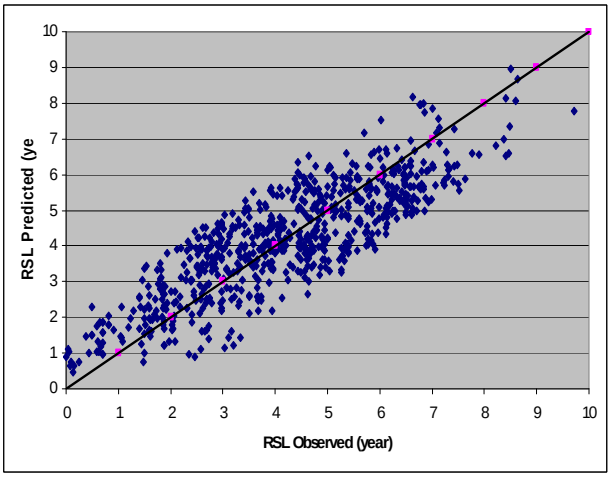

(b) District 2

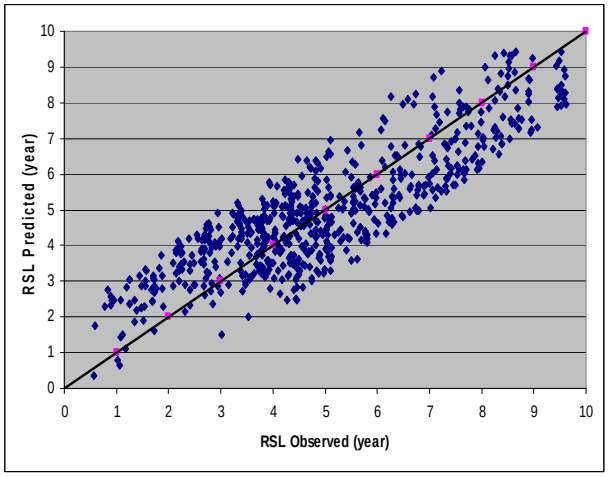

(c) District 3

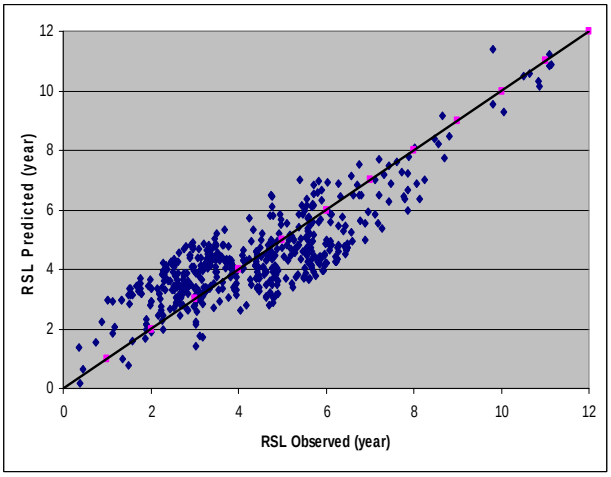

(d) District 4

Figure 5-7 Sigmoidal RSL Model with Linear Sub-Models for Districts 1 to 4

Observed and predicted RSL are balanced around the 45^{o} slope line except that predicted RSL is greater than observed RSL when RSL is low and vice versa for Districts 5, 6, and the state as shown in Figure 5-8. Sigmoidal RSL models with linear sub-models that include cracking data show a better fit than the ones without cracking data.

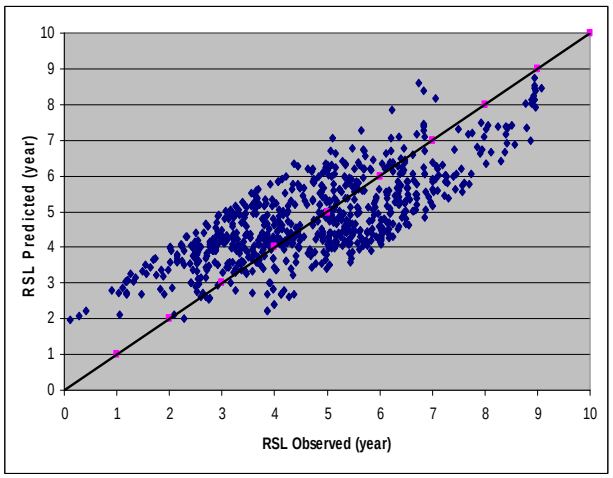

(a) District 5

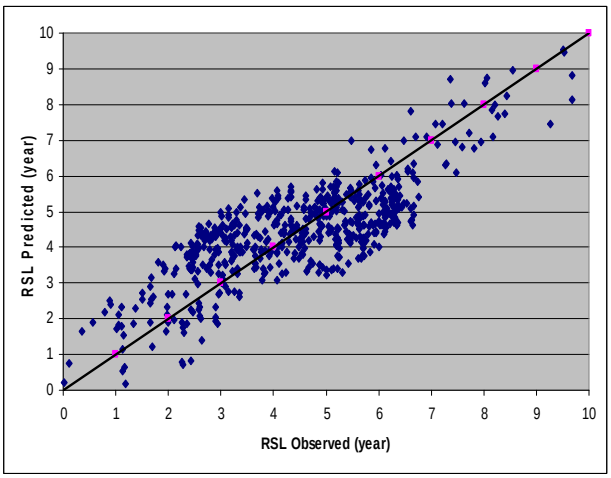

(d) District 6

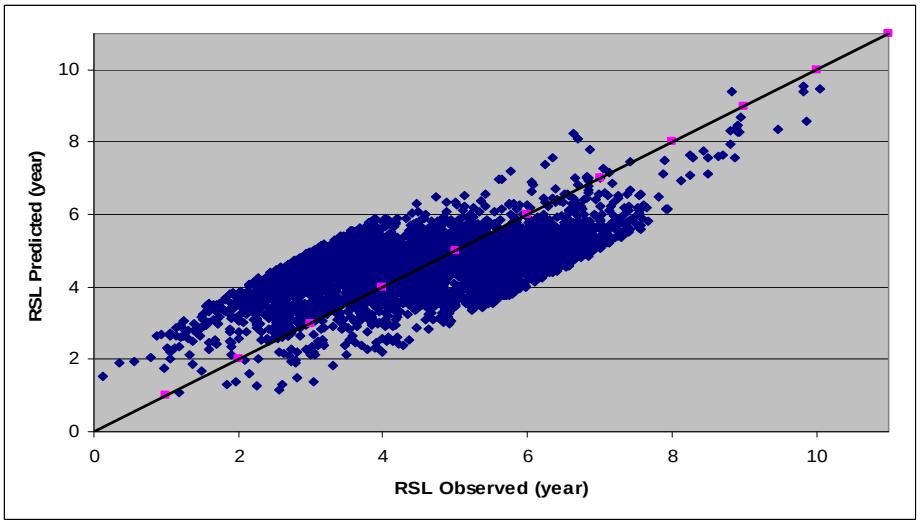

(c) State

Figure 5-8 Sigmoidal RSL Model with Linear Sub-Models for Districts 5, 6, and State

5.3.2.2.2 Validation Plots

Predicted RSL is greater than observed RSL when RSL is low and vice versa, with some scatter away from the 45^{o} slope line for District 1 as shown in Figure 5-9(a). Observed and predicted RSL are well balanced around the 45^{o} slope line for Districts 2, 3, and 4 as shown in Figure 5-9(b), (c), and (d).

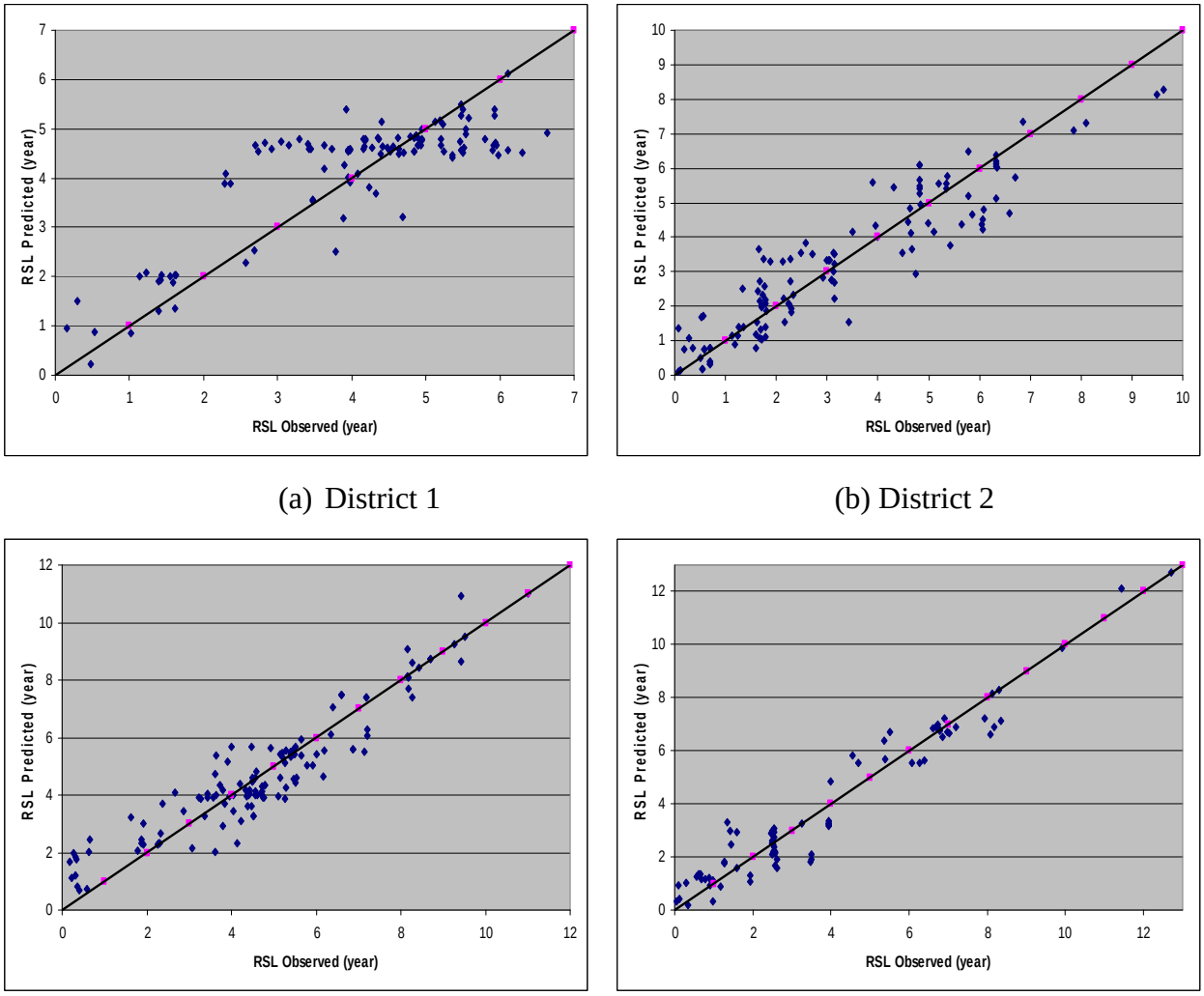

(a) District 1 (b) District 2

(c) District 3 (d) District 4

Figure 5-9 Sigmoidal RSL Models with Linear Sub-Models Validation for Districts 1 to 4

Observed and predicted RSL show good fit for District 5 as shown in Figure 5-10(a), and some points show that RSL is as high as 20 years. Validation plots for District 5 and statewide data show that the model is well fit with the exception of a few points as indicated in Figure 5-10(b) and (c).

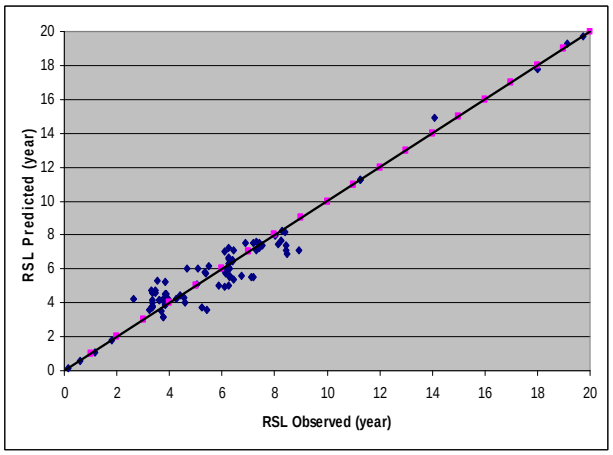

(a) District 5

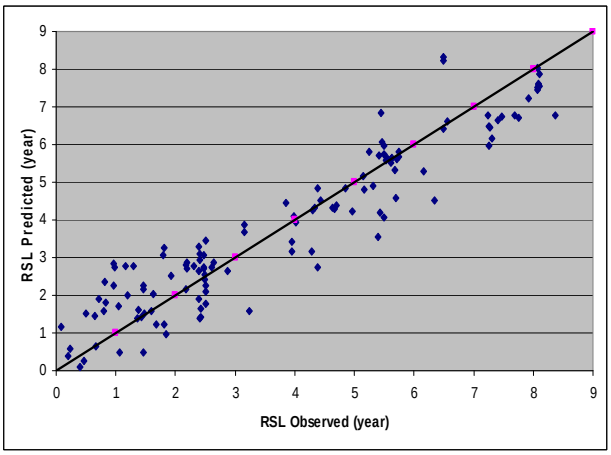

(d) District 6

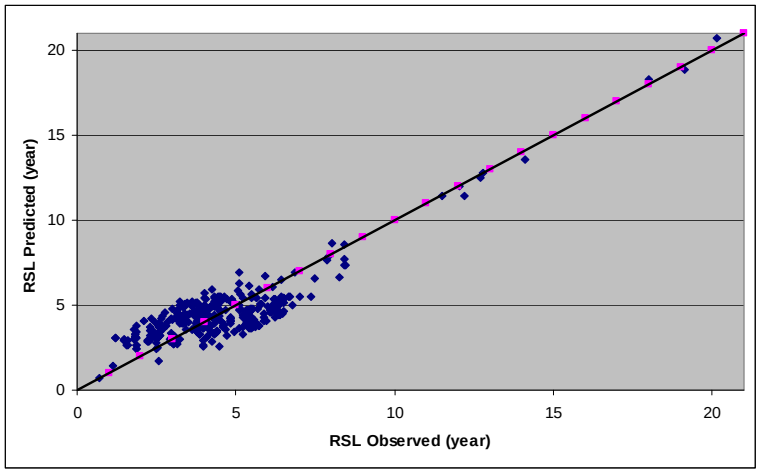

(c) State

Figure 5-10 Sigmoidal RSL Model with Linear Sub-Models Valid. for Dist. 5, 6, and State

5.3.2.3 Mean Absolute Deviation

Mean observed and predicted RSL are very close for all road categories, districts, and the state as shown in Table 5-7. The lower the mean absolue deviation observed and predicted difference, the better the model.

Table 5-7 Mean Absolute Deviation for Sigmoidal RSL Model with Linear Sub-Models

	Mean			Mean Absolute Deviation		
	Observed	**Predicted**	**Difference**	**Observed**	**Predicted**	**Difference**
(a) Road Category-Wise						
12	5.24	5.24	0.00	1.77	1.67	0.10
13	5.20	5.19	0.00	1.75	1.68	0.07
14	4.79	4.82	-0.03	1.73	1.50	0.24
15	4.83	4.83	0.00	2.18	2.04	0.14
16	4.86	4.85	0.00	1.71	1.58	0.12
17	5.05	5.06	-0.01	1.19	0.70	0.49
18	3.66	3.66	0.00	1.38	1.00	0.38
19	4.57	4.58	-0.02	1.63	1.33	0.30
20	3.99	4.02	-0.03	1.77	1.54	0.23
21	3.92	3.98	-0.06	1.81	1.58	0.23
22	4.48	4.50	-0.02	1.61	1.41	0.21
23	4.22	4.24	-0.02	1.53	1.11	0.42
(b) District-Wise and Statewide						
1	4.76	4.74	0.02	1.03	0.29	0.73
2	4.21	4.21	0.01	1.52	1.25	0.27
3	4.95	4.94	0.01	1.69	1.34	0.35
4	4.35	4.36	-0.01	1.47	1.04	0.43
5	4.73	4.79	-0.06	1.38	0.95	0.43
6	4.50	4.50	0.00	1.40	0.97	0.43
State	4.64	4.63	0.01	1.17	0.68	0.49

5.3.3 Sigmoidal RSL Model with Quadratic Sub-Models

The sigmoidal RSL model with quadratic sub-models has been developed only for districts and the state to see the difference with the linear sub-models. Six variables in the linear sub-models have been included. Coefficients for the quadratic part of EAL are zero or close to zero whereas coefficients for quadratic part of rutting is the highest in magnitude for Districts 1 to 3 as shown in Table 5-8. The coefficient of determination varies from 0.31 to 0.54.

Table 5-8 Sigmoidal RSL Model with Quadratic Sub-Models for Districts 1 to 3

Dist.		0	1(D)	2(EAL)	3(ETCR)	4(EFCR)	5(Rut)	6(SNeff)	R^2	N
1	δ	-28.791	7.172	-3.325	-8.262	-20.327	177.192	7.512	0.31	1,235
	α	31.523	-6.911	3.319	7.661	20.371	-174.71	-6.771		
	β	-7.379	0.128	1.071	1.063	9.276	2.513	2.337		
	γ	0.687	0.727	-0.928	0.909	0.980	1.734	0.868		
	δ_{ii}	-	2.628	0.100	45.874	3.618	-5.908	-2.248		
	α_{ii}	-	-2.642	-0.100	-45.61	-3.622	-14.332	2.160		
	β_{ii}	-	-0.102	0.123	-0.072	-0.479	-31.258	-1.073		
	γ_{ii}	-	0.138	0.121	-1.352	-0.071	-3.700	-0.254		
2	δ	2.927	0.543	0.006	-1.753	-0.108	-5.442	-0.225	0.54	1,220
	α	8.229	0.099	0.023	-0.273	-0.261	7.182	-4.191		
	β	-37.293	4.418	0.207	-8.727	3.131	22.267	20.981		
	γ	-6.721	0.611	0.058	0.278	-0.558	0.781	2.330		
	δ_{ii}	-	-0.033	0.000	0.251	0.010	-8.727	0.082		
	α_{ii}	-	-0.005	0.000	0.406	-0.003	4.500	0.362		
	β_{ii}	-	-0.698	-0.001	4.977	-0.380	-99.102	-3.671		
	γ_{ii}	-	-0.073	0.000	-0.072	0.014	-20.126	-0.506		
3	δ	7.202	-2.024	-0.003	0.147	0.835	-19.846	1.134	0.53	1,404
	α	-3.222	1.460	0.022	-0.762	-1.174	0.353	0.835		
	β	-23.751	11.110	0.165	19.652	4.258	40.425	-19.626		
	γ	-3.268	1.636	-0.010	-3.755	0.438	8.934	-0.878		
	δ_{ii}	-	0.333	0.000	-0.925	-0.057	34.357	-0.267		
	α_{ii}	-	-0.286	0.000	1.010	0.069	23.084	-0.083		
	β_{ii}	-	-0.292	0.000	-15.561	-0.107	-98.080	3.052		
	γ_{ii}	-	-0.097	0.000	0.519	-0.013	-34.984	0.111		

The coefficients of the quadratic part of EAL and rutting show the lowest and the highest magnitude, respectively, for Districts 4 to 6 as shown in Table 5-9.

Table 5-9 Sigmoidal RSL Model with Quadratic Sub-Models for Districts 4 to 6

Dist.		0	1(D)	2(EAL)	3(ETCR)	4(EFCR)	5(Rut)	6(SNeff)	R^2	N
4	δ	8.356	-0.785	-0.009	-5.570	-0.242	-49.481	2.221	0.55	1,007
	α	-30.510	-0.125	0.024	13.510	0.432	201.766	-3.163		
	β	2.056	-0.169	0.006	0.008	0.034	27.695	-0.386		
	γ	-0.087	-0.013	0.001	0.019	-0.001	1.186	0.068		
	δ_{ii}	-	0.052	0.000	2.842	0.014	160.709	-0.174		
	α_{ii}	-	0.037	0.000	-10.585	0.001	-374.19	0.256		
	β_{ii}	-	-0.001	0.000	0.317	-0.001	-140.65	-0.021		
	γ_{ii}	-	0.000	0.000	0.005	0.001	-4.255	-0.017		
5	δ	15.261	-0.611	-0.051	-0.796	0.080	-39.575	-1.605	0.61	1,385
	α	-8.199	0.311	0.023	0.116	0.196	26.010	1.133		
	β	-44.497	-0.169	0.022	-8.139	1.119	201.866	19.793		
	γ	0.207	-0.278	0.002	0.101	0.119	11.123	-0.127		
	δ_{ii}	-	0.033	0.000	-0.346	-0.002	114.649	0.297		
	α_{ii}	-	-0.013	0.000	-0.752	-0.074	-78.748	-0.207		
	β_{ii}	-	-0.024	-0.001	5.183	-0.036	-498.97	-2.284		
	γ_{ii}	-	0.013	0.000	-0.423	-0.004	-20.456	0.116		
6	δ	-29.067	7.051	0.375	-8.516	-20.203	171.974	7.602	0.43	1,289
	α	31.948	-7.193	-0.361	7.489	20.136	-179.86	-7.181		
	β	-7.405	0.128	0.175	1.135	8.723	2.537	2.227		
	γ	-0.559	0.002	0.005	0.208	1.175	1.236	0.328		
	δ_{ii}	-	-0.586	-0.006	45.831	3.895	11.780	-0.597		
	α_{ii}	-	0.606	0.006	-45.639	-3.894	3.368	0.568		
	β_{ii}	-	0.036	0.000	-0.111	0.167	-31.254	-1.051		
	γ_{ii}	-	0.002	0.000	-0.026	0.016	-3.771	-0.093		

The coefficient of the quadratic part of EAL is the highest in magnitude for only two of the four sub-models for Districts 4, 5, and 6 as shown in Table 5-9. The coefficient of determination varies from 0.43 to 0.61, which shows an improvement over the sigmoidal RSL model with linear sub-models, mainly due to the increase in the number of parameters.

The coefficients of the linear part of rutting are largest in magnitude for each sub-model using statewide data except the beta sub-model and the largest coefficients for beta and gamma sub-models as shown in Table 5-10. The coefficient of determination is 0.32 and is greater than that of the sigmoidal RSL model with linear sub-models. Some of the coefficients have different signs for different variables in the linear and quadratic sub-models.

The sigmoidal model with quadratic sub-models shows an improvement in R^2 mainly due to the increase in the number of parameters. To clarify coefficients, a sigma (δ) sub-model has been considered as an example. Intercept (δ_0), the coefficient for linear (δ_1), and quadratic (δ_{22}) part of the total pavement thickness above subgrade (D) are -28.66, 7.157, and -0.607, respectively, from Table 5-10. It is to be noted that no coefficients have been given in the table corresponding to the quadratic coefficients, since each sub-model has only one intercept. Fittness of this model has been discussed based on the model and validation plots.

Table 5-10 Sigmoidal RSL Model with Quadratic Sub-Models Using Statewide Data

	0	**1(D)**	**2(EAL)**	**3(ETCR)**	**4(EFCR)**	**5(Rut)**	**6(SNeff)**	**R^2**	**N**
δ	-28.66	7.157	0.374	-8.384	-20.207	172.014	7.765	0.32	8,427
α	32.349	-7.089	-0.371	7.621	20.133	-179.82	-7.030		
β	-7.404	0.128	0.174	1.133	8.723	2.536	2.223		
γ	-0.582	-0.027	-0.026	0.234	1.170	1.238	0.346		
δ_{ii}	-	-0.607	-0.005	45.779	3.896	11.782	-0.619		
α_{ii}	-	0.605	0.005	-45.69	-3.893	3.370	0.522		
β_{ii}	-	0.020	-0.014	-0.116	0.166	-31.254	-1.075		
γ_{ii}	-	0.162	0.049	0.046	0.016	-3.770	0.154		

5.3.3.1.1 Model Plots

Predicted RSL remains more or less constant with an increase in observed RSL, and there is no improvement due to quadratic sub-models as shown in Figure 5-11(a). Observed and predicted RSL match very well for Districts 2, 3, and 4, though predicted RSL is slightly greater than observed RSL when RSL is low and vice versa as shown Figure 5-11(b), (c), and (d).

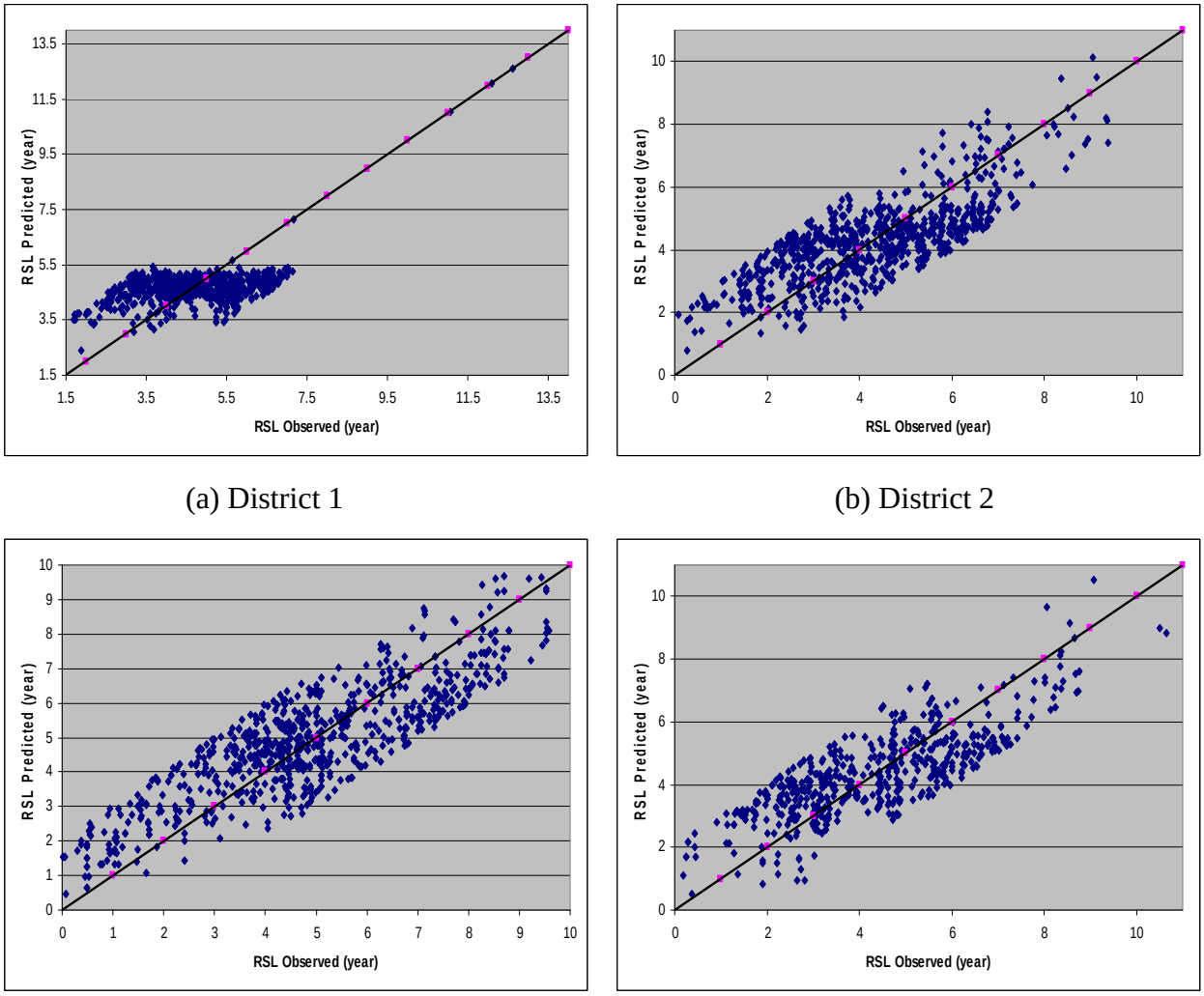

(a) District 1 (b) District 2

(c) District 3 (d) District 4

Figure 5-11 Sigmoidal RSL Model with Quadratic Sub-Models for Districts 1 to 4

Figure 5-12(a) and (b) show a good fit for Districts 5 and 6 except predicted RSL is slightly higher when observed RSL is low and vice versa. Observed and predicted RSL do not fit well for statewide data as shown in Figure 5-12(c). The sigmoidal RSL model with linear sub-models shows a better fit than the sigmoidal RSL model with quadratic sub-models for statewide data.

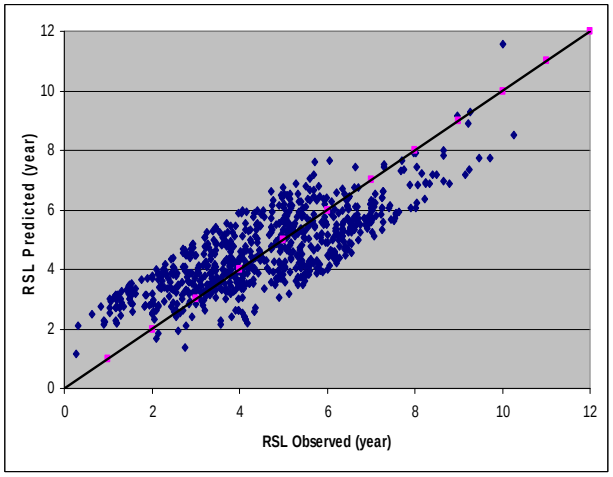

(a) District 5

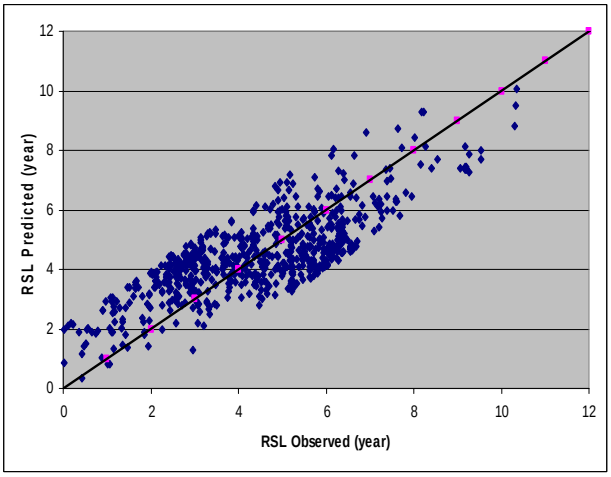

(b) District 6

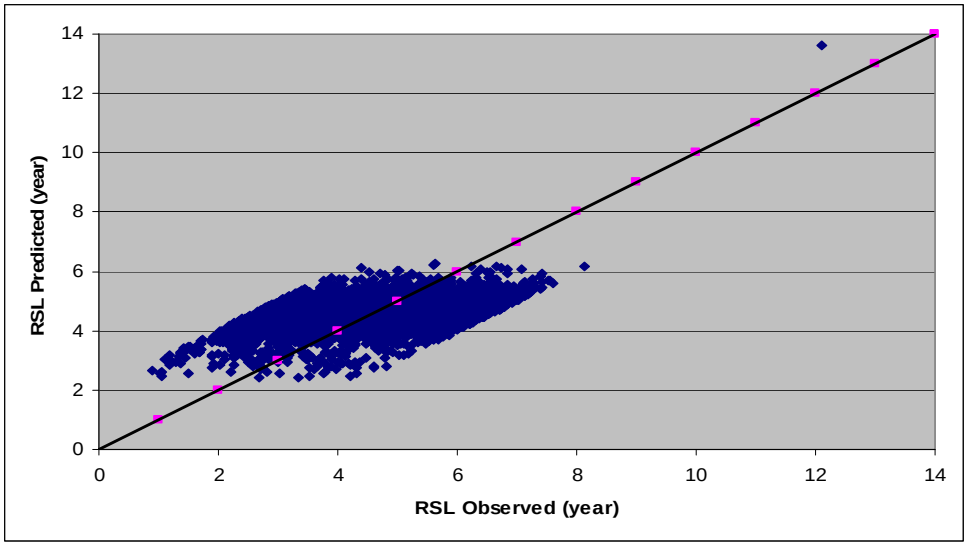

(c) State

Figure 5-12 Sigmoidal RSL Model with Quadratic Sub-Models for Districts 5, 6, and State

5.3.3.1.2 Validation Plots

Validation plots for District 1 show that predicted RSL is zero at two points and there is scatter as shown in Figure 5-13(a). A majority of the points show that predicted RSL is higher than observed RSL when RSL is low and vice versa for District 2 as shown in Figure 5-13(b). Figure 5-13(c) and (d) show that observed and predicted RSL are balanced around the 45^{o} slope line.

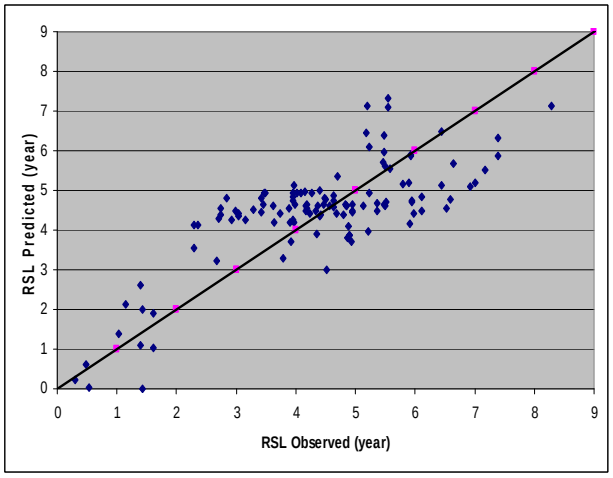

(a) District 1

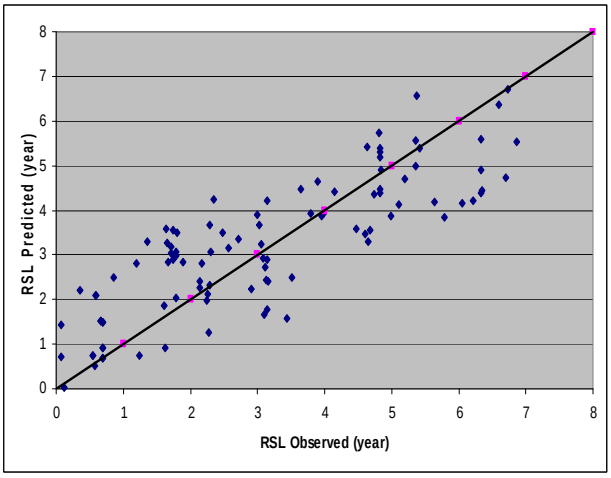

(b) District 2

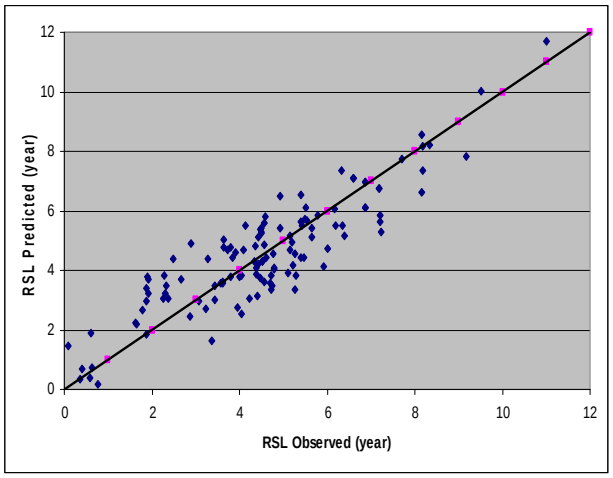

(c) District 3

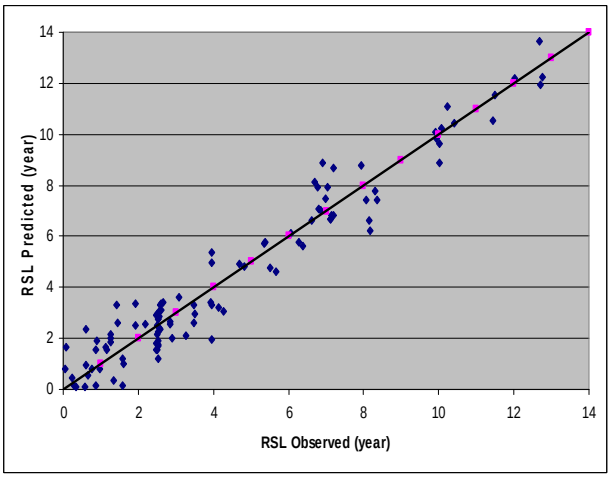

(d) District 4

Figure 5-13 Sigmoidal RSL Model with Quadratic Sub-Models Valid. for Districts 1 to 4

Observed and predicted RSL are in good agreement for Districts 5 and 6 as shown in Figure 5-14(a) and (b). Observed and predicted RSL show somewhat good agreement statewide, though predicted RSL is higher when observed RSL is low or high as shown in Figure 5-14(c). In general, validation plots using the sigmoidal RSL model with quadratic sub-models do not show significant improvement over the sigmoidal RSL model with linear sub-models.

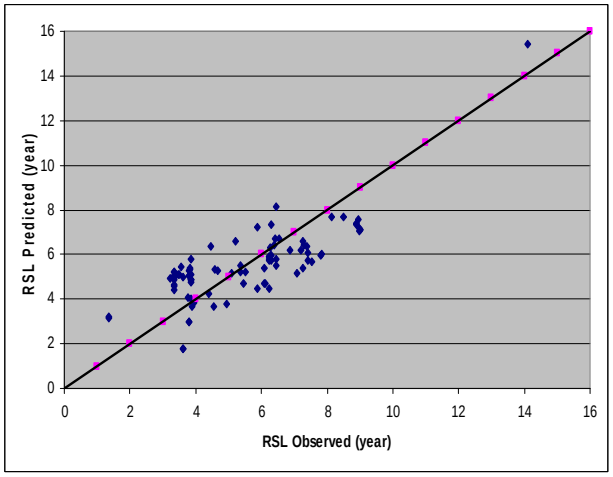

(a) District 5

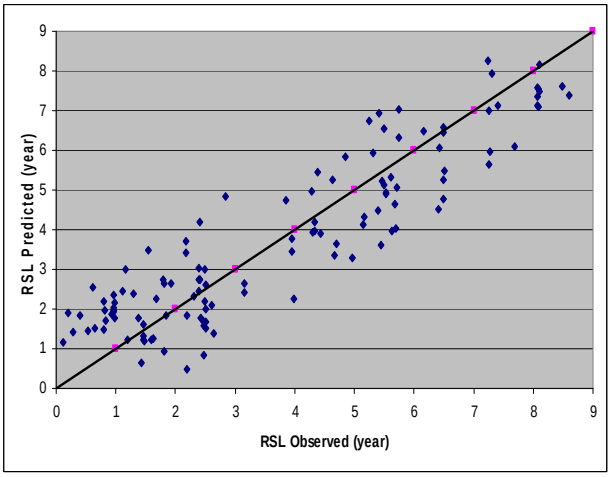

(b) District 6

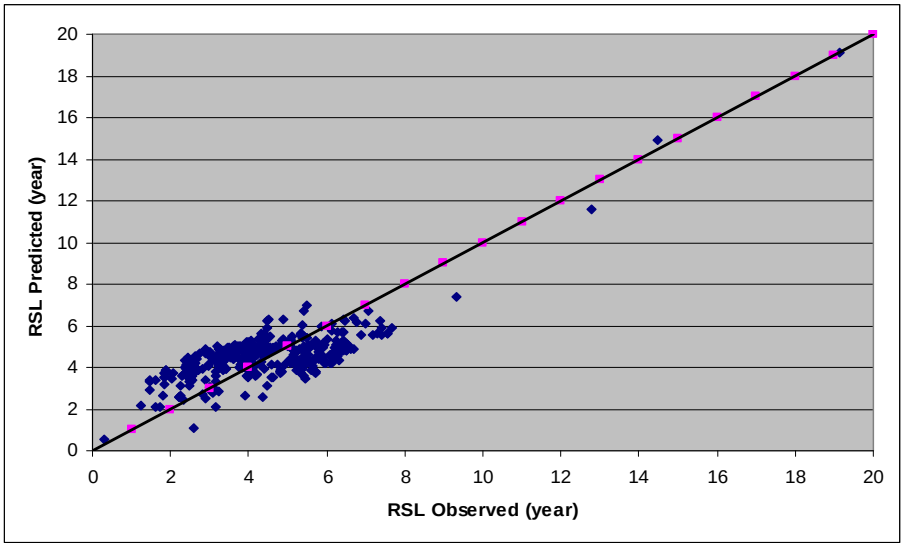

(c) State

Figure 5-14 Sigmoidal RSL Model with Quad. Sub-Models Valid. for Dist. 5, 6, and State

5.3.3.2 Mean Absolute Deviation

Mean difference between observed and predicted RSL is insignificant for all districts and the state as shown in Table 5-11. Mean absolute deviation difference is relatively high if the RSL sigmoidal model is not a good fit.

Table 5-11 Mean Absolute Deviation for Sigmoidal RSL Model with Quad. Sub-Models

District	Mean			Mean Absolute Deviation		
	Observed	Predicted	Difference	Observed	Predicted	Difference
1	4.75	4.68	0.07	1.07	0.36	0.71
2	4.26	4.24	0.01	1.47	0.98	0.49
3	4.83	4.89	-0.06	1.66	1.29	0.38
4	4.33	4.34	-0.01	1.54	1.06	0.48
5	4.51	4.57	-0.06	1.47	1.08	0.39
6	4.42	4.49	-0.07	1.54	1.01	0.53
State	4.60	4.58	0.01	1.09	0.46	0.63

5.3.4 Sigmoidal RSL Model Using Statewide Data

In all RSL sigmoidal models discussed, coefficients for EAL are lowest in magnitude since EAL is largest in magnitude. Three different cases have been considered using a logarithm of EAL (logEAL), and the fourth case is without cracking data. Cases (a) and (b) are sigmoidal RSL models with linear and quadratic sub-models, respectively, with logEAL. Cases (c) and (d) are sigmoidal RSL models with quadratic sub-models without cracking data with EAL and logEAL, respectively. Table 5-12 shows the coefficients for all cases. The coefficient of determination varies from 0.13 to 0.30 for the four cases.

Coefficients for logEAL in the sigmoidal RSL models with linear sub-models are the second highest in magnitude next to the rutting coefficients, whereas there is no specific trend with the quadratic sub-models. Coefficients for EAL are the lowest in magnitude in the sigmoidal RSL model with quadratic sub-models that does not include cracking data.

Table 5-12 Sigmoidal RSL Models Using Statewide Data

		0	1(D)	2(logEAL)	3(ETCR)	4(EFCR)	5(Rut)	6(SNeff)	R^2	N
1[a]	δ	5.738	-0.514	2.085	-0.720	0.044	-10.825	0.769	0.15	7,586
	α	-2.174	0.624	-2.261	-0.113	-0.054	9.039	-0.542		
	β	19.102	-0.698	-4.742	-0.386	-1.225	26.922	-2.702		
	γ	1.615	-0.080	-0.486	-0.105	-0.052	2.573	-0.103		
2[b]	δ	4.608	0.249	-0.548	-1.434	0.184	-6.710	-0.279	0.17	7,586
	α	15.669	-3.843	-24.24	-3.666	-4.351	12.620	13.314		
	β	-9.992	0.557	5.775	2.768	-0.004	-8.701	1.391		
	γ	-1.102	0.059	0.715	0.071	-0.011	-0.906	0.013		
		-	-0.013	-0.017	0.176	-0.005	9.497	0.065		
		-	0.369	8.352	92.308	0.056	-43.368	-2.047		
		-	-0.035	-1.088	-0.517	0.001	6.157	-0.073		
		-	-0.004	-0.137	-0.024	0.000	0.915	0.007		
3[c]	δ	4.510	-0.165	-0.001	-	-	-9.622	0.217	0.30	7,587
	α	2.983	0.587	-0.002	-	-	13.503	-1.463		
	β	-27.93	3.235	0.043	-	-	2.307	5.480		
	γ	-2.460	0.216	0.006	-	-	-1.766	0.652		
	δ	-	0.027	0.000	-	-	17.832	-0.033		
	α	-	-0.063	0.000	-	-	-30.12	0.127		
	β	-	-0.121	0.000	-	-	-6.861	-0.985		
	γ	-	-0.006	0.000	-	-	4.165	-0.121		
4[d]	δ	3.901	0.180	-0.367	-	-	-6.598	-0.083	0.13	7,586
	α	16.681	1.067	-13.77	-	-	32.572	-2.179		
	β	-15.02	3.036	1.137	-	-	14.038	0.409		
	γ	-1.854	0.208	0.542	-	-	0.270	0.231		
	δ	-	-0.014	0.178	-	-	15.329	0.033		
	α	-	-0.061	3.750	-	-	-54.249	0.115		
	β	-	-0.212	0.730	-	-	-49.811	-0.050		
	γ	-	-0.014	-0.053	-	-	-4.384	-0.040		

a- linear sub-model with logEAL; b-quadratic sub-model with logEAL; c-quadratic sub-model with no cracking data; d-quadratic sub-model with no cracking data and logEAL

5.3.4.1 Model Plots

Figure 5-15 shows predicted RSL is higher when RSL is low and lower when RSL is high for all cases considered using statewide data.

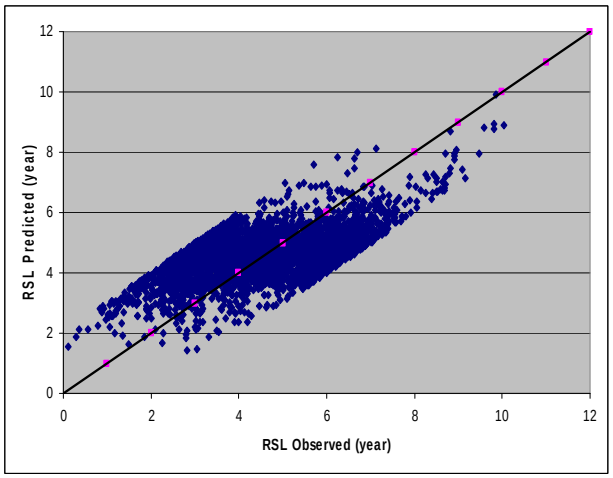

(a) Linear Sub-Models with LogEAL

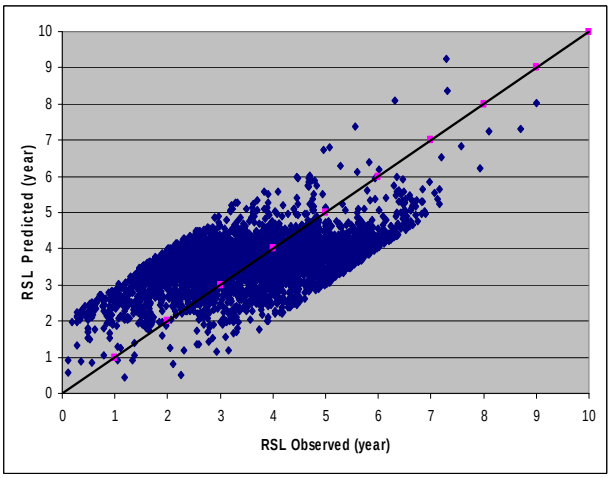

(b) Quadratic Sub-Models with LogEAL

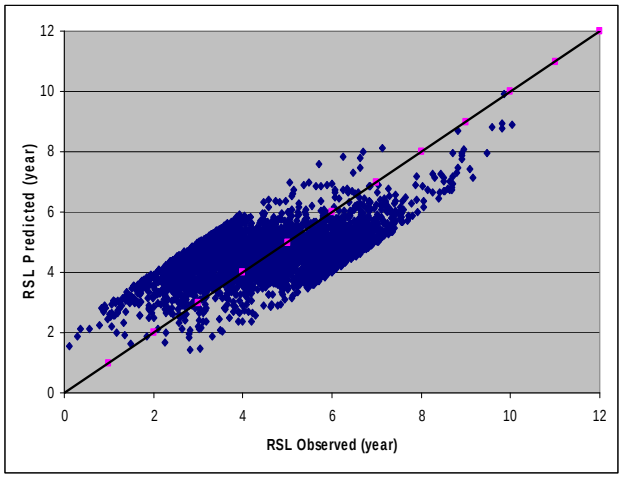

(c) Quadratic Sub-Models with no Cracking Data

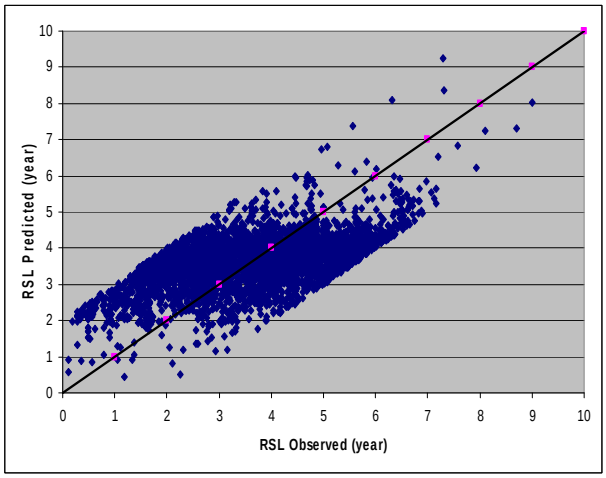

(d) Quadratic Sub-Models with No Cracking and LogEAL

Figure 5-15 Sigmoidal RSL Model Using Statewide Data

5.3.4.2 Validation Plots

Figure 5-16 shows some scatter in the validation plots for all four cases, and predicted RSL is higher at low RSL and vice versa.

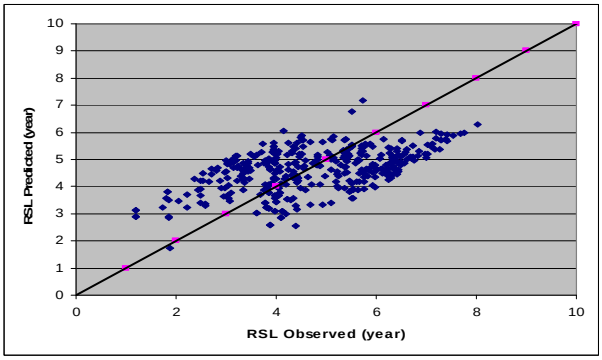

(a) Linear Sub-Models with LogEAL

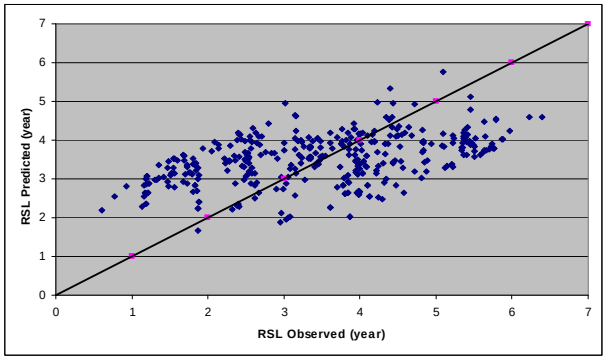

(b) Quadratic Sub-Models with LogEAL

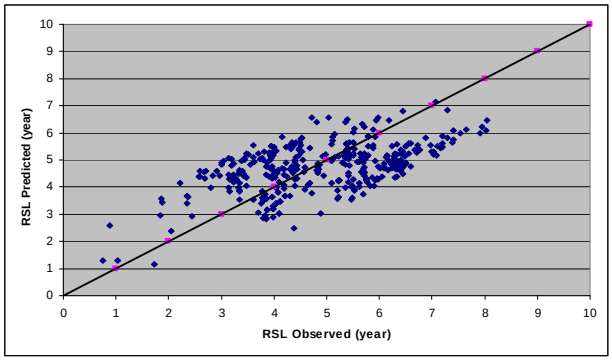

(c) Quadratic Sub-Models with no Cracking Data

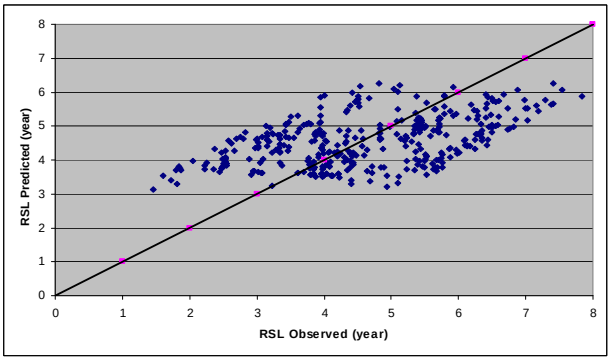

(d) Quadratic Sub-Models with No Cracking and LogEAL

Figure 5-16 Sigmoidal RSL Model Validation Using Statewide Data

5.3.4.3 Mean Absolute Deviation

Table 5-13 shows mean difference between observed and predicted RSL is low. Low mean absolute deviation difference shows a good agreement between observed and predicted RSL values.

Table 5-13 Mean Absolute Deviation for Sigmoidal RSL Model Using Statewide Data

	Mean			Mean Absolute Deviation		
	Observed	**Predicted**	**Difference**	**Observed**	**Predicted**	**Difference**
1[a]	4.62	4.61	0.01	1.20	0.61	0.59
2[b]	4.63	4.61	0.02	1.15	0.56	0.59
3[c]	4.36	4.40	-0.04	1.20	0.72	0.48
4[d]	4.42	4.66	-0.24	1.90	1.94	-0.04

a- linear sub-model with logEAL; b-quadratic sub-model with logEAL; c-quadratic sub-model with no cracking data; d-quadratic sub-model with no cracking data and logEAL

5.3.5 Relationship between RSL and Center Deflection

The relationship between RSL and center deflection has been investigated by keeping other variables constant in the road category-wise, district-wise, and statewide models. A typical relationship is presented in this section.

5.3.5.1 Road Category-Wise

There is a smooth sigmoidal relationship between RSL and the center deflection for road categories 13 and 15, whereas the relationship is not smooth for road categories 12 and 14 mainly due to a lesser number of data points as shown in Figure 5-17.

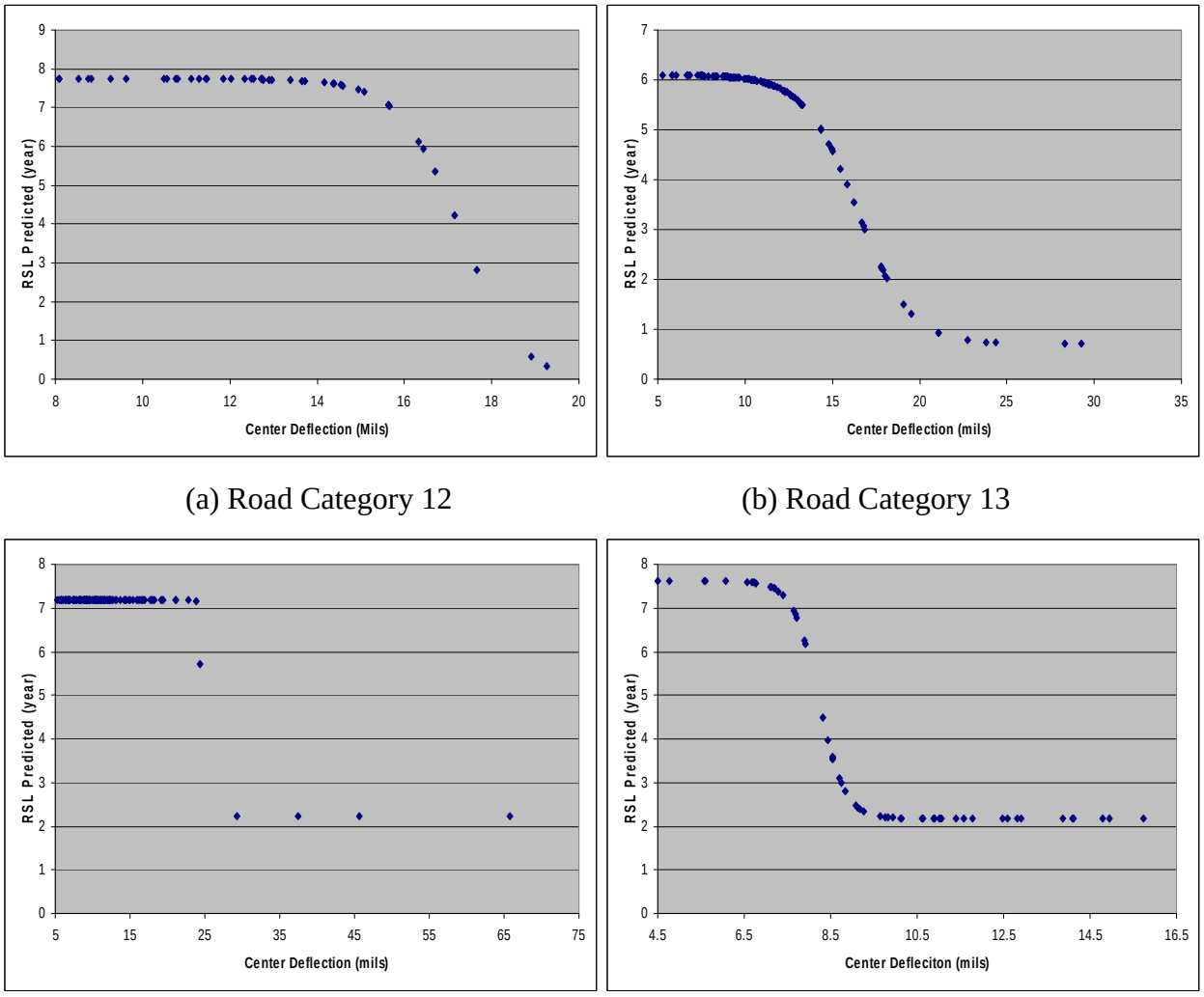

(a) Road Category 12

(b) Road Category 13

(c) Road Category 14

(d) Road Category 15

Figure 5-17 Relationship between RSL and Center Deflection for Road Categories 12 to 15

There is a smooth sigmoidal relationship between RSL and the center deflection for road categories 16 to 19 as shown in Figure 5-18. There is a slight decrease in RSL after a certain threshold value of the center deflection.

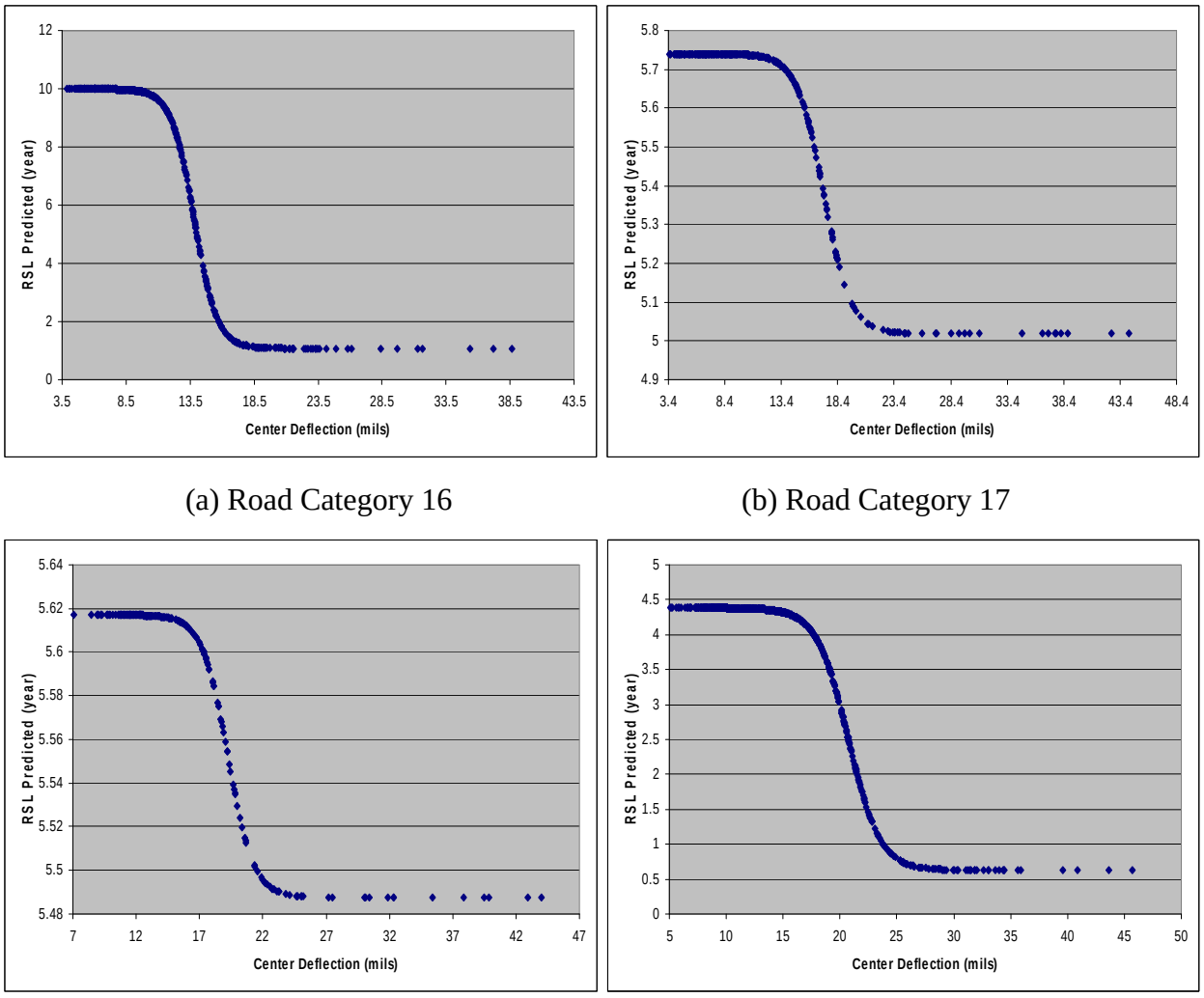

(a) Road Category 16 (b) Road Category 17

(c) Road Category 18 (d) Road Category 19

Figure 5-18 Relationship between RSL and Center Deflection for Road Categories 16 to 19

There is a smooth relationship between RSL and the center deflection for road categories 20, 21, and 22 as shown in Figure 5-19. The relationship is not smooth for road category 23. RSL remains constant at two levels when the center deflection increases for road category 23 as shown in Figure 5-19(d).

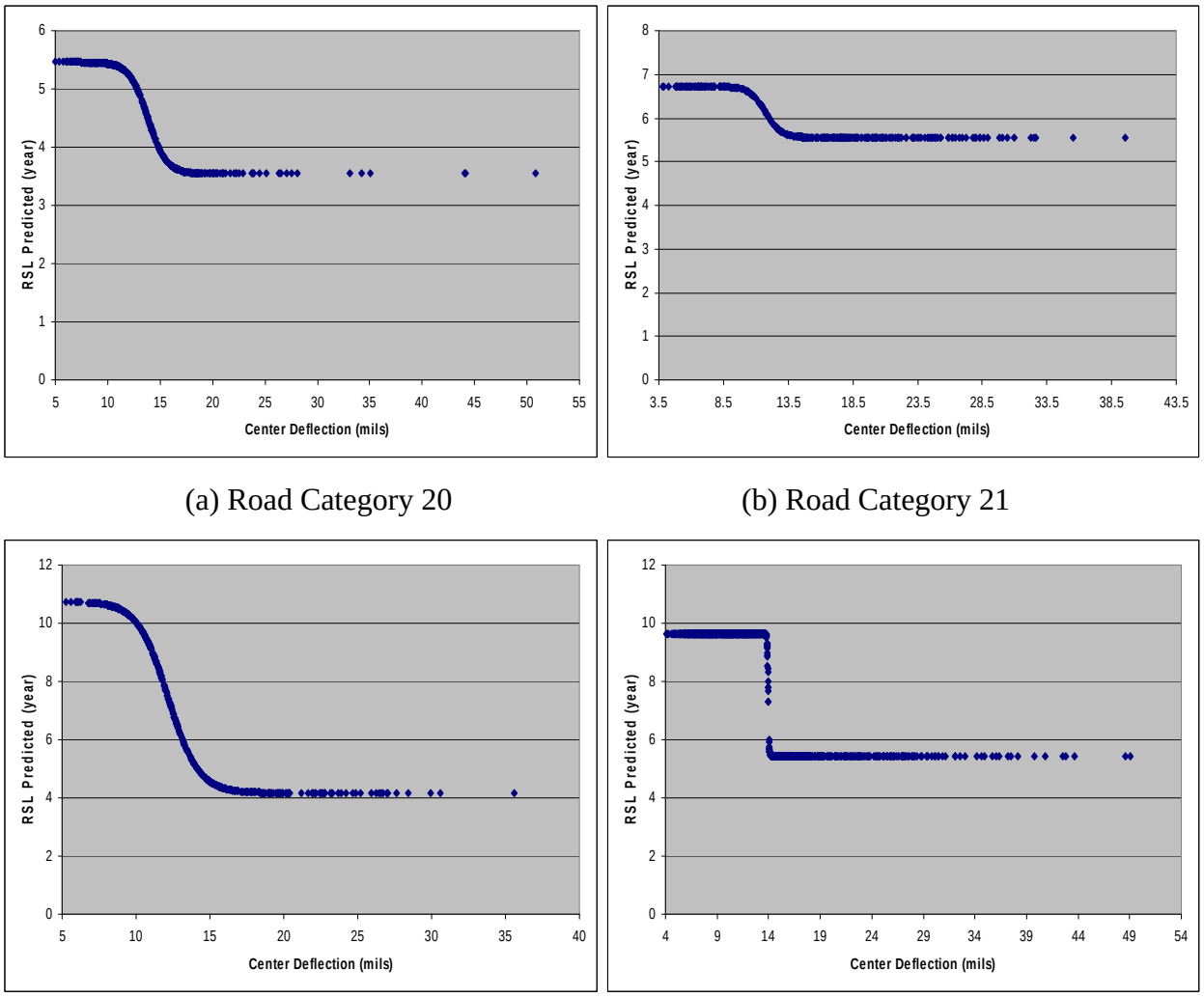

(a) Road Category 20 (b) Road Category 21

(c) Road Category 22 (d) Road Category 23

Figure 5-19 Relationship between RSL and Center Deflection for Road Categories 20 to 23

5.3.5.2 District-Wise and Statewide

Figure 5-20 shows a sigmoidal relationship between RSL and the center deflections for Districts 1 to 4, though the relation is not relatively smooth for Districts 1 and 2. RSL remains more or less constant after a threshold value of the center deflection.

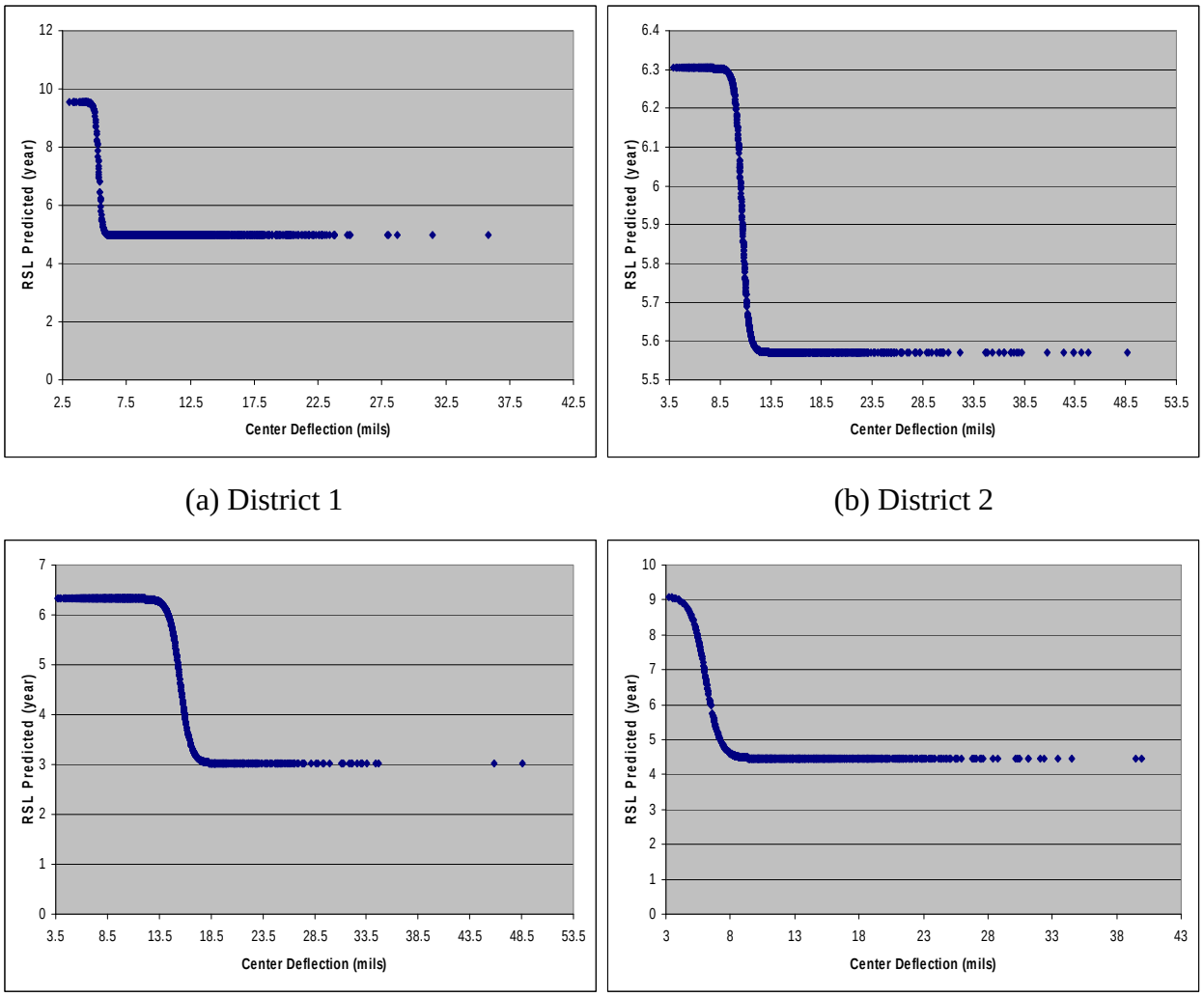

Figure 5-20 Relationship between RSL and Center Deflection for Districts 1 to 4

There is a smooth sigmoidal relationship between RSL and the center deflection for Districts 5, 6, and the state as shown in Figure 5-21.

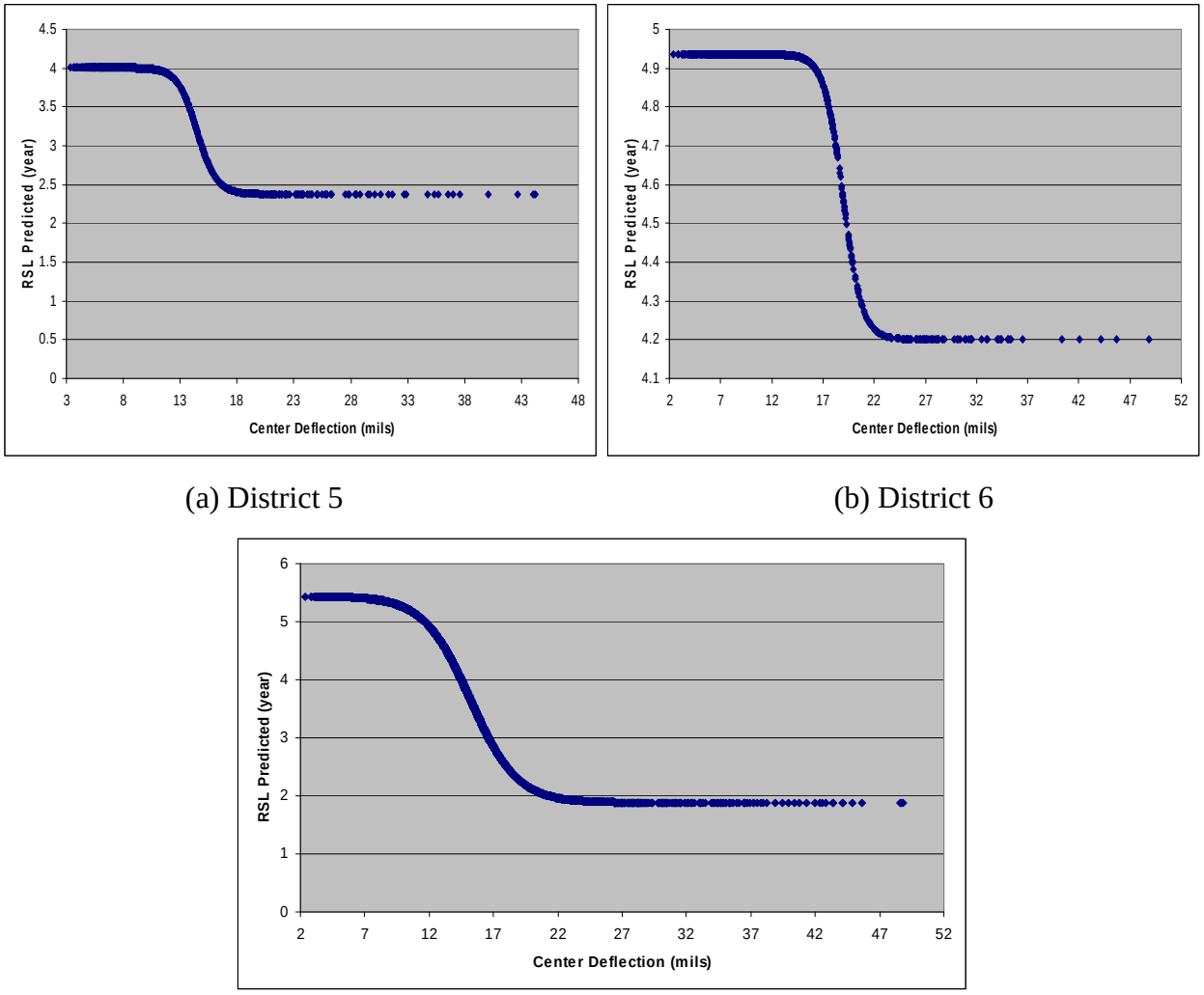

(a) District 5

(b) District 6

(c) State

Figure 5-21 Relationship between RSL and Center Deflection for Districts 5, 6, and State

5.4 Fatigue Cracking Models

Linear models have been developed for road categories 12 to 23, districts, and the state, whereas quadratic models have been developed only for districts and the state. Sigmoidal models with linear sub-models have been developed for road categories 12 to 23, districts, and the state. Sigmoidal models with quadratic sub-models have been developed for districts and the state only. Sigmoidal models have also been developed using logEAL for statewide data only.

5.4.1 Linear Regression

Linear regression has been done road category-wise, district-wise, and statewide, and discussion has also been made separately.

5.4.1.1 Road Category-Wise

Table 5-14 shows a positive linear relationship between equivalent fatigue fracking (EFCR) and center deflection (d_0) only for road categories 17, 18, 21, and 23. The positive relation shows that the higher d_0, the higher EFCR when other variables remain constant. There is no linear relationship between EFCR and any other variable for road categories 13 and 16. Intercept has been found to be insignificant for road categories 12 and 14 and as a result, it has not been included in the models. The highest R^2 value is 0.19 for road category 15, and this shows that much of the variation is not explained.

Table 5-14 Road Category-Wise Linear EFCR Models

RC	Model	R^2	N
12	$EFCR = 0.002AADT - 0.182EAL$	0.15	60
13	NA		
14	$EFCR = 0.292AADT$	0.00	266
15	$EFCR = 3.20 - 2.227PL1 - 8.0166Rut$	0.19	84
16	NA		
17	$EFCR = 0.336 + 0.074d_0 + 3.280Rut$	0.02	4,147
18	$EFCR = 0.632 + 0.007d_0$	0.00	2,135
19	$EFCR = -0.614 + 6.129PL1 + 7.002PL2 + 5.32PL3 + 0.014EAL + 2.258Rut$	0.01	1,465
20	$EFCR = 1.968 - 0.019EAL + 4.12Rut$	0.02	889
21	$EFCR = 0.0576 + 0.003d_0$	0.08	232
22	$EFCR = 1.328 - 0.156D$	0.03	759
23	$EFCR = 0.956 + 0.0353d_0$	0.01	1,789

5.4.1.2 District-Wise and Statewide

There is a positive linear relationship between EFCR and d_0 for Districts 2, 5, 6, and the state as shown in Table 5-15. A positive relationship implies an increase in EFCR with an increase in d_0 when other variables are kept constant. Much of the variation has not been explained since R^2 values are very low and as a result, the models may not be powerful enough to predict EFCR. Intercept is also not significant for District 5.

Table 5-15 District-Wise and Statewide EFCR Linear Regression

District	Model	R^2	N
1	$EFCR = 0.996 + 3.165Rut$	0.00	1,425
2	$EFCR = -2.766 + 0.194d_0 + 0.127D + 3.036Rut$	0.16	1,569
3	$EFCR = -17.90 + 18.246PL1 + 18.804PL2 + 20.131PL3 + 6.477Rut$	0.03	1,956
4	$EFCR = 1.541 - 0.105D + 6.049Rut$	0.02	1,320
5	$EFCR = 0.05d_0$	0.00	1,645
6	$EFCR = 0.730 + 0.0254d_0$	0.00	1,755
State	$EFCR = 0.852 + 0.0185d_0$	0.00	12,865

5.4.1.3 Summary of Linear EFCR Regression

Linear EFCR models have been developed for road categories 12 to 23, districts, and the state. There is a positive linear relationship between EFCR and center deflections in general, though the R^2 values are very low. Low R^2 values show that much of the variation has not been explained. It was decided to develop quadratic EFCR models for districts.

5.4.2 Quadratic Regression

Quadratic regression analysis has been done for the districts and

Table 5-16 shows the results. There is no relationship between EFCR and d_0 for District 1. There are positive and negative linear relationships between EFCR and d_0 for Districts 3, 4, and 6 and Districts 2 and 5, respectively. There are positive and negative quadratic relationships between EFCR and d_0 for Districts 2 and 3, respectively. The highest R^2 value is 0.20, and this

shows that the models are not powerful enough to predict EFCR from other variables. As a result, it was decided to develop sigmoidal EFCR models.

Table 5-16 District-Wise Quadratic EFCR Models

Dist.	Model	R^2	N
1	$EFCR = 0.084D + 12.57Rut - 33.373Rut \times Rut$	0.01	1,423
2	$EFCR = -0.068d_0 + 0.002d_0 \times d_0 - 0.239D + 0.0316d_0 \times D + 3.647Rut$	0.20	1,569
3	$EFCR = -0.819 + 0.111d_0 - 0.0025d_0 \times d_0 - 0.119D + 0.0103D \times D + 14.341Rut - 19.749Rut \times Rut$	0.03	1,951
4	$EFCR = -0.836 + 0.073d_0 + 0.205D - 0.0262d_0 \times D + 25.916Rut - 50.659Rut \times Rut$	0.03	1,300
5	$EFCR = 1.719 - 0.174d_0 - 0.278D + 0.0035D \times D + 0.0347d_0 \times D$	0.03	1,638
6	$EFCR = 0.0313d_0 + 0.221D - 0.015D \times D$	0.00	1,755

5.4.3 Sigmoidal EFCR Model with Linear Sub-Models

A sigmoidal model for EFCR with four linear sub-models has been developed for FDBIT, PDBIT, district-wise, and statewide data. The same sigmoidal model shown in Equation (5.1) has been developed using EFCR as a dependent variable instead of RSL. Each linear sub-model includes four variables, total pavement thickness above subgrade (D), equivalent axle load (EAL), rut depth, and SNeff.

5.4.3.1 Road Category-Wise

Road categories 12 to 17 are FDBIT and road categories 18 to 23 are PDBIT pavements. Table 5-17 shows the coefficients for the four variables included in all four linear sub-models and the intercepts for FDBIT. Coefficients for EAL and rut depth are the smallest and largest in magnitude, respectively. The coefficient of determination varies from 0.19 to 0.99.

Coefficients for the PDBIT pavements are shown in Table 5-18. The coefficients for EAL are generally smallest whereas coefficients for rut depth are generally largest in magnitude. The coefficient of determination varies from 0.15 to 0.93.

Table 5-17 FDBIT Sigmoidal EFCR Model with Linear Sub-Models

RC		**0**	**1(D)**	**2(EAL)**	**3(Rut)**	**4(SNeff)**	**R^2**	**N**
12	δ	0.107	-0.059	0.065	-0.039	-0.124	0.75	36
	α	1.762	-0.196	-0.266	-1.074	1.438		
	β	-330.45	-0.678	-5.913	633.584	100.955		
	γ	-19.973	-0.999	-0.865	39.714	9.930		
13	δ	-3.011	0.395	0.031	-8.110	0.174	0.62	123
	α	2.837	-0.459	-0.013	11.939	-0.220		
	β	-427.60	-10.494	7.785	825.900	57.113		
	γ	-21.444	-0.847	0.334	26.119	6.836		
14	δ	0.746	1.463	-0.074	1.817	-5.461	0.25	240
	α	-1.093	-1.075	0.074	5.847	5.338		
	β	-2.496	0.334	0.016	-4.912	0.022		
	γ	-0.042	-0.030	0.002	-0.936	0.152		
15	δ	64.462	-1.566	-2.638	395.370	-7.022	0.99	63
	α	-64.420	1.490	2.626	-392.936	7.269		
	β	64.511	1.025	-4.383	-987.606	-13.661		
	γ	14.618	0.362	-0.304	-76.196	-4.965		
16	δ	1.882	-0.091	0.006	-1.214	-0.185	0.26	590
	α	65.176	-3.567	-0.803	-239.300	5.300		
	β	72.388	-4.011	-0.554	-200.800	19.912		
	γ	3.006	-0.260	-0.022	-9.642	1.211		
17	δ	41.502	-7.005	0.080	104.300	4.930	0.19	3,729
	α	-39.808	7.047	-0.080	-101.630	-5.160		
	β	-1.601	-0.880	-0.028	-17.976	-3.472		
	γ	0.159	-0.026	-0.001	-0.507	-0.293		

Table 5-18 PDBIT Sigmoidal EFCR Model with Linear Sub-Models

		0	1(D)	2(EAL)	3(Rut)	4(SNeff)	R^2	N
18	δ	-21.212	9.541	-1.166	-29.503	-30.195	0.15	1,910
	α	21.342	-9.349	1.182	34.462	29.814		
	β	-5.707	0.317	0.164	4.602	-0.486		
	γ	-0.053	-0.032	0.010	0.008	0.145		
19	δ	-1.497	-4.837	-0.020	29.625	8.987	0.29	1,299
	α	2.230	4.814	0.031	-26.297	-9.344		
	β	110.300	-3.659	-0.855	-478.200	-23.367		
	γ	8.126	0.035	-0.083	-23.028	-1.843		
20	δ	28.773	-3.274	0.073	-101.100	-15.319	0.21	785
	α	-38.973	5.089	-0.081	160.600	18.735		
	β	-1.880	0.030	0.004	1.411	0.085		
	γ	-0.054	-0.001	0.000	0.025	0.019		
21	δ	0.908	0.006	0.000	-1.358	-0.125	0.93	411
	α	-200.69	36.369	0.093	284.361	-27.250		
	β	-187.15	-0.919	8.563	-179.057	51.587		
	γ	-12.196	-0.008	0.505	-8.608	2.971		
22	δ	-3.455	-1.161	0.515	-33.819	0.075	0.65	655
	α	4.232	1.110	-0.515	32.214	-0.071		
	β	-134.60	-5.805	-3.017	3365.400	-47.139		
	γ	-10.727	1.338	-0.149	235.100	-4.289		
23	δ	0.046	0.085	0.008	3.278	-0.294	0.45	1,605
	α	15.347	1.821	-0.058	-23.483	-0.938		
	β	-32.469	0.964	0.388	177.600	-2.639		
	γ	-4.703	-0.176	0.054	13.019	-0.250		

5.4.3.1.1 Model Plots

The EFCR model predicts some EFCR value when observed EFCR is zero. This discrepancy, shown in Figure 5-22, is not significant from a practical point of view. Figure 5-22(a) shows some scatter where observed EFCR is higher than predicted EFCR for road category 12. Predicted EFCR is zero or less than the observed EFCR for most of the points for road category 13 as shown in Figure 5-22(b). Figure 5-22(c) and (d) show a good fit for road categories 14 and 15, respectively, though there is some scatter for road category 14.

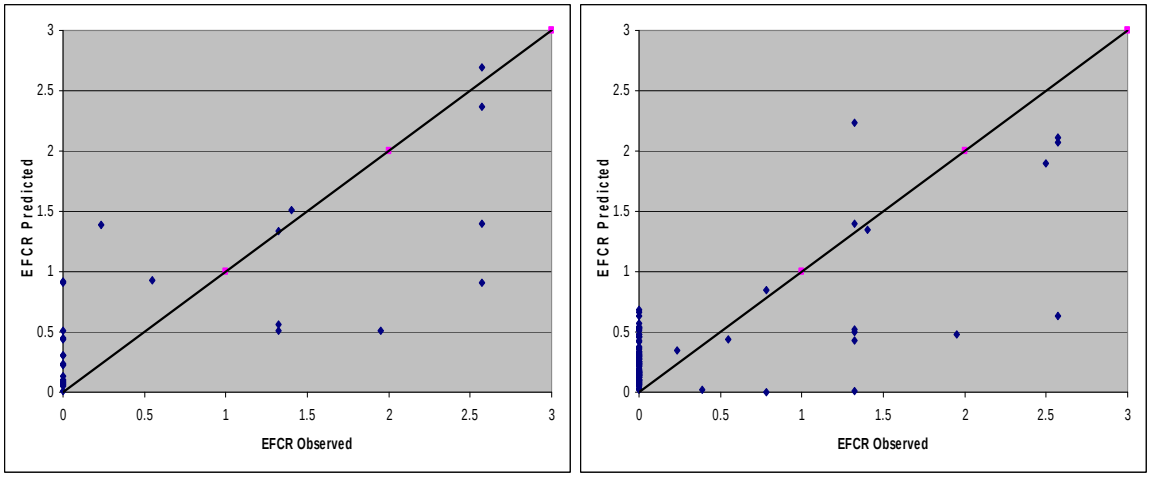

(a) Road Category 12 (b) Road Category 13

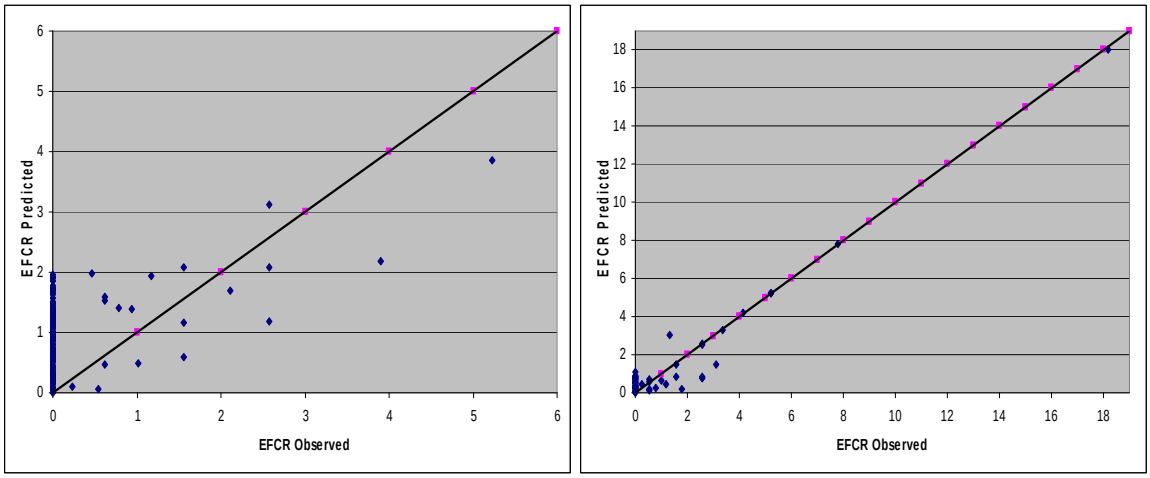

(c) Road Category 14 (b) Road Category 15

Figure 5-22 Sigmoidal EFCR Model with Linear Sub-Models for RC 12 to 15

The model predicts some EFCR values when the observed EFCR is zero for some points as shown in Figure 5-23. Predicted EFCR remains more or less constant as the observed EFCR increases, except for a few points for road categories 16 to 19 as shown in Figure 5-23. Somewhat good fit was observed for road categories 17, 18, and 19, respectively.

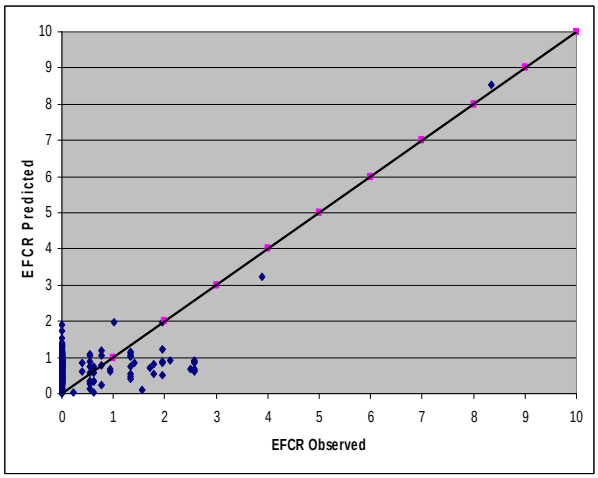

(a) Road Category 16

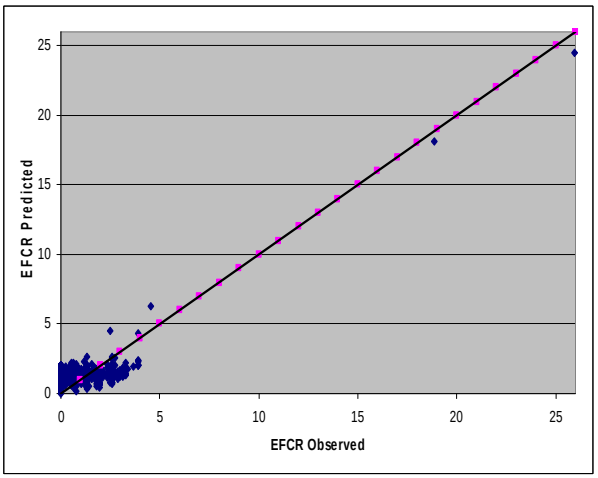

(b) Road Category 17

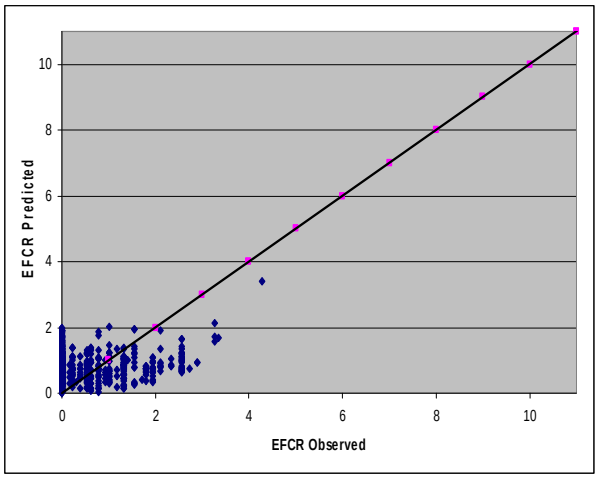

(c) Road Category 18

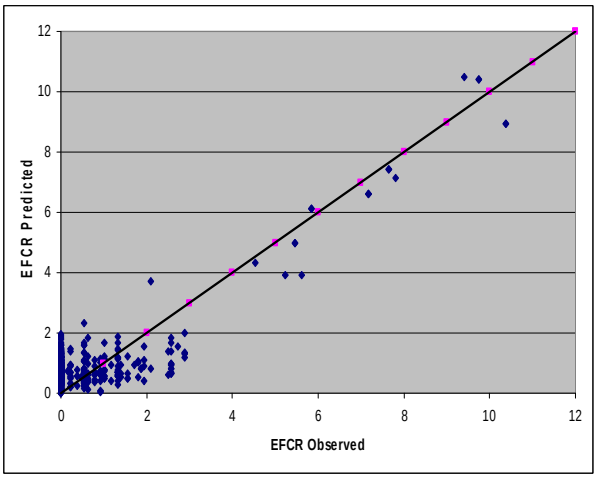

(d) Road Category 19

Figure 5-23 Sigmoidal EFCR Model with Linear Sub-Models for RC 16 to 19

The observed EFCR is zero for some predicted EFCR as shown in Figure 5-24. The predicted EFCR is higher than observed EFCR when EFCR is low and vice versa when EFCR is high for road category 20 as shown in Figure 5-24(a). Predicted EFCR remains more or less constant as observed EFCR for the majority of points for road categories 21 and 22, as shown in Figure 5-24(b) and (c). Figure 5-24(d) shows a good fit for road category 23.

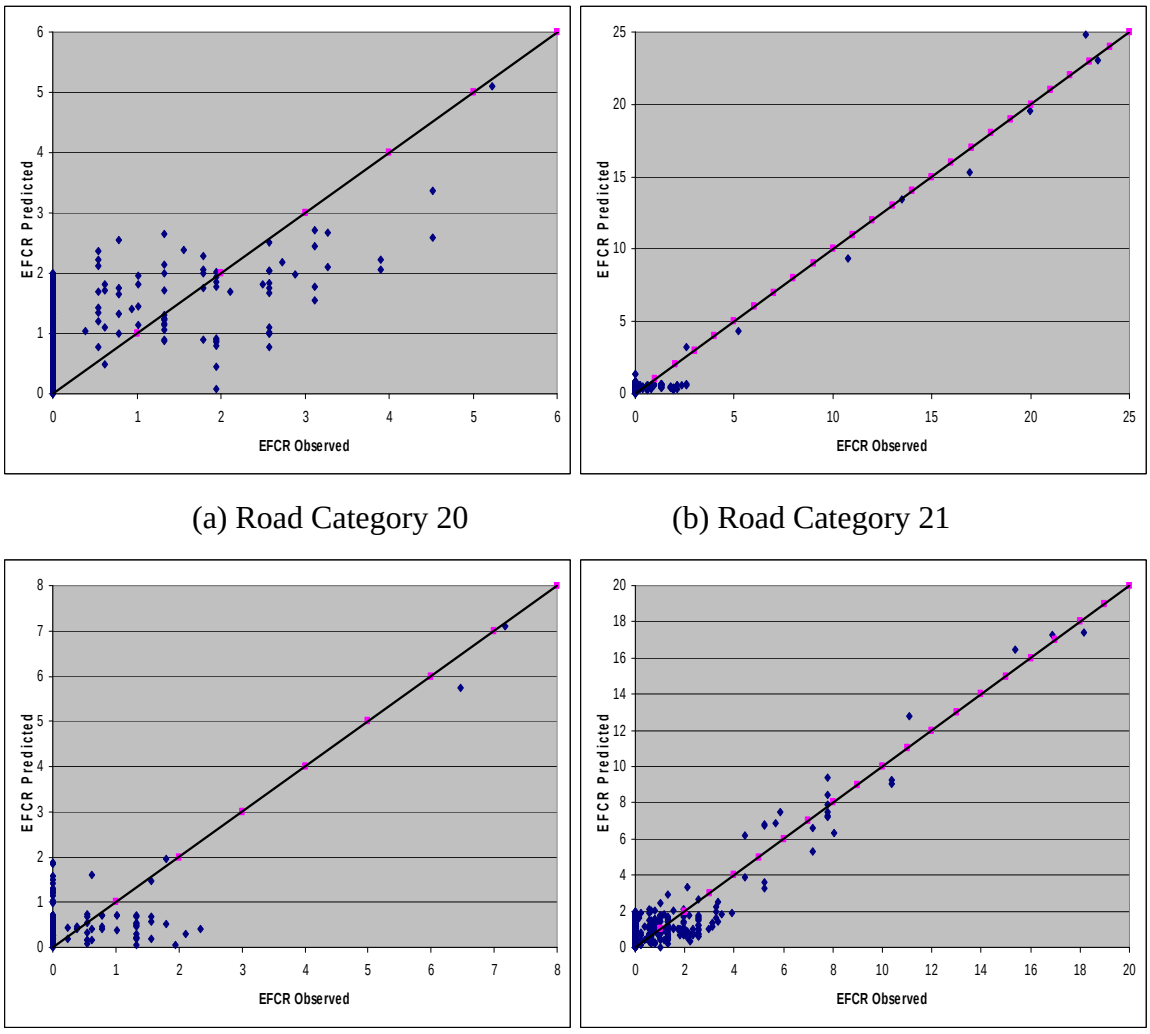

(a) Road Category 20 (b) Road Category 21

(c) Road Category 22 (d) Road Category 23

Figure 5-24 Sigmoidal EFCR Model with Linear Sub-Models for RC 20 to 23

5.4.3.1.2 Validation Plots

Figure 5-25 shows that observed and predicted EFCR match very well for road categories 12, 13, 14, and 15, though the number of data points is small. The model predicts some EFCR values for no observed EFCR at few points for road categories 13 and 14, as shown in Figure 5-25(b) and (c).

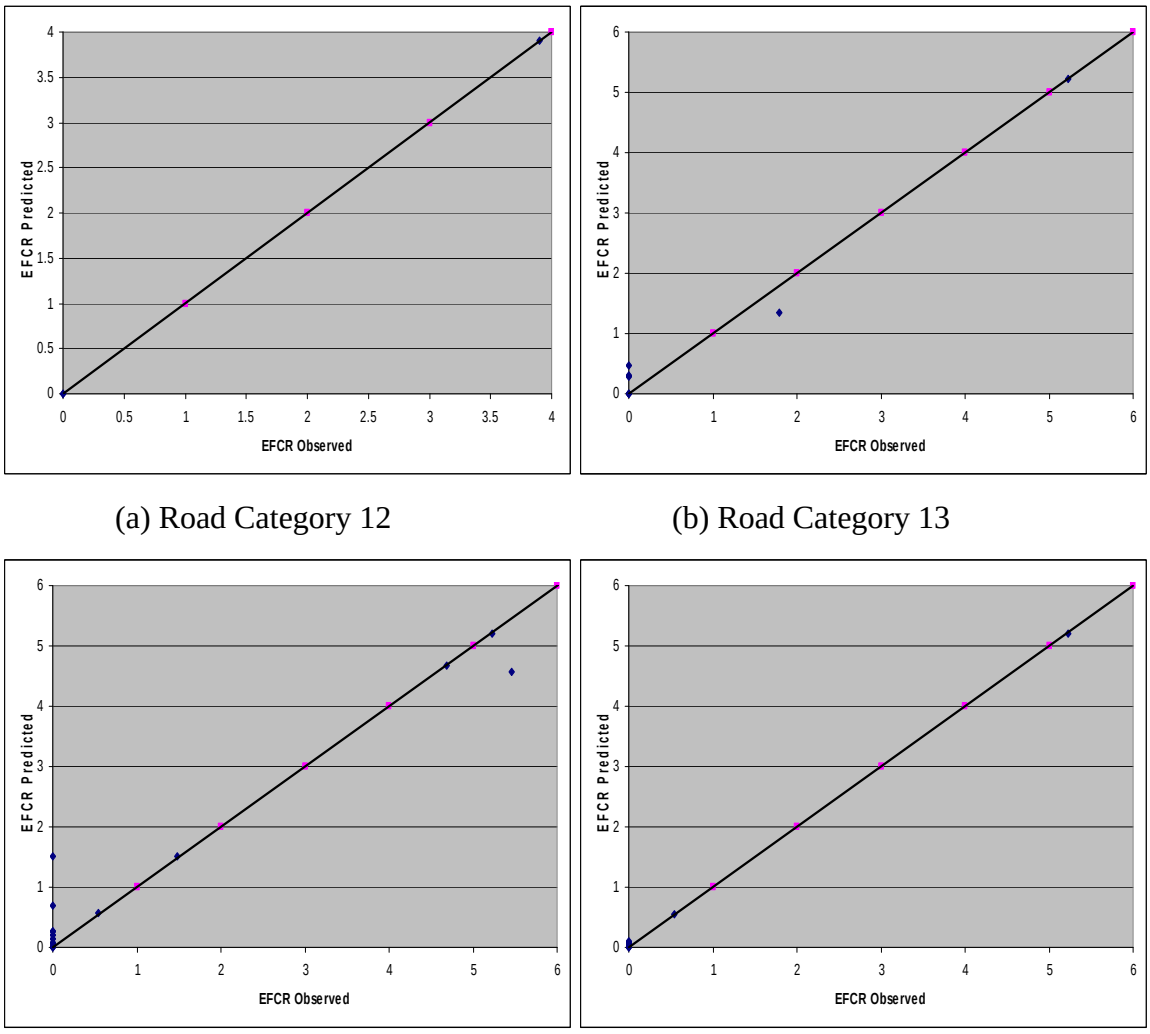

(a) Road Category 12 (b) Road Category 13

(c) Road Category 14 (d) Road Category 15

Figure 5-25 Sigmoidal EFCR Model with Linear Sub-Models Validation for RC 12 to 15

The model predicts EFCR while no EFCR is observed at some points as shown in Figure 5-26. Observed EFCR is higher than the predicted EFCR at one point for road category 16 as shown in Figure 5-26(a). Observed and predicted EFCR fit well around the 45^{o} slope line with some scatter for road categories 17 and 18, as shown in Figure 5-26(b) and (c). There is a good fit between observed and predicted EFCR for road category 19, except the predicted EFCR is very low as compared to the observed EFCR at two points as shown in Figure 5-26(d).

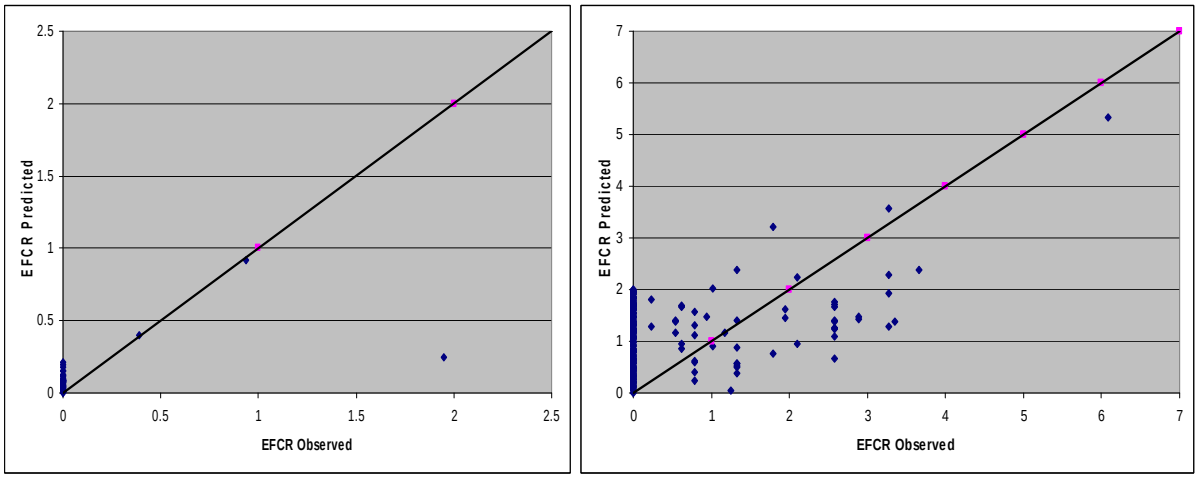

(a) Road Category 16 (b) Road Category 17

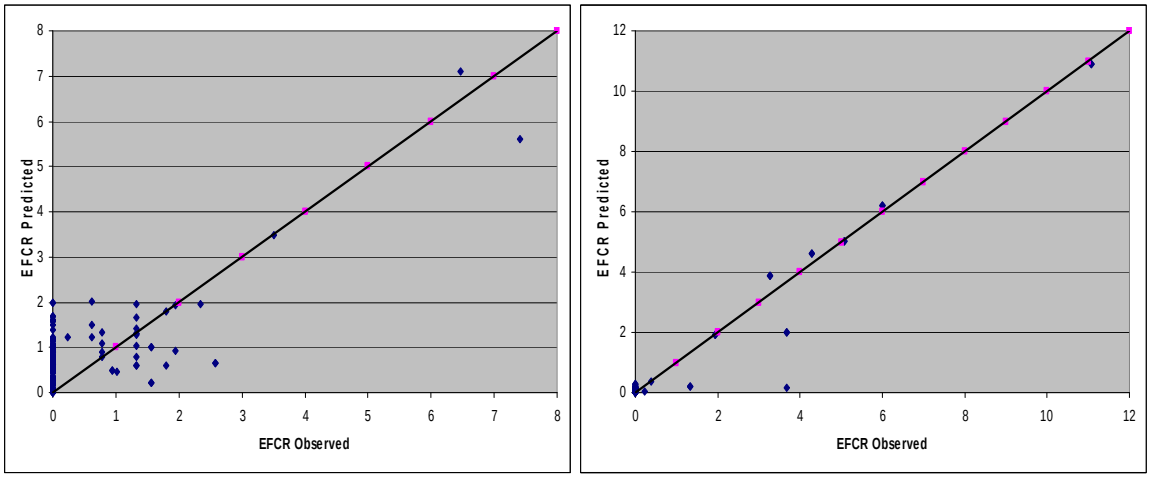

(c) Road Category 18 (d) Road Category 19

Figure 5-26 Sigmoidal EFCR Model with Linear Sub-Models Validation for RC 16 to 19

Observed EFCR is zero corresponding to some predicted EFCR values as shown in Figure 5-27. Observed and predicted EFCR fit well except for one point that shows higher

observed EFCR for road category 20, as shown in Figure 5-27(a). Predicted EFCR remains more or less constant as the observed EFCR increases for road category 21 as shown in Figure 5-27(b). Most of the points show very low observed and predicted EFCR, except for one point for road category 22 as indicated in Figure 5-27(c). Figure 5-27(d) shows somewhat balanced, observed, and predicted EFCR, though there is some scatter.

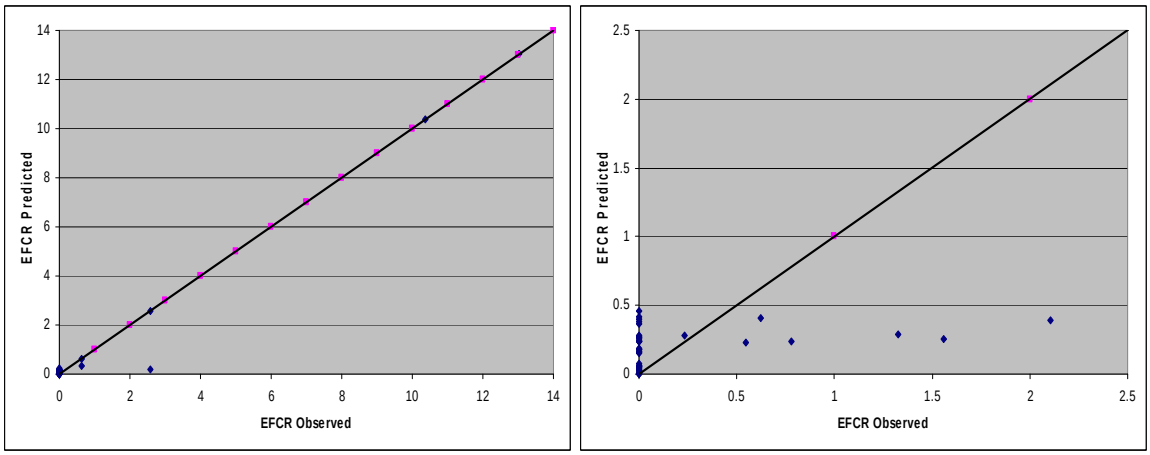

(a) Road Category 20 (b) Road Category 21

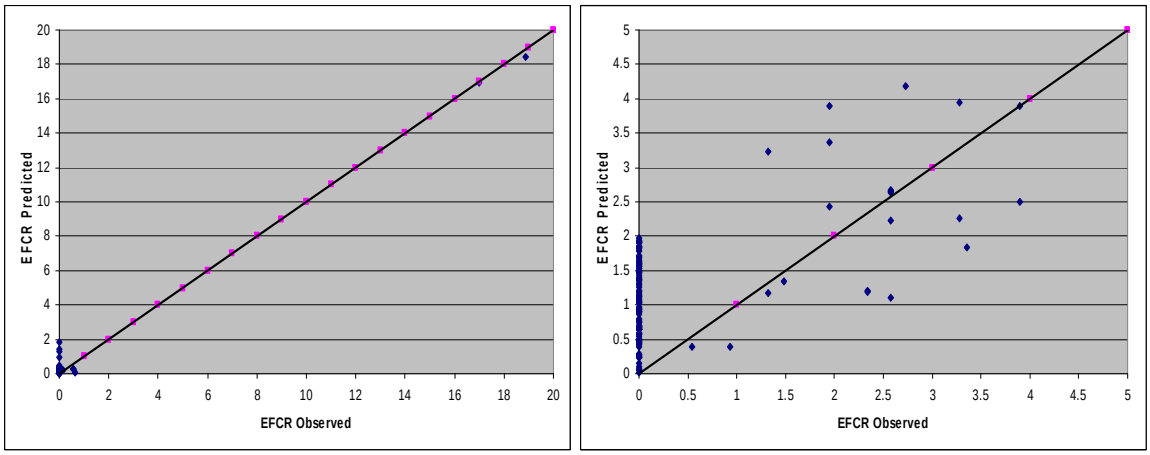

(c) Road Category 22 (b) Road Category 23

Figure 5-27 Sigmoidal EFCR Model with Linear Sub-Models Validation for RC 20 to 23

5.4.3.2 District-Wise and Statewide

Coefficients for different variables of the district-wise and statewide models for each linear sub-model are shown in Table 5-19. Coefficients for EAL and rut depth are highest and lowest in magnitude. The coefficient of determination varies from 0.15 to 0.85.

Table 5-19 District-Wise and Statewide Sigmoidal EFCR Model with Linear Sub-Models

Dist.		0	1(D)	2(EAL)	3(Rut)	4(SNeff)	R^2	N
1	δ	18.302	-6.306	1.552	15.178	4.525	0.26	1,423
	α	-17.675	6.286	-1.547	-10.003	-4.506		
	β	25.516	75.820	-4.101	182.844	-310.515		
	γ	10.339	1.856	0.320	25.874	-8.806		
2	δ	33.945	-1.658	-0.054	18.531	-1.395	0.85	1,569
	α	-33.874	1.703	0.061	-16.520	1.261		
	β	26.455	78.001	-2.214	182.647	-310.156		
	γ	3.752	2.924	-0.183	28.355	-9.882		
3	δ	0.505	0.065	0.006	5.057	-0.276	0.25	1,951
	α	1.937	-2.541	-0.012	-5.408	9.237		
	β	-52.055	13.944	-0.640	138.135	30.574		
	γ	-2.650	0.163	-0.040	13.184	1.320		
4	δ	-1.238	0.161	0.008	9.368	-0.200	0.17	1,300
	α	11.740	-1.039	-0.016	-28.136	1.312		
	β	-4.081	-0.210	0.071	23.690	0.267		
	γ	-0.608	-0.031	0.007	3.007	0.038		
5	δ	0.416	0.047	0.000	0.731	-0.095	0.43	1,638
	α	-5.813	-2.314	0.679	22.154	-0.415		
	β	19.902	-39.374	-0.233	128.700	105.758		
	γ	2.969	-0.163	-0.072	-16.618	-1.975		
6	δ	1.750	5.858	-0.150	-4.976	-4.350	0.15	1,755
	α	-15.256	-191.084	5.181	109.602	131.237		
	β	3.409	0.006	0.000	-0.378	0.008		
	γ	-0.003	0.000	0.000	-0.029	0.001		
State	δ	0.715	0.031	0.003	3.246	-0.183	0.18	13,194
	α	-10.709	-0.699	0.386	-12.737	2.779		
	β	-5.922	-0.055	0.087	20.008	1.428		
	γ	-0.531	-0.012	0.005	1.396	0.078		

5.4.3.2.1 Model Plots

The model predicts existence of some EFCR when there was none observed as shown in Figure 5-28. Predicted EFCR remains more or less constant as observed EFCR increases for District 1 as shown in Figure 5-28(a). Observed and predicted EFCR are well balanced around the 45^{o} slope line for Districts 2, 3, and 4 as shown in Figure 5-28(b), (c), and (d).

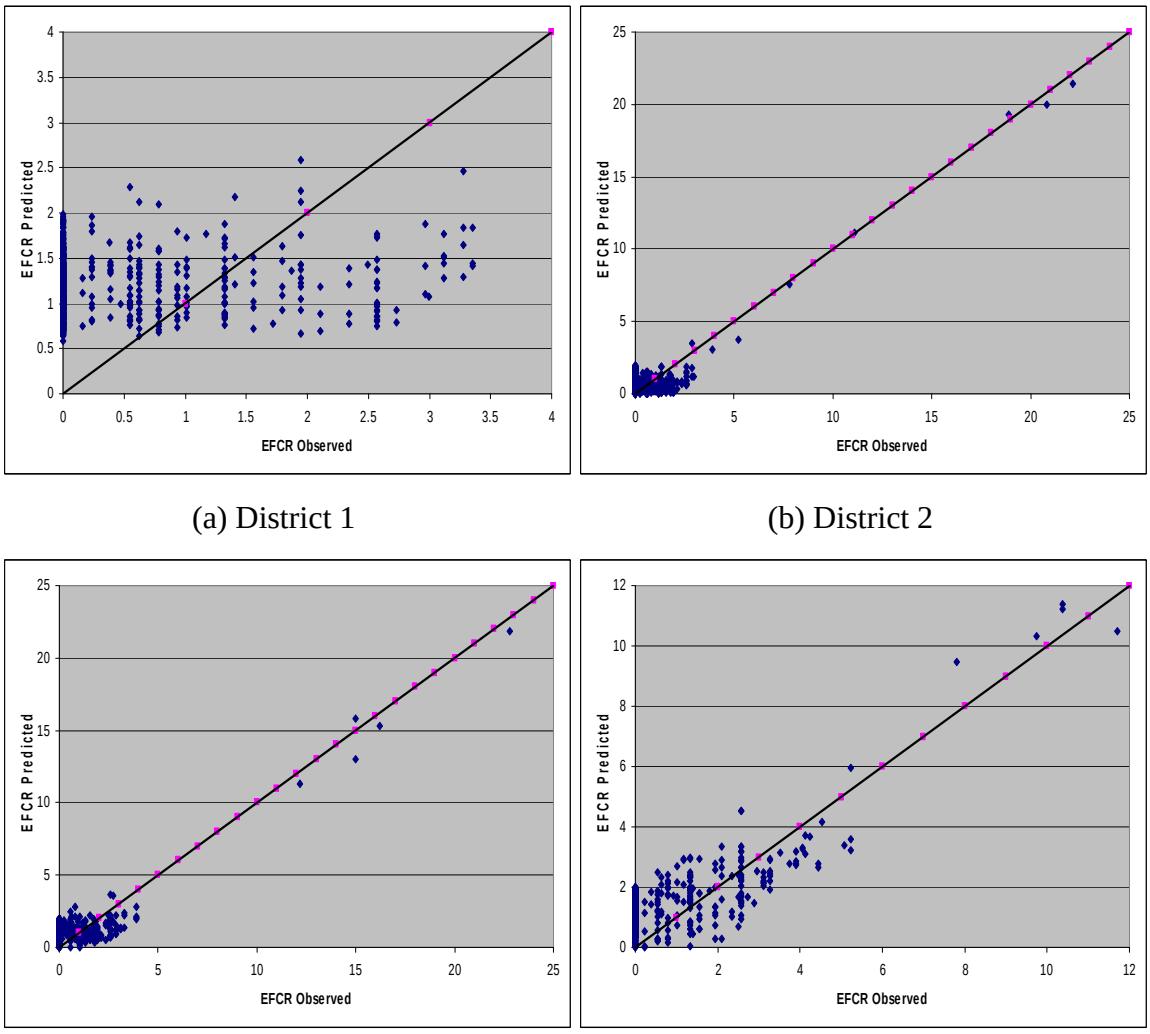

(a) District 1 (b) District 2

(c) District 3 (d) District 4

Figure 5-28 Sigmoidal EFCR Model with Linear Sub-Models for Districts 1 to 4

The model predicts some EFCR when none was observed as shown in Figure 5-29. Figure 5-29(a) shows that predicted EFCR remains somewhat constant as observed EFCR increases. Observed and predicted EFCR are more or less balanced around the 45^{o} slope line, though there is some scatter in District 6 data as shown in Figure 5-29(b).

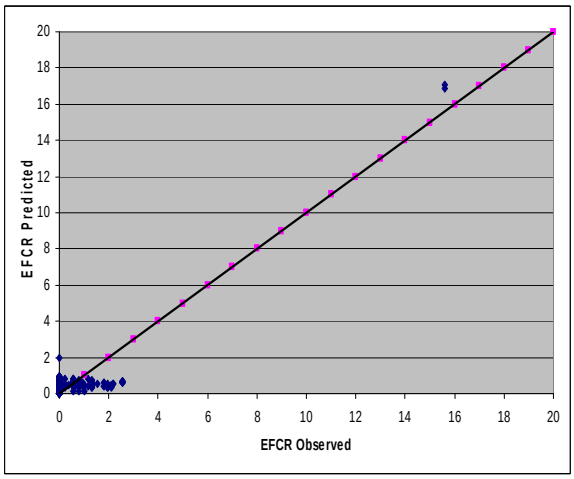

(a) District 5

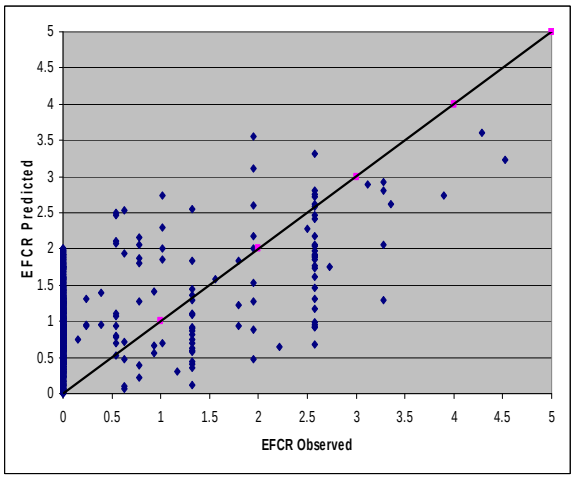

(b) District 6

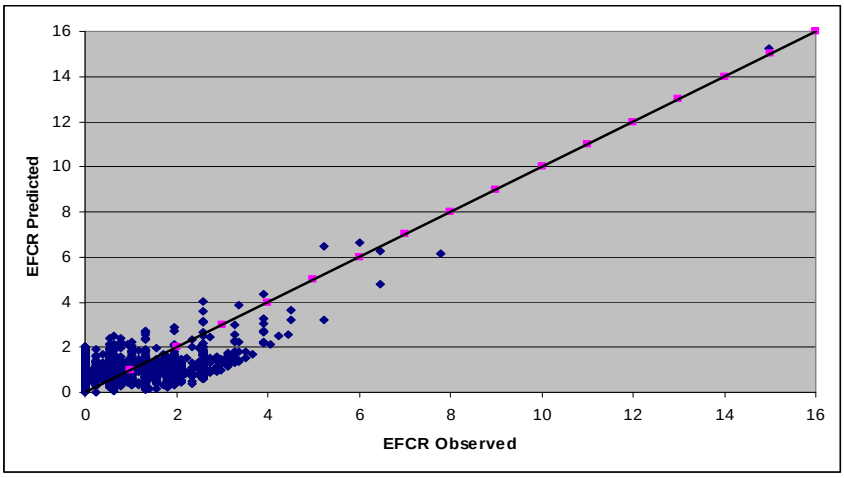

(c) State

Figure 5-29 Sigmoidal EFCR Model with Linear Sub-Models for Districts 5, 6, and State

5.4.3.2.2 Validation Plots

Observed EFCR is greater than predicted EFCR for all points except when there was no observed EFCR for District 1 as shown in Figure 5-30(a). Observed and predicted EFCR fit well for Districts 2 and 3 as shown in Figure 5-30(b) and (c). Predicted EFCR is higher when EFCR is lower and vice versa for District 4 as shown in Figure 5-30(d).

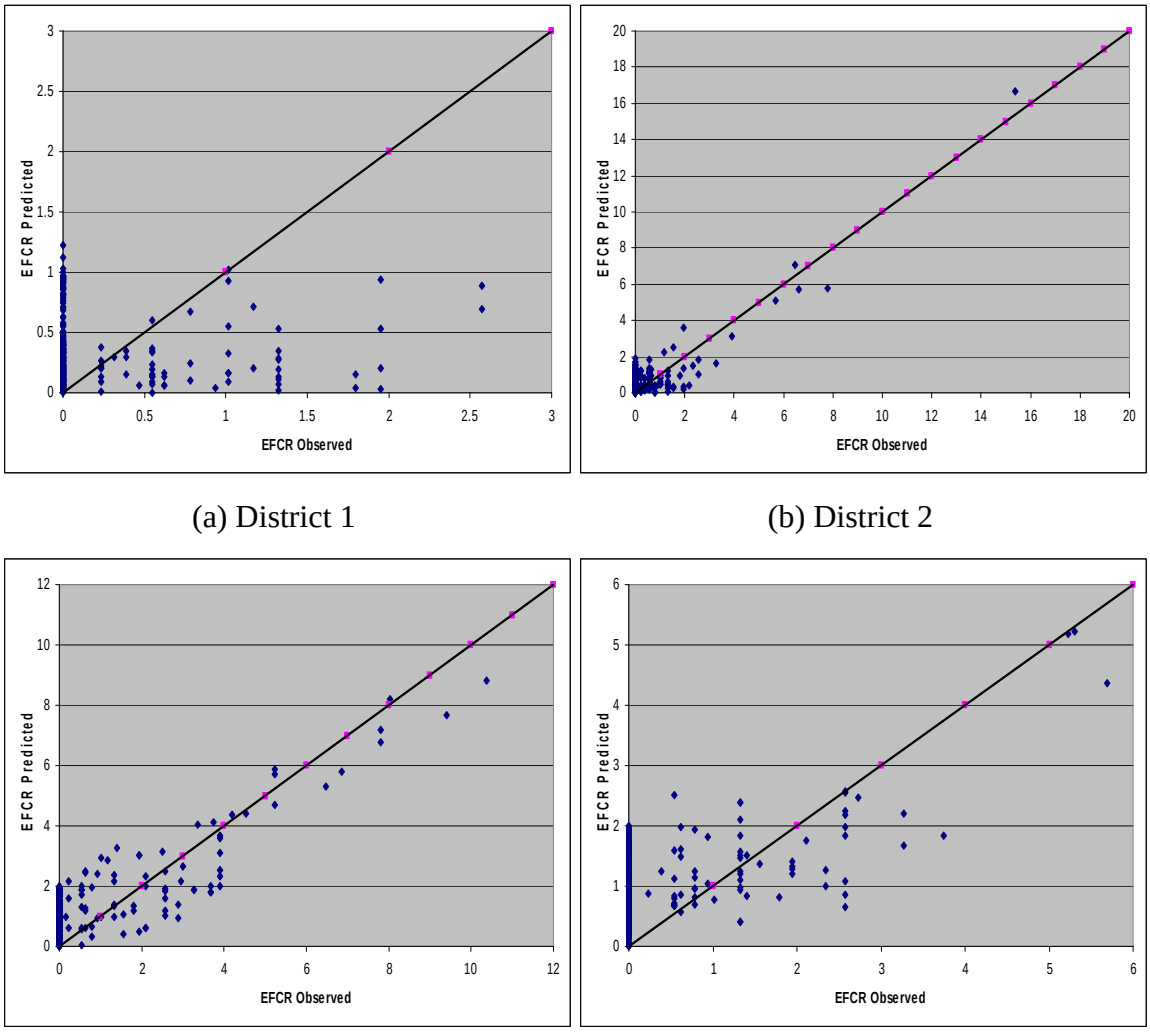

(a) District 1 (b) District 2

(c) District 3 (d) District 4

Figure 5-30 Sigmoidal EFCR Model with Linear Sub-Models Validation for Districts 1 to 4

The model predicts existence of some EFCR when there is no observed EFCR as shown in Figure 5-31. A majority of the points show that predicted EFCR is higher than observed EFCR for Districts 5 and 6, as shown in Figure 5-31(a) and (b). There is a good fit between predicted and observed EFCR for statewide data as shown in Figure 5-31(c).

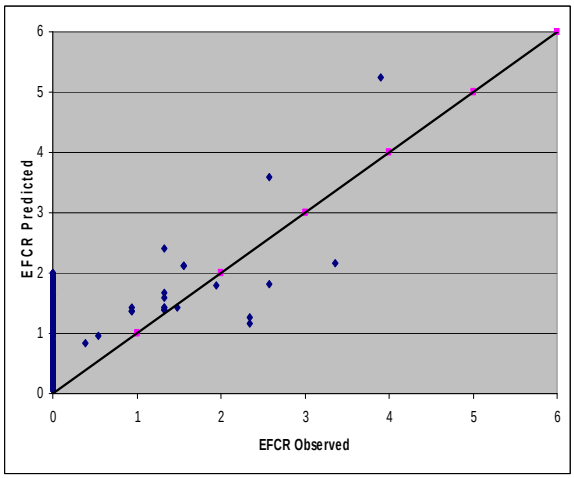

(a) District 5

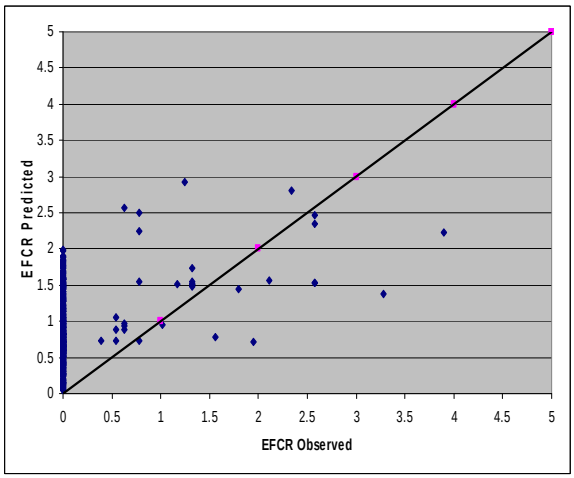

(b) District 6

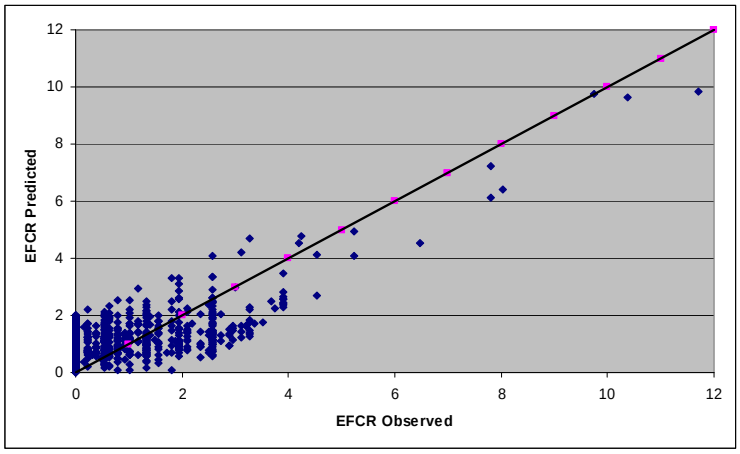

(c) State

Figure 5-31 Sigmoidal EFCR Model with Linear Sub-models Valid. for Dist. 5, 6, and State

5.4.3.3 Mean Absolute Deviation

Mean observed EFCR values are greater than mean predicted EFCR for all road categories, districts, and the state as shown in Table 5-20. This may be due to the existence of some predicted EFCR for zero observed EFCR. Low mean absolute deviation difference shows more mismatch between observed and predicted EFCR.

Table 5-20 Mean Absolute Deviation for Sigmoidal EFCR Model with Linear Sub-Models

	Mean			Mean Absolute Deviation		
	Observed	**Predicted**	**Difference**	**Observed**	**Predicted**	**Difference**
(a) Road Category-Wise						
12	0.66	0.68	-0.02	0.84	0.54	0.30
13	0.24	0.36	-0.12	0.40	0.26	0.14
14	0.17	0.93	-0.75	0.31	0.48	-0.17
15	1.25	1.35	-0.10	1.62	1.40	0.21
16	0.15	0.71	-0.56	0.27	0.27	0.00
17	0.19	1.34	-1.15	0.34	0.29	0.04
18	0.22	0.77	-0.55	0.37	0.32	0.04
19	0.26	0.81	-0.55	0.44	0.40	0.05
20	0.28	1.18	-0.90	0.47	0.47	0.00
21	0.47	0.75	-0.28	0.77	0.57	0.20
22	0.10	0.39	-0.29	0.18	0.18	0.00
23	0.32	1.00	-0.68	0.55	0.53	0.02
(b) District-Wise and Statewide						
1	0.28	1.17	-0.90	0.44	0.26	0.18
2	0.23	0.61	-0.38	0.39	0.36	0.03
3	0.24	1.01	-0.77	0.41	0.41	0.00
4	0.48	1.43	-0.94	0.75	0.58	0.17
5	0.08	0.51	-0.43	0.15	0.15	0.00
6	0.15	0.93	-0.79	0.27	0.42	-0.15
State	0.18	1.01	-0.82	0.32	0.30	0.02

5.4.4 Sigmoidal EFCR Model with Quadratic Sub-Models

The sigmoidal model with quadratic sub-models has been developed using only district and statewide data. Each quadratic sub-model includes total pavement thickness above subgrade (D), equivalent axle load (EAL), rut depth, and SNeff. Table 5-21 shows the coefficients for all four quadratic sub-models for Districts 1, 2, and 3. Coefficients for linear and quadratic parts of EAL and rut depth are smallest and largest for all sub-models. Coefficients for the same variable vary in magnitude and sign for different sub-models for each district. The coefficient of determination varies from 0.12 to 0.92.

Table 5-22 shows coefficients for all variables in both linear and quadratic parts of beta and gamma sub-models are very high for Districts 4 and 5. Rut depth and EAL coefficients are highest and lowest in magnitude for both linear and quadratic parts of all sub-models. The coefficient of determination varies from 0.21 to 0.29. There is an improvement in R^2 as compared to the sigmoidal EFCR model with linear sub-models for Districts 4 and 6, whereas R^2 decreases for District 5.

Table 5-21 Sigmoidal EFCR Model with Quadratic Sub-Models for Districts 1 to 3

Dist.		0	1(D)	2(EAL)	3(Rut)	4(SNeff)	R^2	N
1	δ	-10.011	1.848	0.073	15.254	-0.032	0.38	1,423
	α	8.032	-1.490	0.090	-21.078	0.348		
	β	3.286	-0.338	0.014	-6.955	0.107		
	γ	0.870	-0.170	-0.007	-0.899	0.040		
	δ_{ii}	-	-0.114	0.000	-20.720	-0.067		
	α_{ii}	-	0.094	0.000	115.000	-0.009		
	β_{ii}	-	0.024	0.000	13.001	-0.028		
	γ_{ii}	-	0.011	0.000	-1.720	0.004		
2	δ	0.302	0.108	0.012	5.959	-0.633	0.92	1,569
	α	226.400	-92.046	0.082	-167.800	37.009		
	β	122.500	-29.797	-0.424	-834.800	10.512		
	γ	3.653	-1.097	0.010	-32.688	-0.025		
	δ_{ii}	-	-0.005	0.000	-15.230	0.070		
	α_{ii}	-	7.496	0.007	18.201	-12.662		
	β_{ii}	-	3.977	0.000	3683.500	2.057		
	γ_{ii}	-	0.154	0.000	146.700	0.243		
3	δ	4.354	0.428	0.120	57.508	28.417	0.12	1,951
	α	-4.374	-0.547	-0.103	-45.471	-28.312		
	β	5.823	6.114	0.158	-109.616	2.928		
	γ	0.230	0.578	0.109	-37.532	-0.781		
	δ_{ii}	-	148.410	1.719	-17.016	38.368		
	α_{ii}	-	-148.399	-1.719	-0.803	-38.457		
	β_{ii}	-	-0.614	0.002	0.019	-3.467		
	γ_{ii}	-	-0.037	0.000	464.658	0.118		

Table 5-22 Sigmoidal EFCR Model with Quadratic Sub-Models for Districts 4 to 6

Dist.		0	1(D)	2(EAL)	3(Rut)	4(SNeff)	R^2	N
4	δ	5.324	0.548	0.093	56.615	-1.775	0.29	1,300
	α	-5.745	-0.713	-0.089	-33.022	2.054		
	β	6084.600	1349.700	381.400	-312774	3468.700		
	γ	3462.700	770.300	464.600	259978	87.326		
	δ_{ii}	-	0.008	0.000	-21.818	-0.058		
	α_{ii}	-	0.002	0.000	-25.218	0.011		
	β_{ii}	-	-263.400	17.698	-30360000	1112.200		
	γ_{ii}	-	308.400	59.657	10864158	-90.365		
5	δ	5.594	0.640	0.098	47.187	-1.969	0.22	1,638
	α	-5.515	-0.601	-0.095	-48.431	2.147		
	β	251823	-249740	-20972	396390	-502079		
	γ	-25995	1763.500	494	-17853	40495		
	δ_{ii}	-	0.000	0.000	-2.800	-0.060		
	α_{ii}	-	0.004	0.000	5.449	0.001		
	β_{ii}	-	-429209	-3513	-84750000	-743719		
	γ_{ii}	-	18625	315	3735402	50292		
6	δ	0.470	-0.006	0.006	6.066	-0.025	0.21	1,755
	α	10.704	12.975	0.369	-659.900	-51.499		
	β	61.671	-10.671	0.044	-128.500	7.492		
	γ	0.750	0.062	0.005	-1.380	-0.010		
	δ_{ii}	-	0.001	0.000	-10.878	-0.029		
	α_{ii}	-	-1.139	0.000	2431.900	30.231		
	β_{ii}	-	0.315	0.000	270.100	0.028		
	γ_{ii}	-	-0.034	0.000	0.227	0.103		

Coefficients for linear and quadratic parts of all four variables included in the quadratic sub-models using statewide data are shown in Table 5-23. Coefficients for EAL are significantly small, whereas coefficients for rut depth are the highest in magnitude in all four sub-models. The coefficient of determination is 0.27, which shows an improvement when compared with the sigmoidal model with linear sub-models.

Table 5-23 Sigmoidal EFCR Model with Quadratic Sub-Models Using Statewide Data

	0	**1(D)**	**2(EAL)**	**3(Rut)**	**4(SNeff)**	**R^2**	**N**
δ	0.504	-0.036	0.005	5.043	0.072	0.27	9,636
α	-8.944	8.458	-0.003	66.475	-42.720		
β	80.775	-8.823	0.016	-28.190	-18.576		
γ	2.099	-0.131	0.003	6.161	-1.147		
δ_{ii}	-	0.003	0.000	-9.420	-0.040		
α_{ii}	-	-0.934	0.001	-119.300	24.564		
β_{ii}	-	0.459	0.000	33.647	2.993		
γ_{ii}	-	-0.003	0.000	-14.860	0.203		

5.4.4.1.1 Model Plots

Figure 5-32 shows that a sigmoidal EFCR model with the quadratic sub-model fits well for Districts 1 to 4. It also shows an improvement over the sigmoidal EFCR model with linear sub-models.

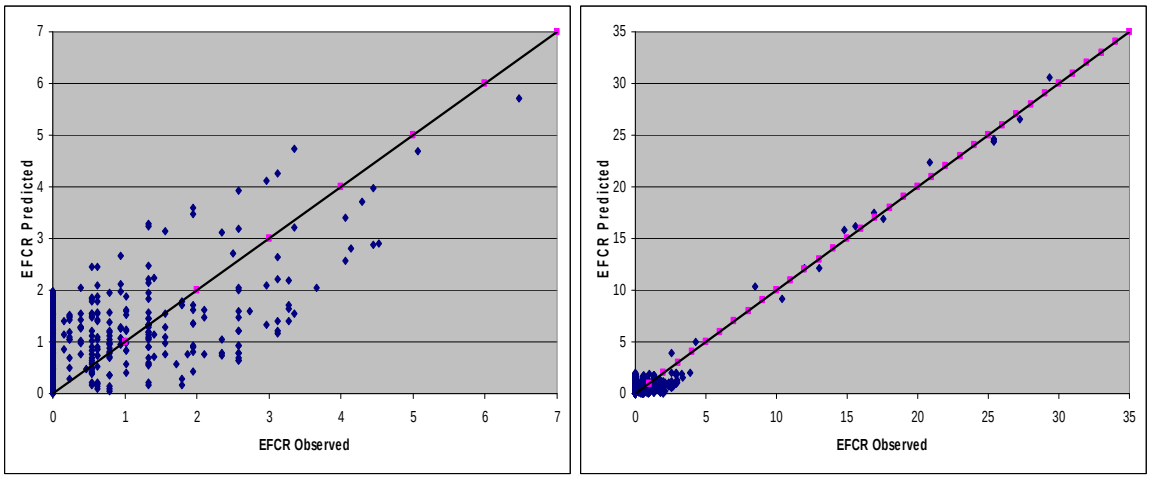

(a) District 1 (b) District 2

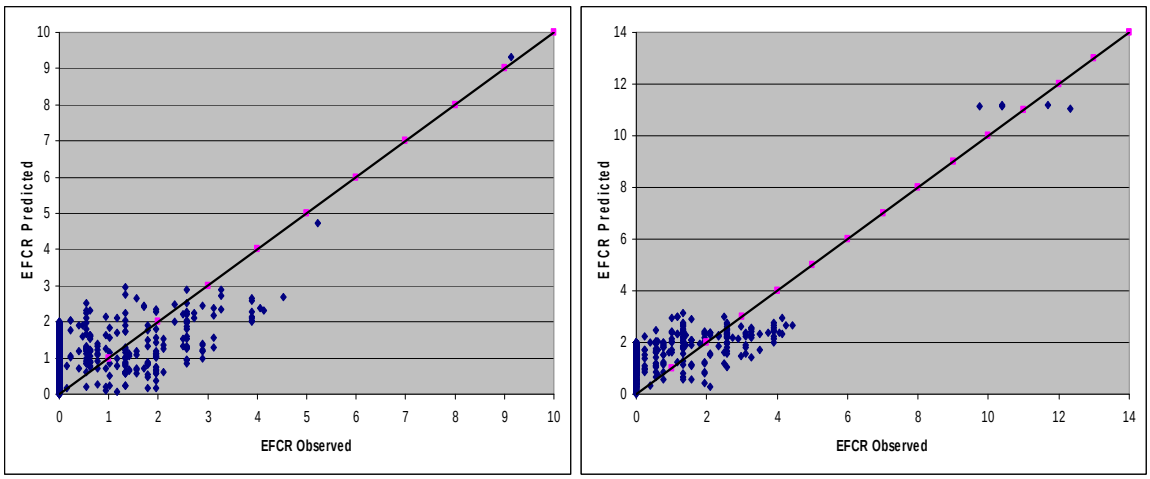

(c) District 3 (d) District 4

Figure 5-32 Sigmoidal EFCR Model with Quadratic Sub-Models for Districts 1 to 4

Figure 5-33(a) shows that a sigmoidal model with quadratic sub-models is not a good fit for District 5. District 5 is the only district which shows a decrease in R^2 when quadratic sub-models are used instead of linear sub-models. Observed and predicted EFCR are well distributed around the 45^o slope line for District 6 and the state, as shown in Figure 5-33(b) and (c).

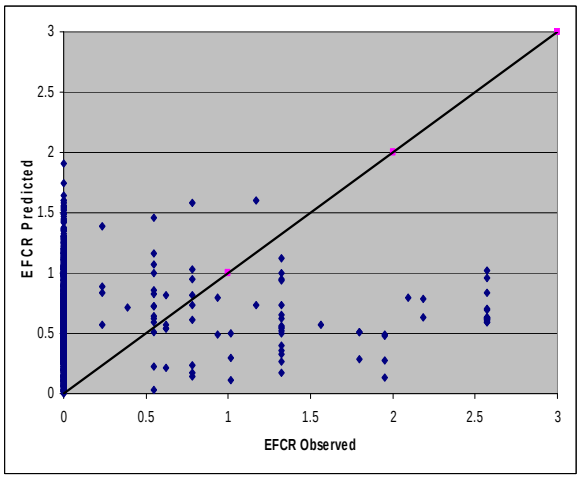

(a) District 5

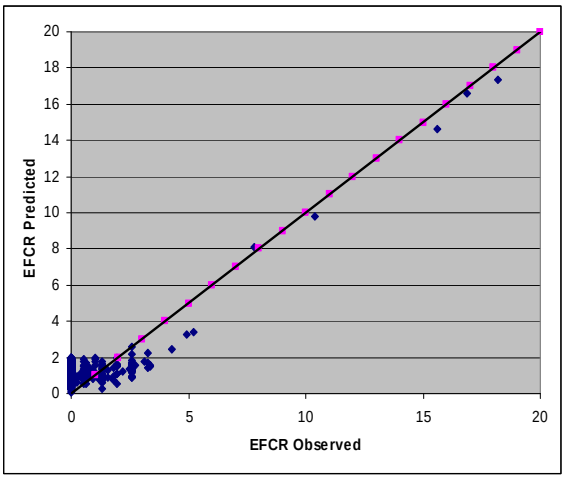

(b) District 6

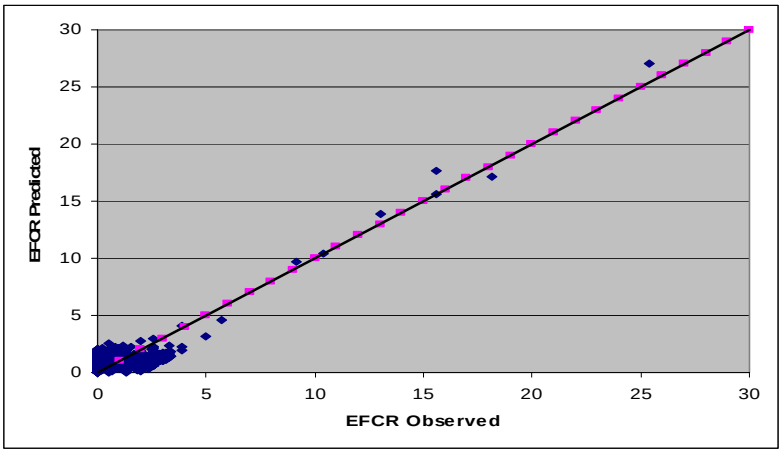

(c) State

Figure 5-33 Sigmoidal EFCR Model with Quadratic Sub-Models for Dist. 5, 6, and State

5.4.4.1.2 Validation Plots

Figure 5-34 shows that observed and predicted EFCR are well balanced with minor scatter signifying a well fit model.

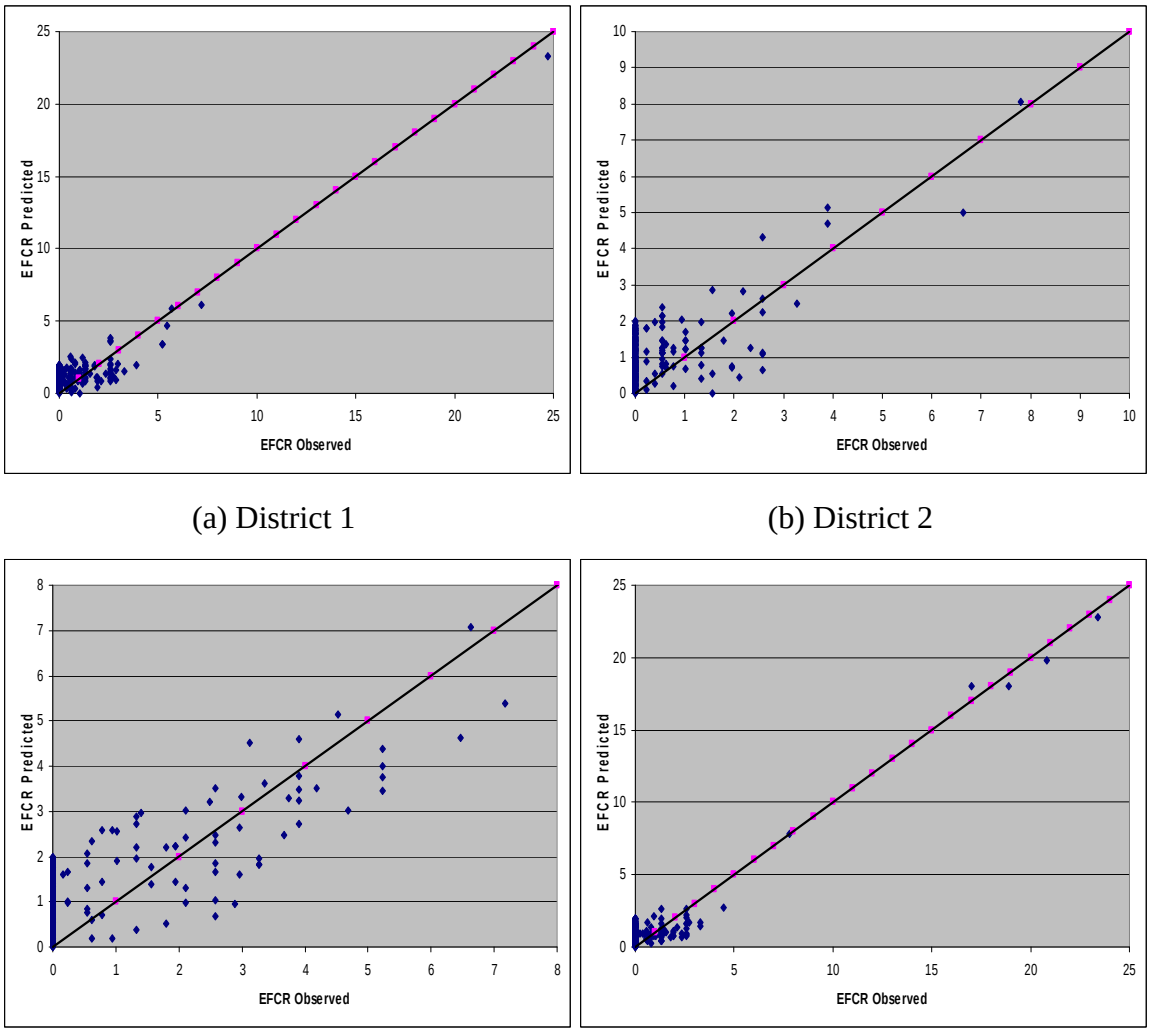

(a) District 1 (b) District 2

(c) District 3 (d) District 4

Figure 5-34 Sigmoidal EFCR Model with Quadratic Sub-Models Valid. for Districts 1 to 4

Predicted EFCR remains more or less constant as the observed EFCR increases for District 5 as shown in Figure 5-35(a). Predicted EFCR is generally less than observed EFCR, and the points are widely scattered for District 6 as shown in Figure 5-35(b). Figure 5-35(c) shows that observed and predicted EFCR do not correspond well for the statewide data.

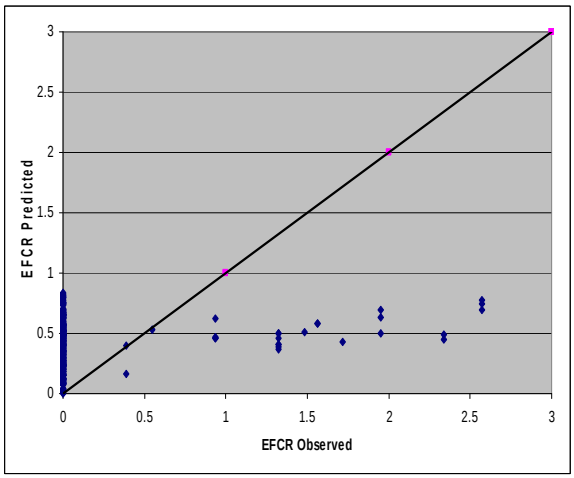

(a) District 5

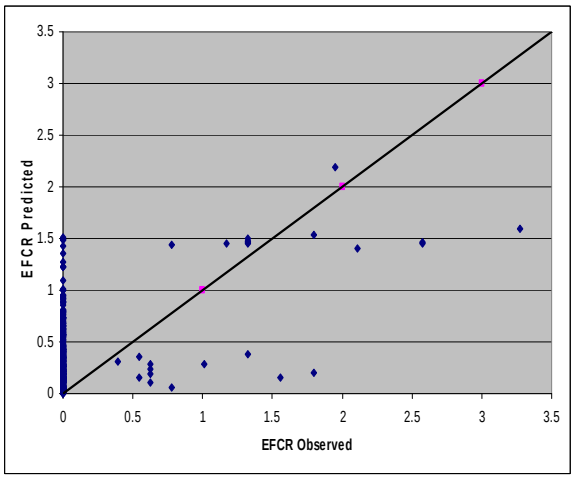

(b) District 6

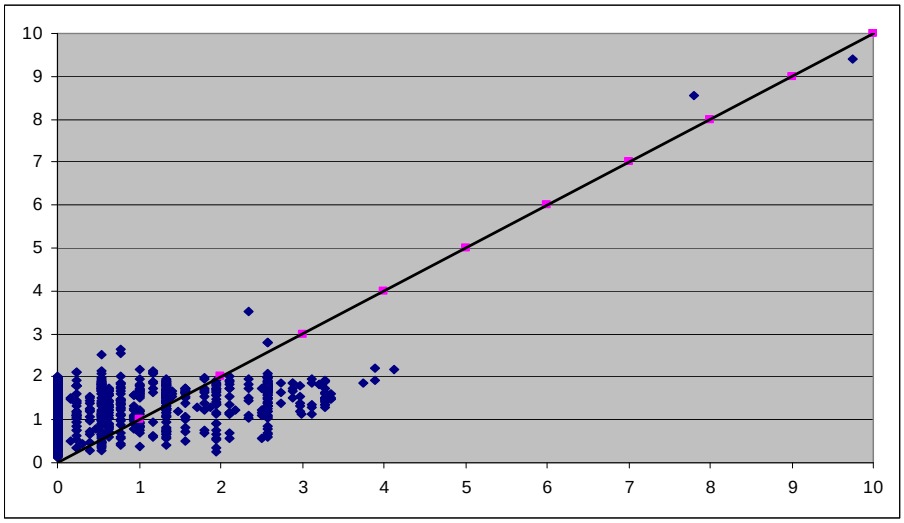

(c) State

Figure 5-35 Sigmoidal EFCR Model with Quad. Sub-Models Valid. for Dist. 5, 6, and State

5.4.4.2 Mean Absolute Deviation

Mean predicted EFCR is greater than mean observed EFCR for all districts and the state since the mode predicts some EFCR for zero observed EFCR as shown in Table 5-24. Low mean absolute deviation difference shows a good fit in general.

Table 5-24 Mean Absolute Deviation for Sigmoidal EFCR Model with Quad. Sub-Models

District	Mean			Mean Absolute Deviation		
	Observed	Predicted	Difference	Observed	Predicted	Difference
1	0.33	1.04	-0.71	0.52	0.47	0.05
2	0.41	0.83	-0.42	0.68	0.59	0.08
3	0.23	1.07	-0.84	0.40	0.46	-0.06
4	0.51	1.51	-1.00	0.77	0.54	0.23
5	0.07	0.60	-0.53	0.13	0.22	-0.08
6	0.18	1.20	-1.02	0.32	0.35	-0.03
State	0.18	1.01	-0.82	0.32	0.28	0.05

5.4.5 Sigmoidal EFCR Model Using Statewide Data

All sigmoidal EFCR models have shown that coefficients for EAL are very small, since EAL is large compared to other variables. Sigmoidal models with linear and quadratic sub-models have been developed using the logarithm of EAL as cases (a) and (b). Table 5-25 shows that the coefficients for logEAL are second highest for all linear sub-models. Coefficients for logEAL is the second highest for all quadratic sub-models, except for the linear part of the beta sub-model. The coefficient of determination is 0.17 for the linear sub-model and 0.07 for the quadratic sub-models. Sigmoidal EFCR model with linear sub-models shows higher R^2, though there are more parameters in sigmoidal EFCR model with quadratic sub-models.

Table 5-25 Sigmoidal EFCR Model Using Statewide Data

		0	1(D)	2(logEAL)	3(Rut)	4(SNeff)	R^2	N
1[a]	δ	-0.234	0.010	0.834	2.646	-0.188	0.17	9,635
	α	257.000	-4.552	-100.500	-160.700	29.057		
	β	-11.193	-0.215	7.839	9.020	2.504		
	γ	-1.789	-0.004	0.890	1.024	0.068		
2[b]	δ	32.389	-0.509	-18.743	-87.207	4.220	0.07	9,635
	α	-32.755	0.579	19.214	95.144	-4.446		
	β	-1452.237	224.320	169.486	862.527	-140.574		
	γ	-4.971	-0.158	-45.804	106.776	-2.934		
	δ_{ii}	-	0.031	7.235	79.327	-0.864		
	α_{ii}	-	-0.036	-7.029	-94.821	0.846		
	β_{ii}	-	-7.548	30.182	-5346.999	12.186		
	γ_{ii}	-	0.190	35.631	-419.441	-0.175		

a- linear sub-models with logEAL; b- quadratic sub-models with logEAL

5.4.5.1 Model Plots

A sigmoidal model with linear and quadratic sub-models shows somewhat a good fit, though the former is a better fit as shown in Figure 5-36.

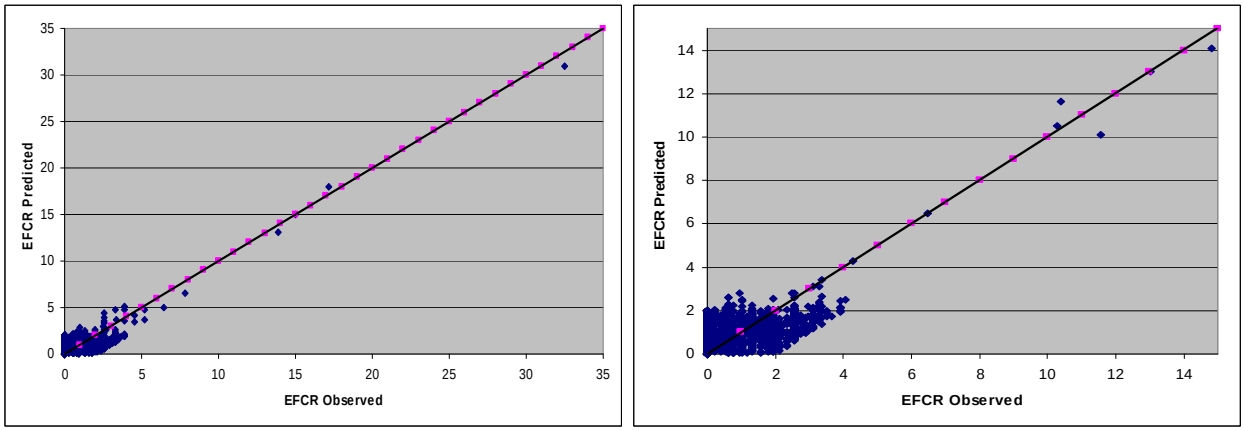

(a) Linear sub-models with logEAL (b) Quadratic sub-models with logEAL

Figure 5-36 Sigmoidal EFCR Model Using Statewide Data

5.4.5.2 Validation Plots

Figure 5-37(a) shows that the simoidal model with linear sub-models is a good fit, since the observed and predicted EFCR are more or less balanced around the 45^{o} slope line. Predicted EFCR using a sigmoidal model with quadratic sub-models remains somewhat constant as the observed EFCR increases as shown in Figure 5-37(b).

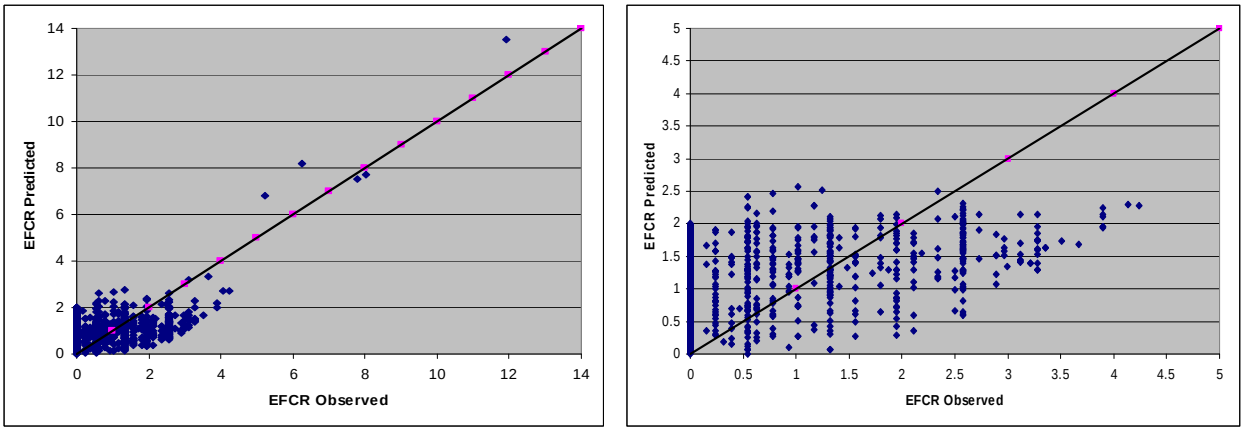

(a) Linear sub-models with logEAL (b) Quadratic sub-models with logEAL

Figure 5-37 Sigmoidal EFCR Model Validation Using Statewide Data

5.4.5.3 Mean Absolute Deviation

Table 5-26 shows mean predicted is greater than mean observed. Mean absolute deviation difference is low, which shows a good match between observed and predicted EFCR.

Table 5-26 Mean Absolute Deviationn for Sigmoidal EFCR Model Using Statewide Data

	Mean			Mean Absolute Deviation		
	Observed	**Predicted**	**Difference**	**Observed**	**Predicted**	**Difference**
1[a]	0.19	1.02	-0.83	0.33	0.34	-0.01
2[b]	0.19	1.08	-0.89	0.33	0.41	-0.08

a- Linear sub-models with logEAL; b- Quadratic sub-models with logEAL

5.5 ETCR Models

Linear, quadratic, and sigmoidal models have been developed using ETCR as a dependent variable and are discussed separately for road categories 12 to 23, districts, and the state.

5.5.1 Linear Regression

Linear ETCR models have been developed for road categories 12 to 23, districts, and the state. Relationships between ETCR and center deflection (d_0) have been discussed in depth.

5.5.1.1 Road Category-Wise

Table 5-27 shows no linear relationship between ETCR and d_0 for road categories 14, 15, and 23. There is a positive relationship between ETCR and d_0 for road categories 12, 13, 17, 18, 21, and 22, whereas there is a negative relationship between ETCR and d_0 for road categories 16, 19, and 20. The coefficient of determination varies from 0.01 to 0.63, and the values show that much of the variation is not explained.

5.5.1.2 District-Wise and Statewide

There is a positive linear relationship between ETCR and d_0 for all districts and the state, except District 6 as shown in Table 5-27. There is no linear relationship between ETCR and d_0 for District 6. The coefficient of determination varies from 0.01 to 0.48. Since R^2 is very low, it was decided to carry out quadratic regression.

Table 5-27 Road Category-Wise Linear ETCR Models

RC	Model	R^2	N
12	$ETCR = 0.019 + 0.010d_0$	0.02	60
13	$ETCR = 0.177 + 0.012d_0 - 0.006EAL$	0.16	134
14	$ETCR = 0.0118D - 0.108AADT + 0.1805EAL + 1.269Rut$	0.11	266
15	$ETCR = 1.655 - 0.02D - 1.002PL1 - 0.0066EAL - 1.437Rut$	0.63	84
16	$EFCR = 0.484 - 0.009d_0$	0.01	658
17	$EFCR = 0.0283 + 0.0044d_0 + 0.011D + 0.471Rut$	0.03	4,134
18	$ETCR = 0.358 + 0.0025d_0$	0.00	2,135
19	$ETCR = 1.321 - 0.001d_0 - 1.028PL1 + 0.147PL2 - 0.271PL3 - 0.001EAL - 0.468Rut$	0.45	1,457
20	$ETCR = 0.994 - 0.006d_0 - 0.527PL1 + 0.582PL2 - 0.002EAL - 0.306Rut$	0.49	879
21	$ETCR = -2.211 + 0.142d_0 + 0.0025AADT$	0.10	232
22	$ETCR = 1.568 + 0.0115d_0 - 1.504PL1 - 0.186PL2$	0.58	750
23	$ETCR = 0.184 + 0.0137D$	0.01	1,791

5.5.1.3 Summary of Linear ETCR Models

Linear models show a positive relationship between ETCR and center deflections for road categories, districts, and the state in general, but R^2 values are relatively low. It was decided to develop quadratic ETCR models for districts since R^2 values for districts particularly very low.

5.5.2 Quadratic Regression

Quadratic models have been developed only for the districts. There is a positive linear relationship between ETCR and d_0 for all districts except District 4, in which the relationship is negative as shown in Table 5-29. There is a negative quadratic relationship between ETCR and d_0 for Districts 1, 3, and 4. Interaction between d_0 and D is positively related with ETCR for District 5 and negatively related for Districts 1 and 6. The coefficient of determination varies

from 0.03 to 0.10, which is significantly low. As a result, it was decided to investigate the sigmoidal relationship between ETCR and d_0.

Table 5-28 District-Wise and Statewide Linear ETCR Models

District	Model	R^2	N
1	$ETCR = 0.282 + 0.0011d_0 + 0.623Rut$	0.01	1,425
2	$ETCR = 0.217 + 0.0092d_0$	0.03	1,573
3	$ETCR = 0.222 + 0.010d_0$	0.01	1,955
4	$ETCR = 0.00622 + 0.152d_0$	0.01	1,305
5	$ETCR = 0.112 + 0.018d_0 - 0.274Rut$	0.04	1,645
6	$ETCR = 1.154 - 0.962PL1 - 0.258PL2$	0.48	1,755
State	$ETCR = 0.248 + 0.003d_0$	0.01	12,865

Table 5-29 District-Wise Quadratic ETCR Models

Dist.	Model	R^2	N
1	$ETCR = 0.114 + 0.0215d_0 - 0.00002d_0 \times d_0 + 0.0106D - 0.0023d_0 \times D + 1.286Rut - 2.752Rut \times Rut$	0.04	1,423
2	$ETCR = 0.156 + 0.0088d_0 + 1.154Rut - 3.573Rut \times Rut$	0.04	1,573
3	$ETCR = 0.0193d_0 - 0.00023d_0 \times d_0 + 0.05D - 0.003D \times D$	0.03	1,951
4	$ETCR = 0.125 - 0.0172d_0 - 0.0003d_0 \times d_0 + 0.0217D - 0.0024D \times D + 1.195Rut - 2.791Rut \times Rut$	0.03	1,300
5	$ETCR = 0.0913 + 0.0023d_0 + 0.0158D - 0.002D \times D + 0.0023d_0 \times D$	0.05	1,638
6	$ETCR = -0.369 + 0.0207d_0 + 0.1014D - 0.007D \times D - 0.0021d_0 \times D + 3.906Rut - 6.92Rut \times Rut$	0.10	1,755

5.5.3 Sigmodal ETCR Model with Linear Sub-Models

ETCR has been used as a dependent variable in Equation (5.1). Four variables have been included in the linear sub-models: total pavement thickness above subgrade (D), equivalent axle load (EAL), rut depth, and SNeff.

5.5.3.1 Road Category-Wise

The higher the magnitude of the variable, the lower the magnitude of the coefficient in the linear sub-models. Table 5-30 shows that R^2 varies from 0.19 to 0.99.

Table 5-30 FDBIT Sigmoidal ETCR Model with Linear Sub-Models

RC		0	1(D)	2(EAL)	3(Rut)	4(SNeff)	R^2	N
12	δ	-1.509	0.135	0.085	-1.648	0.250	0.99	36
	α	1.562	-0.130	-0.081	0.309	-0.241		
	β	-309.89	59.513	56.281	248.187	-434.32		
	γ	-102.53	5.771	7.371	-33.564	-21.792		
13	δ	-0.040	0.000	0.001	-0.103	0.014	0.94	123
	α	0.977	-0.034	-0.043	-0.669	0.456		
	β	-30.833	25.967	-3.761	-168.793	24.868		
	γ	8.414	1.488	-0.394	7.438	-1.231		
14	δ	0.212	-0.001	-0.001	-0.072	-0.004	0.58	240
	α	-0.603	0.026	0.010	1.204	-0.008		
	β	64.479	-11.459	-0.080	190.651	10.648		
	γ	0.689	-0.719	-0.015	19.867	1.995		
15	δ	1.167	0.070	-0.073	-0.705	-0.091	0.96	63
	α	-0.771	0.870	0.093	-4.702	-0.440		
	β	-53.123	10.632	0.060	59.216	1.457		
	γ	-4.474	0.556	0.025	7.422	0.441		
16	δ	0.600	-0.033	-0.015	2.354	0.149	0.38	590
	α	-0.273	0.078	0.024	-3.065	-0.281		
	β	-15.902	-7.740	0.611	12.805	-2.822		
	γ	7.897	-1.208	0.014	6.209	-2.059		
17	δ	0.142	0.099	0.000	-0.131	-0.043	0.19	3,729
	α	-0.260	-0.086	-0.001	0.594	0.092		
	β	0.235	-0.334	0.008	-0.222	-0.776		
	γ	-0.052	0.007	0.000	-0.558	-0.073		

Coefficients of four variables in the linear sub-models for all PDBIT road categories are shown in Table 5-31. In general, the magnitude of the coefficient depends on the magnitude of the variable. The coefficient of determination varies from 0.18 to 0.67.

Table 5-31 PDBIT Sigmoidal ETCR Models with Linear Sub-Models

		0	**1(D)**	**2(EAL)**	**3(Rut)**	**4(SNeff)**	**R^2**	**N**
18	δ	0.491	0.008	0.002	-0.586	-0.055	0.21	1,910
	α	3.658	-0.298	-0.059	-13.007	2.589		
	β	-28.827	-1.630	2.024	36.610	15.422		
	γ	-1.525	-0.152	0.085	2.308	0.788		
19	δ	0.410	-0.035	-0.001	-0.411	0.049	0.19	1,299
	α	-46.972	0.324	0.756	14.610	17.095		
	β	-134.20	14.590	2.844	-69.378	1.157		
	γ	-4.642	1.224	-0.075	-6.097	-0.240		
20	δ	0.374	0.031	-0.004	0.612	0.028	0.25	785
	α	0.885	0.217	0.015	-4.907	-1.129		
	β	13.846	-0.414	-0.303	44.011	0.925		
	γ	1.456	0.024	-0.033	3.887	-0.059		
21	δ	74.450	-2.295	-1.407	-104.400	5.643	0.67	411
	α	-73.012	2.332	1.328	98.313	-5.784		
	β	-4.965	-0.043	0.041	5.326	0.080		
	γ	0.119	-0.002	-0.006	-0.258	0.005		
22	δ	0.828	-0.005	-0.010	-0.474	-0.004	0.57	655
	α	0.086	-1.161	0.157	-0.004	0.782		
	β	113.900	-7.463	-4.036	1111.200	-12.330		
	γ	-7.905	-0.462	-0.160	118.300	-0.877		
23	δ	0.801	0.163	-0.008	-2.679	-0.024	0.18	1,605
	α	-0.797	-0.157	0.009	3.480	0.040		
	β	-3.645	-0.858	-0.018	8.120	2.079		
	γ	0.140	-0.072	-0.002	-0.078	0.204		

5.5.3.1.1 Model Plots

Figure 5-38 shows a somewhat good fit for road categories 12 to 15 with some scatter. The plot for road category 14 shows that predicted ETCR is less than observed ETCR for a majority of the points. In general, the difference is not significant from a practical point of view.

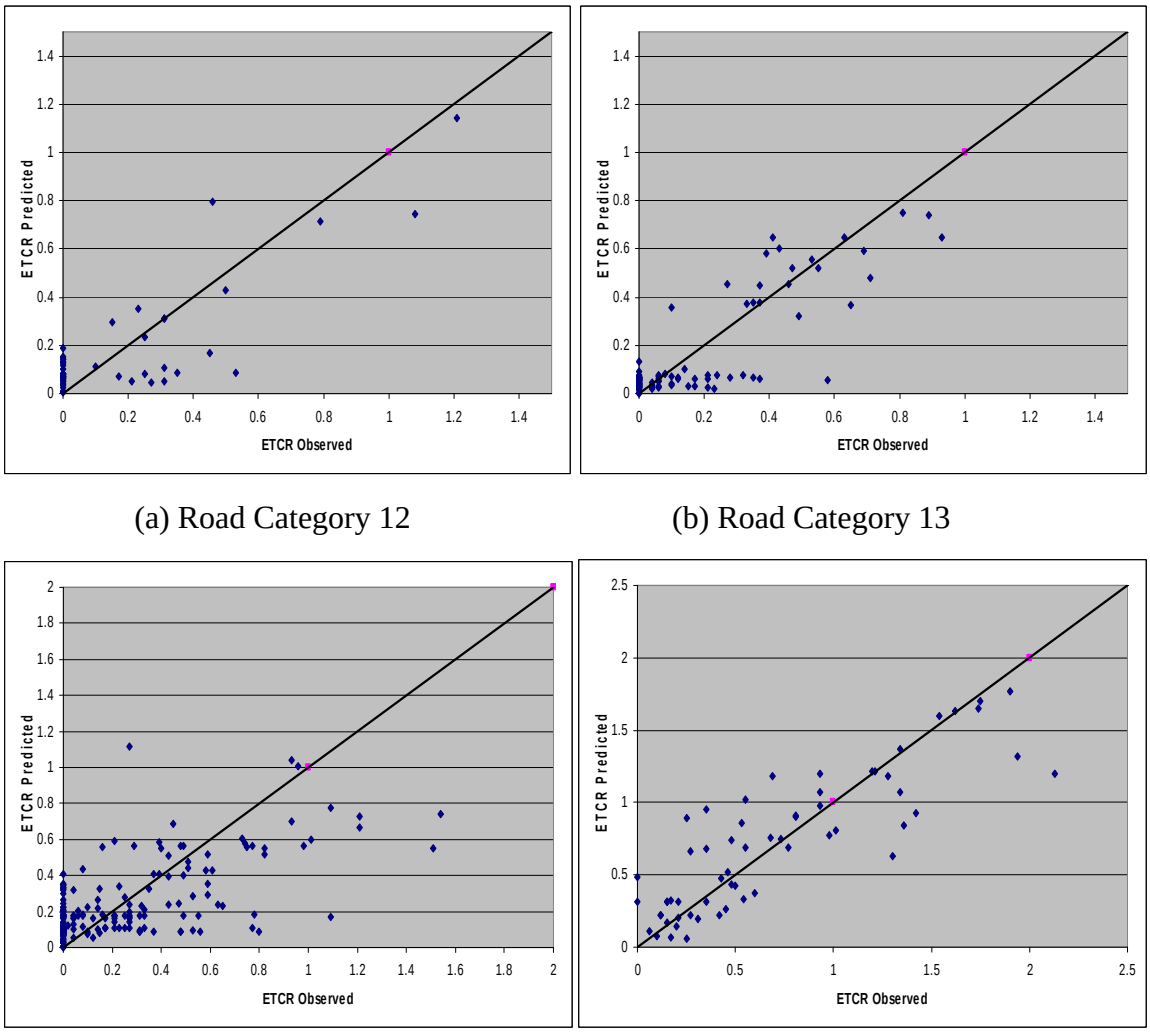

(a) Road Category 12 (b) Road Category 13

(c) Road Category 14 (d) Road Category 15

Figure 5-38 Sidmoidal ETCR Model with Linear Sub-Models for RC 12 to 15

Observed and predicted ETCR are comparable with some scatter around the 45^{o} slope line for road category 16 as shown in Figure 5-39(a). There is a weak or no linear relationship between observed and predicted ETCR for the road categories 17, 18, and 19 as shown in Figure 5-39 (b), (c), and (d).

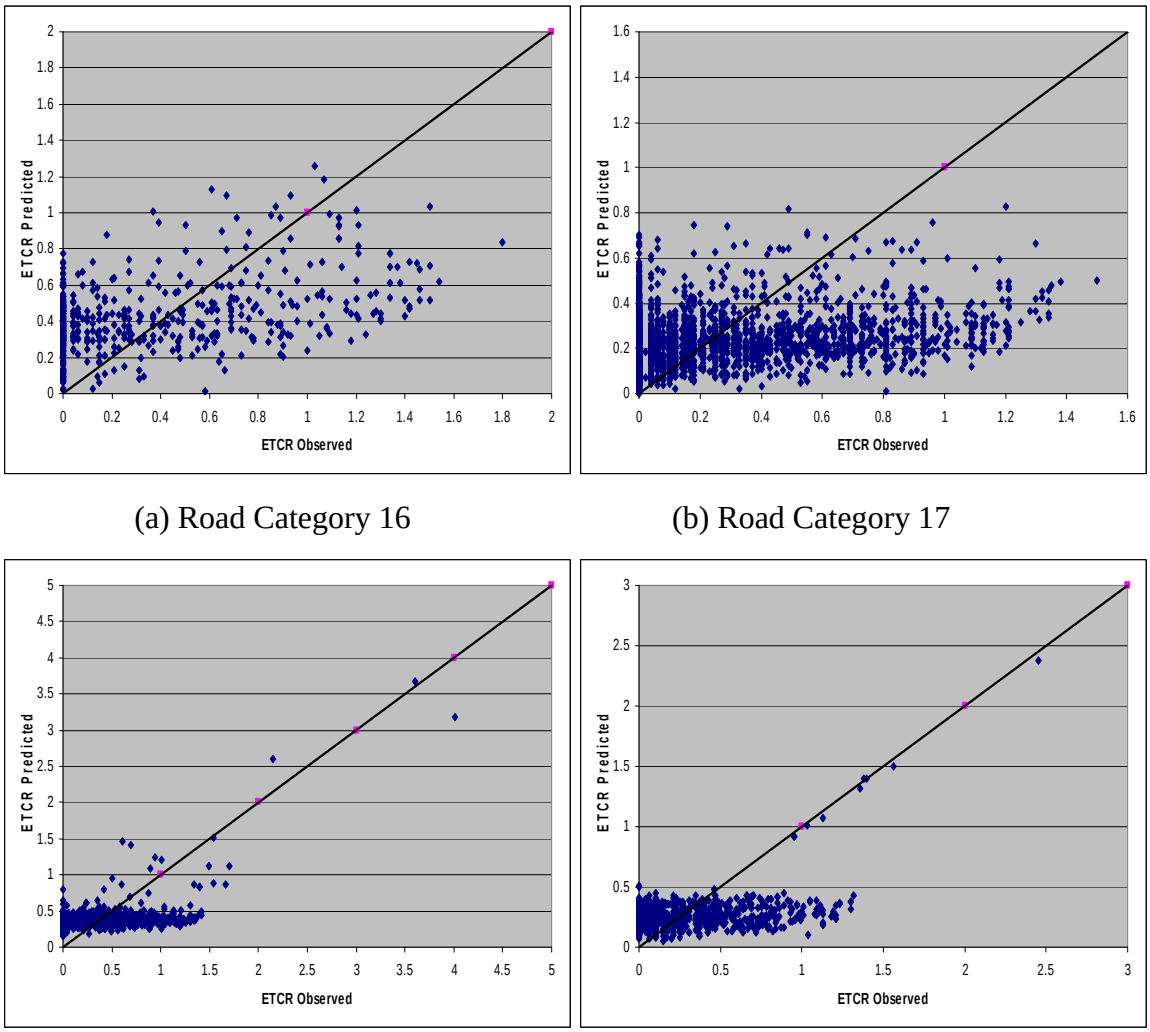

(a) Road Category 16 (b) Road Category 17

(c) Road Category 18 (d) Road Category 19

Figure 5-39 Sidmoidal ETCR Model with Linear Sub-Models for RC 16 to 19

Predicted ETCR increases at a slow rate when observed ETCR increases for road categories 20 and 21, as shown in Figure 5-40(a) and (b). There is a minor linear relationship between observed and predicted ETCR for the road categories 22 and 23, as shown in Figure 5-40(c) and (d).

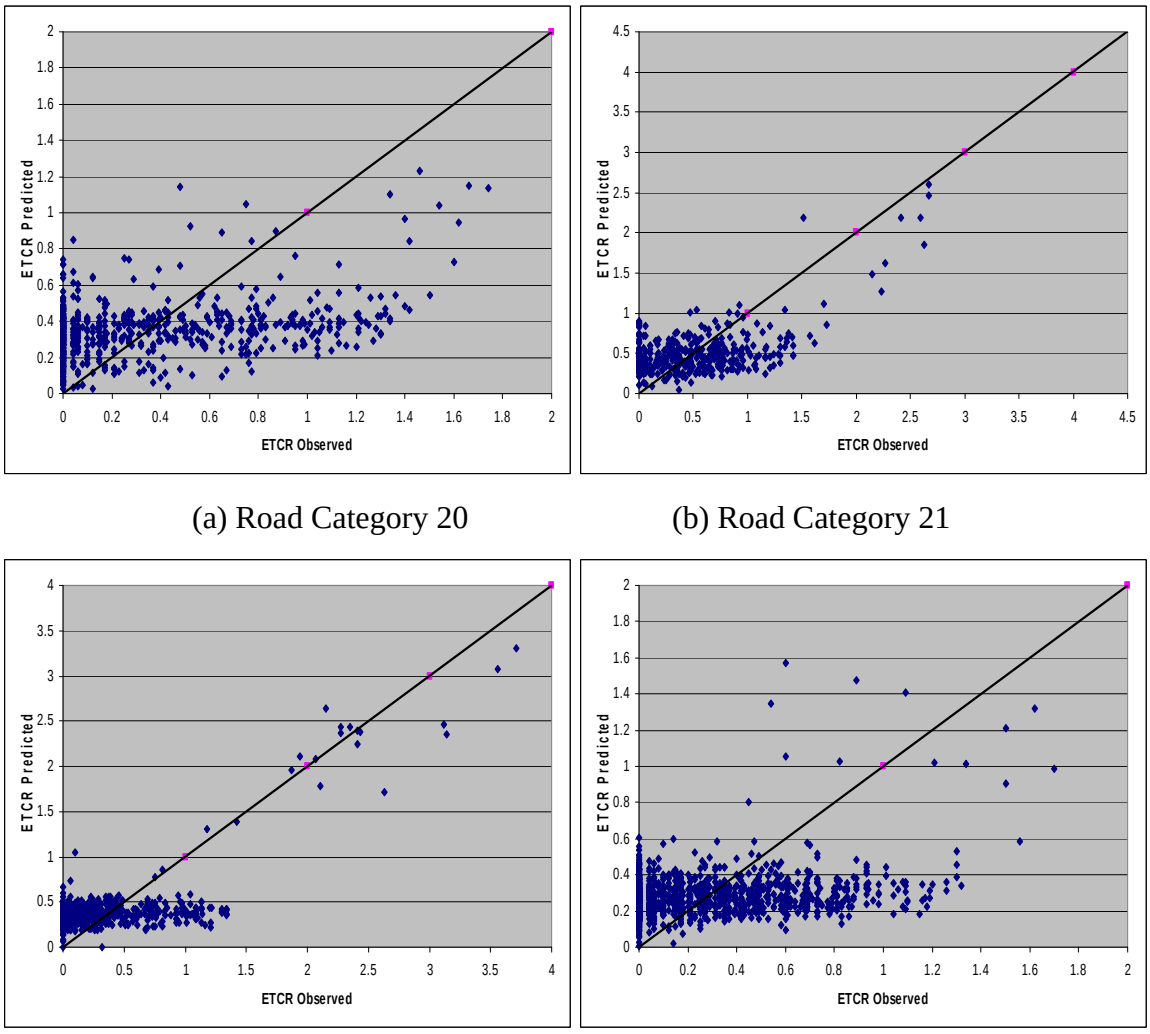

(a) Road Category 20 (b) Road Category 21

(c) Road Category 22 (d) Road Category 23

Figure 5-40 Sidmoidal ETCR Model with Linear Sub-Models for RC 20 to 23

5.5.3.1.2 Validation Plots

Figure 5-41 shows that observed and predicted ETCR match very well for road categories 12 to 15.

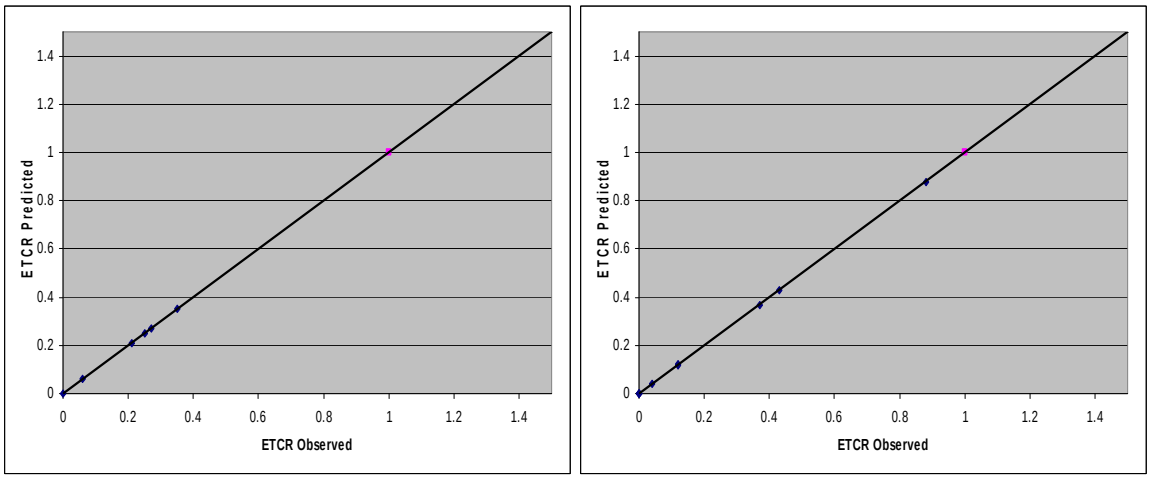

(a) Road Category 12 (b) Road Category 13

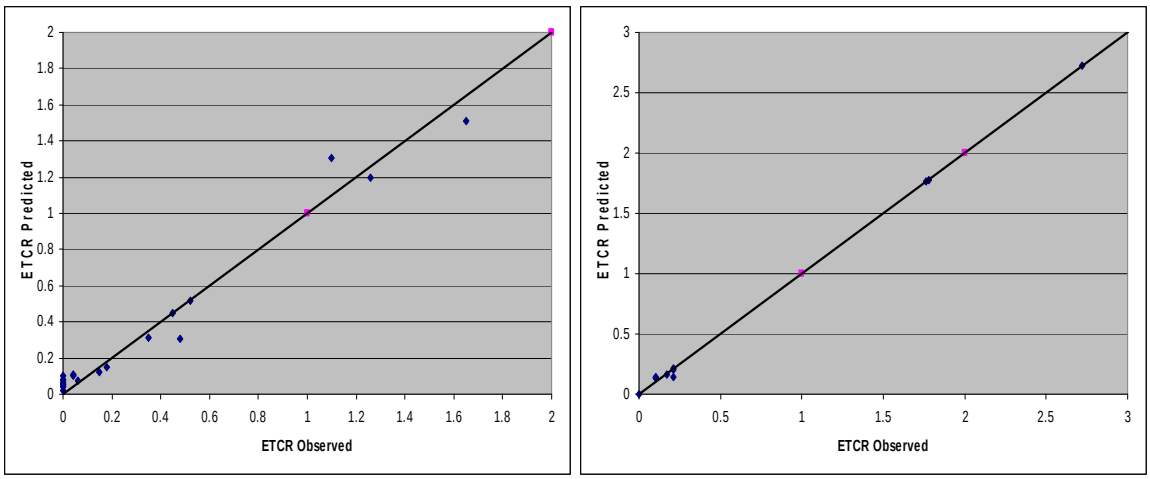

(c) Road Category 14 (d) Road Category 15

Figure 5-41 Sidmoidal ETCR Model with Linear Sub-Models Validation for RC 12 to 15

Predicted and observed ETCR fit well for District 16 as shown in Figure 5-42(a). Figure 5-42(b) shows there is no or a weak linear relationship between observed and predicted ETCR for road category 17. Predicted ETCR increases at a slow rate as the observed ETCR increases for road categories 18 and 19, as shown in Figure 5-42(c) and (d).

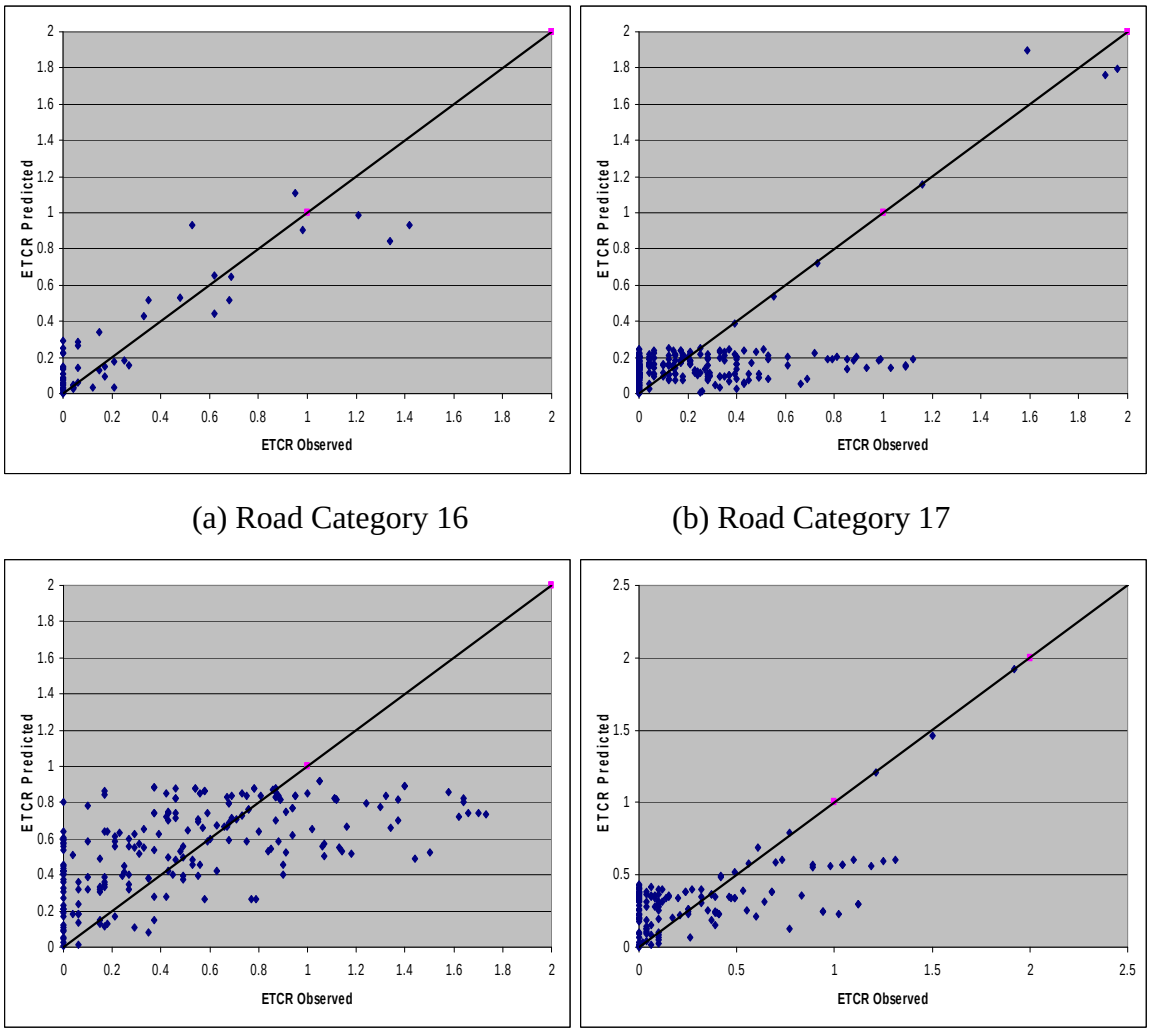

(a) Road Category 16 (b) Road Category 17

(c) Road Category 18 (d) Road Category 19

Figure 5-42 Sidmoidal ETCR Model with Linear Sub-Models Validation for RC 16 to 19

Observed and predicted ETCR are somewhat well matched with some scatter for road categories 20 and 21, as shown in Figure 5-43(a) and (b). This shows that sigmoidal model with linear sub-models is a good fit for road categories 20 and 21. A majority of the points show that observed ETCR is greater than predicted ETCR with significant scatter for road categories 22 and 23, as shown in Figure 5-43(c) and (d).

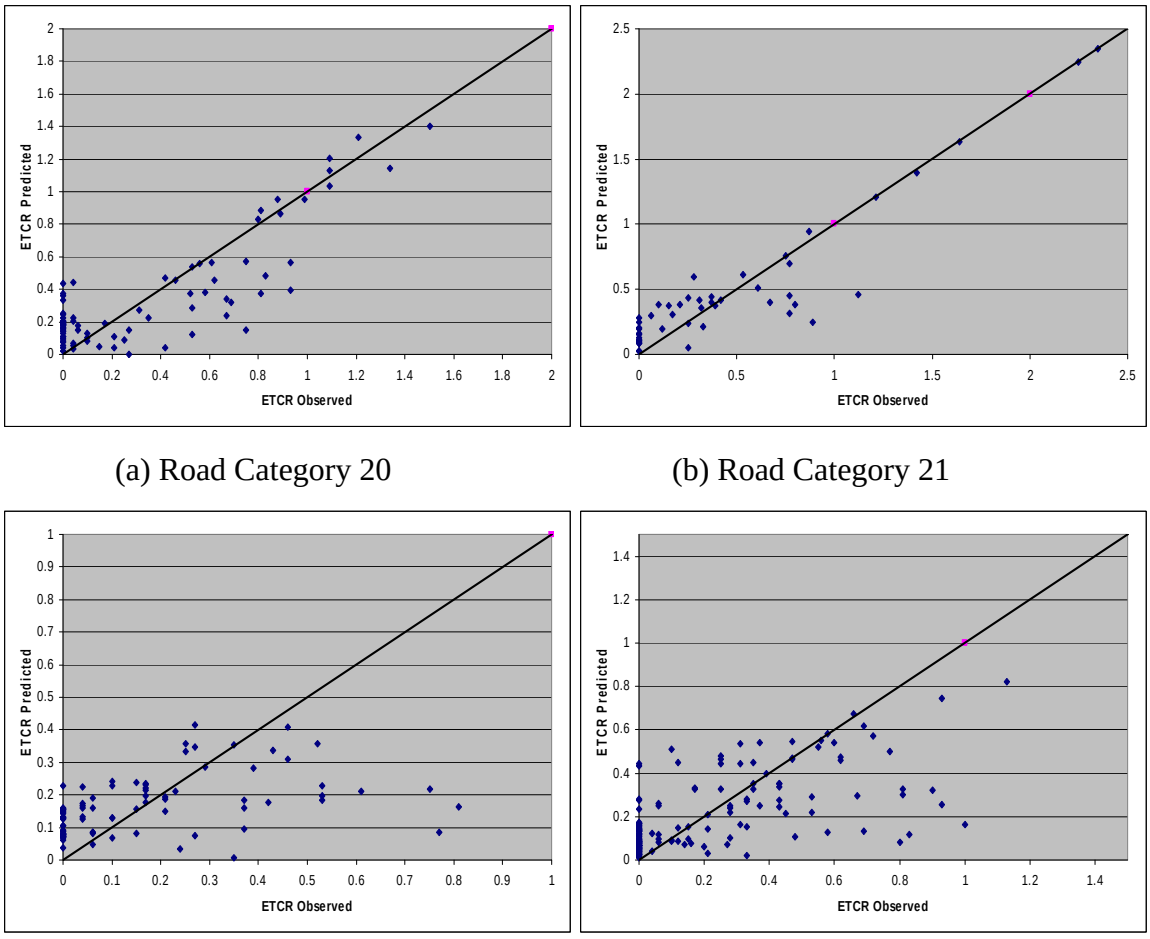

(a) Road Category 20 (b) Road Category 21

(c) Road Category 22 (d) Road Category 23

Figure 5-43 Sidmoidal ETCR Model with Linear Sub-Models Validation for RC 20 to 23

5.5.3.2 District-Wise and Statewide

Table 5-32 shows the intercepts of all linear sub-models are positive for District 4. Magnitude of the coefficients highly depends on magnitude of the variables; low coefficients result in the variables with high magnitude. The coefficient of determination varies from 0.11 to 0.48.

Table 5-32 District-Wise and Statewide Sigmoidal Model with Linear Sub-Models

Dist.		0	1(D)	2(EAL)	3(Rut)	4(SNeff)	R^2	N
1	δ	-0.014	-0.018	0.002	0.676	-0.223	0.23	1,423
	α	1.132	-0.033	-0.002	-1.078	0.225		
	β	2.701	-0.315	0.005	-4.556	-0.405		
	γ	0.127	-0.016	-0.001	-0.056	0.009		
2	δ	0.291	0.009	0.001	-0.610	-0.011	0.48	1,569
	α	0.268	-0.046	-0.010	8.233	0.017		
	β	-3.741	0.443	0.022	17.433	-1.207		
	γ	0.054	0.036	0.002	-0.199	-0.234		
3	δ	-0.789	0.267	0.057	2.382	-0.195	0.47	1,951
	α	1.083	-0.245	-0.057	-2.495	0.142		
	β	-0.109	0.412	0.077	-6.747	-1.791		
	γ	-0.219	0.079	0.021	-0.886	-0.263		
4	δ	0.021	-0.002	0.000	0.081	0.008	0.40	1,300
	α	1.422	-0.049	0.008	-1.974	-0.252		
	β	23.575	1.014	-0.021	-151.600	-4.006		
	γ	1.405	0.138	-0.016	-11.889	-0.233		
5	δ	0.397	0.003	0.000	-0.261	-0.018	0.22	1,638
	α	-1.524	0.281	0.000	-1.790	0.246		
	β	-6.855	3.340	0.010	23.403	-0.680		
	γ	-1.240	0.201	0.001	2.514	0.095		
6	δ	0.291	0.000	0.000	1.314	-0.020	0.42	1,755
	α	2.243	-0.285	-0.008	-9.100	2.146		
	β	-23.288	1.681	0.105	411.600	-13.139		
	γ	-0.490	0.193	-0.019	28.156	-2.595		
State	δ	1.772	-0.126	0.252	-9.284	-0.071	0.11	9,636
	α	-1.468	0.137	-0.252	9.449	0.027		
	β	-8.249	0.165	-0.039	-2.135	0.716		
	γ	-0.152	0.020	0.003	-0.378	-0.065		

5.5.3.2.1 Model Plots

Predicted ETCR increases at a slow rate with an increase in observed ETCR for District 1 as shown in Figure 5-44(a). Predicted ETCR remains more or less constant as the observed ETCR increases for Districts 2 and 4, as shown in Figure 5-44(b) and (d). A sigmoidal model with linear sub-models fits well for District 3, with some scatter as shown in Figure 5-44(c).

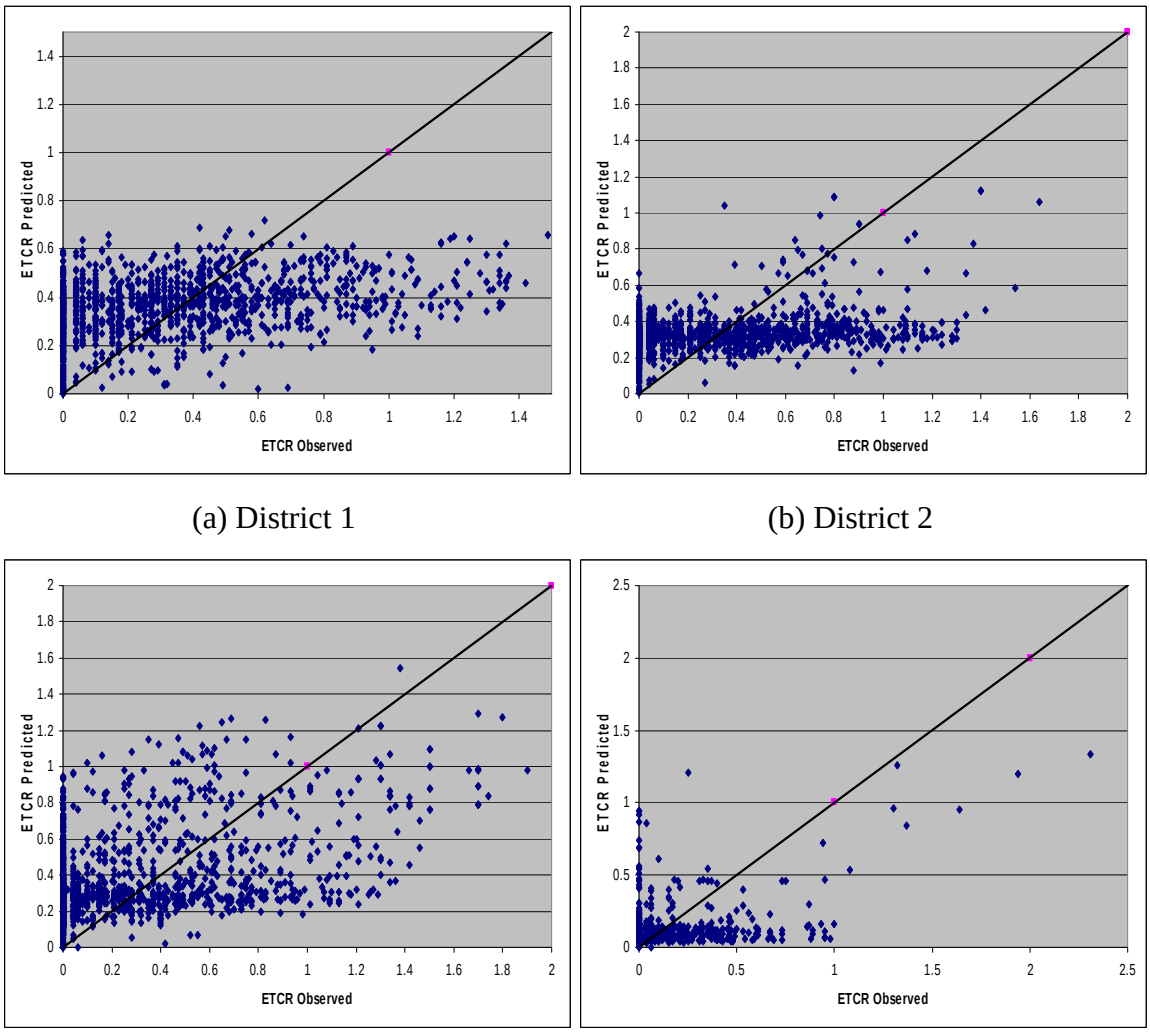

(a) District 1 (b) District 2

(c) District 3 (d) District 4

Figure 5-44 Sidmoidal ETCR Model with Linear Sub-Models for Districts 1 to 4

There is no linear relationship between observed and the predicted ETCR for Districts 5, 6, and the state as shown in Figure 5-45. However, the difference is not significant from a practical point of view. This shows that a sigmoidal model with linear sub-models is not a good fit. As a result, sigmoidal models with quadratic sub-models have been developed and will be discussed in the next section.

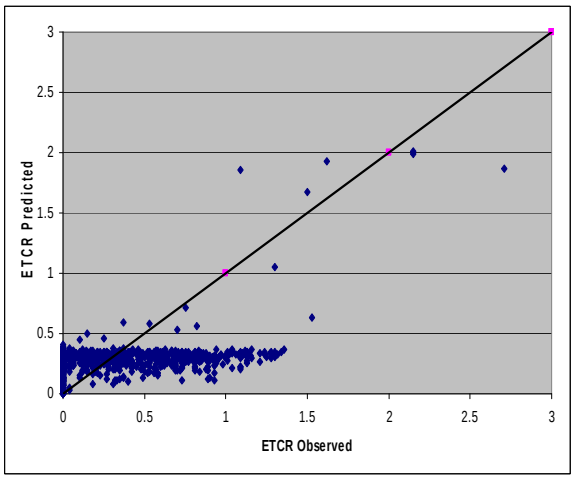

(a) District 5

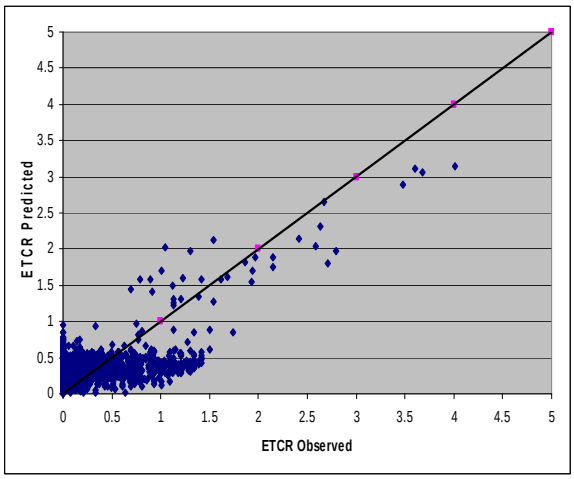

(b) District 6

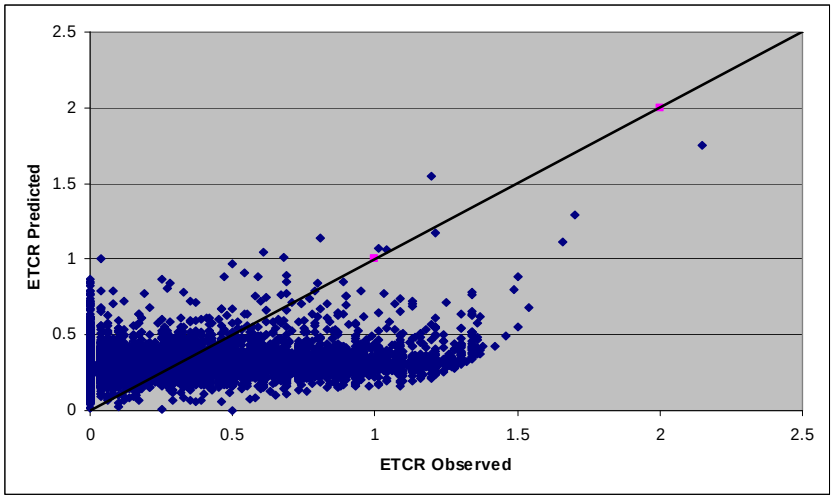

(c) State

Figure 5-45 Sidmoidal ETCR Model with Linear Sub-Models for Districts 5, 6, and State

5.5.3.2.2 Validation Plots

Predicted ETCR remains constant or increases at a slow rate as the observed ETCR increases for Districts 1 to 4 as shown in Figure 5-46.

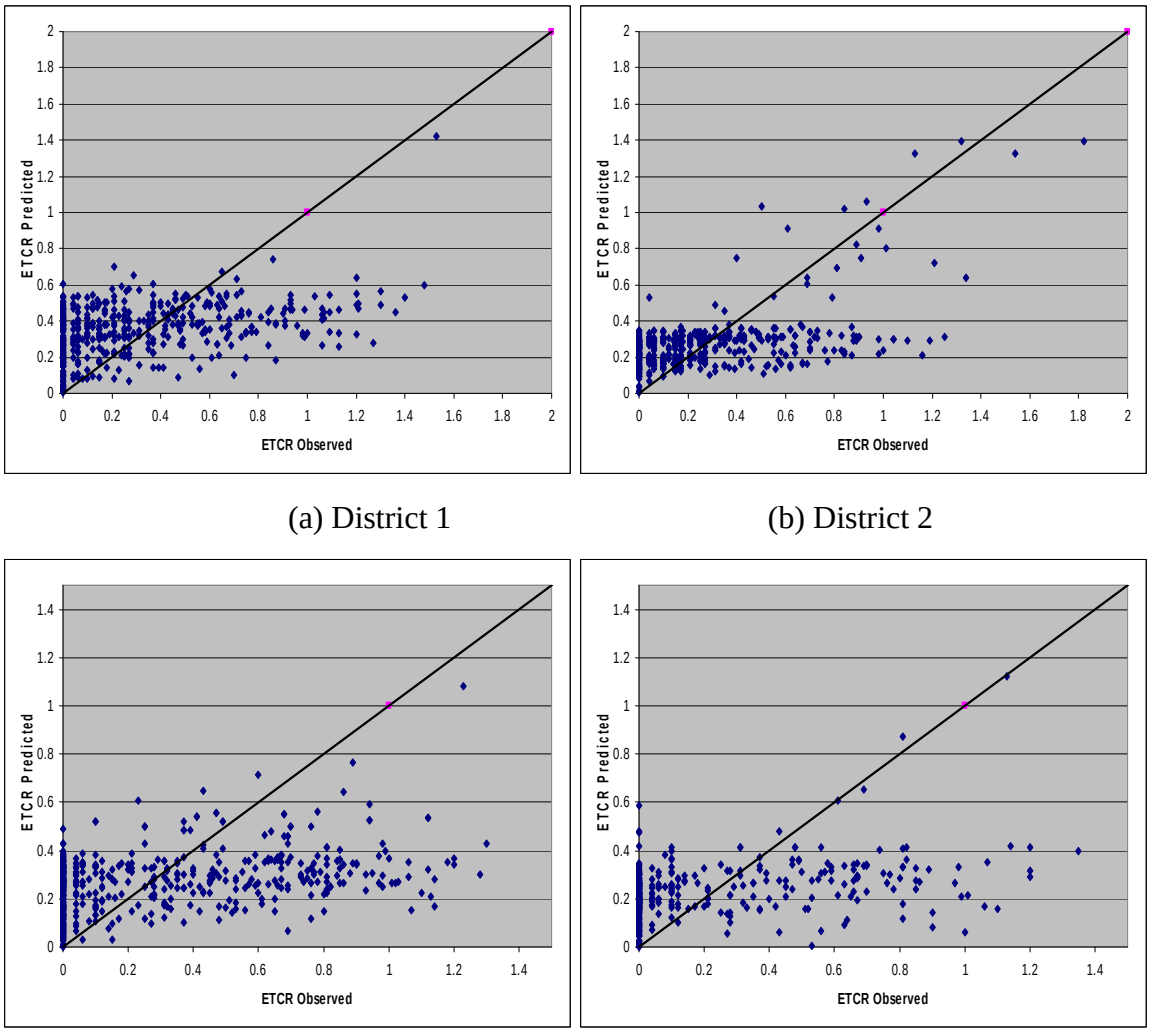

(a) District 1 (b) District 2

(c) District 3 (d) District 4

Figure 5-46 Sigmoidal ETCR Models with Linear Sub-Models Valid. for Districts 1 to 4

Observed and predicted ETCR are independent of each other for District 5 and the state as shown in Figure 5-47(a) and (c), whereas predicted ETCR increases at a slow rate as the observed ETCR increases for District 6 as shown in Figure 5-47(b).

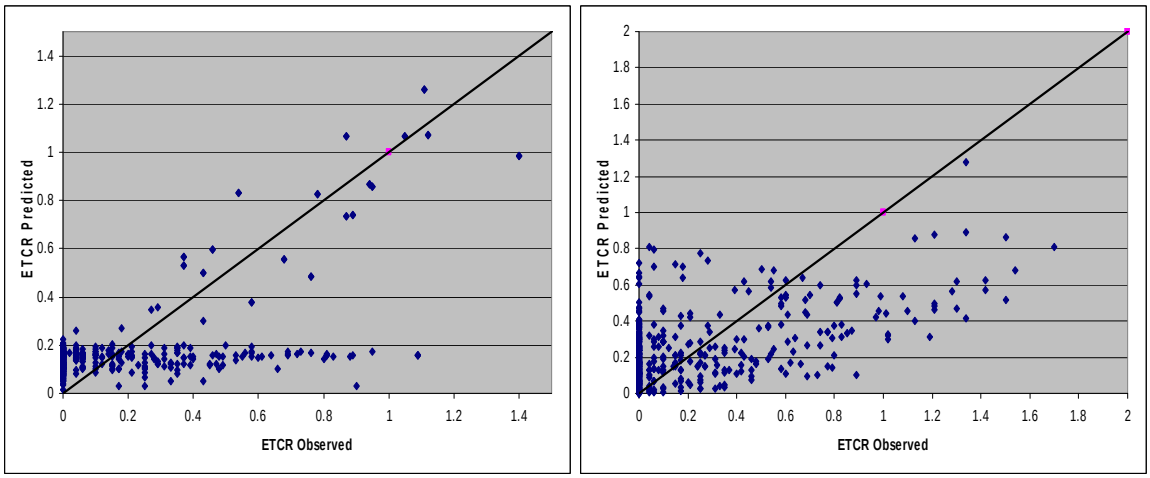

(a) District 5 (b) District 6

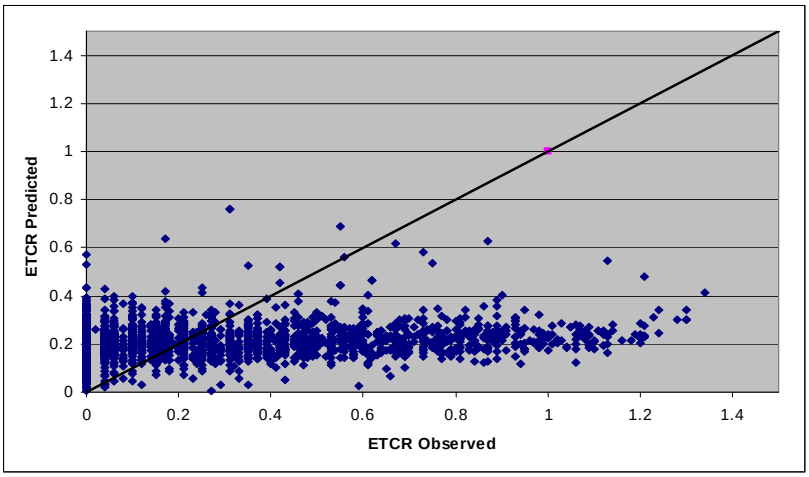

(c) State

Figure 5-47 Sidmoidal ETCR Model with Linear Sub-Models Valid. for Dist. 5, 6, and State

5.5.3.3 Absolute Mean Deviation

Mean predicted ETCR is slightly higher than mean observed ETCR as showb in Table 5-33 since the model predicts existence of some ETCR for zero observed. The lower the mean absolute deviation difference, the better the agreement between observed and predicted ETCR in general.

Table 5-33 Absolute Mean Deviation for Sigmoidal ETCR Models with Linear Sub-Models

	Mean			Mean Absolute Deviation		
	Observed	**Predicted**	**Difference**	**Observed**	**Predicted**	**Difference**
(a) Road Category-Wise						
12	0.172	0.175	-0.003	0.204	0.150	0.054
13	0.130	0.131	-0.001	0.164	0.133	0.031
14	0.198	0.216	-0.019	0.231	0.138	0.092
15	0.709	0.716	-0.007	0.465	0.391	0.075
16	0.365	0.421	-0.056	0.363	0.149	0.214
17	0.177	0.211	-0.033	0.219	0.083	0.137
18	0.305	0.385	-0.080	0.286	0.052	0.234
19	0.197	0.255	-0.058	0.230	0.073	0.157
20	0.295	0.349	-0.054	0.321	0.104	0.217
21	0.486	0.507	-0.021	0.390	0.193	0.197
22	0.331	0.413	-0.082	0.349	0.142	0.207
23	0.208	0.275	-0.067	0.235	0.073	0.162
(b) District-Wise and Statewide						
1	0.324	0.358	-0.034	0.267	0.097	0.170
2	0.302	0.331	-0.029	0.287	0.066	0.221
3	0.279	0.383	-0.104	0.302	0.177	0.125
4	0.080	0.102	-0.022	0.115	0.059	0.056
5	0.226	0.284	-0.058	0.270	0.060	0.210
6	0.284	0.372	-0.087	0.322	0.141	0.181
State	0.239	0.313	-0.073	0.263	0.066	0.197

5.5.4 Sigmoidal ETCR Model with Quadratic Sub-Models

Sigmoidal ETCR models with quadratic sub-models have been developed for districts and the state. Four variables have been included in all sub-models: total pavement thickness above subgrade (D), equivalent axle load (EAL), rut depth, and SNeff. The coefficients are tabulated in three tables: Districts 1 to 3, Districts 4 to 6, and statewide.

Magnitude of the coefficients highly depends on the magnitude of the variable. EAL coefficients are lowest in both linear and quadratic parts of all sub-models for Districts 1 to 3 as shown in Table 5-34. Coefficients for the quadratic part are close to zero. On the other hand, coefficients for rut depth are largest in both linear and quadratic parts of all sub-models. Signs of coefficients for the same variable do not show a consistent trend. The coefficient of determination varies from 0.30 to 0.46.

Intercepts for all quadratic sub-models are positive for District 5 as shown in Table 5-35. Coefficients of EAL are zero or close to zero, both in the linear and quadratic parts of all sub-models. The coefficient of determination varies from 0.31 to 0.67.

Table 5-34 Sigmoidal ETCR Model with Quadratic Sub-Models for Districts 1 to 3

Dist.		0	1(D)	2(EAL)	3(Rut)	4(SNeff)	R^2	N
1	δ	0.206	0.023	-0.003	1.995	-0.009	0.30	1,423
	α	-1.129	2.172	-0.064	-11.297	-3.707		
	β	16.186	-5.592	-0.157	93.327	5.382		
	γ	1.505	-0.611	-0.020	5.899	0.594		
	δ_{ii}	-	-0.001	0.000	-5.289	0.008		
	α_{ii}	-	-0.236	0.005	36.202	1.302		
	β_{ii}	-	0.661	0.000	-347.000	-0.641		
	γ_{ii}	-	0.054	0.000	-19.021	-0.118		
2	δ	0.449	0.051	0.000	2.144	-0.281	0.37	1,569
	α	8.631	-0.597	0.005	-5.550	-4.934		
	β	-31.016	-13.52	0.185	-281.100	29.247		
	γ	-5.458	-0.285	0.018	-9.406	3.090		
	δ_{ii}	-	-0.002	0.000	-7.458	0.039		
	α_{ii}	-	0.036	0.000	14.468	0.938		
	β_{ii}	-	2.372	0.000	1604.200	-3.487		
	γ_{ii}	-	0.082	0.000	64.067	-0.385		
3	δ	-5.184	1.847	-0.054	1.761	-0.252	0.46	1,951
	α	5.645	-1.779	0.047	0.194	0.208		
	β	18.256	-6.334	0.361	-24.188	-1.429		
	γ	2.899	-1.143	0.035	-5.737	0.593		
	δ_{ii}	-	-0.128	0.000	-3.142	0.155		
	α_{ii}	-	0.124	0.000	-0.909	-0.152		
	β_{ii}	-	0.496	-0.002	56.429	-1.197		
	γ_{ii}	-	0.078	0.000	19.189	-0.228		

Table 5-35 Sigmoidal ETCR Model with Quadratic Sub-Models for Districts 4 to 6

Dist.		0	1(D)	2(EAL)	3(Rut)	4(SNeff)	R^2	N
4	δ	35.294	-14.31	0.128	-111.700	-9.277	0.67	1,300
	α	-35.270	14.334	-0.128	112.000	9.262		
	β	-27.873	15.450	2.190	-107.200	-88.393		
	γ	20.251	0.028	0.157	-49.944	-14.586		
	δ_{ii}	-	1.941	0.000	315.200	1.678		
	α_{ii}	-	-1.943	0.000	-316.500	-1.675		
	β_{ii}	-	-3.052	-0.006	182.300	10.737		
	γ_{ii}	-	-0.078	0.000	119.200	1.839		
5	δ	0.401	0.029	0.000	-0.515	-0.082	0.31	1,638
	α	13.032	-0.131	0.021	-4.575	-8.478		
	β	33.017	-20.65	-0.020	129.700	8.801		
	γ	0.537	-1.597	-0.005	21.354	0.879		
	δ_{ii}	-	-0.001	0.000	0.424	0.006		
	α_{ii}	-	-0.009	0.000	9.545	1.563		
	β_{ii}	-	1.528	0.000	-120.400	-0.428		
	γ_{ii}	-	0.125	0.000	-34.347	-0.026		
6	δ	2.876	-0.553	-0.016	-10.788	2.610	0.55	1,755
	α	-2.213	0.568	0.016	12.353	-2.859		
	β	-38.735	5.523	0.066	34.405	9.508		
	γ	-0.498	0.133	0.005	-6.615	0.650		
	δ_{ii}	-	0.023	0.000	5.270	0.071		
	α_{ii}	-	-0.025	0.000	-9.410	-0.043		
	β_{ii}	-	-0.428	0.000	-138.400	-1.414		
	γ_{ii}	-	-0.009	0.000	6.589	-0.105		

Intercepts of all sub-models are positive except for the sigma sub-model using statewide data as shown in Table 5-36. The coefficient of EAL in both linear and quadratic parts of all sub-models are zero or very close to zero, whereas coefficients of rut depth in both linear and quadratic parts of all sub-models are the largest in magnitude. The coefficient of determination is 0.15.

Table 5-36 Sigmoidal ETCR Model with Quadratic Sub-Models Using Statewide Data

	0	**1(D)**	**2(EAL)**	**3(Rut)**	**4(SNeff)**	**R^2**	**N**
δ	2.656	-0.189	0.000	-10.867	-0.913	0.15	9,636
α	-2.268	0.214	0.000	11.617	0.812		
β	-82.477	22.727	0.017	9.926	2.774		
γ	-1.181	0.911	0.001	-9.158	-0.262		
δ_{ii}	-	-0.013	0.000	7.549	2.001		
α_{ii}	-	0.011	0.000	-9.945	-1.989		
β_{ii}	-	-1.701	0.000	-149.939	-0.428		
γ_{ii}	-	-0.068	0.000	8.117	0.022		

5.5.4.1.1 Model Plots

Predicted ETCR increases at a slow rate as the observed ETCR increases for Districts 1 to 3, as shown in Figure 5-48(a), (b), and (c). Predicted ETCR remains somewhat constant as the observed ETCR increases for District 4 as shown in Figure 5-48(d). This shows that the sigmoidal model with quadratic sub-models does not show an improvement over linear sub-models.

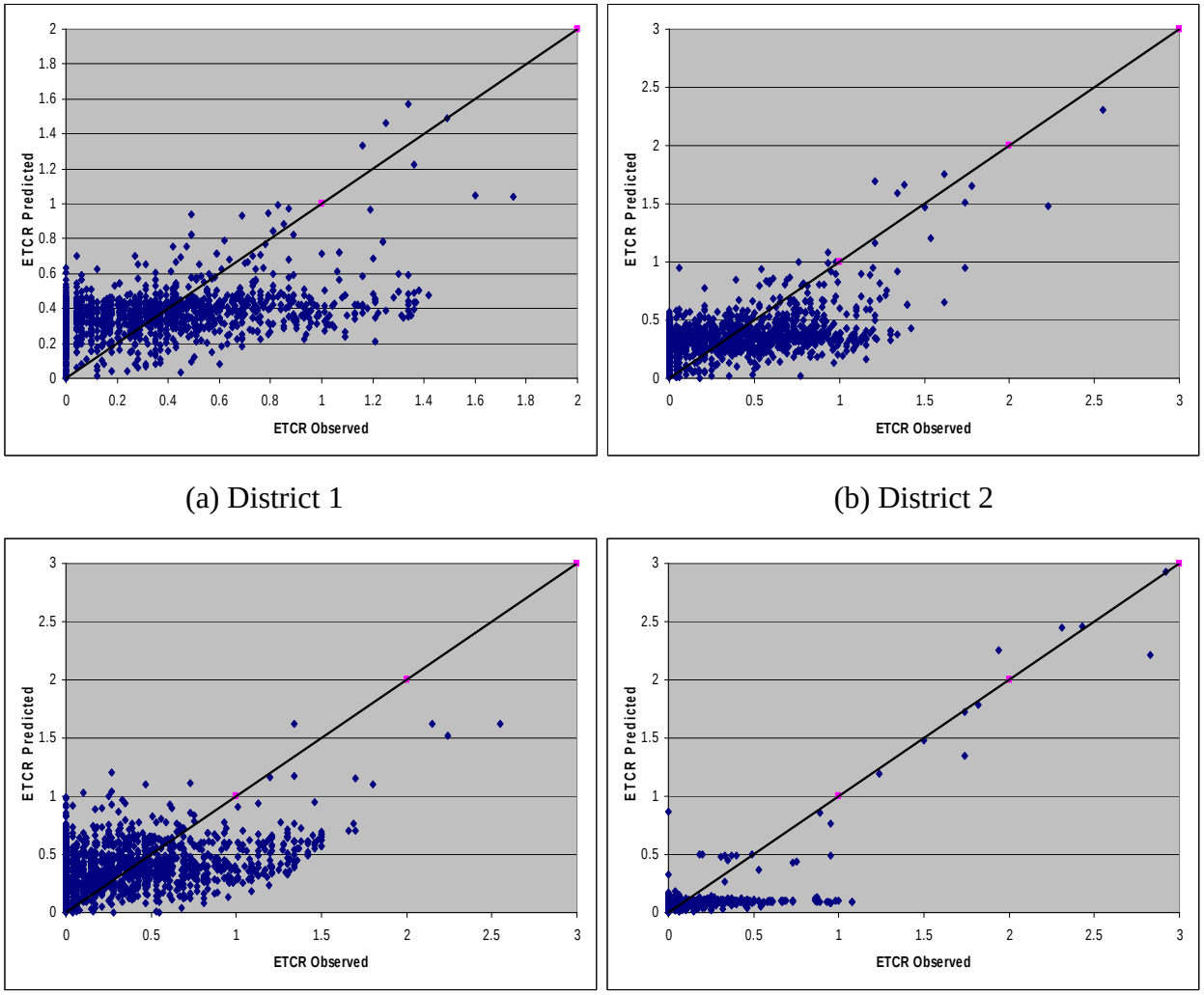

(a) District 1 (b) District 2

(c) District 3 (d) District 4

Figure 5-48 Sigmoidal ETCR Model with Quadratic Sub-Models for Districts 1 to 4

Predicted and observed ETCR do not fit well for District 5 and statewide, as shown in Figure 5-49(a) and (c). This shows that a sigmoidal model with quadratic sub-models is not a good fit. Figure 5-49(b) shows that a sigmoidal model with quadratic sub-models fits well for District 6.

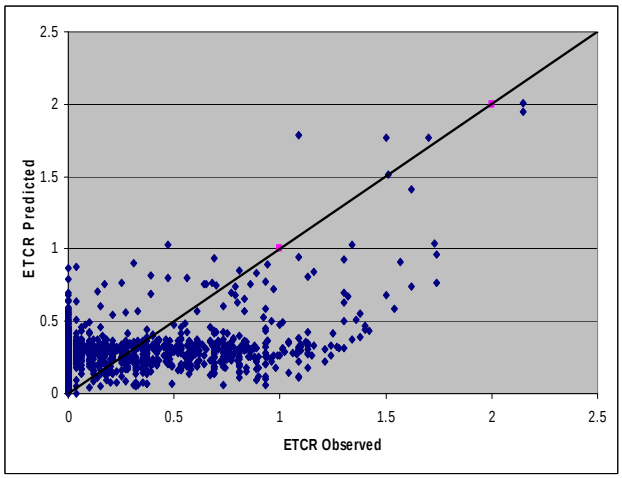

(a) District 5

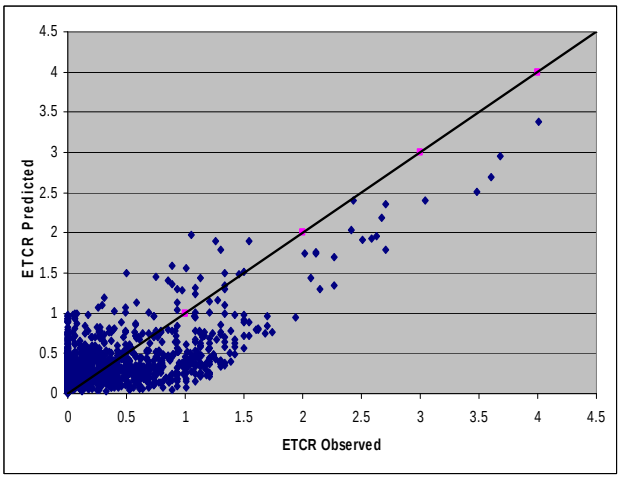

(b) District 6

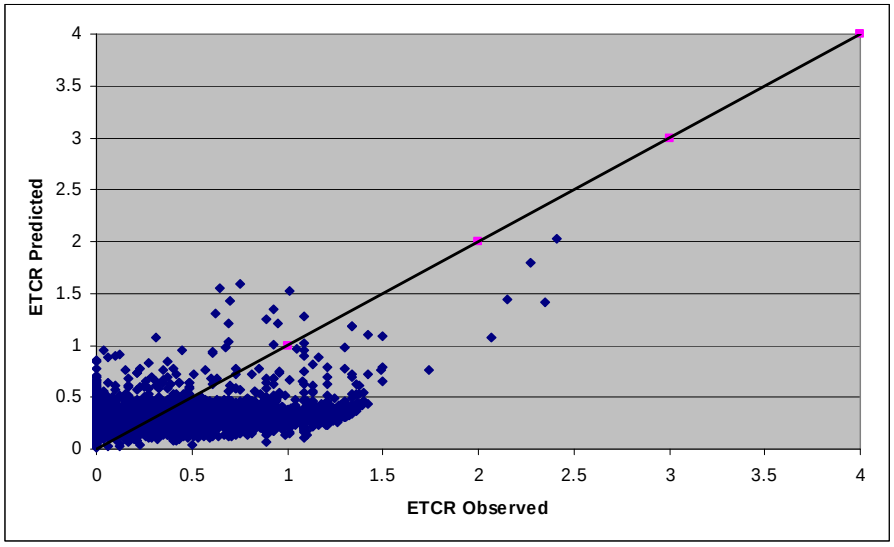

(c) State

Figure 5-49 Sigmoidal ETCR Model with Quadratic Sub-Models for Dist. 5, 6, and State

5.5.4.1.2 Validation Plots

Validation plots for Districts 1 to 3 show that a majority of the points are below the 45^{o} slope line as shown in Figure 5-50(a), (b), and (c). This shows that predicted ETCR increases at a slow rate with an increase in observed ETCR. Most of the points show that observed and predicted ETCR are independent of each other for District 4 as shown in Figure 5-50(d).

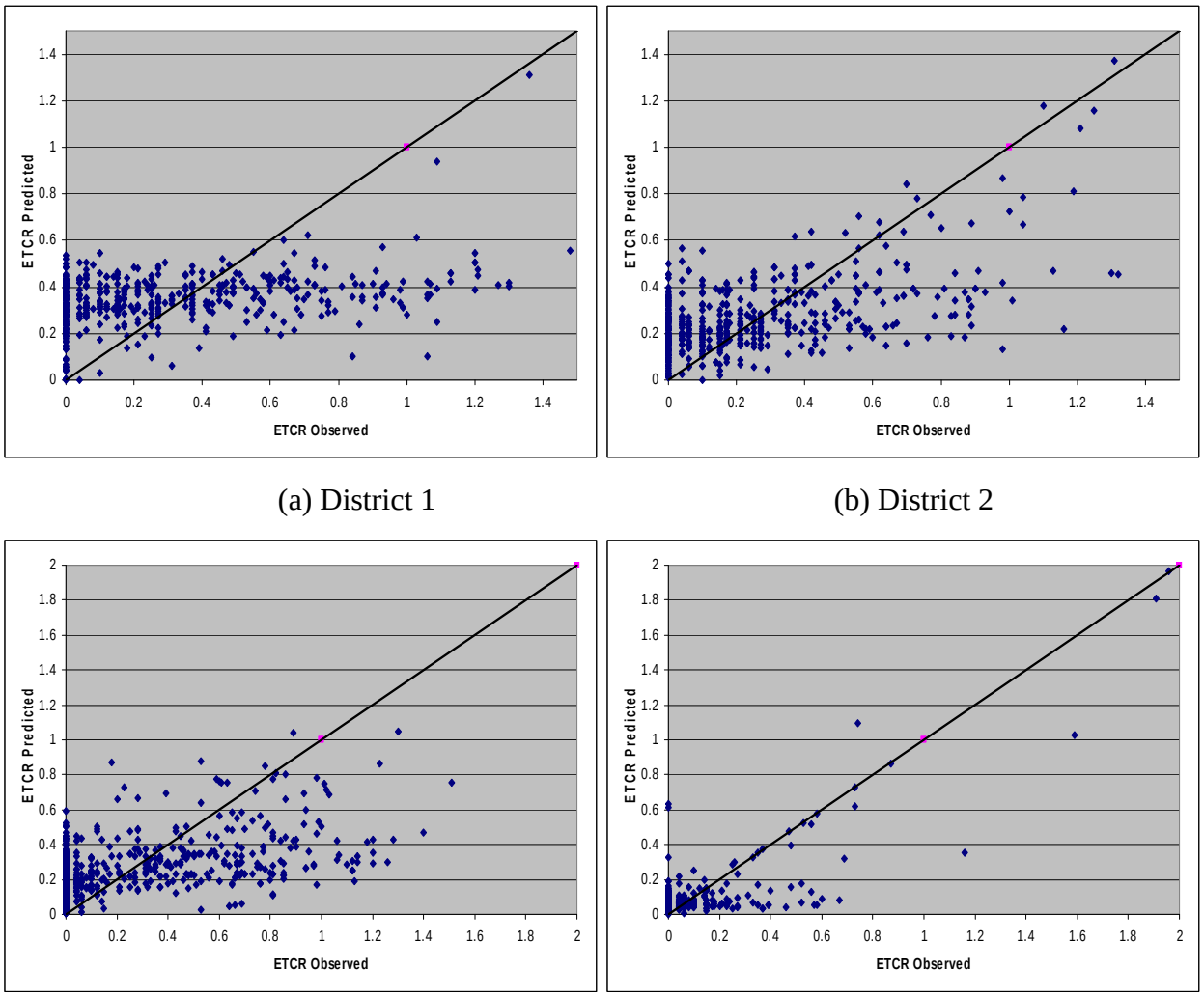

(a) District 1 (b) District 2

(c) District 3 (d) District 4

Figure 5-50 Sigmoidal ETCR Model with Quadratic Sub-Models Valid. for Districts 1 to 4

Observed and predicted ETCR are somewhat well matched with some scatter for Districts 5 and 6, as shown in Figure 5-51(a) and (b), whereas Figure 5-51(c) shows that observed and predicted ETCR are not linearly related for statewide data.

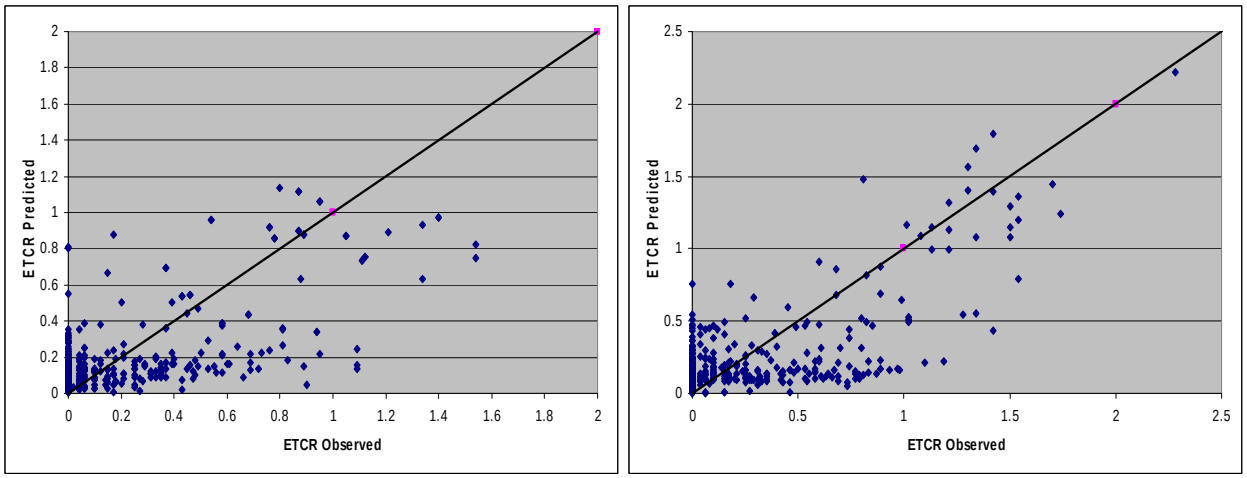

(a) District 5 (b) District 6

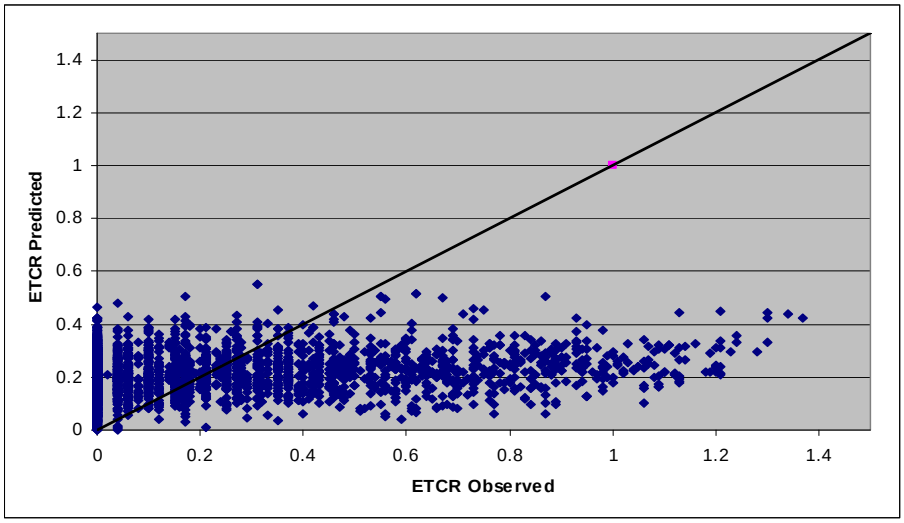

(c) State

Figure 5-51 Sigmoidal ETCR Model with Quad. Sub-Models Valid. for Dist. 5, 6, and State

5.5.4.2 Mean Absolute Deviation

Table 5-37 shows mean predicted ETCR is slightly higher than mean observed ETCR for all districts and the state. Low mean absolute deviation difference shows a better fit in general.

Table 5-37 Mean Absolute Deviation for Sigmoidal ETCR Model with Quad. Sub-Models

	Mean			Mean Absolute Deviation		
	Observed	**Predicted**	**Difference**	**Observed**	**Predicted**	**Difference**
1	0.329	0.362	-0.033	0.270	0.096	0.174
2	0.320	0.348	-0.029	0.301	0.108	0.193
3	0.294	0.373	-0.078	0.306	0.152	0.155
4	0.091	0.107	-0.016	0.131	0.044	0.087
5	0.229	0.278	-0.049	0.276	0.099	0.177
6	0.297	0.371	-0.074	0.336	0.192	0.144
State	0.241	0.310	-0.069	0.265	0.065	0.200

5.5.5 Sigmoidal ETCR Model Using Statewide Data

Since the coefficients of EAL have been smallest due to large magnitudes, a logarithm of EAL (logEAL) has been used to develop models using statewide data. Three cases have been considered: (a) sigmoidal models with linear sub-models (logEAL and no SNeff); (b) sigmoidal models with linear models with logEAL including SNeff, and (c) sigmoidal models with quadratic sub-models with logEAL. Coefficients for these cases are shown in Table 5-38. Coefficients of EAL are no longer smallest when a logarithm is used for all three cases. The coefficient of determination varies from 0.10 to 0.17.

Table 5-38 Sigmoidal ETCR Models Using Statewide Data

		0	1(D)	2(logEAL)	3(Rut)	4(SNeff)	R^2	N
1[a]	δ	0.613	0.014	-0.212	-1.051	-	0.10	9,635
	α	-0.145	-0.031	0.032	5.406	-		
	β	4.491	0.057	-1.443	1.090	-		
	γ	0.102	0.008	0.003	-0.184	-		
2[b]	δ	0.501	0.006	-0.142	0.131	-0.003	0.10	9,635
	α	0.427	-0.078	-0.066	-2.881	1.012		
	β	-14.240	0.396	-0.478	150.900	7.386		
	γ	-1.321	0.028	0.206	7.869	0.268		
3[c]	δ	5.158	0.212	-5.863	5.653	0.140	0.17	9,635
	α	-4.506	-0.225	5.862	-6.123	-0.225		
	β	-27.909	1.217	5.903	-44.488	8.388		
	γ	0.372	0.108	-0.413	-6.149	-0.051		
	δ_{ii}	-	-0.014	1.408	-10.471	-0.031		
	α_{ii}	-	0.015	-1.470	9.904	0.045		
	β_{ii}	-	-0.119	-1.270	96.673	-0.805		
	γ_{ii}	-	-0.009	0.079	12.236	0.025		

a- Linear Sub-Models with logEAL and No SNeff ; b-Linear Sub-Models with logEAL;
c-Quadratic Sub-Models with logEAL

5.5.5.1 Model Plots

A majority of the points show that predicted ETCR remains more or less constant as the observed ETCR increases for all three cases with logEAL as shown in Figure 5-52. This shows that the models do not fit well for the statewide data, though the difference is not significant in magnitude.

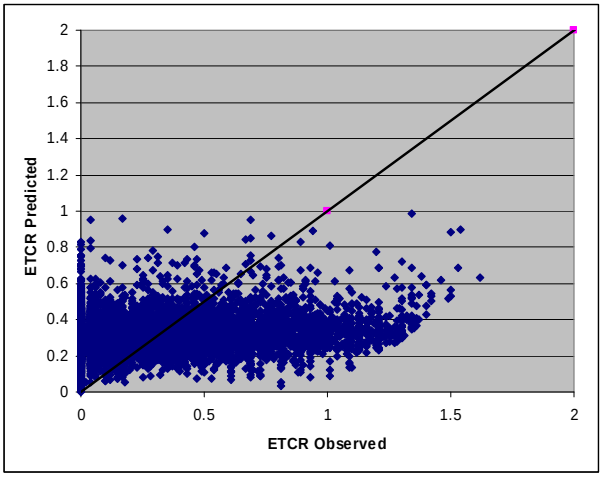

(a) Linear Sub-Models with logEAL and No SNeff

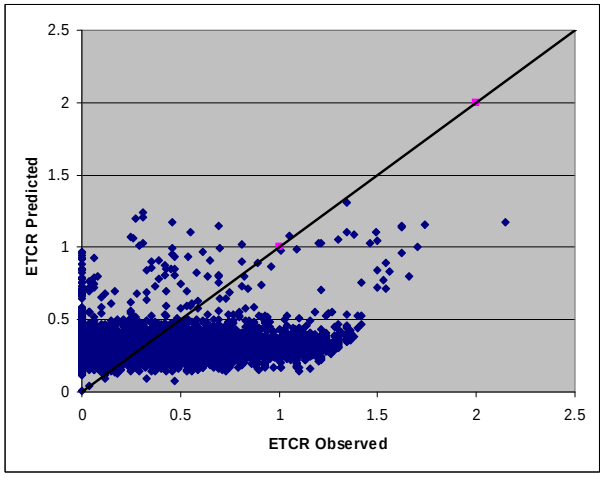

(b) Linear Sub-Models with logEAL

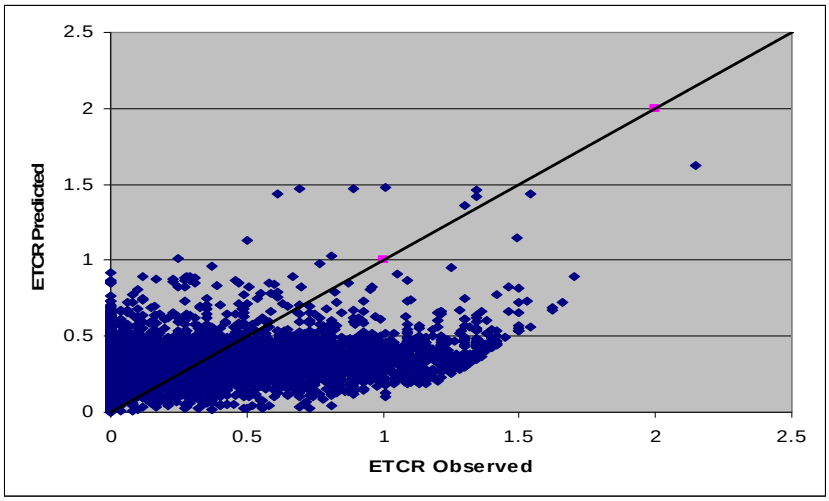

(c) Quadratic Sub-Models with logEAL

Figure 5-52 Sigmoidal ETCR Model Using Statewide Data

5.5.5.2 Validation Plots

Predicted ETCR remains almost constant as observed ETCR increases for all three cases as shown in Figure 5-53.

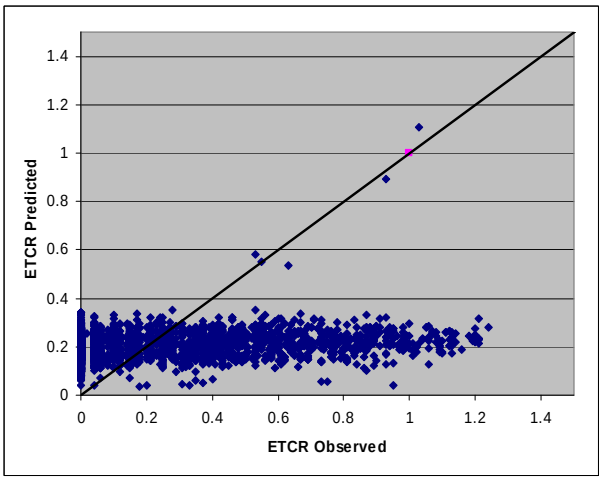

(a) Linear Sub-Models with logEAL and No SNeff

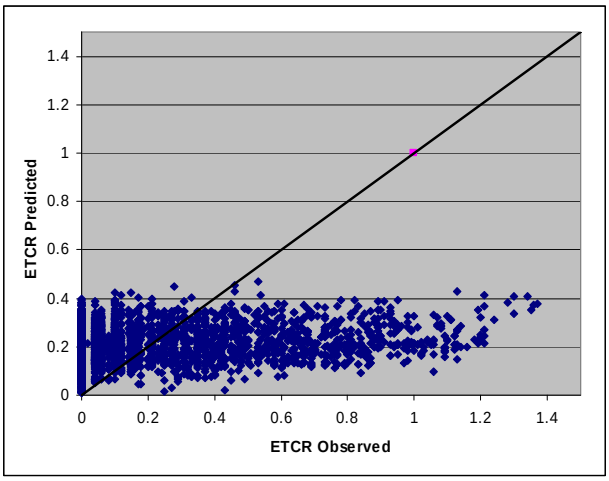

(b) Linear Sub-Models with logEAL

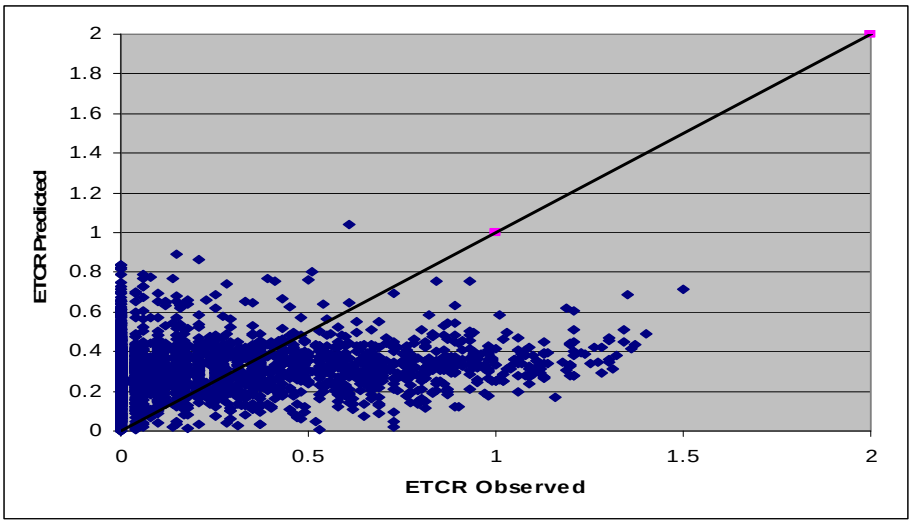

(c) Quadratic Sub-Models with logEAL

Figure 5-53 Sigmoidal ETCR Model Validation Using Statewide Data

5.5.5.3 Absolute Mean Deviation

Mean predicted ETCR is slightly higher than mean observed ETCR as shown in Table 5-39. Low mean absolute deviation difference shows a better agreement between observed and predicted ETCR.

Table 5-39 Mean Absolute Deviation for Sigmoidal ETCR Model Using Statewide Data

	Mean			Mean Absolute Deviation		
	Observed	**Predicted**	**Difference**	**Observed**	**Predicted**	**Difference**
1[a]	0.240	0.313	-0.073	0.263	0.077	0.187
2[b]	0.241	0.312	-0.071	0.265	0.062	0.203
3[c]	0.246	0.311	-0.065	0.269	0.093	0.176

a- Linear Sub-Models with logEAL and No SNeff; b-Linear Sub-Models with logEAL;
c- Quadratic Sub-Models with logEAL.

CHAPTER 6 CONCLUSIONS AND RECOMMENDATIONS

6.1 Conclusions

Based on this study, the following conclusions can be made:

(1) There is no significant difference between FWD and RWD center deflections and corresponding SNeff for most of the projects with rehabilitation actions and all projects without rehabilitation action. This shows that effects of rehabilitation action on center deflections and corresponding SNeff are not evident for most of the projects. RWD can be used to collect deflection data at the network-level instead of FWD. This notion is reinforced by the fact that there is no significant difference in FWD and RWD center deflections and corresponding SNeff for all perpetual pavement sections on US-75. It is to be noted that this is a more reasonable comparison of FWD and RWD center deflections, since data was taken on the same day using two devices. Also analysis of different RWD runs on perpetual pavement sections on US-75 shows that RWD has a reasonably good repeatability.

(2) There is a significant difference between calculated and measured mid-depth pavement temperatures for all perpetual pavement sections on US-75. However, BELLS3 equation gives a mid-depth pavement temperature close to the measured one. There is a significant difference between FWD center deflections and corresponding SNeff using two temperature-correction methods for most Kansas and US routes. It appears that method I (Watson and Chen) results in higher center deflections and lower corresponding SNeff for thicker sections, whereas method II (BELLS3 and AASHTO) results in higher center deflections and lower corresponding SNeff for thinner sections. The results signify that the effect of the method of temperature-correction factor at times can be very pronounced. In general, most Kansas and US routes show a linear relationship between FWD center deflections and corresponding SNeff using two temperature-correction methods with a slope close to 1.00 and an R^2 value greater than 0.90.

(3) There is a significant difference between FWD center deflections and corresponding SNeff over two test years (separated by four to five years) for most of the projects with a rehabilitation action such as thin overlays. However, there is no significant difference between FWD center deflections over the test years for projects without rehabilitation action. Thus the frequency of deflection data collection is a four-year cycle. In other words, 25% of the network can be tested each year for a four-year test cycle.

(4) In general, a sigmoidal RSL model with linear sub-models shows a good fit for all road categories, whereas a sigmoidal RSL model with linear sub-models shows a somewhat good fit for all districts and the state. A sigmoidal RSL model with quadratic sub-models is a better fit than the one with linear sub-models for most of the districts, and it also shows an improvement in R^2 values. There is a sigmoidal relationship between the RSL and the center deflection for road categories, districts, and the state.

(5) There is a positive linear relationship between equivalent fatigure cracking (EFCR) and center deflection for some of the road categories, districts, and the state and a sigmoidal EFCR model with linear sub-models is a good fit for most of the road categories, districtss and the state. However, a sigmoidal EFCR model with quadratic sub-models is a better fit than the one with linear sub-models for most districts and the state.

(6) There is a positive linear relationship between equivalent transverse cracking (ETCR) and center deflections for most road categories, districts, and the state, though R^2 values are low. There is a negative quadratic relationship between ETCR and center deflections for half of the districts. A sigmoidal ETCR model with linear sub-models shows a somewhat good fit for a few road categories and districts, though the difference is insignificant from a practical point of view. However, a sigmoidal ETCR model with quadratic sub-models shows an improvement over the one with linear sub-models for some of the districts and vice versa. Low mean absolute deviation difference shows a good fit in general.

6.2 Recommendations

Based on this study, the following recommendations are presented:

- Method I (Watson and Chen) temperature-correction method is easier to use and is recommended for temperature correction at the network level.
- It is recommended to use the BELLS3 method to calculate mid-depth pavement temperature when there is no measured mid-depth pavement temperature.
- Nonlinear ETCR models other than sigmoidal should be investigated.
- Structural information should be included in the KDOT PMS.

References

AASHTO. *AASHTO Interim Guide for Design of Pavement Structures.*AASHTO, Washington, D.C.,1972.

AASHTO. *Guide for Design of Pavement Structures*. AASHTO, Washington, D.C., 1986.

AASHTO. *AASHTO Guidelines for Pavement Management Systems*. AASHTO, Washington, D.C., 1990.

AASHTO. *Guide for Design of Pavement Structures*. AASHTO, Washington, D.C., 1993.

AASHTO. *Standard Method of Test for Determining Dynamic Modulus of Hot-Mix Asphalt Concrete Mixtures*. AASHTO Designation: TP 62-03, Washington, D.C., 2001.

AASHTO. *AASHTO Provisional Standards. Interim Edition*. AASHTO, Washington, D.C., 2001.

Abdallah, I., D. Yuan, and S. Nazarian. Integrating Seismic and Deflection Methods to Estimate Pavement Moduli. In *Transportation Research Record 1755*, 2001, pp.43-50.

Al-Khoury, R., A. Scarpas, and C. Kasbergen. Dynamic Interpretation of FWD Test Results. In *Transportation Research Record 1716*, 2000, pp.49-54.

Allison, J.T. *A Combined Serviceability and Distress Pavement Performance Model for Estimating Remaining Service of Flexible Pavements*. Ph.D. Dissertation, Texas A & M University, College Station, TX, 1983.

Amekudzi, A.A. and N. O. Attoh-Okine. Institutional Issues in Implementation of Pavement Management Systems by Local Agencies. In *Transportation Research Record 1524*, 1996, pp. 10-15.

ARA. *Rolling-Wheel Deflectometer (RWD) Demonstration for the Kansas Department of Transportation (KDOT)*. Final Report, Kansas Department of Transportation , Topeka, KS, 2007.

Baladi, G. *Analysis of Pavement Distress Data, Pavement Distress Indices, and Remaining Service Life. An Advanced Course in Pavement Management Systems*, FHWA, Boston, MA, 1991.

Bentsen, R.A., S. Nazarian, and A. Harrison. Reliability Testing of Seven Nondestructive Pavement Testing Devices. *Nondestructive Testing of Pavements and Back-Calculation of Moduli, ASTM STP 1026,* American Society of Testing and Materials, Philadelphia, 1989, pp.41-58.

Bergen, A.T. and C.L. Monismith. Some Fatigue Considerations in the Design of Asphalt Pavements. In *Proceedings of Canadian Technical Asphalt Association*, Polyscience Publications, Laval, Québec, Canada, Vol. 27, 1972, pp. 241-284.

Chen, X., J. Weirrmann, T. Dorsey, and W.R. Hudson. URMS: A Graphical Urban Roadway Management System at Network Level. In *Transportation Research Record 1397*, 1993, pp. 103-111.

Chen, D.H., J. Bilyeu, H.H. Lin, and M. Murphy. Temperature Correction on Falling-Weight Deflectometer Measurements. In *Transportation Research Record 1716*, 2000, pp.30-39.

Choubane, B., S. Gokhale, N.M. Jackson, and A. Nazef. Assessing the Precision of FWD for Field Measurements. In *Journal of ASTM International*, Vol. 3, No. 3, 2006.

Choubane, B., S. Gokhale, N.M. Jackson, and A. Nazef. Assessing the Precision of Falling Weight Deflectometer for Field Measurements. In *Journal of ASTM International*, Vol. 3, Issue 3, March 2006.

Croney, D. Is the Measured Deflection of a Flexible Pavement a Reliable Guide to Life Prediction and Overlay Design? In *Journal of Highways*, Vol. 58, 1990, pp.24-26.

Croney, D., and P. Croney. *The Design and Performance of Road Pavements*. McGRAW-HILL Book Company Europe, England, 1991.

Damnjanovic, I. and Z. Zhang. Determination of Required Falling-Weight Deflectometer Testing Frequency for Pavement Structural Evaluation at the Network Level. In *Journal of Transportation Engineering*, Vol. 132, No. 1, 2006, pp. 76-85.

Darter, M.I. Requirements for Reliable Predictive Pavement Models. In *Transportation Research Record 776*, 1980, pp.25-31.

Dicdican, R.Y., Y.Y. Haimes, and J.H. Lambert. *Risk-Based Asset Management Methodology for Highway Infrastructure Systems.* Final Contract Report No. VTRC 04-CR11, Virginia Transportation Research Council, Charlottesville, Virginia, 2004.

Elton, D. J. and M.E. Harr. New Nondestructive Pavement Evaluation Method. In *Journal of Transportation Engineering*, Vol. 114, No.1, 1988, pp.76-92.

Fernando, E.G., D.R. Luhr, and D.A. Anderson. *Development of an Overlay Design Procedure for Flexible Pavements*. Final Report, FHWA Report No. FHWA/PA-84/024, Fourth Cycle of Pavement Research, Vol.2, Pennylvania Transportation Research Facility, 1984.

Ferrel, F. B., and H. R. Paterick. Life Characteristics of Highway Surfaces. In *Highway Research Board Proceedings*, Highway Research Board, Washington, D.C., Vol. 24, 1948, pp. 40–52.

FHWA. *Road Surface Management for Local Governments*. FHWA, DOT-1-85-37, Washington, D.C., 1985.

FWHA. *Automated Pavement Condition Data Collection Equipment Resource Paper*. FHWA Pavement Division, Washington, D.C., 1989.

FHWA. *Advanced Course on Pavement Management*, Course Notebook, FHWA, Washington, D.C., 1990.

FHWA. *Selected Highway Statistics and Charts*. FHWA, U.S. Department of Transportation, Washington, D.C., 1993.

FHWA. *Advanced Course on Pavement Management*, Course Notebook, FHWA, Washington, D.C., 1998.

FHWA. Temperature Predictions and Adjustment Factors for Asphalt Pavement. Publication No. FHWA-RD-98-085, FHWA, Research and Development, McLean, VA, 2000.

Finn, F. N., C. Saraf, R. Kulkarni, K. Nair, W. Smith, and A. Abdullah. *Development of Pavement Structural Subsystems.* Final Report, NCHRP Project 1-10B. Washington,D.C., Feb. 1977.

Garcia-Diaz, A., R. L. Lytton, and J. T. Allison. Estimation of Network Rehabilitation and Maintenance Costs over an Extended Planning Horizon (Abridgement). In *Transportation Research Record 943*, 1983, pp. 9-12.

George, K. P. *Pavement Management Information System*. Final Report. MDOT Report No. MSHD-RD-90-87. Mississippi Department of Transportation, 1989.

Golabi, K., R. B. Kulkarni, and G. B. Way. A Statewide Pavement Management System. *Interfaces,*Vol. 12, No.6, 1982, pp. 5-21.

Haas, R. *A Guide to Pavement Management*. Good Roads Association, Canada, 1977.

Haas, R., W.R. Hudson, and J.P. Zaniewski. *Modern Pavement Management.*Krieger, Malabar, FL, 1994.

Haas, R. Reinventing the (Pavement Management) Wheel. In *Proceedings of 5th International Conference on Managing Pavements,* Seattle, WA, 2001.

Hand, A.J., P. E. Sebaaly, and J. A. Epps. Development of Performance Models Based on Department of Transportation Pavement Management System Data. In *Transportation Research Record 1684,* 1999, p. 215-222.

Harper, W. V. and K. Majidzadeh. Integrated Pavement and Bridge Management Optimization. In *Transportation Research Record 1397,* 1993, pp. 83-89.

Harr, M. E. and N. Ng-A-Qui. *Noncontact, Nondestructive Determination of Pavement Deflection under Moving Loads*. FAA Report FAA-RD-77-127, Federal Aviation Administration, Washington, D.C., 1977.

Herr, W. J., J. W. Hall, Jr., T. D. White, and W. Johnson. Continuous Deflection Basin Measurement and Back-calculation under a Rolling-Wheel Load Using Scanning Laser Technology. In *Proceedings of the 1995 Transportation Congress,* San Diego, California, Vol.1, 1995, pp. 600-611.

Hoffman, M.S. and M.R. Thompson. Comparative Study of Selected NDT Devices. In *Transportation Research Record 852*, 1982, pp.32-41.

Hoffman, M.S. Direct Method for Evaluating Structural Needs of Flexible Pavements with Falling-Weight Deflectometer Deflections. In *Transportation Research Record 1860*, 2003, pp. 41-47.

Hossain, M., T. Chowdhury, S. Chitrapu, and A. Gisi. Network-Level Pavement Structural Evaluation. In *ASTM Journal of Testing and Evaluation*, Vol. 28, No. 3, 2000, pp. 199-207.

Huang, Y. H. *Pavement Analysis and Design*. Pearson Prentice Hall, NJ, 2004.

Hudson, W. R., F. N. Finn, B. F. McCullough, K. Nair, and B. A. Vallerga. *Systems Approach to Pavement Design, Systems Formulation, Performance Definition, and Materials Characterization.* Final Report, NCHRP Project 1-10, TRB, National Research Council Washington, D.C., March 1968.

Hudson, W.R., R. Haas, and R.D. Pedigo. *Pavement Management System Development.* NCHRP Report 215, TRB, National Research Council, Washington, D.C., 1979.

Hugo, F., W. J. Scholtz, M. Sinclair, and P. C. Curtayne. *Management of Pavement Rehabilitation*. Elsevier Science Publishers B.V., North-Holland, 1989.

Hveem, F.F. Pavement Deflections and Fatigue Failures. In *Highway Research Board Bulletin 114*, Highway Research Board, Washington, D.C., 1955.

Inge, E. H., Jr., and Y. R. Kim. Prediction of Effective Asphalt Layer Temperature. In *Transportation Research Record 1473*, 1995, pp. 93–100.

Jameson, G. W. *Development of Philippines Asphalt Overlay Procedures-Pavement Management System.* Technical Assistance Project TA 1426-PHI. Asian Development Bank, 1992.

Jameson, G. W. *Development of Procedures to Predict Structural Number and Subgrade Strength from Falling-Weight Deflectometer Deflections*, 1993.

Khogali, W.E.I., and K. O. Anderson. Evaluation of Seasonal Variability in Cohesive Subgrades Using Backcalculation. In *Transportation Research Record 1546*, 1996, pp. 140-150.

KDOT. *Kansas Pavement Design Manual*. Kansas Department of Transportation, Topeka, KS.

KDOT. *ICC-Operation Manual for the MDR 4080/4097.* Bureau of Materials & Research, Kansas Department of Transportation, Topeka, 1996.

KDOT. *Traffic Monitoring System for Highways*. Bureau of Transportation Planning Traffic and Field Operation Unit, Kansas Department of Transportation, Topeka, KS, December 2003.

KDOT. *Pavement Management System, Field Operations Manual*. Bureau of Materials and Research, Kansas Department of Transportation, Topeka, KS, Revised January 2006.

Kilareski, W. P. Heavy Vehicle Evaluation for Overload Permits. In *Transportation Research Record 1227*, 1989, pp. 194–204.

Kim, Y. R. and Y.-C. Lee. Interrelationships among Stiffnesses of Asphalt-Aggregate Mixtures. In *Journal of the Association of Asphalt Paving Technologies*, Vol. 64, 1995, pp. 575-609.

Kim, Y.R., B. O. Hibbs and Y. C. Lee. Temperature Correction of Deflections and Back-calculated Asphalt Concrete Moduli. In *Transportation Research Record 1473*, 1995, pp.55-62.

Kulkarni, R., K. Golabi, F. Finn, and E. Alviti. *Development of a Network Optimization System*. Arizona Department of Transportation, Phoenix, 1980.

Kulkarni, R., F. Finn, E. Alviti, J. Chuang, and J. Rubinstein. *Development of a Pavement Management System*. Report to the Kansas Department of Transportation, Woodward-Clyde Consultants, Oakland, Calif., 1983.

Kulkarni, R., F. Finn, E. Alviti, and S. Seeds. *Development of a Project Optimization System*. Prepared for Kansas Department of Transportation, Woodward-Clyde Consultants, Oakland, Calif., 1983.

Kulkarni, R.B. and R.W. Miller. PMS Past, Present, and Future. In *Transportation Research Record 1853*, 2003, pp.65-71.

Kuo, W.H., E.C. Novak and G. Baladi. Development of Optimal Long-Term Network Strategies Using Remaining Service Life, Pavement Management Implementation. In *ASTM STP 1121*, Philadelphia, PA, 1992.

Lee, H., and W. R. Hudson. Reorganizing the PMS Concept. In *Proceedings of PMS-North American Conference on Managing Highways*, Ontario, Canada, 1985, pp. 59–80.

Leland, W., M. Hill, J. P. Welna, and G. K. Birkenbeuel. *SYSTAT for Windows: Statistics*. Version 5 ed. SYSTAT, Inc., Evanston, Ill., 1992.

Lister, N.W. and C.K. Kennedy. A System of Prediction of Pavement Life and Design of Pavement Strengthening. In *Proceedings of 4th International Conference on Structural Design of Asphalt Pavements*, Vol. 1, University of Michigan, Ann Arbor, pp. 629-648, 1977.

Lukanen, E. O., R. Stubstad, and R. C. Briggs. *Temperature Predictions and Adjustment Factors for Asphalt Pavements.* Report FHWA-RD-98- 085. FHWA, U.S. Department of Transportation, 2000.

Lytton, R.L. Concepts of Pavement Performance Prediction and Modeling. In *Proceedings of 2nd North American Conference on Managing Pavements*, Vol. 2, Toronto, Ontario, 1987, pp. 3-19.

Lytton, R. L. Back-calculation of Pavement Layer Properties. In *ASTM STP 1026,* Philadelphia, Pa., 1989, pp. 7–38.

Majidzadeh, K. and G. Ilves. *Flexible Pavement Overlay Design Procedures.* Vols. I & II, Report No. FHWA/RD-81/032 and 033, Federal Highway Administration, McLean, VA.

Mamlouk, M. S., J. P. Zaniewski, W. N. Houston, and S. L. Houston. Overlay Design Method for Flexible Pavements in Arizona. In *Transportation Research Record 1286*, 1990, pp. 112–122.

Marchionna, A., M. A. Fornaci, and M. Malgarini. Evaluation of Flexible Pavements and Overlay Design Based on F.W.D. Tests. In *Proceedings of the 6th International Conference on Structural Design of Asphalt Pavements*, Department of Civil Engineering, Michigan University, Ann Arbor, Vol. 1, 1987.

Markov, M.J. Life-Cycle Cost Evaluations of the Effects of Pavement Maintenance. In *Transportation Research Record 1276*, 1990, pp. 37-47.

Meshkani, A., I. N. Abdallah, and S. Nazarian. Feasibility of Back-Calculation of Nonlinear Flexible Pavement Layer Parameters from Nondestructive Testing. In *Transportation Research Record 1860*, 2003, pp.16-25.

Millard, R. S., C. B. White, N. W. Hudson, F. A. Sharman, E. D. Tingle, R. L. Wilson, and E. H. Woodrow. Lightly Trafficked Roads–Great Britain. In *Proceeding of Permanent International Association Road Congress*, Vol. 2, 1971.

Miller, R.W., K. Vedula, M. Hossain, and G. Cumberledge. Assessment of AASHTO Provisional Standards for Profile Data Collection and Interpretation. In *Transportation Research Record 1889*, 2004, pp. 134-143.

Mitchell, M. F. and J. H. Maree. Pavement Management as Part of Strategic Road Management. In *Proceeding of 3rd International Conference on Managing Pavements*, Vol. 2, TRB, National Research Council, Washington, D.C., 1994, pp. 64-73.

Mohseni, A., M. I. Darter, and J. P. Hall. Illinois Pavement Network Rehabilitation Management Program. In Transportation Research Record 1272, 1990, pp. 85-95.

Noureldin,A.S., K. Zhu, S. Li, and D. Harris. Network Pavement Evaluation with Falling-Weight Deflectometer and Ground-Penetrating Radar. In *Transportation Research Record 1860*, 2003, pp. 90-99.

Panigraphi, D. *Developing Analytical Tools for a Local Agency Pavement Management System*. M.S. Thesis, University of Missiouri, Columbia, MO, 2004.

Park, S. W. and Y.R. Kim. Temperature Correction of Back-Balculated Moduli and Deflections Using Linear Viscoelasticity and Time-Temperature Superposition. In *Transportation Research Record 1570*, 1997, pp. 108-117.

Park, H.M., Y. R. Kim, and S. Park. Temperature Correction of Multiload-Level, Falling-Weight Deflectometer Deflections. In *Transportation Research Record 1806*, 2002, pp.3-8.

Park, H.M.P. and Y.R. Kim. Prediction of Remaining Life of Asphalt Pavement with Falling-Weight Deflectometer Multiload-Level Deflections. In *Transportation Research Record 1860*, 2003, pp.48-56.

Parvini, M. *Pavement Deflection Analysis Using Stochastic Finite-Element Method*. Ph.D. Dissertation, McMaster University, Hamilton, Ontario, 1997.

Paterson, W.D.O. *Road Deterioration and Maintenance Effects*. Models for Planning and Management. Highway Design and Maintenance Standards Series. The Johns Hopkins University Press, Baltimore and London, Dec. 1987.

Richter, C.A. and L.H. Irwin. Application of Deflection Testing to Overlay Deisgn: A Case Study. In *Transportation Research Record 1196*, 1988, pp.193-200.

Rocha, S., S. Nazarian, and V. Tandon. *A Comprehensive Protocol to Improve Reproducibility of Txdot Falling Weight Deflectometer Fleet*. Center for Transportation Infrastructure Systems, The University of Texas At El Paso, TX, 2003.

Roesset, J.M. and K. Shao. Dynamic Interpretation of Dynaflect and FWD Test. In *Transportation Research Record 1022*, 1985, pp. 7-16.

Rohde, G. T. Determining Pavement Structural Number from FWD Testing. In *Transportation Research Record 1448*, 1994, pp. 61-68.

Romanoschi, S. and J. B. Metcalf. Simple Approach to Estimation of Pavement Structural Capacity. In *Transportation Research Record 1652*, 1999, pp. 198–205.

Romanoschi, S.A. and J. B. Metcalf. Evaluation of Probability Distribution Function for the Life of Pavement Structures. In *Transportation Research Record 1730*, 2000, pp. 91-98.

Romanoschi, S. A., A. J. Gisi, M. Portillo and C. Dumitru. The First Findings from the Kansas Perpetual Pavements Experiment. In *Transportation Research Board Annual Meeting*. CD-ROM. Transportation Research Board of the National Academies, Washington, D.C., 2008.

Santha, B. L., W. Yang, and R. L. Lytton. Microcomputer Application to Determine the Load Zoning for Low-Volume Roads. In *Transportation Research Record 1260*, 1990, pp. 226–245.

Scullion, T. and M. Chester. *Nondestructive Test Procedures for Analyzing the Structural Condition of Pavements*. Texas Transportation Institute, Texas State Department of Highways and Public Transportation, 1995.

Sebaaly, B.E. and M.S. Mamlouk. Typical Curves for Evaluation of Pavement Stiffness from Dynaflect Measurements. In *Transportation Research Record 1070*, 1986, pp.42-52.

Shahin, M.Y. *Pavement Management for Airports, Roads, and Parking Lots*. Second Edition, Springer Science, New York, 2005.

Shao, L., S.W. Park, and Y.R. Kim. Simplified Procedure for Prediction of Asphalt Pavement Subsurface Temperatures Based on Heat Transfer Theories. In *Transportation Research Record 1568*, 1997, pp.114-123.

Smith, R.E. *Structuring a Microcomputer-Based Pavement Management System for Local Agencies*. Ph.D. Dissertation, University of Illinois Urbana-Champion, IL, 1986.

Smith, R.E. and R.L. Lytton. Operating Characteristics and User Satisfaction of Commercially Available NDT Equipment. In *Transportation Research Record 1007*, 1985, pp.1-10.

Solaimanian, M. and T. W. Kennedy. Predicting Maximum Pavement Surface Temperature Using Maximum Air Temperature and Hourly Solar Radiation. In *Transportation Research Record* 1417, 1993, pp. 1 - 11.

Steele, D., J. Hall, R. Stubstad, A. Peekna, and R. Walker. Development of a High-Speed, Rolling-Wheel Deflectometer. http://pms.nevadadot.com/2002presentations/17.pdf#search=%22Development%20of%20a%20HighSpeed%20Rolling%20Wheel%20Deflectometer%22.

Thompson, P. D., L. A. Neumann, M. Miettinen, and A. Talvitie. A Micro-Computer Markov Dynamic Programming System for Pavement Management in Finland. In *Proceeding of 2nd North American Conference on Managing Pavements*, Vol. 2, Toronto, Ontario, Canada, 1987.

Thompson M. *Perpetual Pavement Review: Kansas DOT US-75 Project Fairview-Sabetha.* Prepared for the Kansas Asphalt Pavement Association, May 2003.

Til, V., B. F. McCullough, B. A. Vallerga, and R. G. Hicks. *NCHRP Report 128: Evaluation of AASHTO Interim Guides for Design of Pavement Structures.* TRB, National Research Council, Washington, D.C., 1972.

Ullidz, P. *Pavement Analysis*. Elsevier, New York, 1993, pp.306-307.

URS Corp. *Pavement Performance Prediction Models*. Interim Report for Kansas Department of Transportation. Jan. 21, 2000.

USDOT. *An Advanced Course in Pavement Management Systems*. Federal Highway Administration. U.S. Department of Transportation, Washington, D.C., 1991.

Vepa, T.S., K. P. George, and A. R. Shekharan. Prediction of Pavement Remaining Life. In *Transportation Research Record 1524*.1996. pp. 137-144.

Wang, K. C. P., J. Zaniewski, and J. Delton. Analysis of Arizona Department of Transportation's New Pavement Network Optimization System. In *Transportation Research Record 1455*, 1994, pp. 91–100.

Watson, D.E., J. Zhang, and R.B. Powell. Analysis of Temperature Data for the National Center for Asphalt Technology Test Track. In *Transportation Research Record 1891*, 2004, pp. 68–75.

Way, G.B. Network Optimization System for Arizona. In *Proceedings of North American Pavement Management Conference*, Vol. 1, Toronto, Ontario, Canada, 1985.

Werkmeister, S. and D. Alabaster. Estimation of Remaining Pavement Life of Low-Volume Roads with Falling-Weight Deflectometer Results: A Practical Method, In *Transportation Research Record 1989*, Vol. 2, 2007, pp. 261–269.

Winfrey, R. and F. B. Ferrel. Life Characteristics of Surfaces Constructed on Primary Rural Highways. In *Proceeding of Highway Research Borad*, Highway Research Borad, Vol. 20, 1940, pp. 165–199.

Winfrey, R. and P. D. Howell. Highway Pavements–Their Service Lives. In *Highway Research Record 252*, 1968, pp. 1-23.

Witczak, M.W. *Determination of Flexible Pavement Life*. Executive Summary, Vol. I. FHWA Report No. FHWA/MD/R-79/1.FHWA, U.S. Department of Transportation, 1978.

Witczak, M. and E. J. Yoder. *Principles of Pavement Design.* 2nd Edition, John Wiley and Sons, New York, 1975.

Zaghloul, S. and M. Elfino. Pavement Rehabilitation Selection Based on Mechanistic Analysis and Field Diagnosis of Falling-Weight Deflectometer Data Virginia Experience. In *Transportation Research Record 1730*, 2000, pp. 177-186.

Appendix A - Data Analysis

Deflection Data

FWD and RWD Center Deflection

Without Rehabilitation Actions

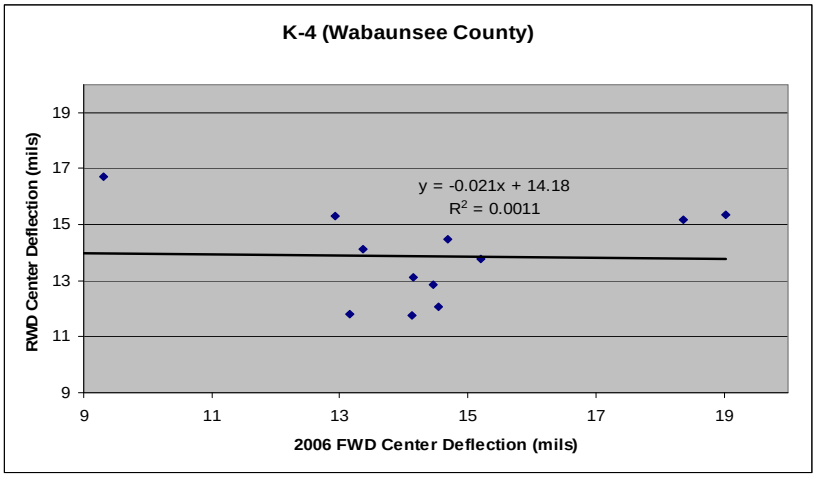

(a)

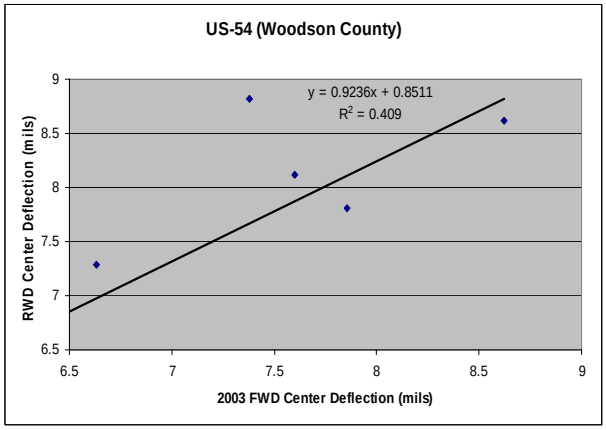

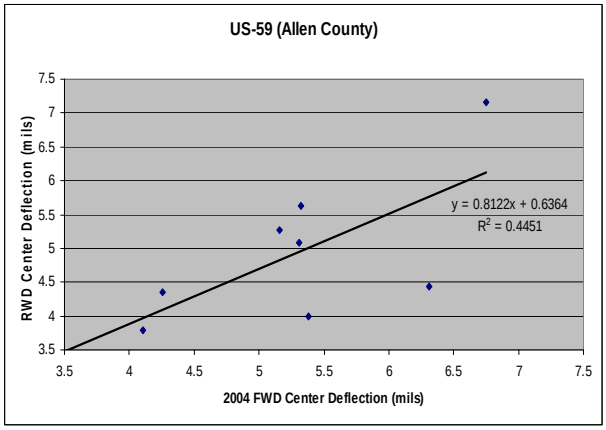

(b) (c)

Figure A-1 FWD and RWD Center Deflections for K-4, US-54, and US-59

With Rehabilitation Actions

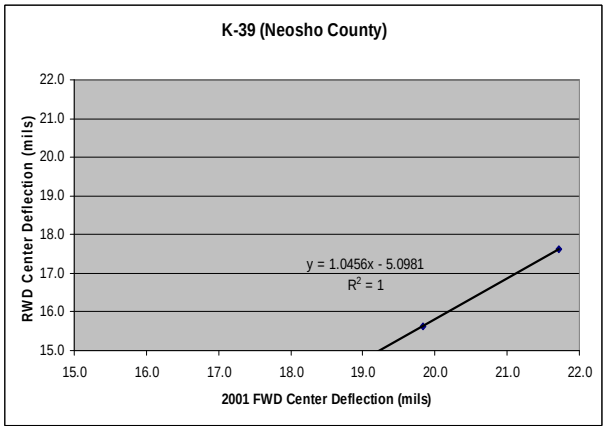

(a)

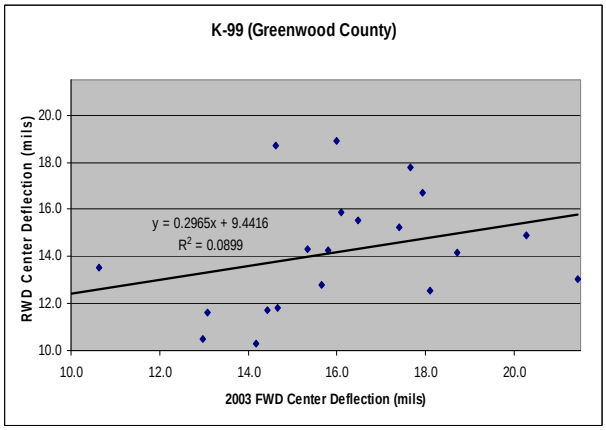

(b)

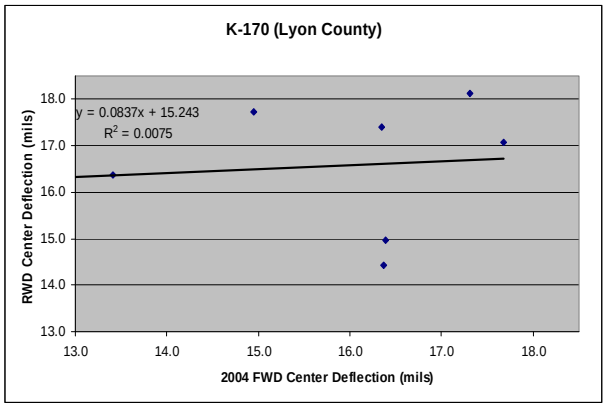

(c)

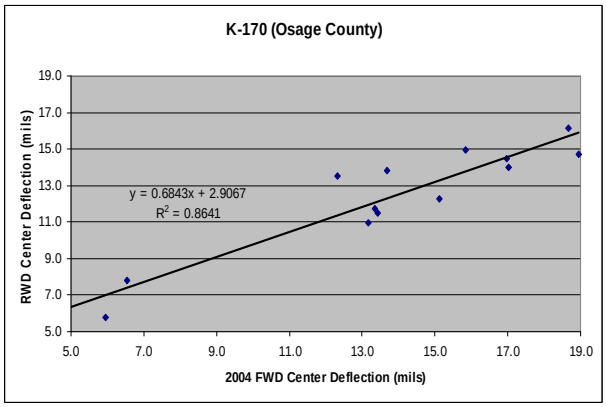

(d)

Figure A-2 FWD and RWD Center Deflections for K-39, K-99, and K-170

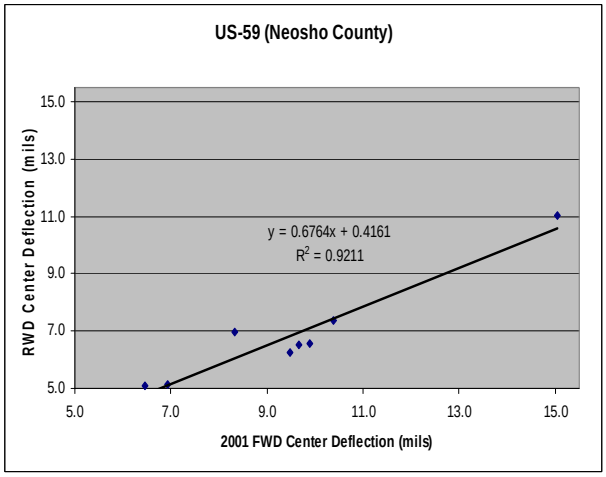

(a)

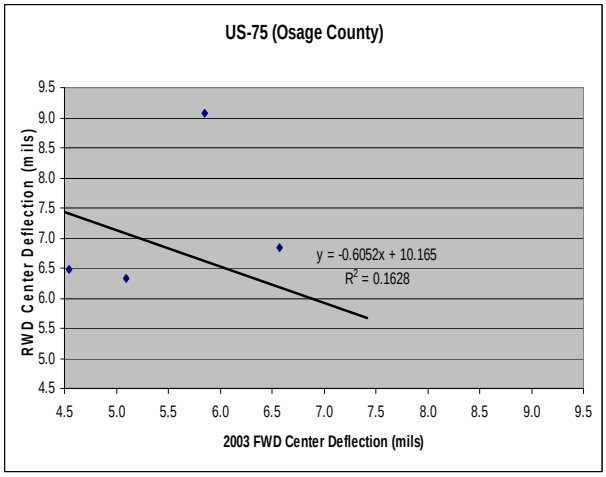

(b)

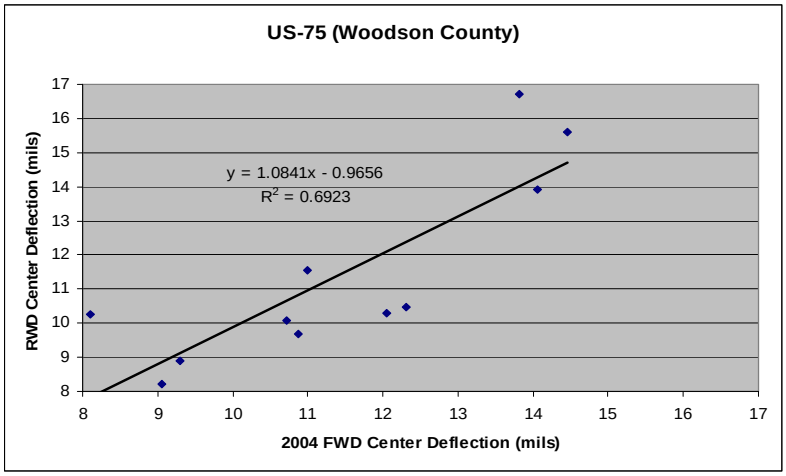

(c)

Figure A-3 FWD and RWD Center Deflections for US-59 and US-75

Effect of Temperature-Correction Method on Center Deflection

Route and County-Wise

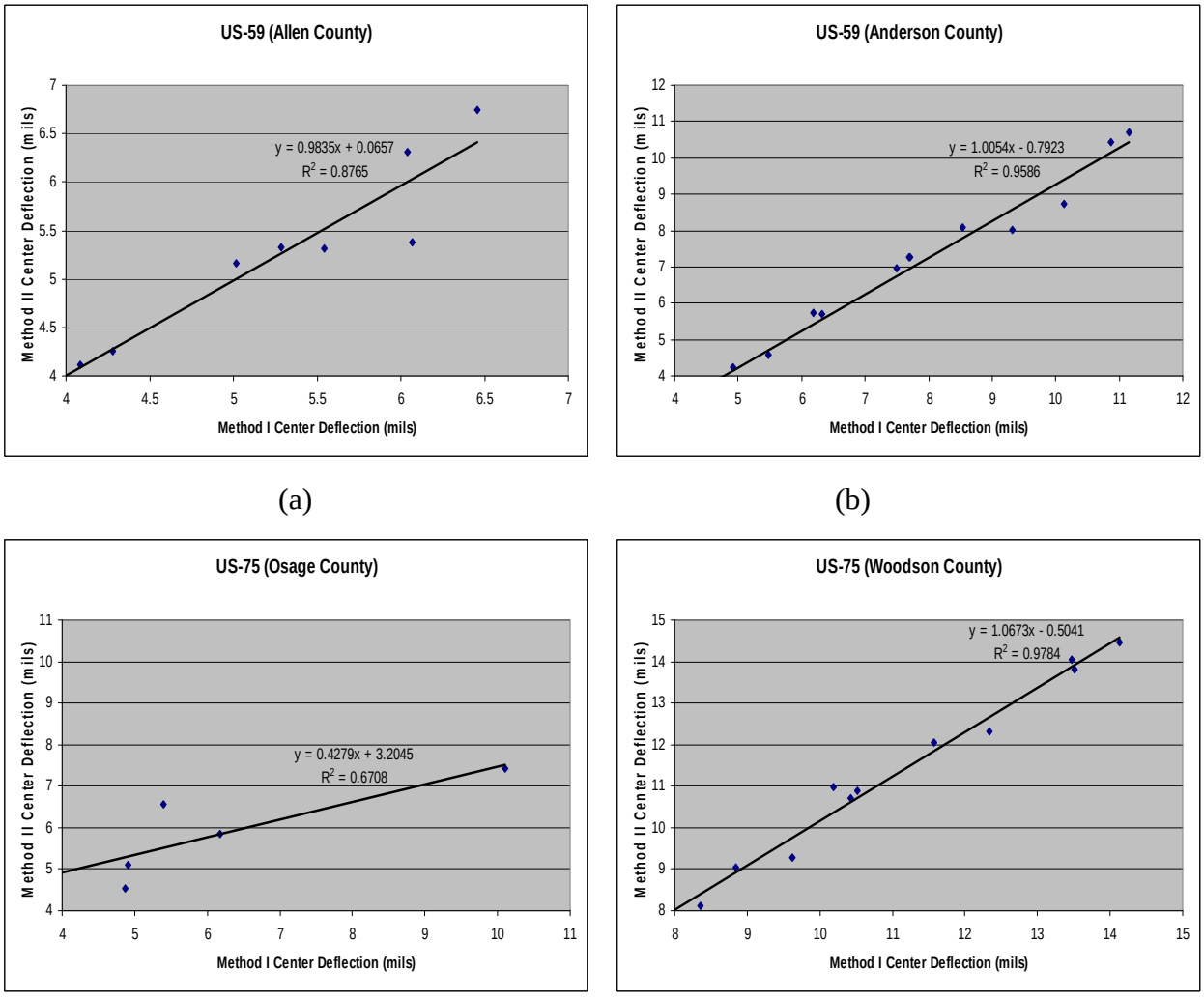

Figure A-4 Effect of Temperature-Correction on FWDd_0 for US-59 and US-75

Route-Wise

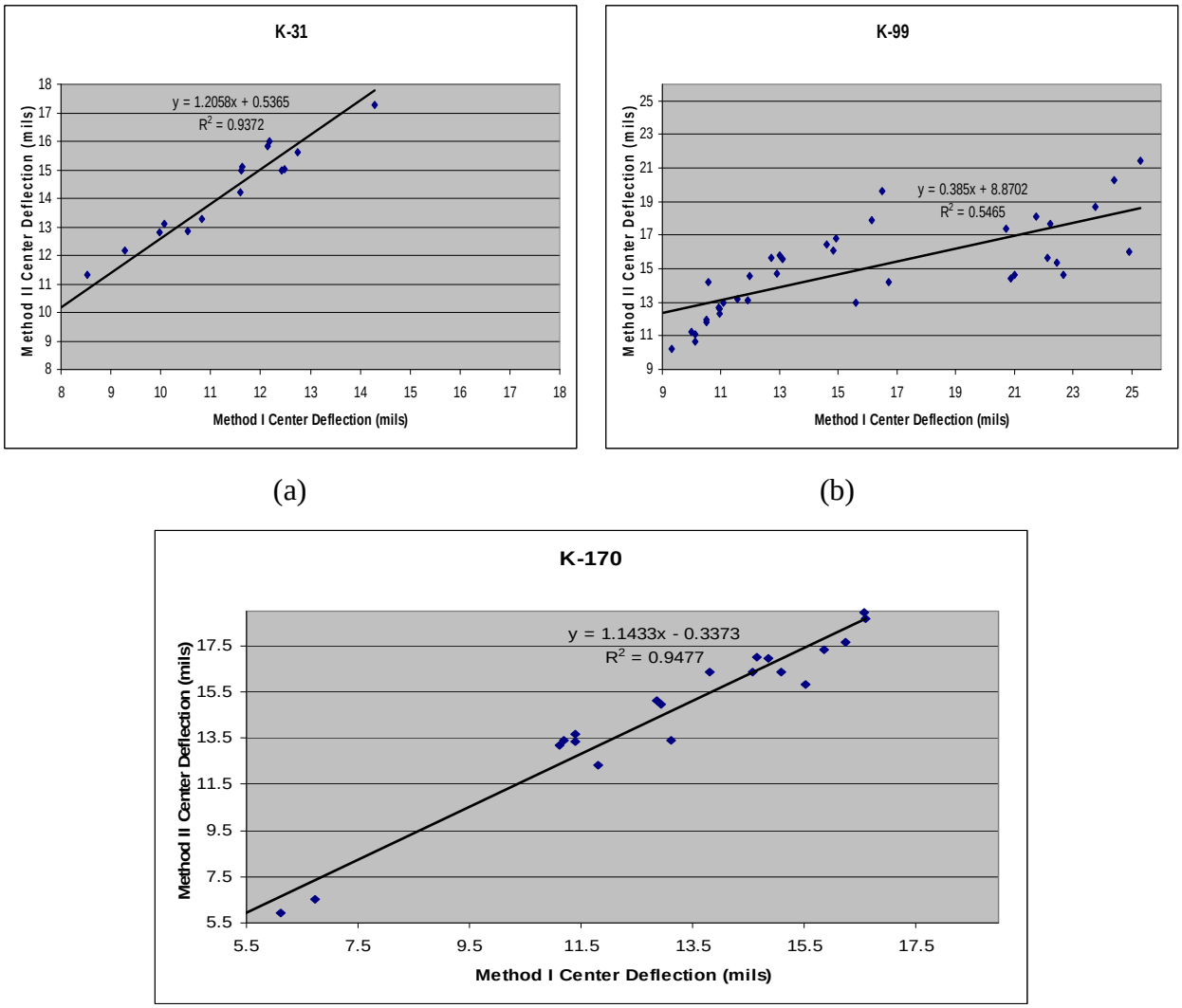

Figure A-5 Effect of Temperature-Correction on $FWDd_0$ for K-31, K-99, and K-170

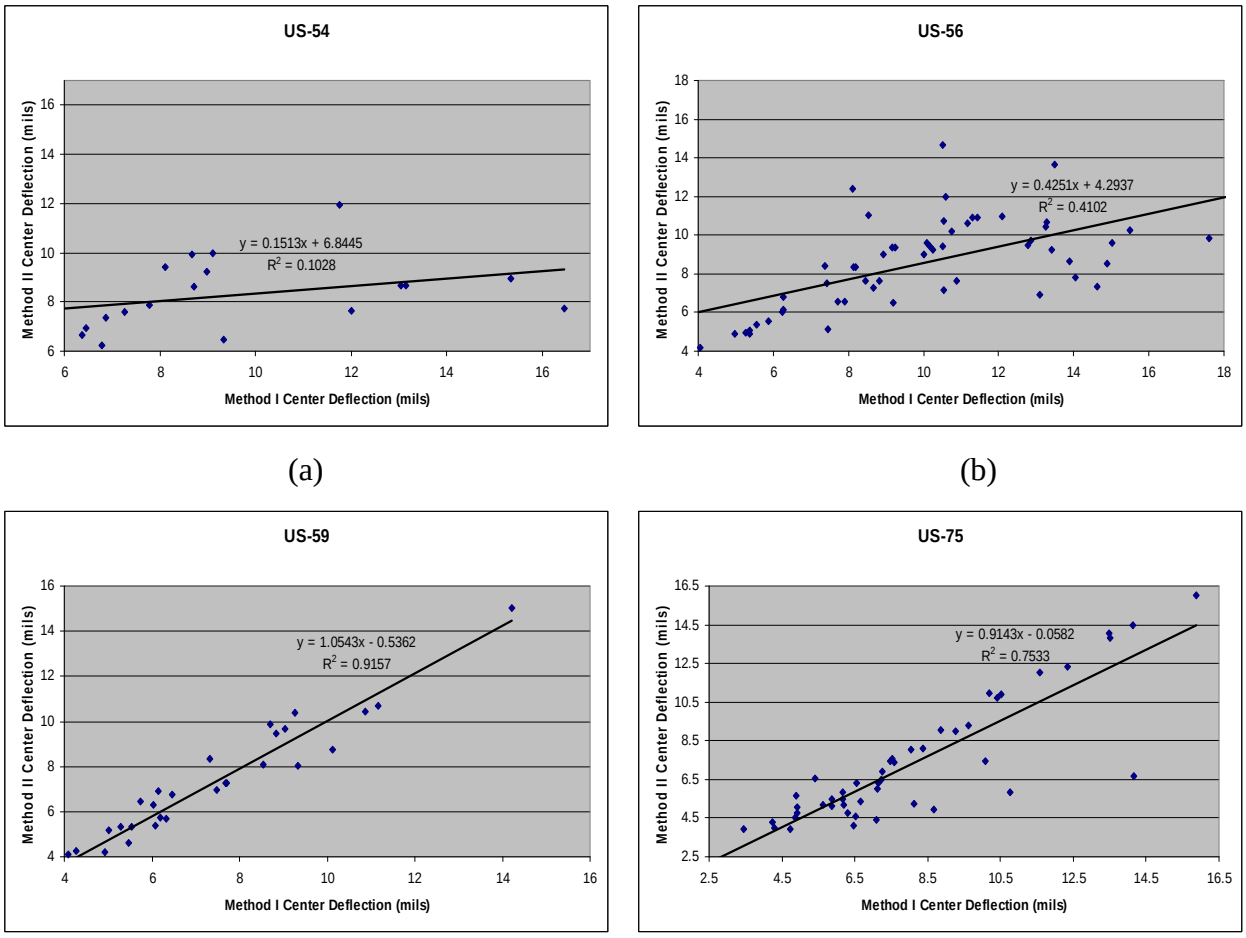

(a) (b)

(c) (d)

Figure A-6 Effect of Temp.-Correction on $FWDd_0$ for US-54, US-56, US-59, and US-75

County-Wise

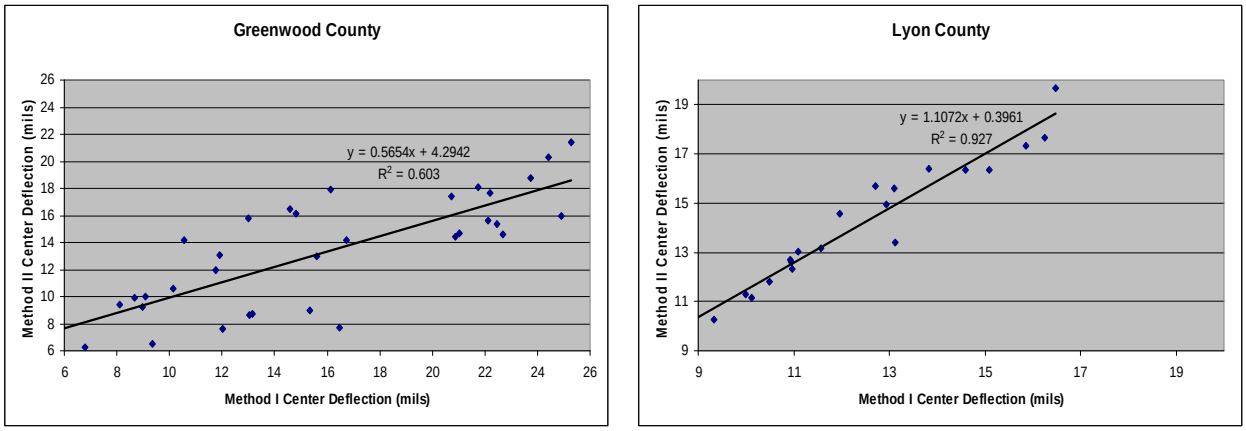

(a) (b)

Figure A-7 Effect of Temperature-Correction on Routes in Greenwood and Lyon Counties

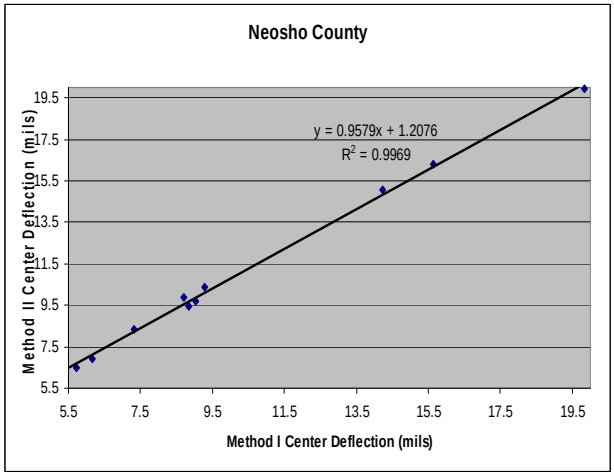

(a)

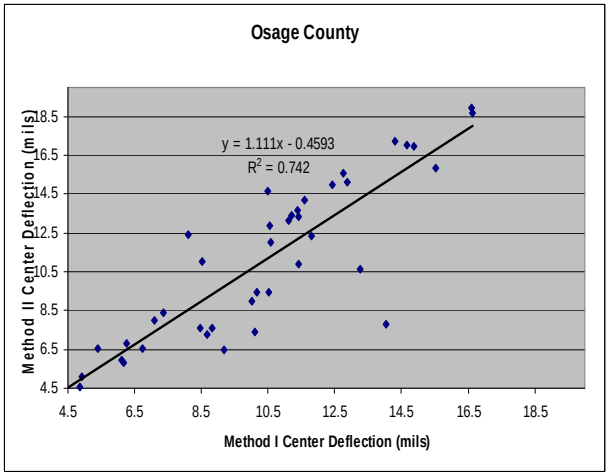

(b)

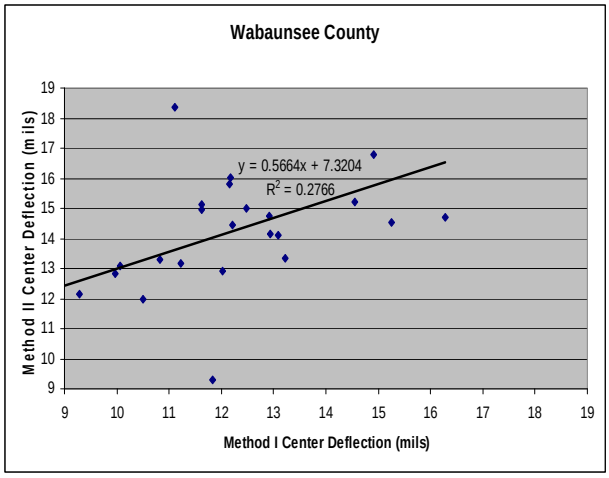

(c)

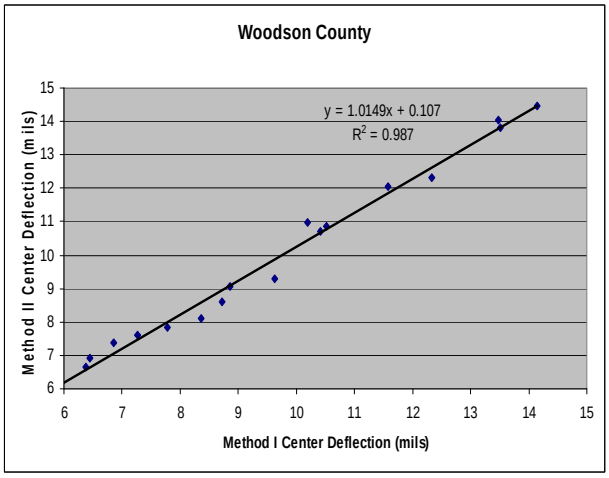

(d)

Figure A-8 Effect on Routes in Neosho, Osage, Woodson, and Wabaunsee Counties

District-Wise

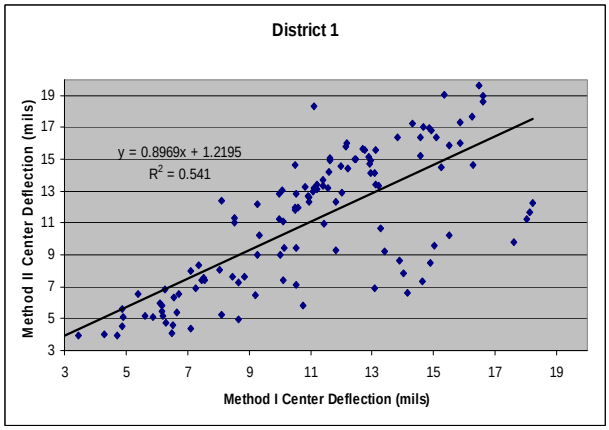

(a)

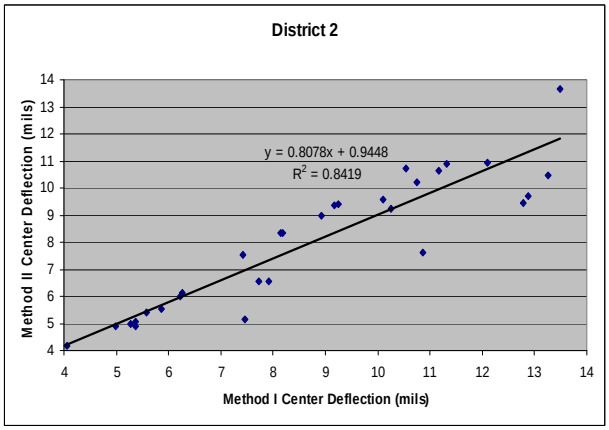

(b)

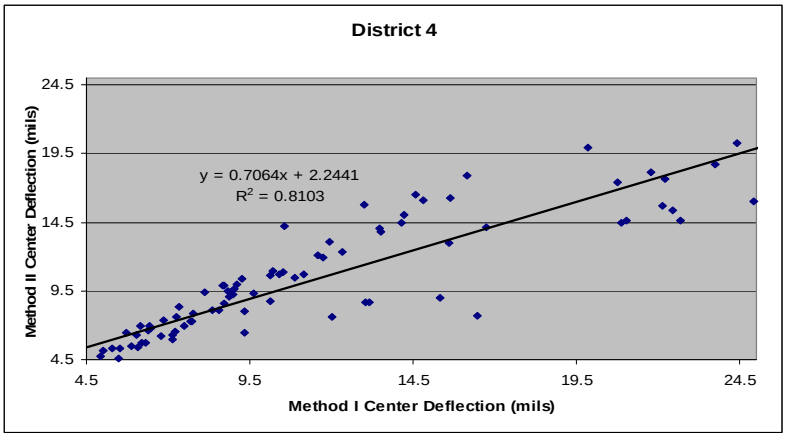

(c)

Figure A-9 Effect of Temperature-Correction Method on Routes in Districts 1, 2, and 4

Significant-Difference Test

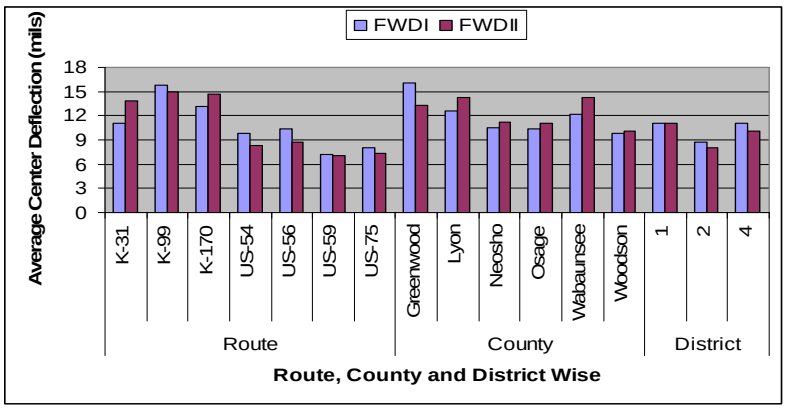

Figure A-10 Effect of Temperature-Correction Method on Average $FWDd_0$

Table A-1 Significant-Difference Test for Effect of Temp.-Correction Method on $FWDd_0$

	Avg. $FWDd_0$		Paired T-Test for Difference (I-II)					N
	I	II	Lower	Mean	Upper	Pr>|t|	Similar	
(a) Route-wise								
K-31	11.09	13.91	-3.177	-2.819	-2.462	<.0001	No	16
K-99	15.78	14.94	-0.409	0.8332	2.0759	0.1823	Yes	37
K-170	13.13	14.67	-1.962	-1.543	-1.124	<.0001	No	20
US-54	9.79	8.33	-0.015	1.4639	2.9427	0.0521	Yes	18
US-56	10.37	8.70	0.9507	1.6678	2.3848	<.0001	No	58
US-59	7.17	7.02	-0.137	0.1474	0.4321	0.2988	Yes	31
US-75	8.01	7.27	0.2804	0.7445	1.2086	0.0023	No	47
(b) County-Wise								
Greenwood	16.01	13.35	1.382	2.6658	3.9496	0.0002	No	33
Lyon	12.57	14.31	-2.081	-1.743	-1.405	<.0001	No	20
Neosho	10.47	11.24	-0.988	-0.766	-0.544	<.0001	No	10
Osage	10.43	11.12	-1.374	-0.699	-0.023	0.043	No	40
Wabaunsee	12.25	14.26	-2.825	-2.009	-1.194	<.0001	No	25
Woodson	9.79	10.04	-0.406	-0.252	-0.099	0.0031	No	17
(c)District-Wise								
1	11.01	11.09	-0.603	-0.084	0.4346	0.7486	Yes	122
2	8.75	8.02	0.3237	0.7377	1.1516	0.001	No	30
4	11.11	10.09	0.4757	1.0192	1.5628	0.0003	No	89

Linear Regression

Table A-2 Linear Regression for Effect of Temperature-Correction Method on $FWDd_0$

	Intercept	Slope	C.I.* for Slope		Pr>|t|	Linear Relation	R^2	Length (mi)
			lower	upper				
(a) Route-Wise								
K-31	0.54	1.21	1.03	1.38	0.00	Yes	0.94	16
K-99	8.87	0.38	0.26	0.51	0.00	Yes	0.55	37
K-170	-0.34	1.14	1.01	1.28	0.00	Yes	0.95	20
US-54	6.85	0.15	-0.09	0.39	0.20	No	0.10	18
US-56	4.29	0.43	0.29	0.56	0.00	Yes	0.41	58
US-59	-0.53	1.05	0.93	1.18	0.00	Yes	0.92	31
US-75	-0.06	0.91	0.76	1.07	0.00	Yes	0.75	47
(b) County-Wise								
Greenwood	4.30	0.57	0.40	0.73	0.00	Yes	0.60	33
Lyon	0.39	1.11	0.95	1.26	0.00	Yes	0.93	20
Neosho	1.21	0.96	0.91	1.00	0.00	Yes	1.00	10
Osage	-0.46	1.11	0.90	1.33	0.00	Yes	0.74	40
Wabaunsee	7.32	0.57	0.17	0.96	0.01	Yes	0.28	25
Woodson	0.11	1.01	0.95	1.08	0.00	Yes	0.99	17
(c)District-Wise								
1	1.22	0.90	0.75	1.05	0.00	Yes	0.54	122
2	0.94	0.81	0.67	0.94	0.00	Yes	0.84	30
4	2.24	0.71	0.63	0.78	0.00	Yes	0.81	89

* confidence interval for slope at 95% confidence level

Frequency of Deflection Measurement Using Center Deflection

Without Rehabiltation Actions

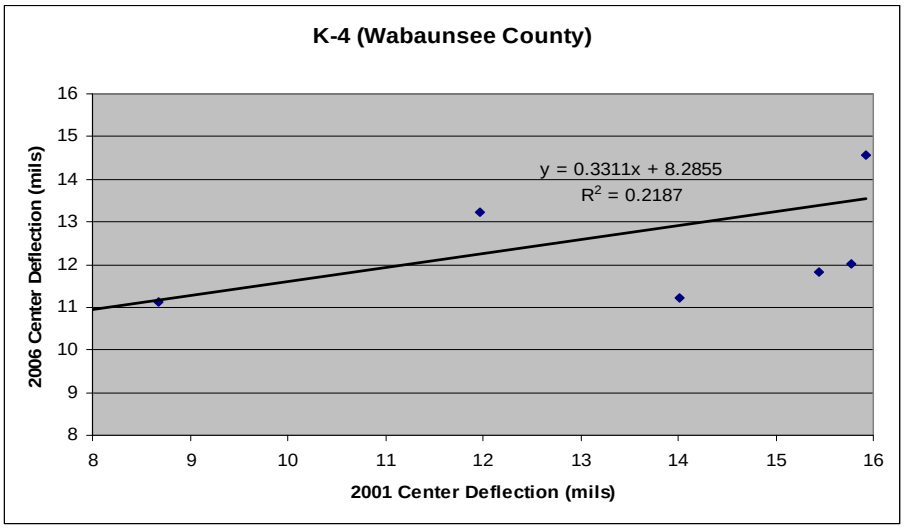

Figure A-11 FWD Center Deflection over Years for K-4

With Rehabilitation Actions

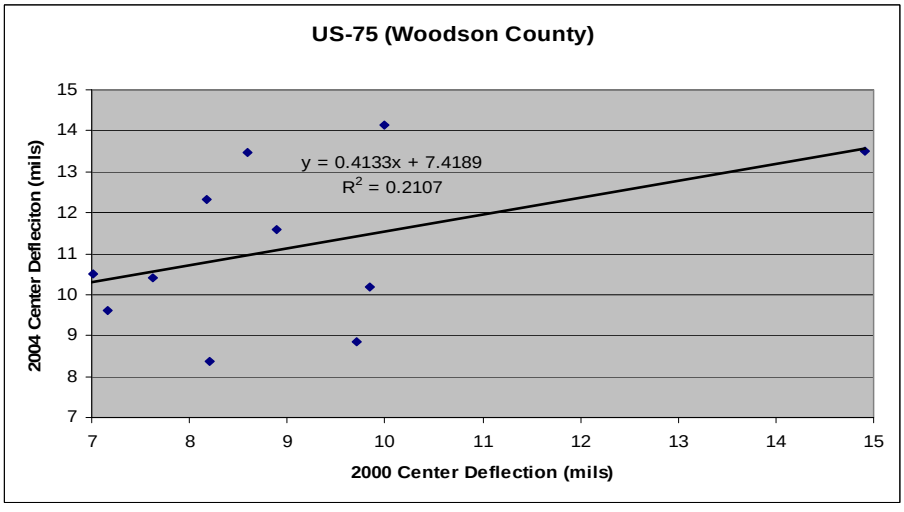

Figure A-12 FWD Center Deflection over Years for US-75

Measured and Calculated Pavement Temperature

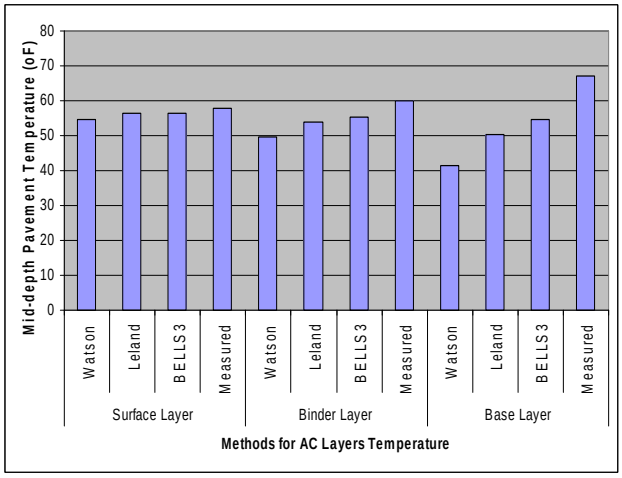

(a) Section 1

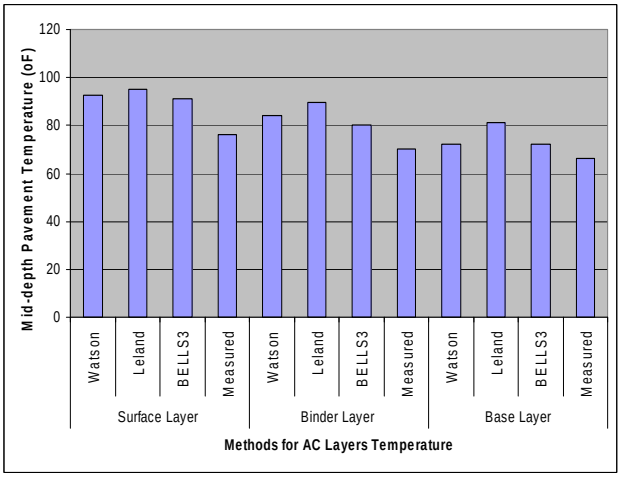

(2) Section 2

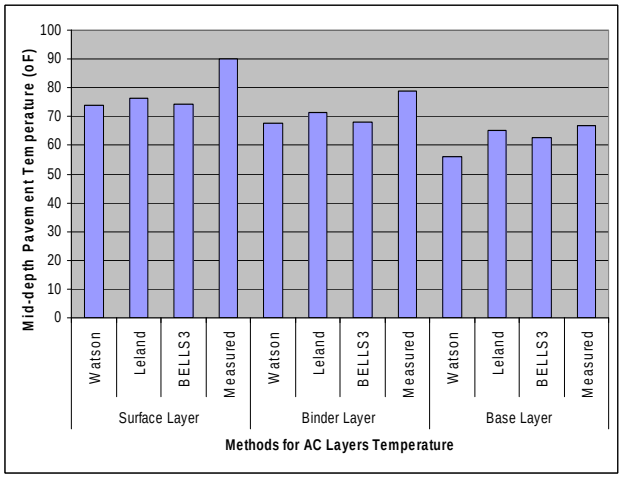

(c) Section 3

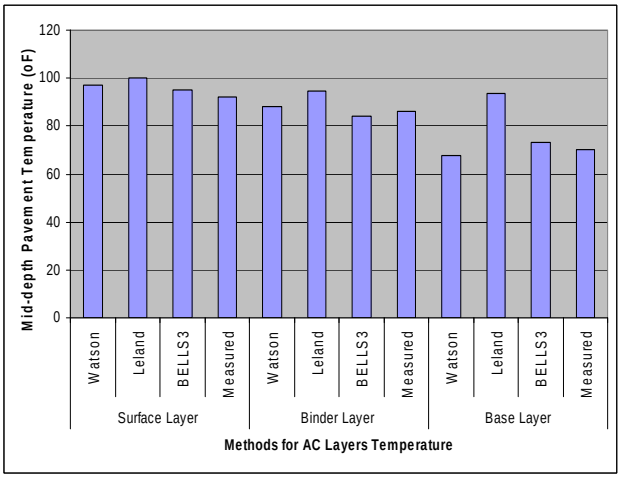

(d) Section 4

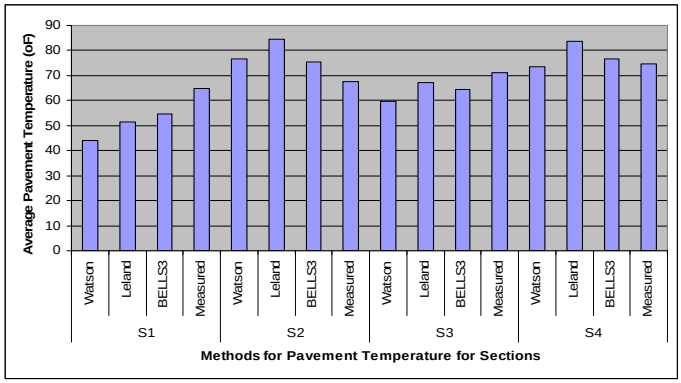

(e) Average Pavement Temperature for All Sections

Figure A-13 Comparison of AC-Layer Temperature (Test Date: 09/25/2005)

Table A-3 Significant-Difference Test for AC-Layer Temperature (Test Date: 09/25/2005)

Section			Surface Layer		Binder Layer		Base Layer		Overall	
			Pr>|t|	Similar	Pr>|t|	Similar	Pr>|t|	Similar	Pr>|t|	Similar
1	Watson	Leland	<.0001	No	<.0001	No	<.0001	No	<.0001	No
		BELLS3	<.0001	No	<.0001	No	<.0001	No	<.0001	No
		Measured	0.0064	No	<.0001	No	<.0001	No	<.0001	No
	Leland	BELLS3	0.6475	Yes	0.0006	No	<.0001	No	<.0001	No
		Measured	0.1368	Yes	0.0001	No	<.0001	No	<.0001	No
	BELLS3	Measured	0.0941	Yes	<.0001	No	<.0001	No	<.0001	No
2	Watson	Leland	<.0001	No	<.0001	No	<.0001	No	<.0001	No
		BELLS3	<.0001	No	<.0001	No	0.2197	Yes	<.0001	No
		Measured	<.0001	No	<.0001	No	<.0001	No	<.0001	No
	Leland	BELLS3	<.0001	No	<.0001	No	<.0001	No	<.0001	No
		Measured	<.0001	No	<.0001	No	<.0001	No	<.0001	No
	BELLS3	Measured	<.0001	No	<.0001	No	<.0001	No	<.0001	No
3	Watson	Leland	<.0001	No	<.0001	No	<.0001	No	<.0001	No
		BELLS3	<.0001	No	<.0001	No	<.0001	No	<.0001	No
		Measured	<.0001	No	<.0001	No	<.0001	No	<.0001	No
	Leland	BELLS3	<.0001	No	<.0001	No	<.0001	No	<.0001	No
		Measured	<.0001	No	<.0001	No	<.0001	No	<.0001	No
	BELLS3	Measured	<.0001	No	<.0001	No	<.0001	No	<.0001	No
4	Watson	Leland	0.2352	Yes	0.1874	Yes	<.0001	No	<.0001	No
		BELLS3	<.0001	No	<.0001	No	<.0001	No	<.0001	No
		Measured	0.0017	No	0.0423	No	0.0166	No	0.2791	Yes
	Leland	BELLS3	0.7047	Yes	0.0002	No	<.0001	No	<.0001	No
		Measured	0.0002	No	<.0001	No	<.0001	No	<.0001	No
	BELLS3	Measured	0.0156	No	0.013	No	<.0001	No	0.0032	No

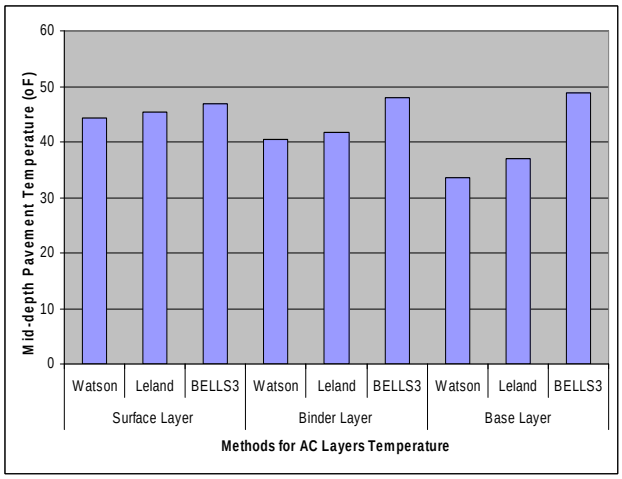

(a) Section 1

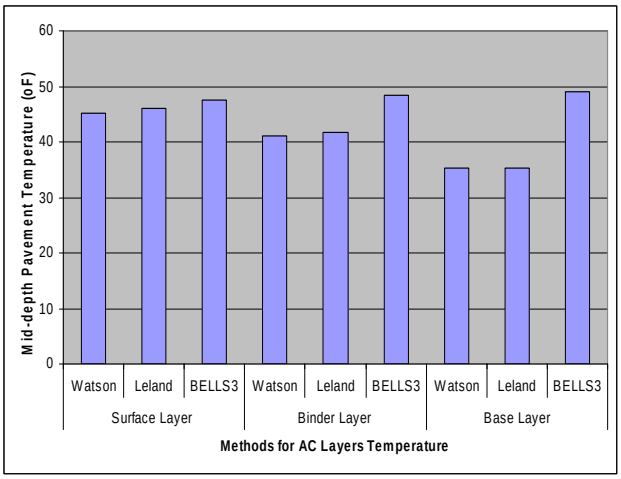

(b) Section 2

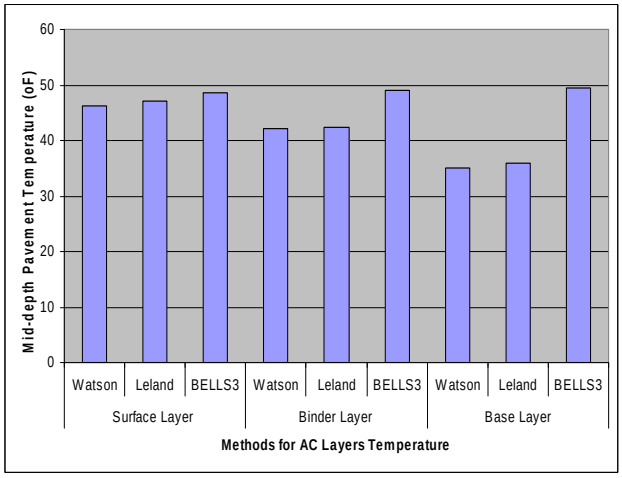

(c) Section 3

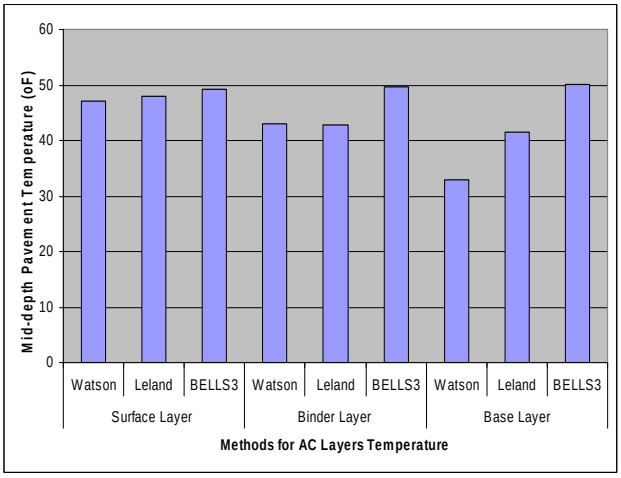

(d) Section 4

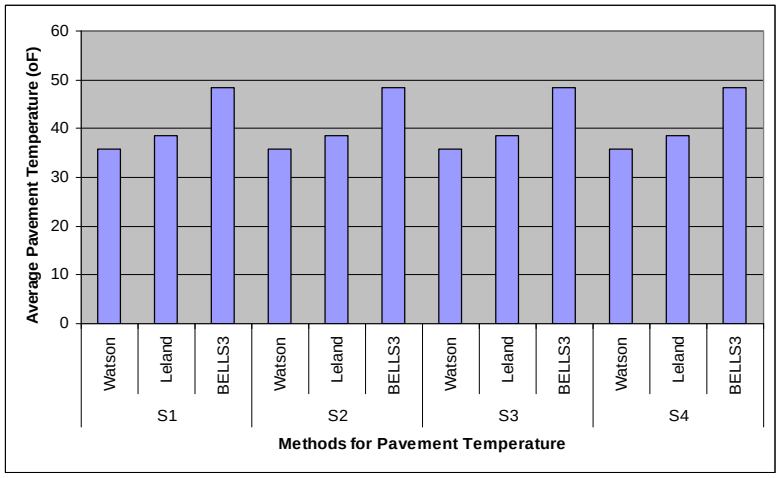

(e) Average Pavement Temperature for All Sections

Figure A-14 Comparison of AC-Layer Temperature (Test Date: 04/26/2007)

Table A-4 Significant-Difference Test for AC-Layer Temperature (Test Date: 04/26/2007)

Section			Surface Layer		Binder Layer		Base Layer		Average	
			Pr>|t|	Similar	Pr>|t|	Similar	Pr>|t|	Similar	Pr>|t|	Similar
1	Watson	Leland	<.0001	No	<.0001	No	<.0001	No	<.0001	No
		BELLS3	<.0001	No	<.0001	No	<.0001	No	<.0001	No
	Leland	BELLS3	<.0001	No	<.0001	No	<.0001	No	<.0001	No
2	Watson	Leland	<.0001	No	<.0001	No	0.4802	Yes	0.0479	No
		BELLS3	<.0001	No	<.0001	No	<.0001	No	<.0001	No
	Leland	BELLS3	<.0001	No	<.0001	No	<.0001	No	<.0001	No
3	Watson	Leland	<.0001	No	<.0001	No	0.0002	No	<.0001	No
		BELLS3	<.0001	No	<.0001	No	<.0001	No	<.0001	No
	Leland	BELLS3	<.0001	No	<.0001	No	<.0001	No	<.0001	No
4	Watson	Leland	<.0001	No	<.0001	No	<.0001	No	<.0001	No
		BELLS3	<.0001	No	<.0001	No	<.0001	No	<.0001	No
	Leland	BELLS3	<.0001	No	<.0001	No	<.0001	No	<.0001	No

Pavement Structural Capacity

FWD and RWD SNeff

Without Rehabilitation Actions

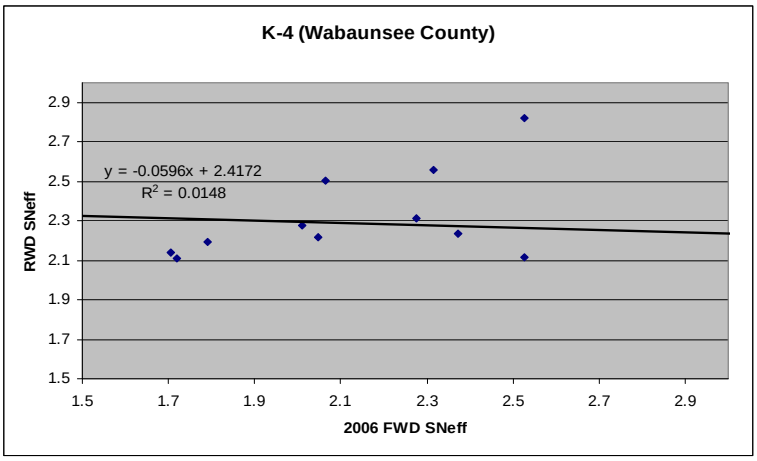

(a)

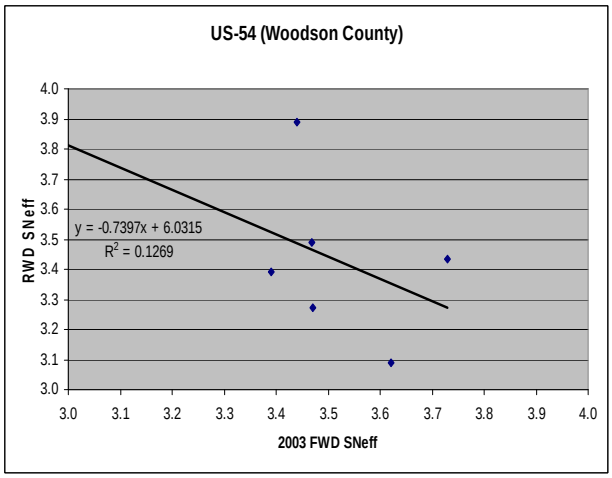

(b)

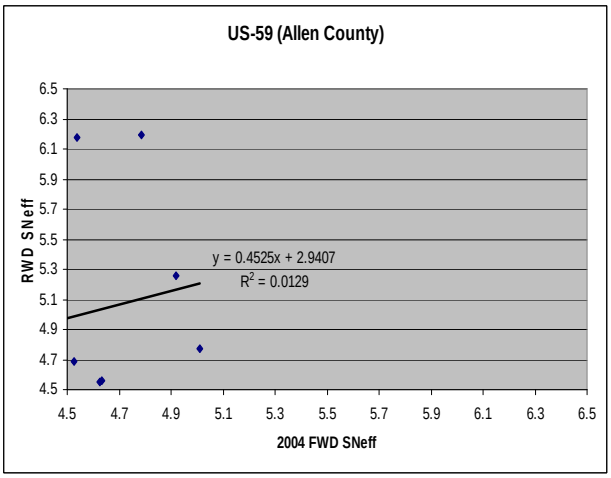

(c)

Figure A-15 FWD and RWD SNeff for K-4, US-54, and US-59

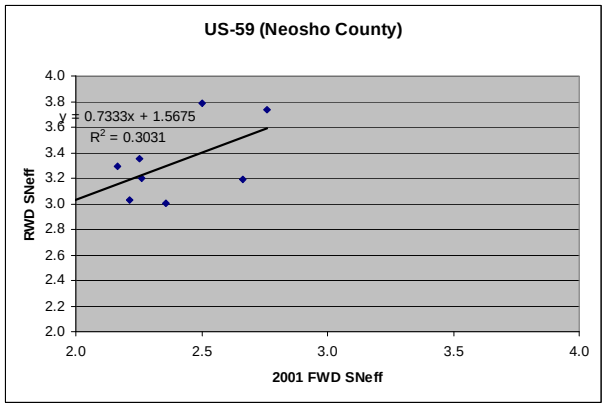

(a)

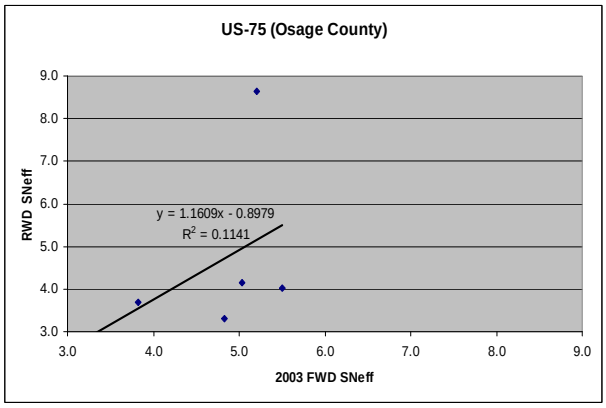

(b)

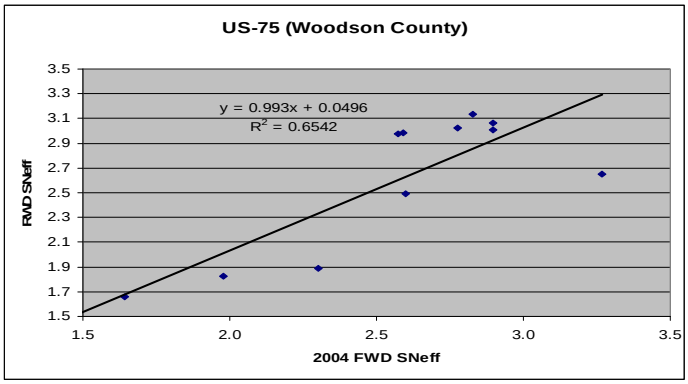

(c)

Figure A-16 FWD and RWD SNeff for US-59 and US-75

With Rehabilitation Actions

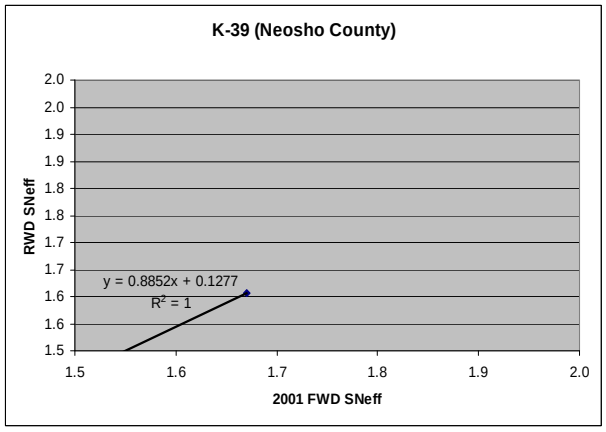

(a)

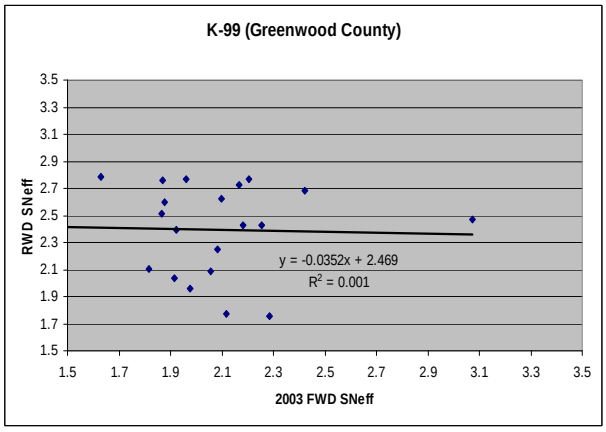

(b)

Figure A-17 FWD and RWD SNeff for K-39 and K-99

Effect of Temperature-Correction Method on SNeff

County and Route-Wise

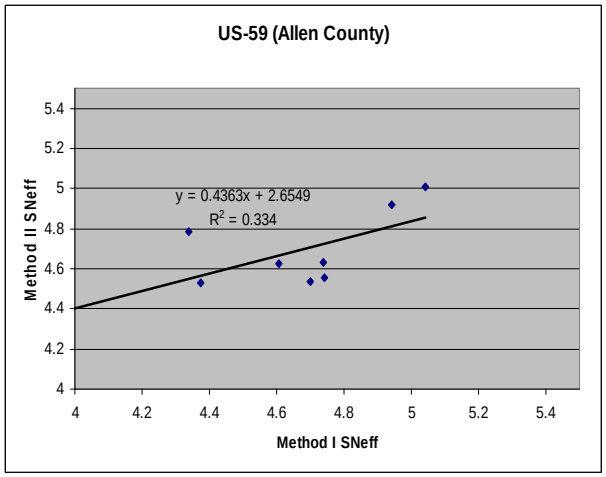

(a)

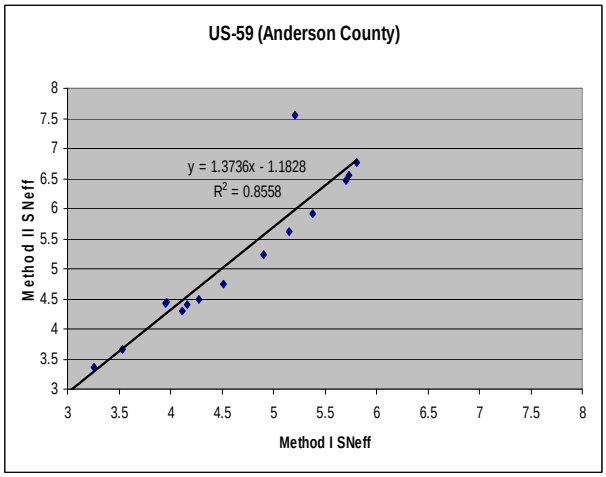

(b)

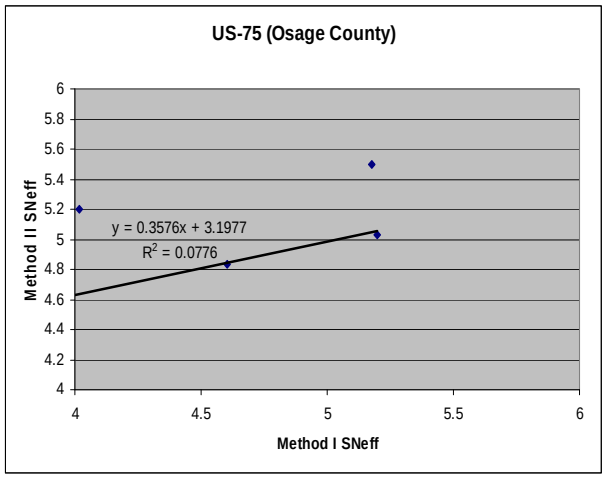

(c)

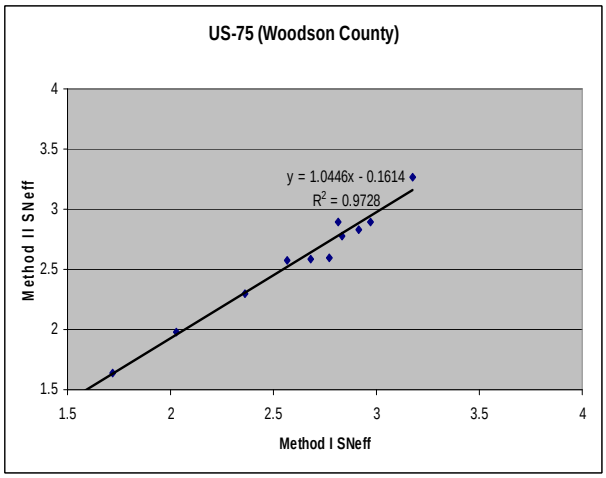

(d)

Figure A-18 Effect of Temperature-Correction Method on SNeff for US-59 and US-75

Route-Wise

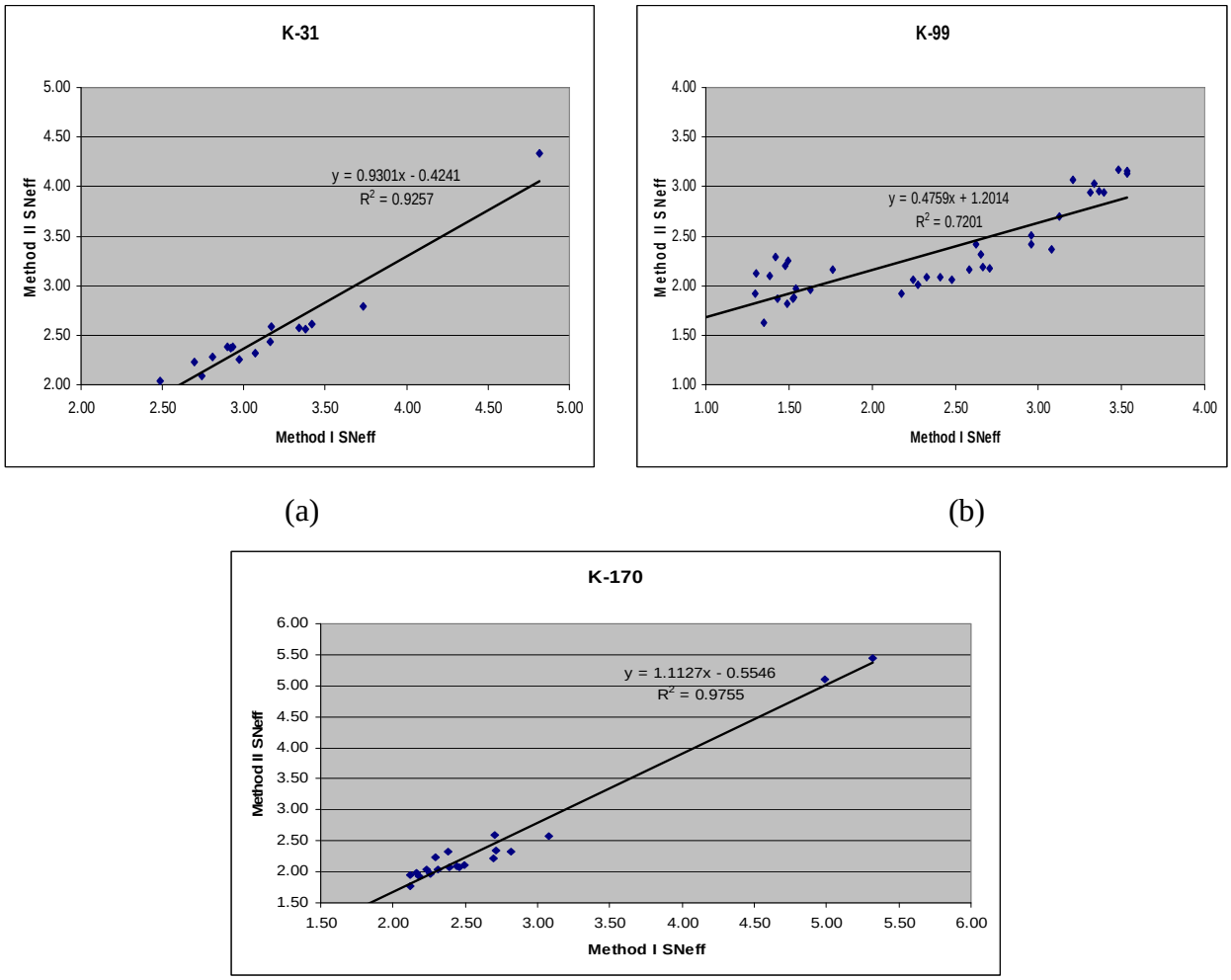

Figure A-19 Effect of Temperature-Correction Method on SNeff for K-31, K-99, and K-170

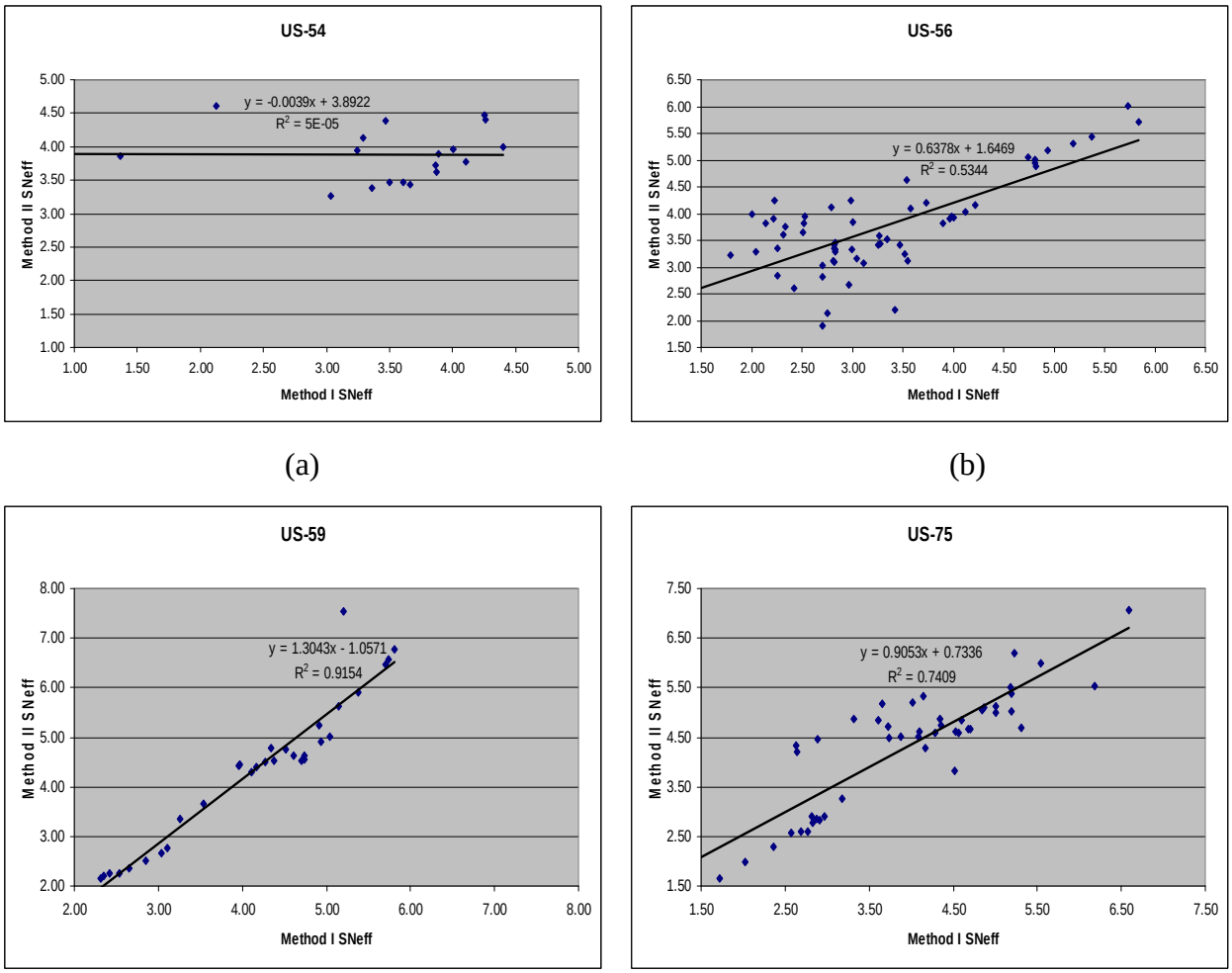

Figure A-20 Effect of Temp.-Correction Method on SNeff US-54, US-56, US-59, and US-75

County-Wise

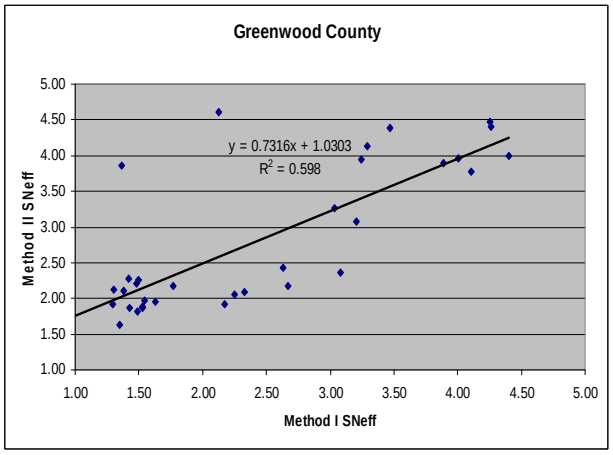

(a)

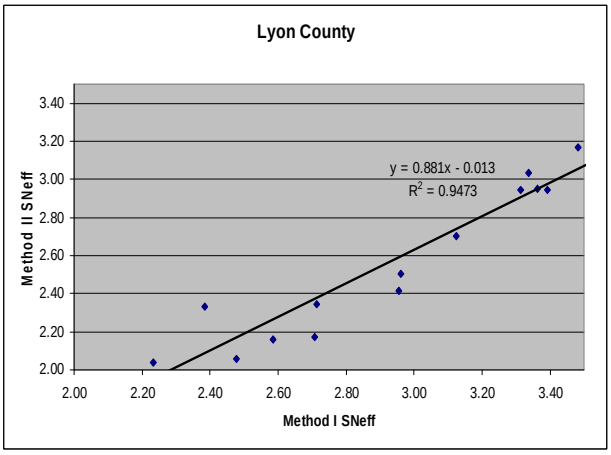

(b)

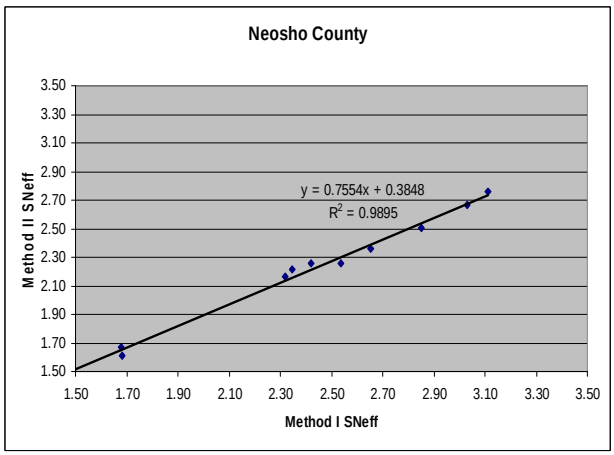

(c)

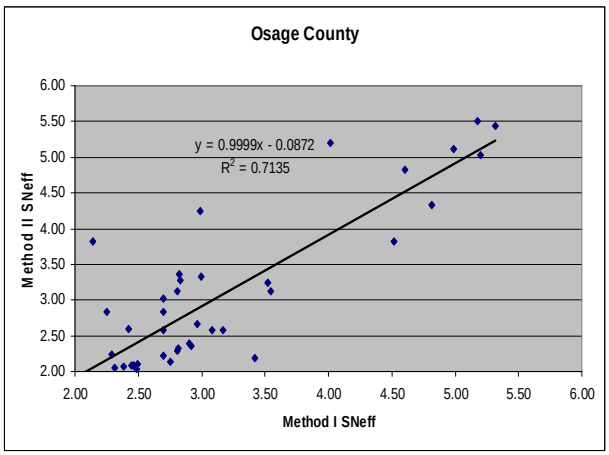

(d)

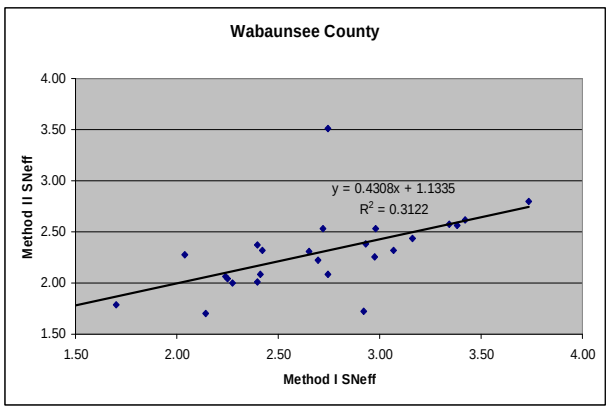

(e) Wabaunsee County

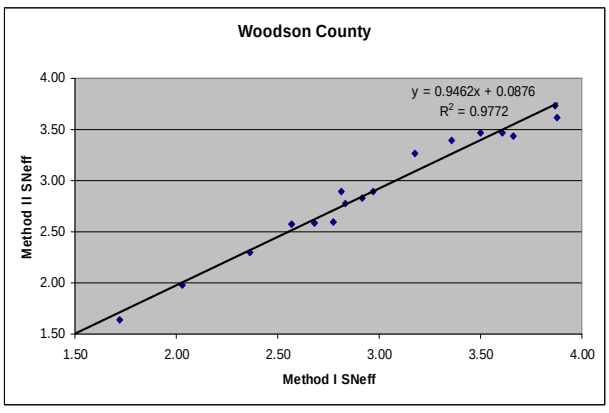

(f) Woodson County

Figure A-21 Effect on Green., Lyon, Neosho, Osage, Wabaunsee, and Woodson Counties

District-Wise

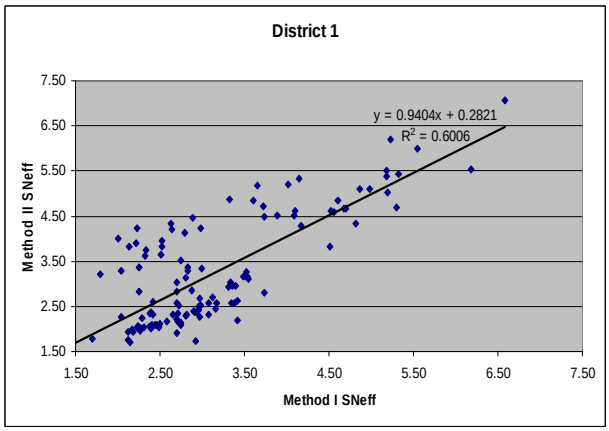

(a)

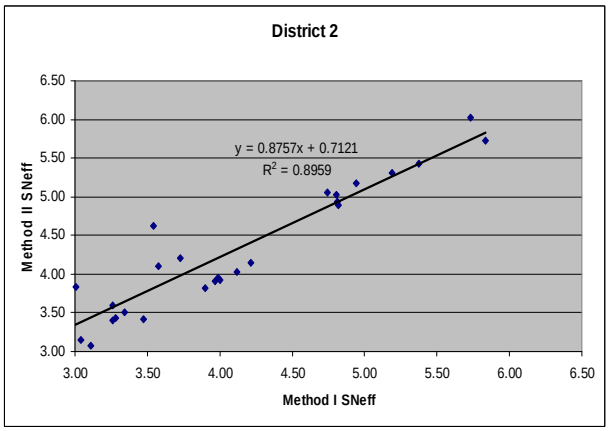

(b)

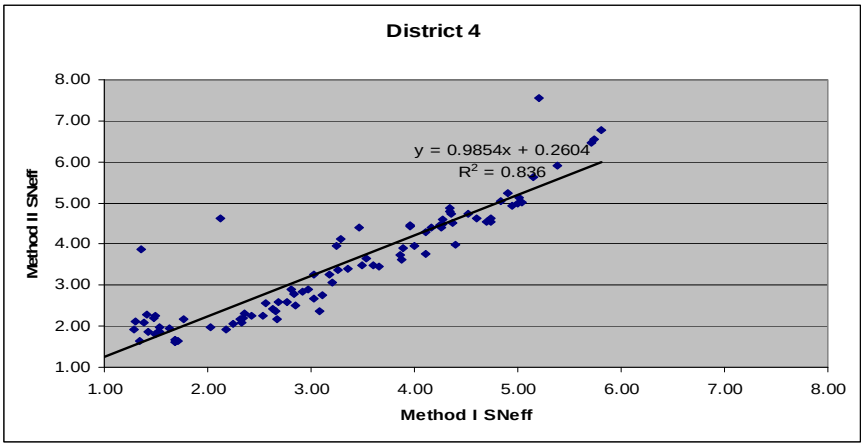

(c)

Figure A-22 Effect of Temperature-Correction Method on SNeff in Districts 1, 2, and 4

Significant-Difference Test

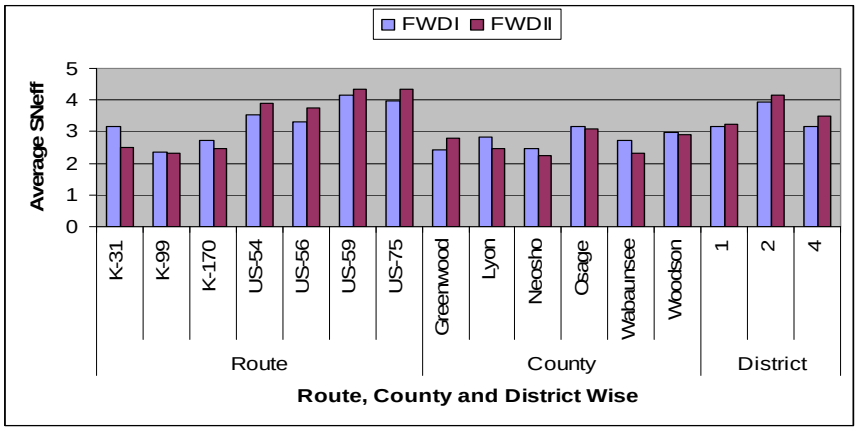

Figure A-23 Effect of Temperature-Correction Method on Average SNeff

Table A-5 Significant-Difference Test for Effect of Temp.-Correction Method on SNeff

	Avg. SNeff		Paired T-Test for Difference (I-II)					Length
	I	II	Lower	Mean	Upper	Pr>|t|	Similar	(mi)
(a) Route-Wise								
K-31	3.16	2.51	0.5661	0.645	0.7239	<.0001	No	16
K-99	2.35	2.32	-0.125	0.0327	0.1903	0.6764	Yes	37
K-170	2.71	2.46	0.1627	0.2485	0.3343	<.0001	No	20
US-54	3.52	3.88	-0.788	-0.358	0.0711	0.0963	Yes	18
US-56	3.30	3.75	-0.631	-0.45	-0.27	<.0001	No	58
US-59	4.14	4.35	-0.399	-0.203	-0.006	0.0439	No	31
US-75	3.98	4.34	-0.536	-0.358	-0.18	0.0002	No	47
(b) County-Wise								
Greenwood	2.44	2.81	-0.623	-0.375	-0.126	0.0043	No	33
Lyon	2.83	2.48	0.291	0.35	0.409	<.0001	No	20
Neosho	2.46	2.25	0.1277	0.219	0.3103	0.0004	No	10
Osage	3.16	3.07	-0.1	0.0873	0.2742	0.351	Yes	40
Wabaunsee	2.71	2.30	0.2356	0.4084	0.5812	<.0001	No	25
Woodson	2.98	2.91	0.023	0.0724	0.1217	0.0068	No	17
(c)District-Wise								
1	3.16	3.25	-0.231	-0.095	0.0418	0.1724	Yes	122
2	3.95	4.17	-0.33	-0.22	-0.111	0.0003	No	30
4	3.17	3.48	-0.329	-0.212	-0.095	0.0005	No	89

Linear Regression

Table A-6 Linear Regression for Effect of Temperature-Correction Method on SNeff

	Intercept	Slope	C.I.* for Slope		Pr>|t|	Linear Relation	R^2	Length (mi)
			lower	upper				
(a) Route-Wise								
K-31	-0.41	0.93	0.77	1.08	0.00	Yes	0.93	16
K-99	1.20	0.48	0.37	0.58	0.00	Yes	0.72	37
K-170	-0.55	1.11	1.02	1.20	0.00	Yes	0.98	20
US-54	3.89	-0.00	-0.28	0.28	0.98	No	0.00	18
US-56	1.65	0.64	0.48	0.80	0.00	Yes	0.54	58
US-59	-1.06	1.31	1.15	1.46	0.00	Yes	0.92	31
US-75	0.74	0.90	0.74	1.07	0.00	Yes	0.74	47
(b) County-Wise								
Greenwood	1.03	0.73	0.51	0.95	0.00	Yes	0.60	33
Lyon	-0.01	0.88	0.78	0.98	0.00	Yes	0.95	20
Neosho	0.39	0.75	0.69	0.82	0.00	Yes	0.99	10
Osage	-0.08	1.00	0.79	1.21	0.00	Yes	0.71	40
Wabaunsee	1.13	0.43	0.16	0.71	0.00	Yes	0.31	25
Woodson	0.09	0.95	0.87	1.03	0.00	Yes	0.98	17
(c)District-Wise								
1	0.28	0.94	0.80	1.08	0.00	Yes	0.60	122
2	0.71	0.87	0.76	0.99	0.00	Yes	0.90	30
4	0.26	0.99	0.89	1.09	0.00	Yes	0.84	89

* confidence interval for slope at 95% confidence level

Frequency of Deflection Measurement Using SNeff

With Rehabilitation Actions

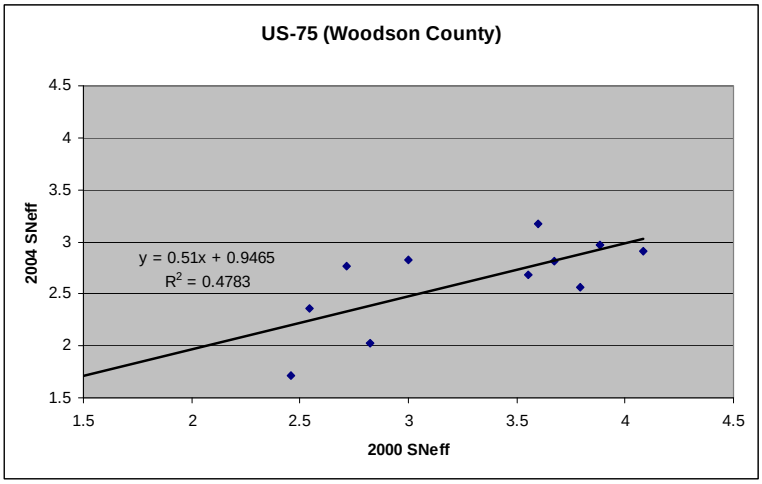

Figure A-24 FWD SNeff over Years for US-75

Without Rehabilitation Actions

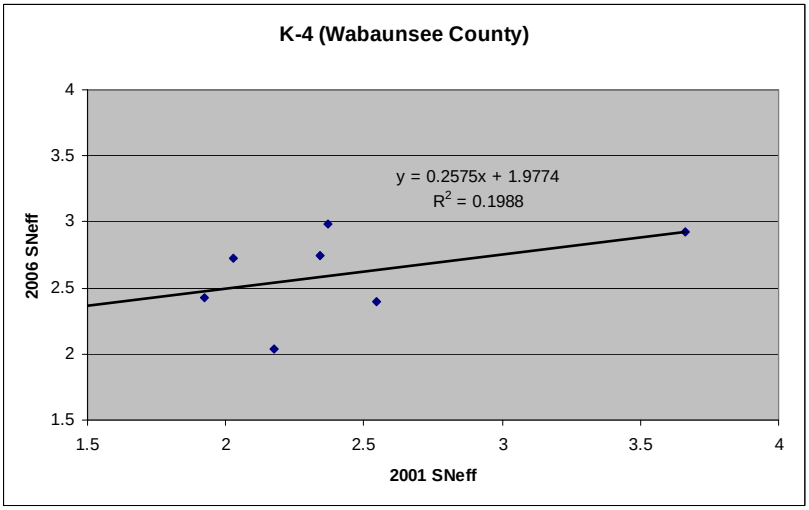

Figure A-25 FWD SNeff over Years for K-4

Linear Regression

Table A-7 Linear Regression of FWD SNeff over Years

Routes	County	Intercept	Slope	C.I.* for Slope		Pr>|t|	Linear Relation	R^2	Length (mi)
				Lower	Upper				
(a)With Rehabilitation Actions									
K-31	Wabaunsee	3.68	-0.30	-1.59	0.98	0.60	No	0.04	10
K-99	Lyon	3.08	0.13	-0.18	0.44	0.35	No	0.14	8
K-170	Lyon	0.03	1.10	-9.84	12.03	0.71	No	0.09	4
	Osage	-0.15	0.99	0.69	1.30	0.00	Yes	0.84	12
US-56	Morris	2.05	0.52	0.38	0.65	0.00	Yes	0.75	23
	Osage	3.50	-0.34	-0.90	0.22	0.21	No	0.11	16
US-75	Woodson	0.95	0.51	0.11	0.91	0.02	Yes	0.48	11
(b)Without Rehabilitation Actions									
K-4	Wabaunsee	1.98	0.26	-0.34	0.85	0.32	No	0.20	7
US-54	Woodson	0.44	0.75	0.55	0.95	0.00	Yes	0.86	13
US-59	Allen	-1.18	1.29	0.03	2.54	0.04	Yes	0.34	12
	Anderson	0.19	0.80	0.24	1.35	0.00	Yes	0.43	15
US-75	Brown	3.02	0.13	-0.04	0.30	0.11	No	0.33	9
	Coffey	8.41	-0.79	-2.80	1.23	0.30	No	0.34	5
	Jackson	3.00	0.43	-0.31	1.16	0.23	No	0.13	13

* confidence interval for slope at 95% confidence level

SNeff AASHTO and KDOT

District-Wise and Statewide

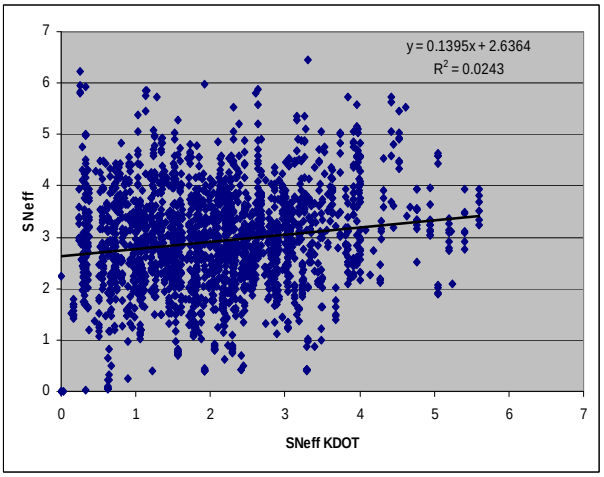

(a) District 5

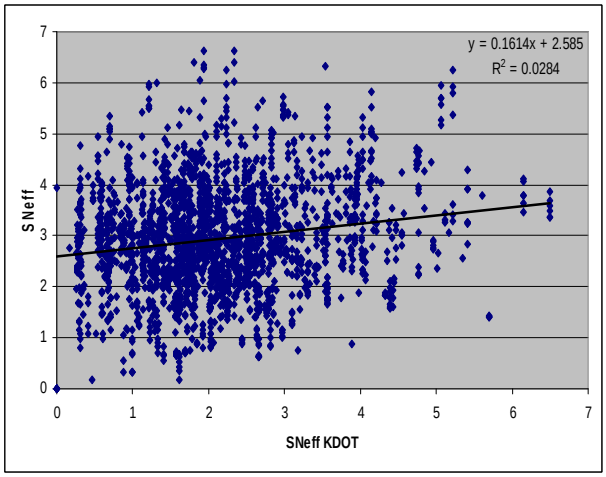

(b) District 6

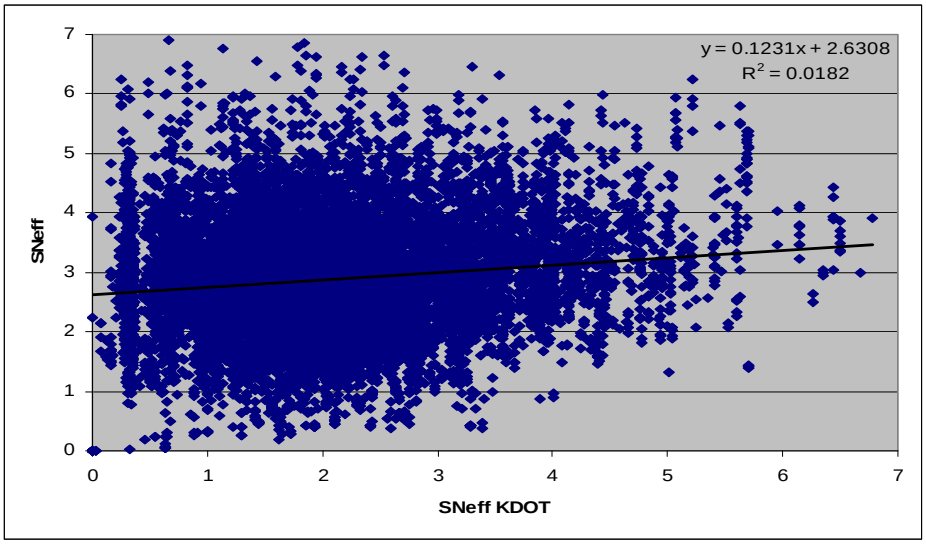

(c) State

Figure A-26 SNeff AASHTO and KDOT for Districts 5, 6, and State

Linear Regression

Table A-8 Linear Regression for SNeff AASHTO and KDOT

	Intercept	Slope	C.I.* for Slope		Pr>|t|	Linear Relation	R^2	Length (m)
			Lower	Upper				
(a)Road Category-Wise								
12	2.27	0.23	0.08	0.38	0.00	Yes	0.15	59
13	1.98	0.06	-0.04	0.15	0.26	No	0.01	134
14	2.88	0.06	-0.09	0.22	0.42	No	0.00	136
15	3.28	0.02	-0.09	0.14	0.68	No	0.00	204
16	2.83	0.16	0.09	0.24	0.00	Yes	0.03	657
17	3.00	0.12	0.09	0.15	0.00	Yes	0.01	3992
18	2.16	0.08	0.06	0.11	0.00	Yes	0.02	1871
19	2.43	0.05	0.02	0.09	0.00	Yes	0.01	1348
20	2.65	0.05	0.01	0.09	0.01	Yes	0.01	952
21	2.45	0.12	0.05	0.18	0.00	Yes	0.02	563
22	2.47	0.12	0.06	0.18	0.00	Yes	0.02	761
23	2.57	0.20	0.16	0.25	0.00	Yes	0.05	1790
(b)District-Wise								
1	3.11	-0.01	-0.05	0.04	0.73	No	0.00	1843
2	2.44	0.18	0.14	0.22	0.00	Yes	0.03	2020
3	2.39	0.17	0.14	0.20	0.00	Yes	0.05	2527
4	2.72	0.05	0.01	0.10	0.02	Yes	0.00	1657
5	2.64	0.14	0.10	0.18	0.00	Yes	0.02	2145
6	2.59	0.16	0.12	0.20	0.00	Yes	0.03	2262
State	2.63	0.12	0.11	0.14	0.00	Yes	0.02	12454

* confidence interval for slope at 95% confidence level

Appendix B - Prediction Models

Strain

Longitudinal Strain

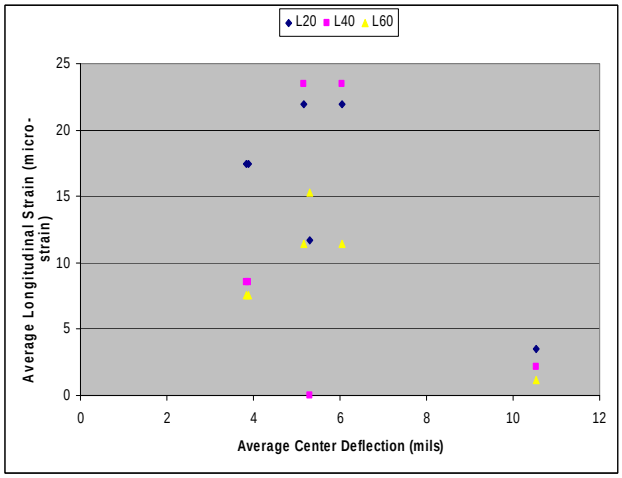

(a) Section 1

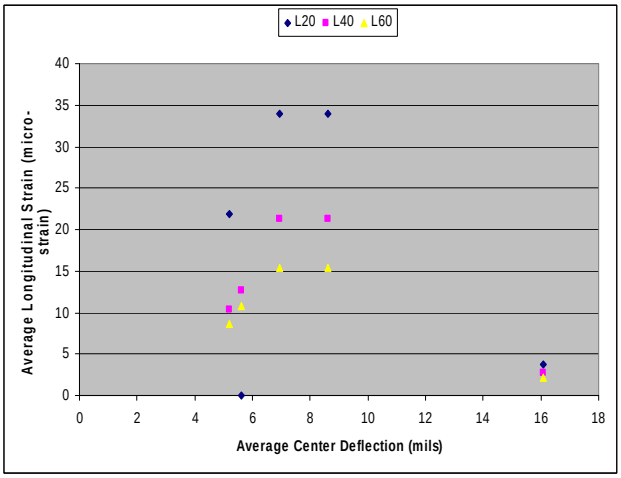

(b) Section 2

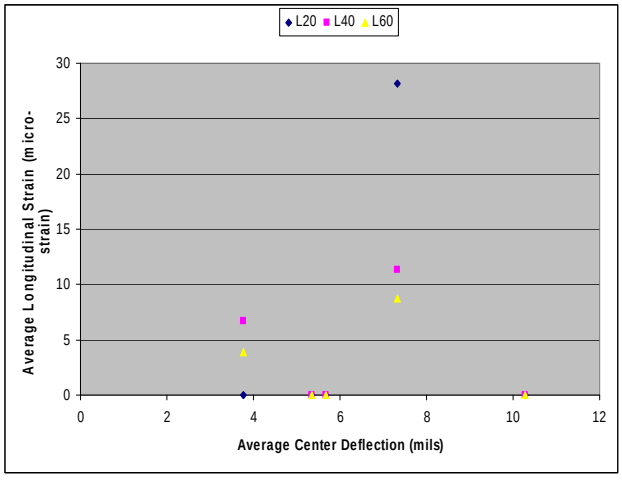

(c) Section 3

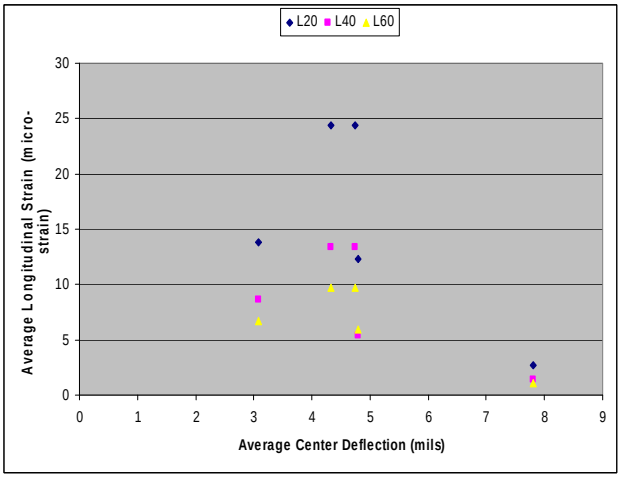

(d) Section 4

Figure B-1 Average Longitudinal Strain and Center Deflection

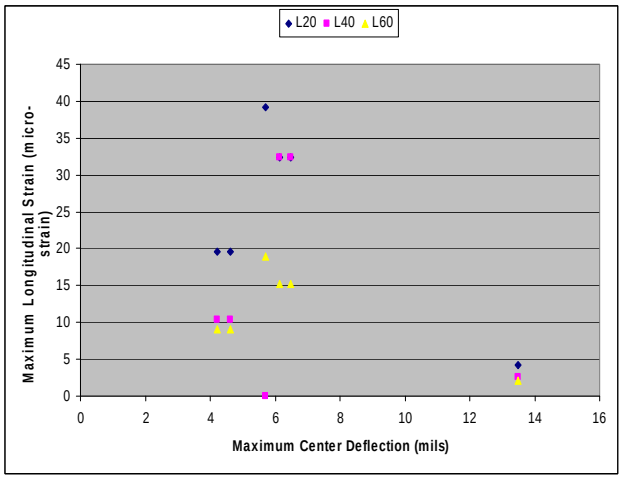

(a) Section 1

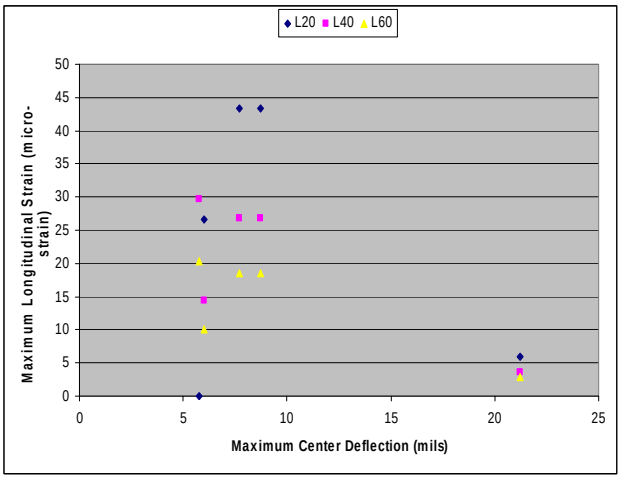

(b) Section 2

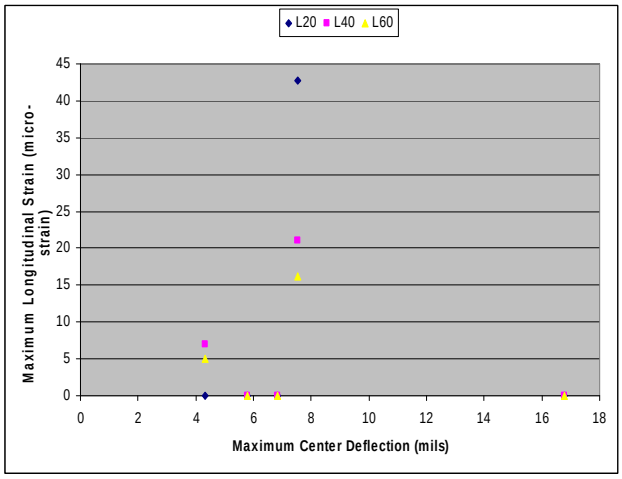

(c) Section 3

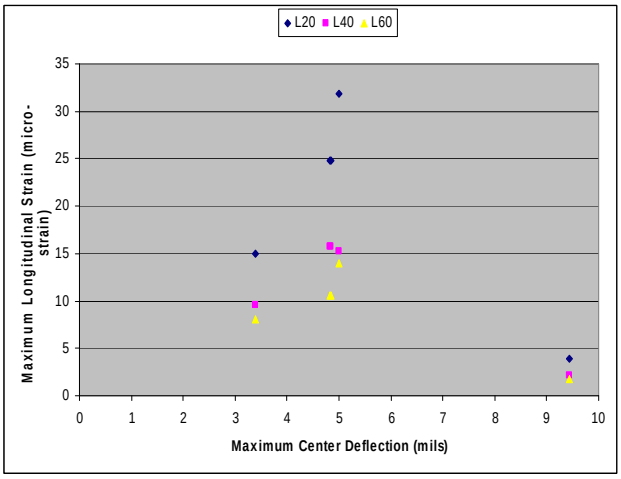

(d) Section 4

Figure B-2 Maximum Longitudinal Strain and Center Deflection

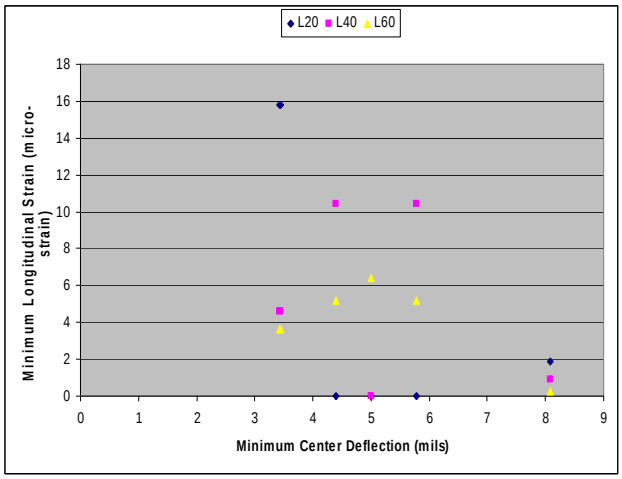

(a) Section 1

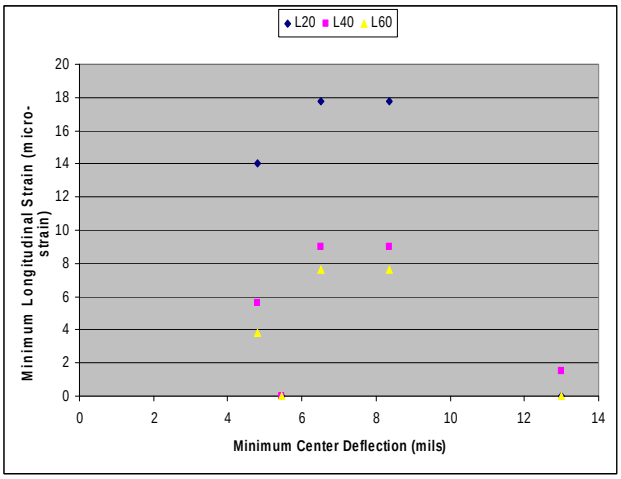

(d) Section 2

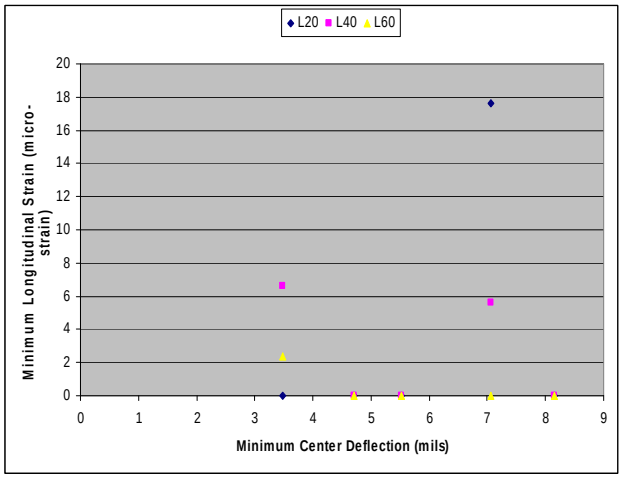

(c) Section 3

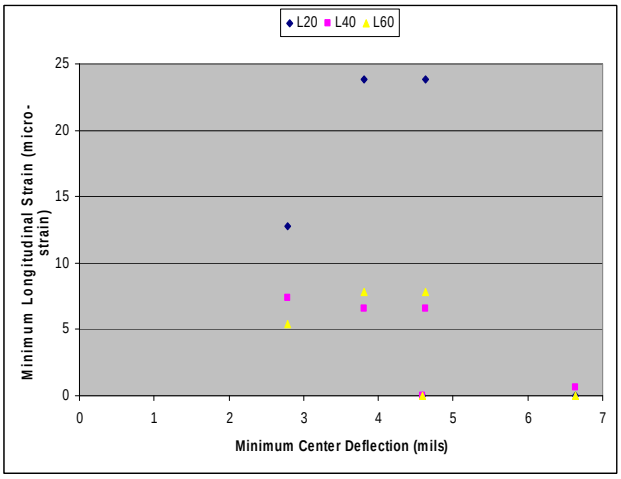

(d) Section 4

Figure B-3 Minimum Longitudinal Strain and Center Deflection

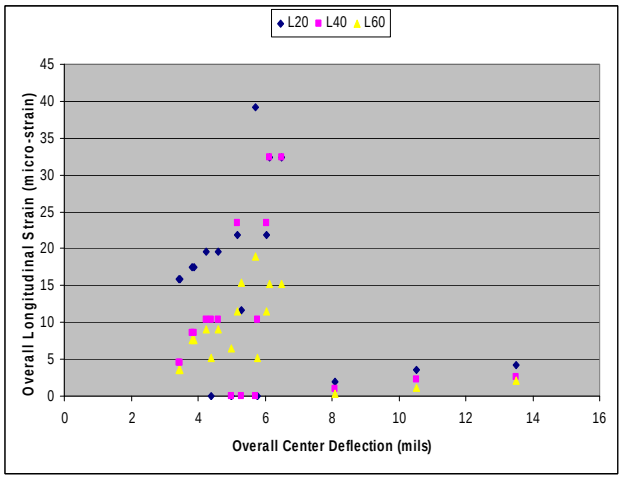

(a) Section 1

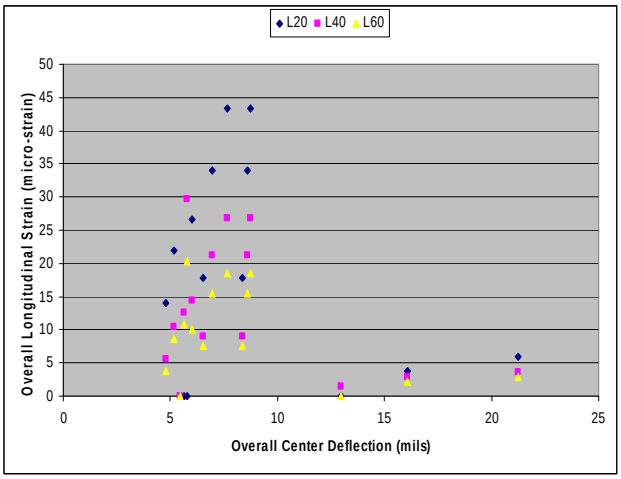

(b) Section 2

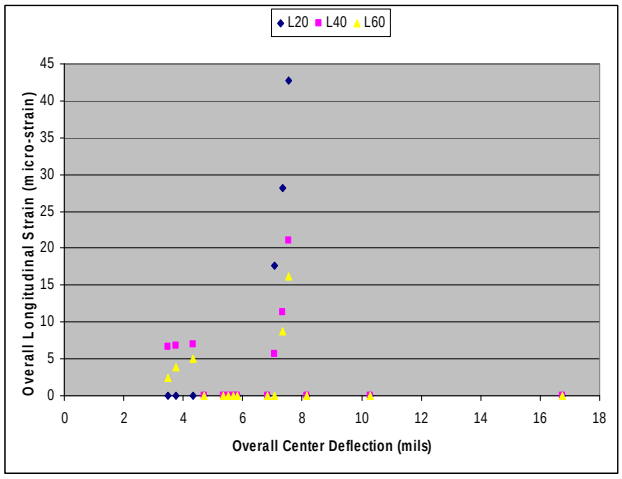

(c) Section 3

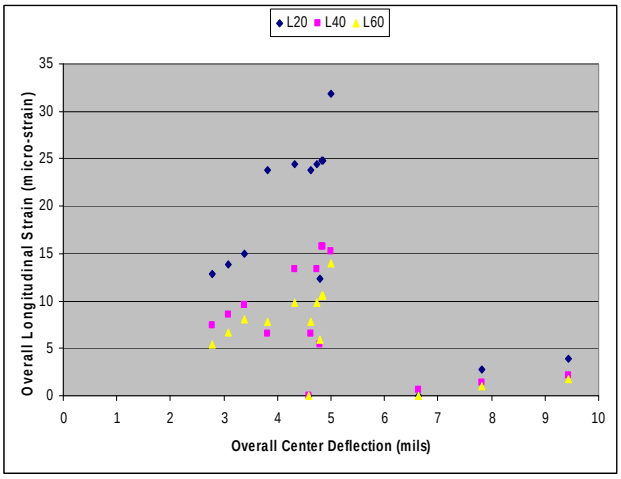

(d) Section 4

Figure B-4 Overall Longitudinal Strain and Center Deflection

Transverse Strain

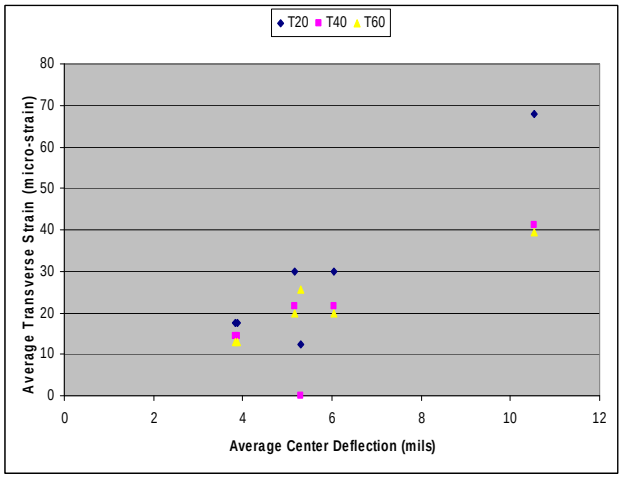

(a) Section 1

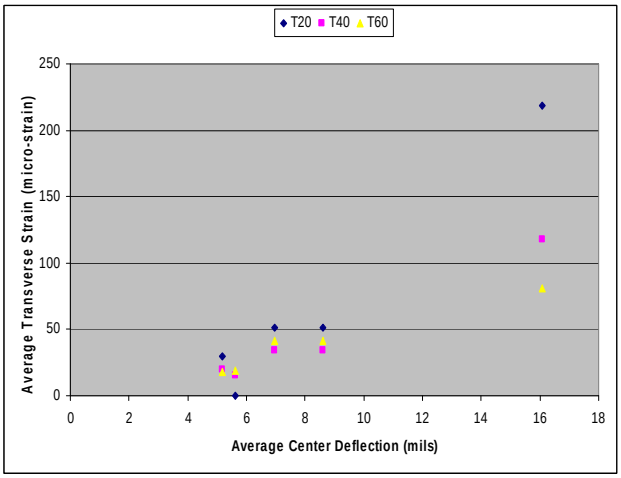

(b) Section 2

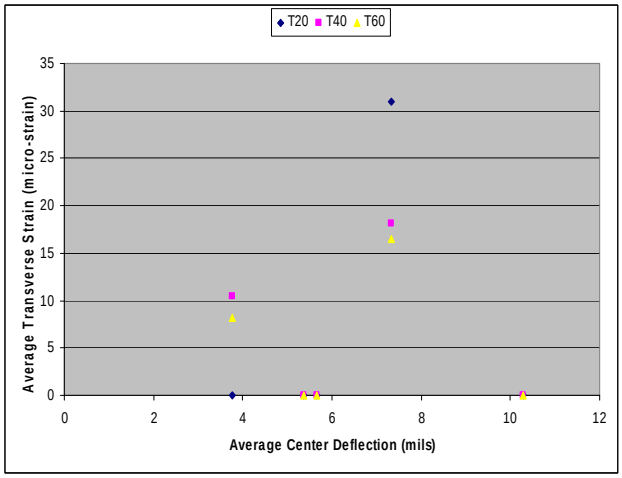

(c) Section 3

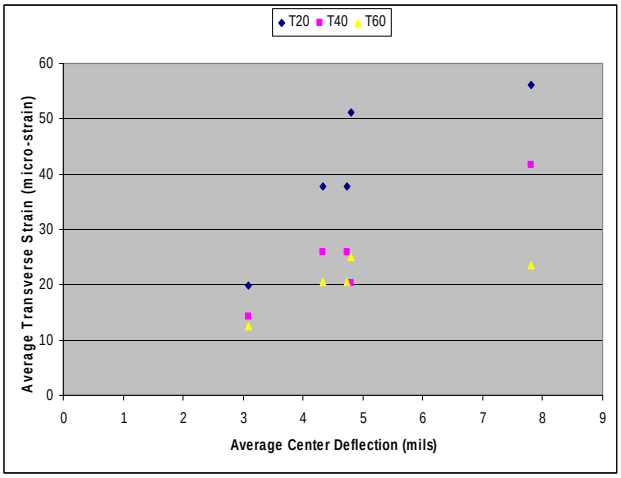

(d) Section 4

Figure B-5 Average Transverse Strain and Center Deflection

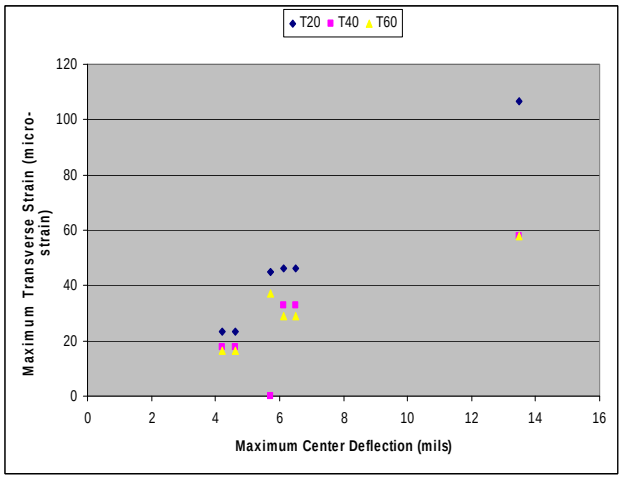

(a) Section 1

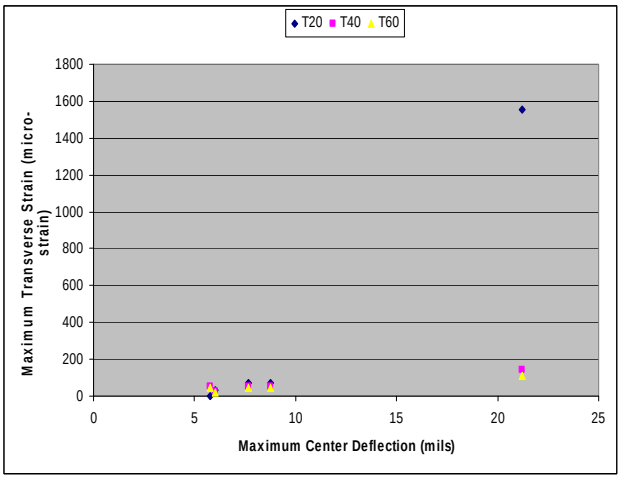

(b) Section 2

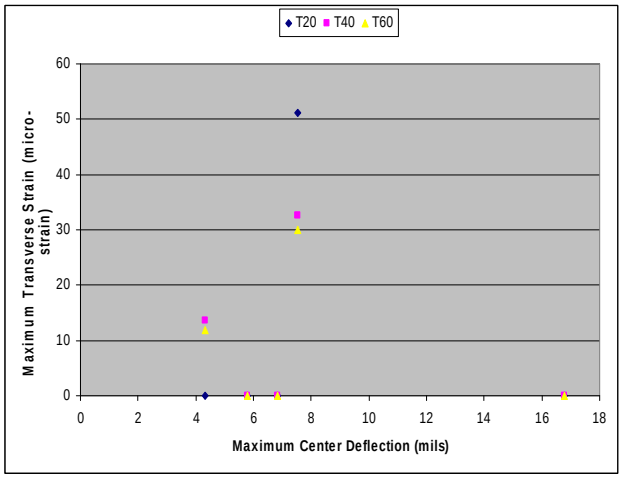

(c) Section 3

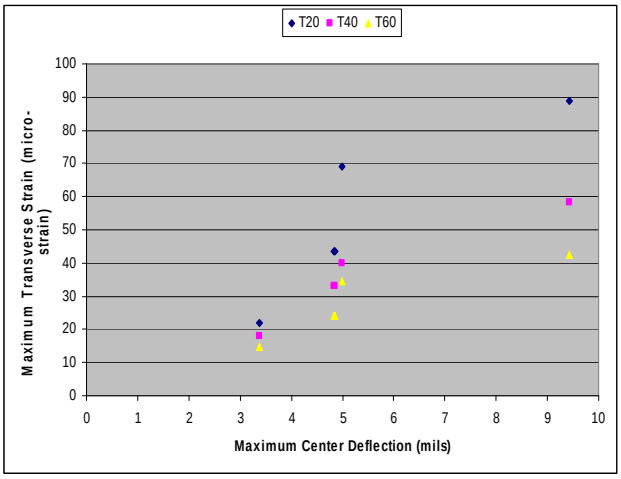

(d) Section 4

Figure B-6 Maximum Transverse Strain and Center Deflection

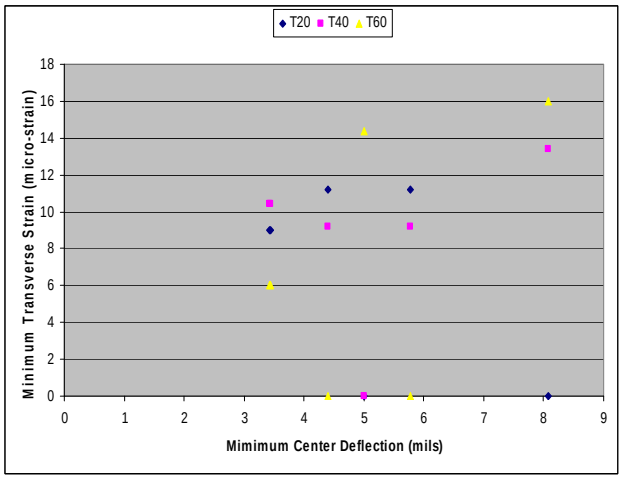

(a) Section 1

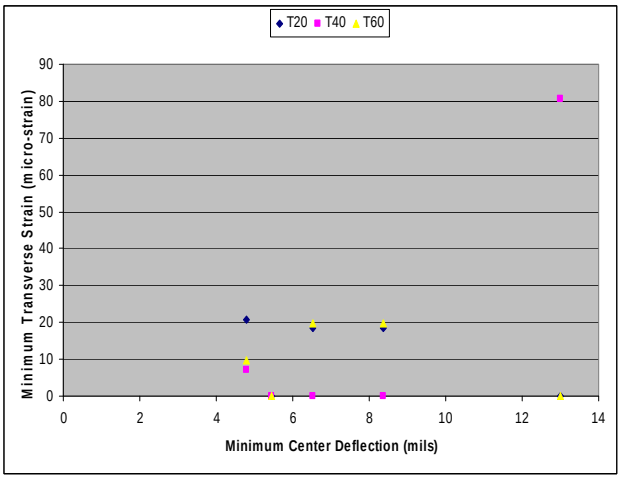

(b) Section 2

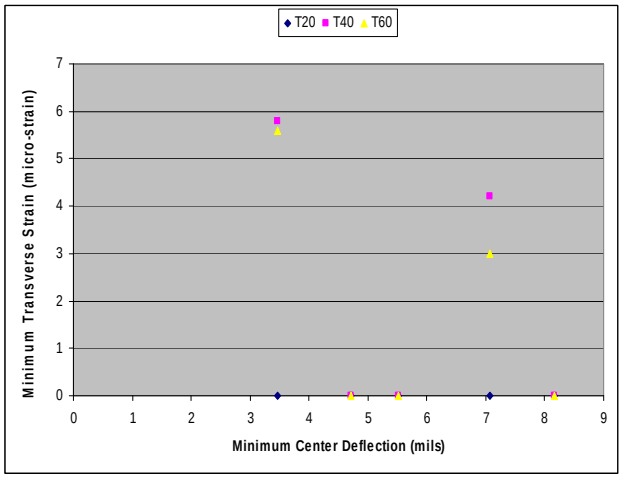

(c) Section 3

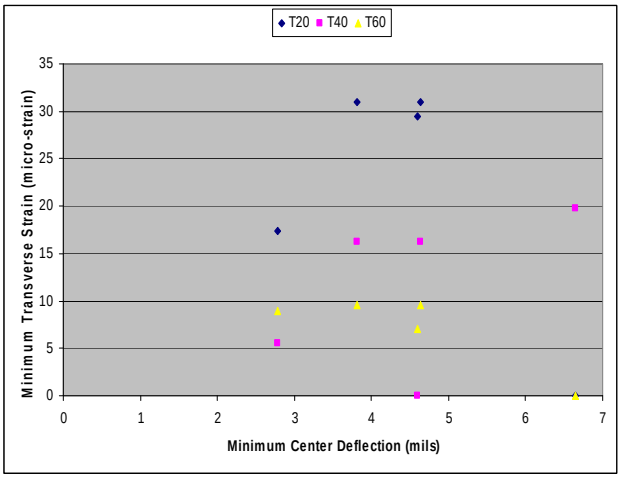

(d) Section 4

Figure B-7 Minimum Transverse Strain and Center Deflection

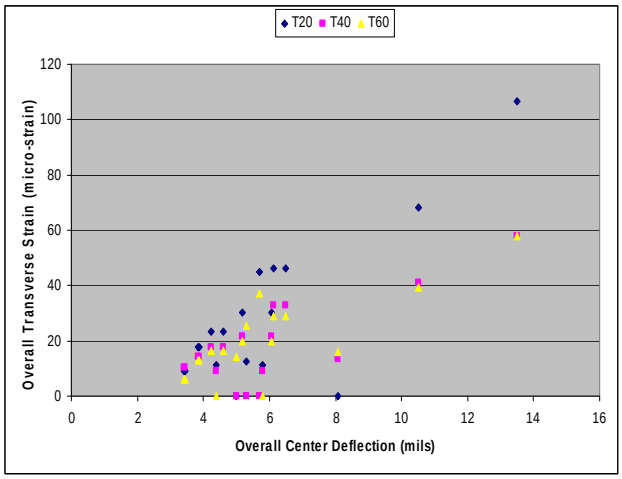

(a) Section 1

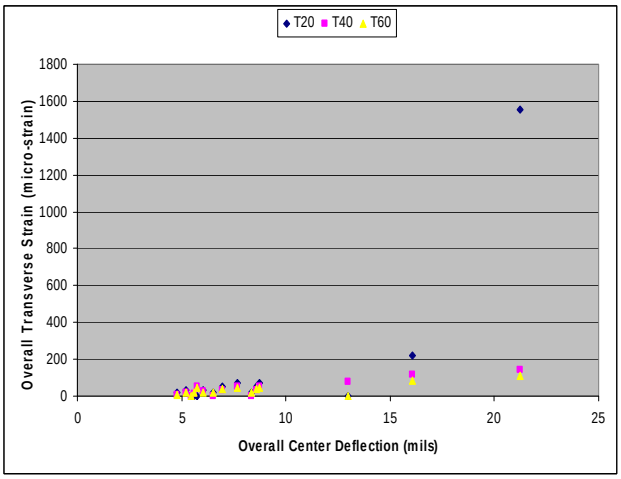

(b) Section 2

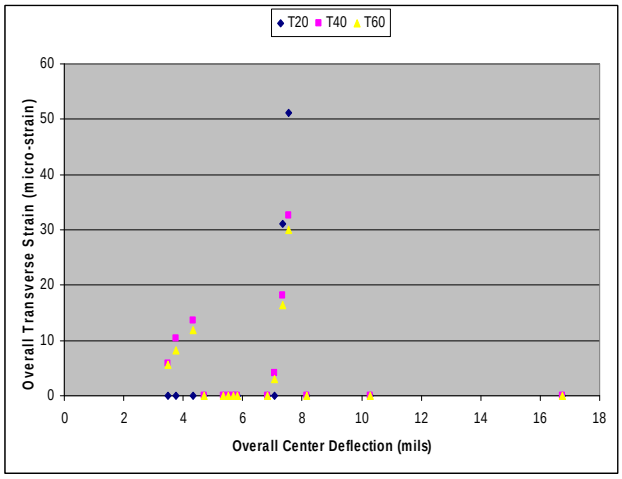

(c) Section 3

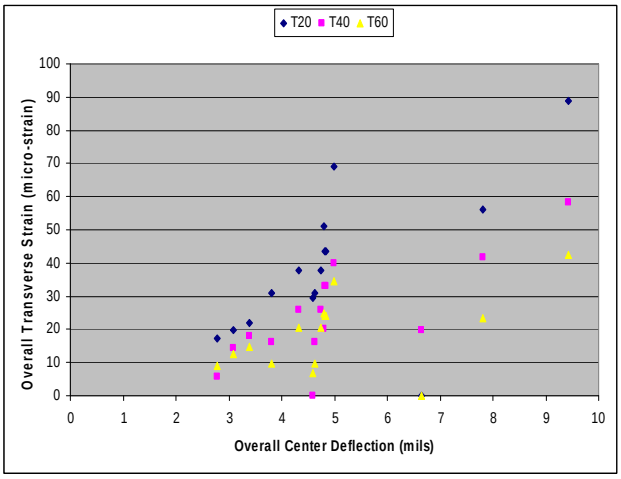

(d) Section 4

Figure B-8 Overall Transverse Strain and Center Deflection

Stress on Subgrade

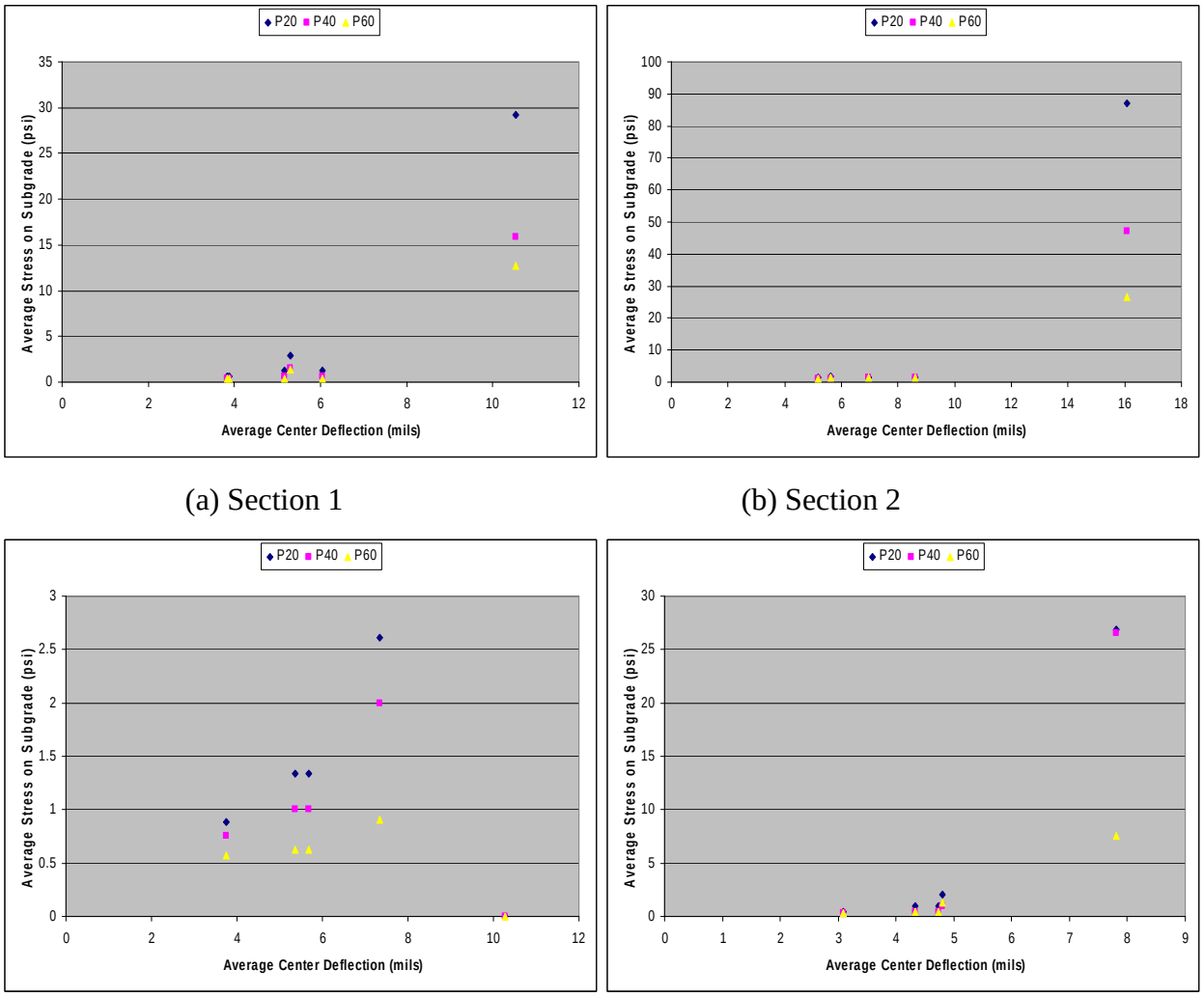

(a) Section 1 (b) Section 2

(c) Section 3 (d) Section 4

Figure B-9 Average Stress on Subgrade and Center Deflection

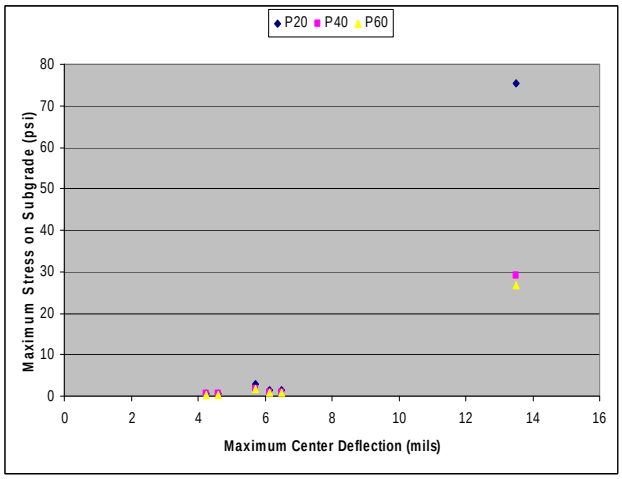

(a) Section 1

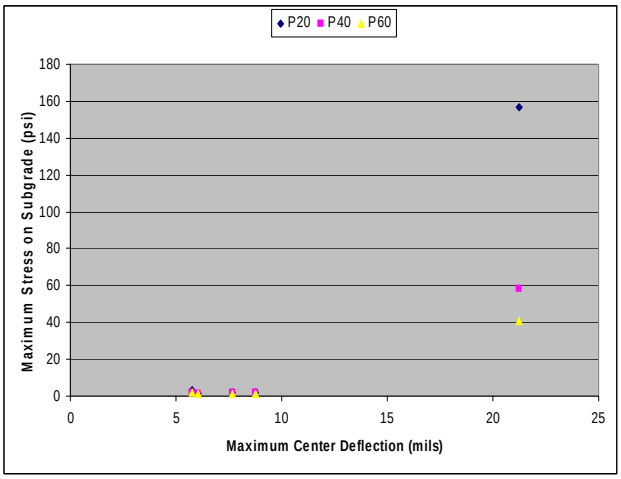

(b) Section 2

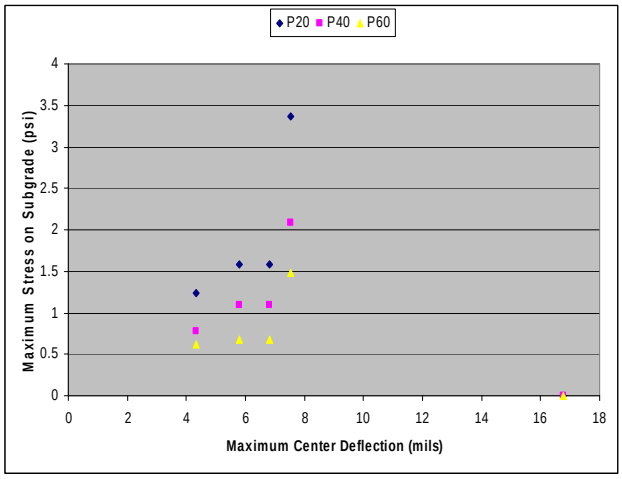

(c) Section 3

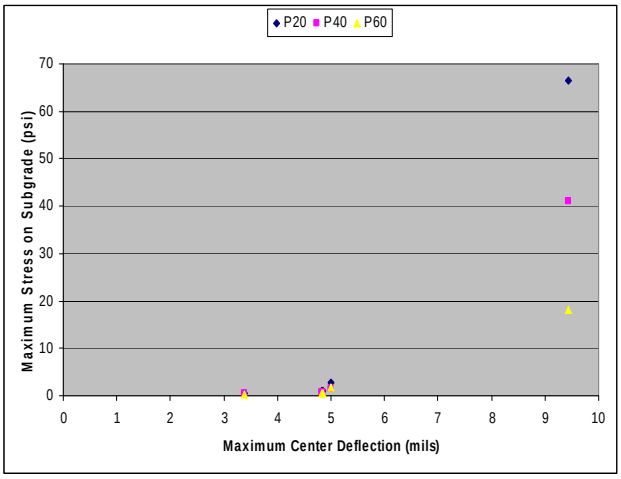

(d) Section 4

Figure B-10 Maximum Stress on Subgrade and Center Deflection

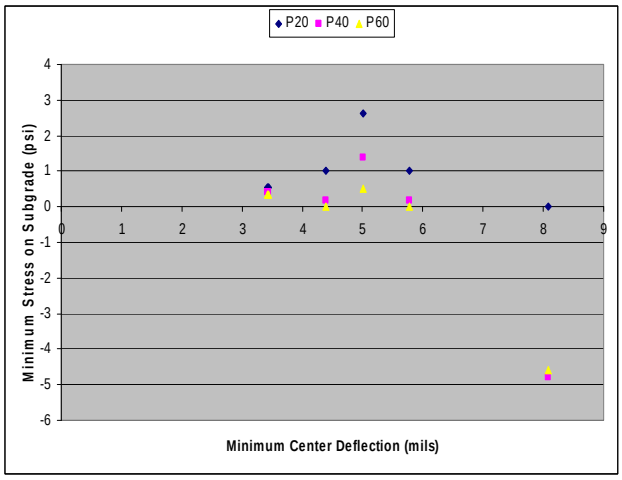

(a) Section 1

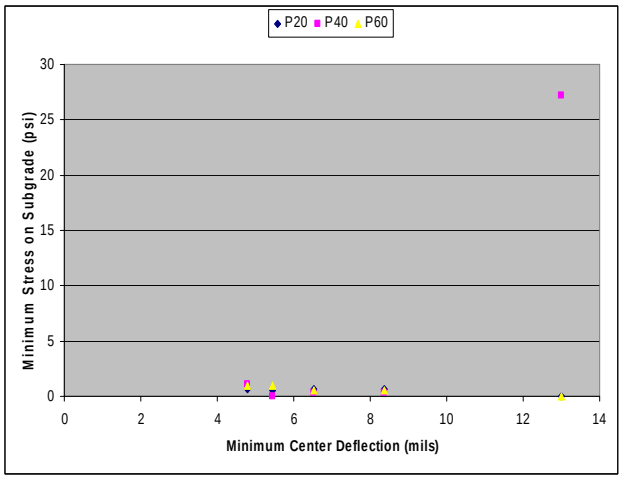

(b) Section 2

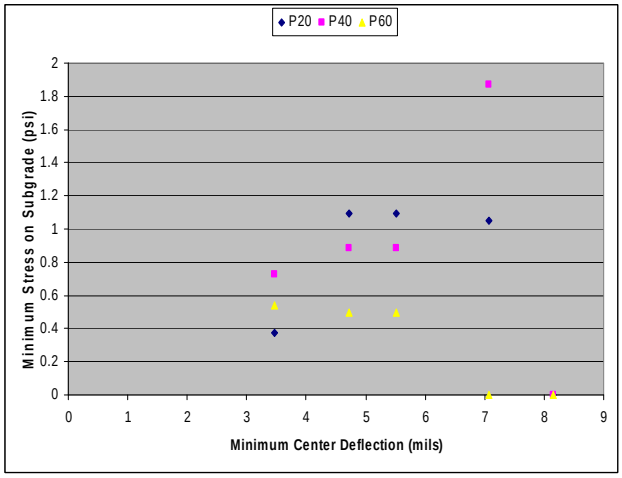

(c) Section 3

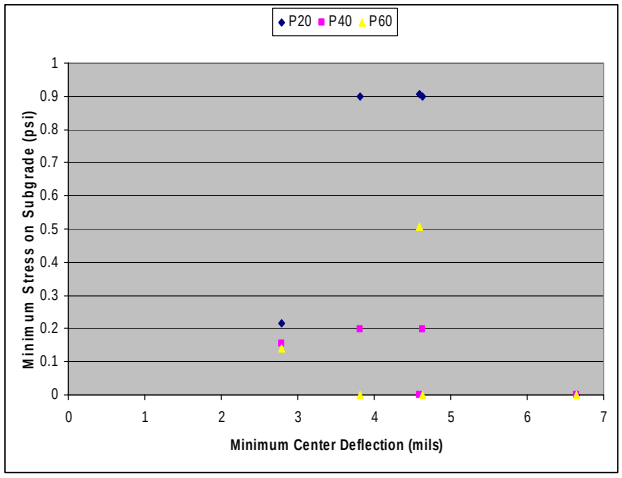

(d) Section 4

Figure B-11 Minimum Stress on Subgrade and Center Deflection

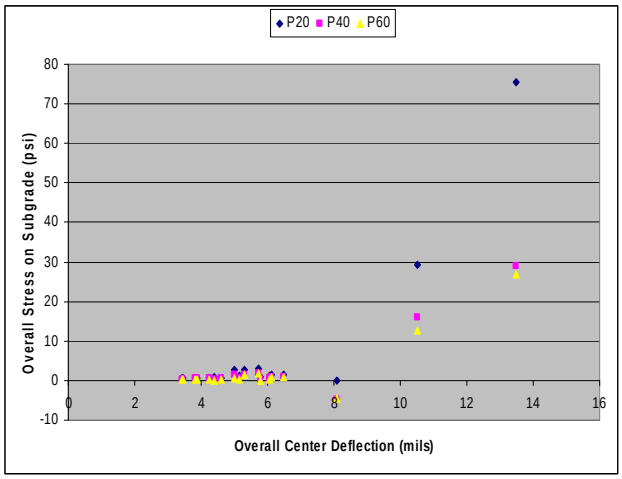

(a) Section 1

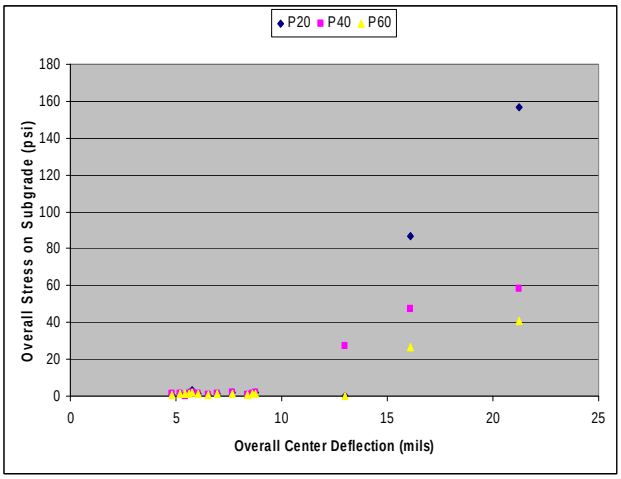

(b) Section 2

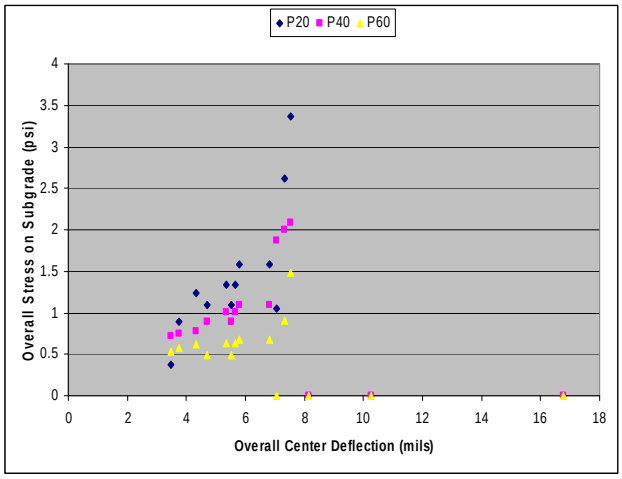

(c) Section 3

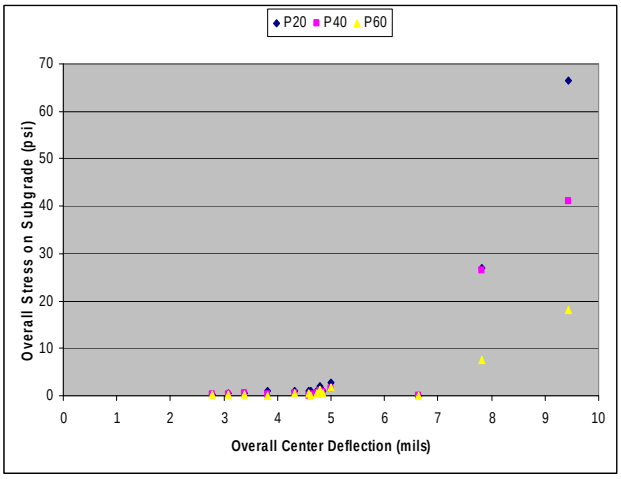

(d) Section 4

Figure B-12 Overall Stress on Subgrade and Center Deflection

Significant-Difference Test

Strain

Longitudinal Strain

Table B-1 Significant-Difference Test for Longitudinal Strain at Various Speeds

			Average		Maximum		Minimum		Overall	
			P-value	**Similar**	**P-value**	**Similar**	**P-value**	**Similar**	**P-value**	**Similar**
1	L20	L40	0.1127	Yes	0.1683	Yes	0.9192	Yes	0.0708	Yes
		L60	0.0417	No	0.0048	No	0.6852	Yes	0.0022	No
	L40	L60	0.6547	Yes	0.5926	Yes	0.5494	Yes	0.3655	Yes
2	L20	L40	0.3656	Yes	0.6978	Yes	0.1018	Yes	0.1761	Yes
		L60	0.2175	Yes	0.3148	Yes	0.0705	Yes	0.0274	No
	L40	L60	0.0425	No	0.0175	No	0.0177	No	0.0006	No
3	L20	L40	NA	NA	0.5785	Yes	0.7382	Yes	0.2592	Yes
		L60	NA	NA	0.4874	Yes	0.454	Yes	0.1432	Yes
	L40	L60	0.0326	No	0.2228	Yes	0.1836	Yes	0.0127	No
4	L20	L40	0.0183	No	0.0275	No	0.1188	Yes	0.0002	No
		L60	0.0247	No	0.0176	No	0.0925	Yes	<.0001	No
	L40	L60	0.1016	Yes	0.0578	yes	0.9517	Yes	0.0141	No
Over	L20	L40	0.0032	No	0.0373	No	0.0629	Yes	0.0001	No
		L60	0.0021	No	0.001	No	0.0138	No	<.0001	No
	L40	L60	0.2872	Yes	0.0479	No	0.0738	Yes	0.0025	No

Transverse Strain

Table B-2 Significant-Difference Test for Transverse Strain at Various Speeds

			Average		Maximum		Minimum		Overall	
			P-value	**Similar**	**P-value**	**Similar**	**P-value**	**Similar**	**P-value**	**Similar**
1	T20	T40	0.0337	No	0.0409	No	0.4278	Yes	0.0144	No
		T60	0.231	Yes	0.0447	No	0.9488	Yes	0.034	No
	T40	T60	0.5516	Yes	0.5242	Yes	0.6629	Yes	0.5108	Yes
2	T20	T40	0.2559	Yes	0.3777	Yes	0.7707	Yes	0.3056	Yes
		T60	0.3357	Yes	0.3698	Yes	0.4998	Yes	0.2808	Yes
	T40	T60	0.6508	Yes	0.1079	Yes	0.7023	Yes	0.2896	Yes
3	T20	T40	NA	NA	0.8549	Yes	0.185	Yes	0.7875	Yes
		T60	NA	NA	0.7427	Yes	0.2028	Yes	0.6202	Yes
	T40	T60	0.0945	Yes	0.1871	Yes	0.2962	Yes	0.0189	No
4	T20	T40	0.0246	No	0.0357	No	0.2766	Yes	0.001	No
		T60	0.0096	No	0.0201	No	0.0307	No	<.0001	No
	T40	T60	0.2339	Yes	0.0175	No	0.3886	Yes	0.0092	No
Over	T20	T40	0.0117	No	0.261	Yes	0.9937	Yes	0.1837	Yes
		T60	0.0923	Yes	0.2502	Yes	0.1458	Yes	0.1549	Yes
	T40	T60	0.7195	Yes	0.2005	Yes	0.4376	Yes	0.1363	Yes

Stress on Subgrade

Table B-3 Significant-Difference Test for Stress on Subgrade at Various Speeds

			Average		Maximum		Minimum		Overall	
			P-value	**Similar**	**P-value**	**Similar**	**P-value**	**Similar**	**P-value**	**Similar**
1	P20	P40	0.2575	Yes	0.3314	Yes	0.123	Yes	0.1334	Yes
		P60	0.2558	Yes	0.327	Yes	0.0757	Yes	0.1175	Yes
	P40	P60	0.2514	Yes	0.2484	Yes	0.2441	Yes	0.0463	No
2	P20	P40	0.3626	Yes	0.3653	Yes	0.3903	Yes	0.3134	Yes
		P60	0.364	Yes	0.3617	Yes	0.5062	Yes	0.1775	Yes
	P40	P60	0.3667	Yes	0.3416	Yes	0.3992	Yes	0.0887	Yes
3	P20	P40	0.0365	No	0.0576	Yes	0.4847	Yes	0.0834	Yes
		P60	0.0626	Yes	0.0467	No	0.1316	Yes	0.0006	No
	P40	P60	0.0862	Yes	0.0401	No	0.1638	Yes	0.0037	No
4	P20	P40	0.0435	No	0.3329	Yes	0.0625	Yes	0.2171	Yes
		P60	0.3219	Yes	0.3508	Yes	0.079	Yes	0.1628	Yes
	P40	P60	0.3825	Yes	0.3718	Yes	0.8842	Yes	0.1698	Yes
Over	P20	P40	0.1516	Yes	0.1101	Yes	0.5578	Yes	0.068	Yes
		P60	0.1558	Yes	0.0948	Yes	0.0164	No	0.0202	No
	P40	P60	0.327	Yes	0.1145	Yes	0.2854	Yes	0.0118	No

Linear Regression

Strain

Longitudinal Strain

Table B-4 Linear Regression for Longitudinal Strain at 20 kmh

Data	Section	Model	R^2	N
Average	1	$L_{20} = 27.92229 - 2.1156 d_0 + 0.09935 L_{60}$	0.55	6
	2	$L_{20} = 56.86189 - 0.53308 T_{pav}$	0.30	5
	3	$L_{20} = NA$		
	4	$L_{20} = NA$		
	Overall	$L_{20} = NA$		
Maximum	1	$L_{20} = NA$		
	2	$L_{20} = 909.95627 - 9.03123 S - 3.30017 T_{pav}$	1.00	5
	3	$L_{20} = NA$		
	4	$L_{20} = -6.39546 d_0 + 0.87612 T_{pav}$	0.99	5
	Overall	$L_{20} = 30.40266 - 1.28244 d_0$	0.13	20
Minimum	1	$L_{20} = NA$		
	2	$L_{20} = NA$		
	3	$L_{20} = 49.50780 + 6.42828\ d_0 - 1.31722\ T_{pav}$	1.00	4
	4	$L_{20} = NA$		
	Overall	$L_{20} = 0.63882 D$	0.47	20
Overall	1	$L_{20} = NA$		
	2	$L_{20} = NA$		
	3	$L_{20} = 8.84616 P_{20}$	0.71	9
	4	$L_{20} = 29.55241 - 2.74389 d_0$	0.22	15
	Overall	$L_{20} = NA$		

Table B-5 Linear Regression for Longitudinal Strain at 40 kmh

Data	Section	Model	R^2	N
Average	1	$L_{40} = NA$		
	2	$L_{40} = NA$		
	3	$L_{40} = NA$		
	4	$L_{40} = NA$		
	Overall	$L_{40} = 40.63882 - 1.02894 d_0 - 1.72678 D$	0.22	17
Maximum	1	$L_{40} = NA$		
	2	$L_{40} = 187.72630 - 1.95324 d_0 - 1.99556 S$	0.92	5
	3	$L_{40} = NA$		
	4	$L_{40} = -3.44360\ d_0 + 0.48252\ T_{pav}$	0.96	5
	Overall	$L_{40} = NA$		
Minimum	1	$L_{40} = NA$		
	2	$L_{40} = NA$		
	3	$L_{40} = 15.75248 + 2.04536 d_0 - 0.41911 T_{pav}$	1.00	4
	4	$L_{40} = NA$		
	Overall	$L_{40} = NA$		
Overall	1	$L_{40} = NA$		
	2	$L_{40} = NA$		
	3	$L_{40} = 3.98163 P_{20}$	0.70	9
	4	$L_{40} = 15.03903 - 1.38842 d_0$	0.19	15
	Overall	$L_{40} = NA$		

Table B-6 Linear Regression for Longitudinal Strain at 60 kmh

Data	Section	Model	R^2	N
Average	1	$L_{60} = NA$		
	2	$L_{60} = NA$		
	3	$L_{60} = NA$		
	4	$L_{60} = NA$		
	Overall	$L_{60} = 33.24510 - 0.93351 d_0 - 1.39081 D$	0.45	17
Maximum	1	$L_{60} = NA$		
	2	$L_{60} = 128.79748 - 1.32386 d_0 - 1.36858 S$	0.92	5
	3	$L_{60} = NA$		
	4	$L_{60} = 4.94674 - 2.69341 d_0 + 0.30004 T_{pav}$	0.99	5
	Overall	$L_{60} = 15.33036 - 0.68285\, d_0$	0.19	20
Minimum	1	$L_{60} = NA$		
	2	$L_{60} = NA$		
	3	$L_{60} = NA$		
	4	$L_{60} = NA$		
	Overall	$L_{60} = 0.25264 D$	0.54	20
Overall	1	$L_{60} = NA$		
	2	$L_{60} = NA$		
	3	$L_{60} = -9.11804 + 0.59899 d_0 + 5.26991 P_{20}$	0.82	9
	4	$L_{60} = 12.43855 - 1.16978 d_0$	0.23	15
	Overall	$L_{60} = 9.96274 - 0.40455\, d_0$	0.06	57

Transverse Strain

Table B-7 Linear Regression for Transverse Strain at 20 kmh

Data	Section	Model	R^2	N
Average	1	$T_{20} = 5.40615 d_0$	0.94	6
	2	$T_{20} = -89.37848 + 18.75978 d_0$	0.95	5
	3	$T_{20} = NA$		
	4	$T_{20} = -21.94151 + 1.00976 T_{pav}$	0.96	5
	Overall	$T_{20} = -120.73843 + 15.03669 d_0 + 5.16575 D$	0.83	17
Maximum	1	$T_{20} = -11.81415 + 8.89663 d_0$	0.98	6
	2	$T_{20} = -6781.23245 + 104.71216 d_0 + 67.17803 S + 16.89621 T_{pav}$	1.00	5
	3	$T_{20} = NA$		
	4	$T_{20} = -45.35451 + 5.69416 d_0 + 1.07450 T_{pav}$	0.97	5
	Overall	$T_{20} = -301.06469 + 54.08259 d_0$	0.51	20
Minimum	1	$T_{20} = 0.05613 S$	0.84	6
	2	$T_{20} = 47.71934 - 0.5871 T_{pav}$	0.76	5
	3	$T_{20} = NA$		
	4	$T_{20} = 19.71226 - 2.93926 d_0 + 26.14203 P_{20}$	1.00	5
	Overall	$T_{20} = 2.05997 d_0 - 0.212 T_{pav}$	0.61	20
Overall	1	$T_{20} = -20.79114 + 8.34756 d_0$	0.65	18
	2	$T_{20} = -450.6672 + 68.40332 d_0$	0.65	15
	3	$T_{20} = -29.48058 + 1.94031 d_0 + 17.13136 P_{20}$	0.83	9
	4	$T_{20} = 7.72353 d_0$	0.85	15
	Overall	$T_{20} = -184.46426 + 36.3576 d_0$	0.39	57

Table B-8 Linear Regression for Transverse Strain at 40 kmh

Data	Section	Model	R^2	N
Average	1	$T_{40} = 3.39435 d_0$	0.88	6
	2	$T_{40} = -35.04109 + 9.31387 d_0$	0.97	5
	3	$T_{40} = NA$		
	4	$T_{40} = 5.19724 d_0$	0.99	5
	Overall	$T_{40} = -18.65720 + 7.28622 d_0$	0.81	17
Maximum	1	$T_{40} = 4.05196 d_0$	0.89	6
	2	$T_{40} = -53.25293 + 5.58531 d_0 + 0.95582 T_{pav}$	0.99	5
	3	$T_{40} = NA$		
	4	$T_{40} = -14.22412 + 4.34267 D_0 + 0.42777 Watson$	0.97	5
	Overall	$T_{40} = -32.03934 + 3.99357 d_0 + 0.49116 T_{pav}$	0.50	20
Minimum	1	$T_{40} = NA$		
	2	$T_{40} = -55.16718 + 9.532 d_0$	0.79	5
	3	$T_{40} = 11.81436 + 1.53402 d_0 - 0.31434 T_{pav}$	1.00	4
	4	$T_{40} = NA$		
	Overall	$T_{40} = -53.13054 + 6.17419 d_0 + 2.17290 D$	0.53	20
Overall	1	$T_{40} = 3.29490 d_0$	0.82	18
	2	$T_{40} = -30.37098 + 8.34763 d_0$	0.82	15
	3	$T_{40} = -17.23042 + 1.15524 d_0 + 10.44526 P_{20}$	0.82	9
	4	$T_{40} = 5.08798 d_0$	0.89	15
	Overall	$T_{40} = -31.85808 + 4.93545 d_0 + 0.31557 T_{pav}$	0.54	57

Table B-9 Linear Regression for Transverse Strain at 60 kmh

Data	Section	Model	R^2	N
Average	1	$T_{60} = 3.76471 d_0$	0.99	6
	2	$T_{60} = 4.87083 d_0$	0.98	5
	3	$T_{60} = NA$		
	4	$T_{60} = 0.32987 T_{pav}$	1.00	5
	Overall	$T_{60} = 4.25748\, d_0$	0.95	17
Maximum	1	$T_{60} = 4.51376\, d_0$	0.98	6
	2	$T_{60} = 5.43313 d_0$	0.98	5
	3	$T_{60} = NA$		
	4	$T_{60} = 2.56502 d_0 + 0.22817 T_{pav}$	0.99	5
	Overall	$T_{60} = 3.89307 d_0$	0.75	20
Minimum	1	$T_{60} = NA$		
	2	$T_{60} = NA$		
	3	$T_{60} = 8.43883 + 1.09573 d_0 - 0.22453 T_{pav}$	1.00	4
	4	$T_{60} = 16.17286 - 0.22297 T_{pav} + 7.57152 P_{20}$	0.99	5
	Overall	$T_{60} = NA$		
Overall	1	$T_{60} = 3.58067 d_0$	0.87	18
	2	$T_{60} = 4.22887 d_0$	0.82	15
	3	$T_{60} = -16.06440 + 1.07185 d_0 + 9.62920 P_{20}$	0.82	9
	4	$T_{60} = 3.65475 d_0$	0.81	15
	Overall	$T_{60} = 3.27945 d_0$	0.69	57

RSL Models

Quadratic Regression

Table B-10 District-Wise Quadratic RSL Models

Dist.	Model	R^2	N
1	$RSL = 8.562 - 0.201d_0 + 0.0003d_0 \times d_0 - 0.186D + 0.0144d_0 \times D$ $- 0.964ETCR - 4.443Rut$	0.11	1321
2	$ETCR = 6.664 + 0.0314d_0 - 0.001d_0 \times d_0 - 0.049D + 0.0066d_0 \times D$ $- 2.549ETCR + 0.455ETCR \times ETCR - 0.111EFCR + 0.0034EFCR \times EFCR$ $+ 0.051ETCR \times EFCR - 3.255Rut$	0.20	1354
3	$ETCR = 8.655 - 0.249d_0 - 0.003d_0 \times d_0 + 0.081D - 0.02D \times D + 0.016d_0 \times D$ $- 1.858ETCR + 0.326ETCR \times ETCR - 0.201EFCR + 0.007EFCR \times EFCR$ $- 8.224Rut + 7.214Rut \times Rut$	0.20	1624
4	$RSL = 8.468 - 0.158d_0 - 0.269D - 0.017D \times D + 0.017d_0 \times D$ $- 4.559ETCR + 1.586ETCR \times ETCR - 15.172.224Rut + 13.689Rut \times Rut$	0.26	1164
5	$RSL = 7.667 - 0.0613d_0 - 0.125D + 0.009D \times D - 1.556ETCR$ $- 0.756ETCR \times ETCR - 0.141EFCR + 0.0067EFCR \times EFCR$ $- 11.943Rut + 19.035Rut \times Rut$	0.09	1509
6	$RSL = 7.348 - 0.0715d_0 + 0.098D - 0.016D \times D + 0.0076d_0 \times D - 0.258ETCR$ $- 0.076EFCR - 14.956Rut + 25.934Rut \times Rut$	0.11	1455

Sigmoidal RSL Model with Linear Sub-Models without Cracking Data

Road Category-Wise

Table B-11 FDBIT Sigmoidal RSL Model with No Cracking Data

RC		0	1(D)	2(EAL)	3(Rut)	4(SNeff)	R^2	N
12	δ	7.878	-0.208	-0.050	-9.115	0.874	0.98	46
	α	-10.249	0.842	0.067	-1.591	0.110		
	β	647.700	-15.703	-17.346	-2697.00	-51.228		
	γ	36.872	-0.830	-1.155	-187.300	-0.975		
13	δ	6.537	-0.727	0.044	6.330	0.311	0.97	79
	α	-8.343	1.739	-0.091	6.303	0.101		
	β	706.895	-15.554	-4.471	-118.307	-157.178		
	γ	75.333	-1.401	-0.301	-33.260	-18.939		
14	δ	18.254	-0.267	-0.094	-64.003	0.251	0.91	115
	α	-15.963	-0.206	0.072	99.084	0.120		
	β	-28.060	1.001	0.330	-51.110	1.982		
	γ	-1.400	0.016	0.027	-3.755	-0.002		
15	δ	27.499	-1.241	0.481	-54.667	-1.369	0.80	109
	α	-14.333	0.862	-0.635	36.975	-0.149		
	β	11.672	-0.202	-0.044	-6.439	-2.042		
	γ	2.442	-0.091	-0.014	-0.506	-0.326		
16	δ	-654.434	13.170	6.455	-2073.282	65.714	0.49	447
	α	663.408	-13.404	-6.428	2057.395	-65.527		
	β	-8.200	-0.118	0.088	-36.823	0.154		
	γ	0.132	-0.003	0.004	-1.612	-0.138		
17	δ	2.650	0.082	0.002	0.776	0.142	0.09	2425
	α	11.207	-1.014	-0.008	-10.840	1.506		
	β	-4.197	0.369	0.009	0.638	0.754		
	γ	-0.352	0.051	0.001	0.160	-0.018		

Table B-12 PDBIT Sigmoidal RSL Model with No Cracking Data

		0	1(D)	2(EAL)	3(Rut)	4(SNeff)	R^2	N
18	δ	62.875	-0.880	-1.689	379.800	-7.026	0.23	1200
	α	-61.654	1.303	1.642	-372.100	6.394		
	β	-4.634	0.050	0.117	-18.366	0.733		
	γ	-0.112	0.013	0.002	0.197	0.021		
19	δ	3.774	0.405	0.019	-21.980	-0.665	0.34	931
	α	2.479	-0.815	-0.101	16.722	2.819		
	β	-43.682	-4.781	0.046	70.756	16.740		
	γ	-2.580	-0.516	0.019	12.824	0.777		
20	δ	14.307	0.295	0.166	-57.110	-6.032	0.54	542
	α	-10.680	0.137	-0.185	50.986	6.060		
	β	13.612	0.578	0.088	-11.272	-8.639		
	γ	1.647	0.050	0.009	0.686	-0.946		
21	δ	1.997	1.333	0.099	5.383	-2.334	0.67	281
	α	11.658	-4.505	-0.522	-32.697	8.248		
	β	-5.902	0.649	0.161	-13.100	0.481		
	γ	-0.475	0.058	0.008	-0.717	0.032		
22	δ	-8.614	0.131	0.215	18.253	0.606	0.42	455
	α	15.426	-0.232	-0.286	-34.114	0.607		
	β	-28.026	0.632	0.092	27.825	5.759		
	γ	-1.893	0.073	0.005	2.214	0.364		
23	δ	2.160	0.440	0.007	5.423	-0.177	0.29	951
	α	2.653	-0.491	-0.015	-9.063	0.476		
	β	7.449	-3.081	0.081	-93.072	0.630		
	γ	-0.922	0.169	-0.001	-3.774	0.016		

Model Plots

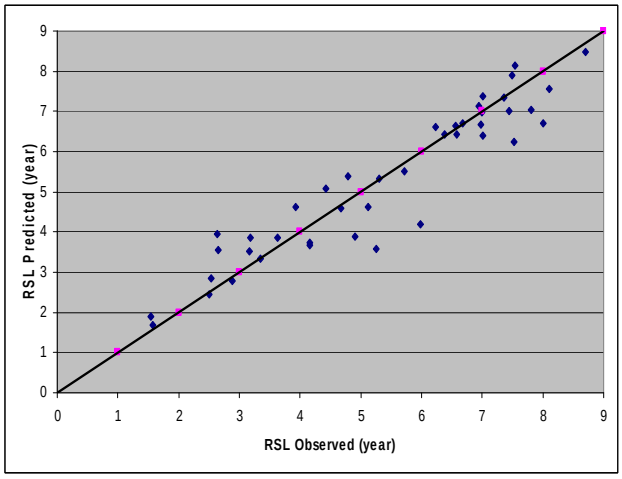

(a) Road Category 12

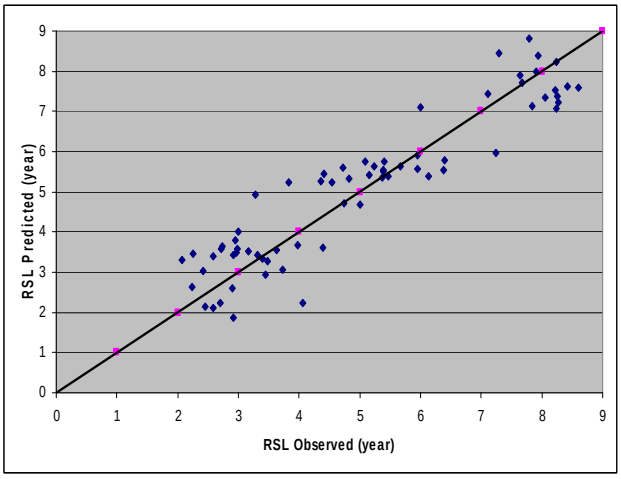

(b) Road Category 13

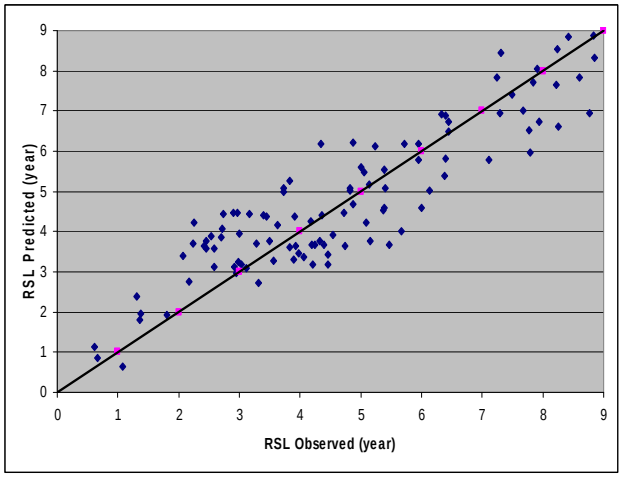

(c) Road Category 14

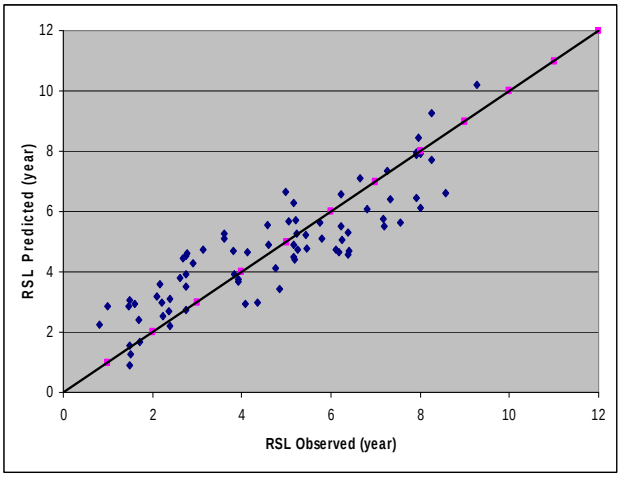

(d) Road Category 15

Figure B-13 Sigmoidal RSL Model with No Cracking Data for Road Categories 12 to 15

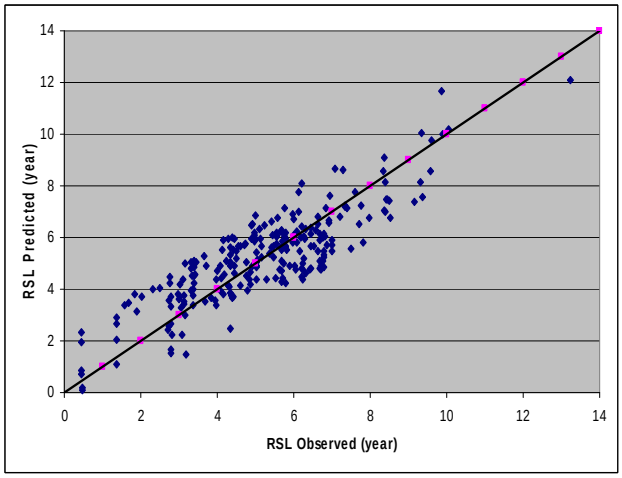

(a) Road Category 16

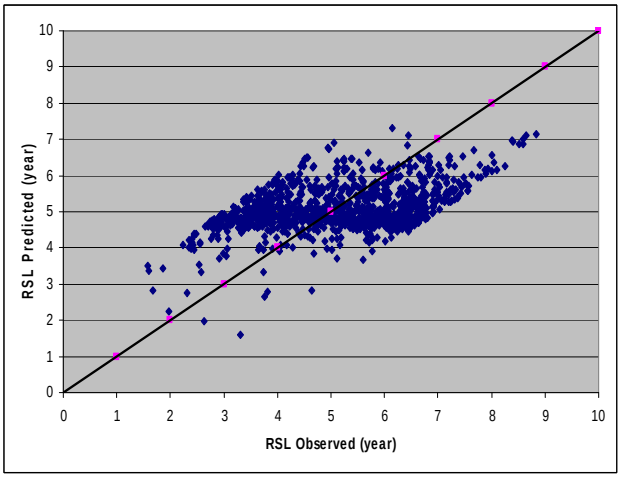

(b) Road Category 17

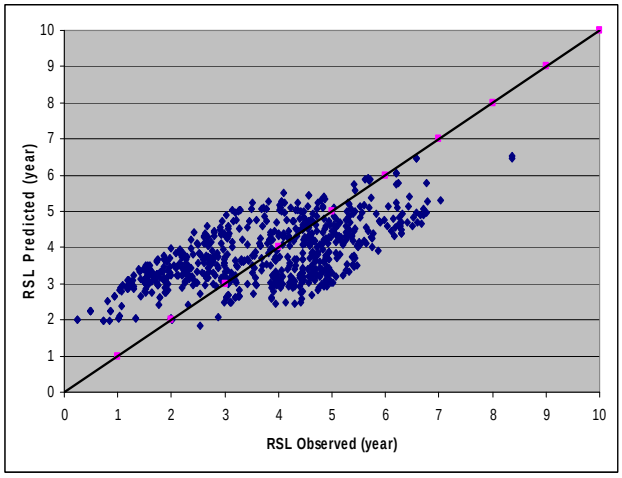

(c) Road Category 18

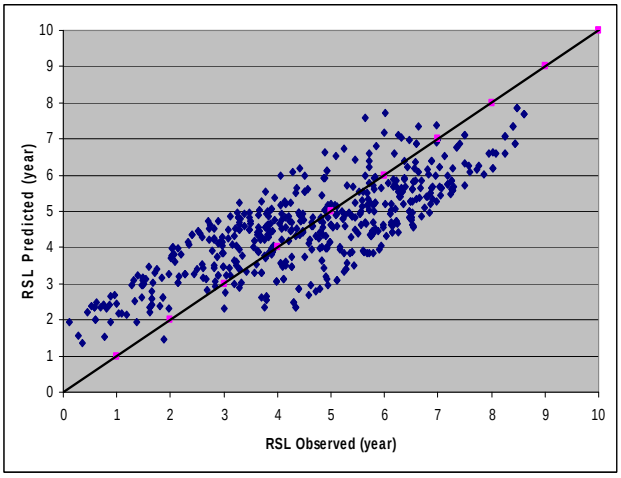

(d) Road Category 19

Figure B-14 Sigmoidal RSL Model with No Cracking for Road Categories 16 to 19

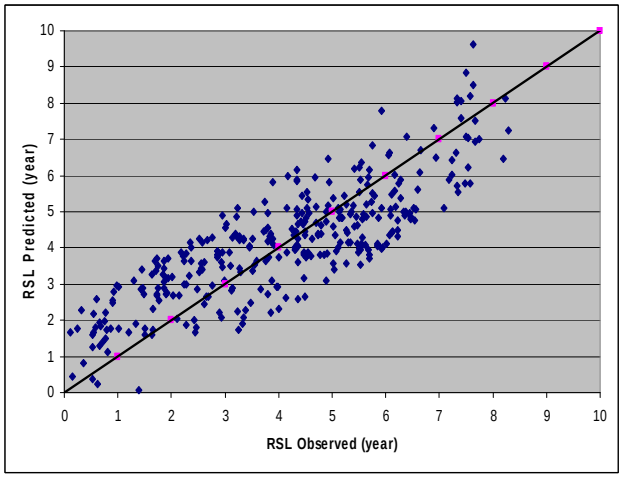

(a) Road Category 20

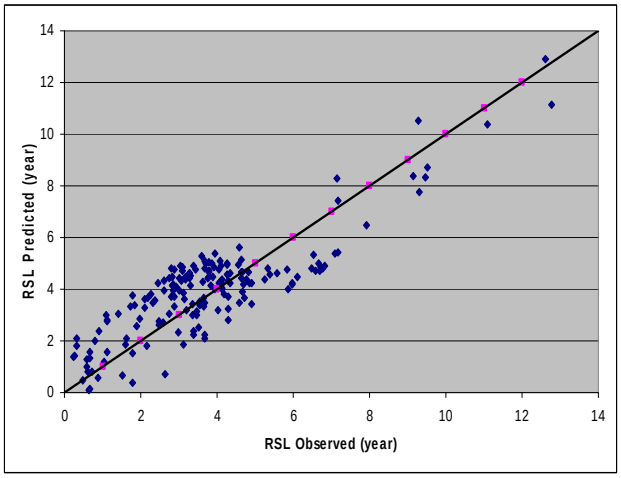

(b) Road Category 21

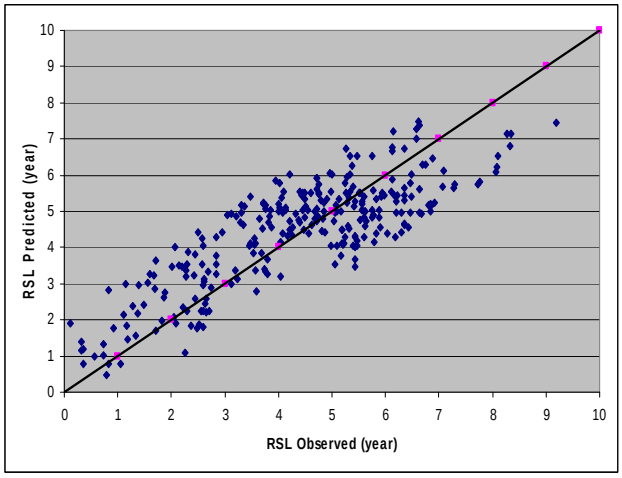

(c) Road Category 22

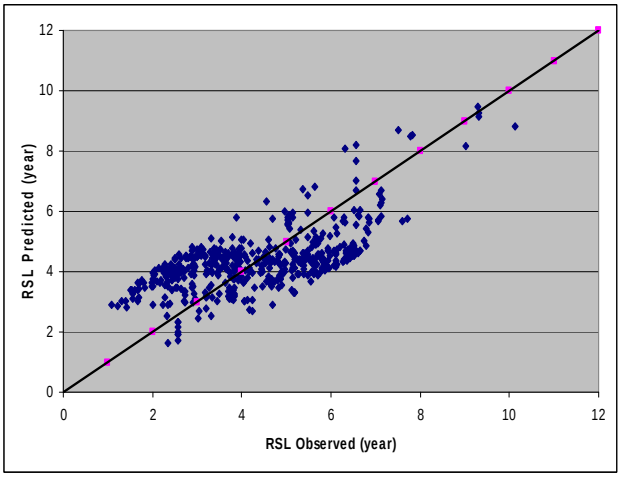

(d) Road Category 23

Figure B-15 Sigmoidal RSL Model with No Cracking for Road Categories 20 to 23

Validation Plots

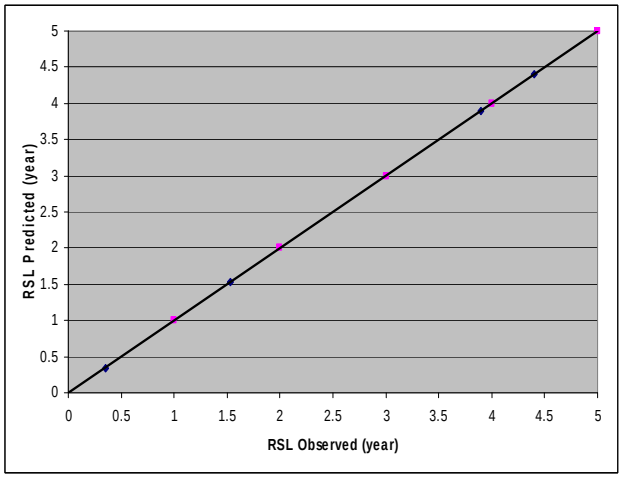

(a) Road Category 12

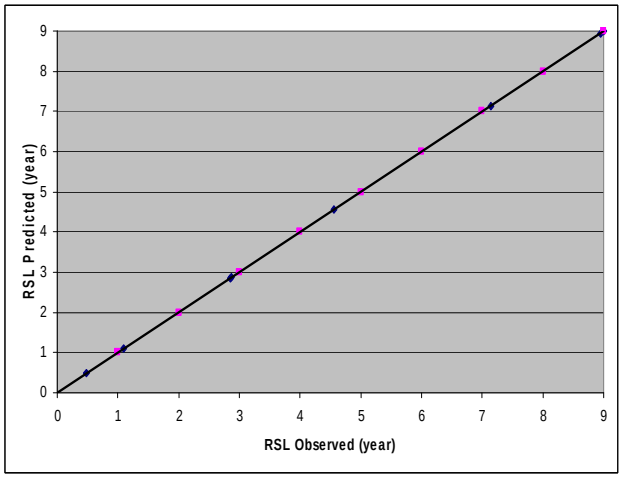

(b) Road Category 13

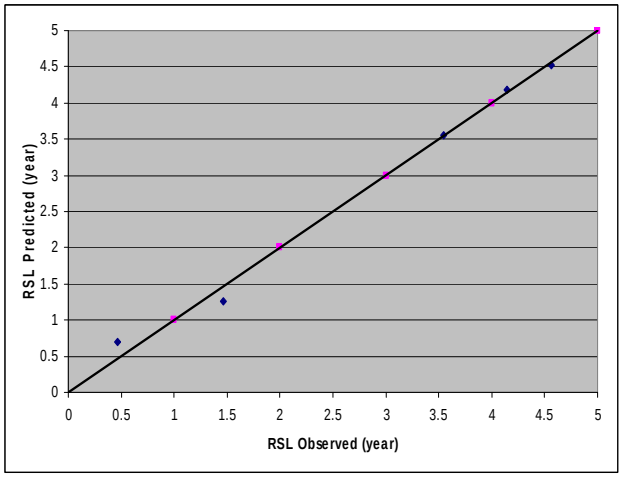

(c) Road Category 14

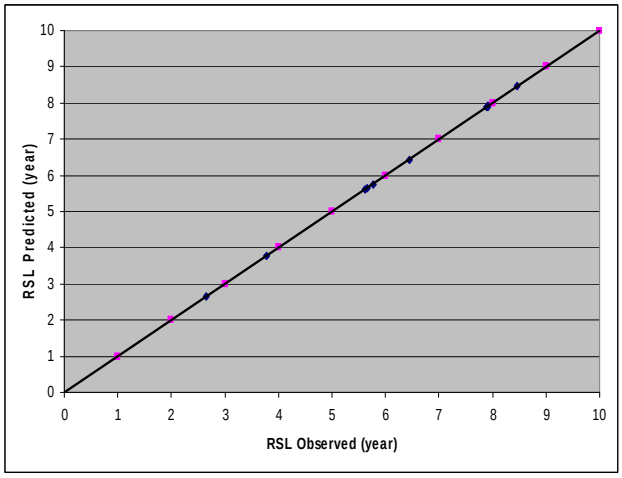

(d) Road Category 15

Figure B-16 Sigmoidal RSL Model with No Cracking Valid. for Road Categories 12 to 15

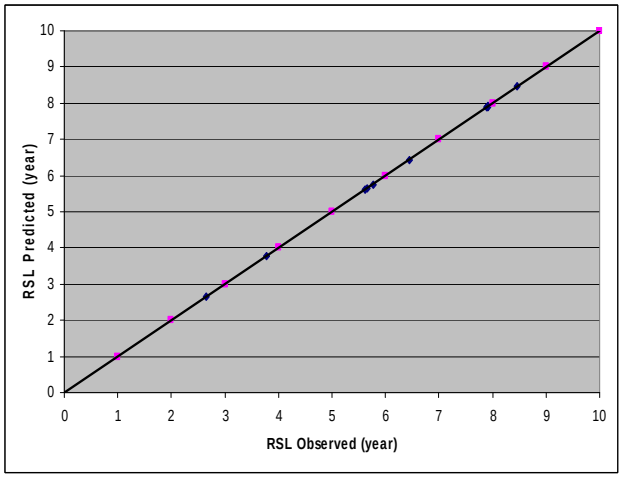

(a) Road Category 16

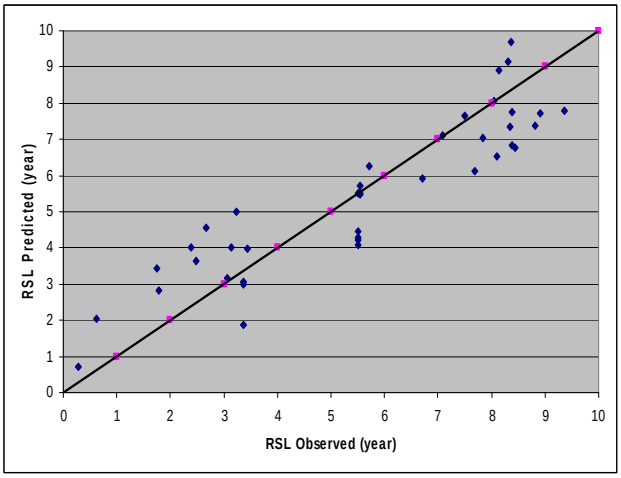

(b) Road Category 17

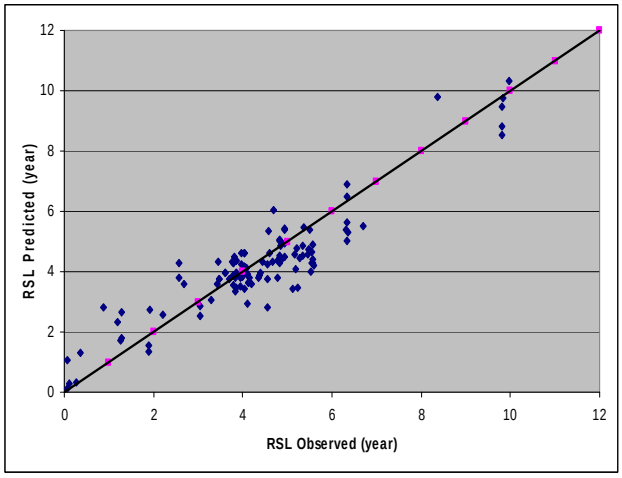

(c) Road Category 18

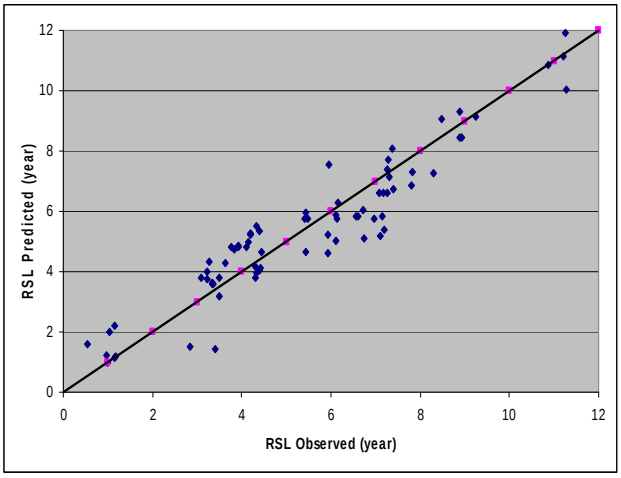

(d) Road Category 19

Figure B-17 Sigmoidal RSL Model with No Cracking Valid. for Road Categories 16 to 19

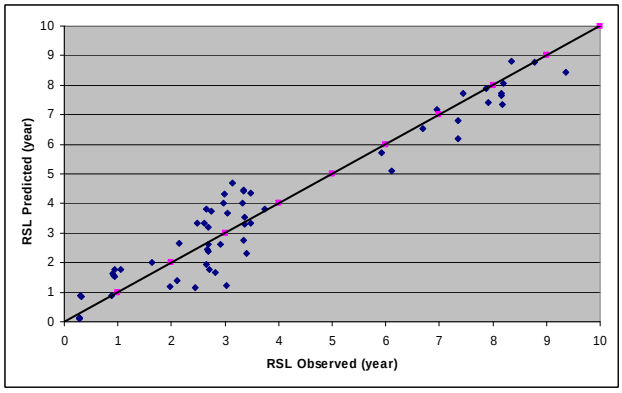

(a) Road Category 20

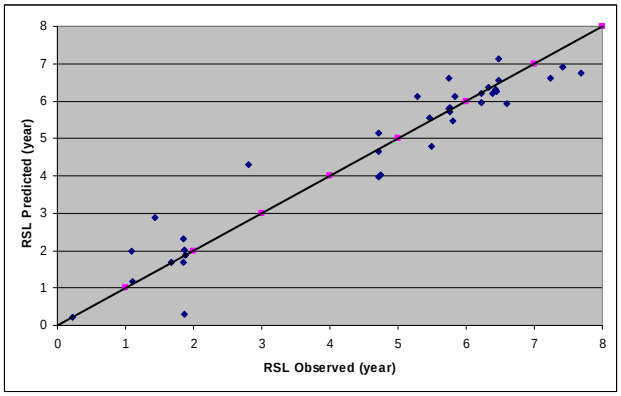

(b) Road Category 21

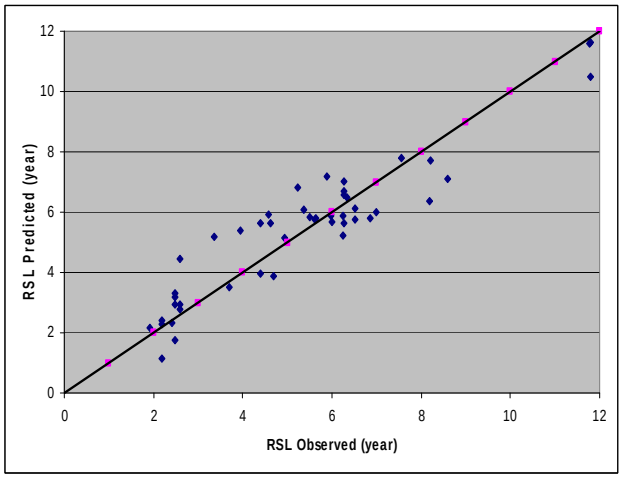

(c) Road Category 22

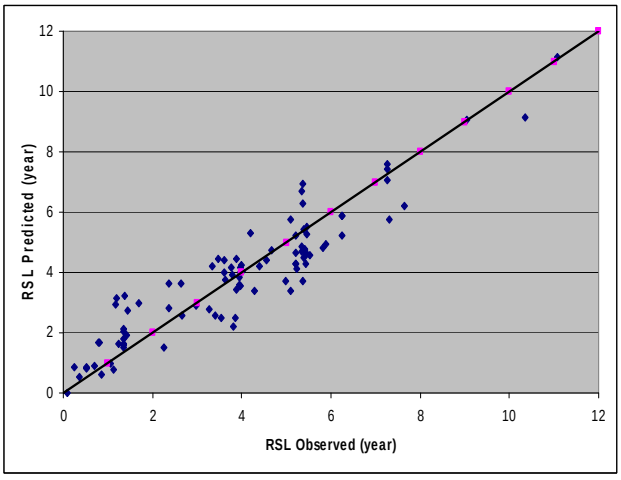

(d) Road Category 23

Figure B-18 Sigmoidal RSL Model with No Cracking Valid. for Road Categories 20 to 23

District-Wise and Statewide

Table B-13 District-Wise and Statewide Sigmoidal RSL Model with No Cracking Data

District		**0**	**1(D)**	**2(EAL)**	**3(Rut)**	**4(SNeff)**	**R^2**	**N**
1	δ	-0.927	1.597	-0.032	94.934	-0.518	0.19	1235
	α	5.549	-1.510	0.031	-98.280	0.436		
	β	170.401	-26.704	-3.392	301.316	-12.222		
	γ	12.937	-1.617	-0.064	40.864	-2.294		
2	δ	2.466	0.169	0.079	5.741	-7.440	0.28	1220
	α	7.385	-0.424	-0.086	-11.903	7.384		
	β	0.504	-0.251	-0.007	3.010	-0.243		
	γ	-0.010	-0.011	0.000	0.100	0.032		
3	δ	-0.371	-0.330	0.041	2.449	2.474	0.34	1404
	α	7.051	0.242	-0.016	-14.961	-3.217		
	β	1.198	3.683	-0.101	-40.602	-3.383		
	γ	-0.560	0.135	-0.003	-4.202	0.359		
4	δ	1.573	0.363	0.000	-2.209	0.339	0.35	1007
	α	-5.355	0.475	-0.005	41.235	1.569		
	β	-105.053	15.231	-0.015	174.837	18.551		
	γ	-2.919	0.471	0.002	-3.731	0.989		
5	δ	1.709	0.085	0.100	0.856	0.345	0.23	1385
	α	2.756	-0.099	-0.093	-2.872	-0.571		
	β	14.785	-1.319	-0.093	21.182	-1.701		
	γ	1.467	-0.146	0.004	2.847	-0.351		
6	δ	1.660	0.857	0.001	-3.766	0.529	0.23	1289
	α	0.892	-0.783	-0.003	2.635	-0.059		
	β	12.829	3.243	-0.083	44.475	-6.150		
	γ	-0.767	0.277	-0.007	3.610	0.193		
State	δ	5.208	-0.193	0.004	-5.789	0.692	0.10	7587
	α	-1.746	0.221	-0.003	4.110	-0.481		
	β	40.626	-0.879	-0.138	86.096	-7.445		
	γ	2.3333	-0.1639	-0.012	8.7703	-0.0853		

Model Plots

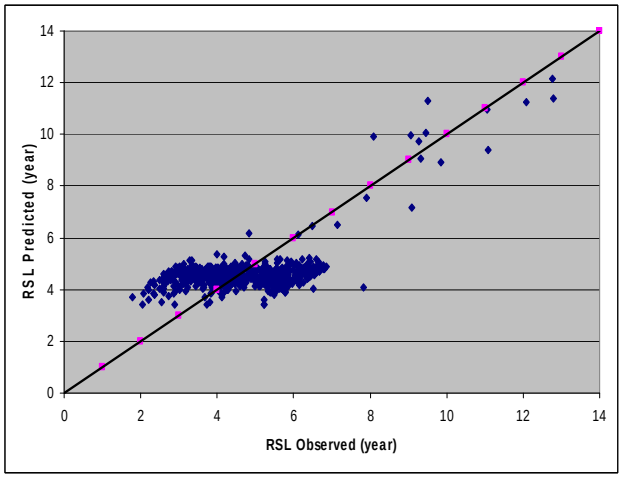

(a) District 1

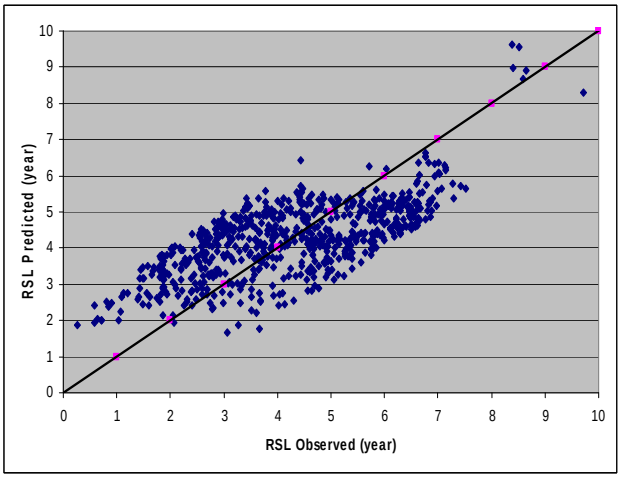

(b) District 2

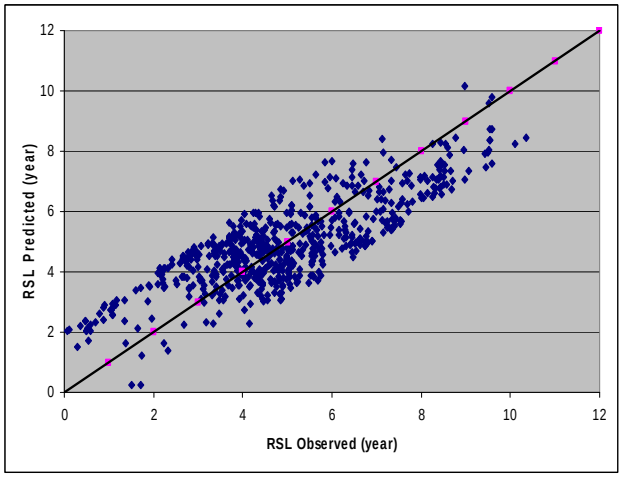

(c) District 3

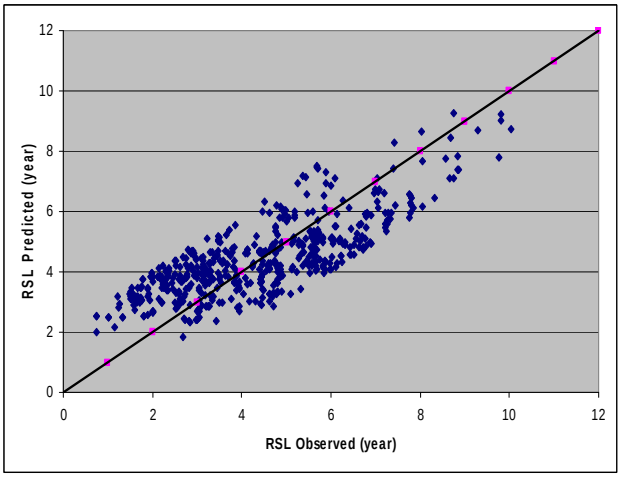

(d) District 4

Figure B-19 Sigmoidal RSL Model with No Cracking for Districts 1 to 4

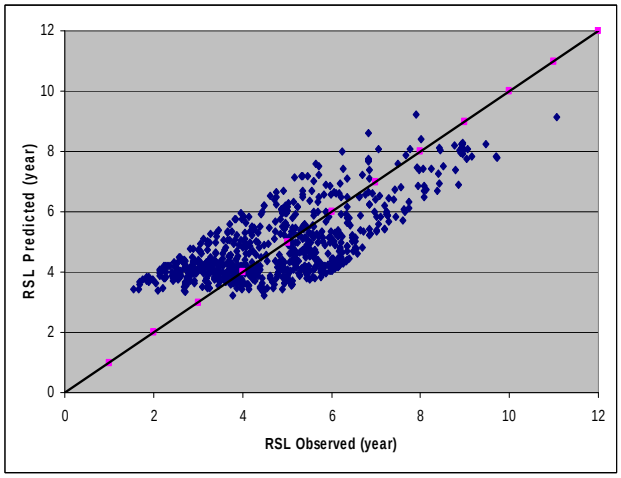

(a) District 5

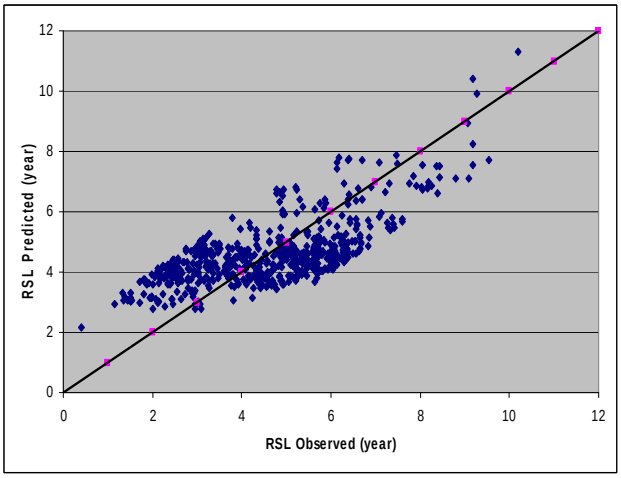

(b) District 6

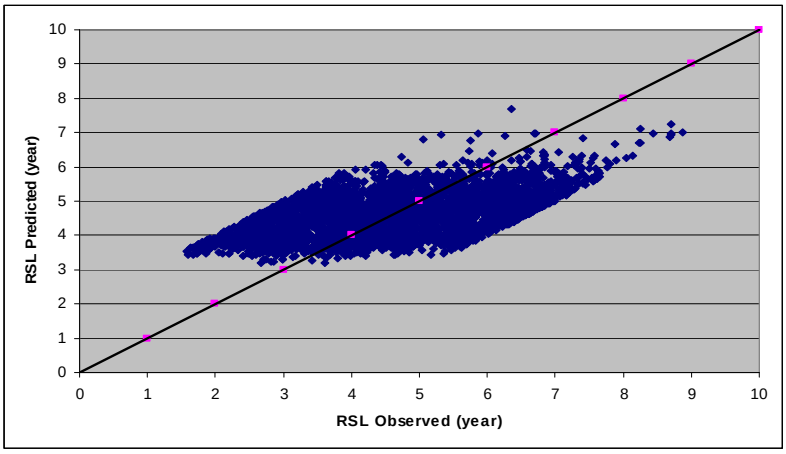

(c) State

Figure B-20 Sigmoidal RSL Model with No Cracking for Districts 5, 6, and State

Validation Plots

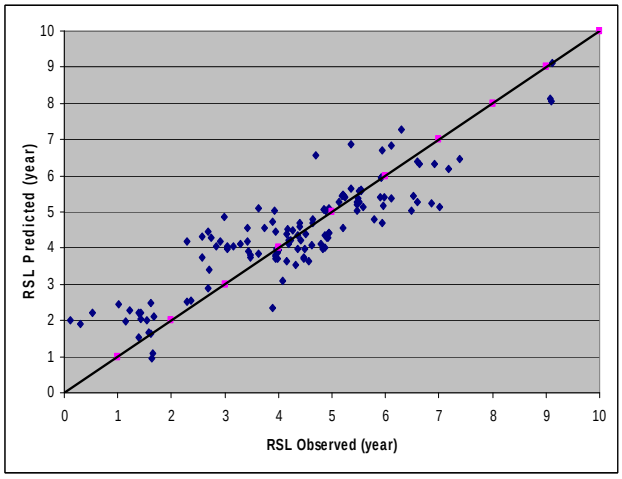

(a) District 1

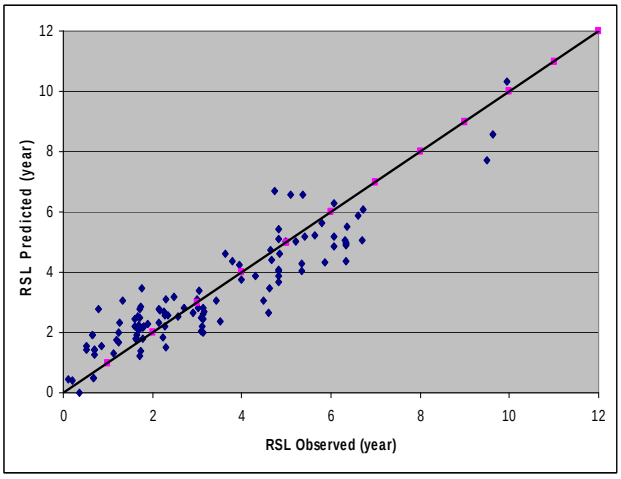

(b) District 2

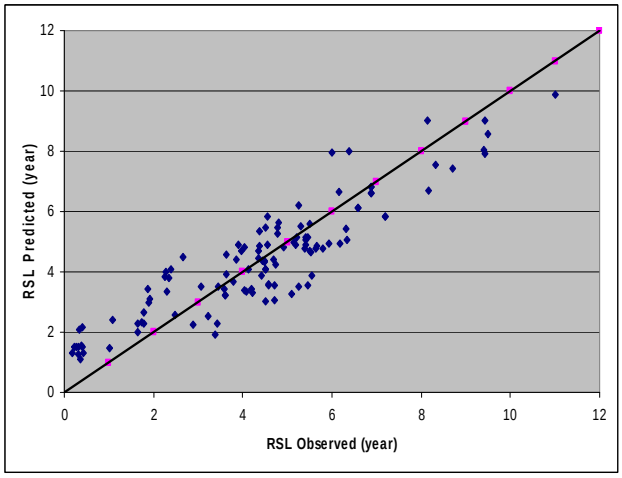

(c) District 3

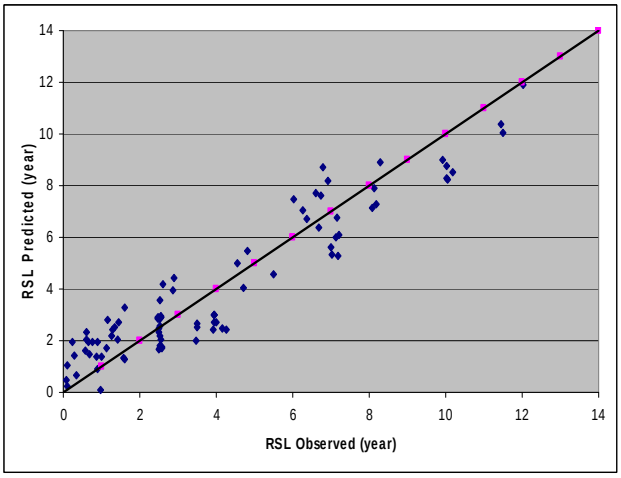

(d) District 4

Figure B-21 Sigmoidal RSL Model with No Cracking Validation for Districts 1 to 4

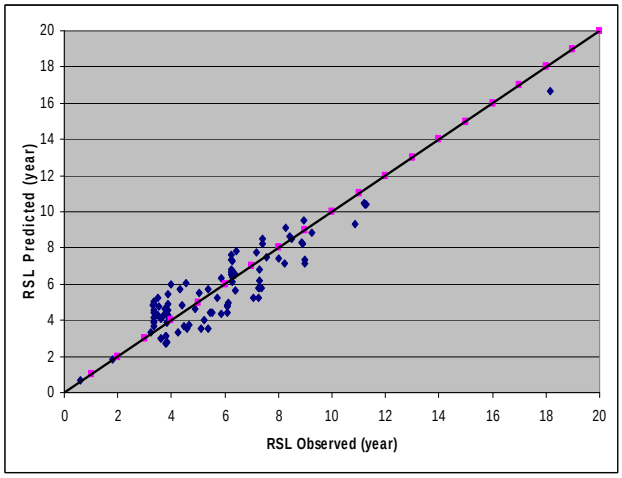

(a) District 5

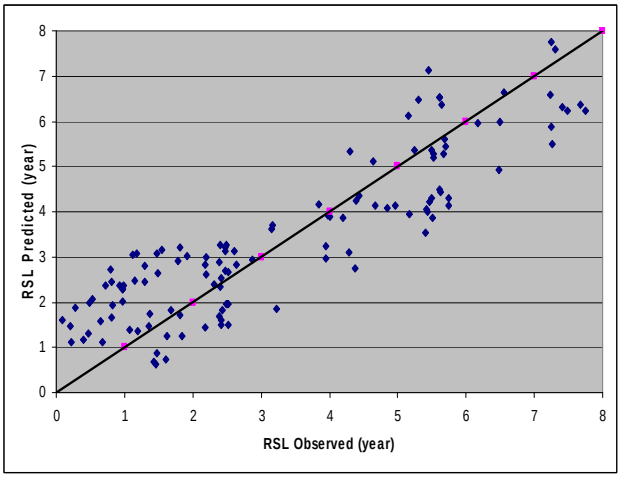

(b) District 6

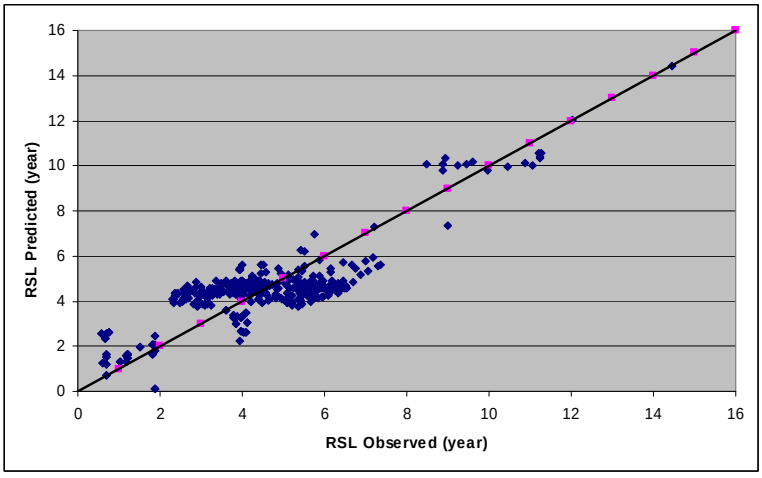

(c) State

Figure B-22 Sigmoidal RSL Model with No Cracking Valid. for Districts 5, 6, and State

Absolute Mean Deviation

Table B-14 Absolute Mean Deviation for Sigmoidal RSL Model with No Cracking Model

	Mean			Mean Absolute Deviation		
	Observed	**Predicted**	**Difference**	**Observed**	**Predicted**	**Difference**
(a) Road Category-Wise						
12	5.37	5.28	0.09	1.73	1.61	0.12
13	5.02	5.10	-0.08	1.74	1.58	0.16
14	4.70	4.79	-0.09	1.70	1.48	0.22
15	4.78	4.84	-0.06	1.98	1.49	0.48
16	5.20	5.28	-0.08	1.54	1.28	0.26
17	5.09	5.09	0.01	1.11	0.46	0.65
18	3.67	3.78	-0.11	1.26	0.71	0.56
19	4.57	4.55	0.02	1.53	1.01	0.53
20	4.11	4.16	-0.05	1.63	1.19	0.43
21	3.80	4.00	-0.20	1.54	1.25	0.29
22	4.38	4.46	-0.07	1.49	1.12	0.37
23	4.32	4.35	-0.03	1.33	0.68	0.66
(b) District-Wise and Statewide						
1	4.77	4.64	0.14	1.11	0.35	0.76
2	4.25	4.26	-0.01	1.36	0.78	0.58
3	4.91	4.90	0.01	1.50	1.10	0.40
4	4.31	4.40	-0.08	1.49	0.96	0.53
5	4.81	4.85	-0.05	1.31	0.93	0.38
6	4.54	4.56	-0.02	1.37	0.71	0.66
State	4.60	4.62	-0.02	1.14	0.52	0.62

ETCR Models

Sigmoidal ETCR Models with Linear Sub-Models without SNeff

Road Category-Wise

Table B-15 FDBIT Sigmoidal ETCR Model with No SNeff in Linear Sub-Models

RC		0	1(D)	2(EAL)	3(Rut)	R^2	N
12	δ	0.066	0.006	-0.002	0.458	0.89	36
	α	36.508	-4.984	-0.529	-1.273		
	β	554.821	13.022	-23.907	-2122.155		
	γ	35.593	0.809	-1.597	-130.348		
13	δ	-4.914	-0.069	0.248	-1.750	0.88	123
	α	4.952	0.063	-0.247	1.775		
	β	-15.157	-5.455	0.929	79.265		
	γ	-2.356	-0.414	0.126	4.576		
14	δ	0.180	0.001	-0.002	-0.178	0.51	240
	α	0.472	0.032	-0.006	3.327		
	β	34.245	-1.950	-0.308	-11.416		
	γ	1.153	-0.105	-0.010	0.819		
15	δ	1.017	0.052	-0.072	-0.916	0.87	63
	α	-1.073	0.306	0.073	1.298		
	β	15.413	1.274	-2.940	-129.727		
	γ	26.879	-5.765	-0.446	7.776		
16	δ	0.378	-0.056	0.006	-1.349	0.30	590
	α	0.680	0.005	-0.015	4.483		
	β	-10.476	-1.478	0.376	21.757		
	γ	-0.762	-0.053	0.020	1.007		
17	δ	0.925	-0.079	0.000	2.482	0.19	3729
	α	-1.229	0.137	-0.001	-3.002		
	β	-1.110	-0.114	0.002	1.163		
	γ	-0.025	-0.018	0.000	0.189		

Table B-16 PDBIT Sigmoidal ETCR Model with No SNeff in Linear Sub-Models

RC		0	1(D)	2(EAL)	3(Rut)	R^2	N
18	δ	0.262	0.079	-0.004	0.960	0.13	1910
	α	-0.233	-0.011	-0.003	-1.012		
	β	29.772	-8.949	0.527	-79.643		
	γ	0.333	-0.120	-0.012	-1.303		
19	δ	0.409	-0.002	-0.005	-0.161	0.15	1299
	α	-0.186	-0.027	0.004	7.640		
	β	-3.074	0.555	-0.483	163.500		
	γ	0.113	-0.023	-0.025	5.775		
20	δ	1.368	0.098	-0.012	1.465	0.25	785
	α	-1.093	-0.060	0.010	-1.589		
	β	-22.075	-24.600	0.559	-12.166		
	γ	-1.353	-0.939	0.032	-0.969		
21	δ	20.164	-1.183	-0.215	-24.594	0.62	411
	α	-19.576	1.184	0.203	24.411		
	β	4.078	-0.488	-0.286	-6.782		
	γ	0.989	-0.023	-0.036	-1.591		
22	δ	0.803	-0.008	-0.010	-0.404	0.55	655
	α	1.697	-0.398	0.089	-5.784		
	β	-112.971	-15.645	0.395	1385.910		
	γ	-23.737	-1.332	0.193	136.990		
23	δ	0.129	0.011	0.000	0.479	0.16	1605
	α	0.980	0.034	-0.003	1.083		
	β	27.371	2.541	-0.241	162.487		
	γ	-0.677	0.266	-0.007	5.914		

Model Plots

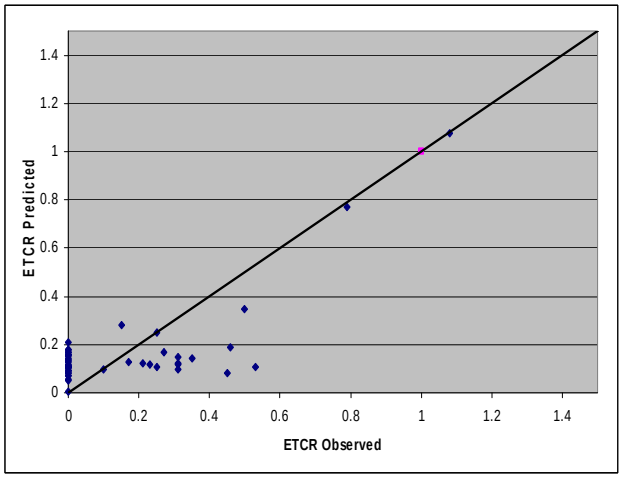

(a) Road Category 12

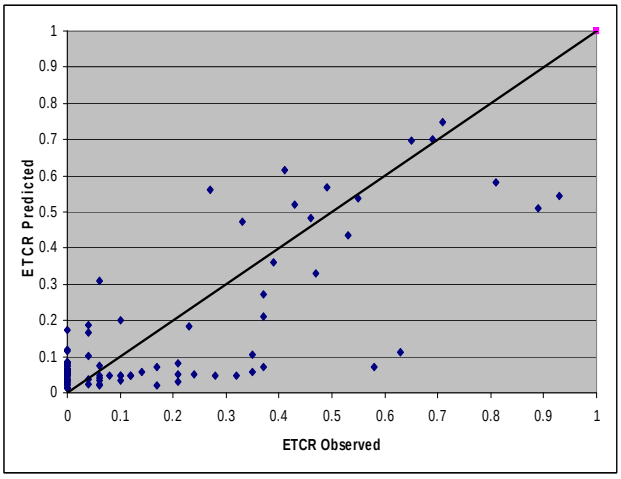

(b) Road Category 13

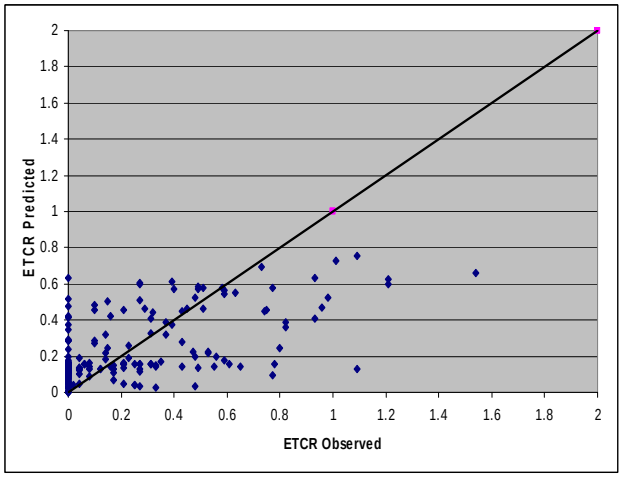

(c) Road Category 14

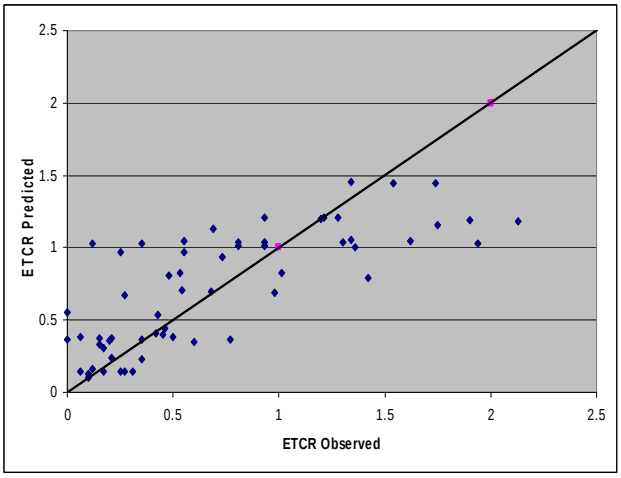

(d) Road Category 15

Figure B-23 Sigmoidal ETCR Model with No SNeff for Road Categories 12 to 15

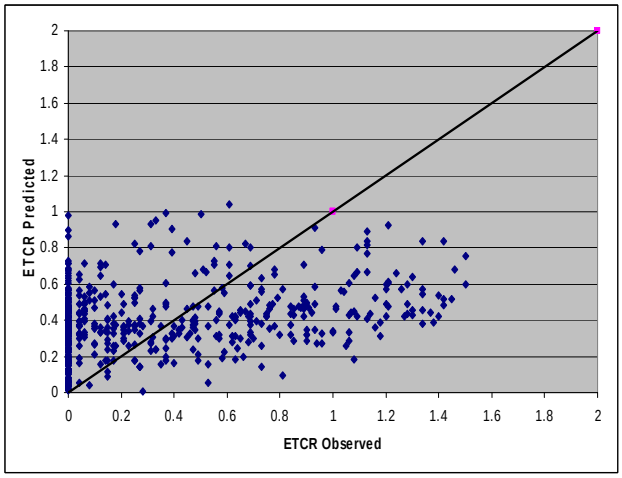

(a) Road Category 16

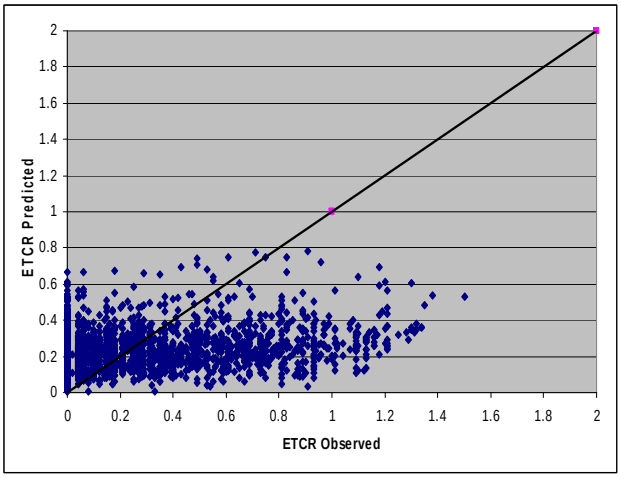

(b) Road Category 17

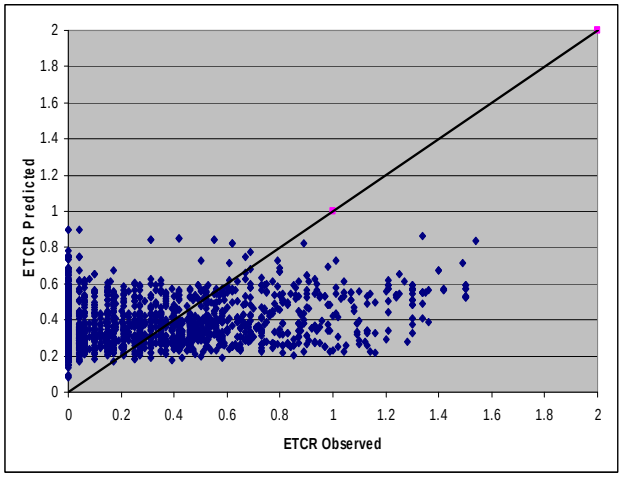

(c) Road Category 18

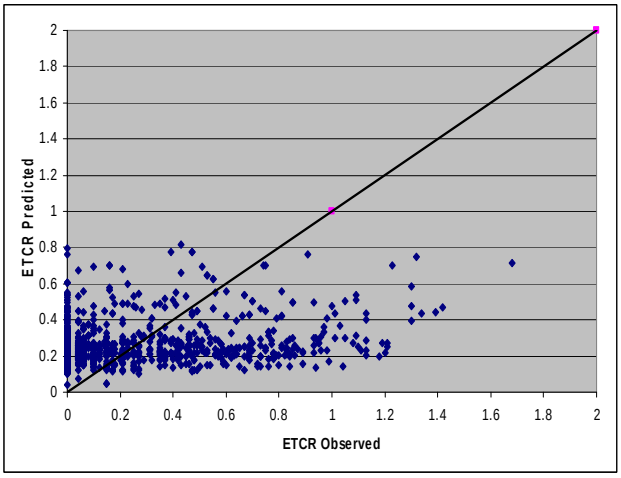

(d) Road Category 19

Figure B-24 Sigmoidal ETCR Model with No SNeff for Road Categories 16 to 19

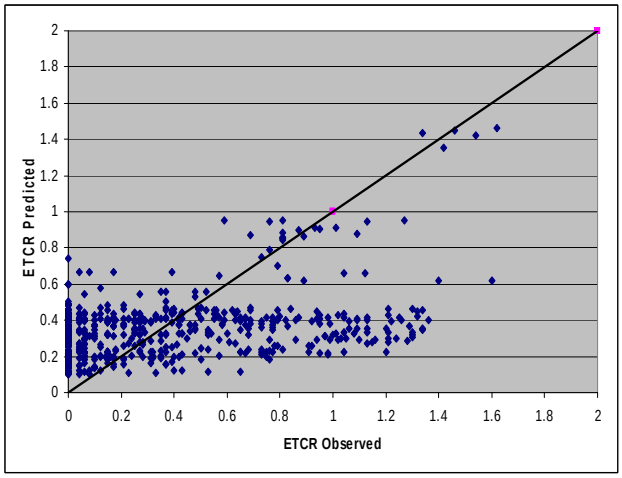

(a) Road Category 20

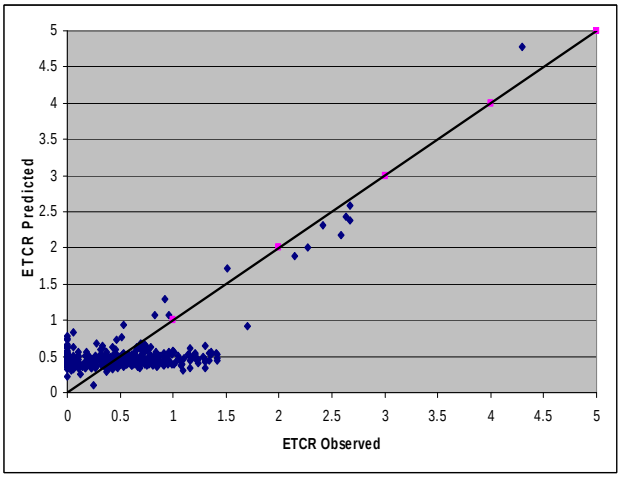

(b) Road Category 21

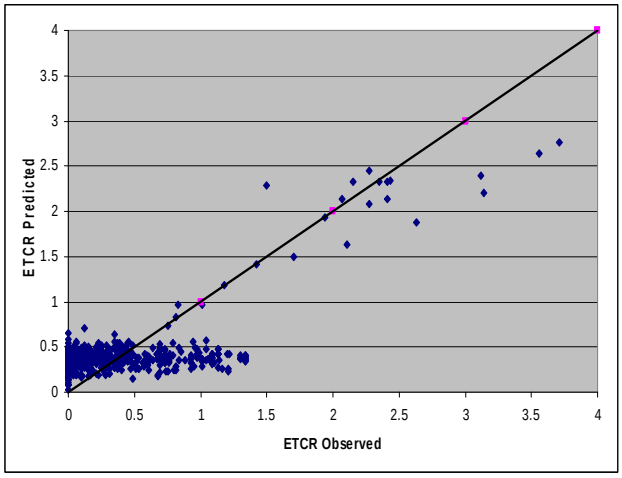

(c) Road Category 22

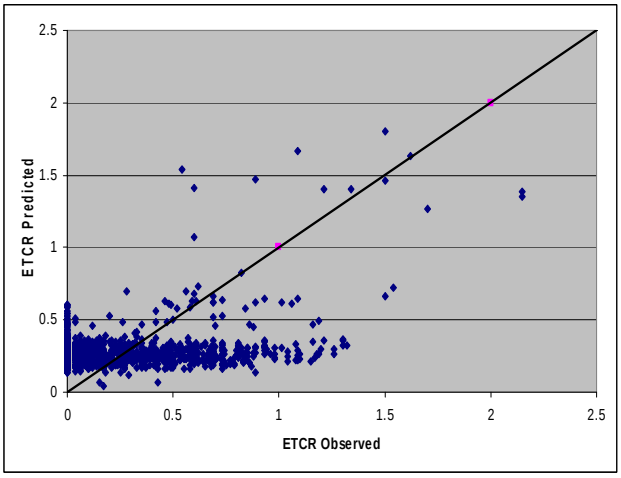

(d) Road Category 23

Figure B-25 Sigmoidal ETCR Model with No SNeff for Road Categories 20 to 23

Validation Plots

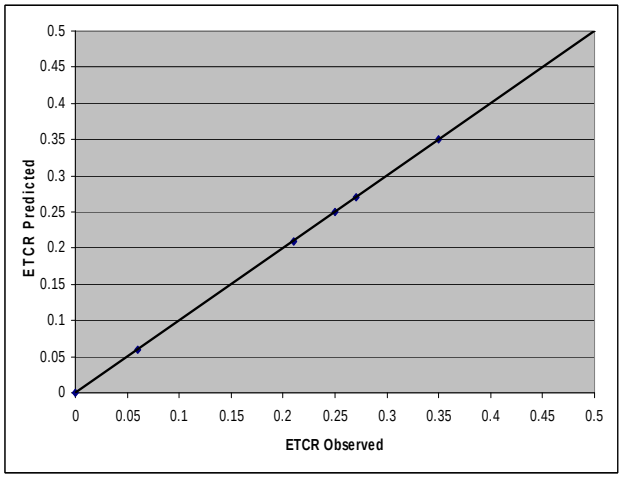

(a) Road Category 12

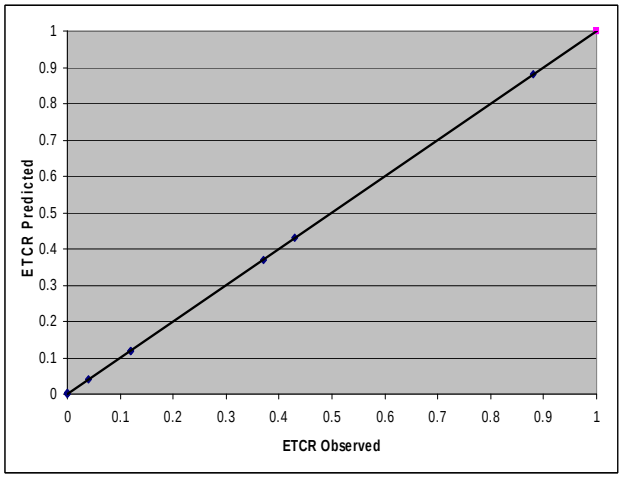

(b) Road Category 13

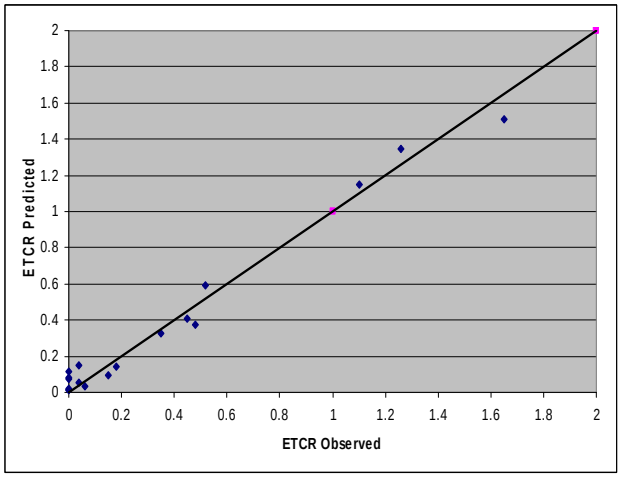

(c) Road Category 14

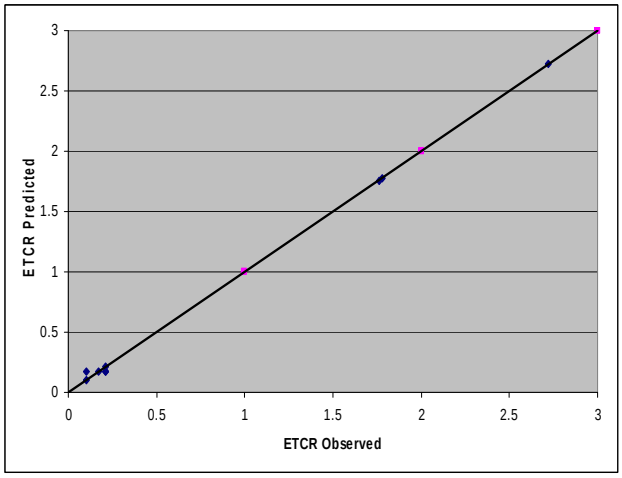

(d) Road Category 15

Figure B-26 Sigmoidal ETCR Model with No SNeff Valid. for Road Categories 12 to 15

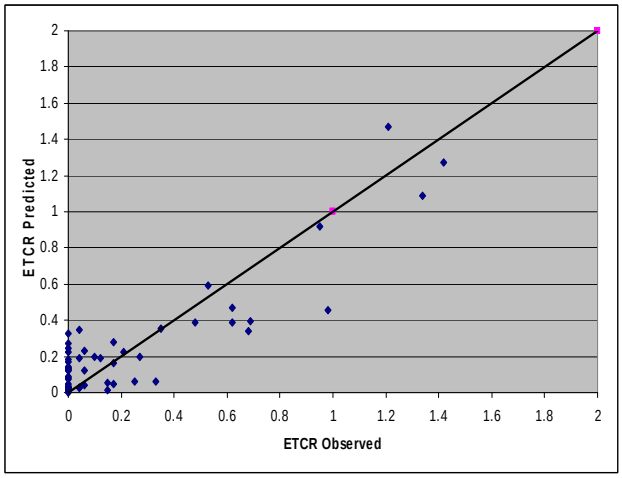

(a) Road Category 16

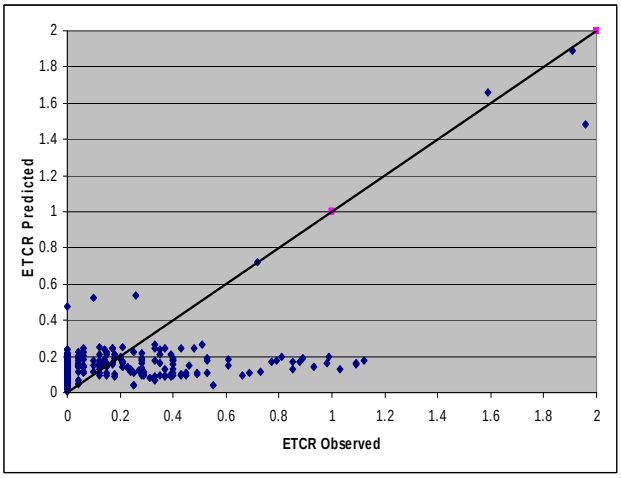

(b) Road Category 17

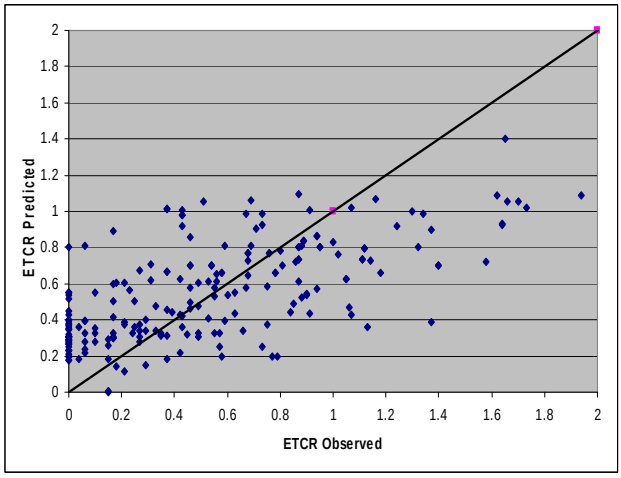

(c) Road Category 18

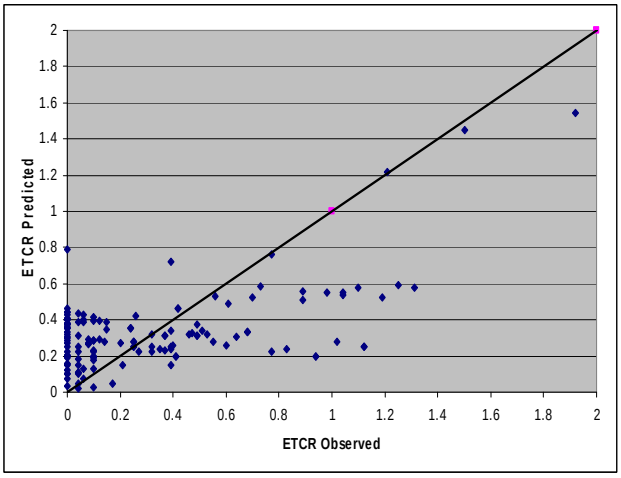

(d) Road Category 19

Figure B-27 Sigmoidal ETCR Model with No SNeff Valid. for Road Categories 16 to 19

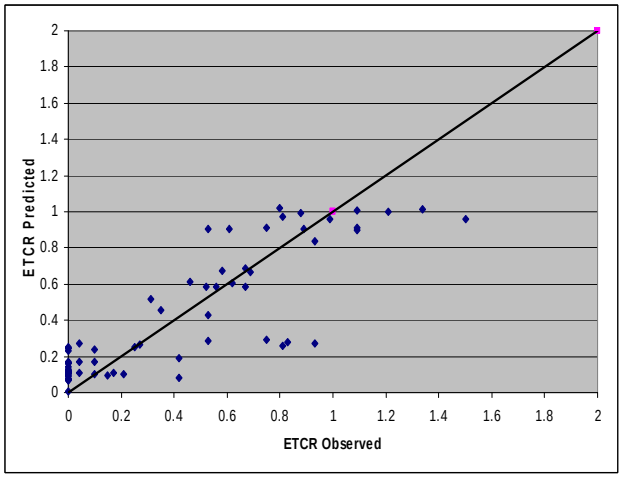

(a) Road Category 20

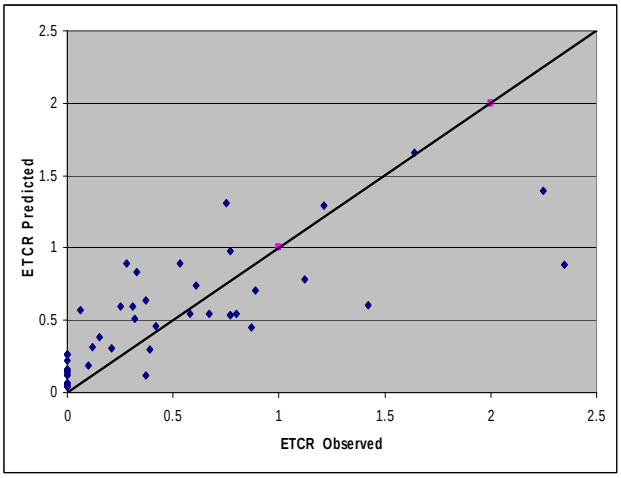

(b) Road Category 21

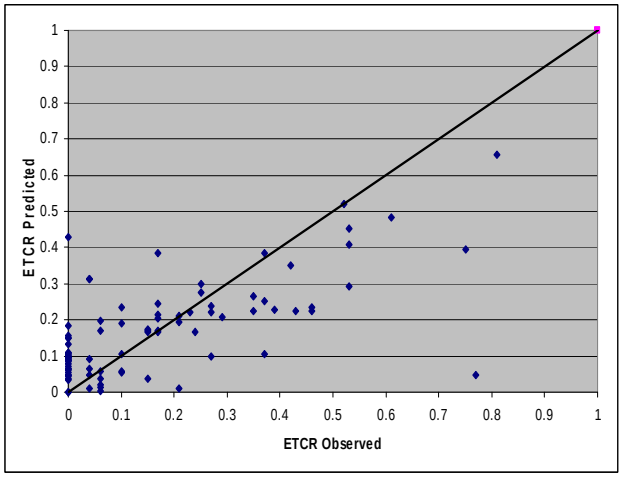

(c) Road Category 22

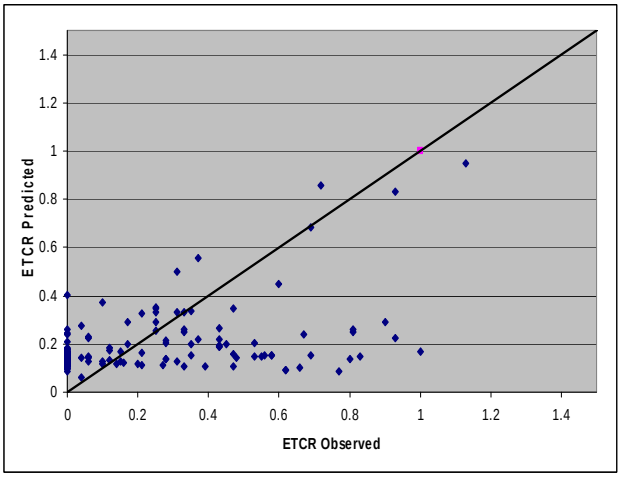

(d) Road Category 23

Figure B-28 Sigmoidal ETCR Model with No SNeff Valid. for Road Categories 20 to 23

District-Wise and Statewide

Table B-17 District-Wise and Statewide Sigmoidal ETCR Model with No SNeff

Dist.		0	1(D)	2(EAL)	3(Rut)	R^2	N
1	δ	0.206	0.007	0.000	0.316	0.21	1423
	α	-0.484	0.204	0.031	-1.091		
	β	3.353	-0.420	0.010	-6.244		
	γ	0.528	-0.093	-0.007	0.121		
2	δ	0.409	-0.009	-0.001	-0.181	0.46	1569
	α	0.454	-0.028	0.000	1.666		
	β	622.934	-46.039	-0.753	18.132		
	γ	22.093	-1.537	0.001	-25.765		
3	δ	0.357	0.010	-0.002	-0.692	0.45	1951
	α	0.531	-0.032	0.003	0.424		
	β	6.239	-3.273	-0.061	-158.179		
	γ	0.939	-0.194	-0.090	6.509		
4	δ	0.084	0.002	0.000	-0.092	0.24	1300
	α	37.175	-12.073	0.565	-12.138		
	β	10.038	-0.636	0.007	-53.102		
	γ	0.315	-0.127	0.001	-6.216		
5	δ	0.222	0.007	0.000	-0.315	0.19	1638
	α	14.940	-1.387	0.130	-24.422		
	β	2.571	-0.051	0.045	2.239		
	γ	-0.251	0.017	0.002	0.632		
6	δ	1.810	-1.784	-0.003	-4.720	0.33	1755
	α	-1.231	1.735	0.003	6.894		
	β	0.950	-0.240	-0.008	-2.694		
	γ	0.028	0.092	-0.001	-0.341		
State	δ	0.385	-0.010	-0.001	1.162	0.09	9636
	α	0.122	0.009	-0.003	-1.674		
	β	-8.872	0.325	0.041	7.115		
	γ	-0.377	-0.006	0.001	0.758		

Model Plots

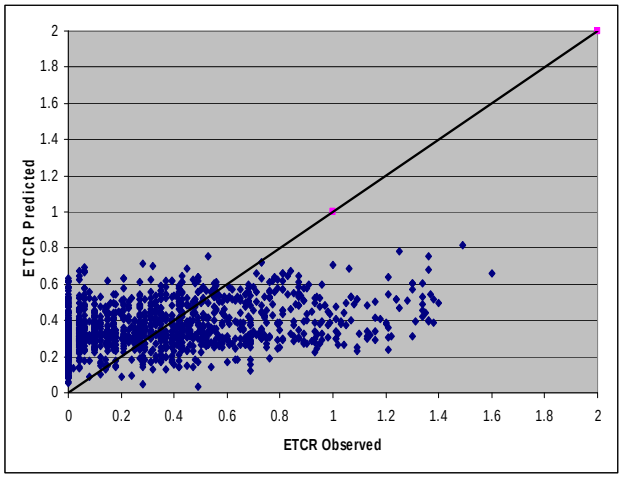

(a) District 1

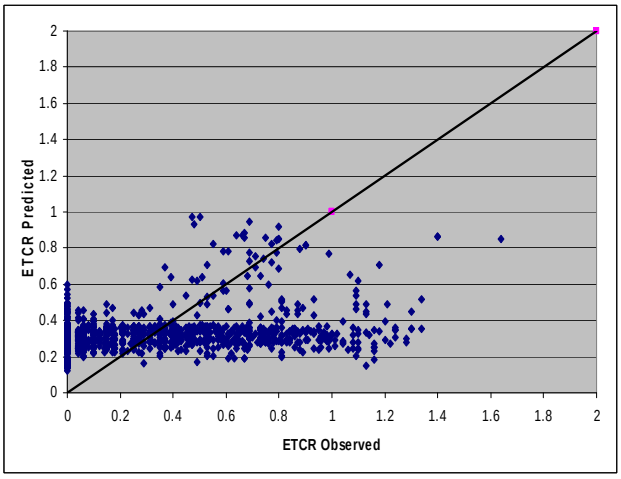

(b) District 2

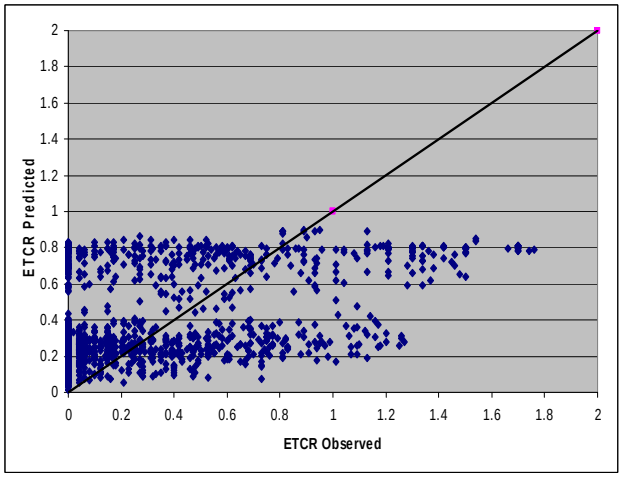

(c) District 3

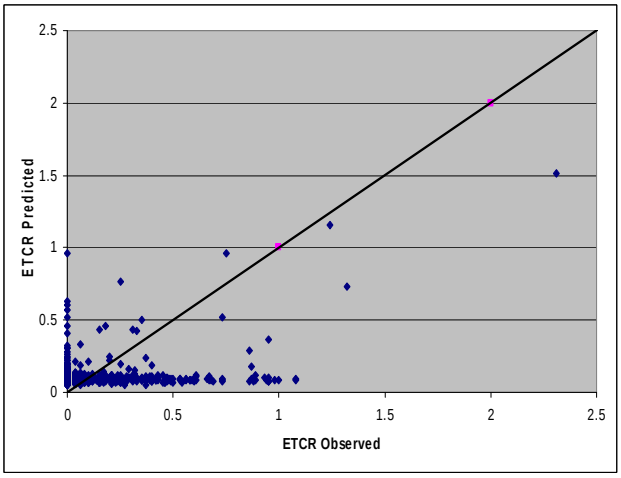

(d) District 4

Figure B-29 Sigmoidal ETCR Model with No SNeff for Districts 1 to 4

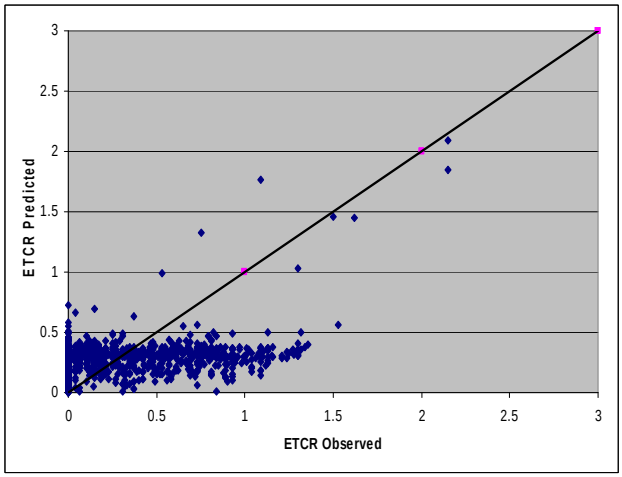

(a) District 5

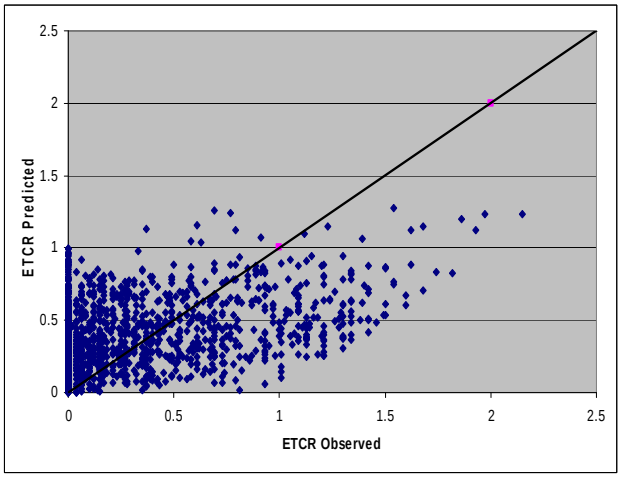

(d) District 6

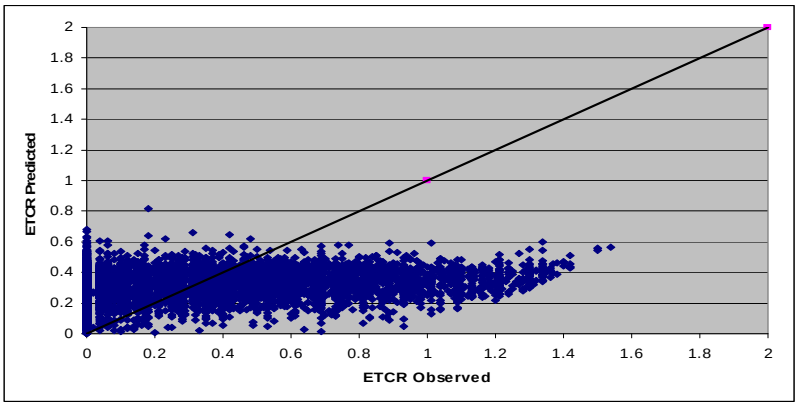

(c) State

Figure B-30 Sigmoidal ETCR Model with No SNeff for Districts 5, 6, and State

Validation Plots

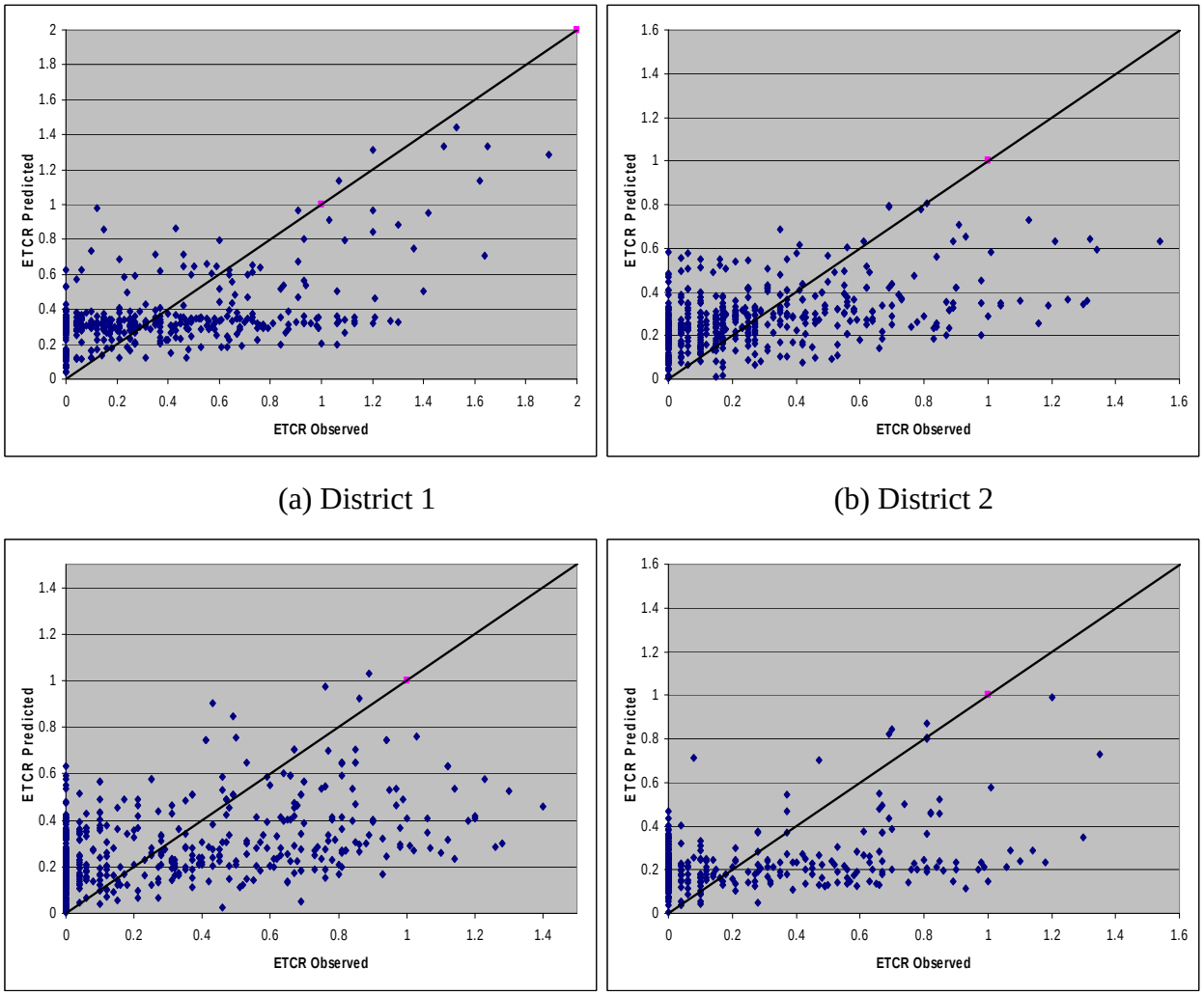

(a) District 1

(b) District 2

(c) District 3

(d) District 4

Figure B-31 Sigmoidal ETCR Model with No SNeff Validation for Districts 1 to 4

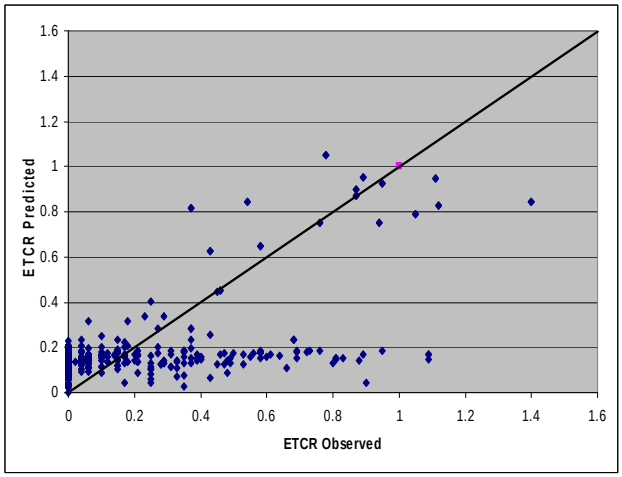

(a) District 5

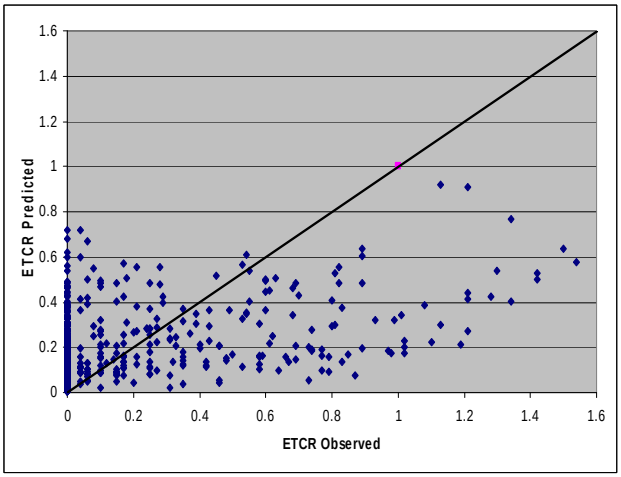

(b) District 6

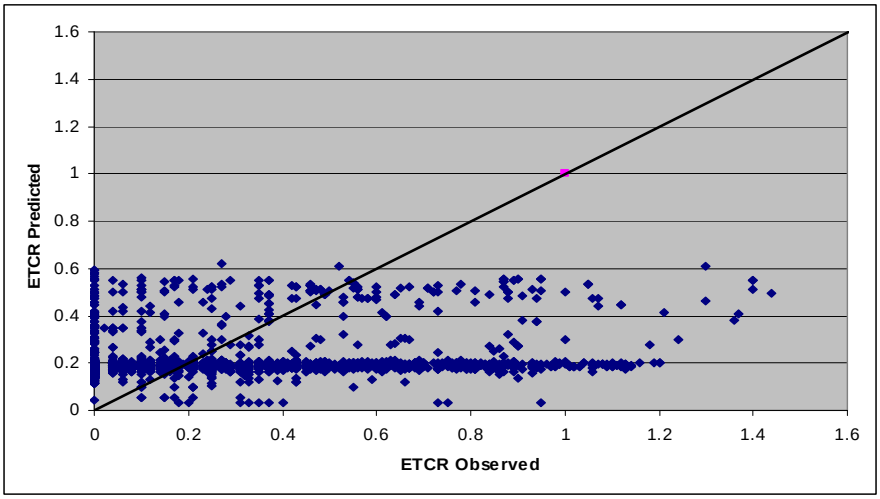

(c) State

Figure B-32 Sigmoidal ETCR Model with No SNeff Valid. for Districts 5, 6, and State

Mean Absolute Deviation

Table B-18 Mean Absolute Deviation for Sigmoidal ETCR Model with No SNeff

	Mean			Mean Absolute Deviation		
	Observed	**Predicted**	**Difference**	**Observed**	**Predicted**	**Difference**
(a) Road Category-Wise						
12	0.141	0.162	-0.022	0.176	0.081	0.094
13	0.129	0.130	-0.002	0.165	0.120	0.045
14	0.195	0.217	-0.023	0.226	0.137	0.089
15	0.701	0.716	-0.015	0.471	0.362	0.109
16	0.342	0.395	-0.054	0.352	0.145	0.207
17	0.177	0.210	-0.033	0.218	0.082	0.137
18	0.302	0.382	-0.081	0.283	0.109	0.174
19	0.194	0.254	-0.059	0.226	0.075	0.151
20	0.283	0.342	-0.059	0.311	0.111	0.201
21	0.472	0.507	-0.036	0.376	0.132	0.244
22	0.334	0.410	-0.076	0.352	0.139	0.213
23	0.211	0.273	-0.062	0.239	0.065	0.174
(b) District-Wise and Statewide						
1	0.321	0.354	-0.033	0.267	0.100	0.167
2	0.298	0.327	-0.030	0.284	0.061	0.222
3	0.285	0.377	-0.092	0.308	0.203	0.105
4	0.077	0.101	-0.024	0.110	0.029	0.081
5	0.218	0.273	-0.054	0.265	0.083	0.183
6	0.284	0.393	-0.109	0.316	0.190	0.125
State	0.241	0.314	-0.073	0.264	0.079	0.185